Durham E-Theses

Theory and performance of high frequency lattice mixers

Korolkiewicz, E.

How to cite:

Use policy

THEORY AND PERFORMANCE OF HIGH

FREQUENCY LATTICE MIXERS

by

E. Korolkiewicz, B.Sc(Hons), M.Sc.

A thesis submitted to the Faculty of Science,
University of Durham, for the degree of
Doctor of Philosophy

Department of Applied Physics   December 1982
    and Electronics,
University of Durham, U.K.

ABSTRACT

Restricting the local oscillator to a sinusoidal current drive the performance of four types of lattice mixers is examined by deriving closed form equations (as compared with the usual numerical computer-aided approach), the effects of the diode parasitics being included.

It is shown that the duality between Z and Y and between G and H mixers is not generally valid (as has been assumed by several workers) except when the diode is regarded as having bi-linear or exponential characteristics and in addition the effect of the diode parasitics is neglected. It is concluded that the H lattice mixer offers the best possibility of producing the lowest conversion loss in practice.

The effect of the diode reactive parasitics (diode package and junction capacitances) on the performance of lattice mixers is also examined. In all the known literature, the diode capacitance parasitics are only included in small-signal analysis and their effect on the local oscillator waveform is ignored. It is shown, however, that the main effect of the diode capacitive parasitics is to modify the local oscillator current waveform present at each diode. It is further shown that this effect has a considerable influence on the performance of lattice mixers.

Microstrip coupled-lines constitute a fundamental building block for the realization of filters associated with image-rejection mixers. The design information on such lines is normally presented in graphical form and only for particular values of relative permittivities of the substrate. To overcome this problem an analytical solution has been developed which relates the physical dimensions of the lines to the odd and even-mode impedances.

Based on the theoretical analysis presented, broadband and narrow-band microstrip lattice mixers were realized and their performance investigated for different terminations at the i.f. port. A good agreement was obtained between the theoretically predicted results and those obtained in practice.

As a result of the above work, four papers have been published by the Institution of Electrical Engineers and one by the International Journal of Electrical Engineering Education and these are listed in Appendix X.

ACKNOWLEDGEMENTS

CONTENTS

Background Review of Mixer Theory and Aims

1.1 Introduction

A heterodyne technique of converting a high frequency (r.f.) signal to a lower intermediate frequency (i.f.) to ease the problem of amplification and frequency selection is often used in communication receivers. Such frequency conversion is obtained by coupling a local oscillator drive and r.f. signal into a non-linear circuit to generate (amongst others) an i.f. frequency. A network containing the non-linear element(s), the means of injecting an r.f. signal, the local oscillator drive, and the means of extracting the i.f. is called a mixer. An important consideration in the design of a communication system receiving low-level r.f. signals is its noise performance.

It has been shown by Friis [1] that the overall noise factor of a receiver consisting of a mixer followed by an i.f. amplifier, assuming that the local oscillator noise is suppressed, is given by,

$$F = L\ (t_N + F_{i.f.} - 1) \qquad\qquad 1.1$$

where L is the conversion loss of the mixer, t_N is the noise temperature ratio of the mixer, and $F_{i.f.}$ is the noise factor of the i.f. amplifier. Equation 1.1 indicates that a low overall noise factor of a receiver is obtained if the mixer has a low conversion loss and low noise temperature ratio. Over the years, a considerable amount of attention has been devoted to the design and analysis of high frequency mixers and a general review of this work is presented here.

Frequency conversion maybe obtained by using elements which exhibit either non-linear resistance or non-linear reactance characteristics. Edwards [2] has shown that devices having non-linear reactance characteristic should be used in frequency up-conversion whilst devices having non-linear

resistance characteristics should be used in frequency down-conversion.

Consequently varactor diodes are used in parametric frequency up-conversion of power from a lower to a higher frequency, whilst resistive diodes, junction transistors or field effect transistors are employed in mixers to convert power from a higher to a lower frequency. Point-contact diodes were used extensively in high-frequency mixer circuits before the advent of Schottky-barrier diodes. The advantages of the Schottky-barrier diodes are that they have a nearly ideal exponential current-voltage characteristic and a high reverse resistance. These desirable properties of the Schottky-barrier diodes have led to a renewed interest in mixer circuits resulting in a substantial improvement in mixer performance. Bipolar microwave transistors are also to be found as non-linear elements in mixer circuits. Although they offer the possibility of conversion gain rather than conversion loss, their noise figure is higher than that of the Schottky-barrier diode. Recently, considerable attention has been focused on the development of GaAs FETs and MESFETs as they appear to offer performances at least comparable with that of the Schottky-barrier diodes. At present, however, because of their nearly ideal properties, Schottky-barrier diodes are still widely used as non-linear elements in mixers.

The behaviour of diodes under the influence of a local oscillator drive and r.f. signal maybe described by non-linear equations. Although solutions to such general equations can be attempted using analytical or numerical techniques, it is extremely difficult to determine the general properties of mixers using this method. The diode in a mixer is driven however by a local signal which is much greater than the r.f. signal and consequently, the drive across each diode is essentially that of the local oscillator with small superimposed perturbations of the r.f.

signal. To a first approximation, it is therefore possible to analyse

the performance of mixers by treating the pumped diode as a time-varying

parameter rather than a non-linear element. Linear theory can then be

applied to the small perturbations produced by the r.f. signal.

A number of authors [3-7] have analysed the performance of single-diode

mixers by assuming that the diode has bi-linear characteristics, i.e.

low forward resistance and high reverse resistance. As a result, the

time-varying resistance of the pumped diode is independent of the

magnitude of the local oscillator drive and has a rectangular waveform.

The theory and performance of mixers have also been developed by several

workers [8-12] on the assumption that a diode obeys an exponential law.

Consequently the waveform of the time varying resistance of the pumped

diode is no longer independent of the local oscillator drive, and is

therefore no longer rectangular. A simpler representation of the diode

was suggested by Strum [13] in his analysis of a single diode mixer.

He proposed that the diode in its reverse characteristic has a constant

high resistance, but in its forward characteristics the relationship

between the current i and voltage v is expressed in the form $i = Kv^x$

where K and x are constants.

The effects of diode parasitics on the performance of single and multi-

diode mixers has been considered by several authors [8, 10, 14-20]. An

important multi-diode mixer is one where the diodes are arranged in a

lattice configuration. Ideally, only even modulation-harmonics appear

at the r.f. port and odd modulation-harmonics appear at the i.f. port

[12]. The properties of this type of mixer driven by a sinusoidal voltage

local oscillator have been investigated by several authors [3-6], assuming

that the diodes have bi-linear characteristics. Kulesza [21] included

in his analysis the effect of the diodes' series resistance for a current-

driven lattice mixer, assuming that the diodes obeyed an exponential law.

The noise performance of mixers using a resistive diode model was initially investigated by Strutt [22], and later by Messenger and McCoy [9]. In both cases, the effects of the diodes' series resistance and the diode reactance parasitics were neglected. A more general analysis of noise in mixers which included the effect of diode series resistance and diode junction capacitance was given by Barker [10]. The noise performance of a mixer in terms of a time-varying conductance and time temperature was initially analysed by Dragone [23]. Stracca [24] then applied these concepts to predict the noise performance of common mixer circuits, and his work was extended by Rustom and Howson [25] who used an improved model of a diode. They concluded, following a computer-based analysis, that H or G mixers with a local oscillator current drive show most promise in relation to low-noise performance of a communication system.

1.2 Mixer Terminology

1.2.1 Frequency Nomenclature

A distortion-free mixer generates modulation products which are in the form $\omega_n = n\omega_p \pm \omega_q$ where ω_p and ω_q are the pump and signal frequencies, respectively, and n is an integer having values $n = 1$, 2, 3,.... The frequency, ω_n, corresponding to $n = 1$ has a form, $\omega_p + \omega_q$ or $\omega_p - \omega_q$. To distinguish between the two cases, if the frequency is $\omega_p + \omega_q$ then the process is called non-inverting conversion, but if it is $\omega_p - \omega_p$ then the process is called inverting conversion. A modulator can be used to translate frequencies either up or down the frequency spectrum. If the output frequency is higher than the signal frequency then the modulator is called an up-converter while if it is less, the modulator is called a mixer. Due to its position in the frequency spectrum an important frequency component in a mixer corresponds to n equal to two and is called an image frequency. The frequency notation used for a down converter mixer is shown in Figure 1.1.

1.2.2 Diode Configurations of Mixers

The single-ended mixer uses one diode situated in the mount of a waveguide-coaxial transformer. The local oscillator drive and the r.f. signal are coupled into a waveguide section, while the i.f. frequency is extracted via co-axial outlet. This type of mixer is very simple in construction but suffers from the disadvantage of poor frequency selection as it maybe difficult to reject the local oscillator and signal frequencies at the i.f. port due to the level differences involved.

In a single-balanced mixer, the local oscillator switching action is such that the unfiltered output does not contain even modulation products of the local oscillator, or the local oscillator frequency. This suppression

of the even modulation products is obtained by using two diodes and a balancing transformer. At high frequencies the balancing transformer is replaced by a magic T for a waveguide structure or a hybrid ring in microwave integrated circuit technology. An advantage of a single balanced mixer is that the noise produced by the local oscillator is minimised if two matched diodes are used.

For a double-balanced or a lattice mixer, the local oscillator drive acts on a lattice network of diodes so as to alternately reverse the path of the carrier. The unfiltered output theoretically does not contain even modulation products, local oscillator or signal frequencies. A further advantage is that owing to the symmetry of the circuit, only even-order modulation products are present at the input port, and only odd-order modulation products are present at the output port. The separation of the even and odd products aids the filtering process of the mixer. Formerly lattice mixers were only used at low frequencies, as it was difficult at r.f. frequencies to select a matched quad of diodes. However, with recent technology, a single package of four matched Schottky barrier diodes is available and, as a consequence it is possible to obtain low noise figures for lattice mixers. The diode mixer circuits for the three basic configurations just discussed are shown in figure 1.2.

1.2.3 Mixer Classification

The mixer, as far as the small signals are concerned may be physically represented as a linear time-varying two-port network. Functionally, however, because selective terminations are normally employed, the mixer behaves as a three-port network having separate ports for the signal, intermediate and image frequencies. It is possible in practice to offer different terminations at the image port which considerably affects the

performance of a mixer.

Three types of image terminations are normally considered, leading to three basic types of mixers.

1. If the termination at the image port of the mixer is the same as that at the r.f. signal port, but all other frequency products are filtered out, then it is called a broadband mixer [12]. This circuit theoretically has a minimum conversion loss of 3 db.

2. A narrow-band image open-circuit mixer has a termination which presents an open-circuit at the image port. For this circuit the theoretical minimum conversion loss is zero db.

3. A narrow-band image short-circuit mixer has a termination which presents a short circuit at the image port. For this type of mixer the minimum theoretical conversion loss is again zero db.

Three other types of mixer have also attracted attention.

In the <u>Harmonic Mixer</u>, the desired output frequency is $n\omega_p - \omega_q$, where n is usually two [20].

In the <u>Image Recovery Mixer</u>, the power at image frequency is converted to intermediate frequency. The conversion is obtained by reflecting the image frequency by a filter back into the mixer, and mixing again with the local oscillator frequency producing the required intermediate frequency [26].

Finally, in the <u>Image Cancelling Mixer</u>, two non-linear elements or mixers are arranged so that the image power generated in one is converted to intermediate frequency in the other, and vice-versa [27].

Balanced mixers have also been classified according to the terminations offered to the undesired out-of-band frequencies [12]. Different configurations of frequency-selective terminations of the input and output ports to the out-of-band modulation frequencies lead to four types

of mixer, Z, Y, G and H. The letter notation corresponds to the type of two-port network parameters which must be used to describe the mixer (see Figure 1.3).

For the Z mixer all out-of-band modulation products at the input and output ports are filtered out by tuned circuits which behave ideally as open circuits at these frequencies. The matrix equation describing the Z mixer is given by,

$$\begin{bmatrix} V_1 \\ V_2 \end{bmatrix} = \begin{bmatrix} Z \end{bmatrix} \begin{bmatrix} I_1 \\ I_2 \end{bmatrix}$$

In the Y mixer the tuned circuits at the input and output ports act as short circuits for all out-of-band modulation products, and the mixer is described by the following matrix equation.

$$\begin{bmatrix} I_1 \\ I_2 \end{bmatrix} = \begin{bmatrix} Y \end{bmatrix} \begin{bmatrix} V_1 \\ V_2 \end{bmatrix}$$

For the H mixer, all odd-order out-of-band modulation products at the input port see an open circuit while all even-order out-of-band modulation products at the output port see a short circuit. The matrix equation describing the 'H' mixer is given below.

$$\begin{bmatrix} V_1 \\ I_2 \end{bmatrix} = \begin{bmatrix} H \end{bmatrix} \begin{bmatrix} I_1 \\ V_2 \end{bmatrix}$$

The G mixer is a dual of the H mixer in that all odd-order out-of band modulation products at the input port see a short-circuit, while all even-order out-of-band modulation frequencies at the output port see an open circuit. The matrix equation describing the G mixer is therefore,

$$\begin{bmatrix} I_1 \\ V_2 \end{bmatrix} = \begin{bmatrix} G \end{bmatrix} \begin{bmatrix} V_1 \\ I_2 \end{bmatrix}$$

1.2.4 Mixer Performance Criteria

The desirable mixer performance is low conversion power loss, noise figure and distortion.

The conversion power loss (c.p.l.) is a measure of the losses that occur in the process of frequency conversion in a mixer. It is defined as the ratio of the available power at r.f. frequency to the output power at intermediate frequency.

$$c.p.l. = 10 \; \log_{10} \frac{\text{Available Input Power at Radio Frequency}}{\text{Output Power at Intermediate Frequency}} \qquad 1.2$$

$$= 10 \; \log_{10} L$$

The available power conversion defined by Friis [1] is also sometimes used to describe the performance of a mixer and is defined as

$$c.p.l._{opt} = 10 \; \log_{10} \frac{\text{Available Power at the r.f. Frequency}}{\text{Available Power at i.f. Frequency}} \qquad 1.3$$

To distinguish between the conversion loss for different types of mixers the following nomenclature [8] is generally adopted;

L_0 mixer is matched to the L.O. and has the same terminations at signal and image frequencies.

L_1 = mixer is matched to the signal but the image sees a short-circuit.

L_2 = mixer is matched to the signal and the image frequencies.

L_3 - mixer is matched to the signal but the image sees an open-circuit.

The sensitivity of a receiver determines the smallest signal which can be detected and is governed by the noise figure of the receiver. If a receiver is considered as consisting of two, two-port networks connected in tandem, corresponding to the mixer and i.f. amplifier, then the overall noise figure is given by,

$$F = F_m + \left[\frac{F_{i.f.} - 1}{G} \right] \qquad 1.4$$

F_m is the noise figure of the mixer, $F_{i.f.}$ is the noise figure of the i.f. amplifier and $G(= 1/L)$ is the 'gain' of the mixer. Equation 1.4 can also be expressed in the form,

$$F = L \left[\frac{F_m}{L} + F_{i.f.} - 1 \right] \qquad 1.5$$

If the noise temperature t_n of the mixer is defined as,

$$t_n = F_m/L \qquad 1.6$$

and substituted in equation 1.5, equation 1.1 is obtained.

The major noise contributions in a semi-conductor diode are ,1/f or flicker noise which is characteristic of all semi-conductors, thermal noise produced by the diode series resistance, and shot-noise produced by electrons moving with random velocities in an electric field. Flicker or 1/f noise is inversely proportional to frequency [13], and its effect may be neglected at normal intermediate frequencies. Thermal noise is caused by the random motion of electrons in a conductor and the resulting mean square open-circuit voltage, $\overline{v_n^2}$ developed is given by,

$$\overline{v_n^2} = 4kTRdf$$

R is the resistance of the conductor, df is the bandwidth, T is the temperature and k is the Boltzman's constant. The variation of the average current I due to the random arrival of the electrons at the anode of a diode was investigated by Schottky. He showed that the mean square noise current $\overline{i_n^2}$ due to this effect is given by,

$$\overline{i_n^2} = 2qI \; df$$

where the bandwidth is df and q is the charge of the electron.

Messenger and McCoy [9] have shown that the relationship between noise figure of a mixer and conversion loss is,

$$F = (L/2) + 1/2 \quad \text{for narrow band mixers} \qquad 1.7$$

and $\qquad F = (L/2) + 1 \quad \text{for a broad band mixer} \qquad 1.8$

Equations 1.7, and 1.8 are derived on the assumption that parasitic effects of the diode are ignored, and indicate that there is a linear relationship between the two mixer parameters F and L. It is found that whereas conversion loss reaches a broad minimum and then starts to increase with increasing local oscillator drive, the noise figure continues to decrease with increasing local oscillator drive. There is therefore an optimum local oscillator level which minimises both the conversion loss and the noise figure of the mixer. However, as the noise figure for modern mixers is significantly lower than that of the i.f. amplifier, the minimum receiver noise figure occurs when the conversion loss is a minimum.

Dragone [23] has developed a new method for determining the noise performance of a resistive mixer which does not involve a detailed analysis of shot or thermal noise sources. His method describes the terminal noise performance of a diode in terms of time-varying conductance $g(t)$ and time-varying temperature $T(t)$. He showed that the noise of the terminals of a single diode is equal to that of two diodes connected in parallel, having time independent temperatures T_1 and T_2 and time-varying conductances $g_1(t)$ and $g_2(t)$ where

$$g(t) = g_1(t) + g_2(t) \qquad\qquad 1.9$$

and $$G(t)\, T(t) = g_1(t)\, T_1 + g_2(t)\, T_2 \qquad\qquad 1.10$$

The temperatures T_1 and T_2 are the minimum and maximum values of $T(t)$ so that,

$$T_1 \leqslant T(t) \leqslant T_2$$

Stracca [24], using this method, analysed the noise performance of common mixer circuits but neglected the effects of diode reactive parasitics.

1.3 Non-Linear Elements used in Mixer Circuits

A linear element is defined as one whose value (resistance, capacitance or inductance) remains constant when the input level of the signal is applied. A non-linear element, however, has a characteristic $I = f(V)$, $Q = f(V)$ or $\phi = f(I)$, which normally is a single-valued function for the three cases respectively. As a consequence of such a non-linear characteristic, the resulting response will contain frequency components which will not be present in the applied stimulus. It is this harmonic generation property of non-linear elements which is exploited in mixers and parametric converters.

A non-linear element commonly used in mixers is a diode whose equivalent circuit at high frequencies is shown in Figure 1.4 where,

L_L is the lead inductance

L_p is the inductance of the whisker contact

r_S is the series resistance

C_p is the package capacitance

G_j is the junction conductance

C_j is the barrier capacitance

The relationship between the diode junction voltage v_j and the current i through the diode is,

$$i = I_s (e^{\alpha v_j} - 1) \tag{1.11}$$

where I_s is the saturation current whose value depends on the diode material and production process and $\alpha (= q/nkT)$ is a diode constant. The junction conductance of a diode is given by,

$$G_j = di/dv_j = \alpha(i + I_s) \tag{1.12}$$

A diode is normally driven by periodically-varying local oscillator and hence G_j is also a periodically-varying function of time. The diode barrier capacitance (C_j) is also a function of diode junction voltage, i.e.

$$C_j = \frac{C_j(o)}{\left[1 - V/V_D\right]^n} \qquad 1.13$$

where $C_j(o)$ is the barrier capacitance at zero junction voltage and V_D is the diffusion potential. For a periodic local oscillator drive the barrier capacitance, just like the junction resistance, is a periodic function of time.

Point-contact diodes which are made by having a wire whisker pressed against a semiconductor surface (usually p+ epitaxial silicon) have been historically used for detection of high-frequency signals. The series resistance of a point contact diode arises from the restriction of current flow caused by the small contact area of the wire, i.e.

$$r_s = \rho/2a$$

where 'a' is the radius of the contact and ρ is the resistivity of the semiconductor.

A considerable improvement in the mixer performance was obtained with the development of the Schottky-barrier diode. These diodes are fabricated by depositing a metal on a semiconductor surface by a process of evaporation, sputtering or electromechanical methods. Schottky-barrier diodes have a V-I characteristic which is nearly exponential. They also have a lower saturation current, series resistance and barrier capacitance than contact diodes. Backward diodes also used in mixer circuits are a special kind of tunnel diode where the tunnelling process is considerably reduced. The V-I characteristics for the three types of diodes are shown in Figure 1.5. MESFET's and GaAsFET's are also used

as non-linear elements in mixers   up to frequencies of 10 GHz

The high frequency operation of the GaAsFET is obtained by replacing

the diffusion process of a pn junction by a Schottky-barrier contact

which has a very-short-time storage. The noise performance of mixers

using FETs is   competitive with all but the best diode mixers and

they are linear up to higher input signal power levels than the diode

mixers. The reason for this greater linearity is the square-law

relationship between drain current and gate-source voltage over a wide

range of the latter. Since f.e.t. s also produce conversion gain rather

than conversion loss, the performance of the i.f. amplifier becomes

less important. The greatest problem with f.e.t. mixers is, however,

one of stability.

1.4 General Mixer Theory

The theory of mixers has been developed on the assumption that the local

oscillator drive is much larger than the signal components present.

Consequently, the non-linearity of the mixer is only affected by the

local oscillator drive. However, signals present in the mixer are at

a much lower level and the interaction between them is linear to a high

degree. A mixer, therefore, may be represented as a linear 'n'-port

network with separate conceptual ports at the signal and all modulation

products. In practice selective networks are used so that the n-ports

of the mixer are reduced to three, corresponding to signal, i.f. and

image frequencies.

1.4.1 Representation of a Mixer by a Linear Network

For a non-linear device the current-voltage characteristic is given by,

$$I = f(V) \qquad\qquad 1.14$$

If the applied voltage consists of a local oscillator drive $V_{LO}(t)$ and

an r.f. signal $V_q(t)$, then,

$$V = V_{LO}(t) + V_q(t) \qquad\qquad 1.15$$

where in normal mixer operation $V_{LO}(t) >> V_q(t)$

Substituting equation 1.15 and 1.14 and expanding the resulting equation by Taylor series, the first two terms are given by,

$$I = f \left[V_{LO}(t) + V_q(t) \right]$$

$$\therefore I_{LO} + i = f \left[V_{LO}(t) \right] + V_q(t) f' \left[V_{LO}(t) \right] + \cdots$$

1.16

The small signal current i can be expressed in the form,

$$i = \left[f' \left[V_{LO}(t) \right] \right] V_q(t) = g(t) V_q(t)$$

1.17

As far as the r.f. signal is concerned, the non-linear element behaves as a linear conductance varying periodically with time which can be expressed in terms of a Fourier series,

$$g(t) = \sum_{-\infty}^{+\infty} g_n e^{jn\omega_p t}$$

1.18

If the local oscillator drive is an even function of time then $g_n = g_{-n}$ and the conductance waveform becomes,

$$g(t) = g_0 + 2 \sum_{n=1}^{\infty} g_n \cos n\omega_p t$$

1.19

where the Fourier coefficients are,

$$g_n = \frac{1}{2\pi} \int_{-\pi}^{+\pi} f' \left[V_{LO}(t) \right] e^{jn\omega_p t} \, d(\omega_p t)$$

1.20

The small-signal performance of a mixer as defined by equation 1.17 results in a matrix which allows the linear relationship between various small signal frequency components to be derived. To determine this matrix, consider Figure 1.6 where the voltage v(t) and current i(t) contain all possible modulation products $n\omega_p \pm \omega_q$ where n=1,2,3 etc.

$$v(t) = \sum_{0}^{\infty} V_n \cos (n\omega_p \pm \omega_q)t$$

1.21

and

$$i(t) = \sum_{0}^{\infty} I_n \cos (n\omega_p \pm \omega_q)t$$

1.22

Equations 1.21 and 1.22 are related by Ohm's law at all instants of time
so that,

$$i(t) = g(t) \, V(t) \qquad\qquad 1.23$$

Equation 1.23 must also be true at each frequency so that,

$$\sum_{\infty}^{\infty} I_n \cos (n\omega_p \pm \omega_q)t = g(t) \sum_{\infty}^{\infty} V_n \cos (n\omega_p \pm \omega_q)t$$

and the resulting matrix equation of the non-linear element is,

$$
\begin{bmatrix} \cdot \\ I_{+1} \\ I_0 \\ I_{-1} \\ \cdot \end{bmatrix}
=
\begin{bmatrix}
\cdot & \cdot & \cdot & \cdot & \cdot \\
\cdot & g_0 & g_1 & g_2 & \cdot \\
\cdot & g_1 & g_0 & g_1 & \cdot \\
\cdot & g_2 & g_1 & g_0 & \cdot \\
\cdot & \cdot & \cdot & \cdot & \cdot
\end{bmatrix}
\begin{bmatrix} \cdot \\ V_{+1} \\ V_0 \\ V_{-1} \\ \cdot \end{bmatrix}
\qquad 1.24
$$

Normally, it is not necessary to consider the infinite number of equations
shown by equation 1.24 and only three frequencies are considered, signal
intermediate and image. Hence equation 1.24 reduces to,

$$
\begin{bmatrix} I_q \\ I_{i.f.} \\ I_I \end{bmatrix}
=
\begin{bmatrix}
g_0 & g_1 & g_2 \\
g_1 & g_0 & g_1 \\
g_2 & g_1 & g_0
\end{bmatrix}
\begin{bmatrix} V_q \\ V_{i.f.} \\ V_I \end{bmatrix}
\qquad 1.25
$$

where $I_q \equiv I_0$, $I_{i.f.} \equiv I_{-1}$ and $I_I \equiv I_{+1}$.

A block diagram of a mixer described by equation 1.25 is shown in Figure
1.7 as having three conceptual ports associated with the signal, image
and intermediate frequencies. The performance of the mixer can now be
evaluated using linear theory.

1.4.2 Evaluation of the Coefficients of the Time-Varying Parameters

For a single-ended diode mixer, where the diode is assumed to have bi-linear
characteristic(see Figure 1.8), the waveform of the time-varying conductance

g(t) is shown in Figure 1.9. The Fourier series of such a waveform

can be expressed in the form,

$$g(t) = g_b + \frac{\tau}{T}(g_f - g_b) + \frac{2}{\pi}(g_f + g_b) \sum_{n=1}^{\infty} \frac{\sin(\frac{n\pi\tau}{T})}{n} \cos n\omega_p t \qquad 1.26$$

where g_b and g_f are the reverse and forward conductances of the diode

respectively and τ/T is the pulse duty ratio.

In the case of a Y mixer having a short-circuit image terminations, or

a Z mixer having an open-circuit image termination, Saleh [12] has

shown that the condition for minimum conversion loss is obtained by

solving the following transcendental equation for τ/T.

$$\tan(\frac{\tau\pi}{T}) = \pi \frac{\tau}{T} + \frac{g_b\pi}{g_f - g_b} \qquad 1.27$$

and occurs when the pulse duty ratio τ/T is very small.

Howson [28] has also determined the required optimum waveform for the

time-varying parameter g(t) for a single ended diode Y mixer with image

open-circuit termination and a single diode Z mixer having an image

short-circuit termination. He showed that the minimum conversion loss

occurs when the second harmonic of g(t) is zero. This optimum condition

is obtained when the ratio of the first harmonic to the average value

of g(t) is maximum.

A more practical model of a diode is one where it is assumed that the

diode has an exponential characteristic rather than the bi-linear characterist-

ic shown in Figure 1.8. For an exponential diode the evaluation of the

conductance or resistance waveforms for two types of local oscillator drives,

a sinusoidal current and sinusoidal voltage, is given below

A sinusoidal local oscillator current drive can be written in the form,

$$i = I_{d.c.} + I_p \cos \omega_p t \qquad 1.28$$

Neglecting the effect of the diode saturation current I_s, the time-varying resistance of the diode is given by [29],

$$r(t) = \frac{dv}{di} = \frac{1}{(\alpha I_{d.c.})\left(1 + \frac{I_p}{I_{d.c.}}\cos \omega_p t\right)}$$

$$= \frac{1 + 2 \sum_{n=1}^{\infty} a_n \cos n\omega_p t}{\alpha I_{d.c.}\left(1 - \left(\frac{I_p}{I_{d.c.}}\right)^2\right)^{\frac{1}{2}}}$$ 1.29

where,

$$a_n = \left[\frac{-I_p / I_{d.c.}}{1 + \left(1 - \left(\frac{I_p}{I_{d.c.}}\right)^2\right)}\right]^n$$ 1.30

Using equations 1.29 and 1.30, the coefficients of equation 1.25 can be evaluated and the performance of a balanced diode mixer determined.

For a local oscillator sinusoidal voltage drive let

$$v = V_{d.c.} + V_p \cos \omega_p t$$

Again assuming an exponential law for the diode and neglecting the effect of diode series resistance it can be shown that [8],

$$g(t) = \frac{di}{dv} = \alpha I_s\, e^{\alpha V_{d.c.}} \mathfrak{I}_0 (\alpha V_p) + 2\mathfrak{I}_1 (\alpha V_p) \cos \omega_p t +$$

$$2\mathfrak{I}_2 (\alpha V_p) \cos 2 \omega_p t + \dots$$ 1.31

where $\mathfrak{I}_0$, $\mathfrak{I}_1$ and $\mathfrak{I}_2$ etc are the modified Bessel functions. The Fourier coefficients g_0, g_1 and g_2 of the time-varying conductance of a diode are,

$$g_0 = I_s\, e^{\alpha V_{d.c.}} \mathfrak{I}_0 (\alpha V_p)$$

$$g_1 = I_s\, e^{\alpha V_{d.c.}} \mathfrak{I}_1 (\alpha V_p)$$

$$g_2 = I_s\, e^{\alpha V_{d.c.}} \mathfrak{I}_2 (\alpha V_p)$$

The effect of the diode series resistance and capacitance on the conversion loss and noise figure for a single-diode mixer was investigated by Barker [10]. He showed that the effect of the diode series resistance is to increase the conversion loss for very high local oscillator drive, and that the only way of reducing this effect is to use reverse d.c. bias.

In the case of a multi-diode lattice mixer the optimum time-varying waveform is a rectangular one where the pulse duty ratio τ/T is a half [12, 13, 27]. For such a mixer the local oscillator drive 'sees' effectively two pairs of diodes back to back and consequently they act as an amplitude limiter, so that a square-waveform is the only one of any practical significance.

The coefficients of the matrix equation describing a lattice mixer have been determined by several authors [3-6] on the assumption that the diode has bi-linear characteristics. Saleh [12] has also analysed a lattice mixer where he assumed that the diode obeyed an exponential law but neglected the effect of the diode series resistance. Kulesza [21] has determined the performance of a current-driven lattice mixer with image open-circuit and included the effect of the diode series resistance in his analysis. A computer-assisted analysis of the response coefficients of a lattice mixer has been obtained by Maiuzzo and Cameron [30] assuming a correlation between the diode series resistance and the diode parameter α. The performance of a K-band integrated lattice mixer has been investigated by Ogwa, Aikawa and Morita [31] where it is assumed that the diode obeys an exponential law but the effect of diode series resistance has been neglected.

1.5 Conclusions

The analysis of mixers consists of two parts: the large-signal analysis and the small-signal analysis. The former analysis is concerned with the behaviour of the diode when pumped by the local oscillator, while the small-signal analysis treats the mixer as a linear two-port network and is largely concerned with the effect of the image termination on the r.f. and i.f. impedances necessary to produce minimum conversion loss.

Early workers [3-5] assumed that the diode pumped by a local oscillator could be considered as having two states, high and low resistance. Later Torry and Whittmer [8] analysed the behaviour of a mixer by assuming that the diode has an ideal exponential characteristic but neglected the effects of the diode parasitics, such as the series resistance and the capacitance. Strum [13] described the behaviour of a diode by a power law, given $I = KV^{\bar{x}}$ where K and $\bar{x}$ are constants for a particular diode. Kulesza [21] analysed the behaviour of a narrow-band image-open circuit lattice mixer pumped by a local oscillator sinusoidal current, and included the effect of the diode series resistance.

The general small signal analysis of resistive mixers and their classification Z, Y, H and G was presented by Saleh [12]. This classification depends on the type of frequency-selective networks used at the r.f. and i.f. ports of the mixer and hence the type of matrix which has to be used to determine its performance. The image-frequency terminations affect the mixer's r.f. and i.f. terminations necessary to produce minimum conversion loss. The i.f. impedance is the output impedance of the mixer and is particularly important as it influences the design of the i.f. amplifier input circuits, and hence the receiver noise figure that can be obtained.

1.6 Aims of the Project

The principal aims of this project are to investigate analytically the effect of the local oscillator drive, image impedance and diode parasitics on the performance of Z, Y, G and H lattice mixers working at high frequencies, and where a practical model of a diode is used. For each of the above four types of mixers (Z, Y, G and H) four distinct cases are to be considered; two narrow-band mixers and two broadband mixers one with matched and the other with mismatched conditions at the r.f. port.

In the large signal analysis of the lattice mixer it is important to use a model of the diode which is sufficiently accurate to represent a true practical mixer, without however being so complex that the mathematics becomes unmanageable. Various numerical methods are therefore normally used in order to determine the Fourier coefficients of the pumped diodes. In this project, however, by restricting the local oscillator to a current drive, it is proposed to obtain an analytical solution, where the effect of the diode's parasitics such as the diode series resistance and capacitance are included.

1.7 <u>References</u>

1. Friis, H.T., Noise Figures of Radio Receivers, Proc. IRE, 1944, 32, pp. 419-422.

2. Edwards, C.F., Frequency Conversion by Means of a Non-Linear Admittance, BSTJ, Nov. 1956.

3. Belevitch, V., Linear Theory of a Bridge and Ring Modulator Circuits, Elec. Comm 25, 1948.

4. Kruse, S., Theory of Rectifier Modulators, Ericsson Techniques 1939.

5. Tucker, D.G., Modulators and Frequency Changers, MacDonald 1953.

6. Howson, D.P. and Tucker, D.G., Rectifier Modulators with Frequency Selective Terminations, Proc. IEE 1960, Vol. 107, Part B, No. 33.

7. Rafuse, R.P., Low Noise and Dynamic Range in Symmetric Mixer Circuits, Proc. of the 1st Viennial Cornell Conf. 1967.

8. Torrey, H.C. and Whitmer, C.A. Crystal Rectifiers, Radiation Laboratory Series Vol. 15 1948.

9. Messenger, G.C. and McCoy C.T., Theory and Operation of Crystal Diode as Mixers, Proc. IRE 1957, Vol. 45, pp. 1269-1283.

10. Barber, M.R., Noise Figure and Conversion Loss of the Schotty-barrier Mixer Diode, Trans. IEEE, Nov. 1967, MIT-15, No 11, pp. 629-635.

11. O'Neill, H.J., Image Frequency Effects in a Microwave Crystal Mixer, Proc. IEEE, Nov. 1965, Vol. 112, No 11.

12. Saleh, A.A.M.S., Theory of Resistive Mixers, MIT Press 1971.

13. Strum, P.D., Some Aspects of Mixer Crystal Performance, Proc. IRE, 1953, Vo. 41, pp. 875-890.

14. Lechti, C.A., Down-Converters using Schottky-barrier Diodes, IEEE Trans on Elec. Devices, Nov. 1970, Vol. ED-17, No 11.

15. Dragone, C., Performance and Stability of Schottky-Barrier Mixers, B STJ, Dec. 1972, Vol. 51, No. 10.

16. Mania, L., Stracca,G.B., Effects of the Diode Junction Capacitance on the Conversion Loss of Microwave Mixers, IEEE Trans. on Comm. Sept. 1974, Vol. COM 22, No 9.

17. Stracca, G.B., et al, Low Noise Microwave Down Converters with Optimum Matching at Idle Frequencies, Trans. IEEE MIT Aug. 1973.

18. Pound, R.V., Microwave Mixers, MIT Press 1948.

19. Van Der Graff, J. Unpublished Report on Modulators, Netherlands Post and Telecom Service.

20. Schneider, M.V., Harmonically Pumped Strip Fine Down Converters Trans. IEEE MIT 8T 23, No. 3, March 1973.

21. Kulesza, B.L.J., General Theory of a Lattice Mixer, Proc. IEE 1 8 1971, No. 7.

22. Strutt, M.J.O., Diode Frequency Chargers, Wireless Eng. Feb. 1936, Vol. 13, No 149, pp. 73-80.

23. Dragone, C., Analysis of Thermal and Shot Noise in Pumped Resistive Diodes, BSTJ Nov. 1968, pp 1883-190.

24. Stracca, G.B., Noise in Frequency Mixers Using Non-Linear Resistors Alta Frequenza 1971, Vol. XL, No. 6.

25. Rustom, S., and Howson, D.P., Mixers Noise Figure Using an Improved Resistive Diode Model, INT. J. Elect. 1976, Vol 41, No. 2.

26. Oxley, T.H., et al., Image Recovery Mixers, E.M.C. Stockholm, Aug 1971.

27. Howson, D.P., Tahim, R.S.,Gardiner,J.G., A Microwave Mixer with Image Cancellation, proc. Fourth Colloq. Microwave Communication, Budapest 1970.

28. Howson, D.P., Ideal Forms of Periodically Varying Conductance for Low Loss Mixers, Int. J. Electronics 1975, Vol. 38, No. 1.

29. Johnson, K.M., X-Band Integrated Circuit Mixer with Reactively Terminated Image, Trans. IEEE Vol. MTT-16, No.7, July 1968.

30. Maiuzzo, M.A., and Cameron, S.H. Response Coefficients of a Double-Balanced Diode Mixer, Trans. IEEE Vol. EMC-21, No.4, Nov 1979.

31. Ogawa, H., A Kawa, M., Morita, K., K-Band Integrated Double-Balanced Mixer, Trans, IEEE Vol. MTT-28, No.3, March 1980.
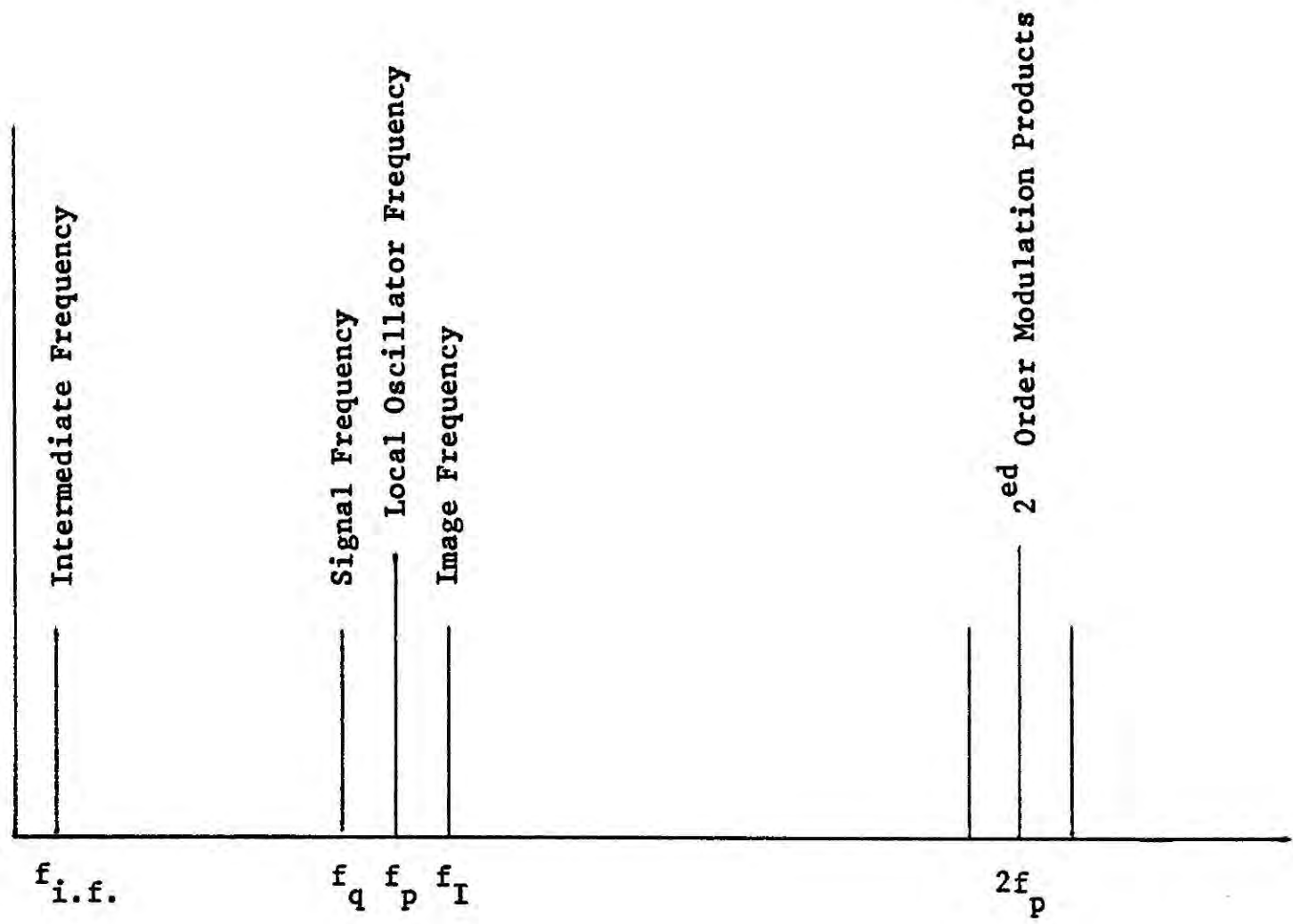
Figure 1.1 Down-Converter Frequency Notation
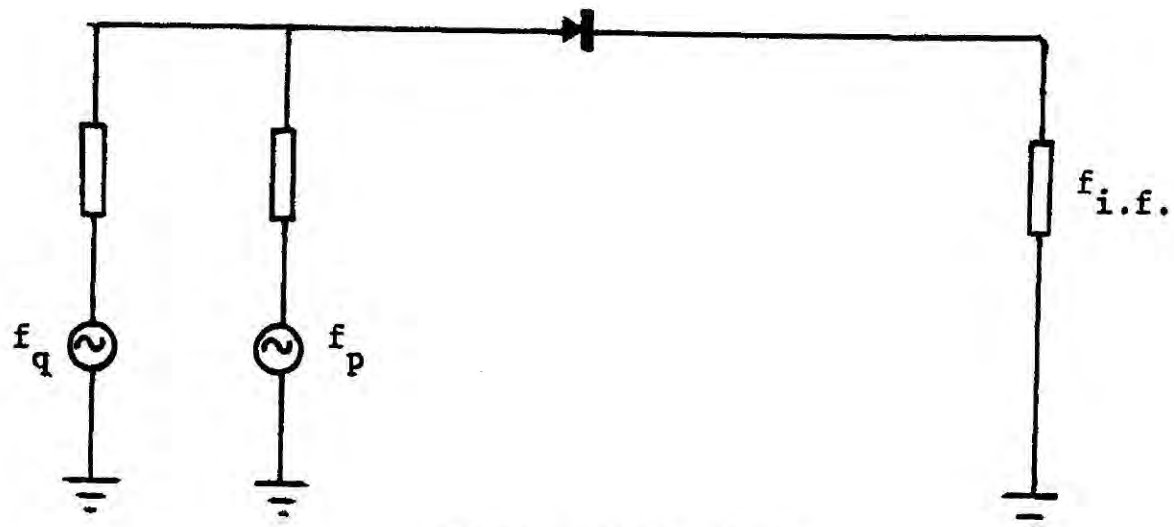
Single-diode mixer
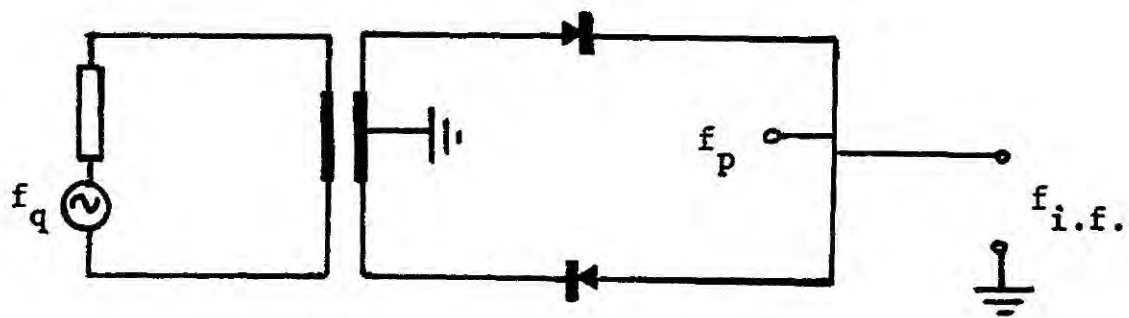
Two-diode balanced mixer
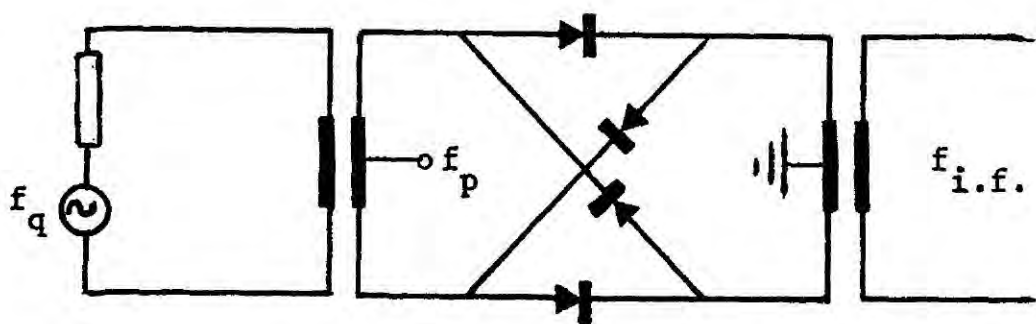
Four-diode double-balanced lattice mixer

Figure 1.2 Diode Mixer Circuits

Series
Tuned
Circuit

Series
Tuned
Circuit

Diode
Network

Signal
Port

Z Mixer

I.F. Port

Parallel
Tuned circuit

Diode
Network

Parallel
Tuned Circuit

Signal
Port

Y Mixer

I.F. Port

Series
Tuned
Circuit

Diode
Network

Parallel
Tuned Circuit

Signal
Port

H Mixer

I.F. Port

Series
Tuned
Circuit

Parallel
Tuned Circuit

Diode
Network

Signal
port

G Mixer

I.F. Port
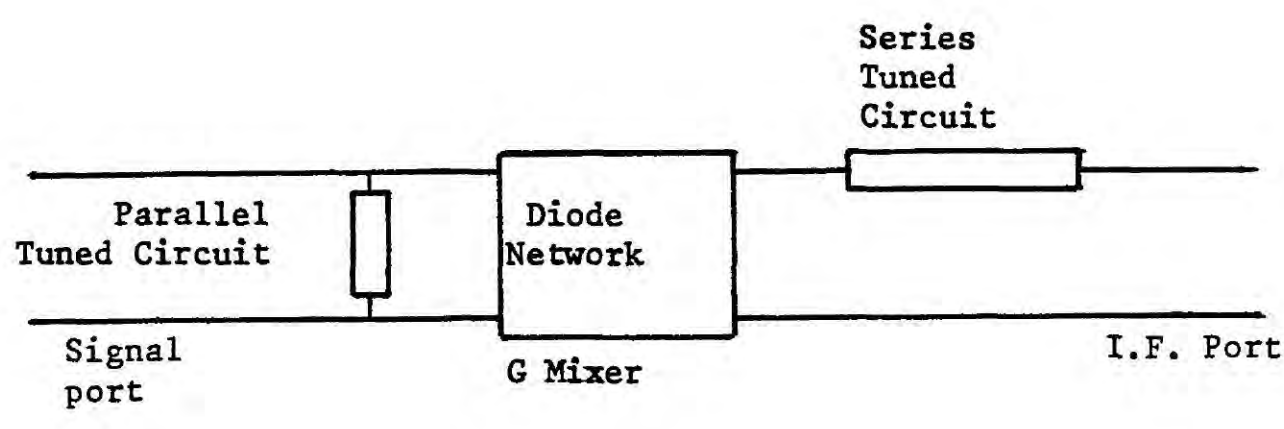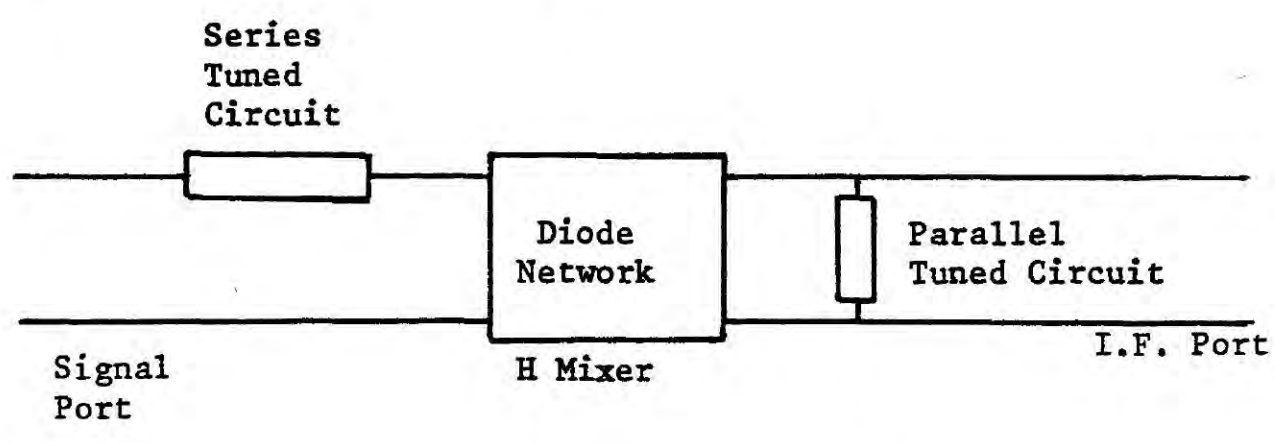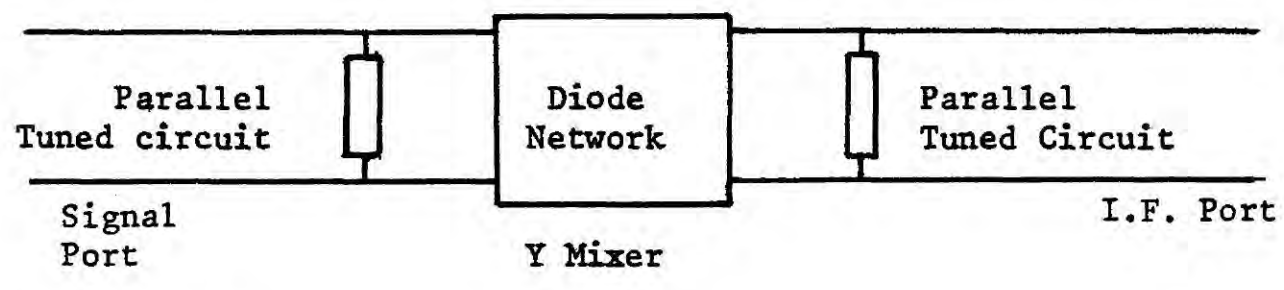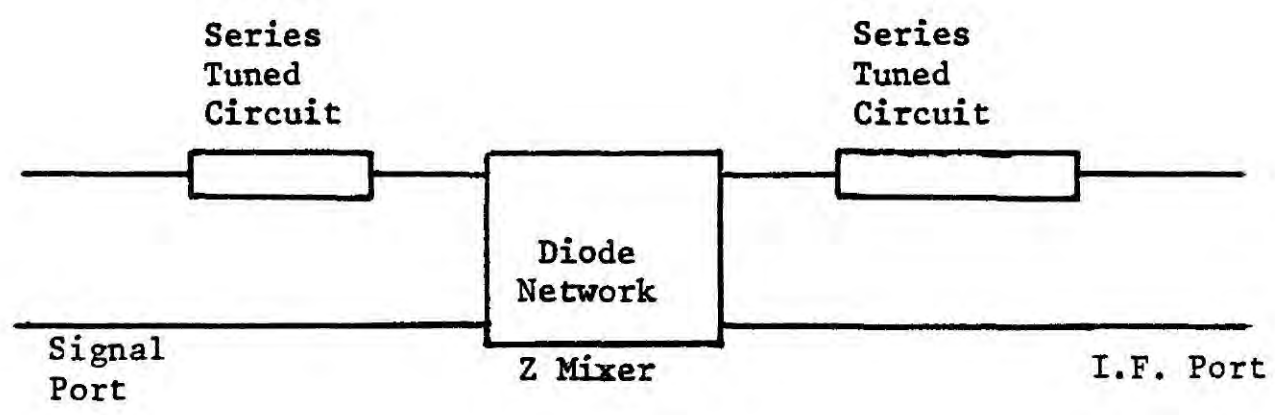
Figure 1.3 Mixer Configurations
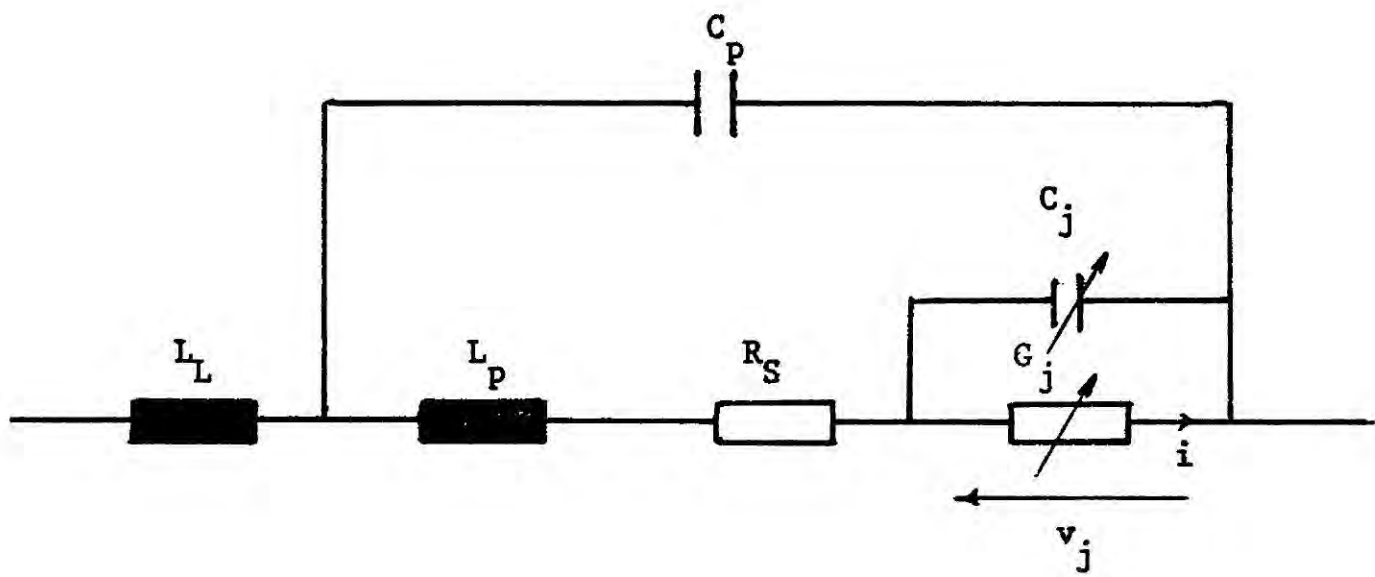
Figure 1.4 An equivalent circuit of a diode
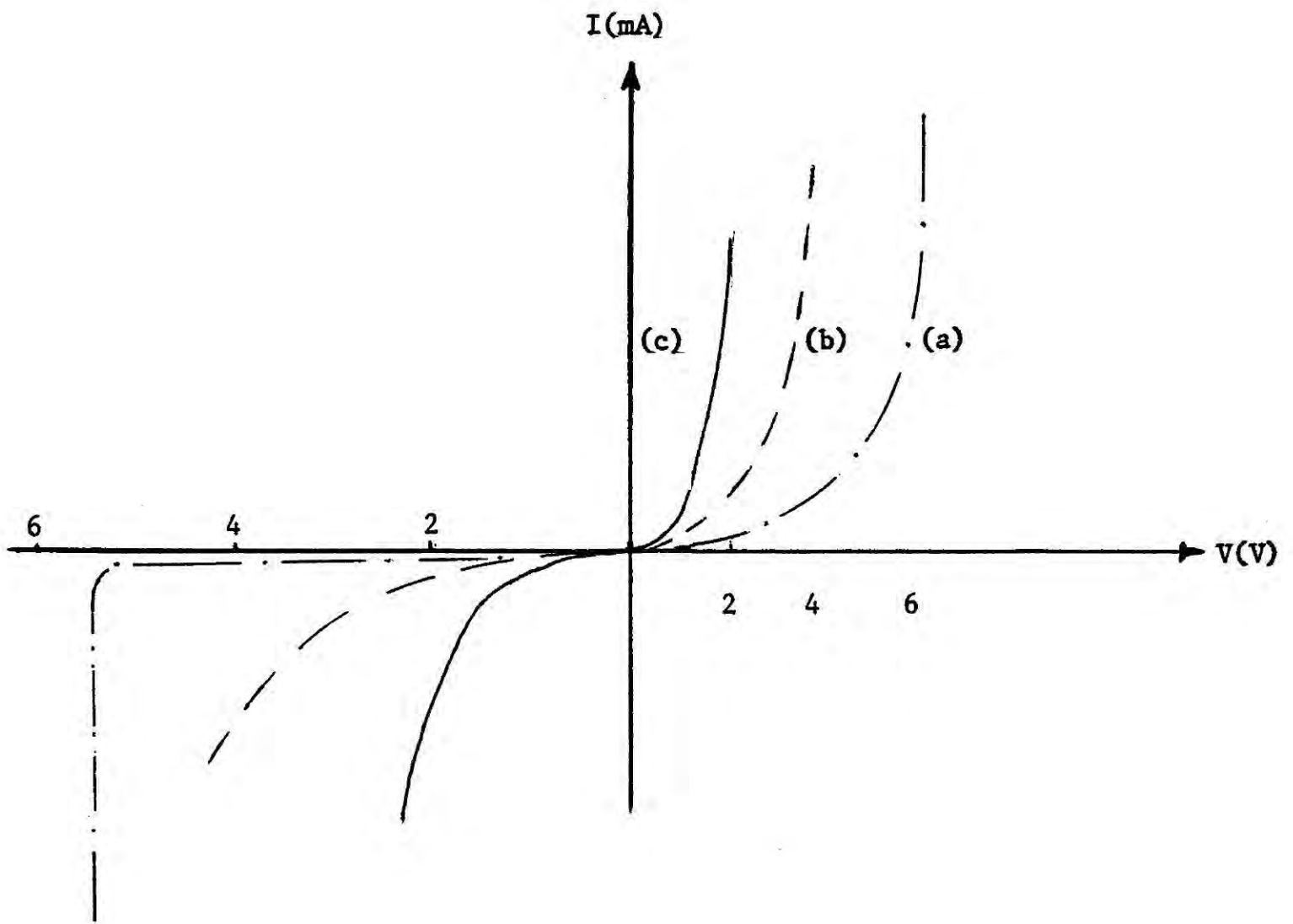
(a) Backward diode
(b) Point-contact diode
(c) Schottky-barrier diode

Figure 1.5 VI characteristics of common diodes
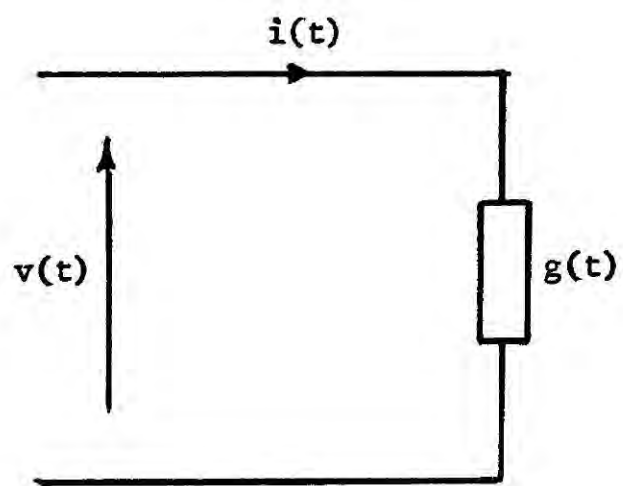
Figure 1.6 Time domain representation of a pumped diode
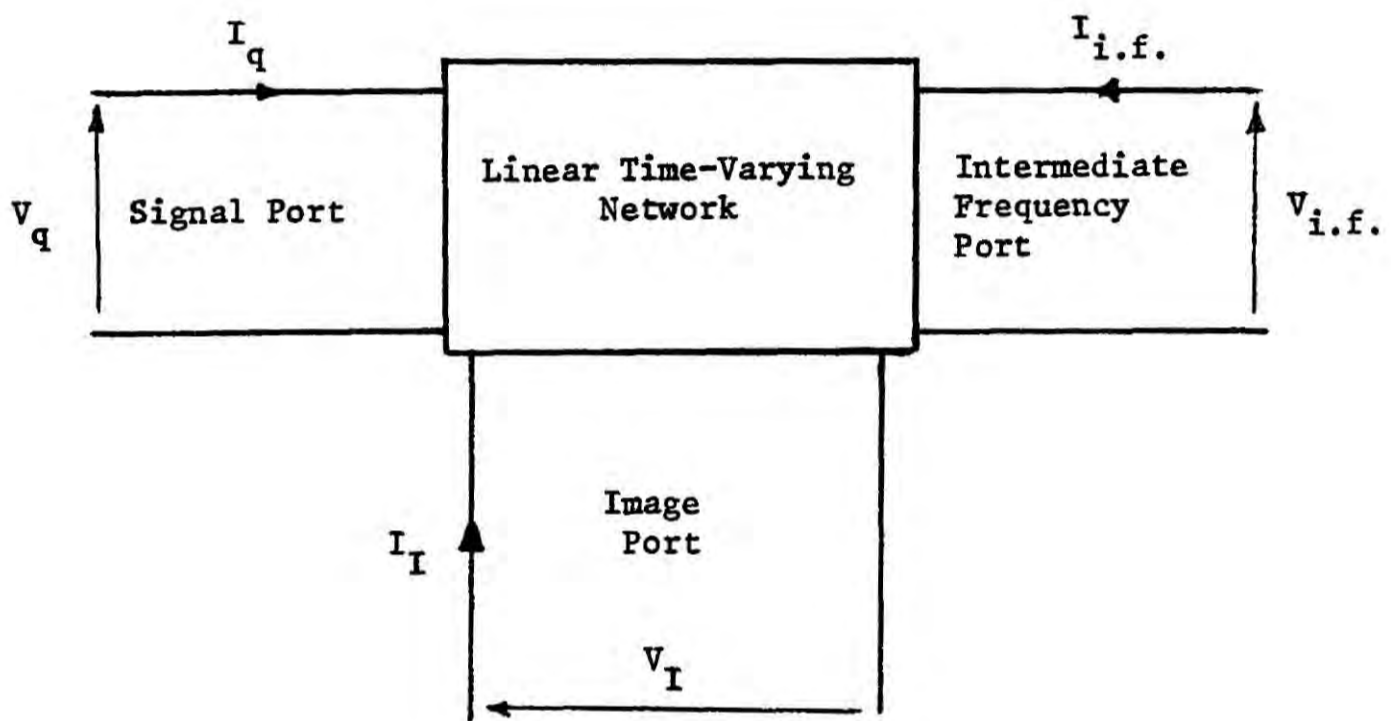
Figure 1.7 Conceptual three-port network of a mixer
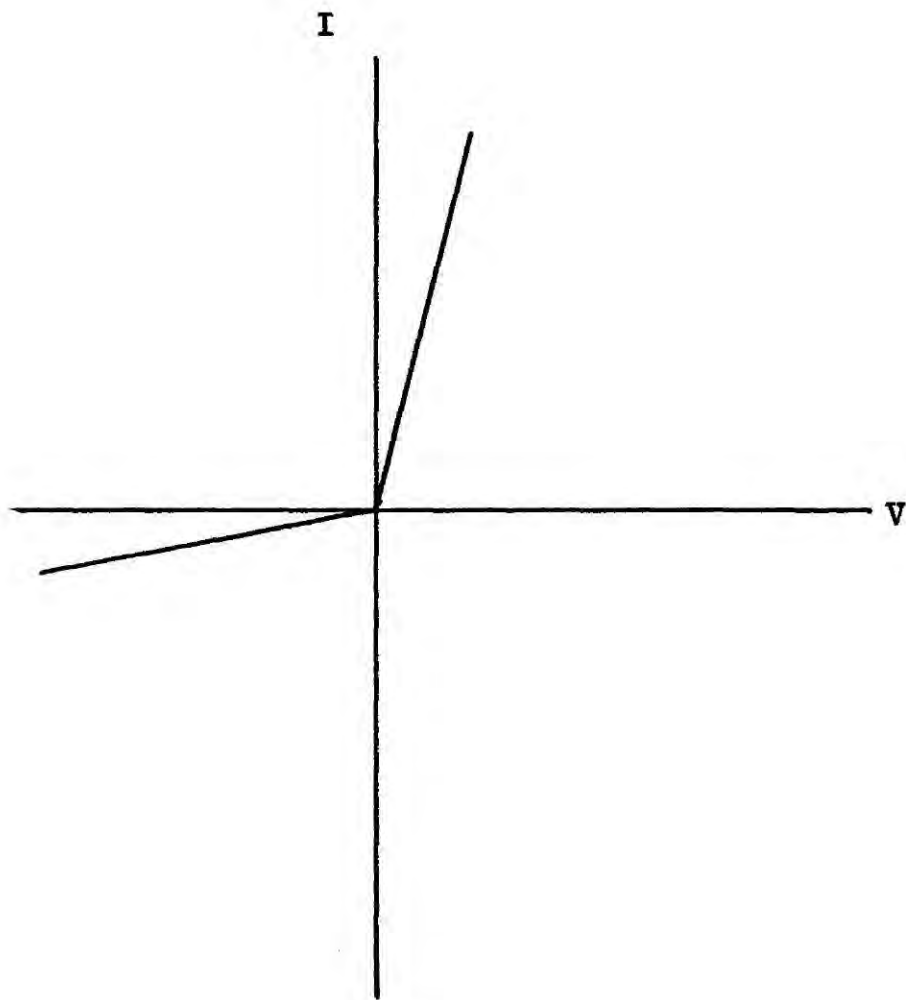
Figure 1.8 VI characteristics of a bi-linear diode
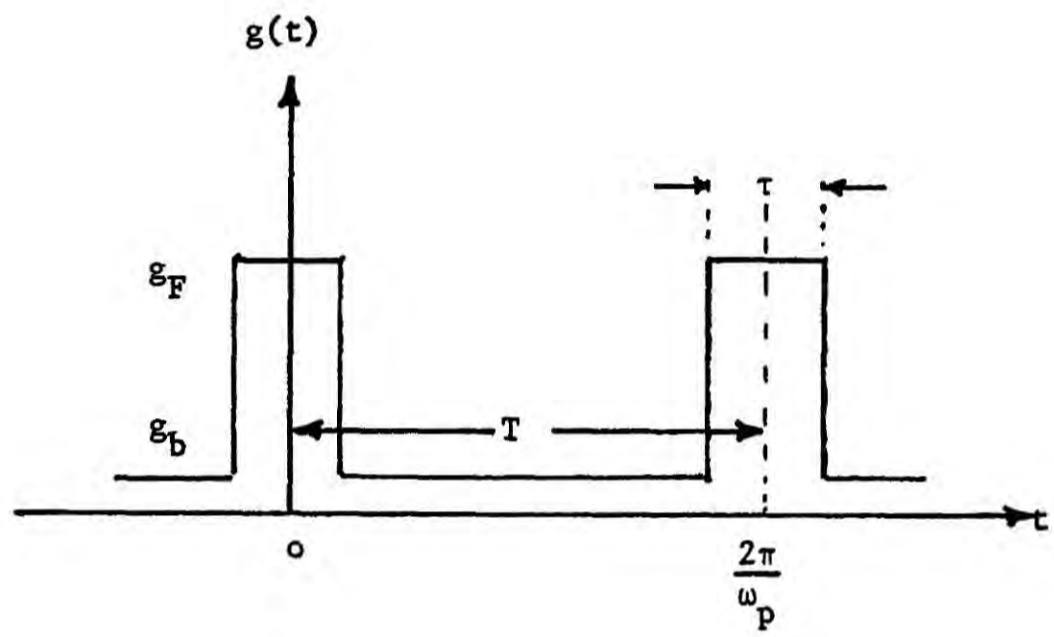
Figure 1.9 Conductance waveform of a pumped bi-linear diode

CHAPTER II

General Theory of Resistive Lattice Mixers

2.1 Introduction

Single balanced and double-balanced lattice mixers are usually preferred
to single diode circuits for high frequency application as they generate
fewer unwanted harmonic products, and therefore reduce associated filtering
problems. They also have the advantage of reducing the noise contribution
from the local oscillator and eliminating the decoupling problems
associated with the local oscillator circuit at the r.f. port of the
mixer. A lattice mixer has a further advantage in that inherent separation
of even and odd harmonic products is obtained, [1], reducing further
filtering problems. The disadvantage, a more complicated diode circuitry
especially at microwave frequencies for multi-diode mixers has largely
been overcome by modern integrated circuit technology [2-6].

Multi-diode mixers have received considerable attention by early
researchers [7-10]. In their analysis, they assumed that the mixer is
pumped by a sinusoidal voltage signal and the diode as having bi-linear
characteristics.

Frequency selective networks can be used to form Z, Y, G and H lattice
mixers according to Saleh's [11] classification. Saleh has also analysed
the performance of Z, Y, G and H lattice mixers, where he assumed that
the diode obeyed an exponential law,but neglected the effect of the diode
series resistance and diode reactive parasitics. Kulesza [12] effectively
analysed the performance of the H lattice mixer with image open-circuit.
He included in his analysis the effect of the diode series resistance
but neglected the effect of diode reactive parasitics. The noise performance
of a lattice mixer has been considered by Stracca [13]. Using a computer
aided analysis Stracca's work has been extended by Rustom and Howson [14]

with an improved model of a diode.

The object of this chapter is to present a general small signal-analysis of Z, Y, G and H resistive lattice mixers for two types of narrow-band (image open and image short-circuit), and two types of broad-band (optimum and matched at the r.f. port) mixers. In this chapter the effect of the diode reactive parasitics has been ignored, and the matrices describing the lattice mixers are therefore real.

2.2 Lattice Mixers

A particular multi-diode mixer considered here is one consisting of
four diodes connected in a lattice configuration and shown in Figure
2.1. During the positive half cycle of a local oscillator drive,
diodes one and two are driven into forward conduction, while diodes
three and four are driven into the reverse region.These processes are
reversed during the negative half-cycle of the local oscillator drive.
The time-varying resistances are designated as $r_+(t)$ and $r_-(t)$ where (+)
and (-) subscripts indicate the relative operation sequence of the pumped diodes
in the lattice mixer. Taking into account the phase difference of the
local oscillator present at the diodes, the time-varying resistances
of the diodes can be expressed in the form,

$$r_+(t) = r(t + 2\pi/\omega_p) = \sum_{n=0}^{\infty} r_n \cos n\omega_p t \qquad \text{2.1(a)}$$

$$r_-(t) = r(t + \pi/\omega_p) = \sum_{n=0}^{\infty} r_n \cos n\omega_p t \qquad \text{2.1(b)}$$

Frequency selective networks can be placed at the r.f. and i.f. ports
shown in Figure 2.2 to produce Z, Y, G and H lattice mixers.

In the case of a Z mixer the filter at the r.f. port constrains the
input current to consist only of two harmonics, at ω_q and ω_I frequencies,
which can be written in the form,

$$i_1 = I_q \cos \omega_q t + I_I \cos \omega_I t \qquad \text{2.2(a)}$$

At the i.f. port of the Z mixer the filter constrains the output current
to be purely sinusoidal i.e.

$$i_2 = I_{i.f.} \cos \omega_q t \qquad \text{2.2(b)}$$

The terminal voltages and currents present at the r.f. and i.f. ports
of a Z mixer are related by the following matrix equation,

$$
\begin{bmatrix} v_1 \\ v_2 \end{bmatrix} = \begin{bmatrix} \dfrac{r_+(t) + r_-(t)}{2} & \dfrac{r_-(t) - r_+(t)}{2} \\ \dfrac{r_-(t) - r_+(t)}{2} & \dfrac{r_+(t) + r_-(t)}{2} \end{bmatrix} \begin{bmatrix} i_1 \\ i_2 \end{bmatrix} \qquad 2.3
$$

If the image frequency is treated differently from the rest of the out-of-band modulation frequencies, then the three terminal voltages present are,

$$
V_q \cos \omega_q t, \quad V_I \cos \omega_I t \quad \text{and} \quad V_{i.f.} \cos \omega_{i.f.} t
$$

Substituting equations 2.2(a) and 2.2(b) into equation 2.3 and performing a frequency balance operation at ω_q, ω_I and $\omega_{i.f.}$ frequencies, the following general three port matrix is obtained.

$$
\begin{bmatrix} V_q \\ V_{i.f.} \\ V_I \end{bmatrix} = \begin{bmatrix} z_{11} & z_{12} & z_{13} \\ z_{21} & z_{22} & z_{23} \\ z_{31} & z_{32} & z_{33} \end{bmatrix} \begin{bmatrix} I_q \\ I_{i.f.} \\ I_I \end{bmatrix} \qquad 2.4(a)
$$

The z parameters of equation 2.4(a) are the Fourier coefficients of the time varying resistances given in equation 2.3.

The other three lattice mixers shown in Figure 2.2(b), Figure 2.2(c) and Figure 2.2(d) can be analysed in a similar manner, and the resulting matrix equations are shown below.

For the Y mixer the three-port matrix equation is given by,

$$
\begin{bmatrix} I_q \\ I_{i.f.} \\ I_I \end{bmatrix} = \begin{bmatrix} y_{11} & y_{12} & y_{13} \\ y_{21} & y_{22} & y_{23} \\ y_{31} & y_{32} & y_{33} \end{bmatrix} \begin{bmatrix} V_q \\ V_{i.f.} \\ V_I \end{bmatrix} \qquad 2.4(b)
$$

For the G mixer the corresponding three-port matrix equation becomes,

$$
\begin{bmatrix} I_q \\ V_{i.f.} \\ I_I \end{bmatrix} = \begin{bmatrix} g_{11} & g_{12} & g_{13} \\ g_{21} & g_{22} & g_{23} \\ g_{31} & g_{32} & g_{33} \end{bmatrix} \begin{bmatrix} V_q \\ I_{i.f.} \\ V_I \end{bmatrix} \qquad 2.4(c)
$$

and for the H mixer it is,

$$
\begin{bmatrix} V_q \\ I_{i.f.} \\ V_I \end{bmatrix} = \begin{bmatrix} h_{11} & h_{12} & h_{13} \\ h_{21} & h_{22} & h_{23} \\ h_{31} & h_{32} & h_{33} \end{bmatrix} \begin{bmatrix} I_q \\ V_{i.f.} \\ I_I \end{bmatrix}
$$

2.4(d)

It is convenient to express the above matrix equations for the four

types of mixers by the following general matrix equation,

$$
\begin{bmatrix} U_q \\ U^*_{i.f.} \\ U_I \end{bmatrix} = \begin{bmatrix} m_{11} & m_{12} & m_{13} \\ m_{21} & m_{22} & m_{23} \\ m_{31} & m_{32} & m_{33} \end{bmatrix} \begin{bmatrix} T_q \\ T^*_{i.f.} \\ T_I \end{bmatrix}
$$

2.5

where U_q, T_q etc. represent either voltage or current signals depending

on the type of mixer considered.

The nine unknown coefficients in equation 2.5 can in practice be reduced

to four. If it is assumed that the lattice network of diodes (but not

necessarily at the mixer terminals) does not contain any tuned circuits

and that the r.f. and image frequencies are much greater than the inter-

mediate   frequency, then from [15]

$$
\left.\frac{U_q}{T_q}\right|_{\substack{T_{i.f.} = 0 \\ T_I = 0}} = \left.\frac{U_I}{T_I}\right|_{\substack{T_{i.f.} = 0 \\ T_I = 0}}
$$

and $m_{11} = m_{33}$. Similarly,

$$
\left.\frac{U_{i.f.}}{T_q}\right|_{\substack{T_{i.f.} = 0 \\ T_I = 0}} = \left.\frac{U_{i.f.}}{T_I}\right|_{\substack{T_{i.f.} = 0 \\ T_I = 0}}
$$

and $m_{21} = m_{23}$.

* For Z and Y mixers. For H and G mixers appropriate voltage or current

signals must be used as given by equations 2.4(c) and 2.4(d).

A further reduction can be made to the number of unknown coefficients of equation 2.5, if it is assumed that the voltage across the diode junction is an even function of time so that reciprocity holds [15], and hence

$$m_{12} = m_{21}$$

$$m_{23} = m_{32}$$

and
$$m_{31} = m_{13}$$

The above relationships are valid for Z and Y mixers, but not in G and H mixers for which,

$$m_{12} = -m_{21}$$

$$m_{23} = -m_{32}$$

$$m_{13} = m_{31}$$

The general matrix equation 2.5 reduces as a consequence to,

$$
\begin{bmatrix} U_q \\ U_{i.f.} \\ U_I \end{bmatrix} =
\begin{bmatrix} m_{11} & m_{12} & m_{13} \\ m_{12} & m_{22} & m_{12} \\ m_{13} & m_{12} & m_{11} \end{bmatrix}
\begin{bmatrix} T_q \\ T_{i.f.} \\ T_I \end{bmatrix}
\tag{2.6}
$$

The three-port equation 2.6 can now be converted into a two-port equation by letting the image frequency have a general real termination W_I where

$$U_I = -W_I T_I \tag{2.7}$$

Substituting equation 2.7 into equation 2.6, the resulting two-port equation is therefore

$$
\begin{bmatrix} U_q \\ U_{i.f.} \end{bmatrix} =
\begin{bmatrix} M_{11} & M_{12} \\ M_{12} & M_{22} \end{bmatrix}
\begin{bmatrix} T_q \\ T_{i.f.} \end{bmatrix}
\tag{2.8}
$$

where,

$$M_{11} = m_{11} \left(1 - \frac{a^2}{W}\right) \qquad\qquad 2.9(a)$$

$$M_{12} = m_{12} \left(1 - \frac{a}{W}\right) \qquad\qquad 2.9(b)$$

$$M_{22} = m_{22} \left(1 - \frac{K_o}{W}\right) \qquad\qquad 2.9(c)$$

and,

$$a = m_{13}/m_{11} \qquad\qquad 2.10(a)$$

$$W = 1 + W_I/m_{11} \qquad\qquad 2.10(b)$$

$$K_o = m_{12}\, m_{21}/m_{11}\, m_{22}$$

i.e. $\qquad K_o = m_{12}^2/m_{11}\, m_{22} \quad$ for Y and Z mixers

$$2.10(c)$$

and $\qquad K_o = -m_{12}^2/m_{11}\, m_{22} \quad$ for G and H mixers

Equation 2.8 can be used to determine the required source and load terminations to obtain the optimum conversion loss for the three types of image terminations, i.e.

(i) image open-circuit $W_I = \infty$,

(ii) image short-circuit $W_I = 0$,

and (iii) image termination equal to the source termination at the r.f. port, $W_I = W_s$.

2.3 The Necessary R.F. and I.F. Terminations to Produce Optimum Conversion Loss

The conversion loss of a mixer defined by equation 1.2 can be conveniently expressed in terms of the general two-port matrix parameters of equation 2.8 as shown below,

$$L = \frac{\left| (M_{11} + W_s)(M_{22} + W_L) - M_{12}M_{21} \right|^2}{4 W_s W_L M_{12}^2} \qquad \qquad 2.11$$

where W_s and W_L are the terminations at the r.f. and i.f. ports of the mixer, respectively. To determine the necessary terminations at the r.f. and i.f. ports to obtain optimum conversion loss, two distinct approaches can be followed.

One method is to set the derivatives of equation 2.11 to zero, i.e.,

$$\frac{dL}{dW_s} = 0 \quad \text{and} \quad \frac{dL}{dW_L} = 0$$

The other technique is to produce matching conditions at the r.f. and i.f. ports, a method usually employed in microwave engineering, i.e.

$$W_{s_{opt}} = W_{IN} \quad \text{and} \quad W_{L_{opt}} = W_{OUT}$$

where W_{IN} is the output impedance (or admittance) of the mixer at the r.f. port while W_{OUT} is the output impedance (or admittance) of the mixer at the i.f. port.

If the coefficients of the two-port matrix are independent of the source and load terminations, the two approaches produce identical results. Equations 2.9(a), 2.9(b) and 2.9(c) show that this is satisfied for narrow-band image-open ($W_I = \infty$) and image short ($W_I = 0$) mixers. For the broad-band mixer ($W_I = W_s$), however, the above condition is not satisfied and the two approaches lead to two different and interesting results.

2.3.1 Optimum R.F., I.F. Terminations and Conversion Loss for Narrow-
       Band Mixers

In the case of narrow-band mixers, setting the derivatives of equation
2.11 with respect to W_s and W_L to zero, which produces matched conditions
at the r.f. and i.f. ports, it may be readily shown that,

$$W_{s_{opt}} = M_{11} \left[1 - K \right]^{\frac{1}{2}} \qquad\qquad 2.12(a)$$

$$W_{L_{opt}} = M_{22} \left[1 - K \right]^{\frac{1}{2}} \qquad\qquad 2.12(b)$$

and

$$L_{opt} = \left[\frac{1 + \left[1 - K \right]^{\frac{1}{2}}}{-1 + \left[1 - K \right]^{\frac{1}{2}}} \right] \left[\pm 1 \right]^{*} \qquad\qquad 2.12(c)$$

where

$$K = \frac{M_{12} M_{21}}{M_{11} M_{22}} \qquad\qquad 2.12(d)$$

In the particular case of a narrow-band image open-circuit mixer
$\left(W_I \rightarrow \infty \right)$ the general parameters of equation 2.8 reduce to,

$$M_{ij} = m_{ij} \text{ for } i,j = 1,2$$

The required terminations at the r.f. and i.f. ports of a mixer (with
image open-circuit) and the resulting minimum conversion loss are,

$$W_{s_{opt}} = m_{11} \left[1 - K_{o} \right]^{\frac{1}{2}} \qquad\qquad 2.13(a)$$

$$W_{L_{opt}} = m_{22} \left[1 - K_{o} \right]^{\frac{1}{2}} \qquad\qquad 2.13(b)$$

and

$$L_{3_{opt}} = \left[\frac{1 + \left[1 - K_{o} \right]^{\frac{1}{2}}}{-1 + \left[1 - K_{o} \right]^{\frac{1}{2}}} \right] \left[\pm 1 \right]^{*} \qquad\qquad 2.13(c)$$

where K_o is defined by equation 2.10(c).

For a narrow-band image short-circuit ($W_I = 0$) mixer, the corresponding
expression for the required terminations at the r.f. and i.f. ports and
the resulting minimum conversion loss, using equations 2.9, 2.10 and
2.12, are

* Positive sign is used for H and G mixers and negative sign is used for
   Z and Y mixers.

$$W_{s_{opt}} = m_{11} \left[1 - a^2 \right] \left[1 - K_s \right]^{\frac{1}{2}} \qquad \text{2.14(a)}$$

$$W_{L_{opt}} = m_{22} \left[1 - K_o \right] \left[1 - K_s \right]^{\frac{1}{2}} \qquad \text{2.14(b)}$$

and

$$L_{1_{opt}} = \left[\frac{1 + \left[1 - K_s \right]^{\frac{1}{2}}}{-1 + \left[1 - K_s \right]^{\frac{1}{2}}} \right] \left[\pm 1 \right] \qquad \text{2.14(c)}$$

where

$$K_s = \left[\frac{K_o}{1 - K_o} \right] \left[\frac{1 - a}{1 + a} \right] \qquad \text{2.14(d)}$$

2.3.2 The Necessary R.F. and I.F. Terminations to Produce Optimum Conversion Loss for Optimum and Matched Broad-Band Mixers

To determine the minimum conversion loss of a broad-band mixer it is necessary to set the derivatives of equation 2.11 with respect to W_L and W_s to zero.

Substituting equations 2.9(a), 2.9(b) and 2.9(c) into equation 2.11 it can be shown that,

$$L = \frac{\left| (1+y) \ (w+a) \ -2K_o \ \right|^2}{4K_o \ (1-W) \ y} \qquad \text{2.15(a)}$$

where

$$y = W_L / m_{22} \qquad \text{2.15(b)}$$

Setting the derivative of equation 2.15(a) with respect to y to zero results in the following expression for y_{opt},

$$y_{opt} = 1 - 2K_o / \left[W+a \right] \qquad \text{2.16(a)}$$

or

$$W_{L_{opt}} = m_{22} \left[1 - 2K_o / \left[W+a \right] \right] \qquad \text{2.16(b)}$$

As the output termination for a two-port network is also given by equation 2.16(b), the condition of minimum conversion loss coincides with the requirement that the i.f. port be matched for maximum power transfer.

Substituting equation 2.16(a) into equation 2.15(a) the following expression for the conversion loss is obtained.

$$L = \frac{\overline{[W+a]}\;\overline{[W+a - 2K_o]}}{K_o\;\overline{[1-W]}}$$ 2.17

Setting the derivative of equation 2.17 with respect to W to zero, results in the following quadratic equation,

$$W^2 - 2W - \overline{[a(2+a) - 2K_o\;(1+a)]} = 0$$ 2.18

where the roots of the quadratic equation 2.18 are,

$$W = 1 \pm \overline{[1+a]}\;\overline{[1 - K_B]}^{\frac{1}{2}}$$ 2.19(a)

and

$$K_B = 2K_o / \overline{[1+a]}$$ 2.19(b)

The required termination at the r.f. port of the mixer using equation 2.19(a) and 2.10(b) then becomes,

$$W_{s_{opt}} = m_{11}\;\overline{[1+a]}\,\overline{[1 - K_B]}^{\frac{1}{2}}$$ 2.20

Equation 2.20 indicated that in order to produce minimum conversion loss the r.f. port of a broad-band mixer must be mismatched.

Finally, substituting equation 2.19(a) into equation 2.17 the expression for the minimum conversion loss can be shown to be,

$$L_{2_{opt}} = \left[\frac{2\;\overline{[1 + (1 - K_B)]}^{\frac{1}{2}}}{-1 + (1 - K_B)^{\frac{1}{2}}}\right]\left[\pm 1\right]$$ 2.21

An alternative approach in the design of a high frequency broad-band mixer is to determine the necessary terminations W_{s_m} and W_{L_m} to produce matching conditions at the r.f. and i.f. ports. It can be shown, using equations 2.9, 2.10 and 2.12(a), that

$$W_{s_m} = m_{11}\;\overline{[1 - \frac{a^2}{W}]}\,\overline{[1 - K_m]}^{\frac{1}{2}}$$ 2.22(a)

where

$$K_m = \left[\frac{K_o}{1 - \frac{K_o}{W}}\right]\left[\frac{(1 - \frac{a}{W})^2}{(1 - \frac{a2}{W})}\right] \qquad 2.22(b)$$

Substituting equation 2.22(b) into equation 2.22(a) results in the following quartic equation in W,

$$W^4 - [K_o+2] W^3 + 3K_o W^2 + a [2a-2K_o-K_o a] W - a^2 [K_o - 2K_o a + a^2] = 0 \qquad 2.23(a)$$

where

$$W = 1 + \frac{W_{s_m}}{m_{11}} \qquad 2.23(b)$$

The solution of the quartic equation 2.23(a) for W and hence W_{s_m} depends on the values of 'Ko' and 'a' and these as will be shown in Chapter III depend on the type of lattice mixer considered.

The termination at the i.f. port W_{L_m} necessary to produce matching condition using equation 2.12(b) can be shown to be,

$$W_{L_m} = m_{22} [1 + K_o] [1 - K_m]^{\frac{1}{2}} \qquad 2.24$$

Finally, the conversion loss of a lattice mixer matched simultaneously at the r.f. and i.f. port is given by,

$$L = \left[\frac{1 + [1 - K_m]^{\frac{1}{2}}}{-1 + [1 - K_m]^{\frac{1}{2}}}\right] \left[\pm 1\right] \qquad 2.25$$

2.4 Conclusions

A general matrix equation describing the four types (Z,Y,G and H) lattice mixers has been derived and it can be used to determine the r.f. and i.f. terminations necessary to obtain optimum conversion loss. For each of the four types of lattice mixers, three types of image terminations have been considered, image open-circuit, image short-circuit and image equal to the r.f. termination.

In the case of narrow-band image open-circuit mixer and image short-circuit mixer, the terminations at r.f. and i.f. ports necessary to obtain minimum conversion loss coincides with the condition of the mixers being matched at the r.f. and i.f. ports. For an optimum broad band mixer, where the image termination is equal to the r.f. termination, it is shown that to produce minimum conversion loss, the i.f. port needs to be matched but the r.f. port must be mismatched. In microwave engineering it is common practice to examine the performance of two-port networks, when both the input and output ports are matched. Consequently, general equations are derived to examine the necessary terminations at the r.f. and i.f. ports and resulting conversion loss when the mixer is matched at both ports.

2.5 References

1. Tucker, D.G., Ellimination of Even-Order Modulation in Rectifier Modulators. J. Brit., IRE, Feb. 1961, Vol. 21, No. 2.

2. Johnson, K.M., X-Band Integrated Circuit Mixer with Reactively Terminated Image. IEEE Trans., MTT-16, July 1968, pp 388-397.

3. Araki, T., and Hirayama, H., A 20 GHz Integrated Balanced Mixer. IEEE Trans., MTT-19, July 1971, pp 638-643.

4. Begemann, G., An X-Band Balanced Fine-Line Mixer IEEE Trans., MTT-26, Dec. 1978, pp 1007-1011.

5. Schneider, M.V., and Snell, W.W., Harmonically Pumped Stripline Down-Converter. IEEE Trans, MTT-23, March 1975, pp 271-275.

6. Cohn, M.,Degnenfold, J.E., Newman, B.A. Harmonic Mixing with an Antiparallel Diode Pair. IEEE Trans, MTT-23, Aug. 1975, pp 667-673.

7. Belevitch, V., Linear Theory of Bridge and Ring Modulator Circuits. Elec. Comm. 1948, Vol. 25.

8. Kruse, S., Theory of Rectifier Modulators, Ericsson Technics, 1939, pp 17-53.

9. Tucker, D.G., Zero-Loss Second Order Ring Modulator. Elec. Letters, 1965, Vol. 1 No. 9 pp 1245-1246.

10. Howson, D.P., and Tucker, D.G. Rectifier Modulators with Frequency Selective Terminations. Proc. IEE, 1960, 107B, pp 261-272.

11. Saleh, A.A.M.S., Theory of Resistive Mixers, MIT Press 1971.

12. Kulesza, B.L.J., General Theory of a Lattice Mixer. Proc. IEE, 1971 Vol. 118, No. 7, pp 864-870.

13. Stracca, G.B., Noise in Frequency Mixers using Non-Linear Resistors, Alta Frequenza 1971, Vol, X1 No. 6.

14. Rustom, S., and Howson, D.P., Mixers Noise Figure Using an Improved Resistive Diode Model. Int. J. Electronics 1975, Vol. 28, No. 1.

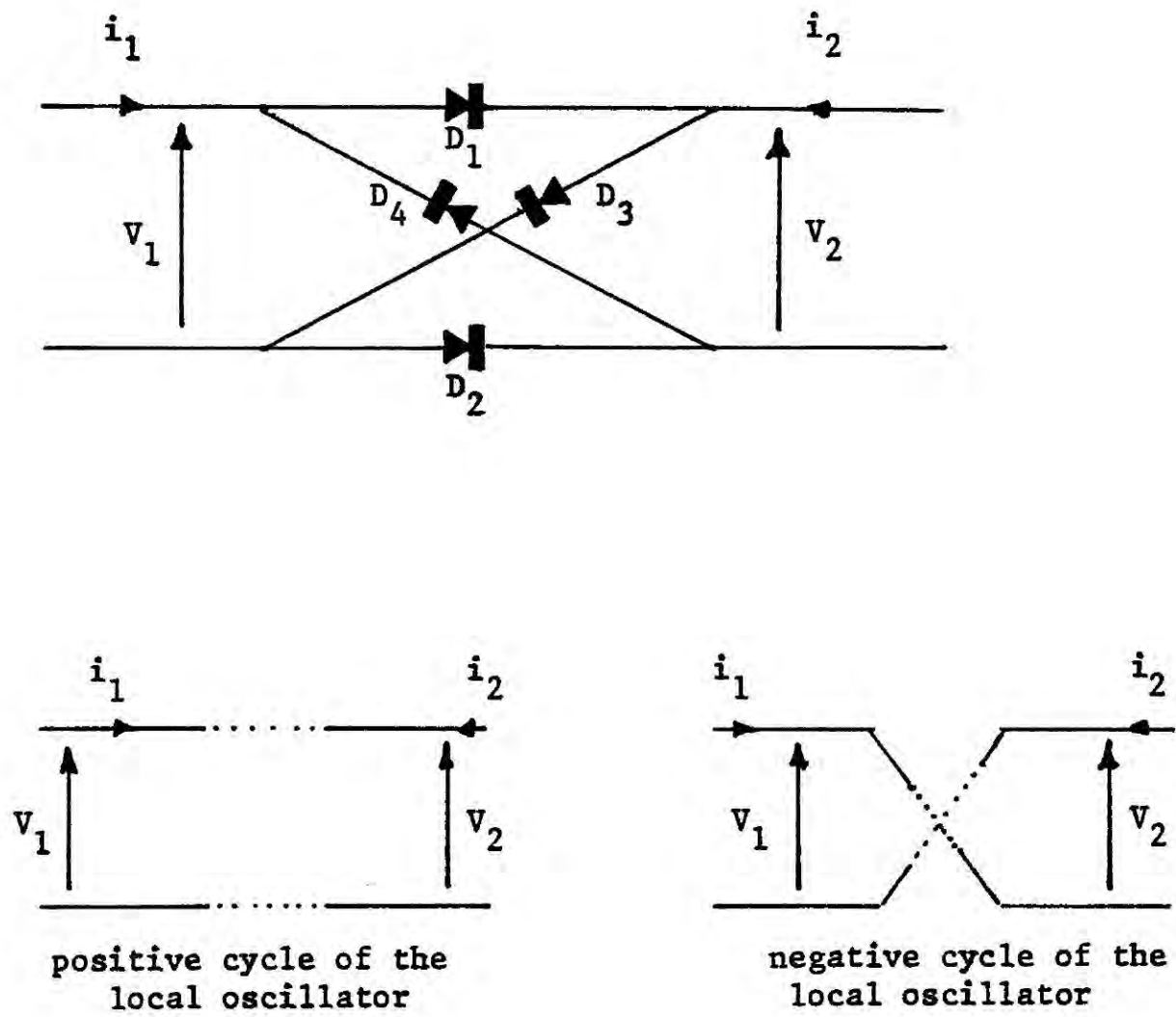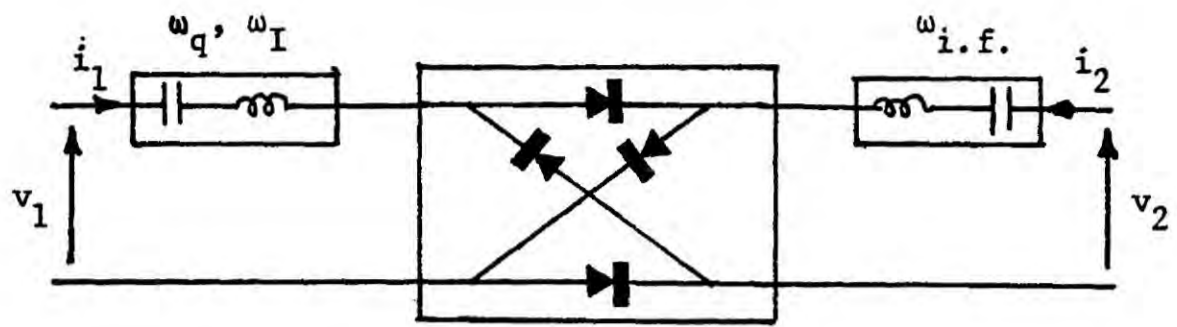15. Torrey, H.C., and Whitmer, C.A., Crystal Rectifiers,Radiation Laboratory Series Vol. 15 1948.
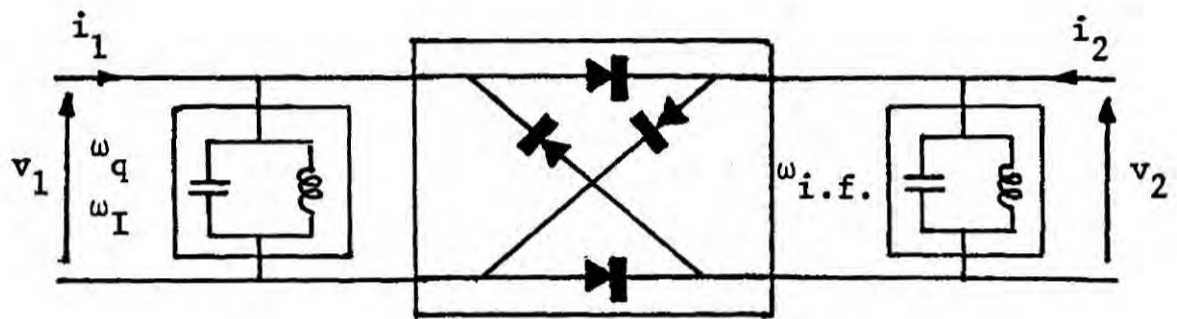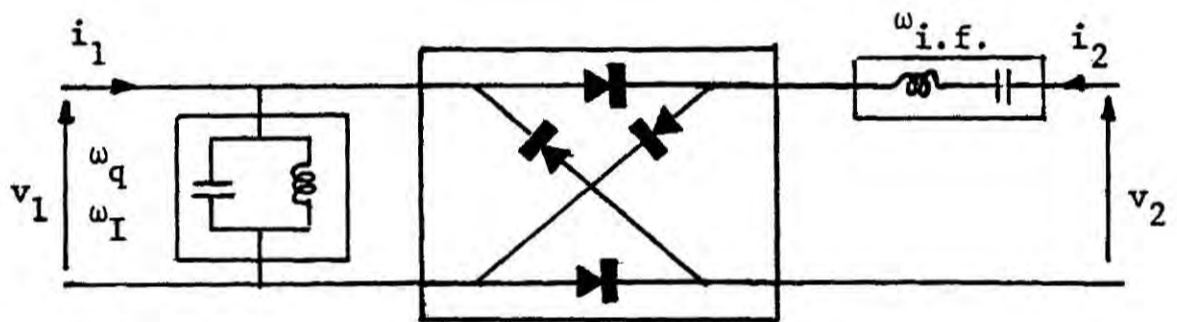
Figure   2.1 Lattice configuration of the diodes and their switching action on the positive and negative cycle of the local oscillator.

(a) Z lattice mixer

(b) Y lattice mixer

(c) G lattice mixer
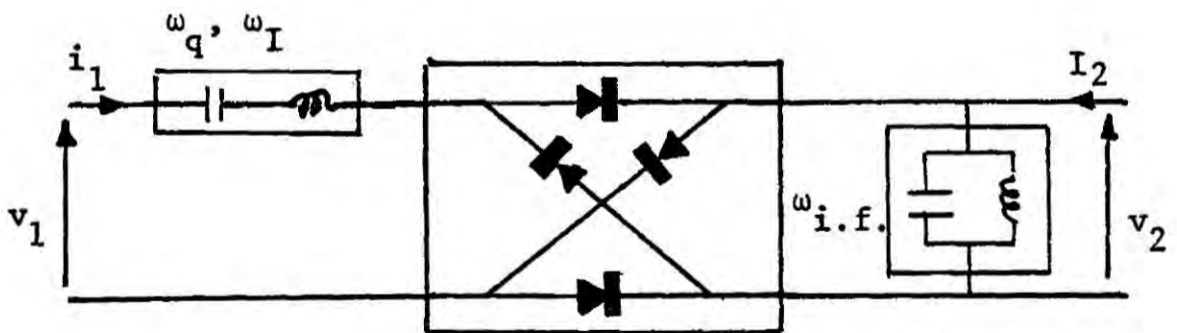
(d) H lattice mixer

Figure 2.2 The Four Fundamental Types of Lattice Mixers

CHAPTER III

Fundamental Limitation in the Conversion Loss

and Optimum Terminations of Resistive Lattice Mixers

3.1 Introduction

In the analysis of mixers, an assumption is normally made that the level of the local oscillator drive is much higher than that of the r.f. signal. Consequently, the pumped non-linear elements can be represented as time-varying parameters and treating the image frequency differently from the rest of the out-of-band modulation products, the mixer circuit can be described in terms of a three-port matrix. To determine the terminations at the r.f. and i.f. ports to obtain minimum conversion loss it is necessary to evaluate the coefficients of the three-port matrix equation. The analysis of mixer, therefore, consists of two parts; one part deals with the interaction of the local oscillator and the non-linear elements which determine the coefficients of the matrix describing the mixer, while the second part deals with the behaviour of the mixer in relation to r.f., image and i.f. signals.

Early researchers analysed the performance of single and multi-diode mixers by assuming that the diode has bi-linear characteristics [1-5]. In recent publications the analysis has been mainly concerned with mixers where the diodes are assumed to have ideal exponential characterisitcs [6-11], but generally the effect of the diode series resistance has been neglected. Stracca [12] has shown that an improvement in the conversion loss of balanced mixers is obtained if the local oscillator is coupled to the diodes through a series resonator. The resonator presents a high impedance to the local oscillator harmonic

frequencies and allows a sinusoidal current, rather than a sinusoidal voltage, drive. The effect of the diode series resistance on the performance of voltage and current driven balanced mixers has been considered by Schneider [13] and Kulesza [14] respectively. Computer assisted methods of analysis have been mainly concerned with the performance of single diode mixers [15-17].

In the mixer analysis presented in this chapter, it is initially assumed that the diode has a bi-linear characteristic, as proposed by many authors. It is found that this model of the diode applies when the lattice is strongly pumped, so that the diode can be assumed to switch from a low forward to a high reverse resistance. The performance of current driven Z, Y, H and G lattice mixers is then determined by assuming that the diodes have exponential characteristics. The performances of the four types of lattice mixers, using the two models of the diode, and for different image terminations, are compared. Such comparison and discussion of the performances has not been dealt with in any of the available published literature.

3.2 The Influence of Image Terminations on the Conversion Loss of Strongly Pumped Resistive Lattice Mixers

A basic circuit of a lattice mixer consisting of four diodes is shown in Figure 3.1. Assuming inherent separation of odd and even modulation harmonics [6], the lattice circuit shown in Figure 3.1 can be described by the following general matrix equation,

$$
\begin{bmatrix} U_1 \\ U_2 \end{bmatrix} = \begin{bmatrix} \sum_{n \text{ even}} a_n \cos n\omega_p t & , & \sum_{n \text{ odd}} b_n \cos n\omega_p t \\ \sum_{n \text{ odd}} c_n \cos n\omega_p t & , & \sum_{n \text{ even}} d_n \cos n\omega_p t \end{bmatrix} \begin{bmatrix} T_1 \\ T_2 \end{bmatrix} \qquad 3.1
$$

U_1, U_2, T_1 and T_2 are the terminal voltages or currents depending on the two-port parameters used to represent the lattice circuit. The general relationships for the four types of lattice mixers are shown in Table 3.1.

Mixer Parameter	Z	Y	H	G
U_1	V_1	I_1	V_1	I_1
U_2	V_2	I_2	I_2	V_2
T_1	I_1	V_1	I_1	V_1
T_2	I_2	V_2	V_2	I_2
$\sum a_n \cos n\omega_p t$	$\dfrac{r_+(t) + r_-(t)}{2}$	$\dfrac{r_+(t) + r_-(t)}{2}$	$\dfrac{2r_+(t)\, r_-(t)}{r_+(t) + r_-(t)}$	$\dfrac{2}{r_+(t) + r_-(t)}$
$\sum b_n \cos n\omega_p t$	$\dfrac{r_-(t) - r_+(t)}{2}$	$\dfrac{r_+(t) - r_-(t)}{2r_+(t)\, r_-(t)}$	$\dfrac{r_-(t) - r_+(t)}{r_+(t) + r_-(t)}$	$\dfrac{r_+(t) - r_-(t)}{r_+(t) + r_-(t)}$
$\sum c_n \cos n\omega_p t$	$\dfrac{r_-(t) - r_+(t)}{2q}$	$\dfrac{r_+(t) - r_-(t)}{2r_+(t)\, r_-(t)}$	$\dfrac{r_+(t) - r_-(t)}{r_+(t) + r_-(t)}$	$\dfrac{r_-(t) - r_+(t)}{r_+(t) + r_-(t)}$
$\sum d_n \cos n\omega_p t$	$\dfrac{r_+(t) + r_-(t)}{2}$	$\dfrac{r_+(t) + r_-(t)}{2r_+(t)\, r_-(t)}$	$\dfrac{2}{r_+(t) + r_-(t)}$	$\dfrac{2r_+(t)\, r_-(t)}{r_+(t) + r_-(t)}$

Table 3.1

An equivalent circuit of a strongly pumped diode having bi-linear characteristic i.e. low forward resistance r_s and high reverse resistance r_b, is shown in Figure 3.2. The time-varying resistances of the pumped diodes used in lattice mixers are,

$$r_+(t) = r_s + r_b \left(1 - s(t)\right) \qquad \text{3.2(a)}$$

and

$$r_-(t) = r_s + r_b\, s(t) \qquad \text{3.2(b)}$$

where $s(t)$ is a switching function defined as,

$$s(t) = 1 \text{ for } -\pi/2 \leqslant \omega_p t \leqslant \pi/2$$

$$\text{3.3(c)}$$

$$s(t) = 0 \text{ for } \pi/2 \leqslant \omega_p t \leqslant 3\pi/2$$

For the Z mixer, filters placed at the r.f. and i.f. ports restrict the input current i_1 to r.f. and image frequencies while the output current i_2 to intermediate frequency only, i.e.

$$i_1 = I_q \cos \omega_q t + I_I \cos \omega_I t \qquad \text{3.4(a)}$$

$$i_2 = I_{i.f.} \cos \omega_{i.f.} t \qquad \text{3.4(b)}$$

Substituting the appropriate two-port parameters from Table 3.1 and equations 3.2 and 3.4 into the general matrix equation 3.1, it may be shown on extracting relations at appropriate frequencies that the following three-port matrix equation is obtained,

$$
\begin{bmatrix} V_q \\ V_{i.f.} \\ V_I \end{bmatrix}
=
\begin{bmatrix}
\dfrac{2r_s + r_b}{2} & , & \dfrac{r_b}{\pi} & , & 0 \\[2ex]
\dfrac{r_b}{\pi} & , & \dfrac{2r_s + r_b}{2} & , & \dfrac{r_b}{\pi} \\[2ex]
0 & , & \dfrac{r_b}{\pi} & , & \dfrac{2r_s + r_b}{2}
\end{bmatrix}
\begin{bmatrix} I_q \\ I_{i.f.} \\ I_I \end{bmatrix}
\qquad \text{3.5}
$$

which corresponds to general equation 2.4(a) derived in Chapter II.

For the Y mixer, the filters restrict the input voltage v_1 to consist of r.f. and image frequency components only while the output voltage v_2 is limited to the intermediate frequency i.e.

$$v_1 = V_q \cos \omega_q t + V_I \cos \omega_I t \qquad \text{3.6(a)}$$

$$v_2 = V_{i.f.} \cos \omega_{i.f.} t \qquad \text{3.6(b)}$$

Performing a similar analysis to that for the Z mixer, the resulting three-port matrix equation for the Y mixer becomes,

$$
\begin{bmatrix} I_q \\ I_{i.f.} \\ I_I \end{bmatrix} = \frac{1}{2r_s(r_s + r_b)}
\begin{bmatrix}
2r_s + r_b, & -\dfrac{2r_b}{\pi}, & 0 \\
-\dfrac{2r_b}{\pi}, & 2r_s + r_b, & -\dfrac{2r_b}{\pi} \\
0, & -\dfrac{2r_b}{\pi}, & 2r_s + r_b
\end{bmatrix}
\begin{bmatrix} V_q \\ V_{i.f.} \\ V_I \end{bmatrix}
$$

which corresponds to equation 2.4(b) derived in Chapter II.

In the case of the H mixer the filters restrict the input and output signals to the following form,

$$i_1 = I_q \cos \omega_q t + I_I \cos \omega_I t \qquad \text{3.7(a)}$$

$$v_2 = V_{i.f.} \cos \omega_{i.f.} t \qquad \text{3.7(b)}$$

and the resulting three-port matrix equation describing the mixer is then,

$$
\begin{bmatrix} V_q \\ I_{i.f.} \\ V_I \end{bmatrix} =
\begin{bmatrix}
2r_s, & 2/\pi, & 0 \\
-2/\pi, & 2/r_b, & -2/\pi \\
0, & 2/\pi, & r_s
\end{bmatrix}
\begin{bmatrix} I_q \\ V_{i.f.} \\ I_I \end{bmatrix}
\qquad \text{3.8}
$$

which corresponds to equation 2.4(d) derived in Chapter II.

Finally, for the G mixer, the corresponding equations for input voltage and output current are,

$$v_1 = V_q \cos \omega_q t + V_I \cos \omega_I t \qquad \qquad 3.8(a)$$

$$i_2 = I_{i.f.} \cos \omega_{i.f.} t \qquad \qquad 3.8(b)$$

and the resulting three-port matrix equation becomes,

$$\begin{bmatrix} I_q \\ V_{i.f.} \\ I_I \end{bmatrix} = \begin{bmatrix} \dfrac{2}{r_b}, & -\dfrac{2}{\pi}, & 0 \\ \dfrac{2}{\pi}, & 2r_s, & \dfrac{2}{\pi} \\ 0, & -\dfrac{2}{\pi}, & \dfrac{2}{r_b} \end{bmatrix} \begin{bmatrix} V_q \\ I_{i.f.} \\ V_I \end{bmatrix} \qquad \qquad 3.9$$

which corresponds to equation 2.4(c) derived in Chapter II.

General equations derived in Chapter II can now be evaluated using the above three-port matrix equations in determining the required optimum terminations at the r.f. and i.f. ports necessary to produce optimum conversion loss for the Z, Y, H and G lattice mixers. Two types of narrow-band (image open circuit and image short-circuit), and two types of broad-band mixers (mismatched and matched) were considered in each case. Tables 3.2 to 3.5 summarise the performances for different terminations at the image port.

'Z' Mixer

Mixer	Optimum Load Resistance ($R_{s_{opt}}$)	Optimum Load Resistance ($R_{L_{opt}}$)	L_{min}	Minimum Power Conversion Loss
Image Open Circuit ($R_I = \infty$)	$\frac{r_b}{2}(1 - \frac{4}{\pi^2})^{\frac{1}{2}}$	$\frac{r_b}{2}(1 - \frac{4}{\pi^2})^{\frac{1}{2}}$	$\frac{1 + (1 - 4/\pi^2)^{\frac{1}{2}}}{1 - (1 - 4/\pi^2)^{\frac{1}{2}}} \approx 7.88$	8.96 db
Image Short Circuit ($R_I = 0$)	$r_b/2\sqrt{3}$	$\sqrt{3}r_b/\pi^2$	$\frac{1 + \frac{1}{\sqrt{3}}}{1 - \frac{1}{\sqrt{3}}} \approx 3.76$	5.75 db
Optimum Broad-Band	$\frac{r_b}{2}(1 - \frac{8}{\pi^2})^{\frac{1}{2}}$	$r_b(1 - \frac{8}{\pi^2})^{\frac{1}{2}}$	$2\frac{1 + \sqrt{2}/\pi}{1 - \sqrt{2}/\pi} \approx 5.2$	7.16 db
Matched Broad-Band	$0.69(\frac{r_b}{2})$	$0.53(\frac{r_b}{2})$	5.7	7.56 db

Table 3.2

'Y' Mixer

Mixer	Optimum Source Resistance ($R_{s_{opt}}$)	Optimum Load Resistance ($R_{L_{opt}}$)	L_{min}	Minimum Power Conversion Loss
Image Short Circuit ($R_I = 0$)	$\dfrac{2r_s}{(1 - \sfrac{4}{\pi^2})^{\frac{1}{2}}}$	$\dfrac{2r_s}{(1 - \sfrac{4}{\pi^2})^{\frac{1}{2}}}$	$\dfrac{1 + (1 - \sfrac{4}{\pi^2})^{\frac{1}{2}}}{1 - (1 - \sfrac{4}{\pi^2})^{\frac{1}{2}}} \approx 7.88$	8.96 db
Image Open Circuit ($R_I = \infty$)	$2r_s/\sqrt{3}$	$\pi^2 r_s/\sqrt{3}$	$\dfrac{1 + (\sfrac{1}{3})^{\frac{1}{2}}}{1 - (\sfrac{1}{3})^{\frac{1}{2}}} \approx 3.76$	5.75 db
Optimum Broad-Band	$\dfrac{2r_s}{(1 - \sfrac{8}{\pi^2})^{\frac{1}{2}}}$	$\dfrac{2r_s}{(1 - \sfrac{8}{\pi^2})^{\frac{1}{2}}}$	$\dfrac{2(1 + \sfrac{\sqrt{2}}{\pi})}{1 - \sfrac{\sqrt{2}}{\pi}} \approx 5.2$	7.16 db
Matched Broad-Band	$2r_s/0.69$	$2r_s/(0.53)$	5.7	7.56 db

Table 3.3

'G' Mixer

Mixer	Optimum Source Resistance ($R_{s\,opt}$)	Optimum Load Resistance ($R_{L\,opt}$)	L_{min}	Minimum Power Conversion Loss
Image Short Circuit ($R_I = 0$)	$\frac{\pi}{2}(r_s\,r_b)^{\frac{1}{2}}$	$\frac{2}{\pi}(r_s\,r_b)^{\frac{1}{2}}$	$\frac{1+(1+K_o^*)^{\frac{1}{2}}}{-1+(1+K_o)^{\frac{1}{2}}} \approx 1$	0 db
Image Open Circuit ($R_I = \infty$)	$\frac{r_b}{2\sqrt{2}}$	$\frac{2r_b\sqrt{2}}{\pi^2}$	$\frac{1+\sqrt{2}}{\sqrt{2}-1} \approx 5.83$	7.66 db
Optimum Broad-Band	$\frac{\pi}{2\sqrt{2}}(r_s\,r_b)^{\frac{1}{2}}$	$\frac{2\sqrt{2}}{\pi}(r_b\,r_s)^{\frac{1}{2}}$	$\frac{2(1+(1+2K_o)^{\frac{1}{2}})}{-1+(1+2K_o)^{\frac{1}{2}}} \approx 2$	3 db
Matched Broad-Band	$\frac{r_b}{4}$	$\frac{4r_b}{3\pi^2}$	3	4.77 db

Table 3.4

* $K_o = r_b/\pi^2 r_s$

'H' Mixer

Mixer	Optimum Source Resistance ($R_{s_{opt}}$)	Optimum Load Resistance ($R_{L_{opt}}$)	L_{min}	Minimum Power Conversion Loss
Image Open Circuit ($R_I = 0$)	$\dfrac{2}{\pi}(r_s\, r_b)^{\frac{1}{2}}$	$\dfrac{\pi}{2}(r_s\, r_b)^{\frac{1}{2}}$	$\dfrac{1 + (1 + K_o)^{\frac{1}{2}}}{-1 + (1 + K_o)^{\frac{1}{2}}} \approx 1$	0 db
Image Short Circuit ($R_I = \infty$)	$2\sqrt{2}\,r_s$	$\dfrac{\pi^2 r_s}{2\sqrt{2}}$	$\dfrac{1 + \sqrt{2}}{-1 + \sqrt{2}} \approx 5.83$	7.66 db
Optimum Broad-Band	$\dfrac{2\sqrt{2}(r_b\, r_s)^{\frac{1}{2}}}{\pi}$	$\dfrac{\pi(r_b\, r_s)^{\frac{1}{2}}}{2\sqrt{2}}$	$\dfrac{2(1 + (1 + 2K_o)^{\frac{1}{2}})}{-1 + (1 + 2K_o)^{\frac{1}{2}}} \approx 2$	3 db
Matched Broad-Band	$4r_s$	$\dfrac{3\pi^2 r_s}{4}$	3	4.77 db

Table 3.5

Several interesting conclusions can be deduced from the results
presented in Tables 3.2 to 3.5.

(i) There is a dual relationship between Z image open-circuit
and Y image open-circuit mixers, and between Z image short-circuit
and Y image open-circuit mixers. There is also equivalent duality
for G and H mixers.

(ii) The conversion loss of Z and Y mixers for most image
terminations is greater than the conversion loss for G and H mixers.*

(iii) It is theoretically possible to obtain zero conversion loss
(in db) for single diode Z and Y mixers, while for lattice Z and Y
mixers it is theoretically impossible to obtain zero conversion loss.

(iv) For practical diodes $r_b \gg r_s$ and the parameter K_o ($= r_b/\pi^2 r_s$)
is much greater than one. Consequently, a conversion loss of zero db can be
obtained by a G mixer with image short-circuit, and an H mixer with image
open-circuit. However, the necessary terminations at the r.f. and i.f.
ports of two mixers to produce the zero conversion loss are large and
are therefore difficult to obtain in practice, especially at high
frequencies. There is, therefore, the inevitable compromise between
the requirement of low conversion loss and the practical realisation
of large resistances at r.f. and i.f. ports. The best possible compromise
between the two conflicting requirements is the H broad-band mixer
matched at the r.f. and i.f. ports. The required terminations for the
above mixer, as shown in Table 3.2, can be readily realized in practice
and the predicted conversion loss is then 4.77 db.

*unless a pulse local oscillator waveform is used.

3.3 Performance of Lattice Mixers with Diodes having Exponential Characteristics and Series Resistance

In section 3.2 general formulae have been obtained which can be used to determine the performance of the four types of lattice mixers, assuming that the diode has bi-linear characteristics. In this section the performance of the four types of current driven lattice mixers is obtained assuming that the diode has exponential characteristics.

The relationship connecting the voltage v developed across the terminals of a diode having exponential characteristics and the current i flowing through the diode is given by

$$v = \frac{1}{\alpha} \log_e \left[1 + i/I_s \right] + i r_s \qquad 3.10$$

where α and I_s are the diode parameters. The incremental resistance from equation 3.10 is shown below.

$$\frac{dv}{di} = r_s + \frac{1}{\alpha I_s} \left[\frac{1}{1 + i/I_s} \right]$$

$$= r_s + \frac{r_b}{1 + i/I_s} \qquad 3.11$$

where $r_b = \frac{1}{\alpha I_s}$ and is the incremental resistance of the diode at the origin.

If the local oscillator is treated as a constant-current source, i.e.

$$i_p = 2I_p \cos \omega_p t$$

then the current i_d flowing through each diode of the lattice mixer can be conveniently expressed in the form,

$$i_d = \frac{1}{2} I_p \left[1 + s(t) \right] \cos \omega_p t \qquad 3.12$$

where s(t) is the switching function defined as,

$$s(t) = 1 \text{ for } -\pi/2 \leqslant \omega_p t \leqslant \pi/2$$

$$3.13$$

$$s(t) = -1 \text{ for } \pi/2 \leqslant \omega_p t \leqslant 3\pi/2$$

Substituting equation 3.12 into equation 3.11, the time-varying resistance of the pumped diode is given by,

$$r(t) = \frac{dv}{di} = r_s + \frac{r_b}{1 + X(t) + X(t)\ s(t)} \qquad 3.14$$

where $X(t) = X \cos \omega_p t$, $X = 2I_p/I_s$.

For a lattice mixer, taking into account the 180° phase difference of the local oscillator waveform for the two pairs of diodes, the time-varying resistances are [14],

$$r_+(t) = r_s + \frac{r_b}{1 + X(t) + X(t)\ s(t)} \qquad 3.15(a)$$

$$r_-(t) = r_s + \frac{r_b}{1 - X(t) + X(t)\ s(t)} \qquad 3.15(b)$$

The expressions for the time-varying resistances shown in equations 3.15(a) and 3.15(b) can be substituted for the two-port parameters shown in Table 3.1, and the performance of the four types of mixers can be determined by using the general formulae derived in Chapter II.

3.3.1 The Z Mixer

A block diagram of a Z mixer is shown in figure 3.3. Substituting equations 3.15(a) and 3.15(b) for the two-port parameters shown in Table 3.1, the following two-port matrix equation is obtained provided $r_b \gg r_s$.

$$\begin{bmatrix} v_1 \\ v_2 \end{bmatrix} = \begin{bmatrix} \dfrac{r_s + r_b \left[1 + X(t)\ s(t)\right]}{1 + 2\left[X(t)\ s(t)\right]} & , & \dfrac{r_b\ X(t)}{1 + 2\left[X(t)\ s(t)\right]} \\[3ex] \dfrac{r_b\ X(t)}{1 + 2\left[X(t)\ s(t)\right]} & , & \dfrac{r_s + r_b \left[1 + X(t)\ s(t)\right]}{1 + 2\left[X(t)\ s(t)\right]} \end{bmatrix} \begin{bmatrix} i_1 \\ i_2 \end{bmatrix} \qquad 3.16$$

Restricting the input and output currents i_1 and i_2 to the form given in equations 3.4(a) and 3.4(b) and equating the terms of the same frequency it is shown in appendix I that the Z parameters of the equation 3.16 are,

$$z_{11} = \frac{r_b}{2} \left[1 + \frac{1}{\pi X} \log_e 4X \right] \simeq r_b/2 \qquad 3.17(a)$$

$$z_{12} = r_b/\pi \qquad\qquad 3.17(b)$$

and

$$z_{13} = \frac{r_b}{2\pi X}\left[2 + \log_e 4X\right] \qquad\qquad 3.17(c)$$

Using the general formulae derived in Chapter II the performance of the Z mixer can now be determined.

For the image open-circuit, it can be shown that

$$R_{s_{opt}} = R_{L_{opt}} = \frac{r_b}{2}\left[1 - K_o\right] \qquad\qquad 3.18(a)$$

and

$$L_{3_{opt}} = \frac{1 + \left[1 - K_o\right]^{\frac{1}{2}}}{1 - \left[1 - K_o\right]^{\frac{1}{2}}} \qquad\qquad 3.18(b)$$

where

$$K_o = \left(\frac{z_{11}}{z_{12}}\right)^2 \simeq 4/\pi^2 \qquad\qquad 3.18(c)$$

For the image short-circuit, the corresponding equations are

$$R_{s_{opt}} = \frac{r_b}{2}\left(1 - K_s\right)^{\frac{1}{2}} \qquad\qquad 3.19(a)$$

$$R_{L_{opt}} = \frac{r_b}{2}\left(1 - 4/\pi^2\right)\left(1 - K_s\right)^{\frac{1}{2}} \qquad\qquad 3.19(b)$$

and

$$L_{1_{opt}} = \frac{1 + (1 - K_s)^{\frac{1}{2}}}{1 - (1 - K_s)^{\frac{1}{2}}} \qquad\qquad 3.19(c)$$

where

$$K_s = \frac{4}{\pi^2}\left[\frac{1}{1 - 4/\pi^2}\right] \simeq \frac{2}{3} \qquad\qquad 3.19(d)$$

In the case of a broad-band mismatched Z mixer the optimum terminating impedances and the resulting minimum conversion loss are

$$R_{s_{opt}} = R_{L_{opt}} = \frac{r_b}{2}\left(1 - K_B\right)^{\frac{1}{2}} \qquad\qquad 3.20(a)$$

and

$$L_{2_{opt}} = \frac{2\left[1 + (1 - K_B)^{\frac{1}{2}}\right]}{1 - (1 - K_B)^{\frac{1}{2}}} \qquad\qquad 3.20(b)$$

where $K_B \simeq {}^8/\pi^2$.

For the broad-band Z mixer simultaneously matched at the r.f. and i.f. ports, the general equation corresponding to equation 2.23(a) is

$$R^4 - R^3 (K_o + 2) + R^2 \, 3K_o - Ra \left[K_o(2 - a) - 2a \right] + a^2 \left[K_o(2a - 1) - a^2 \right] = 0$$

$$3.21(a)$$

where

$$R = 1 + R_{s_m} / z_{11} \qquad\qquad 3.21(b)$$

and

$$a = \frac{z_{13}}{z_{11}} = \frac{1}{\pi X} \left(2 + \log_e 4X \right) \qquad\qquad 3.21(c)$$

For normal oscillator drive $(X > 10^3)$ the parameter 'a' is approximately zero and equation 3.21(a) reduces to a quadratic, i.e.

$$R^2 - R (K_o + 2) + 3K_o = 0 \qquad\qquad 3.22$$

Using the value for K_o given by equation 3.18(c) and the root of equation 3.22 which leads to a realisable value of r.f. resistance it can be shown that

$$R_{s_m} = 0.35 \, r_b \qquad\qquad 3.23(a)$$

$$R_{L_m} = 0.264 \, r_b \qquad\qquad 3.23(b)$$

and the resulting conversion loss is 5.7 or 7.56 db.

It is interesting to note that the performance of the Z mixers for different image terminations is virtually independent of the local oscillator drive X provided X >> 1. The results obtained in this section correspond to those shown in section 3.2 for the Z mixer, where it was assumed that the diode has bi-linear characteristics.

3.3.2. The Y Mixer

Using the two-port parameters given in Table 3.1 and equation 3.15, the circuit of a Y mixer shown in figure 3.4 is described by the following two-port matrix equation.

$$
\begin{bmatrix} i_1 \\ \\ i_2 \end{bmatrix} = \begin{bmatrix} \dfrac{1 + X(t)\ s(t)}{r_b + 2r_s\ X(t)\ s(t)} & , & \dfrac{-\ X(t)}{r_b + 2r_s\ X(t)\ s(t)} \\ \\ \dfrac{-\ X(t)}{r_b + 2r_s\ X(t)\ s(t)} & , & \dfrac{1 + X(t)\ s(t)}{r_b + 2r_s\ X(t)\ s(t)} \end{bmatrix} \begin{bmatrix} v_1 \\ \\ v_2 \end{bmatrix}
\qquad 3.24
$$

Introducing frequency restrictions(see equations 3.6(a) and 3.6(b)) the coefficients of the three-port matrix equation are derived in Appendix II. These coefficients in terms of parameter b,

$$
b = \frac{2r_s\ X}{r_b} \qquad\qquad 3.25
$$

are given below

(i) where $\underline{b = 0}$

$$
y_{11} = {}^{2X}\!/\pi r_b \qquad\qquad 3.26(a)
$$

$$
y_{12} = {}^{-X}\!/2r_b \qquad\qquad 3.26(b)
$$

$$
y_{13} = \frac{2X}{3\pi r_b} \qquad\qquad 3.26(c)
$$

(ii) where $\underline{0 < b < 1}$

$$
y_{11} = \frac{1}{\pi r_b}\left(\frac{X}{b} + (1 - \frac{X}{b})v_1\right) \qquad\qquad 3.27(a)
$$

$$
y_{12} = \frac{-X}{\pi r_b}\left(2 - \frac{1}{b}(\pi + V_1)\right) \qquad\qquad 3.27(b)
$$

$$
y_{13} = \frac{1}{\pi r_b}\left(\frac{X}{b} + \frac{4}{b}(1 - \frac{X}{b})\right.
$$

$$
+ \pi(\frac{2X}{b^3} - \frac{2}{b^2} - \frac{X}{b}) \qquad\qquad 3.27(c)
$$

$$
\left. + (\frac{2}{b^2} - \frac{2X}{b^3} + \frac{X}{b} - 1)V_1\right)
$$

where

$$V_1 = \frac{4}{\left(1 - b^2\right)^{\frac{1}{2}}} \tan^{-1}\left[\frac{1 - b}{1 + b}\right]^{\frac{1}{2}} \qquad \text{3.27(d)}$$

(iii) where **b = 1**

$$y_{11} = \frac{X}{\pi r_b}\left(\pi - 2\right) \qquad \text{3.28(a)}$$

$$y_{12} = \frac{X}{\pi r_b}\left(\pi - 4\right) \qquad \text{3.28(b)}$$

$$y_{13} = \frac{2X}{\pi r_b}\left(\pi - 3\right) \qquad \text{3.28(c)}$$

and   (iv) where **b > 1**

$$y_{11} = \frac{1}{\pi r_b}\left(\frac{X\pi}{b} + (1 - \frac{X}{b})V_2\right) \qquad \text{3.29(a)}$$

$$y_{12} = \frac{-X}{\pi r_b}\left(2 - \frac{1}{b}(\pi + V_2)\right) \qquad \text{3.29(b)}$$

$$y_{13} = \frac{1}{\pi r_b}\left[\frac{X\pi}{b} + \frac{4}{b}(1 - \frac{X}{b}) + \pi(\frac{2X}{b^3} - \frac{2}{b^2} - \frac{X}{b})\right.$$

$$\left. + V_2\,(\frac{2}{b^2} - \frac{2X}{b^3} + \frac{X}{b} - 1)\right] \qquad \text{3.29(c)}$$

where

$$V_2 = \frac{1}{(b^2 - 1)^{\frac{1}{2}}}\ \log_e \left[\frac{[(b + 1) - (b^2 - 1)^{\frac{1}{2}}]\,[b + (b^2 - 1)^{\frac{1}{2}}]}{[(b + 1) + (b^2 - 1)^{\frac{1}{2}}]\,[b - (b^2 - 1)^{\frac{1}{2}}]}\right] \qquad \text{3.29(d)}$$

For a very strongly pumped Y mixer (b >> 1), it can be shown that

equations 3.32(a), 3.32(b) and 3.32(c) simplify to,

$$y_{11} = \frac{-X}{\pi r_b b}\left(2 \log_e 2b + X(\pi - \frac{2}{b^2} \log_e 2b)\right) \simeq \frac{1}{2r_s} \qquad \text{3.30(a)}$$

$$y_{12} = \frac{-X}{\pi r_b b}\left(2 - \frac{\pi}{b} + \frac{2}{b^2} \log_e 2b\right) \simeq - \frac{1}{\pi r_s} \qquad \text{3.30(b)}$$

$$y_{13} = \frac{2X}{\pi r_b b^2} \log_e 2b \simeq 0 \qquad \text{3.30(c)}$$

and correspond to the coefficients of the matrix equation 3.6.

For a narrow-band Y mixer with image short-circuit ($G_I = \infty$) the optimum terminating impedances and the resulting conversion loss using the general results derived in Chapter II, are

$$G_{s_{opt}} = G_{L_{opt}} = y_{11}(1 - K_o)^{\frac{1}{2}} \qquad \text{3.31(a)}$$

$$L_{1_{opt}} = \frac{1 + \left[1 - K_o\right]^{\frac{1}{2}}}{1 - \left[1 - K_o\right]^{\frac{1}{2}}} \qquad \text{3.31(b)}$$

where

$$K_o = \left(\frac{y_{12}}{y_{11}}\right)^2$$

The value of K_o varies from $\pi^2/16$ when b is equal to zero, corresponding to the condition when the diode series resistance r_s is also zero, to $4/\pi^2$ when the Y mixer is strongly pumped. The effect of the local oscillator drive on the conversion loss and the required terminations at the r.f. and i.f. ports to produce optimum conversion loss as shown in Figure 3.5.

The corresponding equations for a Y mixer with image open-circuit are

$$G_{s_{opt}} = y_{11}(1 - a^2)(1 - K_s)^{\frac{1}{2}} \qquad \text{3.32(a)}$$

$$G_{L_{opt}} = y_{11}(1 - K_o)(1 - K_s)^{\frac{1}{2}} \qquad \text{3.32(b)}$$

$$L_{3_{opt}} = \frac{1 + \left[1 - K_s\right]^{\frac{1}{2}}}{1 - \left[1 - K_s\right]^{\frac{1}{2}}} \qquad \text{3.32(c)}$$

where

$$a = (y_{13}/y_{11}) \qquad \text{3.32(d)}$$

and

$$K_s = \left[\frac{K_o}{1 - K_o}\right]\left[\frac{1 - a}{1 + a}\right] \qquad \text{3.32(e)}$$

The parameter 'a' varies from one third when b (and r_s) is equal to zero, to approximately zero when the Y mixer is strongly pumped. The corresponding values of the conversion loss are 4.1 db and 5.75 db. The effect of the local oscillator drive X on the optimum terminating impedances at r.f. and i.f. ports, and the conversion loss for a Y mixer with image open-circuit is shown in Figure 3.6.

For a broad-band Y mixer ($G_I = G_s$) mismatched at the r.f. port in order to produce minimum conversion loss, the following equations apply:

$$G_{s_{opt}} = y_{11} \left(1 + a\right)\left(1 - K_B\right)^{\frac{1}{2}} \qquad \text{3.33(a)}$$

$$G_{L_{opt}} = y_{11} \left(1 - K_B\right)^{\frac{1}{2}} \qquad \text{3.33(b)}$$

$$L_{2_{opt}} = 2\left(\frac{1 + (1 - K_B)^{\frac{1}{2}}}{1 - (1 - K_B)^{\frac{1}{2}}}\right) \qquad \text{3.33(c)}$$

where

$$K_B = \frac{2K_o}{1 + a} \qquad \text{3.33(d)}$$

The conversion loss varies from 5.4 db when r_s is zero to 7.16 db when the mixer is strongly pumped. The effect of the local oscillator drive X on the optimum terminating impedances and the resulting conversion loss is shown in Figure 3.7.

Finally for a broad-band Y mixer designed to produce simultaneous matching conditions at r.f. and i.f. ports, the required r.f. port termination (G_{s_m}) is governed by the following quartic equation, (see equation 2.23(a)):

$$G^4 - G^3\left(2 + K_o\right) + G^2 3K_o + Ga\left(2a - 2K_o - aK_o\right) - a^2\left[\overline{K_o(1 - 2a) + a^2}\right] = 0 \qquad \text{3.34(a)}$$

where

$$G = 1 + G_{s_m}/y_{11} \qquad \text{3.34(b)}$$

A computer based solution for the roots of equation 3.34(a) indicates that it is only the largest positive root which leads to a realisable value for G_{s_m}, the termination necessary to produce matching conditions at the r.f. port. The conversion loss for this mixer varies from 5.5 db where r_s is zero (hence b = 0) to 7.56db when the mixer is strongly pumped. The effect of the local oscillator drive X on the conversion loss, and the necessary terminations at the r.f. and i.f. ports, are shown in Figure 3.8.

In the analysis of the Y mixer it has been assumed that r_s = 10Ω and r_b = 10^7Ω, typical parameters for a Schottky barrier diode.

3.3.3 The H Mixer

Using the same techniques of analysis as for Z and Y mixers, the circuit of the H mixer shown in Figure 3.9 can be described by the following two-port matrix equations.

$$
\begin{bmatrix} v_1 \\ i_2 \end{bmatrix} = \begin{bmatrix} 2r_s + \dfrac{r_b}{1 + X(t)\ s(t)} & , & \dfrac{X(t)}{1 + X(t)\ s(t)} \\ \\ \dfrac{-X(t)}{1 + X(t)\ s(t)} & , & \dfrac{1}{r_b}\left(\dfrac{1 + 2X(t)\ s(t)}{1 + X(t)\ s(t)} \right) \end{bmatrix} \begin{bmatrix} i_1 \\ v_2 \end{bmatrix} \qquad 3.35
$$

The coefficients of the three-port matrix describing an H mixer are derived in Appendix III and are given below,

$$ h_{11} = 2\left(r_s + \frac{r_b}{\pi X} \log_e 2X \right) \qquad\qquad 3.36(a) $$

$$ h_{12} = {}^2/\pi \qquad\qquad 3.36(b) $$

$$ h_{13} = \frac{r_b}{\pi X}\left(2 - \log_e 2X \right) \qquad\qquad 3.36(c) $$

$$ h_{22} = {}^2/r_b \qquad\qquad 3.36(d) $$

To assess the performance of an H lattice mixer for different image terminations, it is initially convenient to examine the influence of the local oscillator drive X and the diode series resistance r_s on the parameters K_o and a, defined by equations 2.10(c) and 2.10(d) respectively in chapter II.

For the parameter K_o, it can be shown that

$$K_o = \frac{h_{12}{}^2}{h_{11}h_{22}} = \frac{r_b}{\pi^2 \left(r_s + \frac{r_b}{\pi X} \log_e 2X \right)} \qquad 3.37$$

A graph of K_o as a function of the local oscillator drive for typical value of the diode incremental resistance at the origin $r_b = 10^7 \Omega$, over a range of diode series resistance r_s (0 to 18Ω) is shown in Figure 3.10. Examination of equation 3.37 indicates that K_o is much greater than one, reaching a limit of $r_b/\pi^2 r_s$ at large local oscillator drive.

The parameter 'a' using equations 3.36(a) and 3.36(c) can be expressed in the form,

$$a = \frac{h_{13}}{h_{11}} = \frac{r_b}{\pi X} \frac{\left(2 - \log_e 2X \right)}{\left(r_s + \frac{r_b}{\pi X} \log_e 2X \right)} \qquad 3.38$$

For zero diode series resistance and a large local oscillator drive the parameter 'a' approaches -1. For a finite diode series resistance and a large local oscillator drive, the parameter 'a' is approximately equal to zero, i.e.

$$a \simeq \frac{r_b}{r_s \pi X} (2 - \log_e 2X) \simeq 0 \qquad 3.39$$

Figure 3.11 shows how the parameter 'a' varies as a function of a local oscillator drive X for a range of diode series resistance.

For a narrow-band image open-circuit H mixer, the effect of the local oscillator drive X on the optimum conversion loss and optimum terminations at the r.f. and i.f. ports for a range of diode series resistance (0 to 18Ω) is shown in Figure 3.12, 3.13 and 3.14. Examining equations 3.36, 3.37, 3.38, it can be seen that the optimum terminations at the r.f. and i.f. ports for a large oscillator drive approach the following limiting values:

$$R_{s_{opt}} \simeq \frac{2}{\pi} (r_s \ r_b)^{\frac{1}{2}} \qquad\qquad 3.40(a)$$

$$G_{L_{opt}} \simeq \frac{2}{\pi} (\frac{1}{r_s \ r_b})^{\frac{1}{2}} \qquad\qquad 3.40(b)$$

The corresponding limiting value for the conversion loss is,

$$L_{3_{opt}} \simeq \frac{1 + (1 + r_b/\pi r_s)^{\frac{1}{2}}}{-1 + (1 + r_b/\pi r_s)^{\frac{1}{2}}} \simeq 1 \ (\text{or } 0 \text{ db}) \ \ 3.40(c)$$

Figure 3.15 shows the effect of the local oscillator drive and that of the diode series resistance on the conversion loss of the H mixer with image short-circuit. In Figure 3.15 it can be seen that for a given local oscillator drive the conversion loss approaches a minimum value. The necessary local oscillator drive X to obtain a minimum conversion loss can be determined as follows.

The conversion loss of the H mixer with image short-circuit using equations 2.14(c) and 2.14(d) is

$$L_{1_{opt}} = \frac{1 + \left(1 - K_s\right)^{\frac{1}{2}}}{-1 + \left(1 - K_s\right)^{\frac{1}{2}}} \qquad\qquad 3.41(a)$$

where

$$K_s = \left[\frac{K_o}{1 + K_o}\right]\left[\frac{1 - a}{1 + a}\right] \qquad\qquad 3.41(b)$$

Substituting equations 3.36(a) to 3.36(d) into equation 3.41(b) and differentiating with respect to the local oscillator drive X, it may be shown that the condition necessary to obtain minimum conversion loss is given by the following transcendental equation in X.

$$\log_e 2X - 3 = \frac{2}{\pi X} \left(\frac{r_b}{r_s}\right) \qquad 3.42$$

For large local oscillator drive X the limiting value of the conversion loss is

$$L_{1_{opt}} \simeq \frac{1 + \sqrt{2}}{-1 + \sqrt{2}} = 5.8 \ (7.6 \ db)$$

The effect of the local oscillator drive on the required terminations at the r.f. and i.f. ports is shown in Figures 3.16 and 3.17. The limiting values of the terminations of the r.f. and i.f. ports for large local oscillator drive are

$$R_{s_{opt}} \simeq 2\sqrt{2} r_s \qquad 3.43(a)$$

$$G_{L_{opt}} \simeq \frac{2\sqrt{2}}{\pi^2 r_s} \qquad 3.43(b)$$

For a broad-band mixer mismatched at the r.f. port to obtain minimum conversion loss, the parameter K_B for large oscillator drive approaches the following limiting value

$$K_B = \frac{K_o}{1 + a} \simeq 2r_b/\pi^2 r_s \qquad 3.44$$

and the corresponding limiting value of the conversion loss is

$$L_{2_{opt}} \simeq \frac{2 \left[1 + (1 + 2r_b/\pi^2 r_s)^{\frac{1}{2}}\right]}{-1 + (1 + 2r_b/\pi^2 r_s)^{\frac{1}{2}}} \simeq 2 \ (3 \ db) \qquad 3.45$$

The limiting values of the required terminations at the r.f. and i.f. ports for large local oscillator drive are

$$R_{s_{opt}} \simeq \frac{2}{\pi} \left(2r_b \ r_s\right)^{\frac{1}{2}} \qquad 3.46(a)$$

$$G_{L_{opt}} \simeq \frac{2}{\pi}\left(\frac{2}{r_b \; r_s}\right) \qquad\qquad 3.46(b)$$

Figures 3.18, 3.19, and 3.20 show the effect of diode series resistance and local oscillator drive on the terminations at the r.f. and i.f. ports and on the resulting conversion loss of a mismatched broad-band H mixer.

Using equation 2.23(a) the resulting quartic equation shown below describes a broad-band H mixer simultaneously matched at the r.f. and i.f. ports.

$$R^4 + R^3\left(K_o - 2\right) - R^2 3K_o + Ra\left[2a + K_o(2 + a)\right] + a^2\left[K_o(1 - 2a) - a^2\right] = 0$$

$$3.47(a)$$

where

$$R = 1 + R_{s_m}/h_{11} \qquad\qquad 3.47(b)$$

R_{s_m} is the required impedance to produce a matching condition at the r.f. port.

Although there are several methods [18] of determining the roots of equation 3.47(a) an insight into its properties can be deduced by obtaining the largest root β using Tillots criterion [19]. This largest root is bounded by the following inequality,

$$\beta < 1 + \frac{|3K_o|}{K_o - 2} \qquad\qquad 3.48$$

As the parameter K_o is much greater than two, the largest root β is less than four. Using this estimate of the largest root, equation 3.47(b) can be approximated to a cubic one shown below.

$$R^3 - 3R^2 + Ra\left[2 + a\right] + a^2(1 - 2a) = 0 \qquad 3.49$$

The roots of equation 3.49 can be determined using Cardan's formulae [19]. It is only the largest root of equation 3.49 that leads to a realisable value of R_{s_m}, and is given by the following equations,

$$R = 1 + 2 \left[\frac{[(a + 3)(a - 1)]^{\frac{1}{2}}}{3} \right] \cos(\theta/3) \qquad 3.50(a)$$

where

$$\cos \theta = \frac{-\sqrt{27}(1 - a^2)(a - 1)}{[(a + 3)(a - 1)]^{3/2}} \qquad 3.50(b)$$

Examination of equations 3.50(a) and 3.50(b) shows that for large local oscillator drive as the parameter 'a' approaches zero, R approaches a value of three. Computer investigations of equations 3.50(a) and 3.50(b) indicated this value of the root remains approximately constant at three for a wide range of local oscillator drive (10^3 to 10^9). Using this value for R, it can be shown that the oscillator drive necessary to obtain minimum conversion loss for a matched mixer is defined by the following transcendental equation in X.

$$\log_e 2X - 3 = \frac{2}{\pi X} \frac{r_b}{r_s} \qquad 3.51$$

The above equation corresponds to equation 3.42 which defines the local oscillator drive necessary to obtain minimum conversion loss for a narrow-band H mixer with image short-circuit. The limiting value of the conversion loss for a matched broad-band mixer at high local oscillator drive is 3 or 4.77 db. Figures 3.21, 3.22 and 3.23 show the effect of local oscillator drive and diode series resistance on the terminations of r.f. and i.f. ports, and the conversion loss of a broad-band matched H mixer. The limiting values of the terminations at the r.f. and i.f. ports for large local oscillator drive are

$$R_{s_m} \simeq 4r_s \qquad 3.52(a)$$

$$G_{L_m} \simeq 4/3\pi^2 r_s \qquad 3.52(b)$$

3.3.4 The G Mixer

A block diagram of a G mixer is shown in Figure 3.24 where r_s has been taken outside the lattice network of diodes by applying the Bisection Theorem. Using equations 3.15(a) and 3.15(b) and the parameters given in Table 3.1 the following two port matrix equation describing a G mixer is obtained.

$$
\begin{bmatrix} i_1 \\ \\ v_2 \end{bmatrix} = \begin{bmatrix} \dfrac{1}{r_b} 2 - \dfrac{1}{1 + X(t)\ s(t)} & , & \dfrac{-X(t)}{1 + X(t)\ s(t)} \\ \\ \dfrac{X(t)}{1 + X(t)\ s(t)} & , & 2r_s + \dfrac{r_b}{1 + X(t)\ s(t)} \end{bmatrix} \begin{bmatrix} v_1 \\ \\ i_2 \end{bmatrix} \qquad 3.53
$$

Restricting the input voltage and output current as defined by equations 3.8(a) and 3.8(b), the coefficients of the three port matrix equation 2.4(c) describing a G mixer are derived in appendix IV. These coefficients are given below

$$ g_{11} = \frac{2}{r_b}\left(1 - \frac{1}{\pi X} \log_e 2X\right) \simeq \frac{2}{r_b} \qquad 3.54(a) $$

$$ g_{12} = - 2/\pi \qquad 3.54(b) $$

$$ g_{13} = \frac{2}{r_b\ \pi X}\left(\log_e 2X - 2\right) \simeq 0 \qquad 3.54(c) $$

$$ g_{22} = 2r_s + \frac{2r_b}{\pi X} \log_e 2X \qquad 3.54(d) $$

The parameter 'a' defined as

$$ a = g_{13}/g_{11} \qquad 3.55 $$

is approximately zero over the whole range of the local oscillator drive, for $X > 10^3$. Consequently, the performance of the narrow-band(image short-circuit and image open-circuit) G mixers and broad-band mixers (mismatched and matched) is similar to that shown in table 3.2.

3.4 Conclusions

The performance of practical lattice mixers considered does depend to a large extent on the quality of the imbedding networks employed. In every case, an assumption has been made that the frequency selective terminations are ideal and non-dissipative outside the required frequencies. To simplify the analysis further, the effect of the diode reactive parasitics is assumed to be negligible at the frequencies of interest. It is apparent, therefore, that only with such constraints it is possible to show that the input and output impedances are purely resistive and a minimum conversion power loss is obtained when the mixer works between optimum terminations.

In this chapter, a general analysis of the four types of lattice mixers for different image terminations using two different diode models has been obtained. It is shown that as the local oscillator current drive increased, the performance of the lattice mixers using an exponential diode model, approaches the performance of the lattice mixers where the diode is assumed to have bi-linear characteristics.

In the case of strongly-pumped lattice mixers there is a dual relationship between the appropriate narrow-band Y and Z and G and H mixers. However, if the diodes are assumed to obey an exponential law where the effects of the diode series resistance is included, the above duality is no longer valid. This conclusion is in agreement with that reached by Glover, Gardiner and Howson [20] who showed the failure of the duality relationship between series and shunt mixers using computer aided analysis and an improved diode model. The analytical solutions showing that the duality between the various mixers is not generally valid has not been derived by researchers working in this field.

The performance of Z and G mixers is not basically affected by the level of the local oscillator drive (provided X >> 1) or by the model of the diode, i.e. whether the diode is assumed to have an exponential or bi-linear characteristic. For Y and H mixers, however, the performance is considered influenced by the model of the diode assumed and by the level of the local oscillator drive.

Generally, the conversion loss of Z and Y lattice mixers is considerably higher than the conversion loss of H and G lattice mixers. The narrow-band H mixer with image open-circuit and the narrow-band conversion loss at practical local oscillator drive levels. It can also be shown that even at the image current rejection ratio of 4:1 with conjugate optimum terminations a loss below 2 db is still possible [14]. A useful practical feature of the above H and G mixers is that the ratios of the optimum input and output impedances remain reasonably constant for any drive level, provided X >> 1. As the drive level is increased, however, the absolute values of the required terminations become lower.

The predicted performance of the narrow-band short-circuit H mixer and the narrow-band open-circuit G mixer does not compare favourably with their respective narrow-band dual mixers, i.e. H mixer with image open-circuit and G mixer with image short-circuit. The optimum terminations and the resulting conversion loss of the narrow-band image open-circuit G mixer is virtually independent of the local oscillator drive for X >> 1. In the case of the H mixer with image short-circuit, it displays an optimisation process that takes place within the lattice network of diodes. For this type of mixer there is a minimum conversion loss which occurs at certain drive levels.

It is normally difficult to approximate the ideal open or short-circuit conditions at the image frequency components in practical mixers. The problem becomes even more acute when the r.f. signal lies in the microwave frequency range (e.g. 10 GHZ) and low values of i.f. are employed (e.g. 70, 45 or 30 MHz). Very often, therefore, because of relatively wide bandwidths of practical filters, the impedance presented to the image frequency components may be very close to or equal in value to the terminating impedance at the r.f. signal frequency. The mixers which satisfy this latter equal-impedance condition are known as broad-band or double-sideband mixers.

One method of design of broad-band mixers is to produce a mismatch at the r.f. port in order to obtain minimum conversion loss. The general relationships for the four types of mixers using two different models of the diode have been derived. Again the conversion loss for the Y and Z lattice mixers is considerably greater than for G and H lattice mixers. In the case of the latter type of lattice mixers they both reach a theoretical limit of 3 db for the conversion loss.

An alternative approach in the design of a broad-band mixer is to obtain matching conditions at the r.f. and i.f. ports. On equating the signal and image terminating impedance a general quartic equation is obtained. This equation must be solved in order to obtain the required terminations at the r.f. and i.f. ports and the conversion loss. For practical diodes in the case of Z and G lattice mixers the quartic equation reduces to a quadratic one and a solution is readily obtained. For practical H mixers the quartic equation reduces to a cubic one and a solution is obtained using Cardan's formulae. The conversion power loss plot shows a presence of the optimisation effect previously encountered in the case of a narrow-band image short-circuit

H mixer. The transcendental equation defining the local oscillator
drive necessary to obtain minimum conversion loss is in fact the
same for the two H mixers. For lossless diodes at infinite drive
the conversion loss for a matched broad-band H mixer reaches a
theoretical limit of 3 db. In the case of the broad-band Y mixer
matched at the r.f. and i.f. ports the resulting quartic equation
is solved with the help of a computer. The effect of the local
oscillator drive and the diode series resistance on the terminations
at the r.f. and i.f. ports and the conversion loss is shown.

3.5 <u>References</u>

1. Belevitch, V., Linear Theory of a Bridge and Ring Modulator Circuits, Elec. Comms. 25, 1948.

2. Kruse, S., Theory of Rectifier Modulators, Ericsson Techniques, 1939.

3. Tucker, D.G. Modulators and Frequency Changers, MacDonald, 1953.

4. Van der Graff, J., Unpublished Report on Modulators, Dr. Neter Laboratory, Netherlands Post and Telecommunication Service.

5. Howson, D.P., and Tucker, D.G., Rectifier Modulators with Frequency-Selective Terminations, Proc. IEE., 1960, 107B, pp 261-272.

6. Saleh, A.A.S., Theory of Resistive Mixers, MIT Press, 1971.

7. Cohn, M., Degenford, J.E., Burton, A.N., Harmonic Mixing with an Antiparallel Diode Pair, IEEE, Vol. MTT-23. August 1975, No. 8, pp 667-673.

8. Buchs, J.D., and Begemann, G., Frequency Conversion Using Harmonic Mixers with Resistive Diodes, Microwaves, Optics and Acoustics, May 1978, Vol. 2, No. 3, pp 71-76.

9. Maiuzzo, M.A., Cameron, S.H., Response Coefficients of a Double-Balanced Diode Mixer, IEEE, Vol. EMC-21. Nov. 1979, No. 4, pp 316-319.

10. Ogawa, H., Aikawa, M., Morita K., K-Band Integrated Double-Balanced Mixer, IEEE, Vol. MTT-28, March 1980, No. 3, pp 180-185.

11. Johnson, K.M., X-Band Integrated Circuit Mixer with Reactively Terminated Image, IEEE, Vol. MTT-16, July 1968, No. 7, pp 388-397.

12. Stracca, G.B., Aspesi, F., D'arcangelo, T. Low Noise Microwave Down-Converter with Optimum Matching at Idle Frequencies, IEEE, MTT, August 1973, pp 544-547

13. Schneider, M.V., and Snell, W.W., Harmonically Pumped Stripline Down-Converter, IEEE, Vol. MTT-23, March 1975, No. 3, pp 271-275.

14. Kulesza, B.L.J., General Theory of a Lattice Mixer, Proc, IEE., July 1971, Vol. 118, No. 7.

15. Egami, S., Non-linear, Linear Analysis and Computer-Aided Designs of Resistive Mixers, IEEE., Vol. MTT-22, March 1974, pp 270-275.

16. Gwarek, W.K., Non-linear Analysis of Microwave Mixers, M.S. Thesis, MIT, Cambridge, Sept 1974.

17. Kerr, A.R., A Technique for Determing the Local Oscillator Waveforms in a Microwave Mixer, IEEE, MTT, October 1975, pp. 828-831.

18. Bois, G.P., Tables of Indefinite Integrals, Dover, 1961.

19. Rektorys, K., Survey of Applicable Mathematics, Iliffe, 1968.

20. Glover, K.J., Gardiner, J.G., and Howson, D.P., Double-Tuned Modulator Calculations using an Improved Diode Model, The Ratio and Electronic Engineer, Vol. 42, No. 1, Jan. 1972, pp. 37-44.
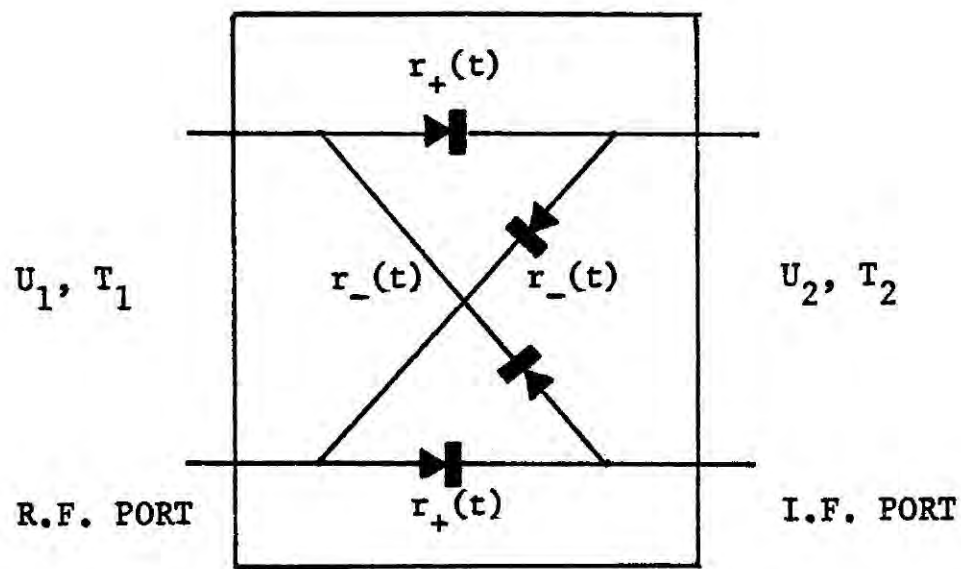
Figure 3.1   General two-port circuit of the lattice mixer
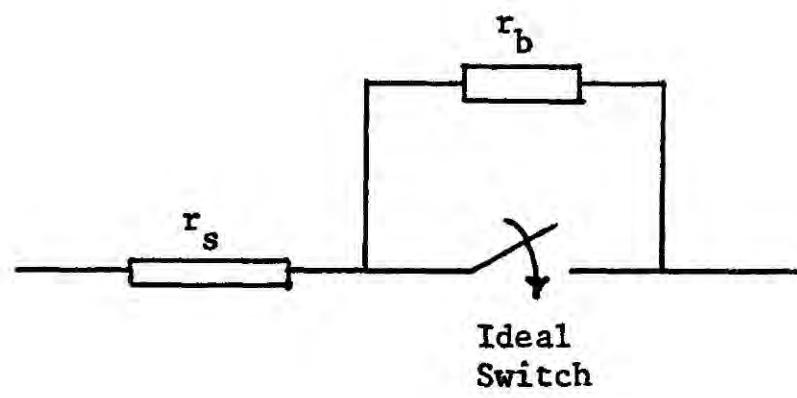
Figure 3.2 Model of a diode having a bi-linear characteristic
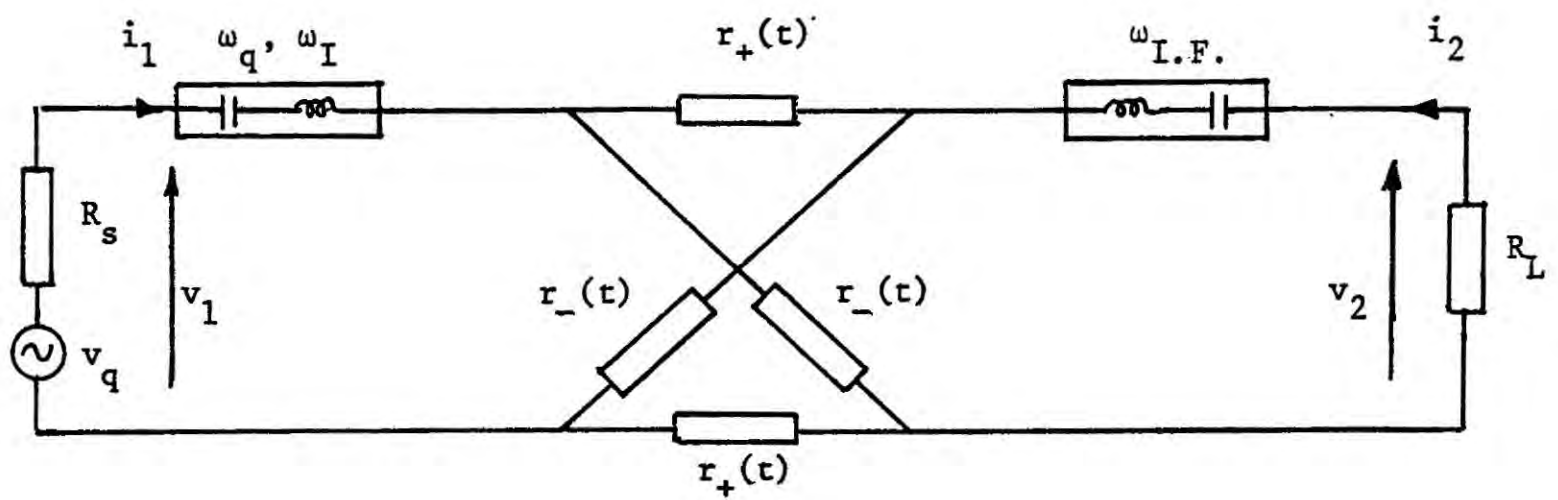
Figure 3.3 Basic equivalent circuit of a Z lattice mixer
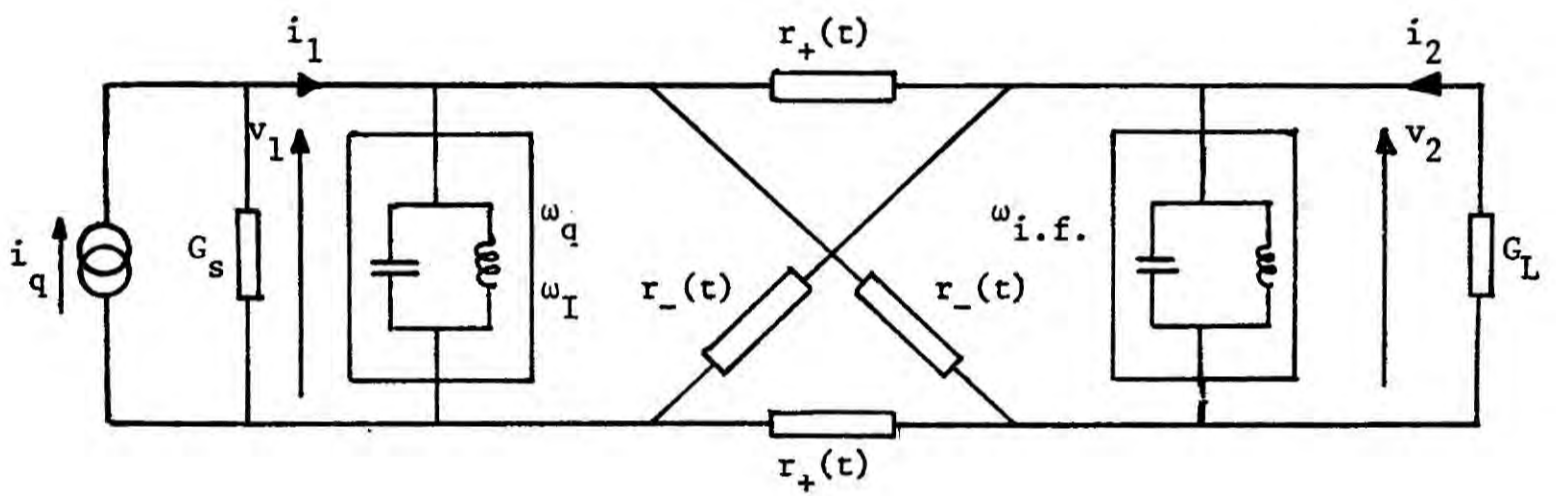
Figure 3.4 Basic equivalent circuit of a Y lattice mixer
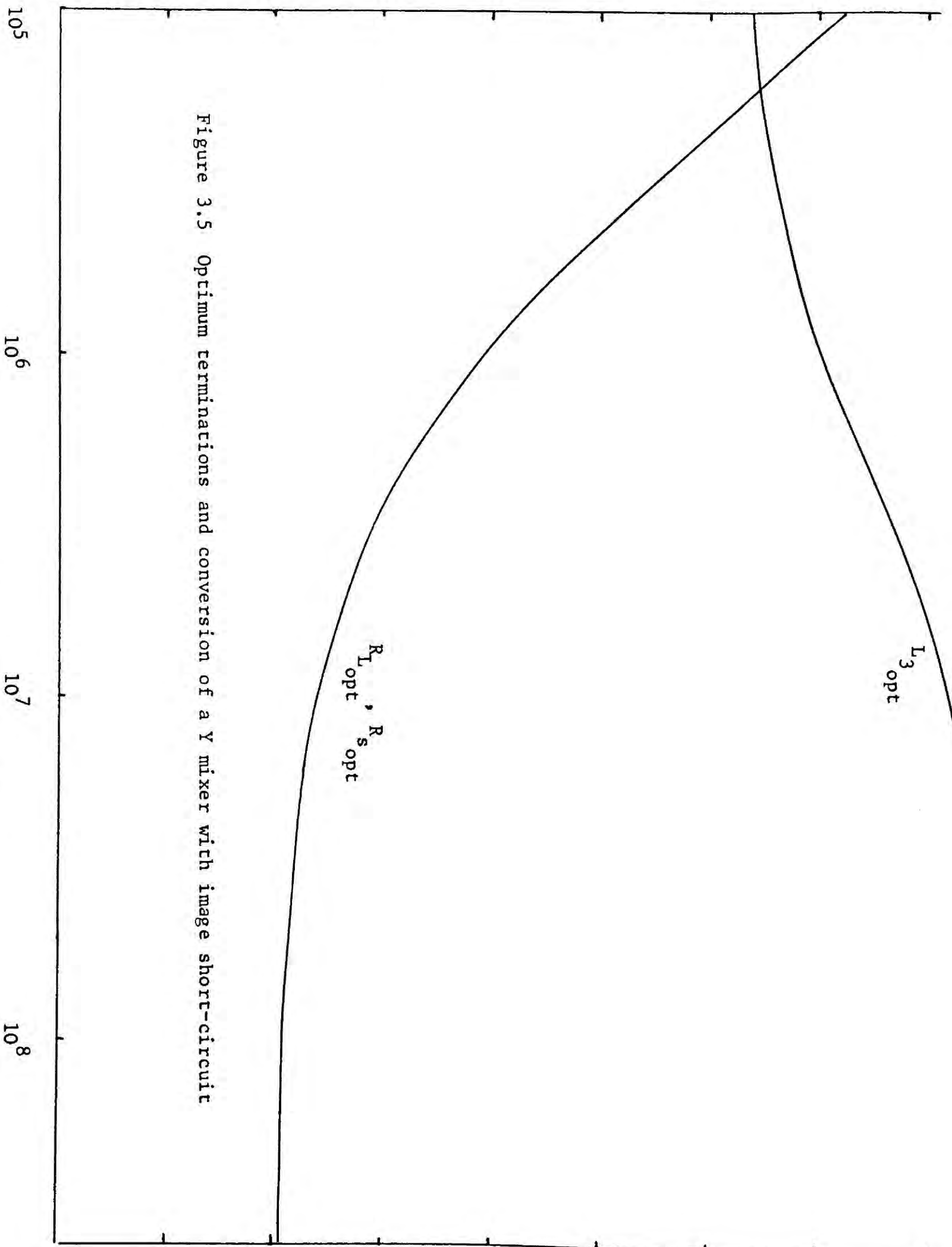
Figure 3.5 Optimum terminations and conversion of a Y mixer with image short-circuit
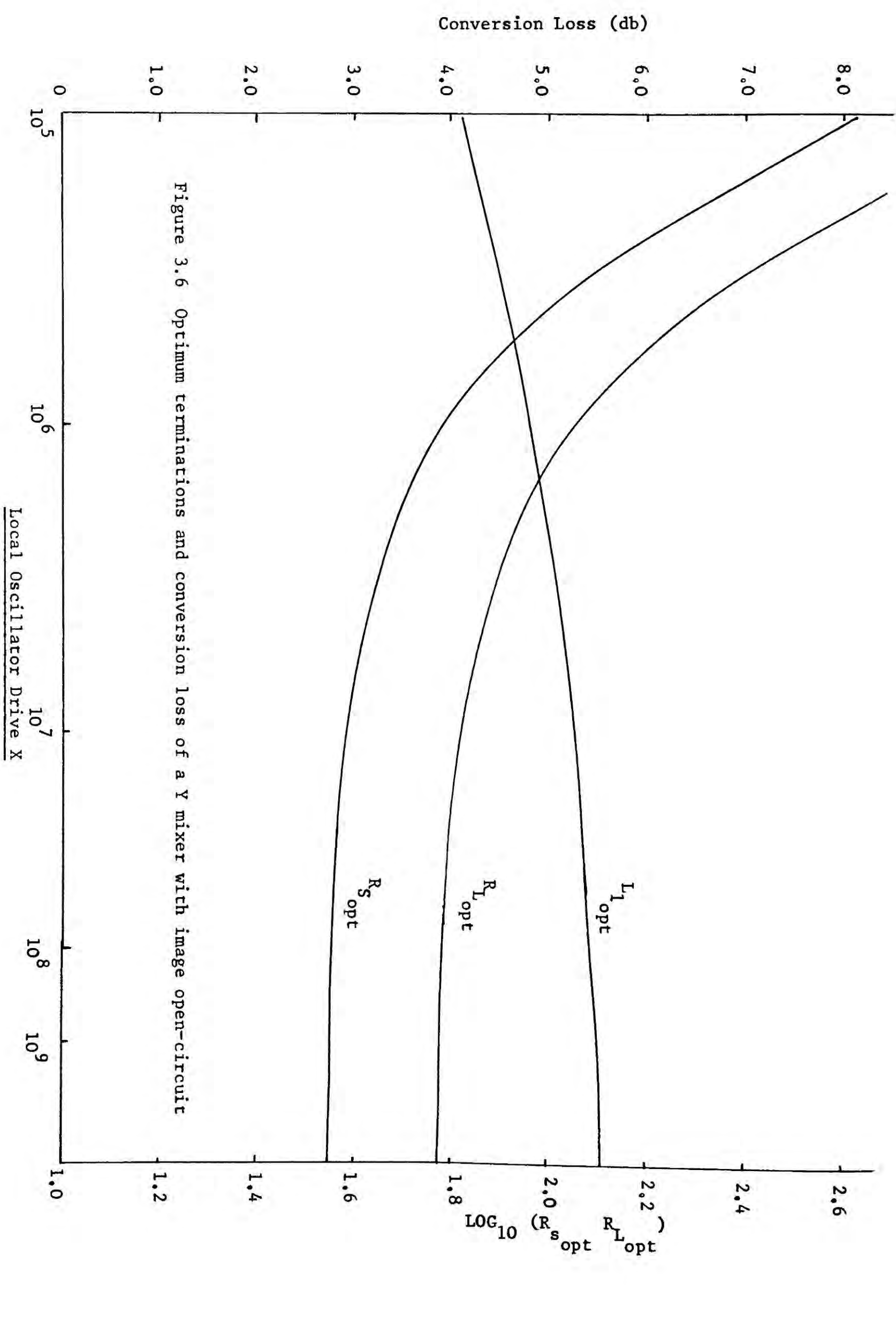
Figure 3.6 Optimum terminations and conversion loss of a Y mixer with image open-circuit
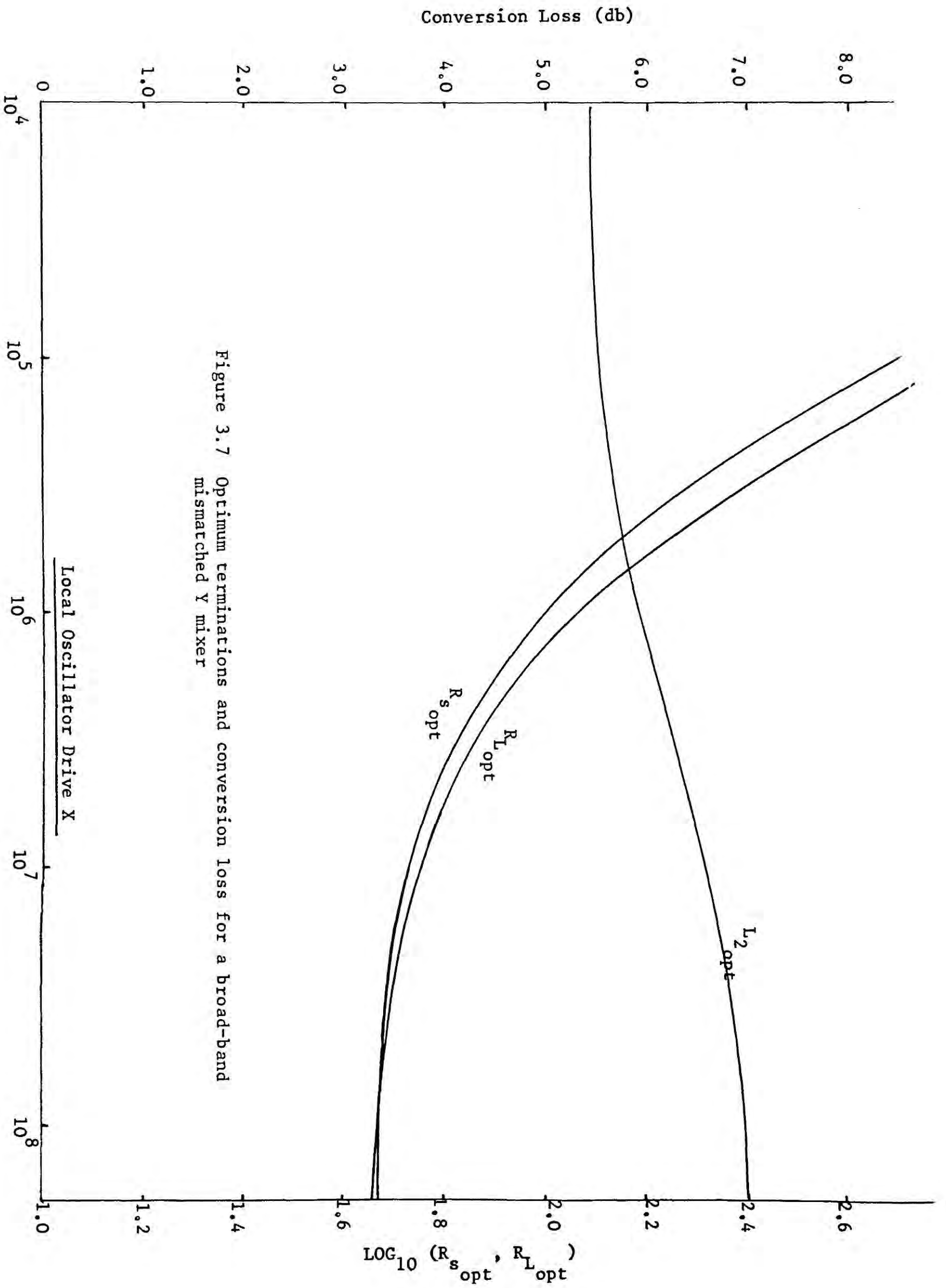
Figure 3.7 Optimum terminations and conversion loss for a broad-band mismatched Y mixer
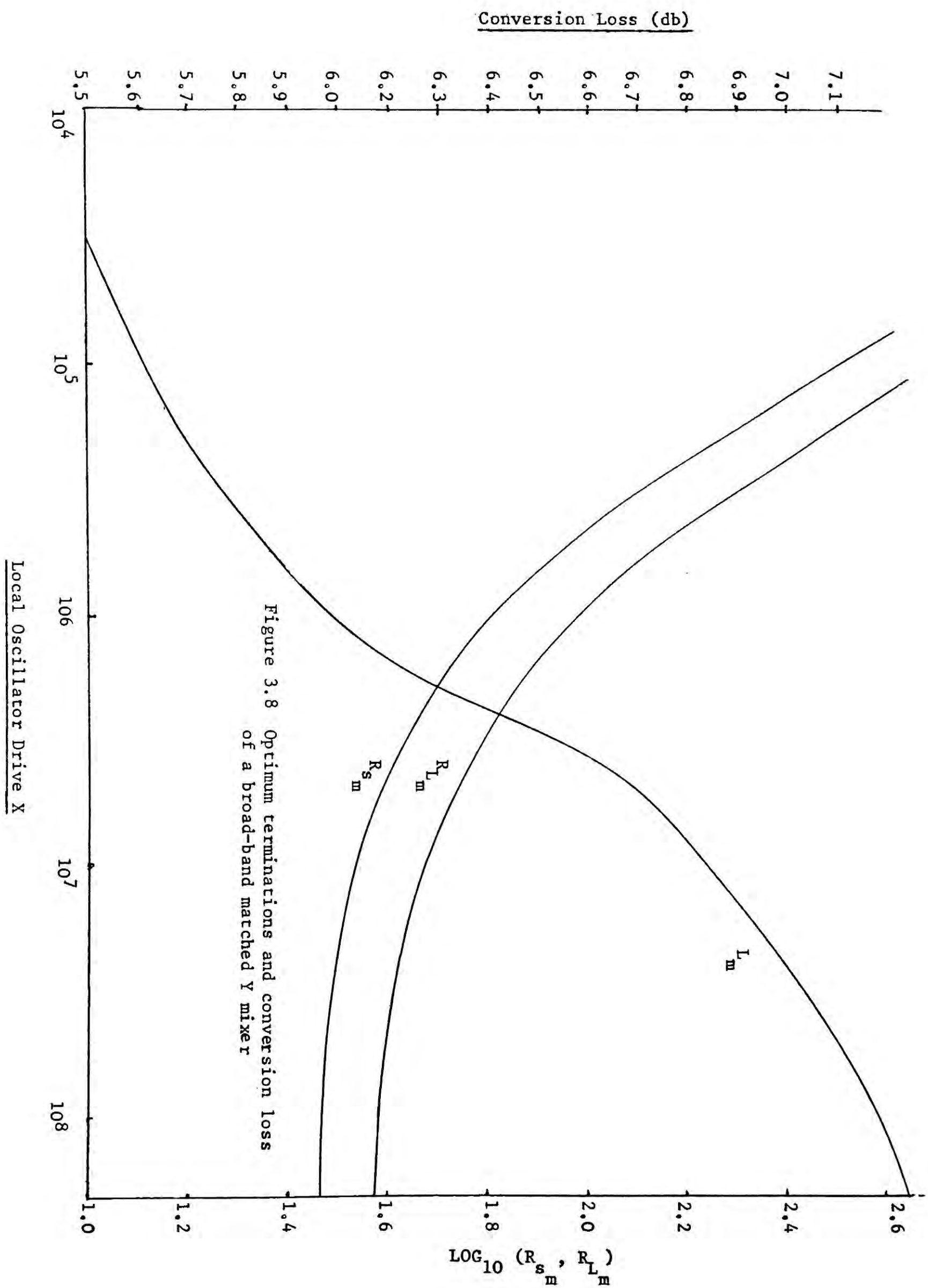
Figure 3.8 Optimum terminations and conversion loss of a broad-band matched Y mixer
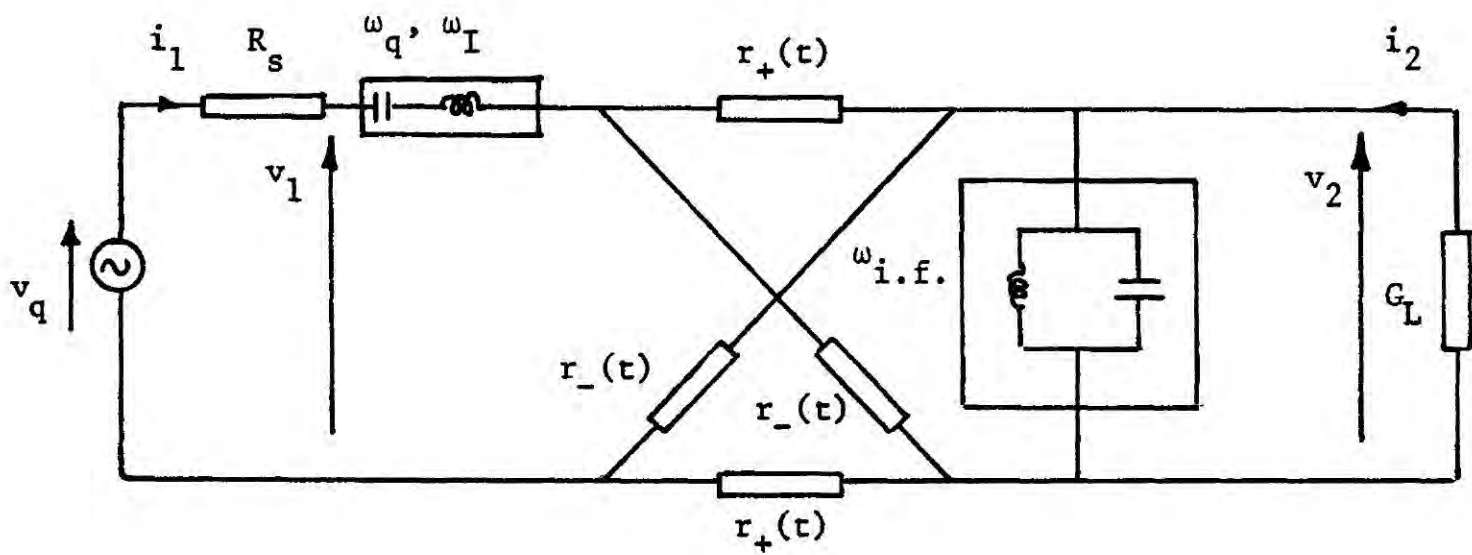
Figure 3.9 Basic equivalent circuit of an H lattice mixer
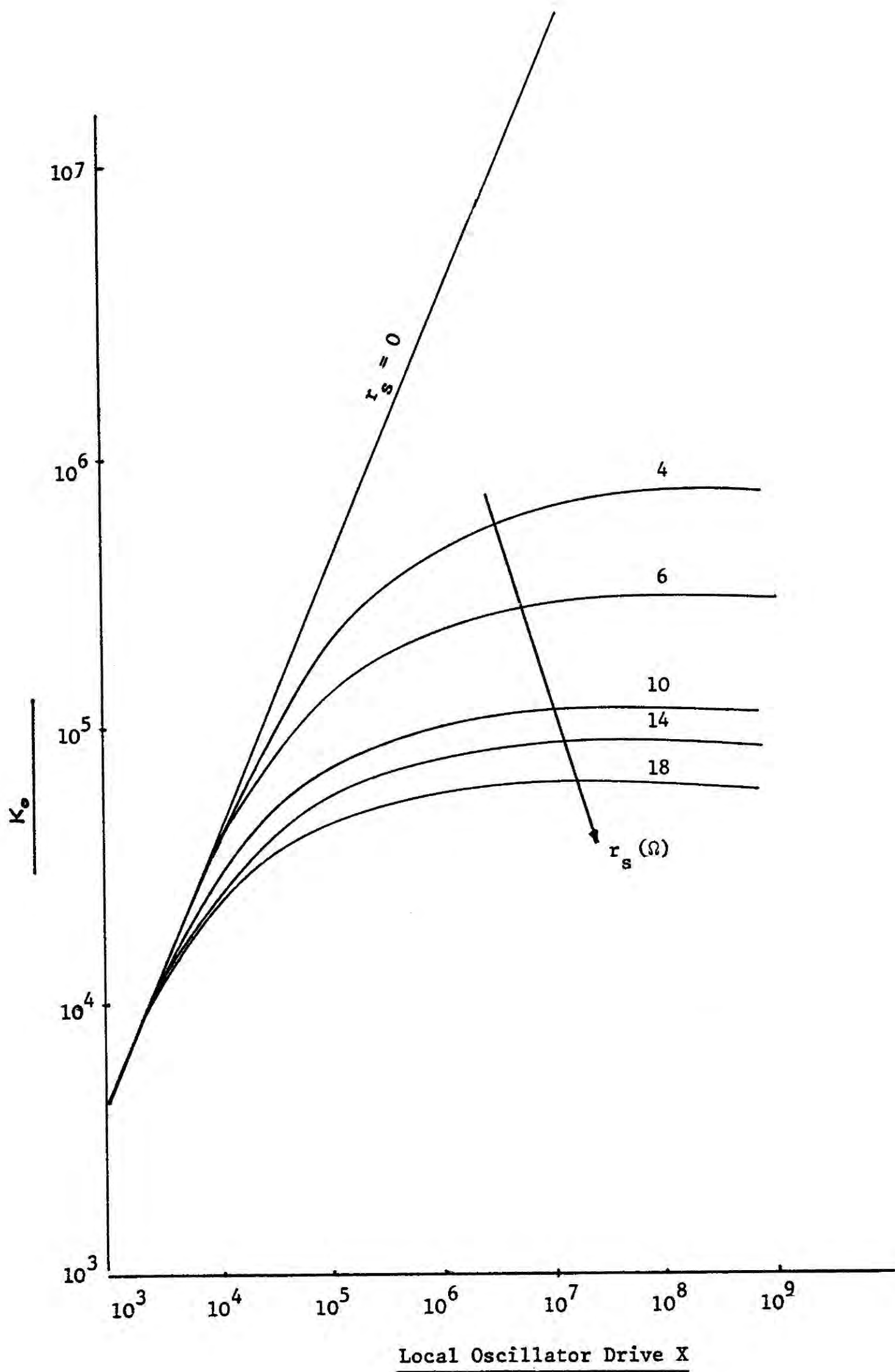
Figure 3.10 The Parameter K_o of an H mixer as a function of local oscillator drive
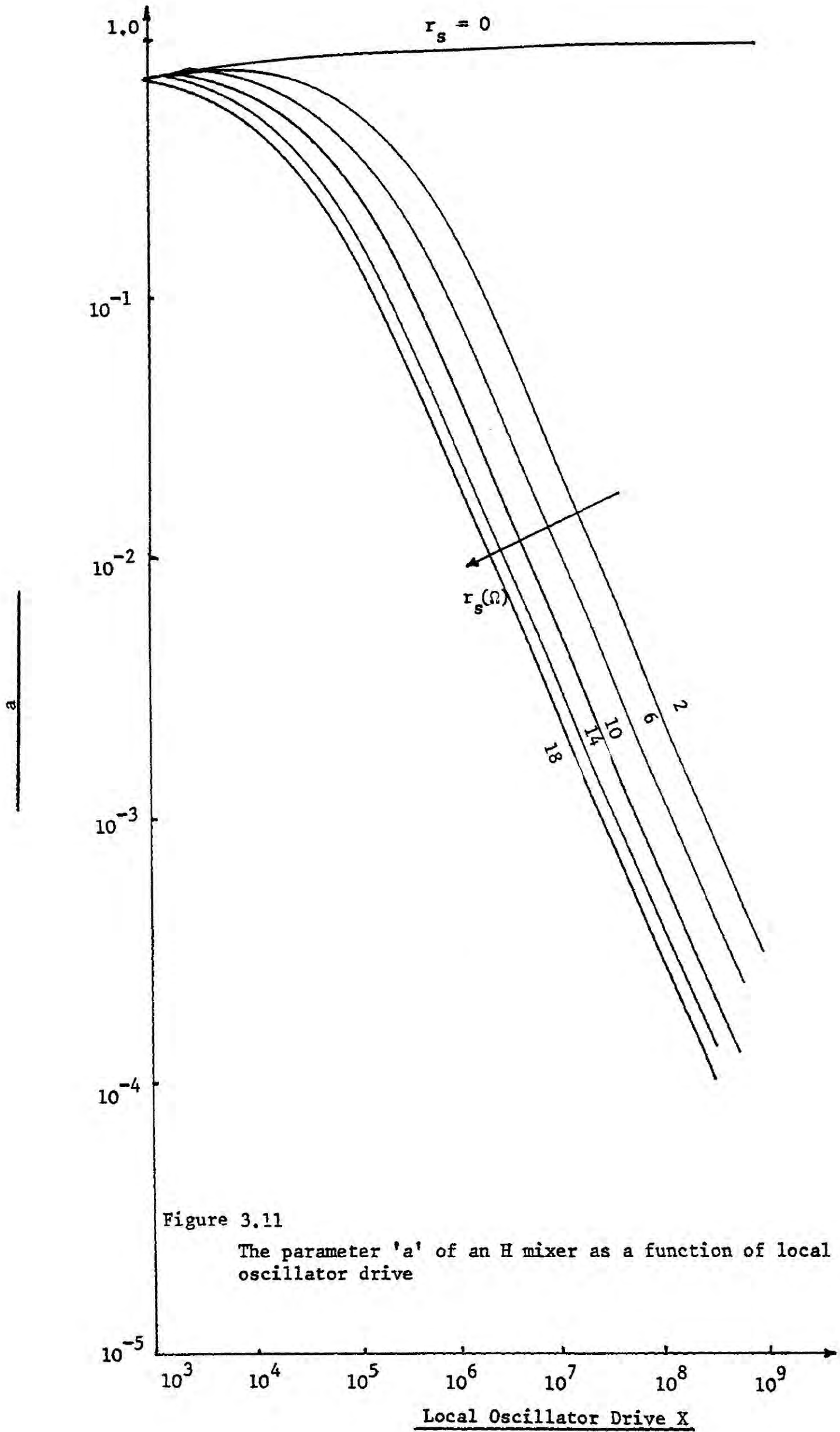
Figure 3.11

The parameter 'a' of an H mixer as a function of local oscillator drive

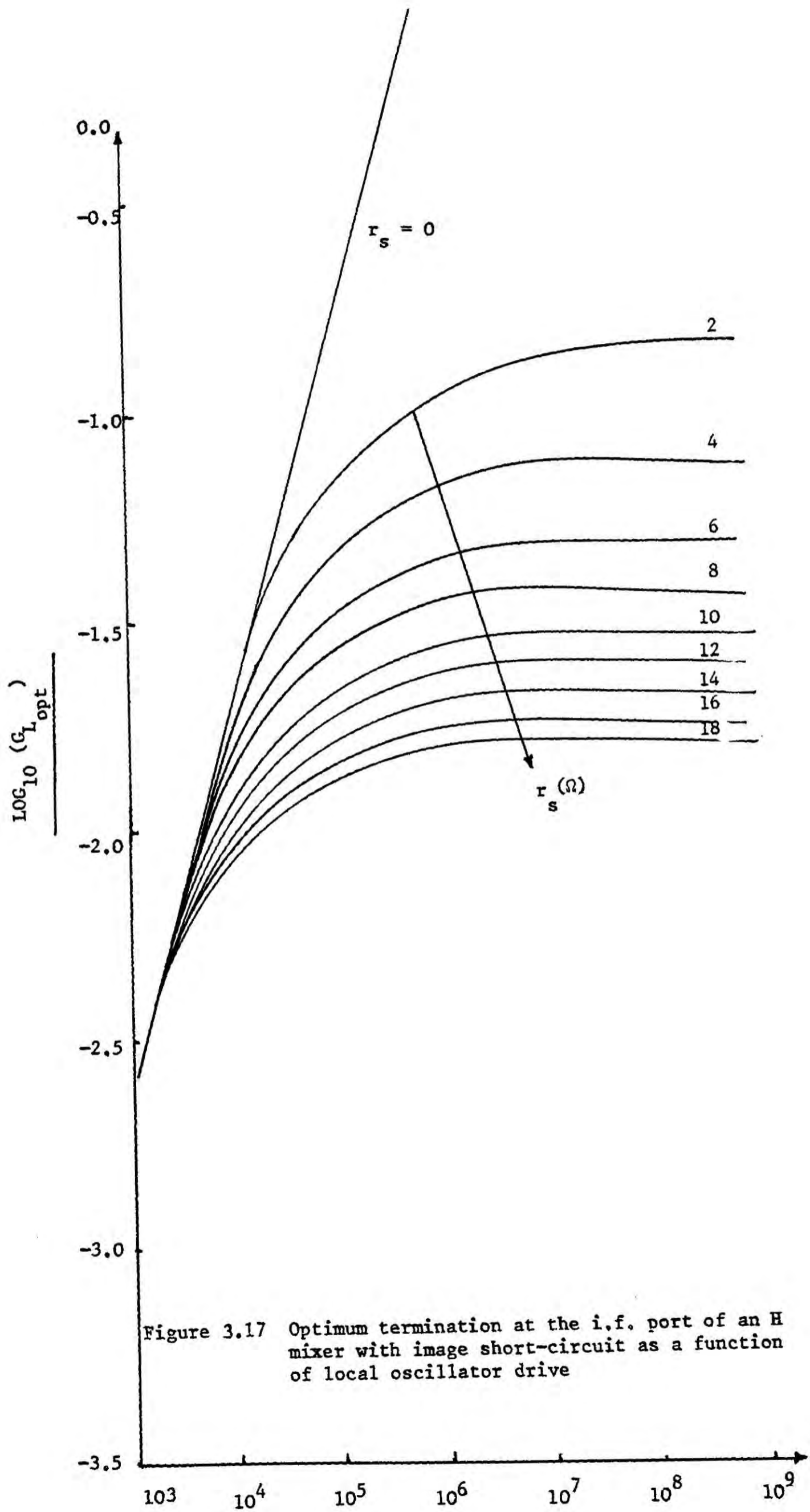Figure 3.12 Optimum conversion loss of an H mixer with image open-circuit as a function of local oscillator drive
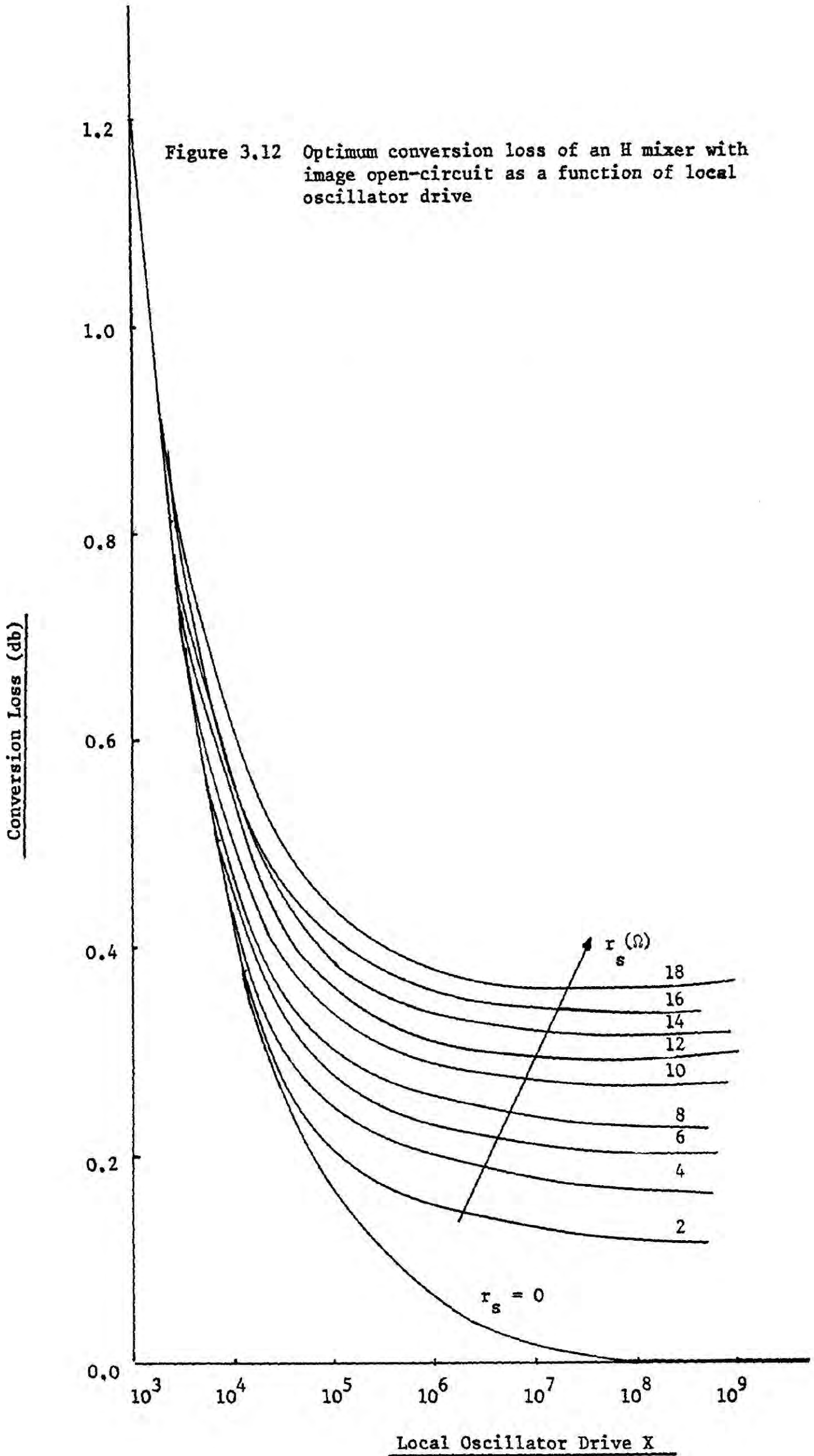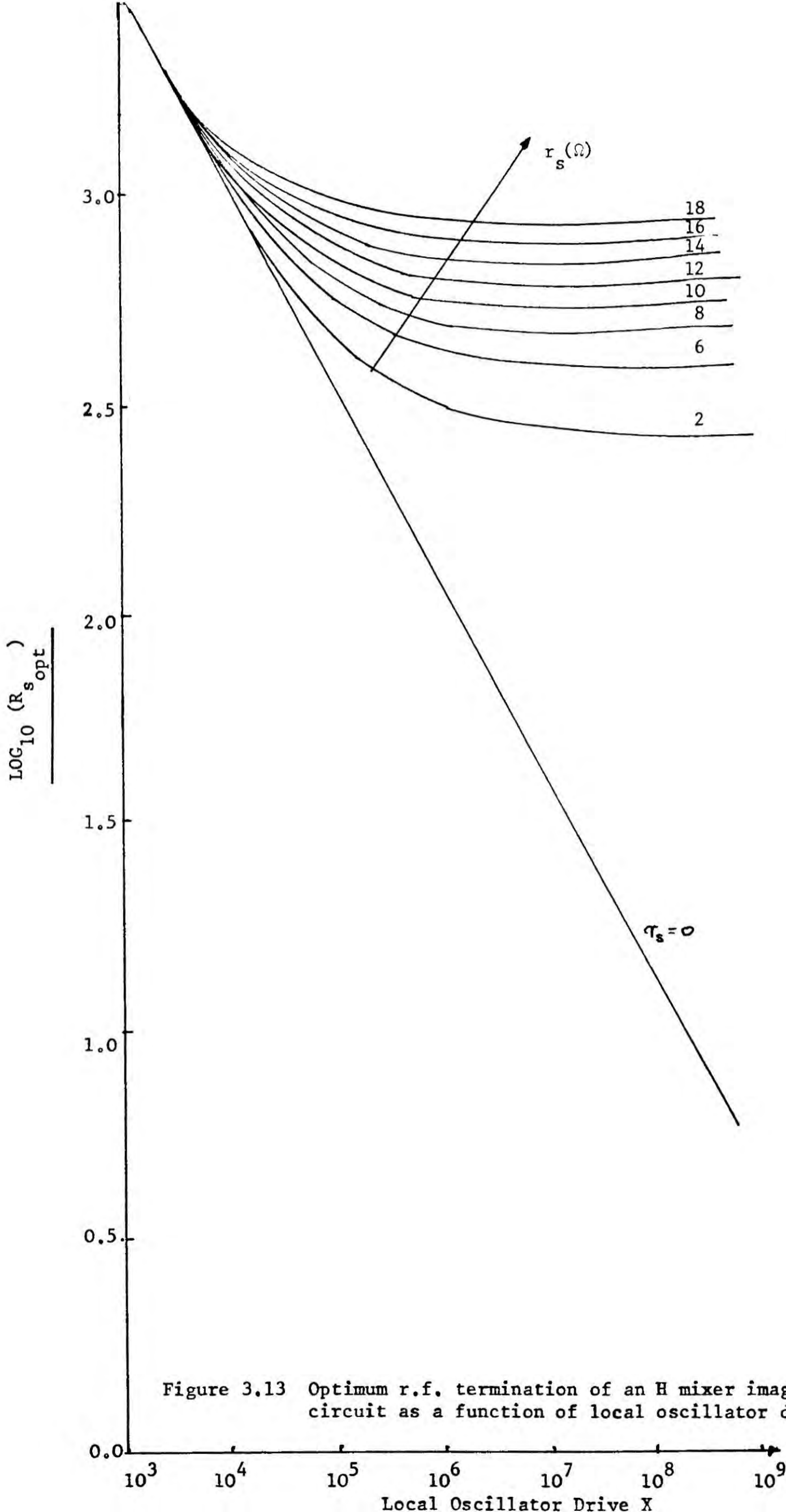
Figure 3.13 Optimum r.f. termination of an H mixer image open-
circuit as a function of local oscillator drive
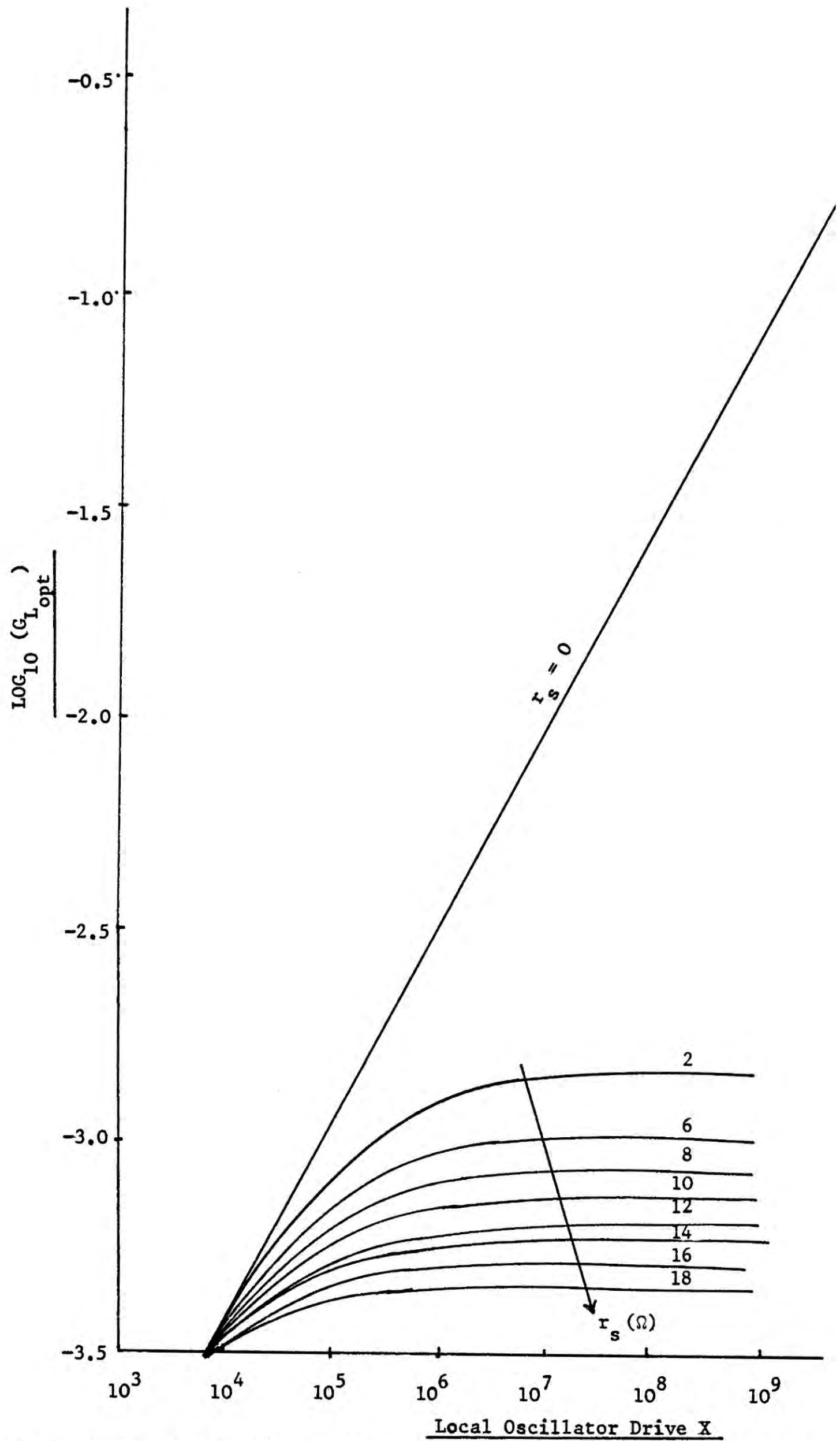
Figure 3.14   Optimum termination at i.f. port of an H mixer with image open-circuit as a function of local oscillator drive
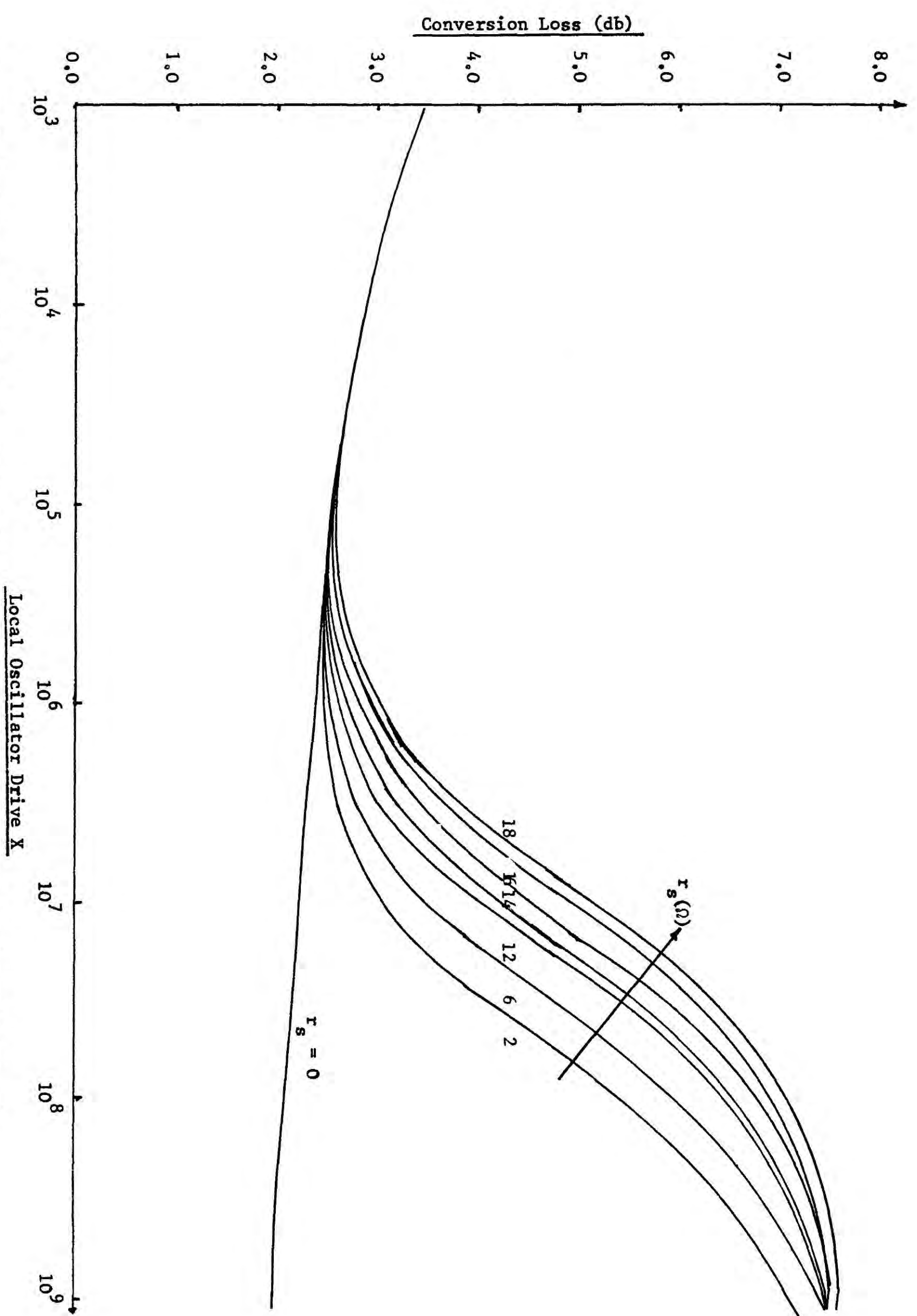
Figure 3.15 Conversion loss of an H mixer image-short circuit as a function of local oscillator drive
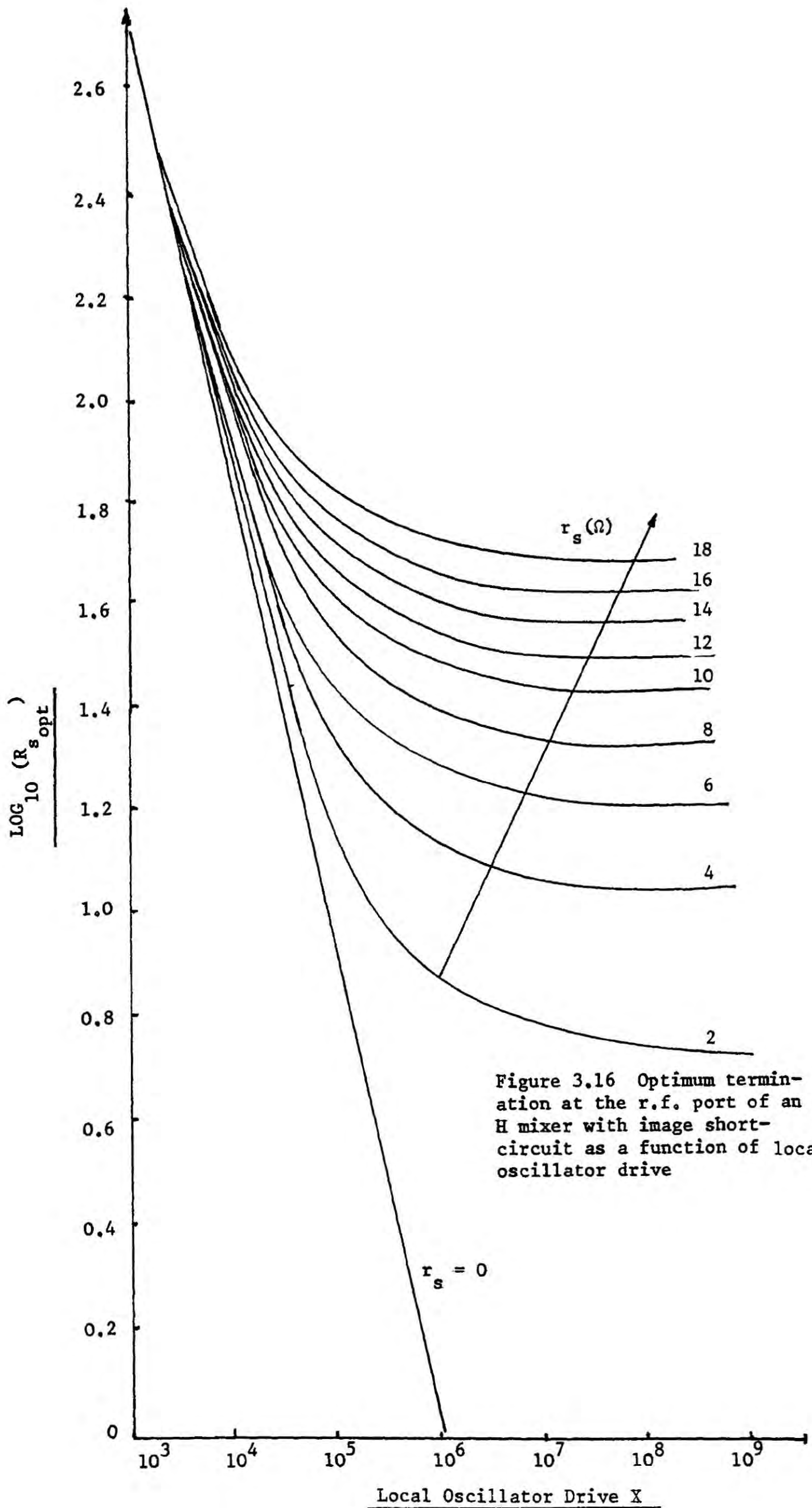
Figure 3.16 Optimum termination at the r.f. port of an H mixer with image short-circuit as a function of local oscillator drive

Figure 3.17   Optimum termination at the i.f. port of an H mixer with image short-circuit as a function of local oscillator drive
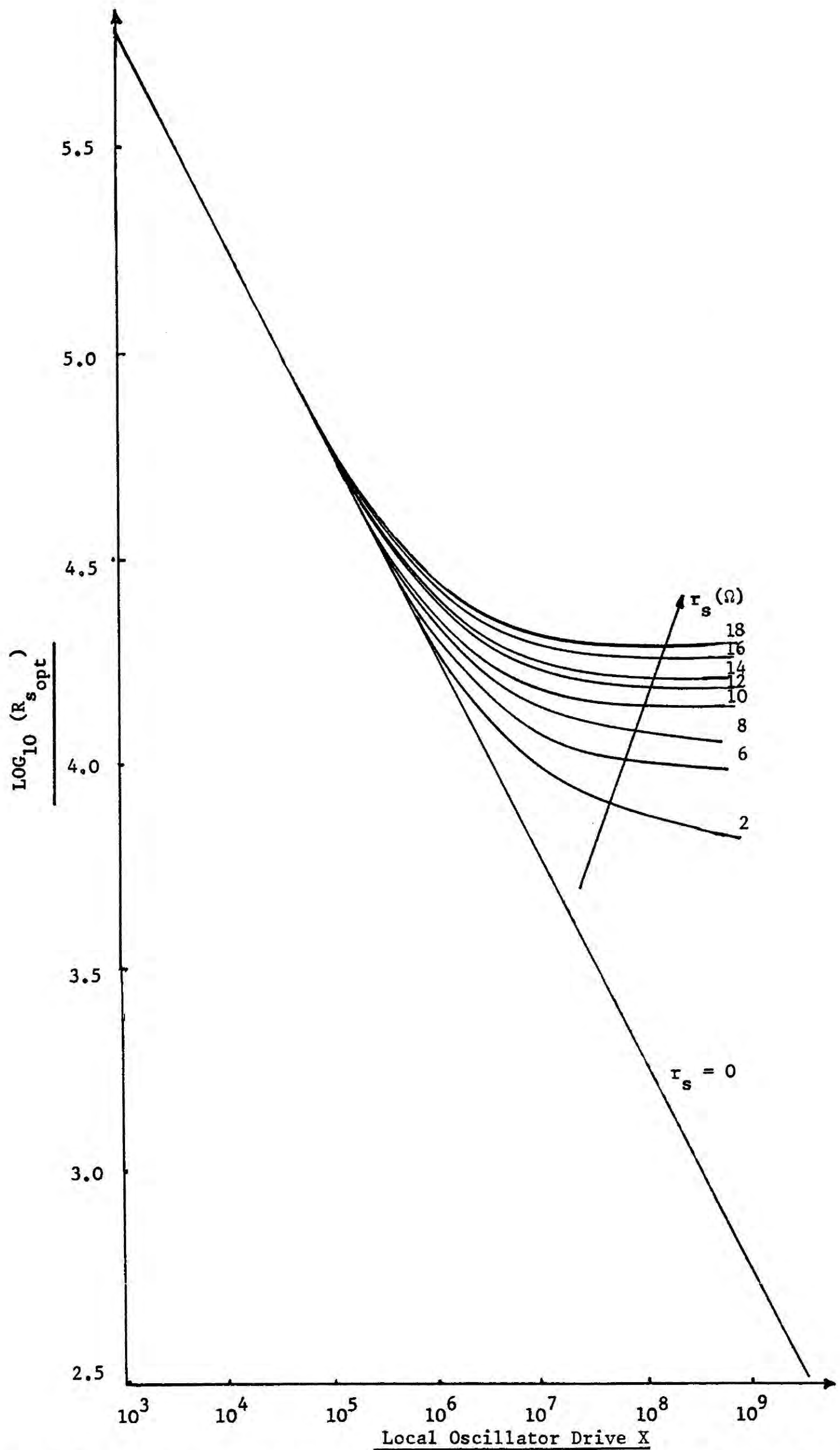
Figure 3.18 Optimum conversion loss of a mismatched
broad-band H mixer as a function of
local oscillator drive
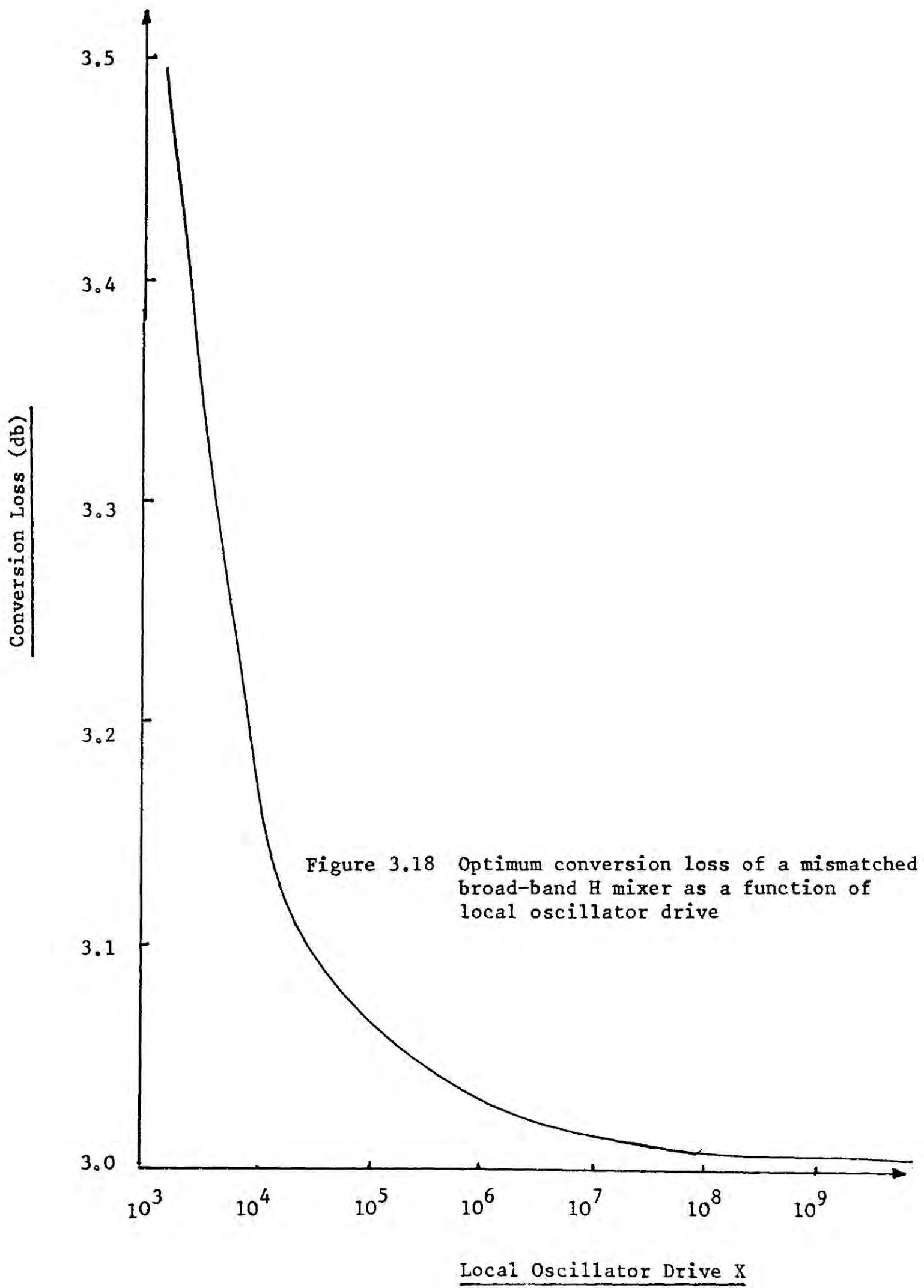
Figure 3.19   Optimum termination at the r.f. port of a broad-band mismatched H
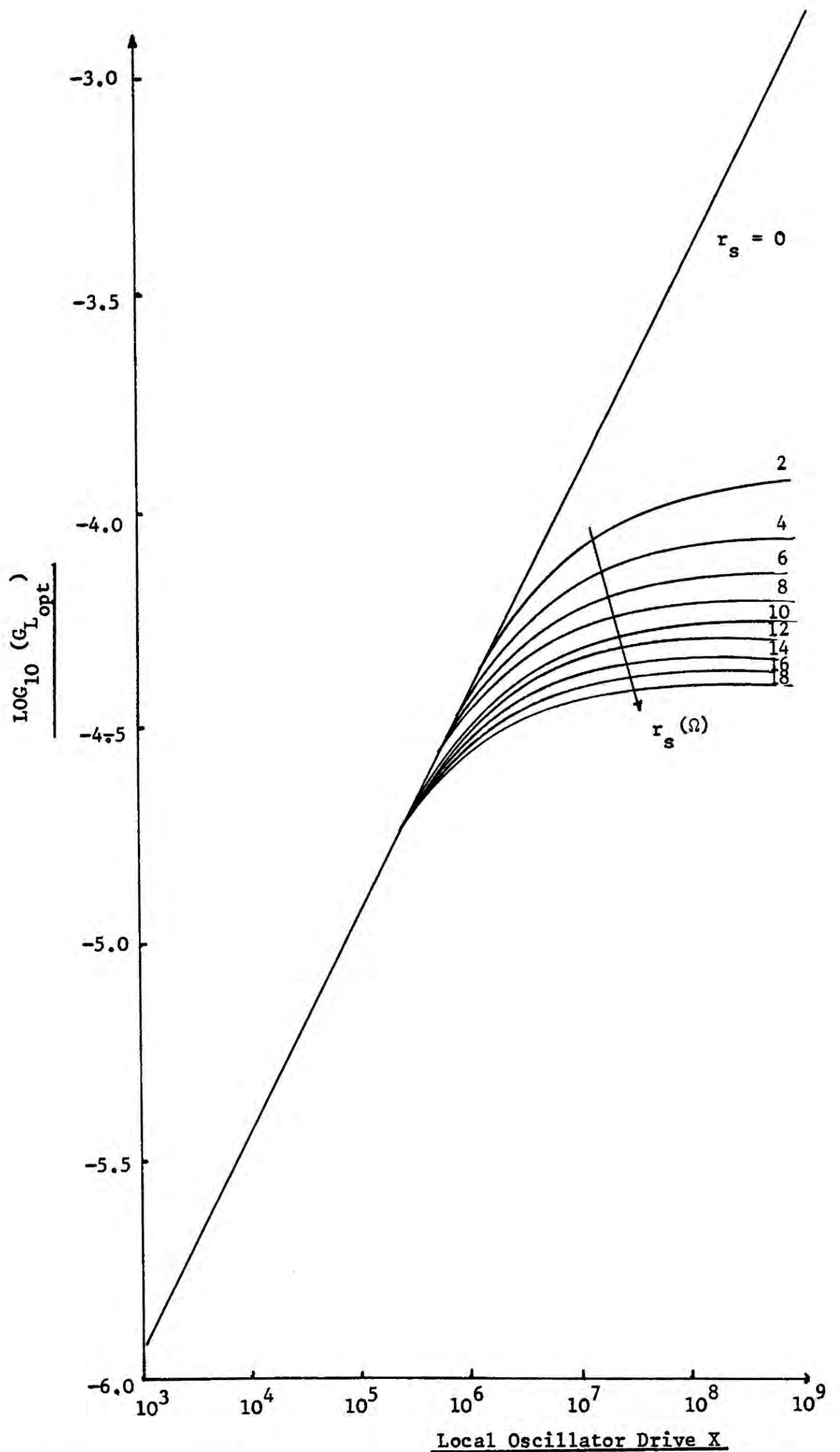mixer as a function of local oscillator drive

Figure 3.20 Optimum termination of the i.f. port of a broad-band mismatched H
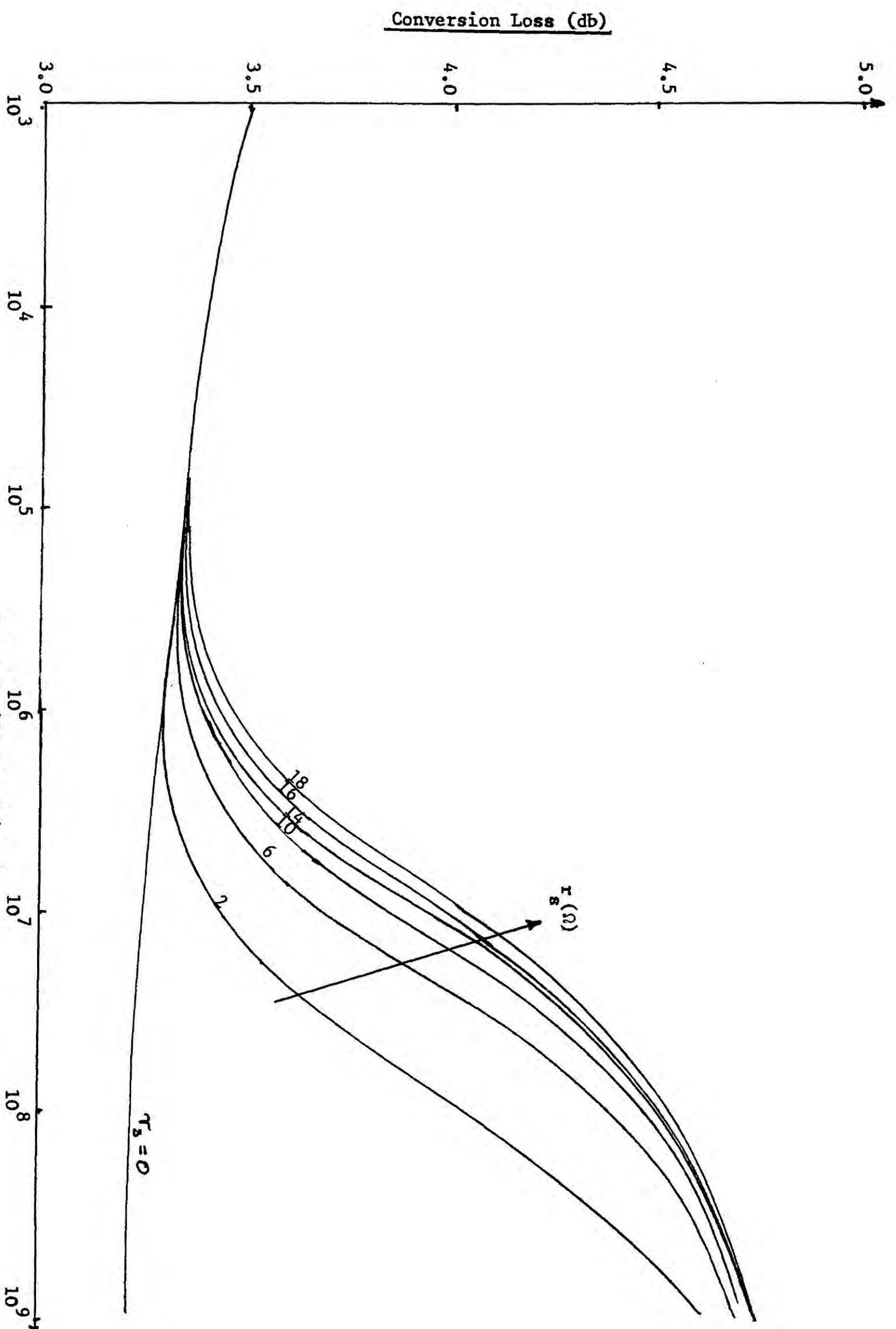mixer as a function of local oscillator drive

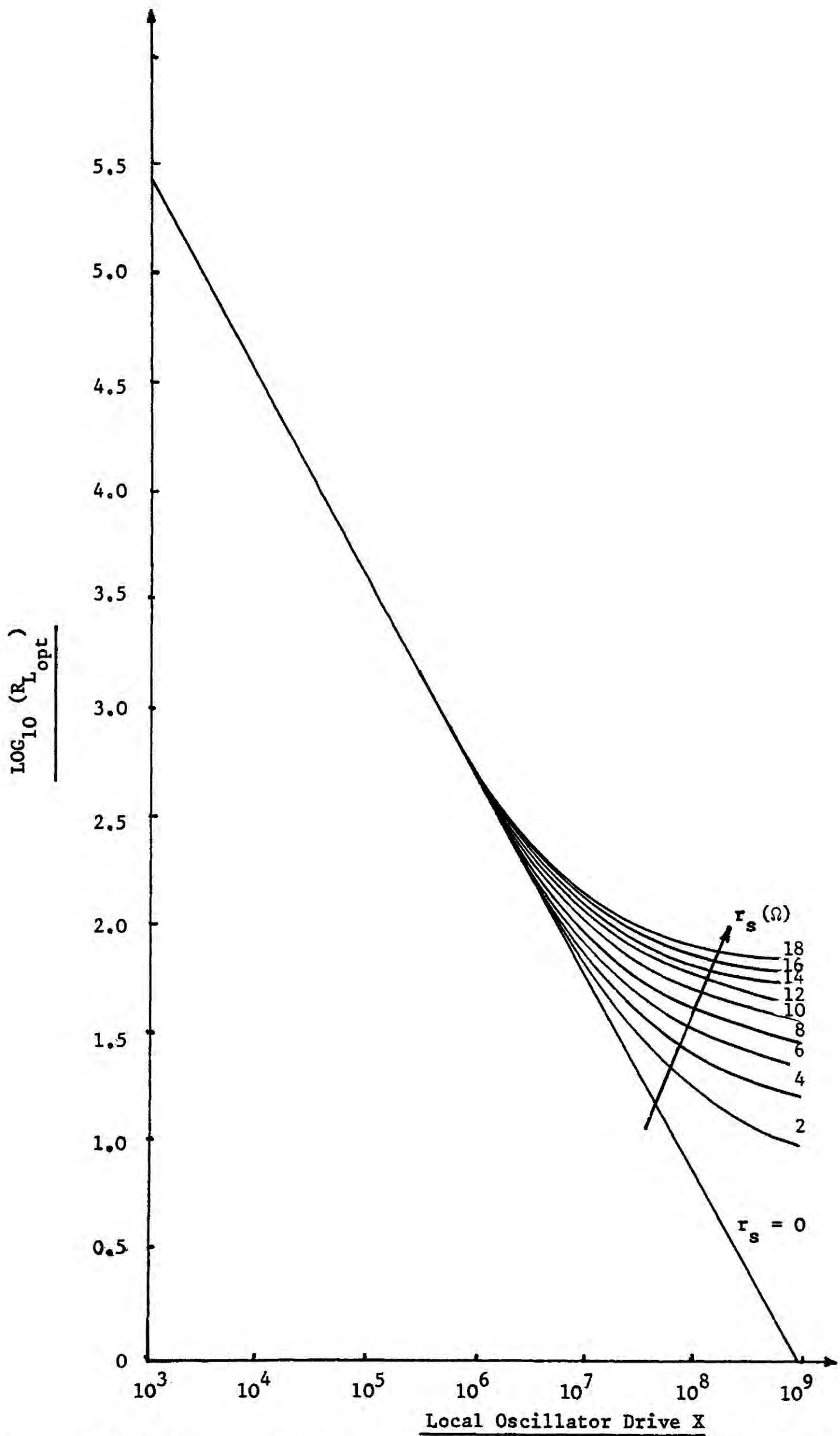Figure 3.21 Conversion loss of a matched broad-band H mixer as a function of local oscillator drive

Figure 3.22 Optimum termination at the r.f. port of a matched broad-band
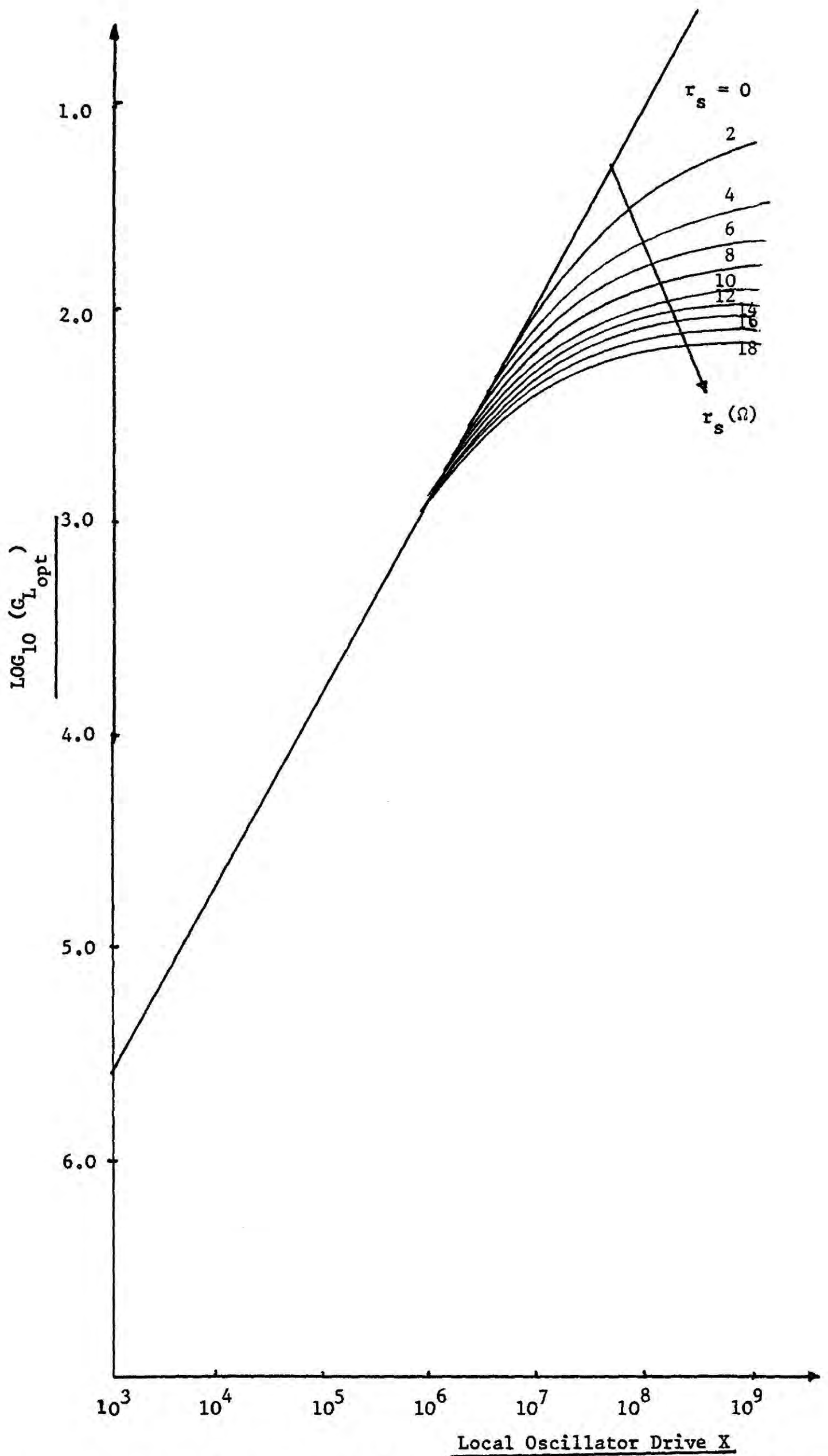H mixer as a function of the local oscillator drive

Figure 3.23 Optimum termination at the i.f. port of a matched broad-band H mixer as a function of local oscillator drive
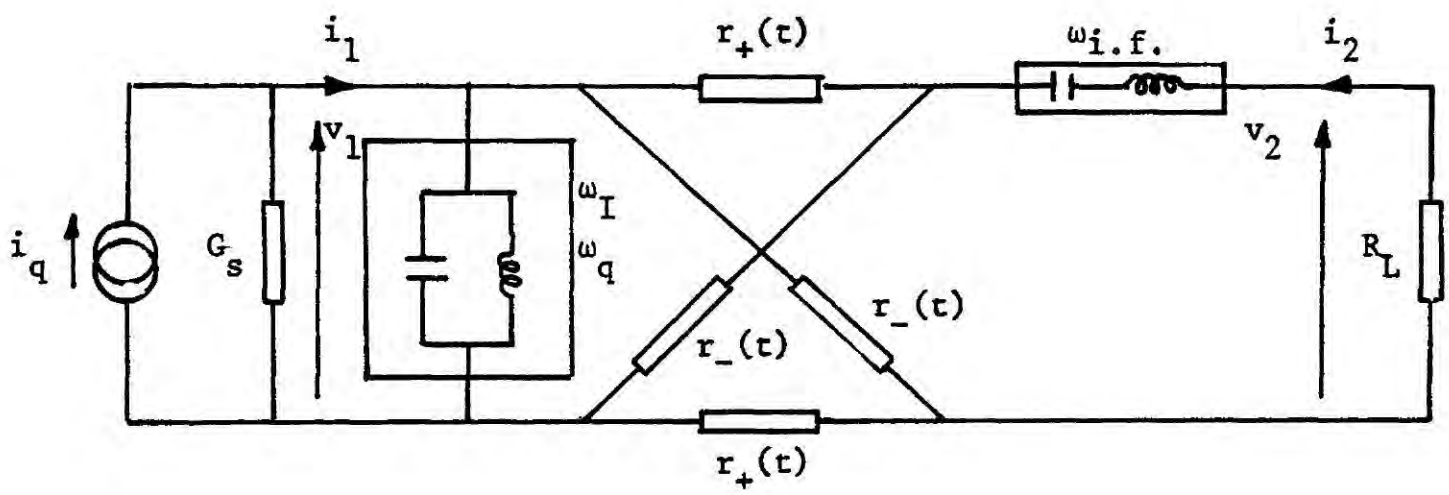
Figure 3.24 Basic equivalent circuit of a G lattice mixer

CHAPTER IV

The Effect of the Diode Capacitance on the
Performance of Lattice Mixers

4.1 Introduction

A number of authors [1-7] have investigated the effect of the diode reactive parasitics (normally junction capacitance) on the performance of single diode mixers. The analysis normally consists of three parts. Firstly it is assumed that the diode junction capacitance and junction resistance are non-linear elements represented as a parallel circuit for which the Fourier coefficients are determined using large signal analysis. Then, using small signal analysis the optimum terminations at the r.f. and i.f. ports are found for the minimum conversion loss. Finally, the noise performance of the mixer is predicted.

The most difficult problem in the analysis of mixers is to determine the Fourier coefficients of the pumped resistance and capacitive waveforms. Very often, it is assumed that the voltage waveform of the local oscillator at the diode junction is sinusoidal and hence the harmonics of the local oscillator are short-circuited. In consequence the Fourier coefficients obtained become only a function of the amplitude of the local oscillator drive. However it is found that the diode parasitics affect the waveform of the local oscillator at the diode junction. The Fourier coefficients of the matrix equation describing the mixer are therefore not only a function of the amplitude but also depend on the shape of the local oscillator waveform present at the diode junction.

Fleri and Cohen [8] investigated the effect of the diode parasitics on the voltage and current waveforms present at the junction of

Schottky-barrier diodes, using the numerical integration algorithm (Runge-Kutta). In their analysis Fleri and Cohen assumed that the embedding network can be treated as a simple lumped circuit.

Egami [9] using a harmonic balance technique has been able to analyse a mixer with arbitrary embedding impedances. He found, however, that the convergence was difficult to obtain when there are a number of local oscillator harmonics present. Gwarek [10] treating the embedding network as a simple lumped circuit element in series with a number of voltage sources, one at each harmonic of the local oscillator,was able to overcome the problem of convergence. Kerr [11] determined the large-signal current and voltage waveforms for a single diode mixer by treating the non-linear problem as a series of reflections between the diode and embedding network. The algorithm treats the diode in the time-domain and the embedding network in the frequency domain.

Based on Kerr's method of analysis the performance of single diode mixers has been obtained by Siegel [12]. Stracca [13] has also investigated the effect of diode parasitics on the performance of a single-diode mixer using fourth-order Kutta-Mason numerical method.

The effect of the diode parasitics on the performance of balanced and double-balanced lattice mixers has also been investigated by a number of authors [14-17]. As in the case of single diode mixers, the effect of the diode parasitics on the waveform of the local oscillator has usually been ignored. Rustom and Howson [18] have investigated the mixer noise figure of Z, Y, H and G resistive mixers using an improved resistive diode model. A computer-based analysis indicated that the best noise figure is obtained if the internal

pump resistance is large. They also confirmed the conclusion reached by Stracca [19] that H and G mixers with a current drive are most promising mixer circuit for low system noise figure.

Both Howson and Stracca used computer based numerical methods and neglected the effect of the diode reactive parasitics on the performance of a mixer. In this chapter an analytical solution has been obtained showing the effect of diode capacitive parasitics on the waveshape of the current flowing in the diodes of a double-balanced lattice mixer. In the analysis it has been assumed that the lattice mixer is driven by a local oscillator having a large internal resistance and a sinusoidal current waveform. Using the analytical expression for the diode current waveform the coefficients of the matrix equation describing the lattice H mixer have been determined. Finally, the effect of the diode parasitic capacitance on the performance of the lattice H mixer was examined.

4.2 Large Signal Waveforms in a Lattice Mixer with Capacitance

The effective circuit of a lattice configuration of diodes seen by the local oscillator current drive is shown in Figure 4.1, where the diode parasitics (diode junction capacitance Cj, diode package capacitance Cp, and diode series resistance r_s) have been included. At low frequencies the reactance of the diode capacitive parasitics is large and their effect on the diode current can be neglected. At high frequencies, however, as the reactance of the diode capacitive parasitics is reduced, the current through each diode is modified. To examine analytically how the diode current is affected by the diode parasitics using the effective circuit shown in Figure 4.1 is a considerable task but it is possible to make the following approximations:-

(i) The diode junction capacitance C_j is a non-linear function of the diode junction voltage but may be approximated to a constant value [20, 21] given by,

$$C_j \simeq C(0)/2 \simeq \left(C_{j_{max}} - C_{j_{min}} \right)/2 \qquad 4.1$$

where $C_{j_{max}}$ and $C_{j_{min}}$ are the diode junction capacitances at extreme values of the operating conditions and C(0) is the diode junction capacitance at zero bias voltage.

(ii) The value of the diode package capacitance is assumed constant and independent of frequency and local oscillator current drive.

(iii) It is assumed that the lattice mixer is pumped by a sinusoidal current drive having a very high internal impedance.

Using the above approximations an analogue model of a high-frequency lattice mixer was constructed and the effects of the diode parasitics on the diode current was examined. For a typical range of diode capacitances the shape of the diode current is as shown in Figure 4.2(a). To a first approximation it was found experimentally that the current through each diode is a truncated half-wave rectified sinewave as shown in Figure 4.2(b).

Further experimental investigations indicated that the diode series resistance had a negligible effect on the angle of truncation. It does not affect the angle of truncation because the product '$I r_s$' is not significant enough during the switching period when all four diodes are held in the 'off' condition by the charged diode capacitance.

As a result of the above approximations and initial experimental investigations, it was decided to analyse the circuit shown in Figure 4.3, where C_e is the effective diode capacitance given by,

$$C_e = 4C_p + 2C_j \qquad\qquad 4.2$$

The effective diode capacitance C_e, by virtue of equation 4.1, can be regarded as constant and only limits the performance of a lattice mixer at high frequencies [22].

The voltage developed across the four diodes in Figure 4.3 is governed by the following differential equation,

$$C_e \frac{dv}{dt} + 2I_s (e^{\alpha v} - e^{-\alpha v}) = 2Ip \sin \omega_p t \qquad\qquad 4.3$$

It is convenient next to introduce the following parameters

$$\theta = \omega_p t \qquad\qquad 4.4(a)$$

$$K = I_s/I_p \;(= \frac{1}{2X}) \qquad\qquad 4.4(b)$$

and a change in a variable,

$$y = Ke^{\alpha v} \qquad \qquad 4.4(c)$$

Equation 4.3 can now be expressed in the form,

$$\epsilon \frac{dy}{d\theta} + y^2 - K^2 = y \sin \theta \qquad \qquad 4.5$$

where

$$\epsilon = \frac{\omega_p C_e}{2\alpha I_p} = \frac{\omega_p C_e r_b K}{2} = \frac{\omega_p C_e r_b}{4X} \qquad \qquad 4.6$$

An analytical solution of the non-linear differential equation 4.5 is still extremely difficult, but an approximate expression for the angle of truncation can be obtained by solving the equation in two regions:

(i) $K^2 \ll y^2$

(ii) $y^2 \ll K^2$

and matching the two solutions to satisfy the condition of periodicity for y.

The condition $K^2 \ll y^2$ corresponds to the part of the cycle of the current when the diode is fully conducting and therefore the diode current is much greater than I_s the diode saturation current. On the other hand, when the diode is in the reverse bias region of the cycle, the condition $y^2 \ll K^2$ is applicable. The solution for the angle of truncation θ_c using equation 4.5 is shown in Appendix V to be

$$\sin^2 (\theta_c/2) = \frac{\epsilon}{2} \log_e \left(4X^2 \left(\frac{2\epsilon}{\pi}\right)^{\frac{1}{2}} \right) \qquad \qquad 4.7$$

The logarithmic term of equation 4.7 varies slowly for large changes in ϵ and hence it can be further simplified to the form,

$$\sin^2 (\theta_c/2) \simeq A \frac{\epsilon}{2} \qquad \qquad 4.8$$

'A' represents the logarithmic term in equation 4.7 and can be regarded as constant.

4.2.1 Experimental Results

A low frequency model of a lattice mixer was constructed and tested at 50 KHz. HP 2833 diodes were used and from preliminary tests performed on these diodes, it was found that $I_s = 8 \times 10^{-10}$A, $r_b = 3.4 \times 10^7 \Omega$. The current drive was adjusted so that the normalised current drive K was 7×10^{-7}, where the parameter K is defined by equation 4.4(b).

Figure 4.4 shows a comparison of the theoretical values given by equation 4.8, with the measured results of the angle of truncation of the diode current for a typical range of capacitances.

The effect of the angle of truncation is that it modifies the frequency spectrum of the diode current by introducing a significant number of odd harmonics. The harmonic content of the diode current was theoretically predicted by assuming that the diode current is zero for angles less than the angle of truncation θ_c and sinusoidal from θ_c to π. The theoretical and measured values of the harmonic components normalised relative to the fundamental are shown in Figure 4.5.

The harmonic content of the voltage across the diodes can be obtained by integration of the expression for the capacitor current. Figure 4.6 shows a comparison between the measured and predicted values of the harmonic content of the voltage both normalised relative to the fundamental. In both cases close agreement between the theoretical and experimental results is evident.

4.3 The Effect of the Diode Parasitic Capacitance on the Coefficients of the H Mixer

It has been shown that the effect of the diode parasitic capacitance on the current waveform through the diodes is to produce

a truncated half-wave rectified sinewave shown in Figure 4.2. The current flowing through each 'on' diode can be expressed in the form,

$$i_1 = \frac{1}{2} \left[1 + s_1(t) \right] I_p \cos \omega_p t \qquad 4.8(a)$$

while the current flowing through each 'off' diode is given by,

$$i_2 = \frac{1}{2} \left[1 + s_2(t) \right] I_p \cos \omega_p t \qquad 4.8(b)$$

where $s_1(t)$ and $s_2(t)$ are two switching functions defined as,

$$s_1(t) = -1 \text{ for } \frac{-\pi}{2} \leqslant \omega_p t \leqslant \frac{-\pi}{2} + \theta_c$$

$$= 1 \text{ for } \frac{-\pi}{2} + \theta_c \leqslant \omega_p t \leqslant \pi/2 \qquad 4.9(a)$$

$$= -1 \text{ for } \frac{\pi}{2} \leqslant \omega_p t \leqslant \frac{3\pi}{2} + \theta_c$$

and

$$s_2(t) = 1 \text{ for } \frac{-\pi}{2} \leqslant \omega_p t \leqslant \frac{\pi}{2} + \theta_c$$

$$= -1 \text{ for } \frac{\pi}{2} + \theta_c \leqslant \omega_p t \leqslant \frac{3\pi}{2}$$

The waveforms of the two switching functions $s_1(t)$ and $s_2(t)$ are shown in Figure 4.7.

The equivalent circuit of the lattice mixer using the bisection theorem is shown in Figure 4.8(a). Taking into account the 180° phase difference of the local oscillator current in the two pairs of diodes, the time-varying resistances can now be expressed in the form,

$$r_+(t) = \frac{r_b}{1 + X(t) + X(t) \ s_1(t)} \qquad 4.10(a)$$

and

$$r_-(t) = \frac{r_b}{1 - X(t) + X(t) \ s_2(t)} \qquad 4.10(b)$$

where $X(t)$ is the normalised local-oscillator current-drive and r_b is the slope resistance of the diode at the origin.

The effective diode capacitance C_e at the i.f. port of the mixer can be incorporated in the parallel tuned circuit, in the case of the H mixer and the equivalent circuit of the lattice mixer reduces from that shown in Figure 4.8(a) to that shown in Figure 4.8(b). The overall general circuit matrix $[a]$ for the circuit shown in Figure 4.8(b) is,

$$[a] = [a_1][a_2][a_3]$$ 4.11(a)

where

$$[a_1] = \begin{bmatrix} 1 & , & r_s & , \\ j\omega C_e, & 1 + j\omega r_s C_e, \end{bmatrix}$$ 4.11(b)

$[a_2]$ is the general circuit matrix of the diode lattice network i.e.

$$[a_2] = \begin{bmatrix} A , B \\ C , D \end{bmatrix}$$ 4.11(c)

and

$$[a_3] = \begin{bmatrix} 1, r_s \\ 0, 1 \end{bmatrix}$$ 4.11(d)

Substituting equation 4.11(b), 4.11(c), 4.11(d) into equation 4.11(a) results in the following expression for the general matrix $[a]$,

$$= \begin{bmatrix} A + Cr_s & , & B + r_s (D + A + C r_s) \\ j\omega C_e (A + r_s C) + C, & j\omega C_e \left[B + r_s (A + C + D) \right] + D + C_{r_s} \end{bmatrix}$$ 4.12(a)

If the cut-off frequency ω_c of the diode is defined as

$$\omega_c = {}^{1}/C_e r_s$$

then equation 4.12(a) becomes,

$$\begin{bmatrix} A + Cr_s & , & B + r_s \left(A + D + Cr_s \right), \\ \dfrac{A}{r_s} j(\omega/\omega_c) & j \left(\dfrac{\omega}{\omega_c}\right) \dfrac{1}{r_s} \left[B + r_s (B + D + C_s) \right] \\ + & + \\ C \left(1 + j \omega/\omega_c \right), & D + C_{r_s} \end{bmatrix}$$ 4.12(b)

Provided $\dfrac{\omega}{\omega_c} \ll 1$ equation 4.12(b) becomes

$$\left[a \right] = \begin{bmatrix} A + Cr_s & , & B + r_s \ (A + D + r_s \ C) \\ \\ C & , & D + C_{r_s} \end{bmatrix}$$

4.13

and the effect of the diode capacitance C_e on the small-signal

analysis can be neglected.

Neglecting the effect of the effective diode capacitance C_e on

the small-signal analysis, the general matrix equation describing

an H mixer is shown below,

$$\begin{bmatrix} V_1 \\ \\ I_2 \end{bmatrix} = \begin{bmatrix} \sum\limits_{n \text{ even}} a_n \ \cos n\omega_p t \ , & \sum\limits_{n \text{ odd}} b_n \ \cos n\omega_p t \\ \\ -\sum\limits_{n \text{ odd}} b_n \ \cos n\omega_p t \ , & \sum\limits_{n \text{ odd}} c_n \ \cos n\omega_p t \end{bmatrix} \begin{bmatrix} I_1 \\ \\ V_2 \end{bmatrix}$$

4.14(a)

where

$$\sum_n a_n \ \cos n\omega_p t = \dfrac{2\left(r_s + r_+(t) \right)\left(r_s + r_-(t) \right)}{2r_s + r_+(t) + r_-(t)}$$

4.14(b)

$$\sum_n b_n \ \cos n\omega_p t = \dfrac{r_-(t) - r_+(t)}{2r_s + r_+(t) + r_-(t)}$$

4.14(c)

and

$$\sum_n c_n \ \cos n\omega_p t = \dfrac{2}{2r_s + r_+(t) + r_-(t)}$$

4.14(d)

Using equations 4.10(a) and 4.10(b) it can be shown that,

$$r_+(t) + r_-(t) = \dfrac{r_b \ (2 + X(t) \ [s_1(t) + s_2(t)])}{1 + X(t)\left(s_1(t) + s_2(t) \right) + X(t)^2 \left(s_1(t)s_2(t) + s_2(t) - s_1(t) - 1 \right)}$$

4.15(a)

$$r_-(t) - r_+(t) = \dfrac{r_b \ X(t)\left(2 + s_1(t) - s_2(t) \right)}{1 + X(t)\left(s_1(t) + s_2(t) \right) + X(t)^2 \left(s_1(t)s_2(t) + s_2(t) - s_1(t) - 1 \right)}$$

4.15(b)

and

$$r_-(t)\, r_+(t) = \frac{r_b^2}{1 + X(t)\left(s_1(t) + s_2(t)\right) + X(t)^2\left(s_1(t)s_2(t) + s_2(t) - s_1(t) - 1\right)}$$

4.15(c)

The various combinations of the two switching functions $s_1(t)$ and $s_2(t)$ used in the above equations are shown in Figure 4.9 where it can be seen that, over a complete cycle of the local oscillator current drive,

$$s_2(t) - s_1(t) + s_1(t)\, s_2(t) - 1 = 0$$

4.16

Substituting equations 4.16, 4.15(a), 4.15(b) and 4.15(c) into equations 4.14(a), 4.14(b), 4.14(c) and provided that $r_b \gg r_s$ then,

$$\Sigma a_n \cos n\omega_p t \simeq 2r_s + \frac{2r_b}{2 + X(t)\left(s_1(t) + s_2(t)\right)}$$

4.17(a)

$$\Sigma b_n \cos n\omega_p t \simeq \frac{X(t)\left(2 + s_1(t) - s_2(t)\right)}{2 + X(t)\left(s_1(t) + s_2(t)\right)}$$

4.17(b)

$$\Sigma c_n \cos n\omega_p t \simeq \frac{2}{r_b}\left[1 - \frac{1}{2 + X(t)\left(s_1(t) + s_2(t)\right)}\right]$$

4.17(c)

It is interesting to note that if the effect of diode capacitance C_e on the diode current waveform is neglected, then $s_1(t) = s_2(t)$ and equations 4.17(a), 4.17(b) and 4.17(c) are given by the matrix equation 3.37 derived in Chapter III.

Substituting equations 4.17(a), 4.17(b) and 4.17(c) into the matrix equation 4.14(a) and on equating components of the same frequency, the coefficients of the H matrix can be expressed in the form,

$$h_{11} = 2r_s + \frac{r_b}{\pi}\int_{-\pi/2}^{3\pi/2} \frac{d(\omega_p t)}{2 + X\left(s_1(t) + s_2(t)\right)\cos \omega_p t}$$

4.18(a)

$$h_{12} = \frac{X}{2\pi} \int_{-\pi/2}^{3\pi/2} \frac{\left(2 + s_1(t) - s_2(t)\right) \cos \omega_p t}{2 + X\left(s_1(t) + s_2(t)\right) \cos \omega_p t} \, d \, (\omega_p t) \qquad 4.18(b)$$

$$h_{22} = \frac{2}{r_b} \left(1 - 2\pi \int_{-\pi/2}^{3\pi/2} \frac{d(\omega_p t)}{2 + X\left(s_1(t) + s_2(t)\right) \cos \omega_p t} \right) \qquad 4.18(c)$$

$$h_{13} = \frac{r_b}{2} \int_{-\pi/2}^{3\pi/2} \frac{\cos (2\omega_p t)}{2 + X\left(s_1(t) + s_2(t)\right) \cos \omega_p t} \, d(\omega_p t) \qquad 4.18(d)$$

The above integrals containing the two switching functions $s_1(t)$ and $s_2(t)$ can be evaluated by carefully choosing the limits of integration. Figure 4.9 shows that;

in the range $-\pi/2$ to $-\frac{\pi}{2} + \theta_c$ $\quad s_1(t) + s_2(t) = 0$

in the range $-\frac{\pi}{2} + \theta_c$ to $\pi/2$ $\quad s_1(t) + s_2(t) = 2$

in the range $\frac{\pi}{2}$ to $\frac{\pi}{2} + \theta_c$ $\quad s_1(t) + s_2(t) = 0$

in the range $\frac{\pi}{2} + \theta_c$ to $\frac{3\pi}{2}$ $\quad s_1(t) + s_2(t) = -2$

Solving the above integrals the following expressions for the coefficients of the H matrix are obtained:-

$$h_{11} = 2r_s + \frac{r_b}{\pi} \left(\theta_c + \frac{U}{X} \right) \qquad 4.19(a)$$

$$h_{12} = \frac{1}{\pi} \left(1 + \cos \theta_c - \frac{1}{X} \left(\pi - \theta_c \right) + \frac{U}{X^2} \right) \qquad 4.19(b)$$

$$h_{22} = \frac{2}{r_b} \left(1 - \frac{\theta_c}{\pi} + \frac{U}{\pi X} \right) \qquad 4.19(c)$$

$$h_{13} = \frac{r_b}{2\pi} \left[-\sin 2\theta_c + \frac{4}{X} \left(1 + \cos \theta_c \right) - \frac{4}{X^2} \left(\pi - \theta_c \right) \right.$$

$$\left. + \frac{2}{X} \left(\frac{2}{X^2} - 1 \right) U \right] \qquad 4.19(d)$$

where

$$U = \log_e \left(\frac{4X^2}{1 + 2X \tan (\theta_c/2)} \right)$$
4.19(e)

It is interesting to note that if the effect of the diode effective capacitance C_e on the diode current waveforms is neglected i.e. $\theta_c \rightarrow 0$, then,

$$h_{11} \simeq 2r_s + \frac{2r_b}{\pi X} \log_e 2X$$
4.20(a)

$$h_{12} \simeq 2/\pi$$
4.20(b)

$$h_{13} \simeq \frac{r_b}{X} \left(4 - \frac{2}{X} \log_e 2X \right)$$
4.20(c)

$$h_{22} \simeq 2/r_b$$
4.20(d)

The above equations correspond to those derived for the resistive H mixer in Chapter III. Finally, for a small but finite angle of truncation, θ_c, the coefficients of the H mixer reduce to,

$$h_{11} \simeq 2r_s + r_b \theta_c/\pi$$
4.21(a)

$$h_{12} \simeq 2/\pi$$
4.21(b)

$$h_{13} \simeq - \frac{r_b}{2\pi} \sin 2\theta_c$$
4.21(c)

$$h_{22} \simeq 2/r_b$$
4.21(d)

It is shown in this section how the angle of truncation θ_c due to the diode capacitance C_e affects the H parameters and the performance of the H mixer is examined in detail in the following section.

4.4 The Performance of the H Lattice Mixers with Capacitance

The effect of the diode capacitance on the performance of the Lattice H mixers having different image terminations can now be deduced using the general results derived in Chapter II and equations 4.21(a), 4.21(b), 4.21(c) and 4.21(d).

The parameter $'K_o'$ is given by

$$K_o = \frac{-h_{12}^2}{h_{11}h_{12}} \simeq \frac{-2}{\pi\theta_c} \qquad \text{4.22(a)}$$

while the parameter 'a' is

$$a = \frac{h_{13}}{h_{11}} \simeq - \frac{\sin 2\theta_c}{2\theta_c} \qquad \text{4.22(b)}$$

For small angle of truncation

$$a \simeq - 1 + \frac{2}{3}\theta_c^2 \qquad \text{4.22(c)}$$

For an H lattice mixer with image open-circuit the optimum terminations at the r.f. and i.f. ports and the resulting conversion loss are,

$$R_{s_{opt}} = h_{11}\left(1 - K_o\right)^{\frac{1}{2}} \simeq \frac{r_b\theta_c}{\pi}\left(1 + \frac{2}{\pi\theta_c}\right)^{\frac{1}{2}} \qquad \text{4.23(a)}$$

$$G_{L_{opt}} = h_{22}\left(1 - K_o\right)^{\frac{1}{2}} \simeq \frac{2}{r_b}\left(1 + \frac{2}{\pi\theta_c}\right)^{\frac{1}{2}} \qquad \text{4.23(b)}$$

$$L_{3_{opt}} = \frac{1 + \left(1 - K_o\right)^{\frac{1}{2}}}{-1 + \left(1 - K_o\right)^{\frac{1}{2}}} \simeq \frac{1 + \left(1 + 2/\pi\theta_c\right)^{\frac{1}{2}}}{-1 + \left(1 + 2/\pi\theta_c\right)^{\frac{1}{2}}} \qquad \text{4.23(c)}$$

In the case of an H lattice mixer with image-short circuit the parameter K_s is given by:-

$$K_s = \left(\frac{K_o}{1 - K_o}\right)\left(\frac{1 - a}{1 + a}\right) \simeq \frac{-8\theta_c}{\left(2 + \pi\theta_c\right)\left(2\theta_c - \sin 2\theta_c\right)} \qquad \text{4.24(a)}$$

For small angle of truncation,

$$K_s \simeq \frac{-3}{\theta_c^2}$$ 4.24(b)

The required terminations at the r.f. and i.f. ports and the resulting conversion loss are,

$$R_{s_{opt}} = h_{11}\left(1 - a^2\right)\left(1 - K_s\right)^{\frac{1}{2}} \simeq \frac{4r_b \theta_c^3}{3\pi}\left(1 + \frac{3}{\theta_c^2}\right)^{\frac{1}{2}}$$ 4.25(a)

$$G_{L_{opt}} = h_{22}\left(1 + K_o\right)\left(1 - K_s\right)^{\frac{1}{2}} \simeq \frac{2}{r_b}\left(1 + \frac{2}{\pi\theta_c}\right)\left(1 + \frac{3}{\theta_c^2}\right)^{\frac{1}{2}}$$ 4.25(b)

$$L_{3_{opt}} = \frac{1 + \left(1 - K_s\right)^{\frac{1}{2}}}{-1 + \left(1 - K_s\right)^{\frac{1}{2}}} \simeq \frac{1 + \left(1 + \frac{3}{\theta_c^2}\right)^{\frac{1}{2}}}{-1 + \left(1 + \frac{3}{\theta_c^2}\right)^{\frac{1}{2}}}$$ 4.25(c)

Finally for a broad-band mixer the parameter K_B is given by,

$$K_B = \frac{2K_o}{1 + a} \simeq \frac{8}{\pi\left(2\theta_c - \sin 2\theta_c\right)}$$ 4.26(a)

For small angle of truncation,

$$K_B \simeq \frac{-6}{\pi\theta_c^3}$$ 4.26(b)

The required terminations at the r.f. and i.f. ports and the resulting conversion loss are,

$$R_{s_{opt}} = h_{11}\left(1 + a\right)\left(1 - K_B\right)^{\frac{1}{2}} \simeq \frac{2r_b}{3}\theta_c^3\left(1 + \frac{6}{\pi\theta_c^3}\right)^{\frac{1}{2}}$$ 4.27(a)

$$G_{L_{opt}} = h_{22}\left(1 - K_B\right)^{\frac{1}{2}} \simeq \frac{2}{r_b}\left(1 + \frac{6}{\pi\theta_c^3}\right)^{\frac{1}{2}}$$ 4.27(b)

$$L_{2_{opt}} = \frac{2\left(1 + \left[1 - K_B\right]^{\frac{1}{2}}\right)}{-1 + \left[1 - K_B\right]^{\frac{1}{2}}} \simeq \frac{2\left(1 + \left[1 + \frac{6}{\pi\theta_c^3}\right]^{\frac{1}{2}}\right)}{-1 + \left[1 + \frac{6}{\pi\theta_c^3}\right]^{\frac{1}{2}}}$$ 4.27(c)

Figures 4.10 to 4.13 show how the conversion loss and the required terminations at the r.f. and i.f. ports vary as a function of local oscillator drive over a typical range of diode effective capacitance (.01 pF to 3.5 pF), for the three types of lattice mixers. It can be seen that the main effects of the diode effective capacitance is to considerably increase the conversion loss for low local oscillator drive and increase in magnitude the required terminations for the three types of lattice H mixers.

To minimise the effect of the diode capacitive parasitics on the performance of lattice mixers, it is necessary to reduce the angle of truncation θ_c and hence reduce the parameter ε (see equation 4.6). Equation 4.8 indicates that the parameter ε is reduced if the local oscillator frequency is lowered and/or the local oscillator drive is increased. However, the local oscillator frequency is normally fixed depending on the application of the mixer and there is a practical limit to how much power can be obtained from the local oscillator.

An alternative method of reducing the angle of truncation of the diode current is to reduce the output resistance of the local oscillator and allow the effective diode capacitance to discharge during the switching action of the four diodes. This reduction of the angle of truncation by lowering the output impedance of the local oscillator was practically verified for the lattice mixer. In practice, a compromise must be made between the need to have a large output impedance of the local oscillator to reduce the noise figure of the mixer as suggested by Howson and Stracca and the need to lower the output impedance of the local oscillator so that the angle of truncation of the diode current is minimised.

4.5 Conclusion

The influence of diode reactance on the noise figure and conversion

loss for single diode 'Y' and 'Z' mixers has been investigated by Gunes,

Howson, and Glover [23, 24]. The results obtained show the mixer's

rank in order of preference for low noise figure and in particular

indicate that the effect of diode reactive components deteriorates the

performance of 'Z' mixers,especially at high frequencies.

A number of authors [18, 19] have analysed the performance of a

lattice mixer where the effects of the diode reactive parasitics have

been neglected. The main conclusion reached is that the current driven

'H' and 'G' lattice mixers produce the best noise figure if the internal

resistance is large. In this chapter, the performance of a current

driven lattice 'H' mixer has been obtained where the effect of the

diode capacitive parasitics has been included. The results obtained

are generally in agreement with the computer predicted performance

obtained by Rustom and Howson [25].

The dominant effect of the diode capacitive parasitics is to produce

a truncated half-wave rectified diode current. The angle of truncation

is a function of the effective diode capacitance, diode incremental

resistance at the origin and current drive but is independent of the

series resistance of the diode. As a result of the angle of truncation,

a significant number of odd harmonics of the local oscillator frequency

are introduced in the frequency spectrum of the diode current waveform.

Using the truncated half-wave rectified diode current, the

coefficients of the H matrix and the performance of three types of

lattice H mixers have been developed. This method of analysis has

not been discussed in any of the available literature. It is shown

that the main effect of the diode capacitance is to considerably

increase the required terminations at the r.f. and i.f. ports

necessary to obtain minimum conversion loss. Such high terminations cannot be realised in practice especially at high frequencies.

It is shown in this chapter that although the angle of truncation can be minimised by decreasing the local oscillator frequency and by increasing the local oscillator drive the most practical method, however, is to reduce the output impedance of the local oscillator. A compromise has therefore to be made between the need to produce a low noise figure and the need to reduce the effect of angle of truncation on the required terminations at the r.f. and i.f. ports of the lattice mixer. Again this point has not been covered in the literature dealing with the performance of lattice mixers.

4.6 References

1. Edwards, C.F., Frequency Conversion by means of a Non-linear Admittance, BSTJ, Nov. 1956, Vol. 35, pp. 1403-1416.

2. Messenger, G.C., McCoy, C.T., Theory and Operation of Crystal Diodes as Mixers, Proc IEEE 1957, pp. 1269-1283.

3. Becker, L., Ernst, R.L., Non-linear Admittance Mixers, RCA Review, Dec. 1964, Vol. 25, No. 4, pp. 662-691.

4. Engelbrecht, R.S., Parametric Energy Conversion by Non-linear Admittances, Proc. IRE 1962.

5. Yoginder, A., Moroney, W. J., Microwave Mixer and Detector Diodes, Proc. IEEE August 1971, Vol. 59, No. 8, pp. 1182-1290.

6. Liechti, C. A., Down-Convertors Using Schottky-barrier Diodes, IEEE Trans. on Electronc Devices, Nov. 1970, Vol. ED-17, pp. 975-983.

7. Dragone, C., Performance and Stability of Schottky-barrier Mixers, BSTJ, Dec, 1972, Vol. 51, No. 10, pp. 2169-2195.

8. Fleri, D. A., Cohen, L.D., Non-linear Analysis of Schotty-barrier Mixer Diode, IEEE Trans. NTT Jan. 1973, Vol. MTT 21, No. 1, pp. 39-43.

9. Egami, S., Non-linear, Linear Analysis and Computer-Aided Designs of Resistive Mixers, IEEE, Vol. MTT-22, March 1974, pp. 270-275.

10. Gwarek, W.K., Non-linear Analysis of Microwave Mixers, M. S. Thesis, M.I.T. Cambridge, Sept. 1974.

11. Kerr, A.R., A Technique for Determining the Local Oscillator Waveforms in a Microwave Mixer, IEEE. Vol. MTT-23, October 1975, pp. 828-831.

12. Siegel, P.H. and Kerr, A.R., A User Oriented Program for the Analysis of Microwave Mixers, and a Study of the Effects of the Series Inductance and Diode Capacitance on the Performance of some simpl Mixer Circuits, NASA Technical Memorandum No. 80324, July 1979.

13. Mania, L., Stracca, G.B., Effects of the Diode Junction Capacitance
    on the Conversion Loss of Microwave Mixers, IEEE Trans. on
    Communication Sept. 1974, Vol. COM 22.

14. Kulesza, B. L. J., General Theory of a Lattice Mixer, Proc. IEE
    July 1971, Vol. 118, No. 7, pp. 864-870.

15. Johnson, K.M., X-Band Integrated Circuit Mixer with Reactively
    Terminated Image, IEEE Trans. on MTT, July 1968, Vol. MTT-16,
    pp. 388-397.

16. Maiuzzo, M.A., Cameron, S.H., Response Coefficients of a Double-
    Balanced Diode Mixer, IEEE Trans. on Electromagnetic Compatability,
    No. 1979, Vol. EMC-21, No. 4, pp. 316-319.

17. Ogawa, H., Aikowa., Morita, K., K-Band Integrated Double-Balanced
    Mixer, IEEE Trans. on MTT, March 1980, Vol. MTT-28, No. 3, pp. 180-185.

18. Rustom, S., Howson, D.P., Mixer Noise Figure using an Improved
    Resistive Model, Int. J. Electronics 1976, Vol. 41, No. 2.

19. Stracca, G.B., Noise in Frequency Mixers using Non-linear Resistors,
    Alta Freq., 1979, No. 6.

20. Fei, F.S., Mattauch, R.J., High Frequency Resistive Mixer Diode
    Capacitance Analysis, Proc. IEEE 1976, 64, pp. 141-143.

21. Saleh, A. A. M. S., Theory of Resistive Mixers, MIT Press 1971.

22. Rafuse, R.P., Low Noise and Dynamic Range in Symmetric Mixer Circuits,
    Proc. of the 1st Bienniol Cornell Conf., 1967.

23. Gunes, F., Howson, D.P., Glover, K.J., Noise Figure Analysis for
    Y and Z Microwave Mixers, Sixth Colloq. Microwave Communications,
    Budapest, 1978.

24. Gunes, F., Howson, D.P., Glover, K.J., Influence of Mixer Diode
    Reactances on Noise Figure and Conversion Loss, Microwaves, Optics
    and Acoustics, Jan. 1979, Vol. 3, No. 1, pp. 34-36.

25. Rustom, S., Howson, D.P., The Conversion Loss of the Balanced H
    Mixer using a Diode Model with Nonlinear Resistance and Capacitance,
    Seventh Colloq, Microwave Communications, Budapest, 1982.
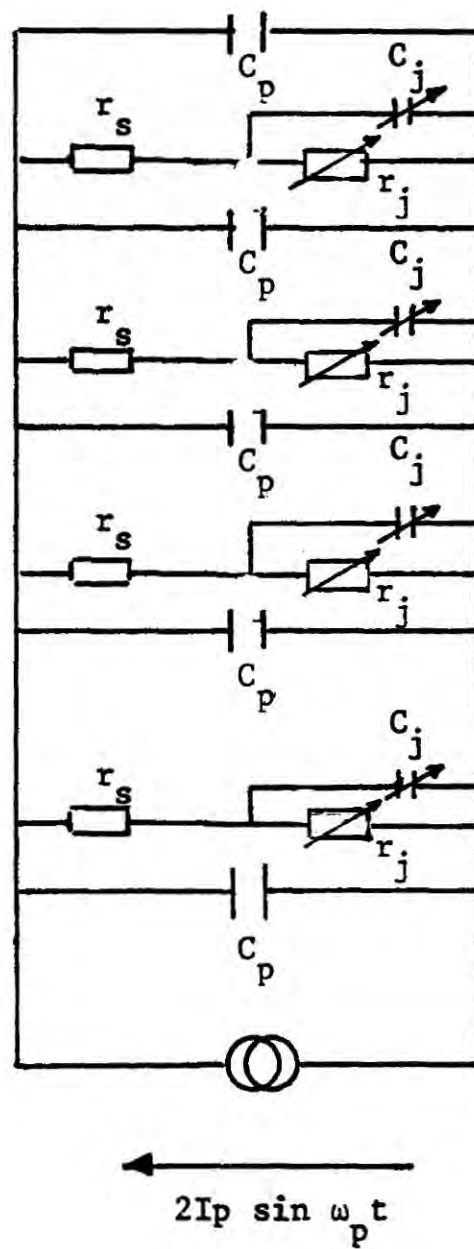
Figure 4.1 Diode circuit 'seen' by the local oscillator current drive
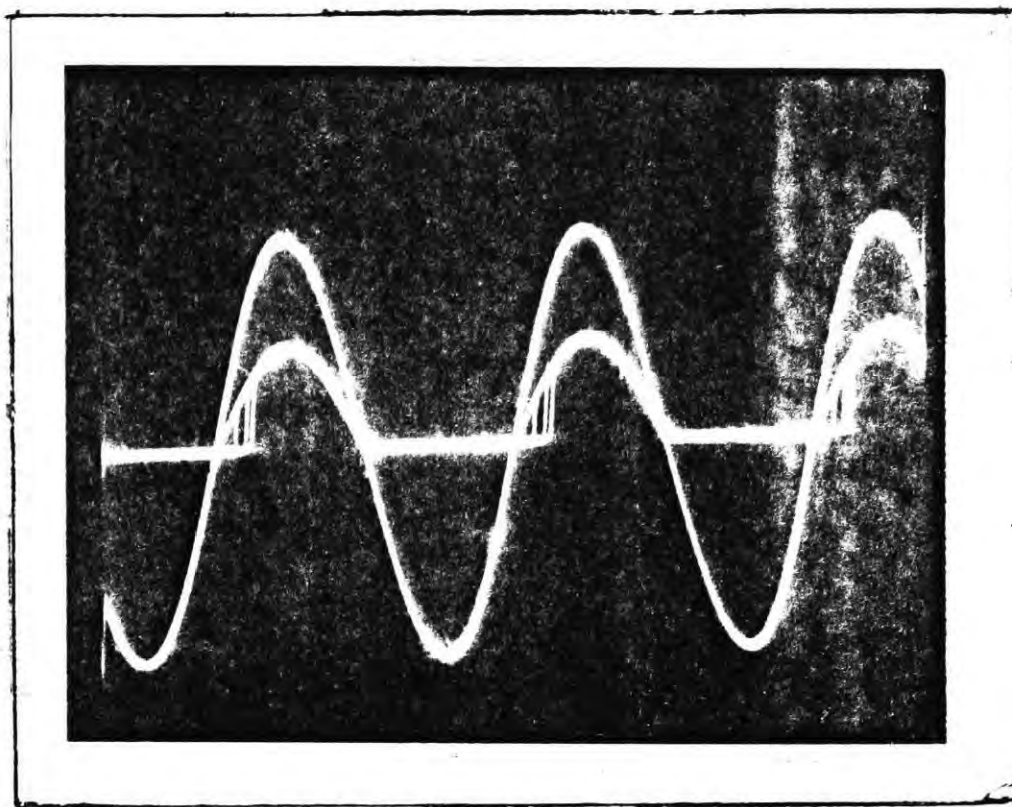
(a)
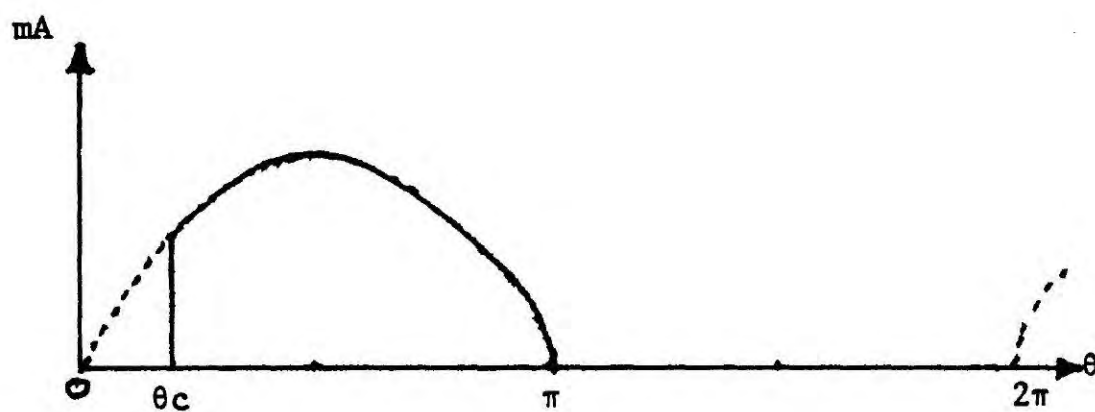
(b)

Figure 4.2 (a) Sinusoidal current drive and diode current waveform for a range of diode capacitance.

(b) Truncated half-wave rectified diode current where θc is the angle of truncation.
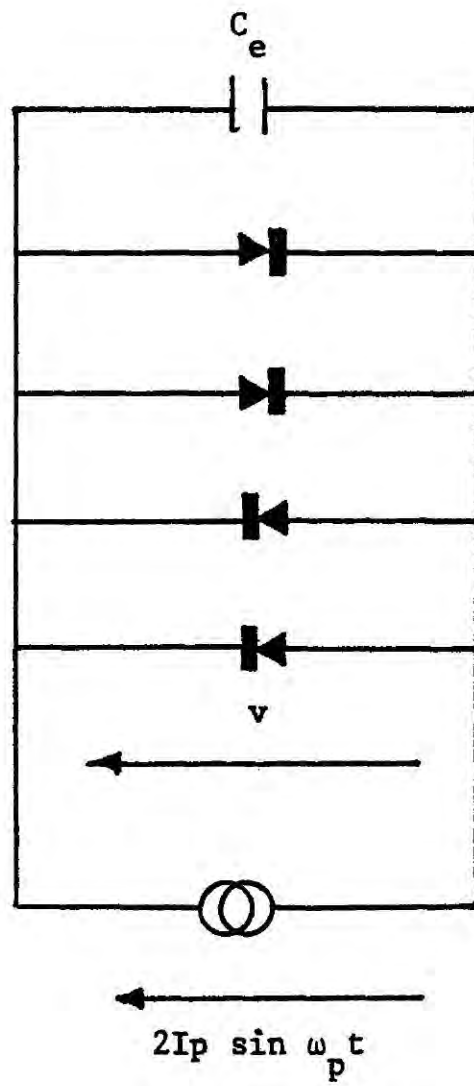
Figure 4.3 Effective diode circuit seen by the local oscillator
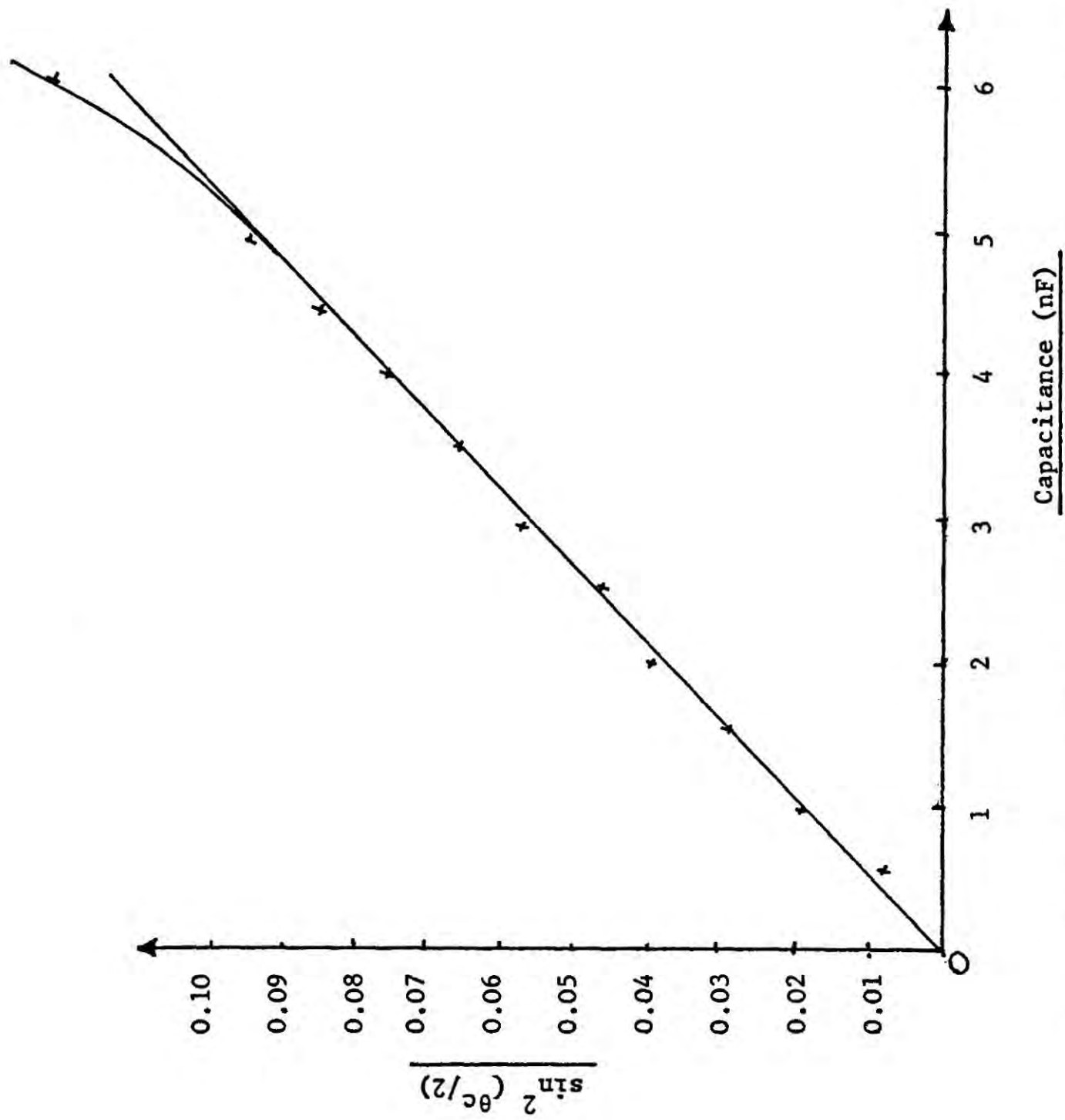
Figure 4.4 Theoretical and measured values of angle of truncation against diode capacitance C_e
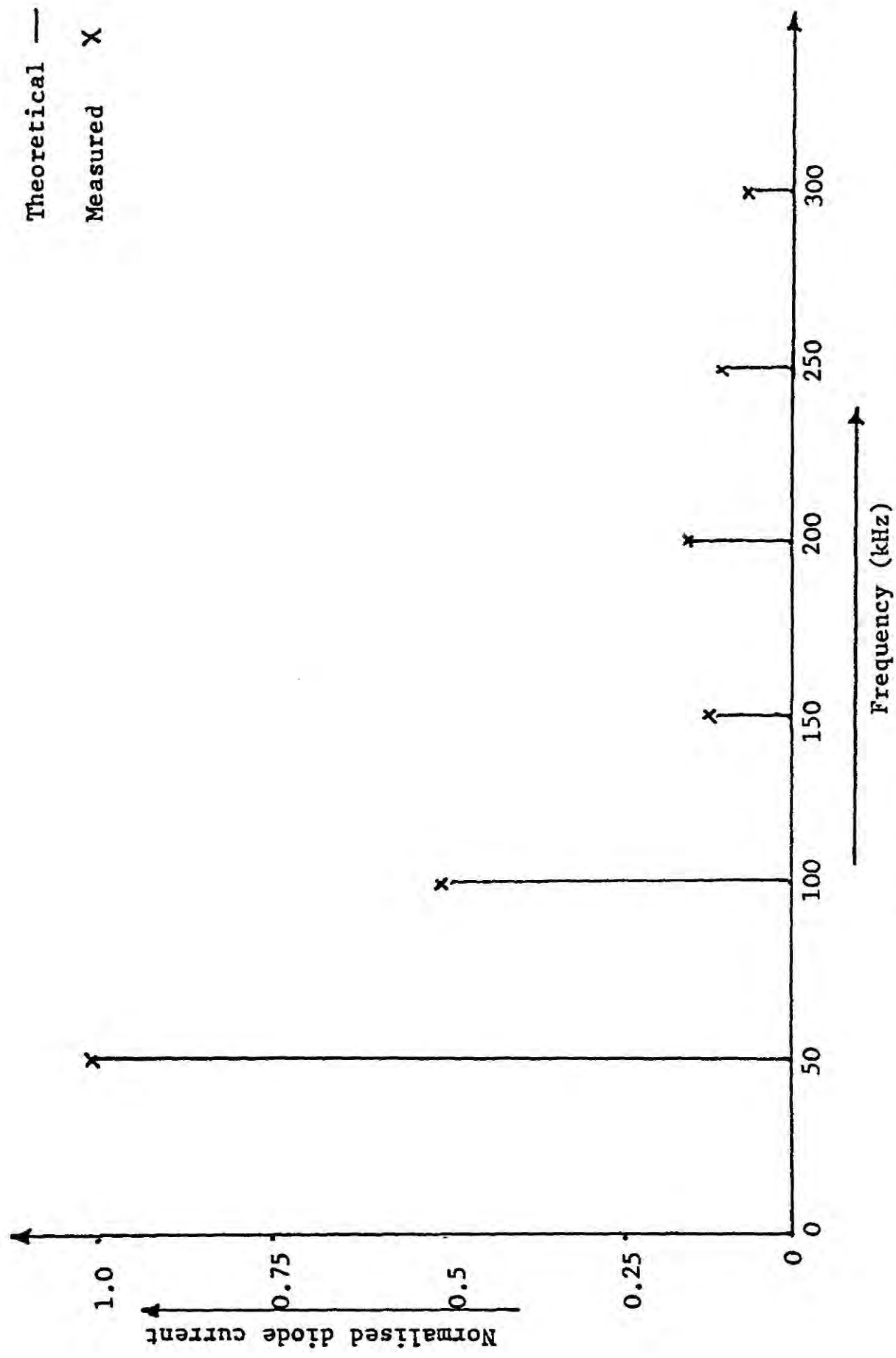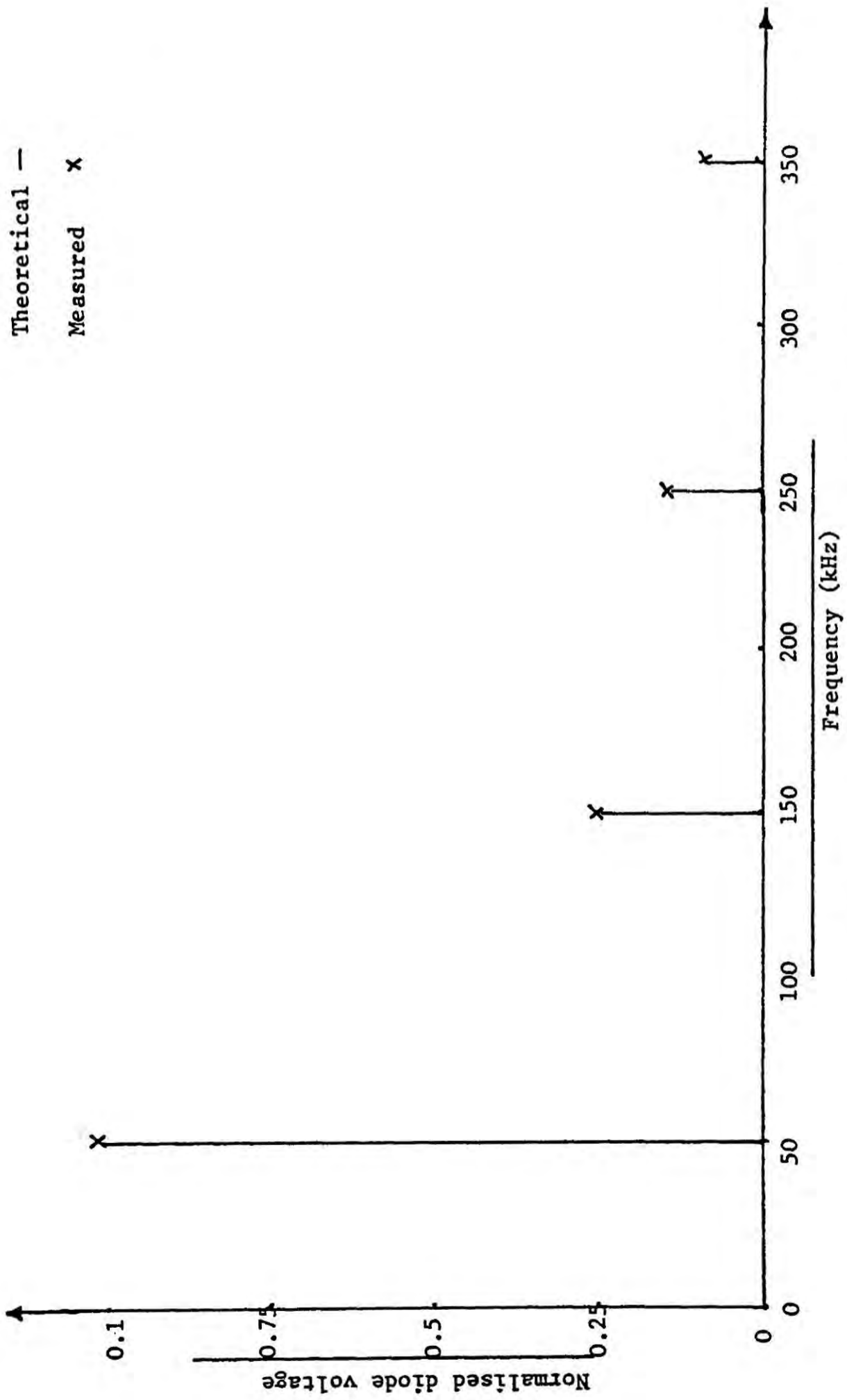
Figure 4.5 Frequency spectrum of the diode current

Figure 4.6 Frequency spectrum of the voltage waveform
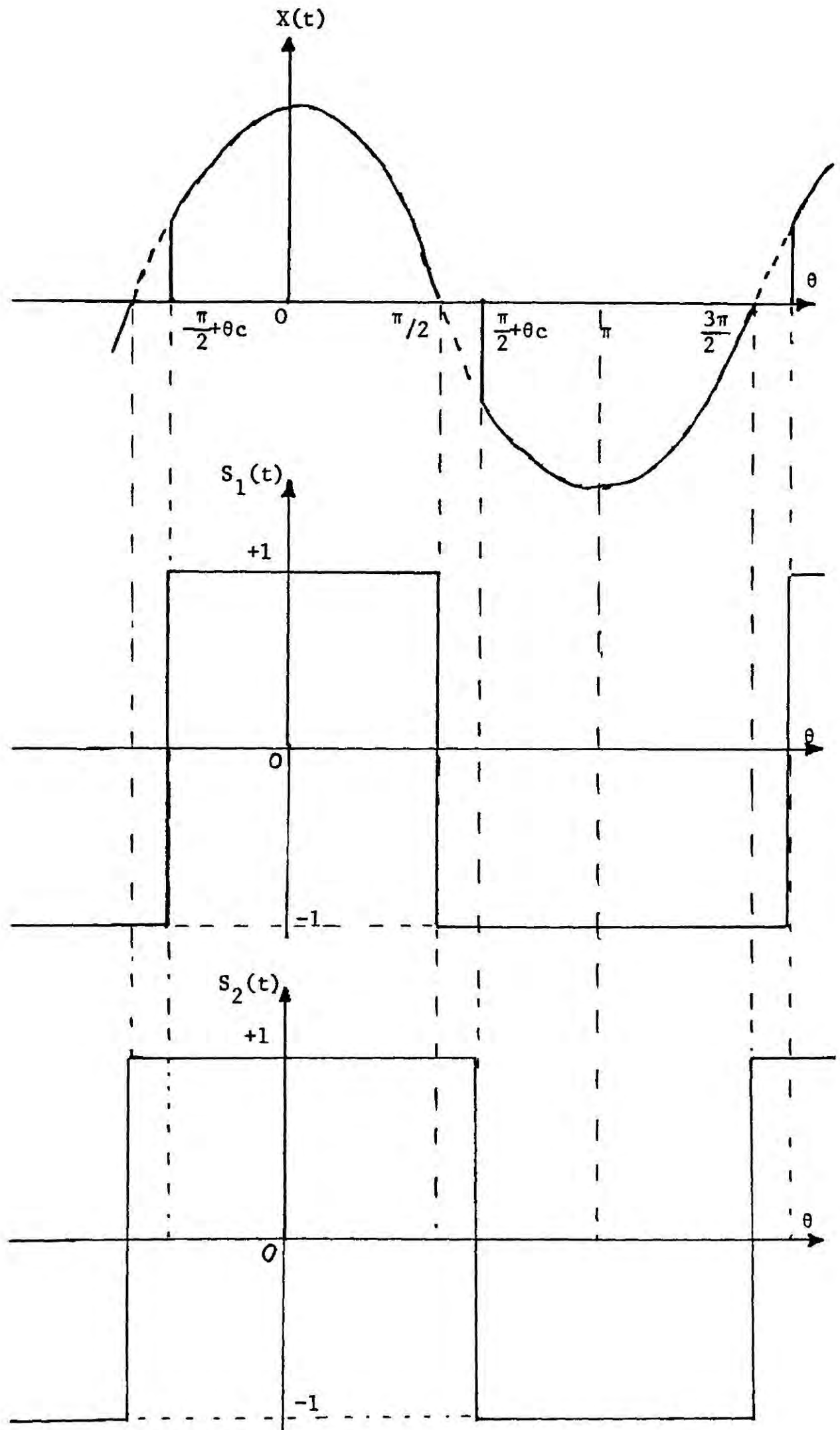
Figure 4.7 Waveforms of the two switching functions $S_1(t)$ and $S_2(t)$
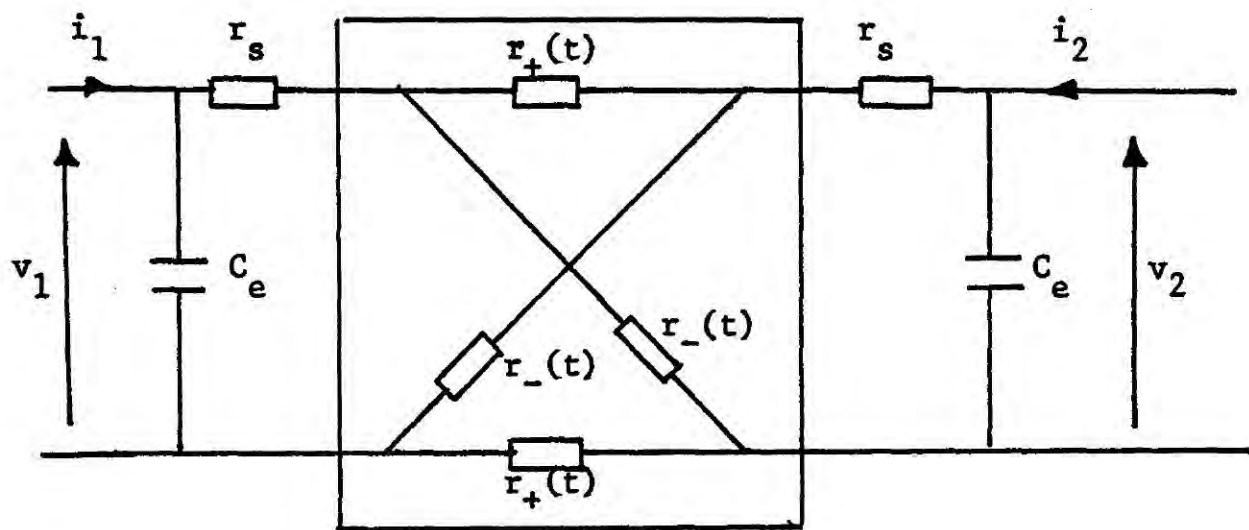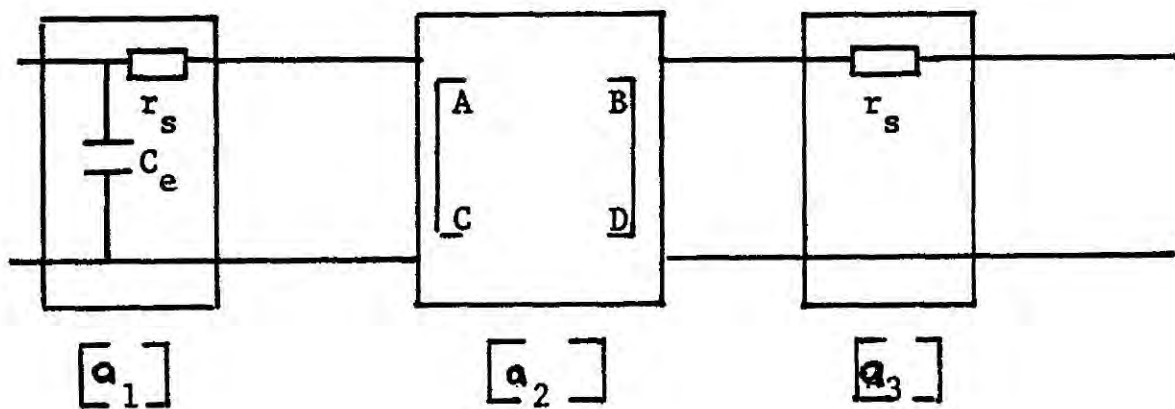
Figure 4.8   (a)   Equivalent circuit of the lattice mixer using the
bisection theorem.

(b)   Three two-port networks representing the lattice mixer.
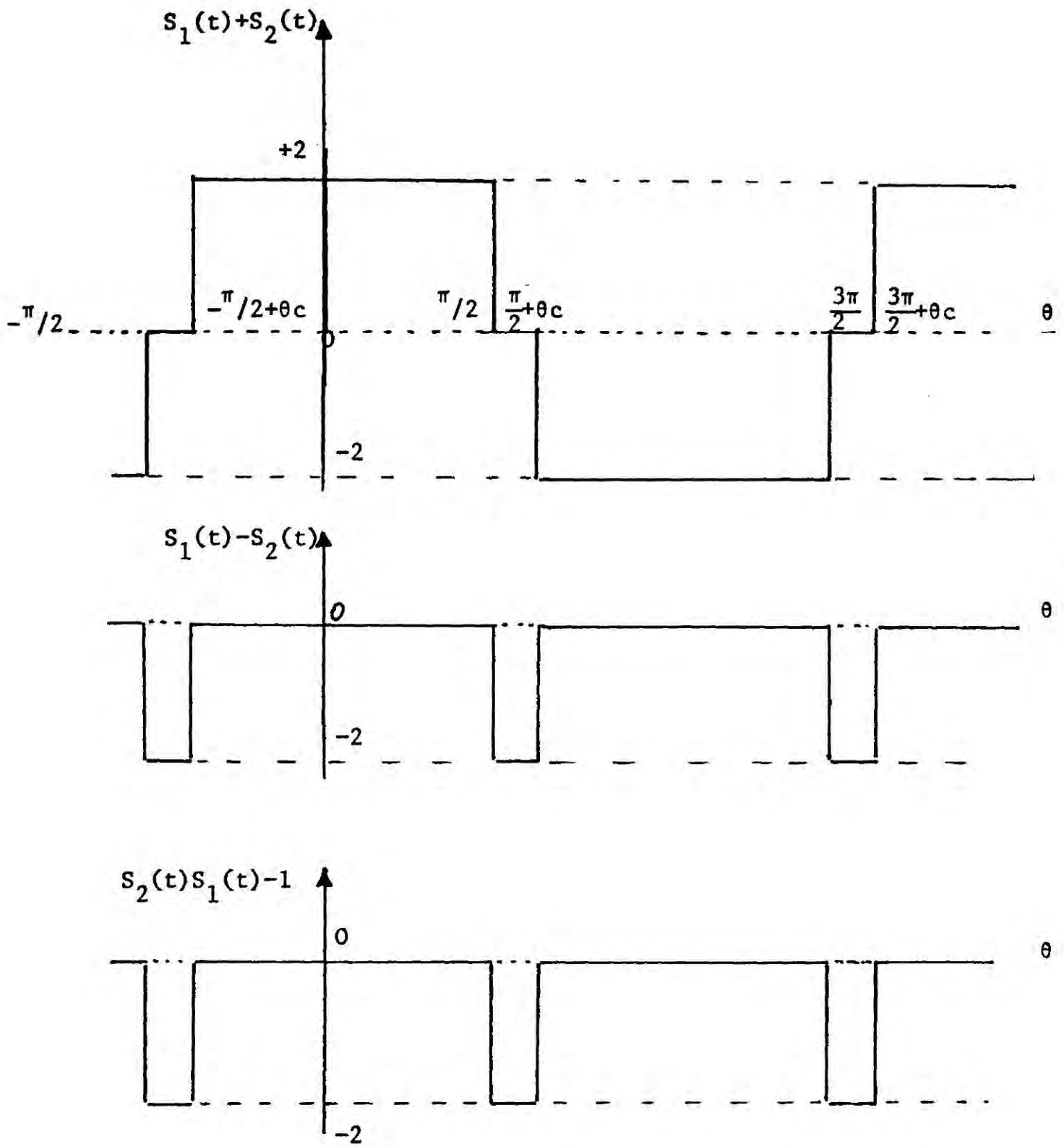
Figure 4.9 Waveforms of different combinations of the two switching functions $S_1(t)$ and $S_2(t)$
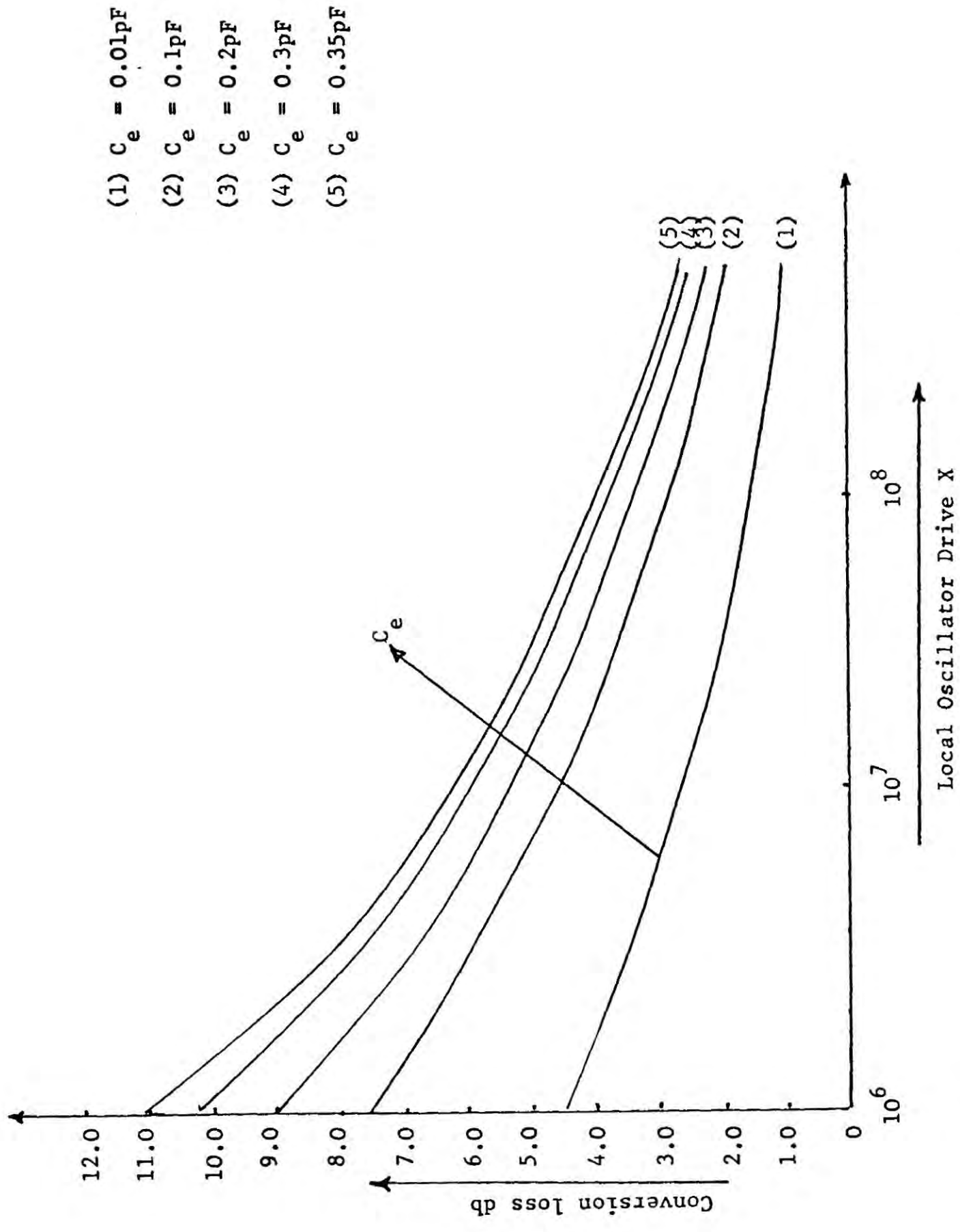
Figure 4.10 Computed conversion loss for an H lattice mixer with image open-circuit for C_e 0.01 – 0.35pF at 1.5525GHz

(1) $C_e = 0.01pF$
(2) $C_e = 0.1pF$
(3) $C_e = 0.2pF$
(4) $C_e = 0.3pF$
(5) $C_e = 0.35pF$

Local Oscillator Drive X

Conversion loss db

Figure 4.11   Computed conversion loss for an H lattice mixer with image short-circuit
for C_e 0.01 - 0.35pF at 1.5525GHz
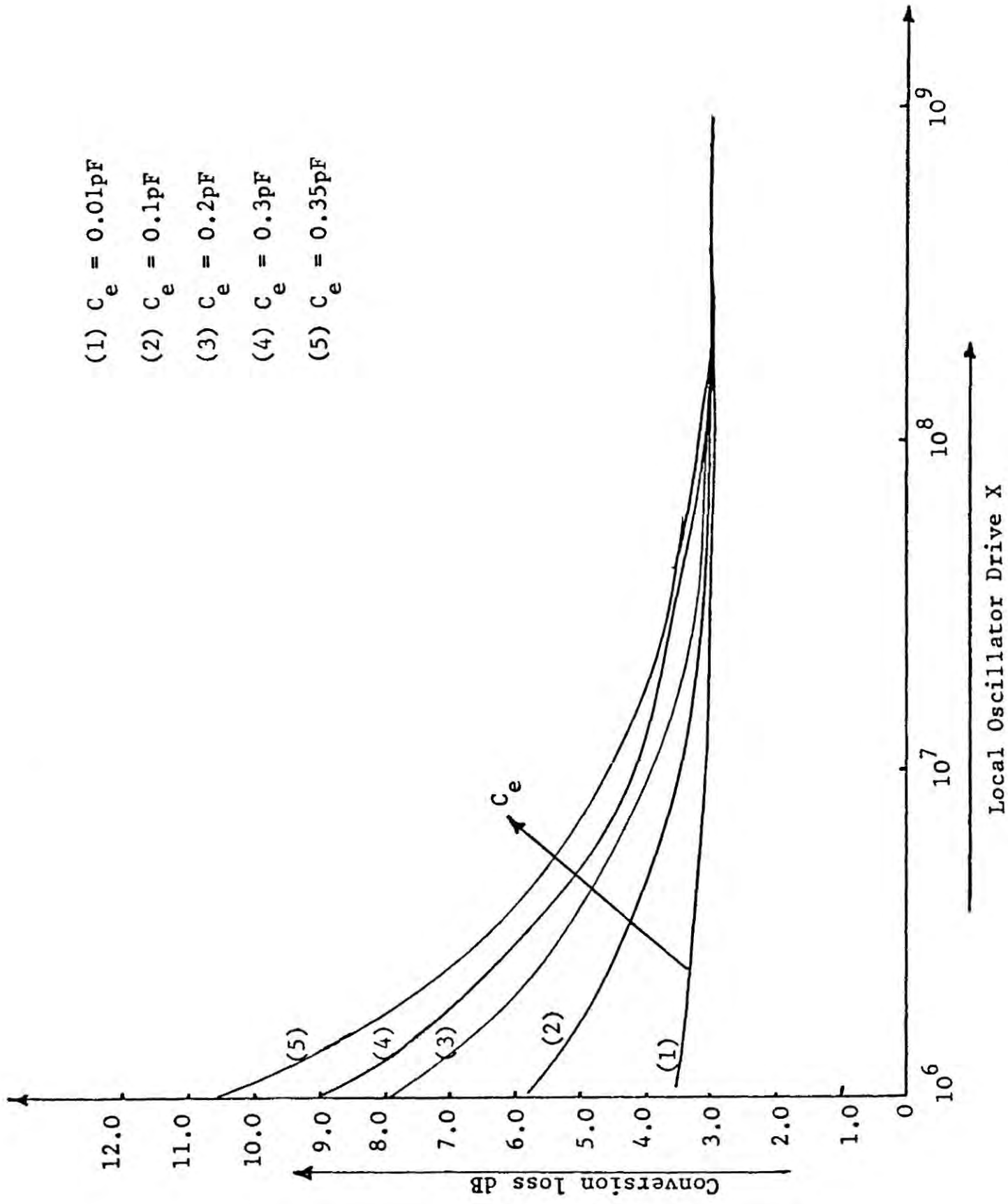
Figure 4.12 Computed conversion loss for an H lattice broad-band mixer for
C_a 0.01 – 0.35pF at 1.5525GHz

Figure 4.13 Computed values of optimum source resistance and load conductance for an H mixer with image open-circuit for C_e 0.01 - 0.35pF at 1.5525GHz
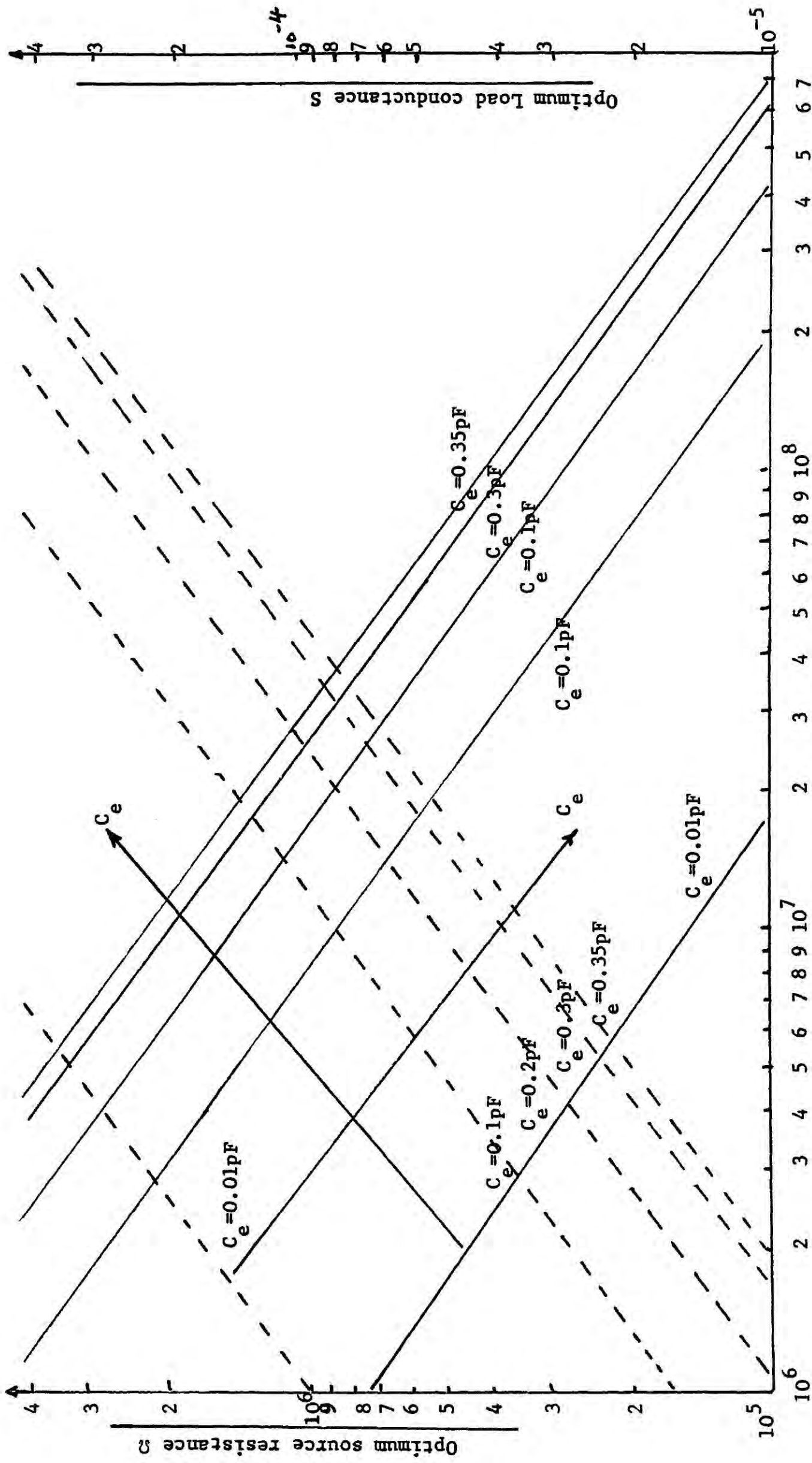
——————— Optimum source resistance

– – – – – – Optimum load conductance

(1) C_e = 0.01pF
(2) C_e = 0.1pF
(3) C_e = 0.2pF
(4) C_e = 0.3pF
(5) C_e = 0.35pF
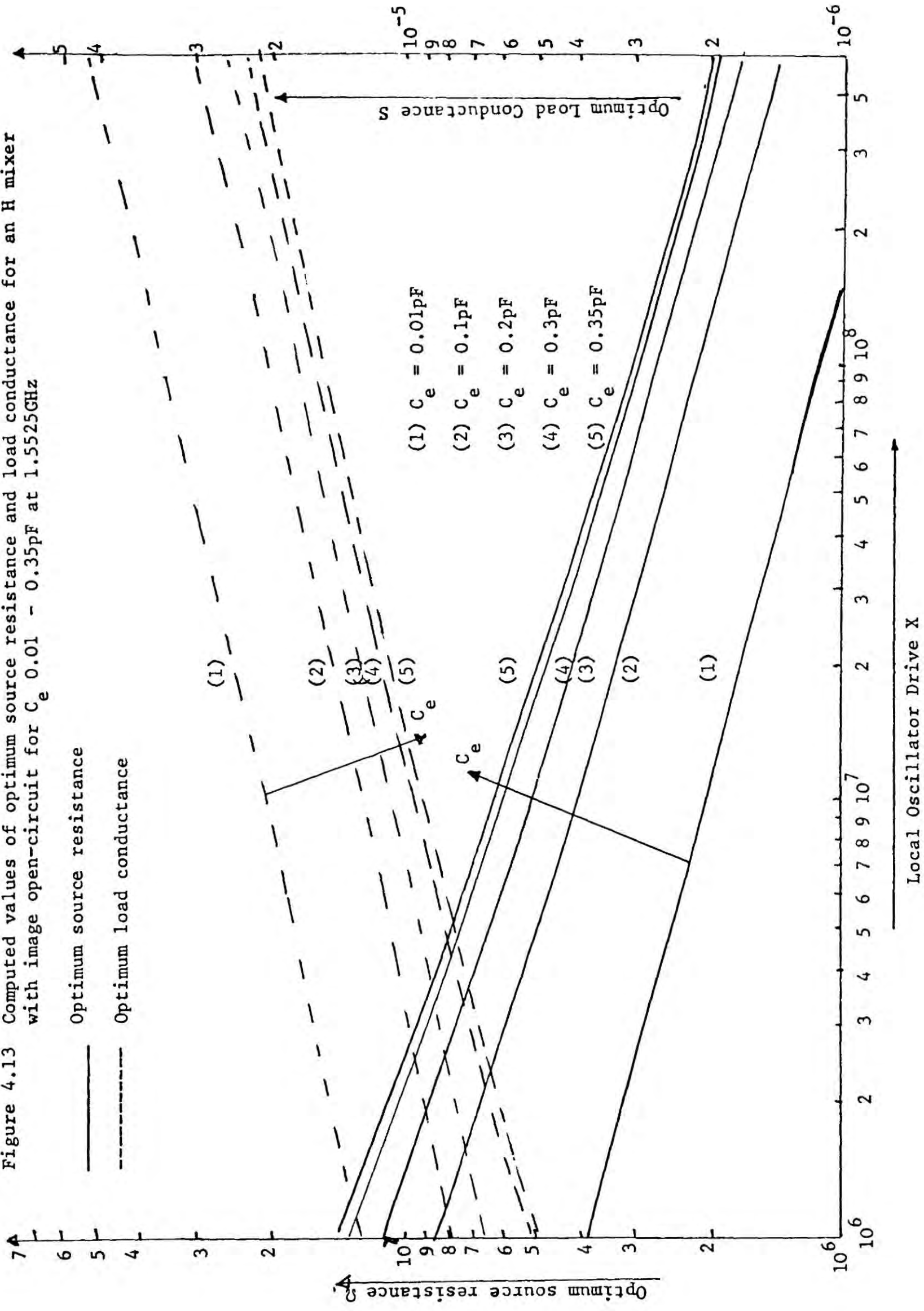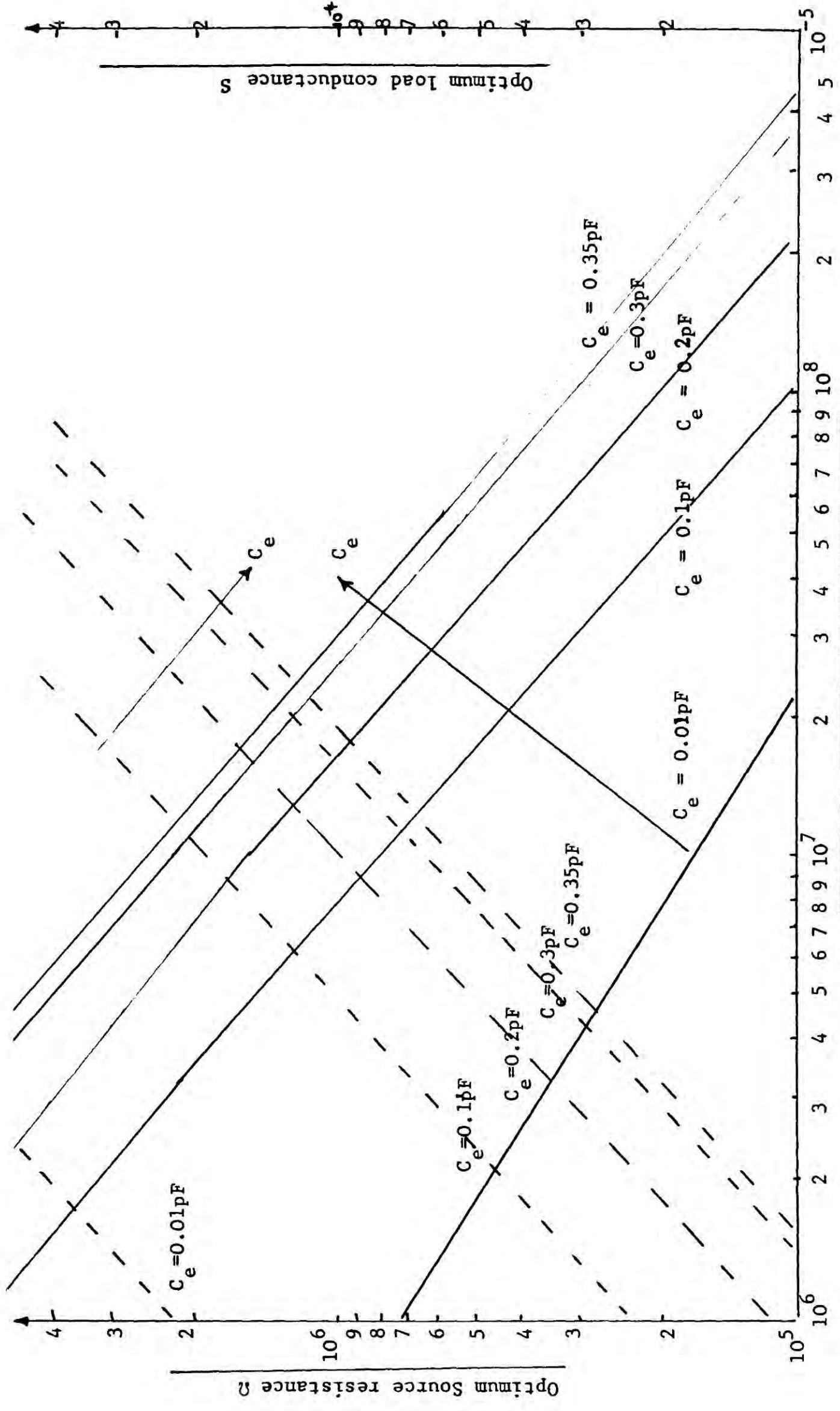
Figure 4.14 Computed values of optimum source resistance and load conductance for an H lattice mixer with image short-circuit for C_e 0.01 - 0.35pF at 1.5525GHz

Figure 4.15 Computed values of optimum source resistance and load conductance for a broad-band H mixer for C_e 0.01 – 0.35pF at 1.5525GHz.

CHAPTER V

Realization of Mixer Embedding Networks

5.1 Introduction

At high frequencies waveguides and coaxial lines have extensively been used in the realization of mixer embedding networks. However, because of the need for high precision engineering necessary in their manufacture, increasing use is being made instead of planar transmission lines. Such lines not only have the advantage they are cheaper to fabricate but also, they are dimensionally small so that compact micro-wave components can be obtained. The analysis and properties of planar transmission lines have been extensively covered in literature [1-8] and are briefly summarized in this chapter.

Coupled microstrip transmission lines constitute a fundamental building block of filters associated with image-rejection mixers. The properties of such lines have been considered by many authors [9-14] but the information is usually presented in graphical forms and only for particular values of relative permittivities of the substrates. To overcome this problem, it was decided to use an analytical solution to relate the dimensions of the coupled lines to the odd and even-mode impedances, for substrates of any relative permittivity. Narrow-band bandpass and band-stop filters were then designed and their performance experimentally examined.

The final part of this chapter is concerned with the realization of a tunable co-axial cavity which will ensure that the configuration of diodes in the lattice mixer is pumped by a sinusoidal current waveform.

5.2 Properties of Planar Microstrip Transmission Lines

Planar transmission lines are now extensively used in the design of components or wide-band circuit elements at high frequencies. Although there are different forms of planar transmission lines they all basically consist of metallic layers separated by dielectric substrate. The physical configurations of the three most common planar transmission lines are shown in Figure 5.1 representing microstrip line, stripline and slot-line. One reason why these lines are so frequently used in microwave integrated circuits (MIC's) is that the line parameters such as characteristic impedance and guide wavelength are conveniently defined in a single plane. This section is primarily concerned with reviewing the properties of microstrip lines as such lines are most easily fabricated using photo-lithographic techniques.

Depending on the operational frequency two analytical approaches are normally made to establish the relationship between the line parameters and the geometry of the microstrip line. If the line is used at the lower end of the microwave frequency range, it is assumed that the mode of propagation is almost TEM* and hence quasi-static methods [1, 2], including conformal transformation or numerical analysis, are applied. The alternative approach [3, 4] assumes that the propagation of waves is a mixture of coupled TEM* and TM** modes and hence demands a more rigorous analysis. This method of analysis is applicable if the micro-strip line is used at high microwave frequencies.

The analysis of propagation of waves along a microstrip line is complicated as parts of the fields are present in a dielectric and parts in air. Wheeler [1] introduced the concept of an effective dielectric constant ($\epsilon_{r_{eff}}$) and showed that it was made up of the dielectric constant in free space ($\epsilon_r = 1$) plus the product of the dielectric constant of the substrate in excess of free space ($\epsilon_r - 1$) and a filling factor q, i.e.,

* Transverse Electric Magnetic Mode

** Transverse Magnetic Mode

$$\varepsilon_{r_{eff}} = 1 + q \ (\varepsilon_r - 1) \qquad\qquad 5.1$$

The filling factor is primarily a function of the width of the conductor strip W, and the height of the substrate, H. Closed-form expressions for the effective dielectric constant have been derived by Wheeler and Schneider [5]. Based on this work but including the effect of the thickness, t, of the conductor strip the expressions for the effective dielectric constant are given below [6].

$$\varepsilon_{r_{eff}} = (\frac{\varepsilon_r + 1}{2}) + (\frac{\varepsilon_r - 1}{2}) \ (1 + 10 \ \frac{H}{W})^{-\frac{1}{2}} \qquad 5.2(a)$$

$$+ \ 0.48 \ (\frac{\varepsilon_r + 0.5}{1.5}) \ (\frac{t}{W})^{\frac{1}{2}}$$

if $\frac{W}{H} \leqslant 2$

and

$$\varepsilon_{r_{eff}} = (\frac{\varepsilon_r + 1}{2}) + (\frac{\varepsilon_r - 1}{2}) \ (1 + 10 \ \frac{W}{H})^{-\frac{1}{2}} \qquad 5.2(b)$$

if $\frac{W}{H} \geqslant 2$.

The closed-form expression for the characteristic impedance Z_{0_m} of the microstrip line is

$$Z_{0_m} = Z_0 / (\varepsilon_{r_{eff}})^{\frac{1}{2}} \qquad\qquad 5.3(a)$$

where

$$Z_0 = 60 \ \log_e (\frac{8H}{W} + \frac{W}{4H}) \quad \text{if} \ \frac{W}{H} \leqslant 1 \qquad 5.3(b)$$

or if $\frac{W}{H} \geqslant 1$

$$Z_0 = 120\pi / \left[\frac{W}{H} + 2.42 - 0.44 \ \frac{H}{W} + (1 - \frac{H}{W})^6\right] \qquad 5.3(c)$$

The microstrip guide wavelength λ_m is related to the free space wavelength λ by the following expression.

$$\lambda_m = \lambda / (\varepsilon_{r_{eff}})^{\frac{1}{2}} \qquad\qquad 5.4$$

Figure 5.2 shows how the characteristic impedance (Z_{0_m}) of a micro-strip line varies as a function of the ratio $\frac{W}{H}$ for the following laminates:

(i) Duroid (trade name) with ε_r = 10.5 and 2.35

(ii) Printed Circuit Board (P.C.B.) with $\varepsilon_r \simeq$ 4.8

The losses in lines are mainly due to the attenuation in the conductor and in the dielectric. The total attenuation constant α of the line is

$$\alpha = \alpha_c + \alpha_d \qquad\qquad 5.5$$

where α_c is the attenuation constant due to the losses in the conductor and α_d is the attenuation constant due to dielectric losses.

If it is assumed that the current distribution is uniform, then the attenuation constant of the conductor can be expressed in the form,

$$\alpha_c = R_s / Z_{0_m} W$$

R_s, the real component of the surface wave impedance, is

$$R_s = \left(\pi f \mu_0 / \sigma \right)^{\frac{1}{2}} \qquad\qquad 5.7$$

where f is the operating frequency and σ the conductivity of the metal strip.

The attenuation constant α_d of the substrate is given by [7],

$$\alpha_d = \frac{27.3}{\lambda_m} \frac{\varepsilon_r}{\varepsilon_{r_{eff}}} \tan \delta \qquad\qquad 5.8$$

where δ is the dielectric loss angle. Values of tan δ for different laminates are shown in Table 5.1 (P.C.B. indicates printed circuit board).

Material	Tan δ	Relative Permittivity ε_r
Duroid	0.006	10.5
Duroid	0.002	2.35
Alumina	0.0001	9.7
P.C.B.	0.025	4.8

It has been shown that with low-loss substrates almost all losses in a microstrip line are conductor losses [8]. Consequently, the conductor loss in a microstrip line is about half that of a stripline of the same width and same characteristic impedance. Thus for the same value of substrate height, H, and characteristic impedance 50Ω, the attenuation constants for the two types of lines are,

$$\alpha_c \lambda_m = 0.088 dB/wavelength - microstrip$$

$$\alpha_c \lambda_m = 0.176 dB/wavelength - stripline$$

5.3 Coupled Microstrip Lines

Coupled microstrip lines as illustrated in Figure 5.3(a) can be used to realize filters and directional couplers which form basic embedding networks in microwave mixers. The properties of such coupled lines are normally expressed in terms of odd and even-mode impedances. The odd-mode impedance, Z_{OO}, is defined as the characteristic impedance of one line when equal but opposite currents are flowing in the two lines. The even-mode impedance, Z_{OE}, is defined as the characteristic impedance of one line when equal currents flow in the same direction in the two li

Analysis of such lines has been suggested by Jones and Bolljahn who showed that the two coupled transmission lines in Figure 5.3(b) be describes in terms of the following four port impedance matrix equation

$$
\begin{bmatrix} V_1 \\ V_2 \\ V_3 \\ V_4 \end{bmatrix} = \begin{bmatrix} Z_{11} & Z_{12} & Z_{13} & Z_{14} \\ Z_{21} & Z_{22} & Z_{23} & Z_{24} \\ Z_{31} & Z_{32} & Z_{33} & Z_{34} \\ Z_{41} & Z_{42} & Z_{43} & Z_{44} \end{bmatrix} \begin{bmatrix} I_1 \\ I_2 \\ I_3 \\ I_4 \end{bmatrix} \quad 5.9(a)
$$

where

$$Z_{11} = Z_{22} = Z_{33} = Z_{44} = - j\ a \cot \theta$$

$$Z_{12} = Z_{21} = Z_{34} = Z_{43} = - j\ b \cot \theta$$

$$\quad 5.9(b)$$

$$Z_{13} = Z_{31} = Z_{42} = Z_{24} = - j\ b \csc \theta$$

$$Z_{14} = Z_{41} = Z_{23} = Z_{32} = - j\ a \csc \theta$$

and

$$a = (Z_{OE} + Z_{OO})/2$$

$$\quad 5.9(c)$$

$$b = (Z_{OE} - Z_{OO})/2$$

θ is the electrical length of the coupled lines and is defined as

$$\theta = \pi f / 2 f_o$$

where f_o is the frequency which causes the length of the coupled lines to be a quarter-wavelength.

In the design of microwave components such as directional couplers and filters [10-12] it is necessary to obtain a relationship between the coupled line parameters ($\frac{W}{H}$ and $\frac{S}{H}$ as shown in Figure 5.3(a)) and the odd and even-mode impedances. This relationship is normally established by making a number of simplifying assumptions: the lines have 'zero' thickness; conductor and dielectric losses are neglected; and the quasi-TEM mode of propagation is assumed. Bryant and Weiss [13] using Green's function have analysed coupled microstrip lines and presented their results in graphical form for substrates having different relative permittivities. Aktarzad [14] has produced a simple set of equations from which the parameters $\frac{W}{H}$ and $\frac{S}{H}$ can be obtained for given values of Z_{OO} and Z_{OE}. Based on the method of Aktarzad, a set of simple monograms have been obtained [15] which allows simultaneous solutions of $\frac{W}{H}$ and $\frac{S}{H}$ relating to the required values of Z_{OE} and Z_{OO}. The basic problem of using the above techniques is that the results are published in graphical form and only for set values of relative permittivities of the substrates. An alternative approach used here is based on the work of Zehentner [16] who applied MSTRIP computer programme [17] to derive a power series for Z_{OE} and Z_{OO} with respect to $\frac{W}{H}$ and $\frac{S}{H}$. The derived results, however, are valid only for values of ϵ_r in the range $8 \leqslant \epsilon_r \leqslant 12$. The characteristic impedance of a microstrip line is proportional to $(\epsilon_{r_{eff}})^{-\frac{1}{2}}$ [18] and therefore odd and even-mode impedances for two substrates having effective relative permittivities $\epsilon_{r_{eff1}}$ and $\epsilon_{r_{eff2}}$ are related by the following equation

$$\frac{Z_{0i_1}}{Z_{0i_2}} = \left[\frac{\varepsilon_{r_{eff\ 2}}}{\varepsilon_{r_{eff\ 1}}}\right]^{\frac{1}{2}} \qquad \qquad 5.11$$

where i represents 0 or E.

Based on the work of Zehentner and equation 5.11 a computer programme, given in appendix VI, was developed to determine the relationship between odd and even-mode impedances and the geometry of the coupled microstrip lines for substrates having any relative permittivity. Tables 5.2 and 5.3 show that the results obtained by this method and those available in the literature [19] are in close agreement.

Computer-predicted relations between odd and even-mode impedances and the parameters $\frac{W}{H}$ and $\frac{S}{H}$ are also shown in graphical form in Figures 5.4, 5.5 and 5.6 for the following laminates.

(i) Duroid with ε_r = 10.5 and ε_r = 2.35

(ii) P.C.B. with $\varepsilon_r \simeq 4.8$

Using either the computer programme or the results shown in graphical form microwave filters using coupled microstrip circuits can be designed.

$$\varepsilon_r = 9.6$$

Dimension		Bryant & Weiss		Method of Text	
$S_{/H}$	$W_{/H}$	Z_{OE}	Z_{OO}	Z_{OE}	Z_{OO}
	0.1	164.1	55.4	165.8	52.7
	0.5	96.2	34.5	96.5	34.0
0.1	1.0	66.5	27.8	66.7	28.2
	2.0	41.7	21.6	41.7	22.4
	0.1	156.0	66.1	155.3	64.5
	0.5	92.2	39.9	92.8	40.0
0.2	1.0	64.5	31.6	65.2	31.9
	2.0	41.0	23.7	41.3	24.5
	0.1	138.4	83.5	138.1	82.4
	0.5	84.5	49.7	85.0	50.1
0.5	1.0	60.5	38.1	61.0	38.5
	2.0	39.4	27.4	40.1	27.7
	0.1	126.0	96.6	125.1	95.44
	0.5	77.4	57.7	77.93	58.1
1.0	1.0	56.5	43.2	56.9	43.8
	2.0	37.6	30.1	37.9	30.7

TABLE 5.2

$$\varepsilon_r = 6$$

Dimension		Bryant & Weiss		Method of Text	
$S_{/H}$	$W_{/H}$	Z_{OE}	Z_{OO}	Z_{OE}	Z_{OO}
	0.2	160	66	159.1	64.7
	0.4	127	54	125.4	52.7
0.2	0.6	105	46.5	105.3	46.6
	1.0	81	39	80.6	39.5
	1.4	66	34	65.5	35.0
	2.0	51.5	29.5	51.2	30.3
	0.2	145	84.7	142.8	82.8
	0.4	115	66.5	114.2	66.6
0.5	0.6	97.5	57.0	96.9	57.8
	1.0	75.0	47.0	75.5	47.6
	1.4	62.0	41.0	62.2	41.2
	2.0	49.5	34.0	49.4	34.6
	0.2	130	99	129.5	96.6
	0.4	105	78	104.3	77.4
	0.6	89	67	89.2	66.8
1.0	1.0	70	53	70.3	54.2
	1.4	57.5	45	58.5	46.2
	2.0	47	38	47.0	38.0
	0.2	120	109	119.0	107.0
	0.4	98	86	96.3	86.0
	0.6	82	74	82.7	73.6
2.0	1.0	65	58	66	58.9
	1.4	56	49	55.6	49.5
	2.0	45	40	45.5	39.9

TABLE 5.3

5.4 Microstrip Bandpass and Bandstop Filters

5.4.1 Introduction

Two types of microstrip filters, band-pass and band-stop can theoretically be used not only to allow r.f. signal to be transmitted with minimum attenuation but also to offer open and short-circuit terminations to unwanted out-of-band modulation products for different configurations. Jones [9] has shown that band-pass and band-stop filters may be realized using coupled lines either by placing an open-or a short-circuit at two of the four available terminal ports, or by inter-connecting two of the terminal pairs. The theoretical performance of coupled microstrip bandpass and bandstop filters are discussed in the following sections.

5.4.2 Microstrip Band-Pass Filters

The basic forms of microstrip band-pass filters are shown in Figure 5.7. An interdigital filter shown in Figure 5.7(a) consists of quarter-wave resonators which are short-circuited at one end and open-circuited at the other end. In Figure 5.7(b) is shown a comb-line filter which is made of adjacent quarter-wave elements having a short-circuit at one end and a lumped capacitance between the other end and ground. Finally in Figure 5.7(c) the edge-coupled filter consisting of adjacent resonators each half-a-wave long and coupled along half of their length.

As an initial investigation, a single-section edge-coupled filter shown in Figure 5.8(a) with equivalent transmission line circuit shown in Figure 5.8(b) was constructed and tested. When the length of the coupled section is a quarter-wavelength the relationship between input and output impedances and the even and odd-mode impedance is

$$(Z_{IN} \, Z_{OUT})^{\frac{1}{2}} = (Z_{OE} - Z_{OO})/2 \qquad 5.12$$

and indicates that the interdigital structure behaves as a quarter-wave impedance transformer. The bandwidth of the filter depends on the ratio Z_{00}/Z_{0E}. For a narrow-band filter this ratio should be as high as possible and the spacing S between the lines is made as narrow as can.be practically realized. Using a laminate whose relative permittivity is 2.35 a filter was designed to operate between 50Ω source and load impedances and to obtain the maximum value of the ratio Z_{00}/Z_{0E}. The design parameters of the filter are shown in table 5.4.

Z_{OE}	Z_{00}	$\frac{W}{H}$	$\frac{S}{H}$
162	58	0.6	0.1

Table 5.4

The transducer loss L_T of the filter is given by

$$L_T = 20 \log_{10} |(A + B + C + D)/2| \qquad 5.13$$

where A, B, C and D are the elements of the normalized overall transmission matrix of the filter. A computer programme was developed based on the above equation to compare the theoretical and practical responses of the filter and the results are shown in Figure 5.9. Excellent agreement is obtained between the predicted and practical results.

Narrow-band, band-pass filters require the addition of redundant network elements to achieve practical impedance levels and appropriate frequency response. The basic building block of a band-pass system is the low-pass prototype filter which can be designed to produce either a maximally flat or Chebyshev frequency response. For a given number of filter sections, the Chebyshev response offers the highest out-of-band attenuation and consequently two narrow-band Chebyshev band-pass filters were designed.
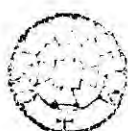
The first filter was designed to have a 0.2dB passband ripple and a fractional bandwidth, w, of 0.8. The normalized filter elements were:

$$g_o = 1.0, \quad g_1 = 1.2275, \quad g_2 = 1.1525, \quad g_3 = 1.2275, \quad g_4 = 1.0$$

The required odd and even mode impedances were obtained using equations given in reference [20]. These impedances cannot be practically realized using the low-loss duroid laminate whose relative permittivity is 2.35 because the separation between the strips would become exceedingly small. Consequently the filter shown in Figure 5.10 was constructed using a PCB whose relative permittivity is approximately 4.8 and its design parameters are given in Table 5.5.

$Z_{OE_{01}} = 71.1$	$Z_{OO_{01}} = 39.1$	$\dfrac{W_{01}}{H} \approx 1.5$	$\dfrac{S_{01}}{H} = 0.2$
$Z_{OE_{12}} = 56.5$	$Z_{OO_{12}} = 44.8$	$\dfrac{W_{12}}{H} = 1.9$	$\dfrac{S_{12}}{H} = 0.9$
$Z_{OE_{23}} = 56.5$	$Z_{OO_{23}} = 44.8$	$\dfrac{W_{23}}{H} = 1.9$	$\dfrac{S_{23}}{H} = 0.9$
$Z_{OE_{34}} = 71.1$	$Z_{OO_{34}} = 39.1$	$\dfrac{W_{34}}{H} = 1.5$	$\dfrac{S_{34}}{H} = 0.2$

Table 5.5

As shown in Table 5.1 the dielectric loss angle of a PCB is high and consequently the dielectric losses are considerably higher than the losses in the copper conductors. For this condition the attenuation loss L_A in the pass-band of the filter is given by [21]

$$L_A = \frac{4.343 \; \text{Tan} \; \delta}{w} \sum_{k=1}^{n} g_k \quad \text{dB} \qquad\qquad 5.14$$

For PCB, tan δ = 0.025 [22] and using the above equation the attenuation loss in the pass-band of the filter is 6.25dB which corresponds closely to that obtained practically.

The second narrow band-pass filter was designed to have a fractional bandwidth equal to 0.1 and a 0.01dB pass-band ripple. The normalized filter elements were:

$$g_0 = 1, \; g_1 = 0.7128, \; g_2 = 1.2003, \; g_3 = 1.3212, \; g_4 = 0.6476, \; g_5 = 1.1007$$

This type of filter cannot be readily constructed using microstrip lines as the separation needed between the conductors becomes extremely small. Consequently, to reduce the size of the filter and to obtain the required separation between the conductors the hair pin filter shown in Figure 5.12 was constructed using strip-lines. To determine the required even and odd mode characteristic impedances monograms given by Matthaei [20] were used, and the design parameters of the filter are shown in Table 5.6

$Z_{0_{01}} = 84.5\Omega$	$Z_{00_{01}} = 37.5\Omega$	$\dfrac{W_{01}}{b} = 0.29$	$\dfrac{S_{01}}{b} = 0.07$
$Z_{OE_{12}} = 59.9\Omega$	$Z_{PO_{12}} = 52.5\Omega$	$\dfrac{W_{12}}{b} = 0.42$	$\dfrac{S_{12}}{b} = 0.27$
$Z_{OE_{23}} = 57.0\Omega$	$Z_{00_{23}} = 44.5\Omega$	$\dfrac{W_{23}}{b} = 0.44$	$\dfrac{S_{23}}{b} = 0.35$
$Z_{OE_{34}} = 59.9\Omega$	$Z_{00_{34}} = 42.5\Omega$	$\dfrac{W_{34}}{b} = 0.42$	$\dfrac{S_{34}}{b} = 0.27$
$Z_{OE_{45}} = 84.5$	$Z_{00_{45}} = 37.5\Omega$	$\dfrac{W_{45}}{b} = 0.29$	$\dfrac{S_{45}}{b} = 0.07$

Table 5.6

The separation between the two copper planes 'b' has a value of 3.175 mm.

The frequency response of the hairpin band-pass filter is shown in Figure 5.13 where it can be seen that extremely sharp cut-off and an attenuation loss of 8dB in the pass-band has been obtained.

The practical results for the three band-pass filters show that the attenuation in the pass-band depends not only on the dielectric losses of the substrate, but also on the fractional bandwidth, w, of the filter as given by equation 5.13. The smaller the fractional bandwidth, the larger is the attenuation in the pass-band of the filter. For this reason narrow-

band, bandpass filters cannot be used in image-rejection mixers because
the attenuation in the passband is unacceptably high.

5.4.3 Microstrip Bandstop Filters

It has been shown in section 5.4.2 that the dielectric loss of the
copper laminates makes it difficult to realize microstrip narrow-band
bandpass filters where the attenuation in the pass-band is very low.
In order to obtain narrow-band mixers, however, the r.f. signal has to
be transmitted with minimum attenuation while the image-frequency has
to be strongly attenuated. Such filtering requirement can be more readily
obtained by using a stopband rather than a bandpass filter, as the latter
provides a low attenuation over a wide-band of frequencies and a high
attenuation over a narrow-band of frequencies.

One method of realizing a microstrip bandstop filter is to use an
open-circuit stub shown in Figure 5.14. Computer analysis of such a
filter indicates that as the characteristic impedance of the open-circuit
increases the bandwidth of the stopband decreases. In order to realize
narrow-band, bandstop filter the characteristic impedance of the open-
circuit stub must be large making it very difficult to realize in this
form.

An alternative method of obtaining a narrow-band bandstop filter is
to use coupled microstrip lines as shown in Figure 5.15(a). The equivalent
transmission line circuit of the bandstop filter is shown in Figure 5.15(b),
where Z_0 and Z_1 are the characteristic impedances of the main line and
stub respectively. The required relationship between Z_0, Z_1 and the odd
and even-mode impedances of the coupled lines maybe obtained using the
impedance matrix of coupled lines derived by Jones [9].

Defining

$$S = j \tan \theta \qquad\qquad 5.15$$

and using equation 5.9(b) it can be shown that

$$Z_{11} = Z_{22} = Z_{33} = Z_{44} = a/S$$

$$Z_{12} = Z_{21} = Z_{34} = Z_{43} = b/S$$

$$\qquad\qquad 5.16$$

$$Z_{13} = Z_{31} = Z_{42} = Z_{24} = b \ (1 - S^2)^{\frac{1}{2}} /S$$

$$Z_{14} = Z_{41} = Z_{23} = Z_{32} = a \ (1 - S^2)^{\frac{1}{2}} /S$$

In practice it is convenient to simulate the short-circuit shown in Figure 5..5(a) by an open-circuit stub as shown in Figure 5.15(c). For port 3 of the filter

$$V_3 = I_s \ Z_3/S \qquad\qquad 5.17$$

where Z_3 is the characteristic impedance of the open-circuit stub, while at port 2 of the filter $I_2 = 0$, so that using equation 5.9(a) results in the following two-port matrix equation

$$
\begin{bmatrix} V_1 \\ \\ V_4 \end{bmatrix}
=
\begin{bmatrix}
Z_{11} - \dfrac{Z_{13}{}^2 \ S}{Z_3 + SZ_{11}} & , & Z_{14} - \dfrac{Z_{13} \ Z_{12} \ S}{Z_3 + SZ_{11}} \\
\\
Z_{14} - \dfrac{Z_{13} \ Z_{12} \ S}{Z_3 + SZ_{11}} & , & Z_{11} - \dfrac{Z_{12}{}^2 \ S}{Z_3 + SZ_{11}}
\end{bmatrix}
\begin{bmatrix} I_1 \\ \\ I_4 \end{bmatrix}
\qquad 5.18
$$

The relationship between Z_0 and Z_1 as defined in Figure 5.15(b) and the odd and even-mode impedances, using equation 5.18, as shown in Appendix VII are

$$Z_0 = (Z_{OE} + Z_{OO})/2$$

5.19

$$Z_1 = \frac{2 (Z_{OE} + Z_{OO})(Z_3 \left[Z_{OE} + Z_{OO} \right]/2 + Z_{OE} Z_{OO})}{(Z_{OE} - Z_{OO})^2}$$

In order to realize the bandstop filter the characteristic impedance Z_3 of the stub shown in Figure 5.15(c) is arbitrary provided

$$Z_3 < Z_0 (Z_0 + Z_1)/Z_1$$

5.20

Based on the design parameters shown in Table 4.7, bandstop filters were realized using PCB and low loss (Duroid) laminates

Laminate	Z_{OE}	Z_{OO}	W/H	S/H
PCB	64.4	32.7	1.7	0.1
Duroid	73.0	41.2	2.2	0.1

Table 5.7

Figures 5.16(a) and 5.16(b) show the frequency responses of single and double-section stopband filters using PCB, while Figure 5.17 shows the frequency response of a single-section stopband filter using the low loss laminate. It is interesting to note from the results obtained, that the effect of the dielectric loss is to increase the bandwidth but to decrease the attenuation in the stopband considerably.

Figures 5.18(a) and 5.18(b) show the predicted frequency responses of the input and output impedances of the single-section stopband filter. They indicate that at the design frequency, the input impedance of the filter is an open-circuit while the output impedance is a short-circuit.
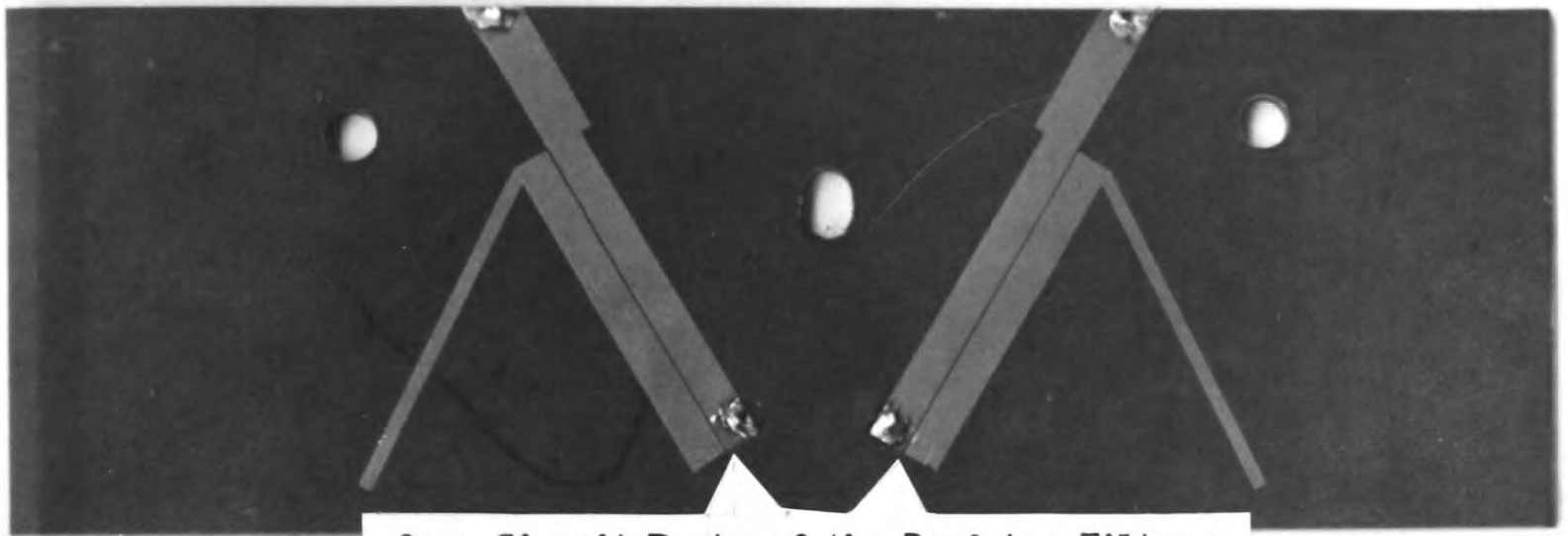
Open-Circuit Ports of the Bandstop Filters
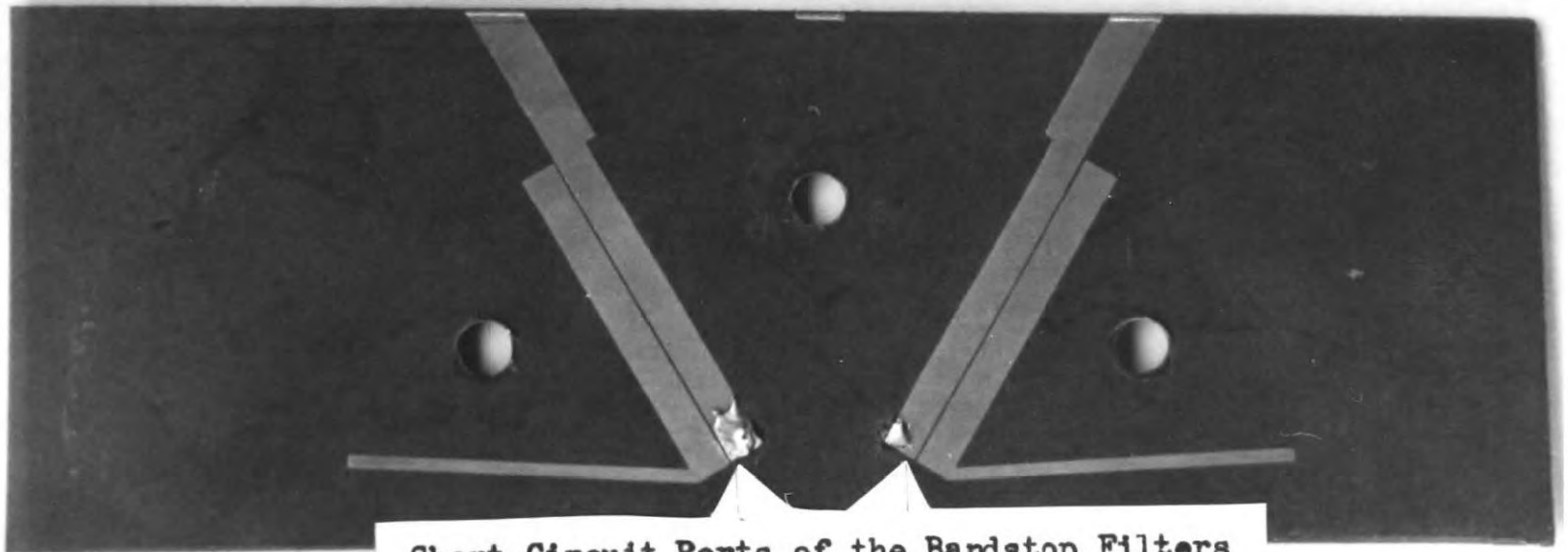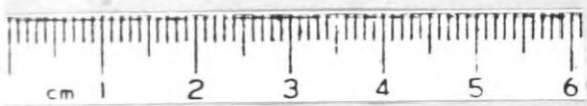
Short-Circuit Ports of the Bandstop Filters

Since a network analyser was not available, the input and output impedance
of the filter were measured using a VSWR meter and a slotted line. It was
found that the results obtained were in agreement with those predicted by
theory. It is therefore possible to use those type of filters to realize
narrow-band image open-circuit or image-short circuit mixers.

It is of obvious interest in realizing microstrip narrow-band mixers
to be able to produce tunable bandstop filters. These type of filters can
be obtained at the lower band of microwave frequencies, by replacing the
open-circuit stub by a variable capacitor as shown in Figure 5.19. The
stopband frequency of such a filter (as shown in Appendix VII) is given
by the following equation

$$\left(\frac{(Z_{OE} + Z_{OO})}{2} \right) X_c \tan \theta + 2Z_{OE} Z_{OO} = 0 \qquad 5.21$$

The properties of the tunable stopband filter were investigated and
results obtained are shown in Figure 5.20 for two computed values of
capacitance while Figure 5.21 show a general frequency response of the
filter over a wide range of capacitance values. The results indicate
that although the attenuation in the stopband has a maximum attenuation
of 13 dB, the filter is tunable as predicted by equation 5.21.

To increase the attenuation in the stopband a double-section filter
was constructed again using a duroid laminate with two variable capacitors
as shown in Figure 5.22. Predicted and practical frequency responses of
the tunable two-section bandstop filter are shown in Figure 5.23 where
the two-sections are tuned to different frequencies. Figure 5.24 shows
the behaviour of the filter if the two-sections are tuned to the same
frequency, while Figure 5.25 shows a general frequency response over a
wide range of frequencies with the two sections again tuned to the same
frequency.

For the two types of stopband filters (fixed and tunable) a good agreement is obtained between the predicted response and that obtained in practice. The tunable stopband filter also offers the possibility to realize narrow-band image rejection mixers which can be tuned over a limited range of frequencies.

5.5. Microstrip Directional Couplers

In order to couple the r.f. signal and the local oscillator to the lattice network of diodes some form of directional coupler is necessary. Three common types of directional couplers suitable for this purpose are shown in Figure 5.26.

For the coupled line directional coupler shown in Figure 5.26(a) the coupling coefficient, K, at the centre frequency is given by,

$$K = (Z_{OE} - Z_{OO})/(Z_{OE} + Z_{OO}) \qquad 5.22$$

The parameters $\frac{W}{H}$ and $\frac{S}{H}$ necessary to obtain a given coefficient of coupling can be conveniently obtained from the developed computer programme given in Appendix VI. This type of coupler, however can only be realized if the coupling is loose (> 3dB) and is normally used in single diode mixers.

In balanced mixers it is necessary to produce tight coupling (3dB) and hence either a two-branch coupler shown in Figure 5.26(b) or a rat-race coupler shown in Figure 5.26(c) can be used. These two couplers are realized by having lines which are an odd number of quarter wavelengths long. It may be shown that a normalized admittance matrix of a line a quarter wavelength long of characteristic admittance Z_{OA} normalized to Y_0 is

$$y = \frac{Y_{OA}}{Y_0} \begin{bmatrix} 0 & , & j \\ j & , & 0 \end{bmatrix} \qquad 5.23(a)$$

and if the line is three-quarter-wavelength long it becomes

$$y = \frac{Y_{OA}}{Y_0} \begin{bmatrix} 0 & , & -j \\ -j & , & 0 \end{bmatrix} \qquad 5.23(b)$$

Using the above equations and taking the admittance matrix of a rat-race coupler to be [23]

$$y = \frac{j}{\sqrt{2}} \begin{bmatrix} 0 & 0 & -1 & 1 \\ 0 & 0 & 1 & 1 \\ 1 & 1 & 0 & 0 \\ 1 - & 1 & 0 & 0 \end{bmatrix}$$
5.24

the relationship between Y_{OA} and Y_O shown in Figure 5.26(c) is

$$Y_{OA} = Y_O/\sqrt{2}$$
5.25(a)

Similarly, for a two-branch coupler the corresponding relationship is

$$Y_{OB} = Y_O\sqrt{2}$$
5.25(b)

where Y_{OB} is defined in Figure 5.26(b).

In the case of the rat-race coupler shown in Figure 5.26(c) the signal applied to port 3 divides equally between ports 4 and 2 where the signals are in phase. If the signal is applied to port 1 once again it divides equally between ports 2 and 4 but the signals in the two ports are opposite in phase. Port 1 is decoupled from port 3. The properties of a rat-race coupler are therefore similar to its low-frequency counter-part, a centre—tapped hybrid transformer and produces the correct phase relationship between the r.f. signal and that of the local oscillator at the lattice network of diodes. Consequently it was decided to use the rate-race coupler as a means of coupling the r.f. signal and the local oscillator to the lattice network of diodes.

Rat-race directional couplers using PCB and low-loss laminate (duroid where ε_r = 2.35) were constructed and their frequency responses are shown in Figures 5.27 and 5.28 respectively. It is interesting to note that the performances of the two couplers are very similar indicating that the losses in the laminates do not play as significant a role as they do in narrow-band bandpass and bandstop filters.

5.6 Co-Axial Cavity Resonator

To ensure that the lattice network of diodes is driven by a sinusoidal current waveform a series tuned resonator has to be used. A convenient form of such a resonator consists of a length of co-axial line which is made a multiple of a quarter-wavelength at the resonant frequency. One end of the line is terminated by a short-circuit while the other end is terminated by a variable capacitor or inductive loading so that tuning can be obtained. To either excite or extract power from the cavity three methods are normally used: capacitive or electric field coupling, inductive or loop coupling, or direct coupling. These three methods are shown in Figure 5.29. The lumped equivalent circuit of the cavity and the cavity length depends on the type of coupling used. The design of such cavities is adeqiately covered in existing literature [24-26].

To realize the resonator in compact form it is possible to use a stepped impedance resonator [27-29] as shown in Figure 5.30. Tuning of the cavity is obtained by a co-axial capacitance C that exists between the two lines. The expression for this tuning capacitance is

$$C_T = \frac{0.0242\ \ell}{\log_e (\frac{b}{a})}\ pF \qquad\qquad 5.26$$

where ℓ is the distance that the two lines overlap in mm, b is the inside radius of the hollow conductor and 'a' is the radius of the inner conductor.

The input impedance looking from the short-circuit end of the line having a characteristic impedance Z_{01} shown in Figure 5.30 is

$$Z_{IN} = j\ Z_{01} \left[\frac{(Z_{02}\ \tan\ \theta_2 - X_c) + Z_{01}\ \tan\ \theta_1}{Z_{01} + \tan\ \theta_1\ (Z_{02}\ \tan\ \theta_2 - X_c)} \right] \qquad 5.28$$

At resonance $Z_{IN} = 0$ and

$$X_c = Z_{01}\ \tan\ \theta_1 + Z_{02}\ \tan\ \theta_2 \qquad\qquad 5.29$$

The impedances Z_{01} and Z_{02} were designed so that there is a minimum loss in the cavity and hence maximum unloaded Q can be obtained.

A series-tuned cavity whose construction details are shown in Figure 5.31 was realized. The frequency response of the cavity when fed from a 50Ω source and terminated by a 50Ω crystal detector is shown in Figure 5.32. It was found that the cavity had a constant response shape and bandwidth between 1.3GHz, and 2 GHz. This cavity can therefore be used in the local oscillator circuit to ensure that the lattice circuit of diodes is driven by a sinusoidal current waveform.

5.7 Conclusions

This chapter has been mainly concerned with the properties of micro-strip transmission lines and their applications to realize directional couplers and narrow-band bandpass and bandstop filters. Initially the relationship between the line parameters such as characteristic impedance and guide-wavelength and the geometry of the microstrip line were established. A computer programme was then developed to determine the relationship between the geometry of the coupled microstrip lines and the odd and even-mode impedances. This was done as such a relationship in not readily available in literature for the type of laminates that are to be used to investigate the properties of microwave integrated circuit double-balanced lattice mixers.

With a view to passing the r.f. and local oscillator signals to the diodes but presenting either open or short-circuit terminations to out-of-band modulation products (mainly image frequency), the properties of narrow-band bandpass and bandstop filters were investigated. It was found that the loss in the case of narrow-band bandpass filters is unacceptably high making it difficult to examine the conversion loss of an image-rejection mixer. A narrow-band bandstop filter can be designed to produce adequate attenuation at the image frequency and pass the r.f. signal with minimum attenuation. A further advantage of the proposed bandstop filter is that open-circuit or short-circuit termination at the image frequency can readily be obtained.

To couple the r.f. signal and the local oscillator to the lattice network of diodes different types of directional couplers were considered. However, because of its properties and ease of construction it was decided to use a rat-race directional coupler.

Finally, a tunable cavity resonator was constructed to ensure that the diodes are fed by a sinusoidal current waveform. The cavity constructed was found to be tunable over the range 1.3 to 2GHz.

5.8 <u>References</u>

1. Wheeler, H.A., Transmission-line Properties of Parallel Strips Separated by a Dielectric Sheet, IEEE Trans., 1965, Vol MTT-13 pp 172-185.

2. Stinehelfer, H.E., An Accurate Calculation of Uniform Microstrip Transmission Lines, IEEE Trans., 1968, Vol MTT-16, No. 7, pp 439-444.

3. Schneider, M.V., Microstrip Dispersion, Proc. IEEE, 1972, Vol 60, pp 144-146.

4. Kompa, G., Mehran R., Planar Waveguide Model for Calculating Microstrip Components, Electron-Letters, 1975, Vol 11, pp 459-460.

5. Schneider, M.V., Microstrip Lines for Microwave Integrated Circuits, B.S.T.J., 1969, pp 1421-1444.

6. Ross, R.F.G., Howes, M.J., Simple Formulas for Microstrip Lines, Electronic Letters, Aug. 1976, Vol 12 No. 16, pp 410.

7. Welch, J.D., Pratt, H.J., Losses in Microstrip Transmission Systems for Integrated Microwave Circuits, NEREM Record, 1966, Vol 8, pp 100-101.

8. Masse, D., Pucel, G.P., Hartwig, C.P., Microstrip Versus Balanced Stripline, Proc. IEEE, Aug. 1968, pp 1359-60.

9. Jones, E.M.T., Bolljahn, J.T., Coupled-Strip Transmission Lines Filters and Directional Couplers, IEEE Trans., Vol MTT-4, 1956, pp 75-81.

10. Napoli, L.S., and Hughes J.J., Characteristics of Coupled-Microstrip Lines, R.C.A. Rev., Sept. 1970, pp 479-498.

11. Snell, W.W., Low-Loss Microstrip Filters Developed by Frequency Scalling, B.S.T.J., Vol 50, No. 6, July-August, 1971, pp 1919-1931.

12. Cohn, S.B., Parallel Coupled Transmission Line Resonator Filters, I.R.E. Trans., Microwave Theory Tech., Vol MTT-6, April 1958, pp 223-231.

13. Bryant, T.G., Weiss, J.A., Parameters of Microstrip Transmission Lines and of Coupled Pairs of Microstrip Lines, IEEE Trans., 1968, Vol MTT-16, pp 1021-1027.

14. Akhtarzad, S., Rowbotham, T.R., Johns, P.B., The Design of Coupled Microstrip Lines, IEEE Trans., June 1975, Vol MTT-23, No. 6, pp 486-492.

15. Shamanna, K.N., Rao, V.S., Kosta, S.P., Parallel-Coupled Microstrip Line, Electronic Design, May 1976, pp 78-81.

16. Zehentner, J., Analysis of Coupled Microstrip Lines, Microwave Journal, May 1978, pp 82-83.

17. Young, L., Sobol, H., Advances in Microwaves, Vol 8, Academic ?. 1974, pp 313-318.

18. Shamasundra, S.D., Singh, N., Design of Coupled Microstrip Lines, IEEE Trans., M.T.T., March 1977, pp 232-233.

19. Sadd, T.S., Microwave Engineers Handbook, Artech House, Vol 1, 1971.

20. Matthaei, G.L., Young, L., Jones, E.M.T., Microwave Filters, Impc? ce Matching Networks and Coupling Structures, McGraw-Hill, 1964.

21. Cohn, S.B., Dissipation Loss in Multiple-Coupled Resonator Filters, Proc., IRE, Vol 47, Aug 1959, pp 1342-1348.

22. Hallford, B.R., Using Plastic Substrates in the Design of Microstrip Components, MSN, June/July 1974, pp 81-91.

23. Altman, J.L., Microwave Circuits, Van Nostrant, London, 1964.

24. Harvard University, Radio Research Lab. Staff, Very High Frequency Techniques, Chaoter 28, McGraw-Hill, 1947.

25. Montgomery, C.G., Rickie, R.H., Purcell E.M., Principles of Microwave Circuits Radiation Lab. Series, McGraw-Hill, 1948, pp 207-239.

26. Emmett, J.R., Microwave Lattice Mixers at 4.5GHz, Ph.D. Thesis, Durham University, Sept. 1974.

27. Private Communication, Trinogga, L.A., Newcastle Polytechnic, Belin, M.J., General Electric Company, Coventry.

28. Makimoto, M., Yamashita, S., Bandpass Filters Using Parallel Coupled Stripline Stepped Impedance Resonators, IEEE Trans., Vol MTT-28, No. 12, Dec 1980, pp 1413-1417.

29. Makimoto, M., Yamashita, S., Compact Bandpass Filters Using Stepped Impedance Resonators, Proc. IEEE, Vol 67, No. 1, Jan 1979, pp 16-19.
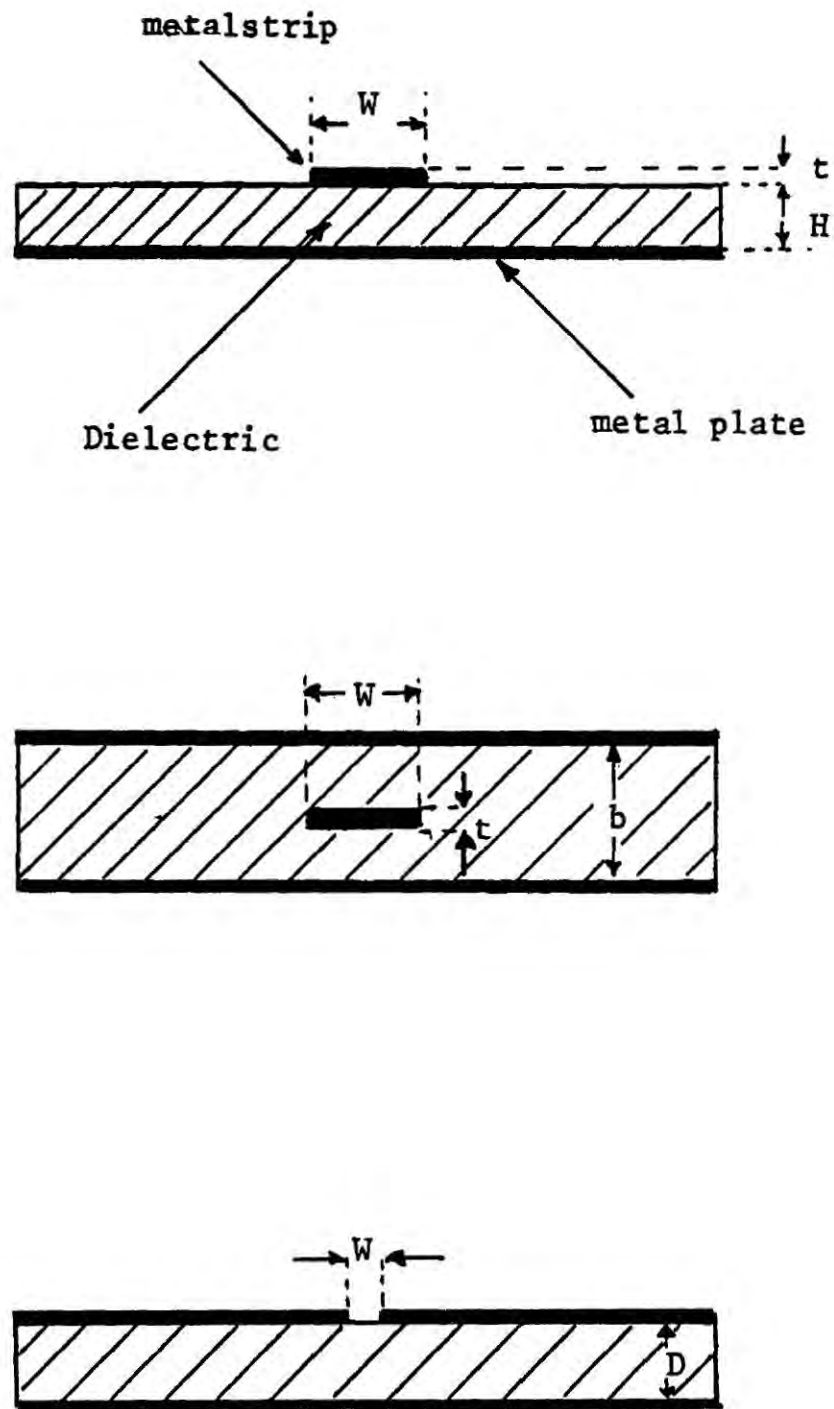
Figure 5.1 Cross-Sectional Views of Common Planar Transmission Lines

        (a) Microstrip
        (b) Stripline
        (c) Slotline
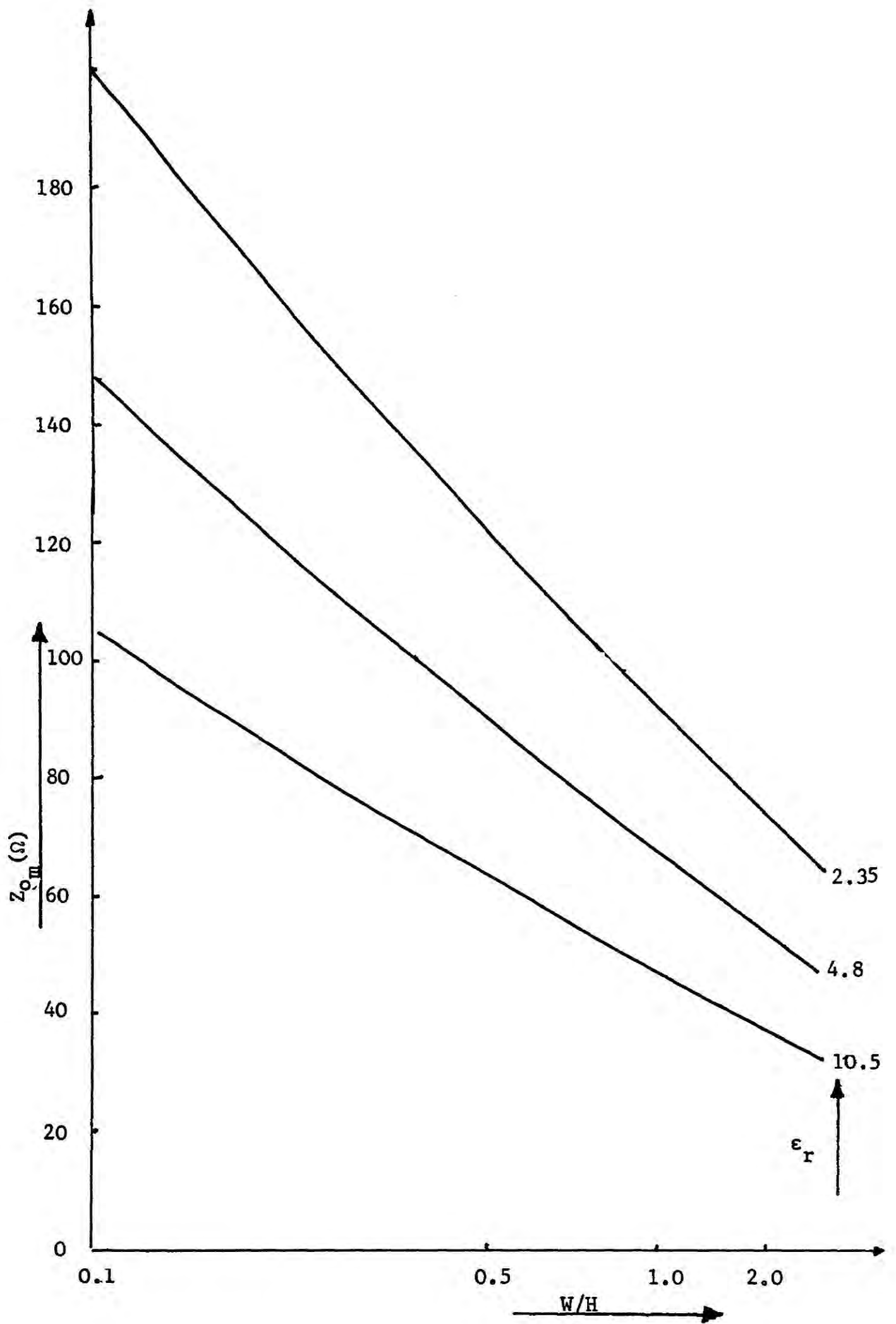
Figure 5.2 Characteristic Impedance of a Microstrip Line as a
of W/H for Laminates having Different Reactive Permittivities
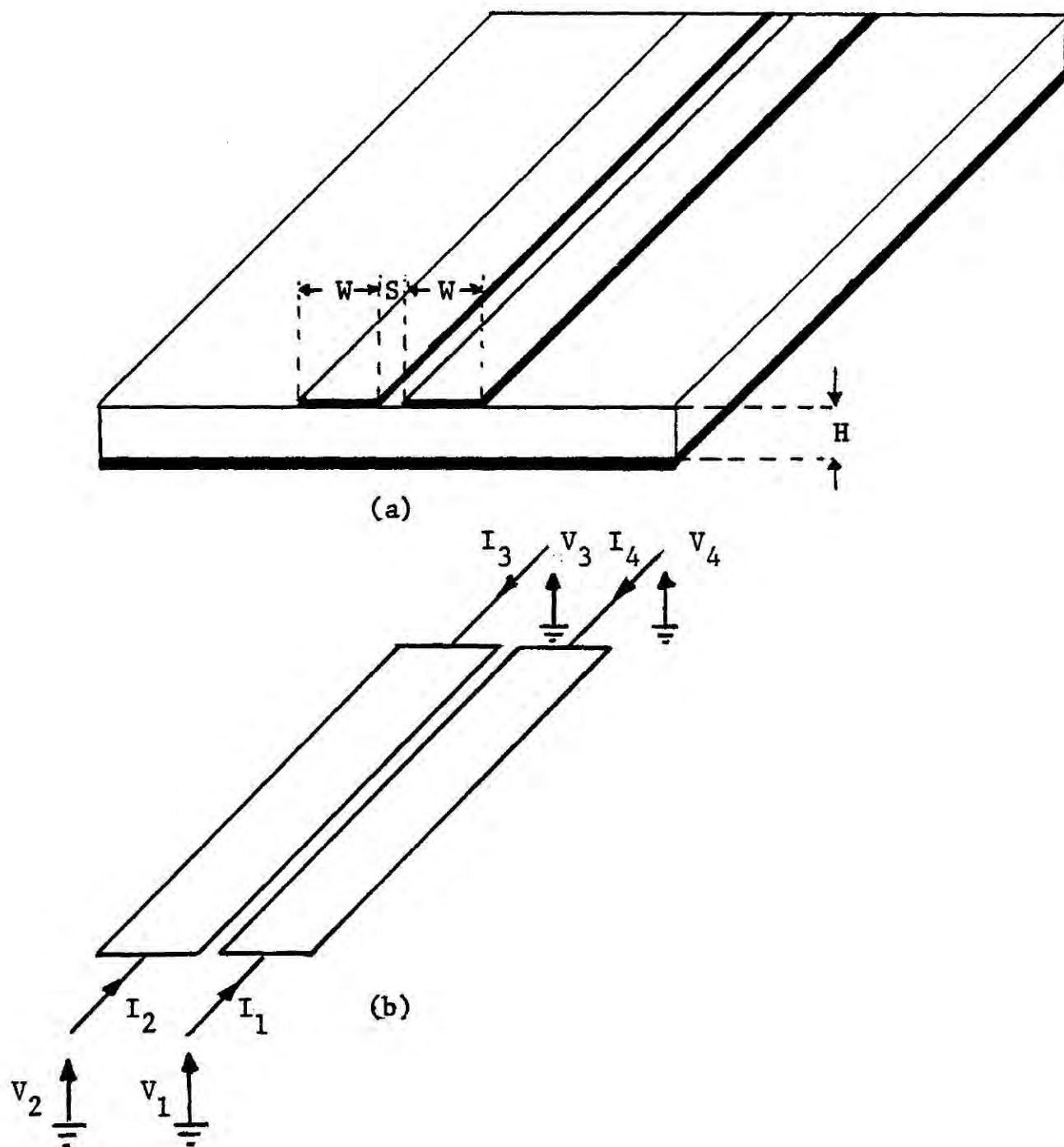
Figure 5.3 Coupled Microstrip Lines
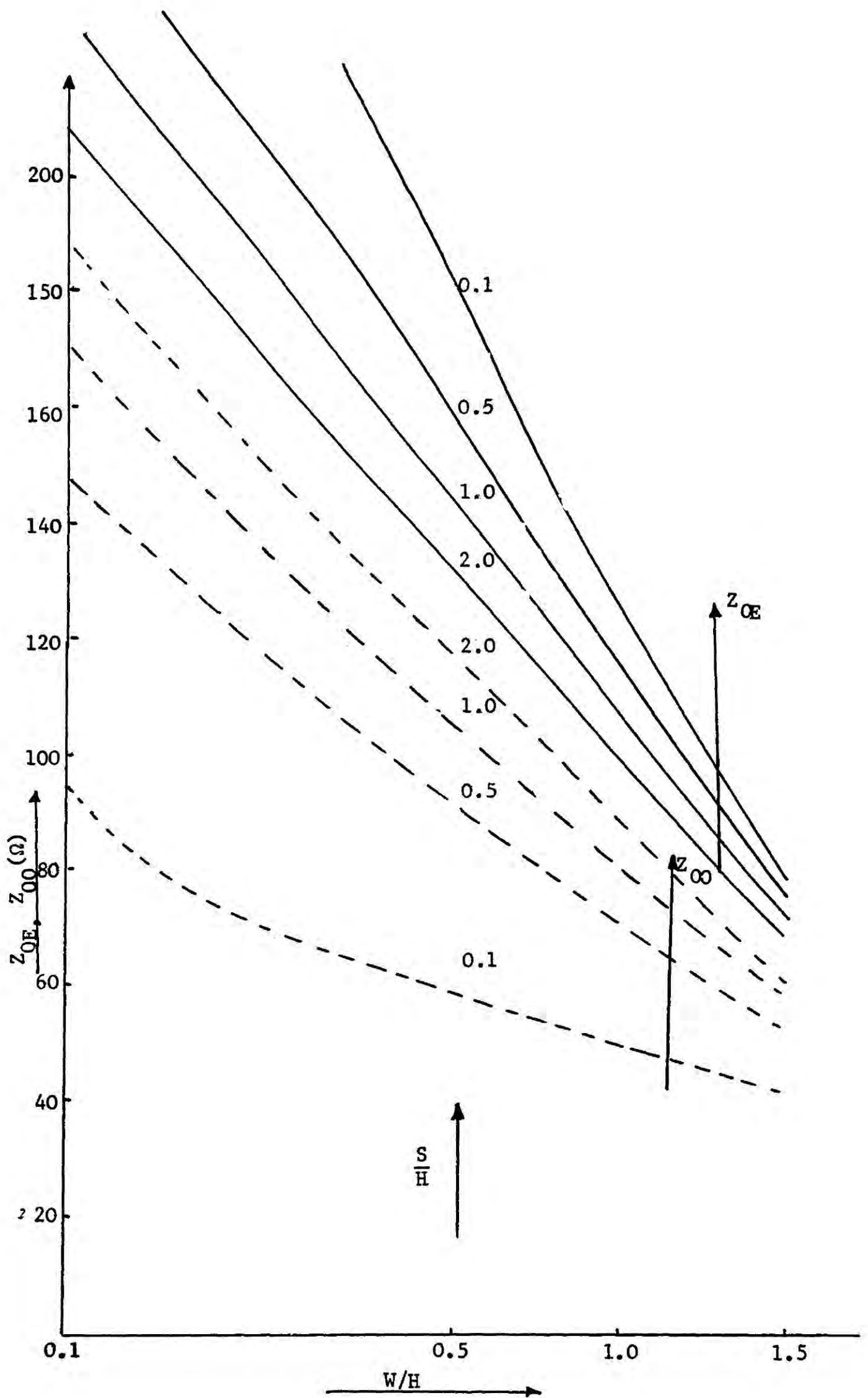
Figure 5.4   Even and odd mode characteristic Impedances as a Function of
W/H and S/H where ε_r = 2.35
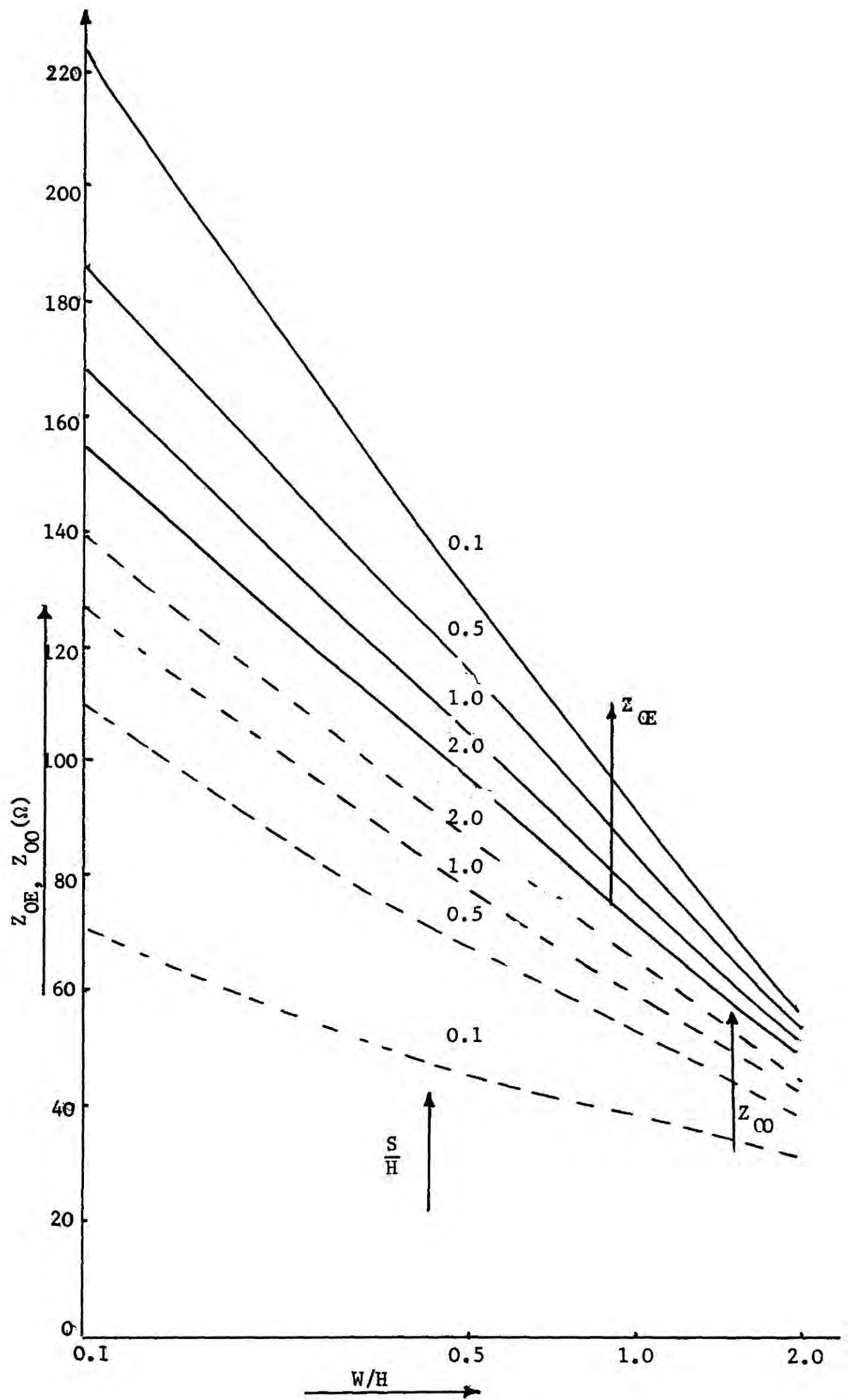
Figure 5.5   Even and odd mode characteristic Impedances as a Function of
W/H and S/H where $\varepsilon_r = 4.8$.
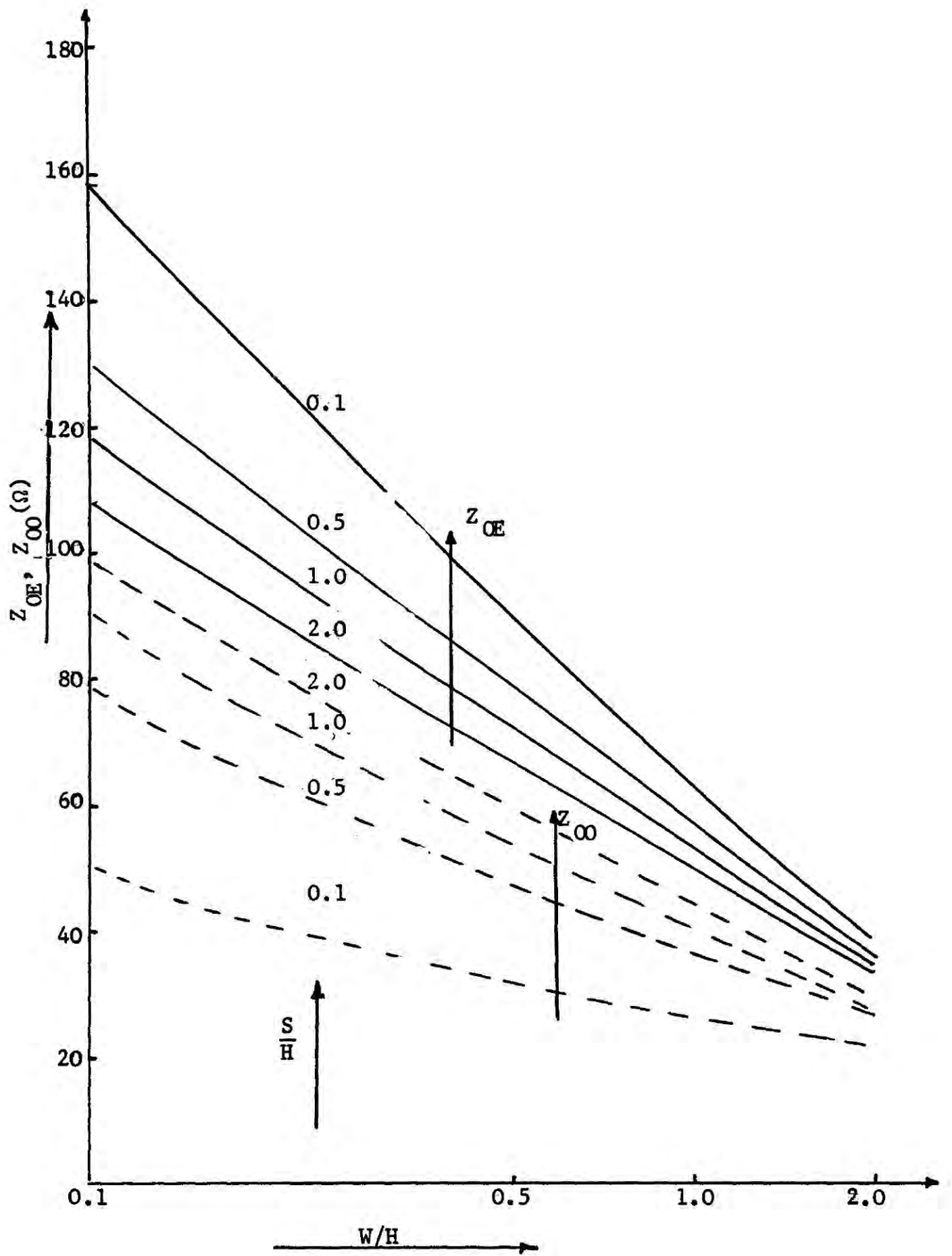
Figure 5.6 Even and odd mode characteristic Impedance as a Function of W/H and S/H where ϵ_r = 10.5
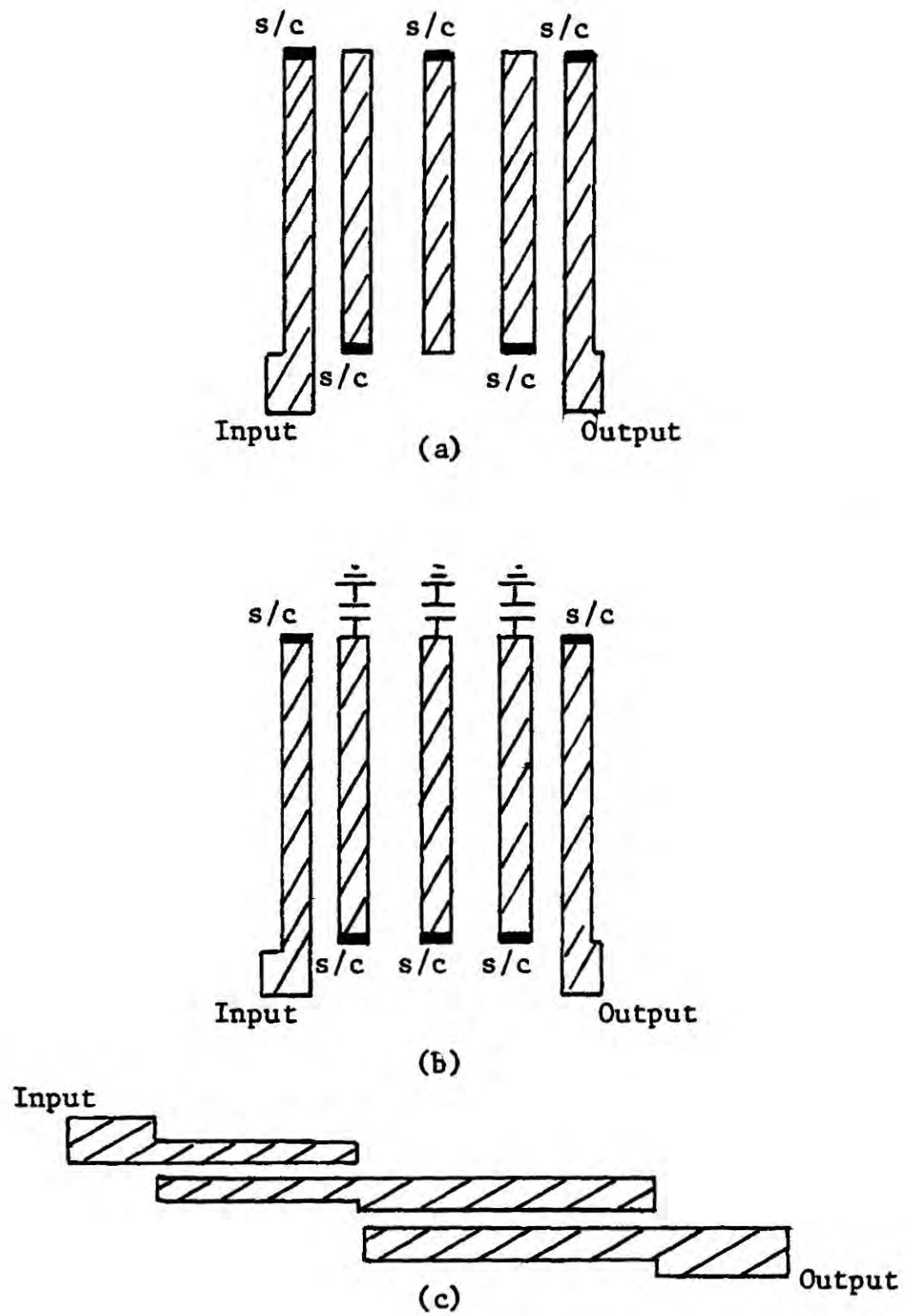
Figure 5.7   Microstrip Band-Pass Filters

(a) Interdigital
(b) Comb-Line
(c) Edge-Coupled
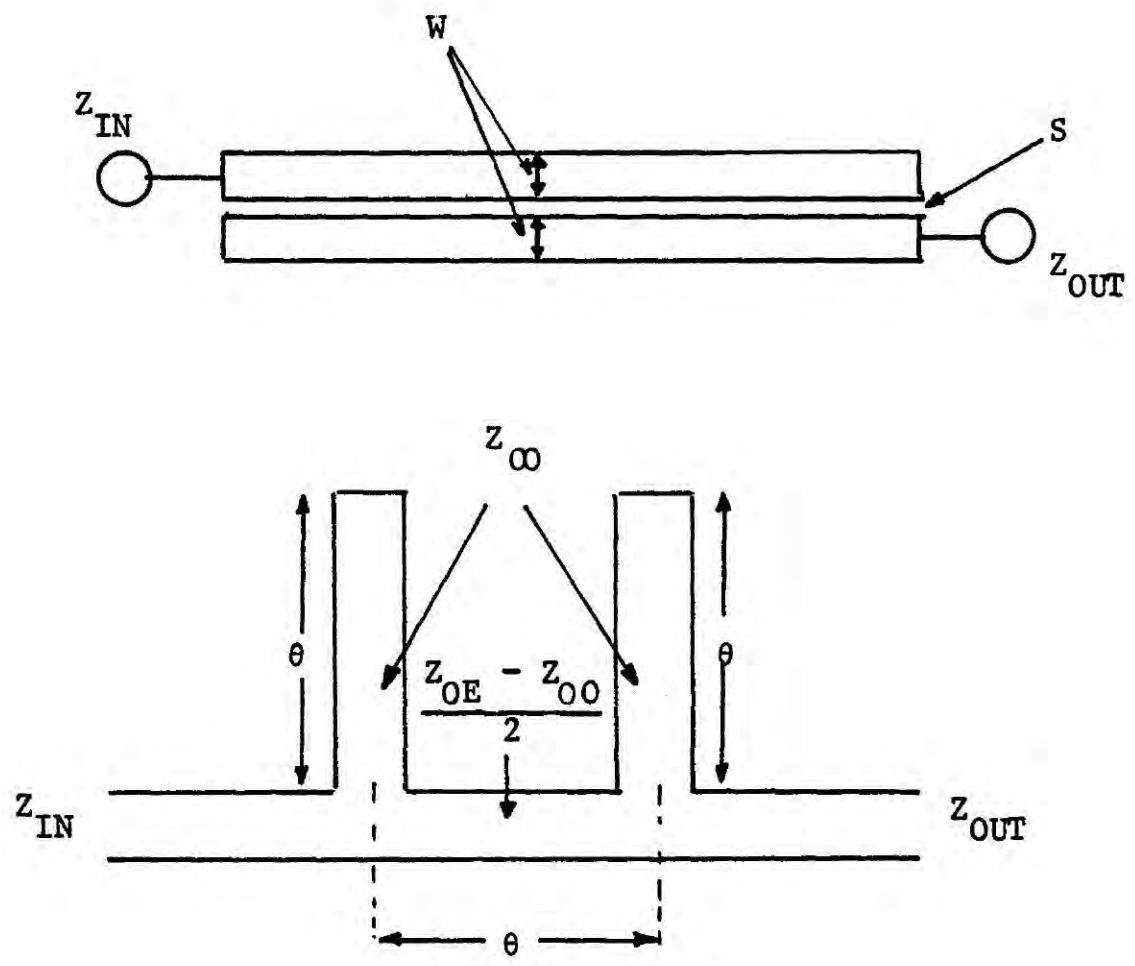
Figure 5.8   Single-Section Band-Pass Filter

(a) Edge-Coupled Filter
(b) Equivalent circuit of the Band-Pass Filter
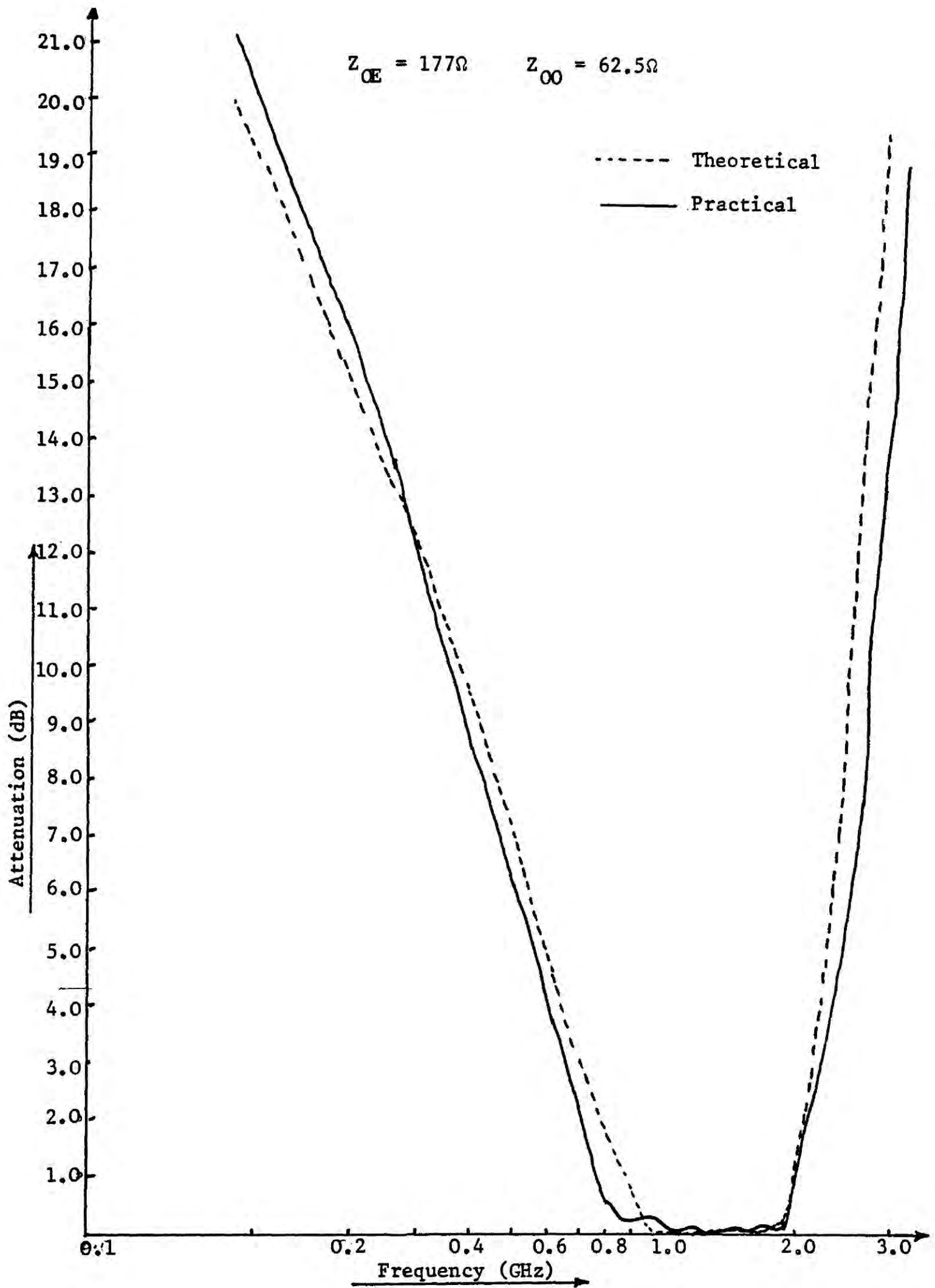
Figure 5.9   Frequency Response of a Single-Section Edge-
Coupled Filter
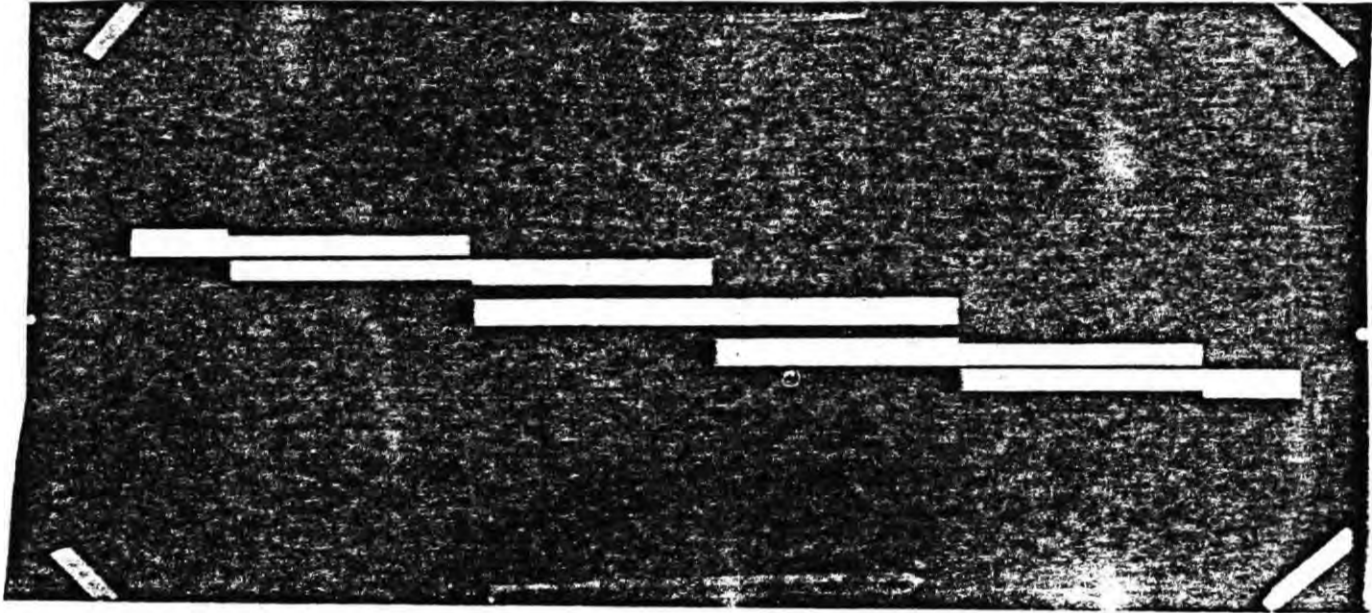
Figure 5.10 Microstrip Three Element Band-Pass Filter
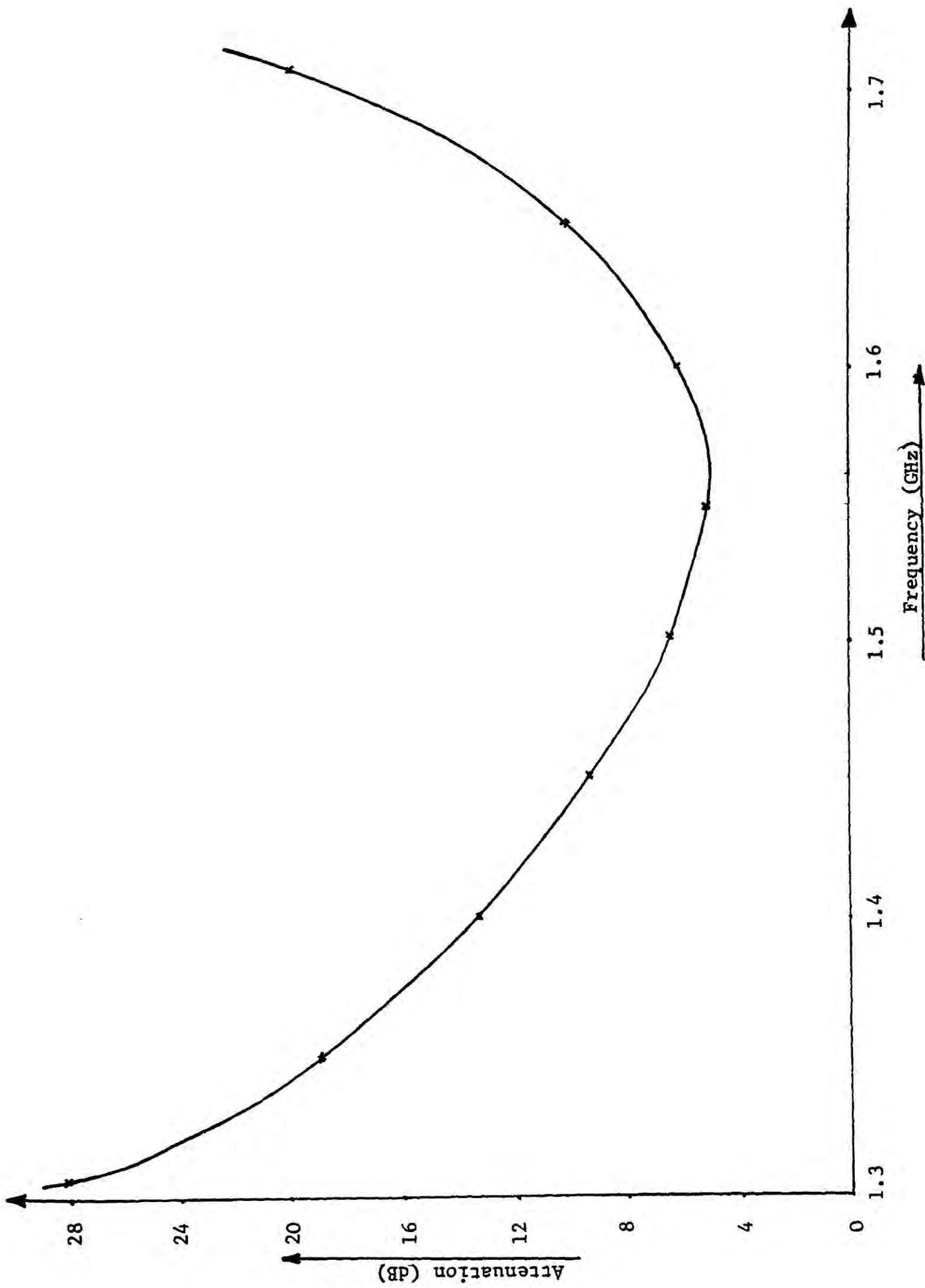
Figure 5.11 Frequency Response of a Three Element Microstrip Band-Pass Filter
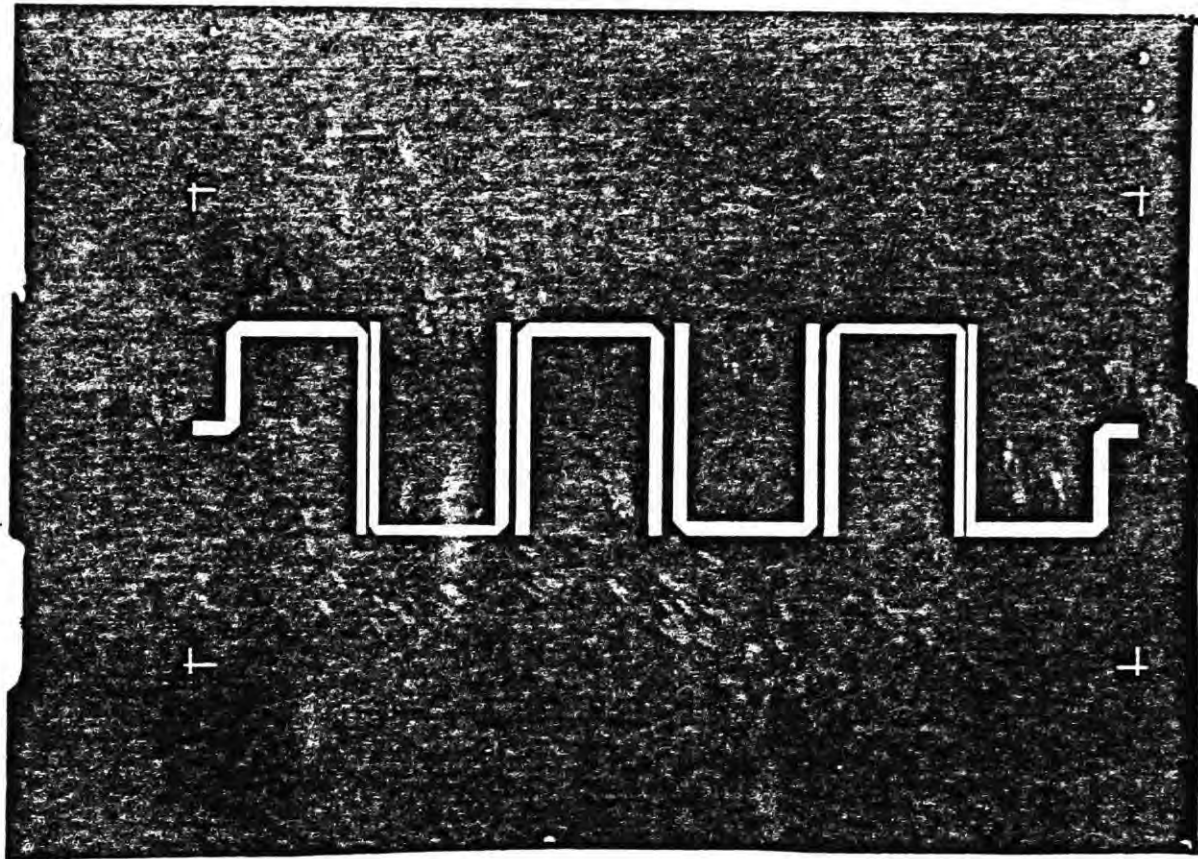
Figure 5.12 Hairpin Stripline Band-Pass Filter
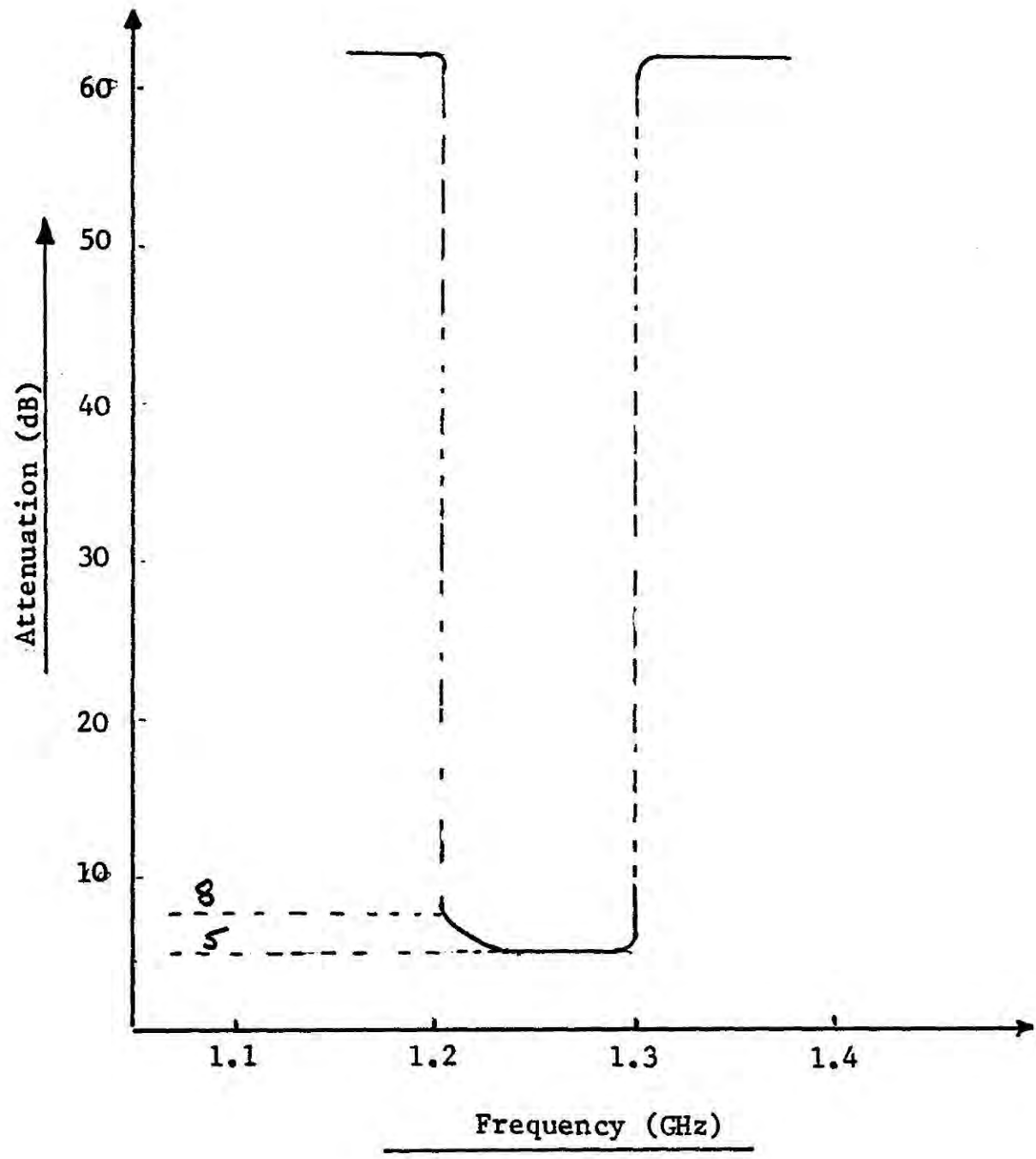
Figure 5.13   Frequency response of the Hairpin Filter
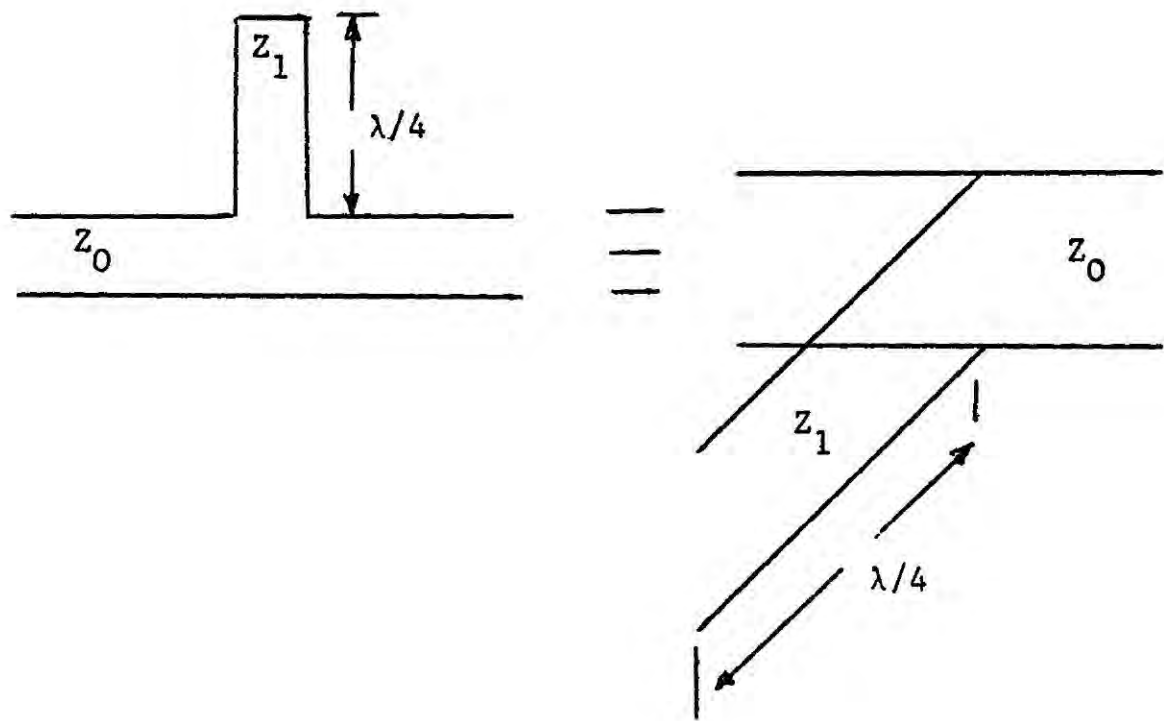
Figure 5.14   Microstrip Open-Circuit Stub Stopband Filter

(a)

(b)

(c)
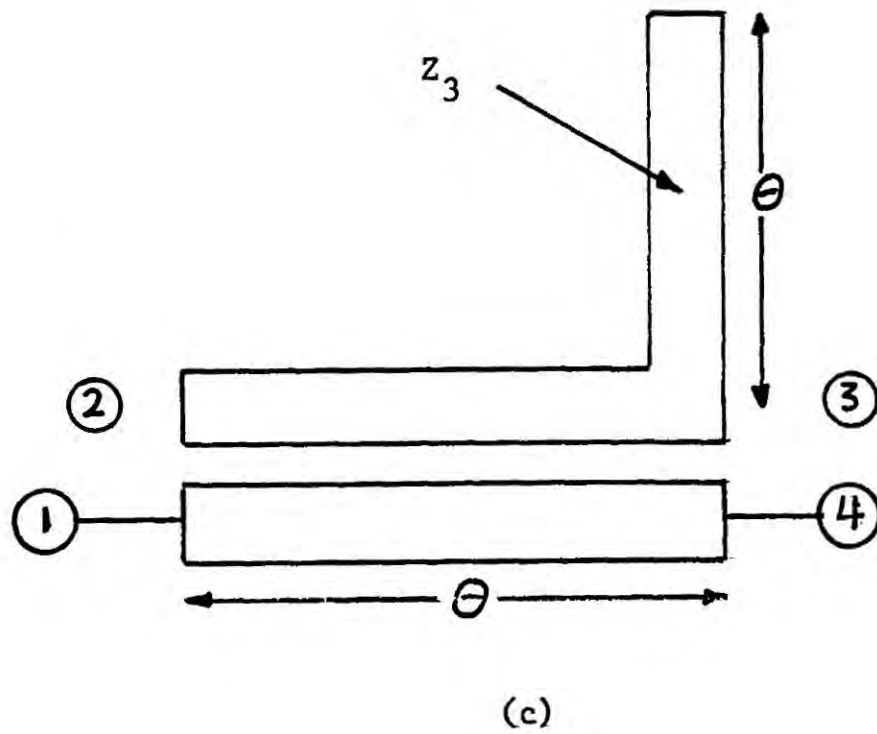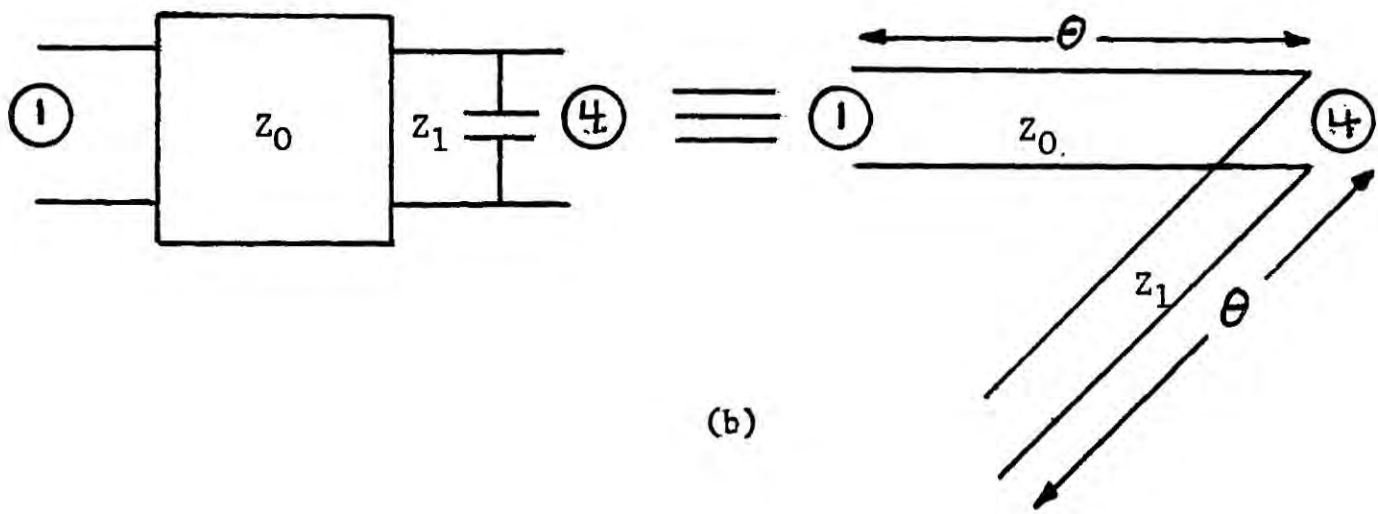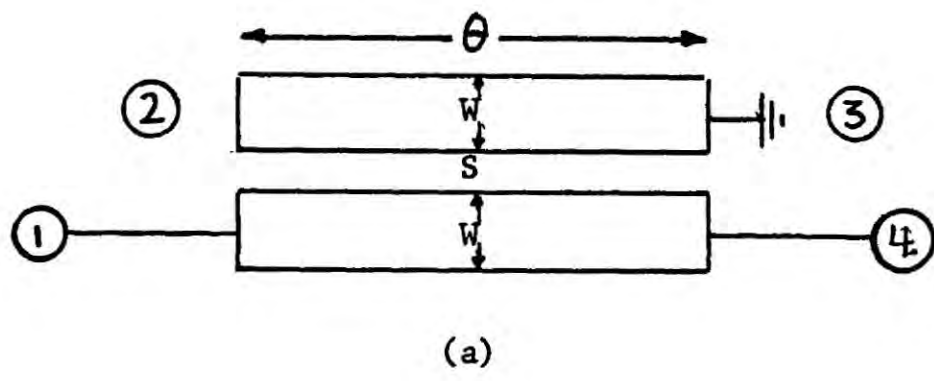
Figure 5.15   Microstrip Band-Stop Filter
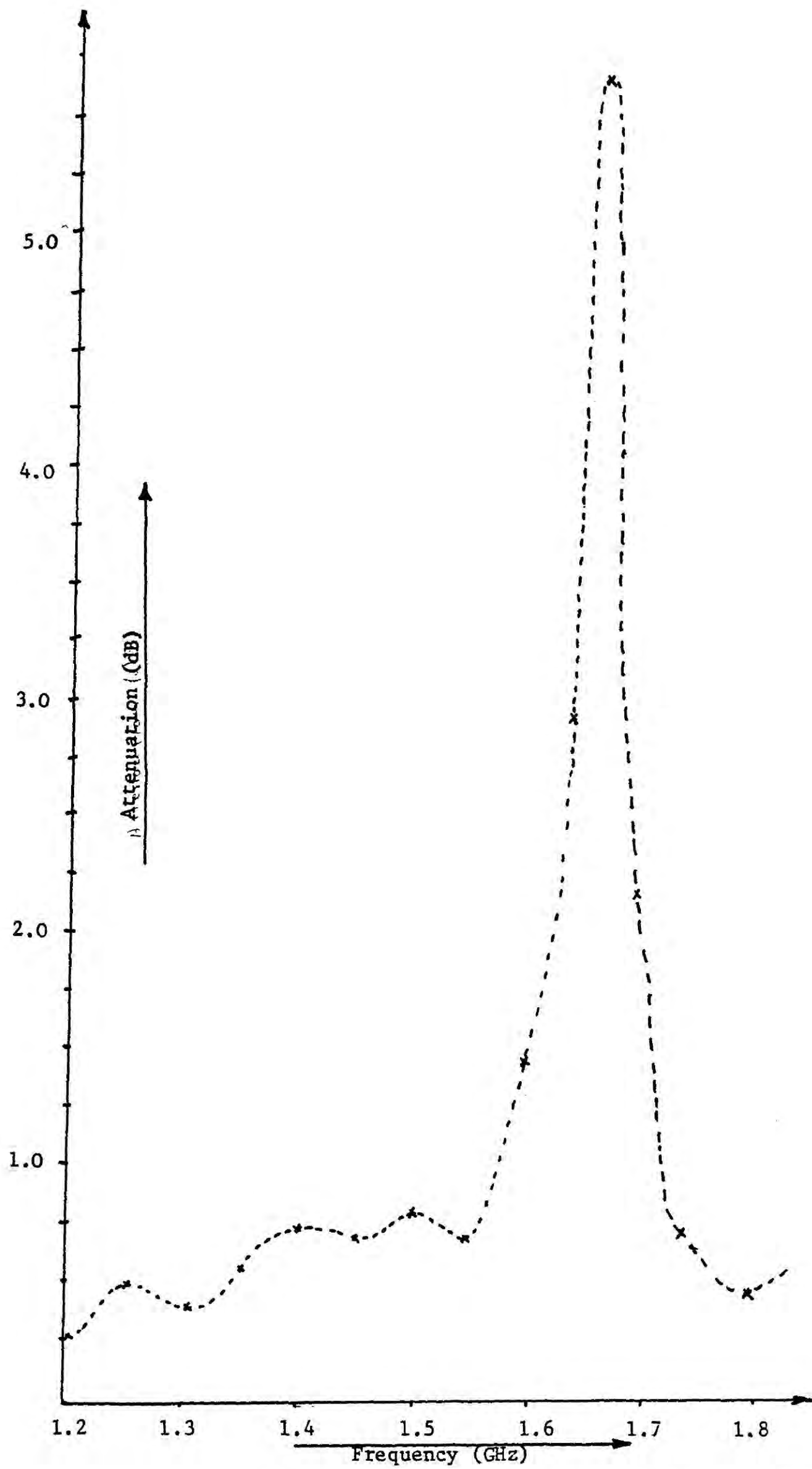
Figure 5.16(a)   Frequency Response of a Single Section Stopband
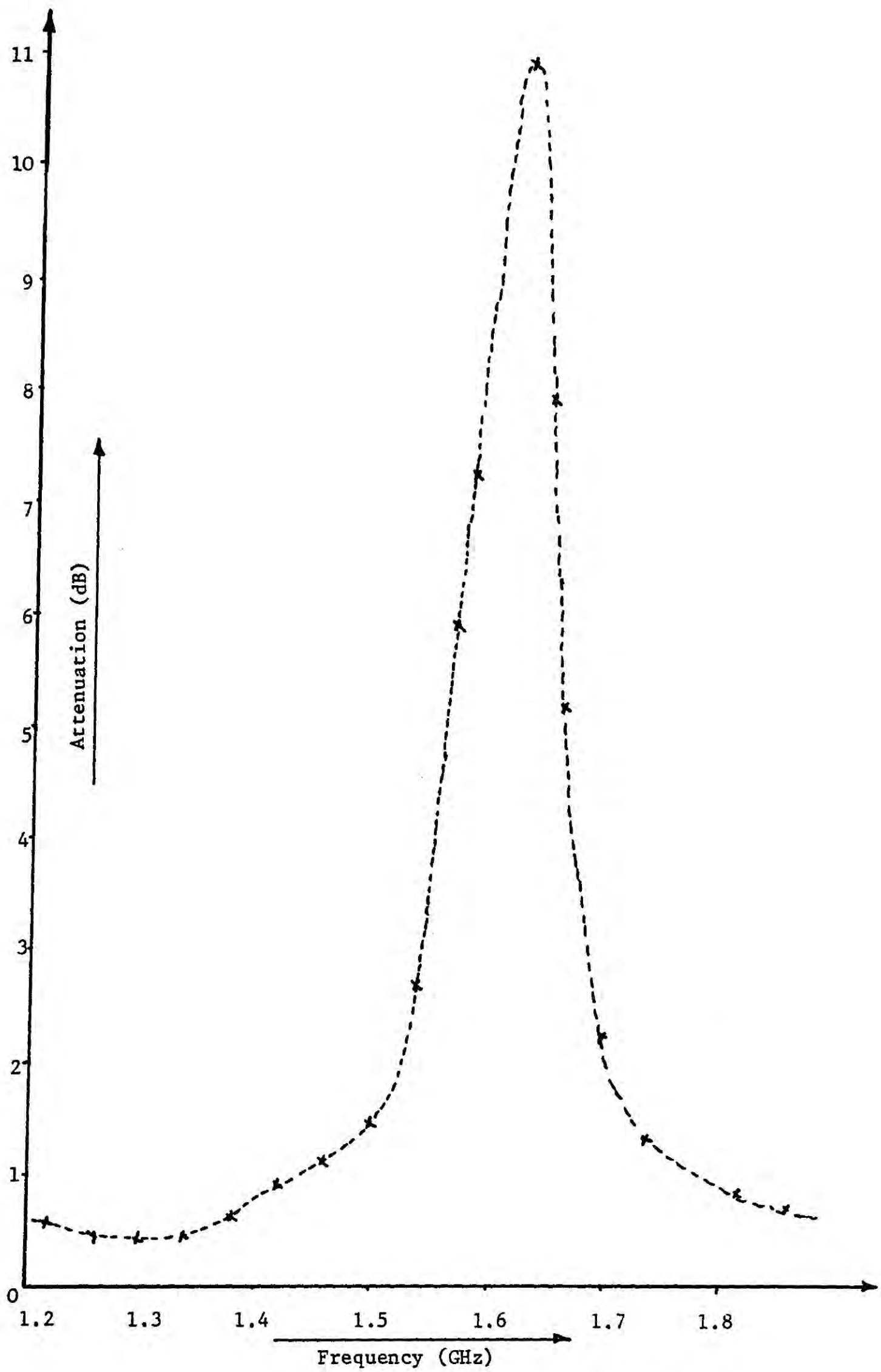
Filter Using PCB.

Figure 5.16(b)   Frequency Response of a Double Section

Stopband Filter Using PCB.
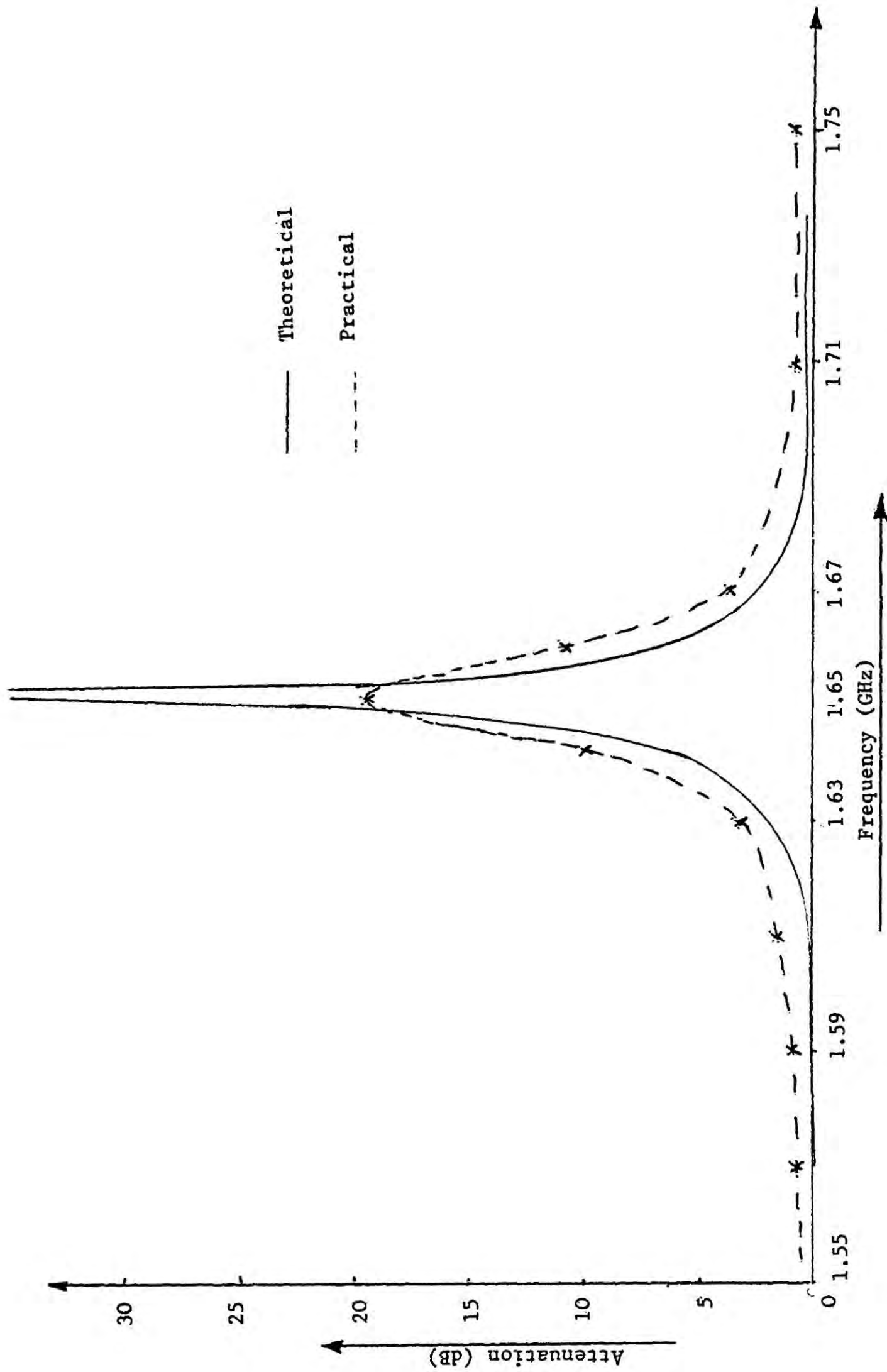
Figure 5.17   Theoretical and Practical Frequency Responses of a SingleSection

Microstrip Stopband Filter using Duroid Substrate
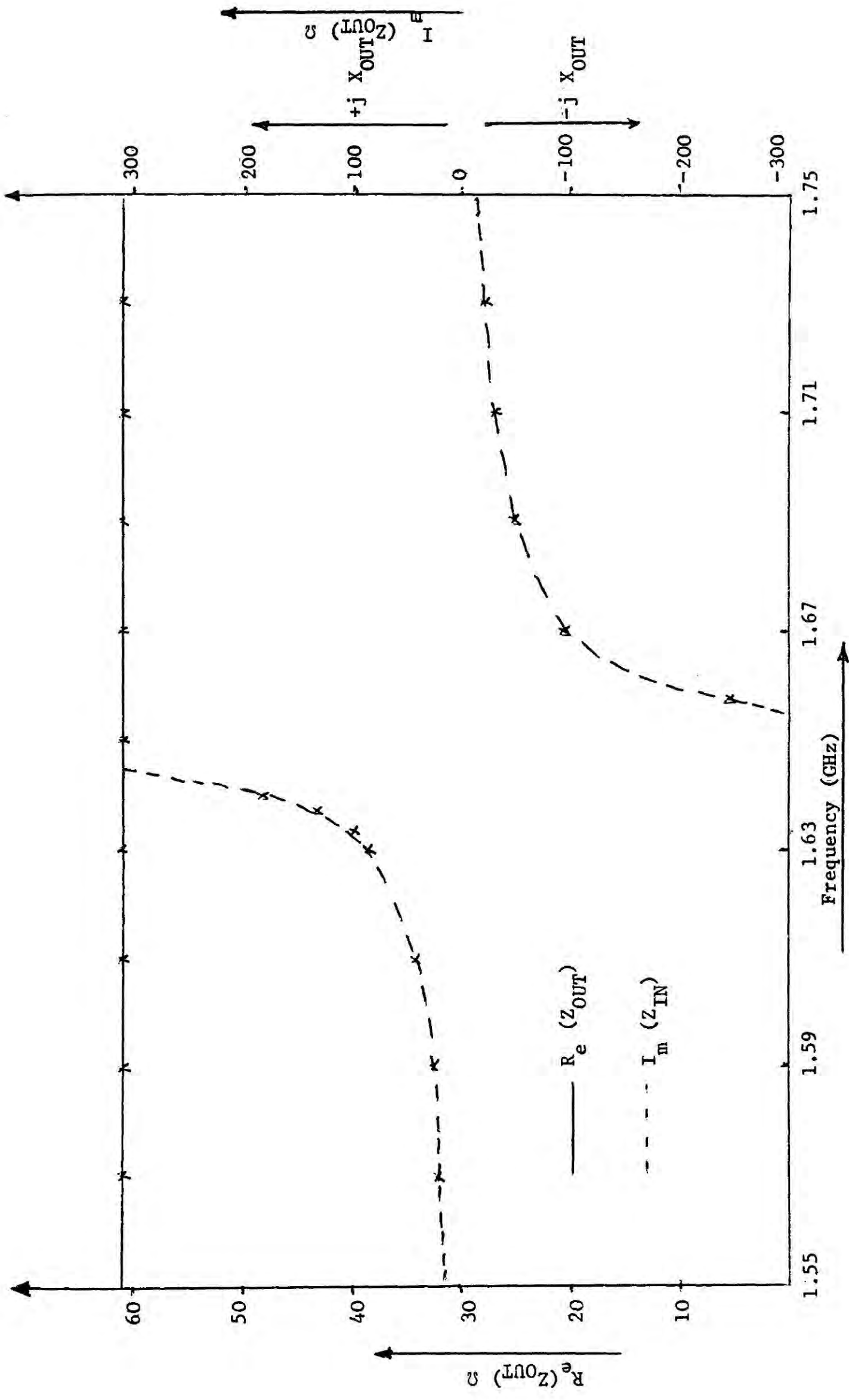
Figure 5.18(a) Frequency Response of the Output Impedance of the Stopband Filter
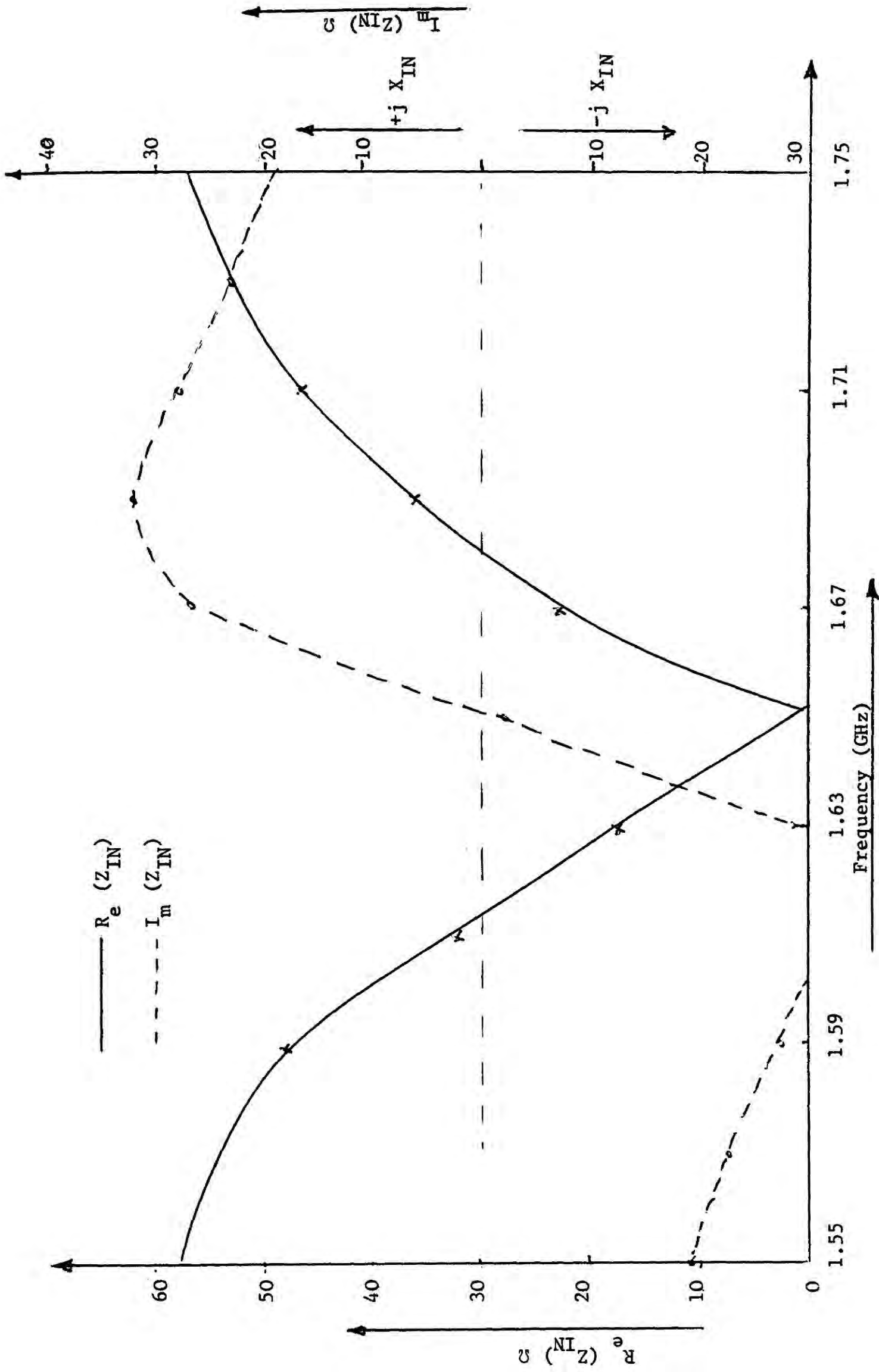
Figure 5.18(b) Frequency Response of the Input Impedance of the Stopband Filter
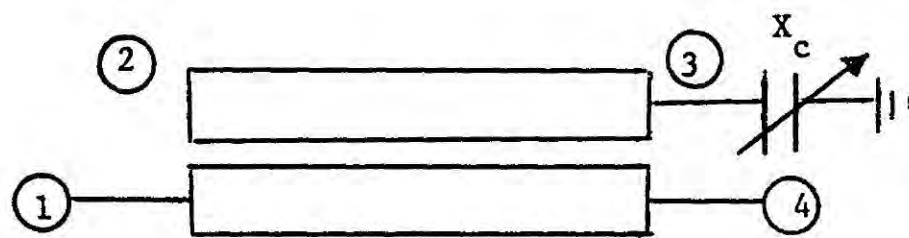
Figure 5.19 Tunable Bandstop Filter
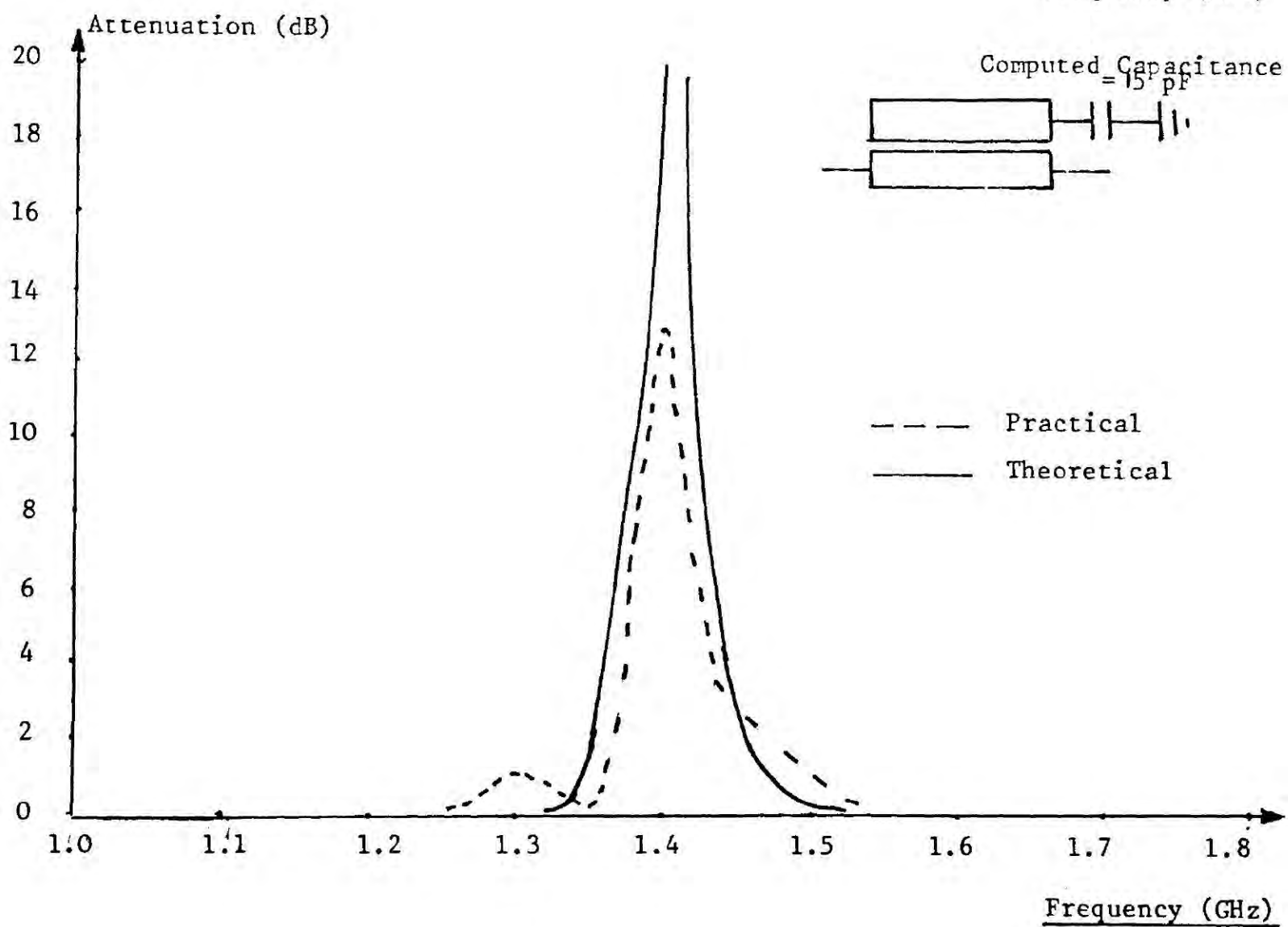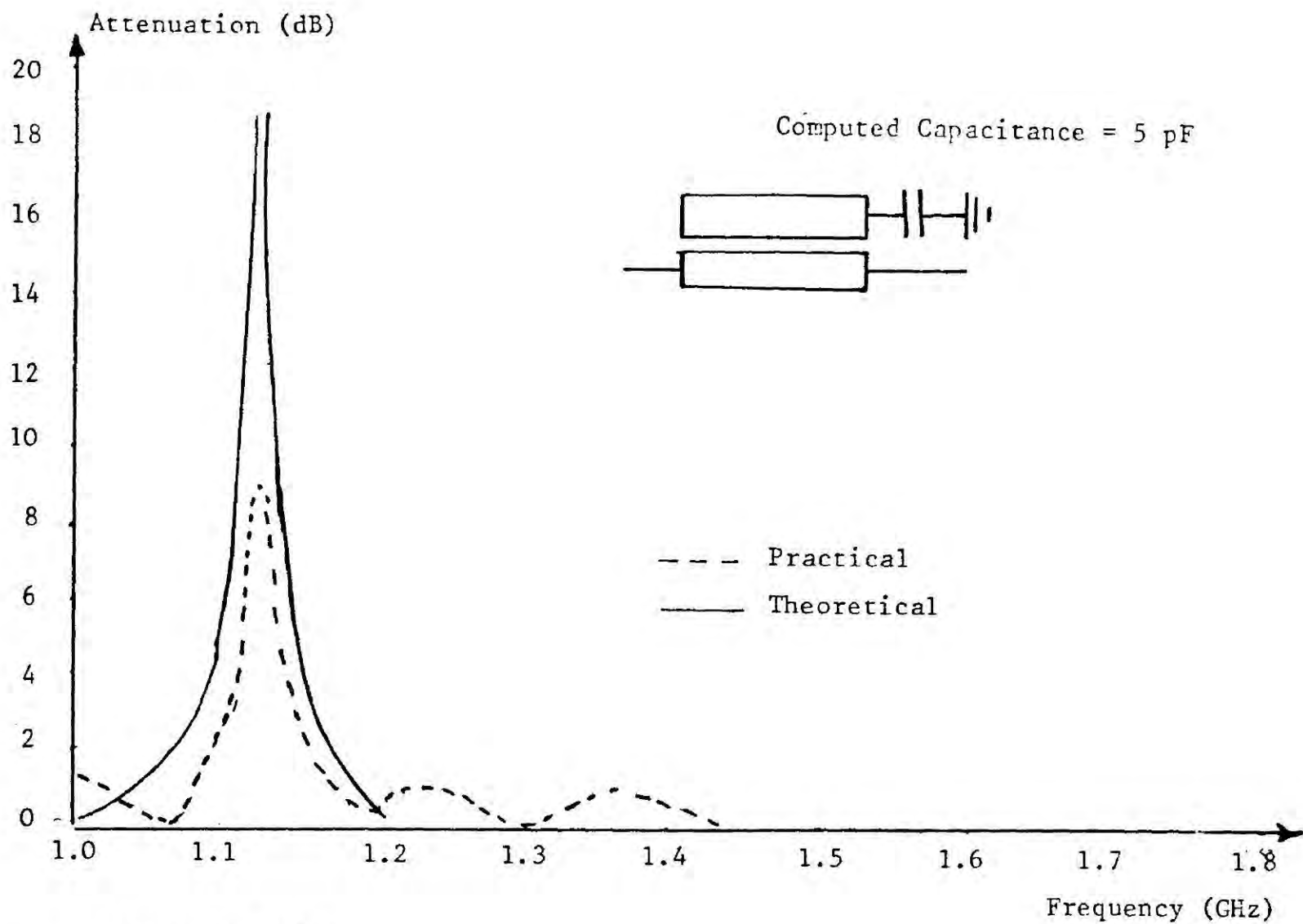
Figure 5.20   Frequency Response of a Tunable Bandstop Filter
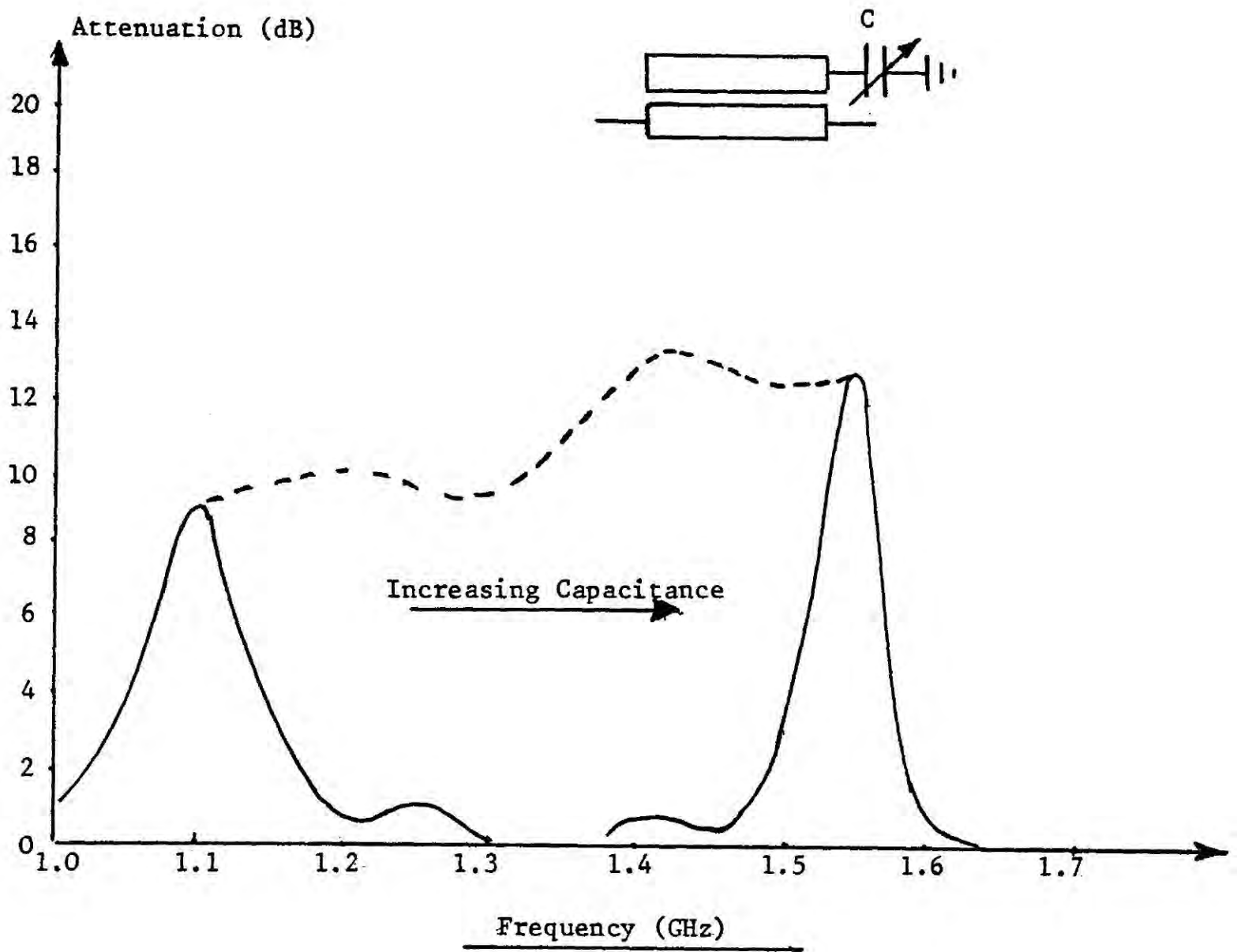
Figure 5.21 General Frequency Response of a Tunable Stopband Filter
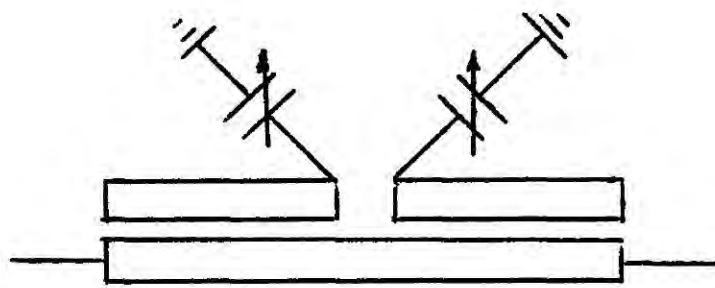
Figure 5.22 Two-section Tunable Bandstop Filter

Attenuation

26
24
22
20
18
16
14
12
10
8
6
4
2
0

1.0 1.1 1.2 1.3 1.4 1.5 1.6 1.7 1.8 1.9 2.0
Frequency (GHz)

Theoretical
Practical

$C_1 = 14$ pF
$C_2 = 30$ pF
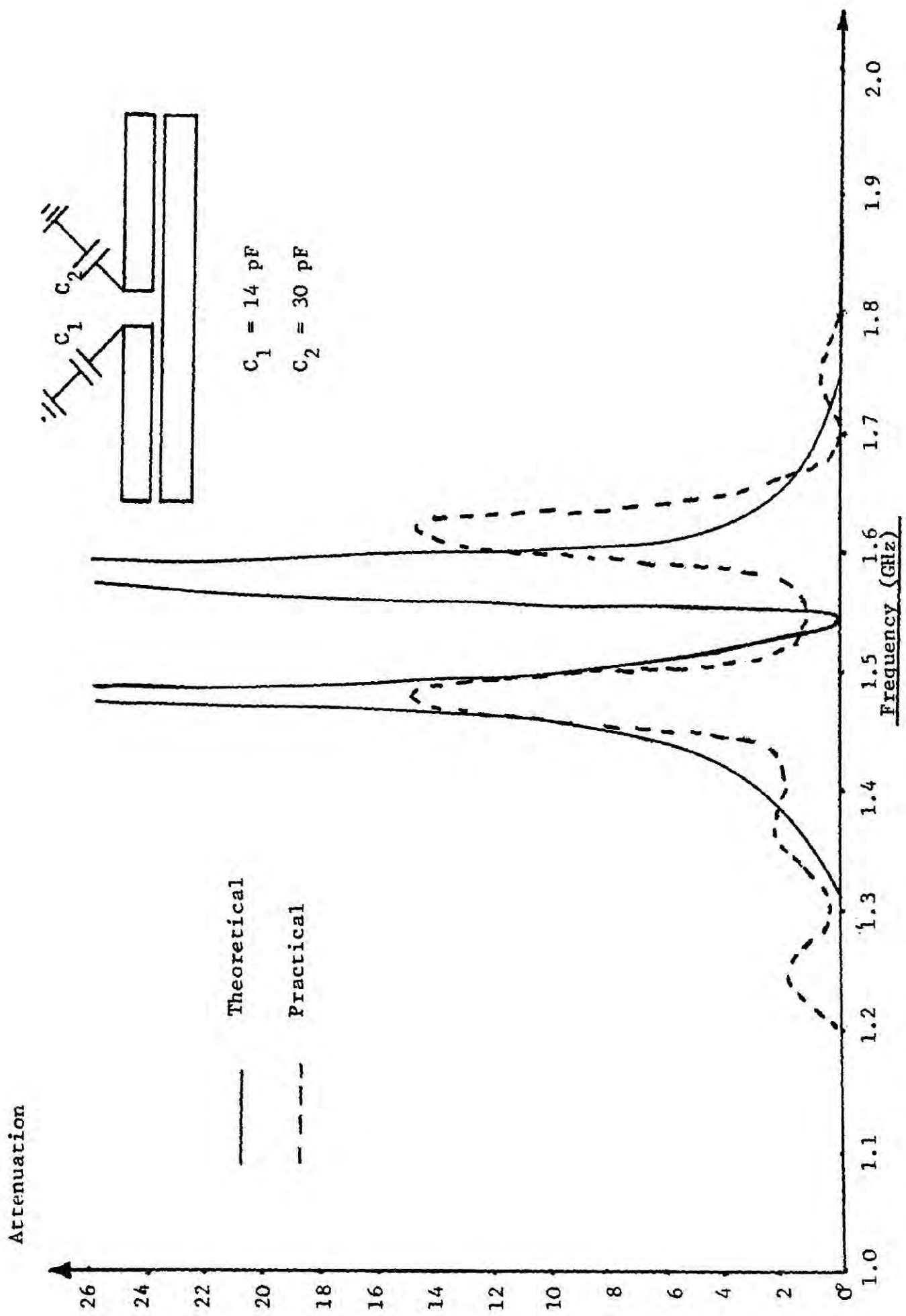
Figure 5.23 Frequency Response of Two-Section Stopband Filter Tuned to Different Frequencies
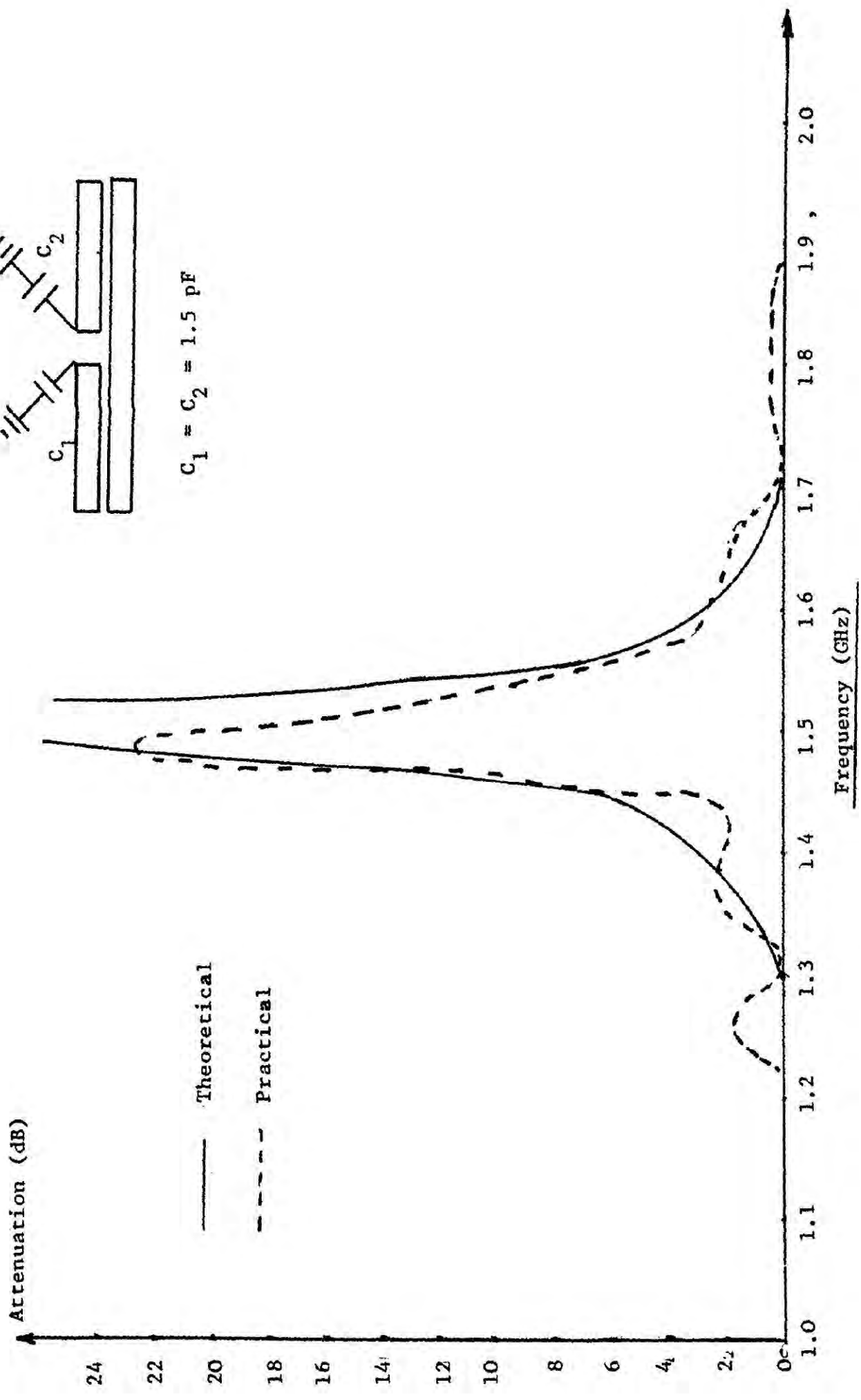
Figure 5.24 Theoretical and Practical Frequency Response of the Two-Section Stopband Filter Tuned to the Same Frequency
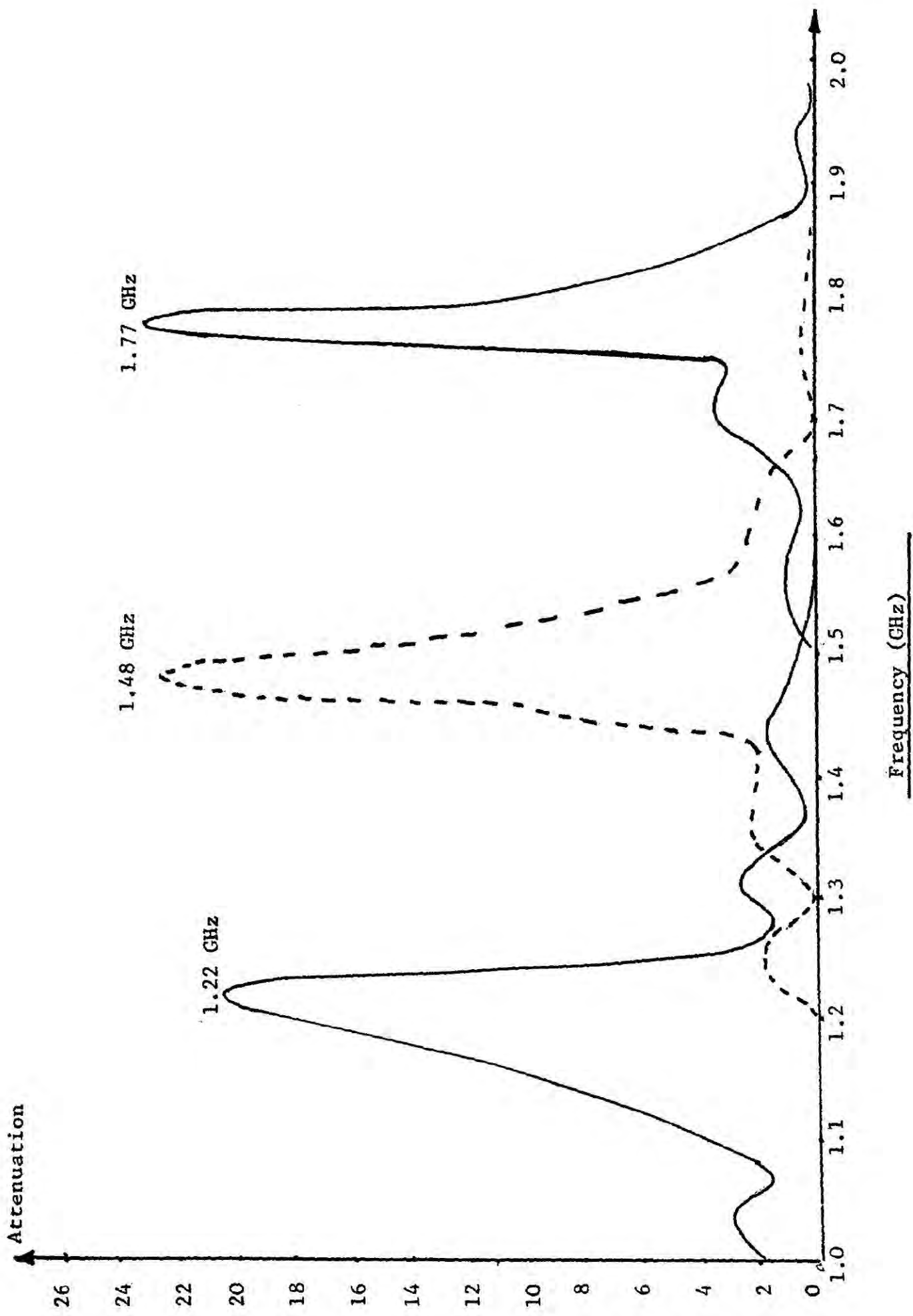
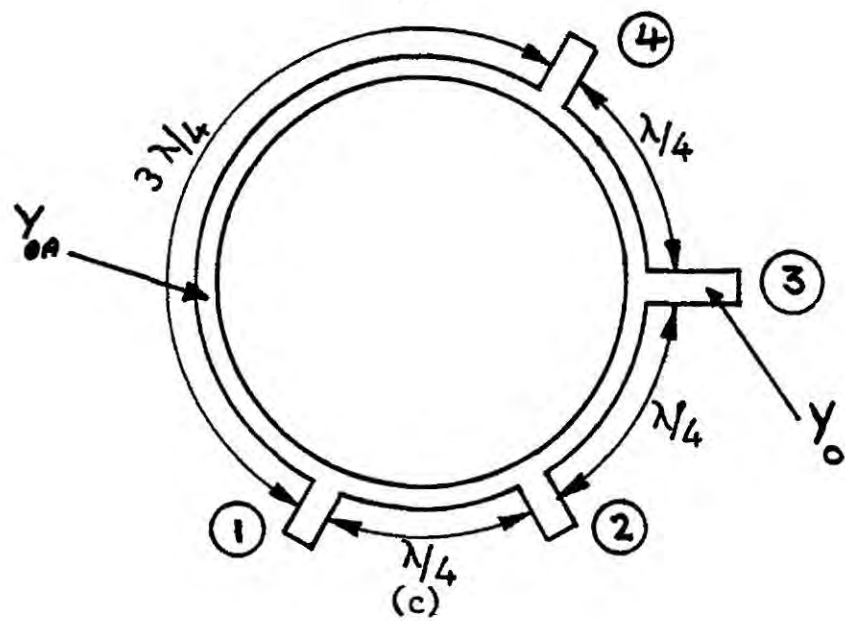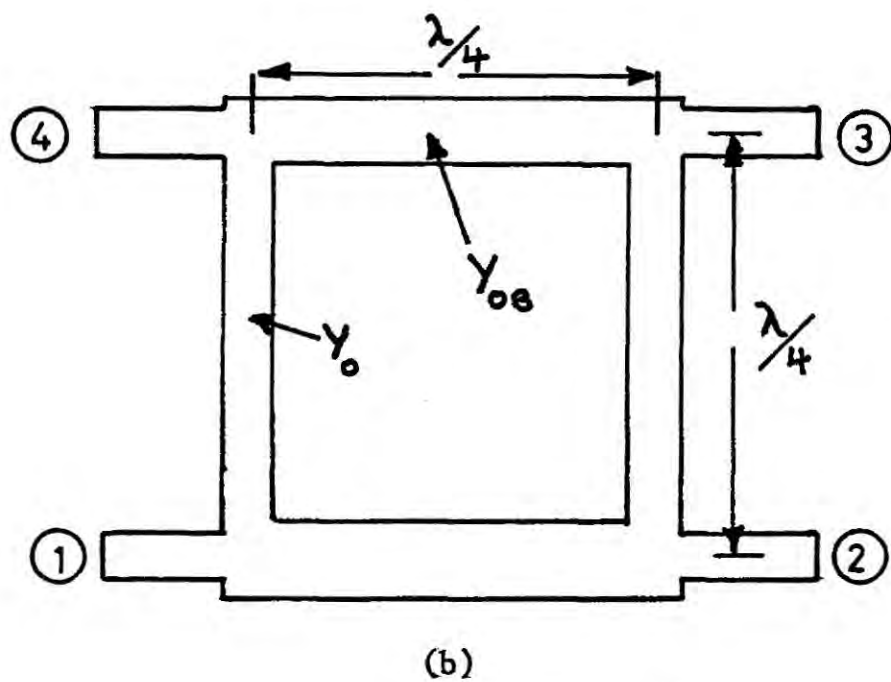Figure 5.25 General Frequency Response of the Two-Section Stopband Filter Tuned to the Same Frequency
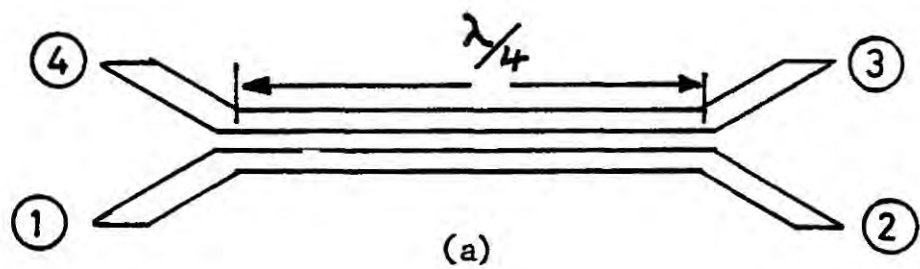
Figure 5.26 Microsrtip Directional Couplers
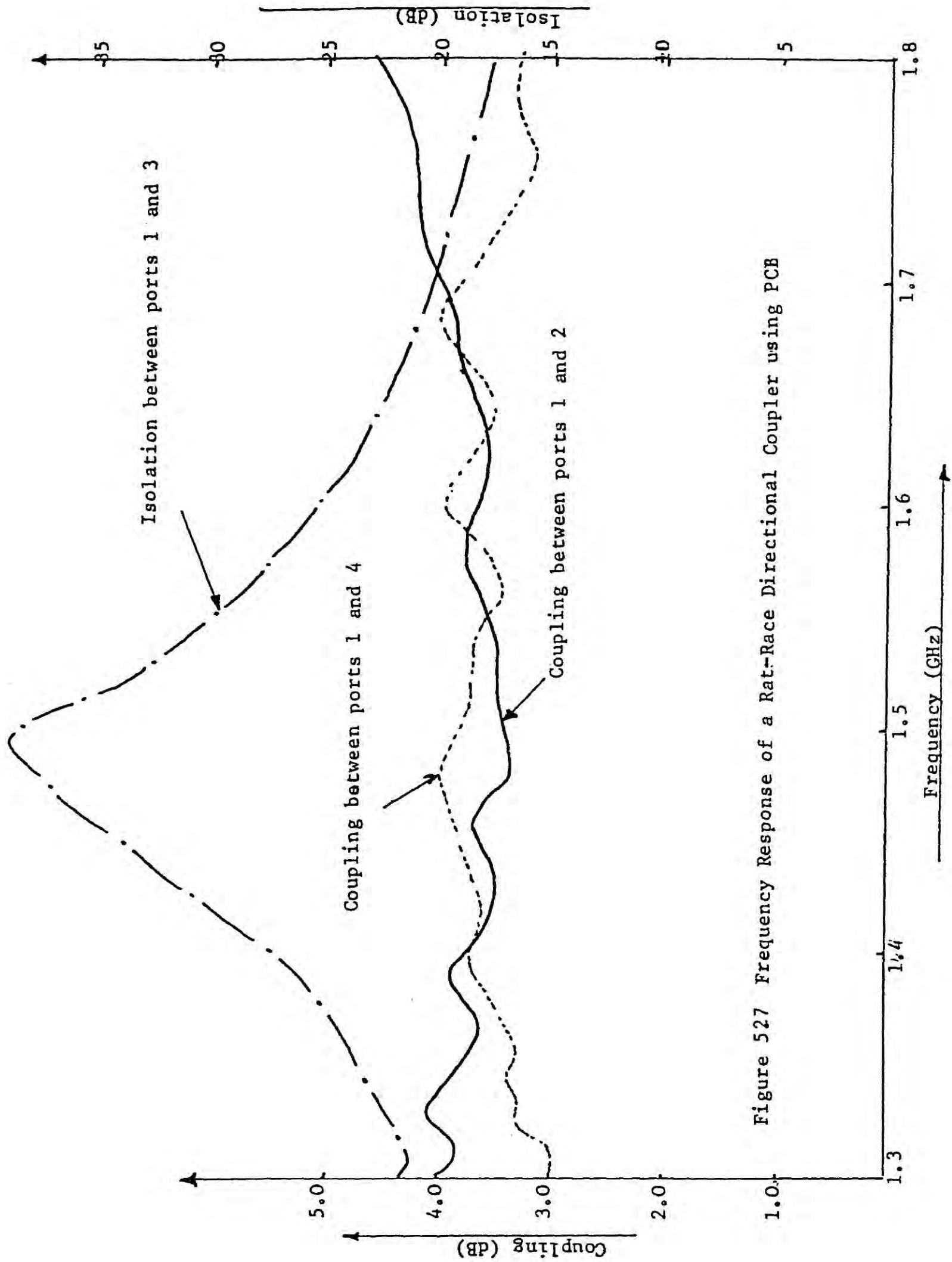
(a) Edge-coupled

(b) Two-Branch

(c) Rate-Race

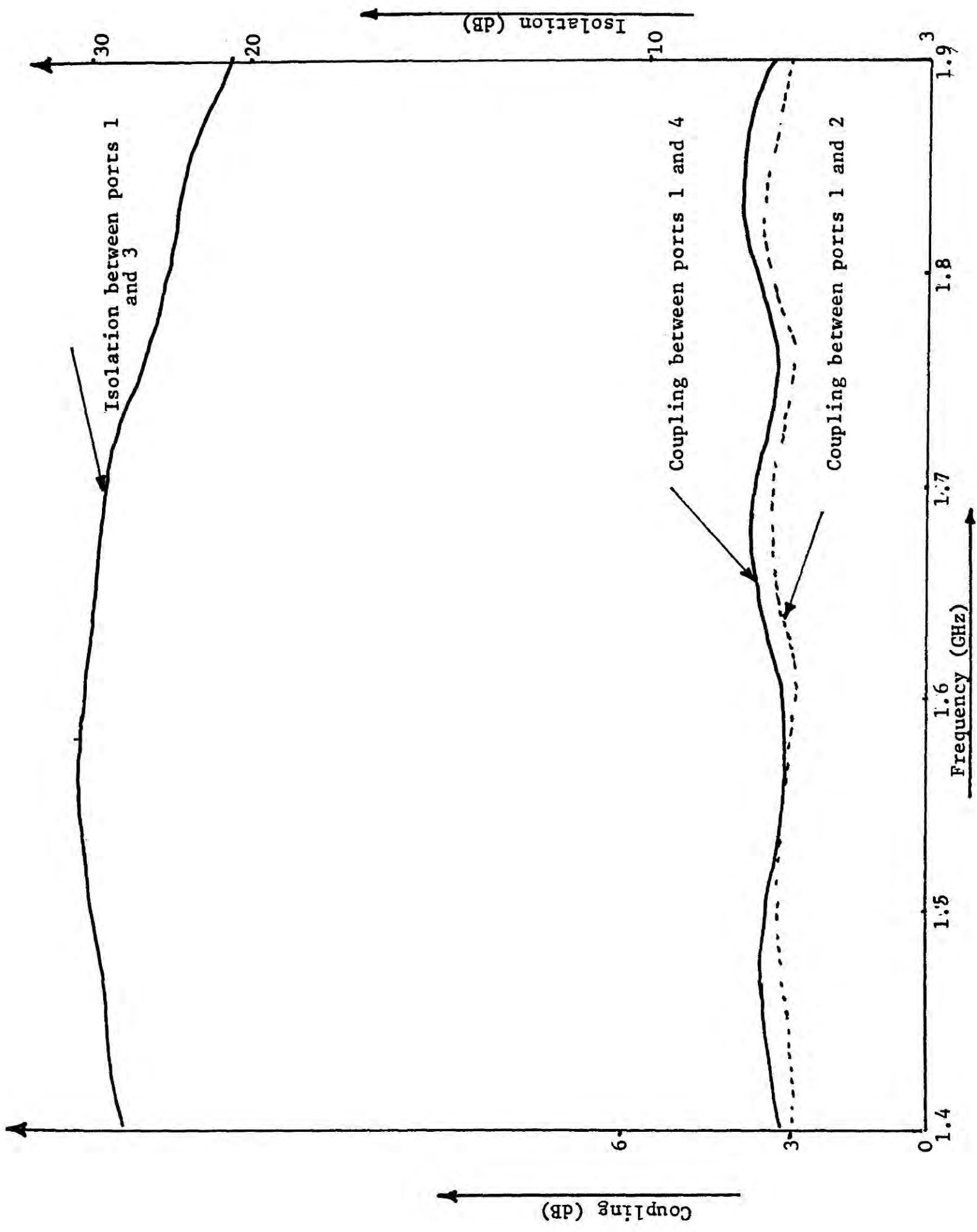Figure 527 Frequency Response of a Rat-Race Directional Coupler using PCB

Figure 5.28, Frequency Response of a Rat-Race Directional Coupler using Duroid
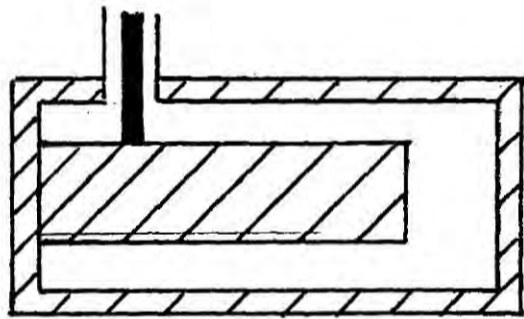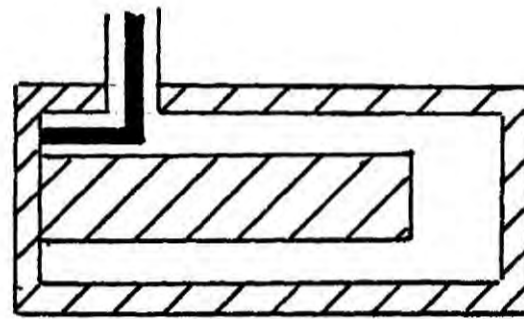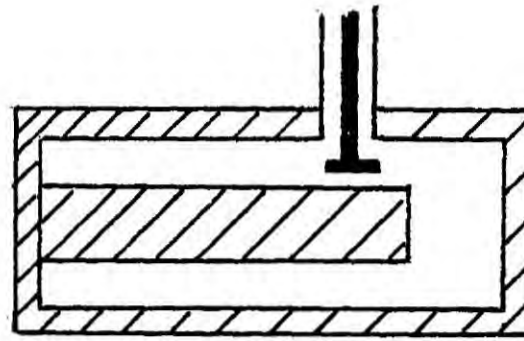
Figure 5.29 Three types of coupling for a co-axial
cavity

(a) capacitive coupling
(b) Inductive coupling
(c) Direct coupling

Figure 5.30 Equivalent Circuit of the Coaxial Cavity

VARIABLE
CAPACITOR

20 MIN. HT.

57·7

22

COUPLING COILS
ø13 SILVER WIRE

10

8

ø23

ø16 FINE
THRD.

ø14

ø9·5

ø6 SCREW

10

1

24·4

36·8

10

1

50

ø 28·5

ø16

18

43

Figure 5.31   Details of the Cavity Filter

Figure 5.32 Frequency Responses of the Variable Coaxial Cavity Filter

CHAPTER VI

Determination of the Diode Parameters and the
Performance of Broadband Lattice Mixers

6.1 Introduction

For the analyses of lattice mixers, r_s, α and r_b play a principal role and the accuracy of their values is of great importance. Initially, therefore, the methods used in the determination o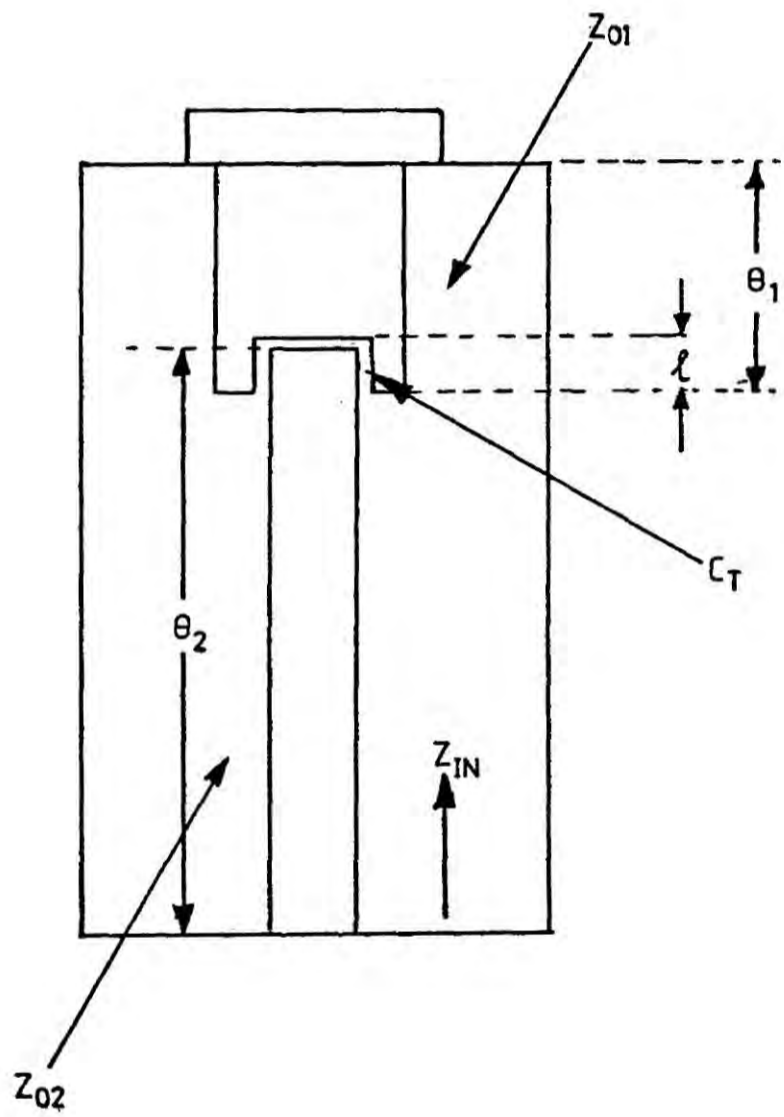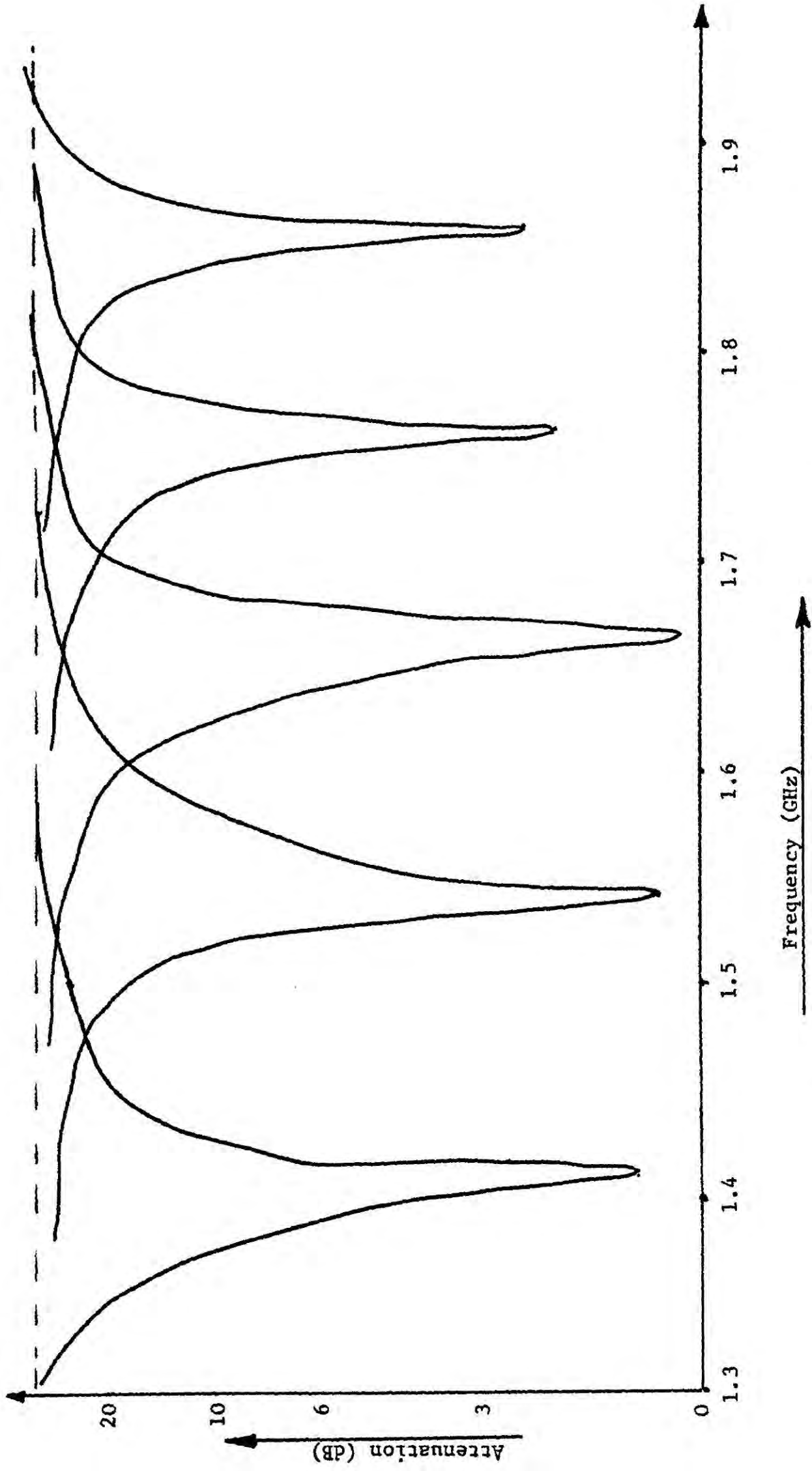f these parameters are discussed in this chapter. Then using these diode parameters a theoretical relationship between the normalized current drive and the available local oscillator power is derived. This is done as it is not possible to measure current directly, especially at very high frequencies, but it is possible in practice to measure available power.

Finally, in terms of the determined diode parameters, this chapter examines how the conversion loss of a broadband lattice varies with local oscillator drive for different terminations at the i.f. port. The results obtained in practice are then compared with the theoretical predictions.

6.2 Experimental Measurement of the Diode Parameters

The relationship between the current, I, flowing through a diode and the diode junction voltage, V_j, is normally expressed in the form [1, 2]

$$I = I_s (e^{qV_j/nKT} - 1) \qquad\qquad 6.1$$

where the constant, n, is a function of the donor density [3]. It is convenient to rewrite equation 6.1 in the form

$$I = I_s (e^{\alpha(V_A - Ir_s)} - 1) \qquad\qquad 6.2$$

where V_A is the voltage measured across the accessible terminals of the diode, r_s is the diode series resistance and $\alpha = {}^q/nKT$ is a constant for a given diode.

The above diode parameters α, r_s and r_b the diode incremental resistance at the origin have been used to establish the performance characteristics of the lattice mixers. To measure these parameters in practice it is convenient to consider two regions, A and B of the diode characteristic shown in Figure 6.1 [4].

In the region A of the diode characteristic the current I flowing through the diode is small so that the following approximations maybe made:

(i) $Ir_s \ll V_A$

(ii) $I \gg I_s$

and equation 6.2 can be expressed in the form

$$\ell n(I) = \ell n(I_s) + \alpha V_A \qquad\qquad 6.3$$

which is that of a straight line from which the parameters, α and I_s
can be easily obtained.

In the region B of the diode characteristic, where $I \gg I_s$ and
the effect of the potential drop Ir_s cannot now be neglected, equation
6.2 can be expressed in the form

$$\ell n \ (I/e^{\alpha V_A}) \simeq \ell n \left(I_s\right) - \alpha r_s I \qquad 6.4$$

Equation 6.4 again is in the form of a straight line from which the
parameter r_s can be determined.

The three diode parameters for a number of diodes, type HP 2811
were obtained using an experimental circuit shown in Figure 6.2. The
voltage V_A was measured with a voltmeter having a high input impedance
while the current I was determined by measuring the voltage across an
accurately known resistor.

Typical results obtained for a given diode are shown in Figures
6.3 and 6.4 and the results obtained for the four diodes are summarized
in Table 6.1.

Diode	$r_s(\Omega)$	α	$I_s(A)$	$r_b(\Omega)$
1	11.49	33.25	$6.5 \ 10^{-9}$	$4.59 \ 10^7$
2	10.87	35.16	$7.8 \ 10^{-9}$	$3.65 \ 10^7$
3	11.47	35.16	$8.85 \ 10^{-9}$	$3.98 \ 10^7$
4	11.83	35.33	$7.15 \ 10^{-9}$	$3.96 \ 10^7$

Table 6.1

The average diode constants for the four diodes were:

$$r_s = 11.42\Omega, \qquad r_b = 4.05 \ 10^7\Omega, \qquad \alpha = 34.72 \ V^{-1}$$

and these were used to determine the performance of the three types of
lattice mixers.

6.3 Analysis of the Local Oscillator Circuit

6.3.1 Introduction

The performance of the different types of the lattice mixers has been obtained as a function of the normalised local oscillator current drive, X. At microwave frequencies, however, it is not possible to measure current directly but the two fundamental quantities that can be measured in practice using available commercial instruments are power and voltage reflection coefficient. To compare the performance of practical mixers with that predicted by theory it is necessary to establish a relationship between normalized current drive, X, and one the voltage reflection coefficient at the local oscillator frequency, ω_p and two the available local oscillator power (P_A).

6.3.2 Relationship Between the Local Oscillator Power Delivered to the Diode Network and the Normalised Current Drive

The equivalent circuit of the lattice network of diodes as 'seen' by the local oscillator is shown in Figure 6.5. The voltage, V(t), developed across the diode is

$$V(t) = 2I_p \left[\cos \omega_p t \right] R(t) \qquad 6.5(a)$$

where

$$R(t) = \frac{r_+(t) \cdot r_-(t)}{2(r_+(t) + R_-(t))} \qquad 6.5(b)$$

Equation 6.5(b) may be expressed in terms of the diode parameters r_b, r_s and the normalised current drive, X(t), and, s(t), the switching function, i.e.

$$R(t) \simeq \frac{1}{4} \left[2r_s + r_b/(1 + X(t) \, s(t)) \right] \qquad 6.6$$

provided $r_b \gg r_s$

Substituting equation 6.6 into equation 6.5(a) for R(t) results

in

$$V(t) = \tfrac{1}{2} \left[I_p \cos \omega_p t \right] \left[2r_s + r_b/(1 + X(t) \ s(t)) \right] \qquad 6.7$$

The fundamental harmonic of the periodic voltage V(t) at the

local oscillator frequency, ω_p, is

$$A_1 = \frac{I_p}{2\pi} \int_{-\pi/2}^{3\pi/2} \left[\cos^2 \omega_p t \right] \left[2r_s + r_b/(1 + X(t) \ s(t)) \right] d(\omega_p t)$$

$$6.8$$

Equation 6.8 can be evaluated by splitting the integral into two

ranges: $- \ ^\pi/2 \leqslant \omega_p t \geqslant \ ^\pi/2$ and $^\pi/2 \leqslant \omega_p t \leqslant \ ^{3\pi}/2$ and results in

$$A_1 = I_p \ (r_s + 2r_b/X\pi) \qquad 6.9$$

Finally, the power P_D delivered to the lattice network of diodes,

at the local oscillator frequency, ω_p, is

$$P_D = (2I_p/\sqrt{2})(A_1/\sqrt{2})$$

$$= \frac{4X^2}{r_b^2 \alpha^2} \ (r_s + 2r_b/\pi X) \qquad 6.10$$

Equation 6.10 agrees with that obtained by Kulesza[5].

6.3.3 Time Domain Analysis of the Local Oscillator Circuit

It is not possible to measure directly the local oscillator power

delivered to the lattice circuit of diodes, but it is possible to measure

the available local oscillator power. Hence, it is necessary to establish

a relationship between these two quantities so that the actual

power delivered to the diodes can be found. This relationship is

more easily obtained by using time-domain analysis of the local oscillator

circuit shown in Figure 6.6, where the non-linear resistance characteristic

of the diodes is replaced by a linear time-varying resistance R(t).

As the local oscillator current is constrained to be sinusoidal by the filter the relationship between incident and reflected voltages is given by

$$a + b_n = v(t) = 2I_p . R(t) . \cos \omega_p t \qquad 6.11$$

The incident voltage 'a' is defined as

$$a = E_p \cos \omega_p t \qquad 6.12(a)$$

and the reflected voltage b_n is defined as

$$b_n = \sum_{n=1}^{\infty} B_n \cos n\omega_p t \qquad 6.12(b)$$

The fundamental harmonic of the periodic voltage $v(t)$ of equation 6.11 is given by equation 6.9, and therefore

$$b_1 = I_p \left[r_s + \frac{2r_b}{\pi X} \right] \cos \omega_p t - a \qquad 6.13$$

The reflection coefficient ρ at the local oscillator frequency, ω_p, is given by

$$\rho = \frac{b_1}{a} = \frac{I_p \left[r_s + \frac{2r_b}{\pi X} \right] - E_p}{E_p} \qquad 6.14$$

For the local oscillator circuit shown in Figure 6.6, and using equation 6.9, the relationship between E_p and I_p at the local oscillator frequency, ω_p, is given by

$$\frac{E_p}{I_p} = R_o + \frac{r_s}{2} + \frac{r_b}{\pi X} \qquad 6.15$$

where R_o is the characteristic impedance.

Combining equation 6.15 and 6.14 results in

$$\rho = \frac{\left(r_s + 2r_b/\pi X\right)}{\left(R_o + \dfrac{r_s}{2} + \dfrac{r_b}{\pi X}\right)} - 1 \qquad\qquad 6.16$$

where the voltage reflection coefficient ρ is now a function of the normalized local oscillator drive X.

Finally, the relationship between the power available from the local oscillator, P_A, and the power delivered to the lattice circuit of diodes, P_D, is given by

$$P_D = P_A \left(1 - |\rho|^2\right) \qquad\qquad 6.17$$

Using equations 6.10, 6.16 and 6.17 it is possible to obtain a relationship between the available power from the local oscillator P_A, the voltage reflection coefficient, ρ, the power delivered to the lattice network of diodes, P_d, as a function of the normalized current drive X. Figure 6.7 shows the predicted relationship between P_D, P_A, and X while Figure 6.8 shows the predicted relationship between the voltage reflection coefficient, ρ, and the available local oscillator power P_A.

6.4 Predicted and Practical Performance of a Broadband Mixer

6.4.1 Introduction

In the case of a broadband mixer, the terminations at the image and r.f. signal ports are the same and the theoretical minimum conversion loss that can be achieved is 3 dB (see section 3.3.3). The necessary terminations at the r.f. and i.f. ports to obtain this minimum conversion loss were shown to be

$$R_{S_{OPT}} = \frac{2}{\pi} (2 \ r_b r_s)^{\frac{1}{2}} \qquad\qquad 3.46(a)$$

$$G_{L_{OPT}} = \frac{2}{\pi} (2/r_b r_s)^{\frac{1}{2}} \qquad\qquad 3.46(b)$$

which, however, are extremely difficult to realize in a mixer using practical diodes operating at microwave frequencies.

An alternative approach in the design of a broadband mixer is to choose terminations so that the r.f. and i.f. ports are matched. At large local oscillator drive it has been shown in section 3.3.3 that the conversion loss obtained is 4.77 dB and the required terminations then are

$$R_{s_m} \simeq 4 \ r_s \qquad\qquad 3.52(a)$$

$$G_{L_m} \simeq 4/3\pi^2 r_s \qquad\qquad 3.52(b)$$

These terminations can be more readily realized in case of a practical mixer, although a deterioration of 1.77 dB in the conversion loss is the penalty.

The object of the next sections is to investigate experimentally the performance of a simple broadband mixer for different terminations at the i.f. ports and to compare the practical results with those predicted by theory.

6.4.2 Effect of the Termination at the I.F. Port on the Conversion Loss of a Broadband Lattice Mixer

A 3 x 3 'h' matrix describing a general mixer

$$
\begin{bmatrix}
h_{11} & h_{12} & h_{13} \\
-h_{12} & h_{22} & -h_{12} \\
h_{13} & h_{22} & h_{11}
\end{bmatrix}
$$

6.18

reduces to the following 2 x 2 matrix when the image port is terminated by a source impedance R_s

$$
\begin{bmatrix}
H_{11} & H_{12} \\
-H_{12} & H_{22}
\end{bmatrix}
$$

6.19(a)

where

$$H_{11} = h_{11} (1 - a^2/R)$$

$$H_{12} = h_{12} (1 - a/R)$$

6.19(b)

$$H_{22} = h_{22} (1 + k_o/R)$$

and

$$a = h_{13}/h_{11}$$

$$R = 1 + R_s/h_{11}$$

6.19(c)

$$K_o = h_{12}^2/h_{11}h_{22}$$

The corresponding expression for the conversion power loss (c.p.l.) of a mixer is given by

$$c.p.l. = 10 \log_{10} |L|$$

where

$$L = \frac{|(R_s + H_{11})(H_{22} + G_L) + H_{12}^2|^2}{4H_{12}^2 R_s G_L}$$

6.20

The H parameters of equation 6.20 are functions of the normalized local oscillator current drive X which in turn can be expressed in terms of the available local oscillator power P_A as discussed in section 6.3. Based on these theoretical relationships a computer programme was developed to show how the conversion loss varies as a function of the available local oscillator power P_A for different terminations at the IF port.

The predicted relationships between the conversion loss as a function of the available local oscillator power for different terminations at the i.f. ports are shown in Figure 6.9.

6.4.3 Practical and Predicted Relationship Between Conversion Loss and Local Oscillator Power

A low-frequency circuit model of the broadband mixer is shown in Figure 6.10. A microstrip rat-race directional coupler was designed to simulate the centre-tapped transformer at the r.f. port and to operate in the L frequency band. A coaxial cavity resonator was used in the local oscillator circuit to ensure a sinusoidal current drive while capacitors C_1 and C_2 were included to ensure that any unbalance in the circuit due to stray impedances or mismatched between the diodes is minimized. Four commercially available MINI-CIRCUITS (trade name) transformers were used in turn at the i.f. port to transform a 50Ω load impedance to: 50Ω; 100Ω; 150Ω; 450Ω as 'seen' by the mixer. The manufacturer's specification of the IF transformers used is shown in Figure 6.11 Experimentally it was found that the insertion loss of each transformer at 70 MHz IF was approximately 1.2 dB.

The conversion loss of a mixer is defined as the ratio of the output power from the mixer at the IF frequency to the input power to the mixer at the RF frequency. A Marconi power meter which is capable of measuring power in the range 1 μW to 10 mW was used to measure r.f. and i.f. power.

To ensure that the only i.f. power was measured an IF filter type F1 85L having a cut-off frequency of 185 MHz was placed between the i.f. port of the mixer and the power meter. The frequency response of the IF filter is shown in Figure 6.12 where it can be seen that an attenuation of 0.7 dB is obtained at 70 MHz.

The method of using a power meter to measure the conversion loss was checked by feeding the output from the mixer into a spectrum analyser having a frequency range from 1 MHz to 500 MHz. The spectrum analyser was calibrated by means of an HP signal generator. It was found that there was a very close agreement between the two methods and consequently the conversion loss measurement was carried out using a spectrum analyser.

For each of the four i.f. terminations the practical and predicted conversion loss as a function of the available local oscillator power are shown in Figures 6.13 to 6.16. As can be seen a good agreement is obtained between the theory and practice.

The predicted and practical results obtained are in fact similar to the conversion loss v local oscillator power characteristic claimed by different manufacturer's (Hewlett Packard, Mini-Circuits, Anzac) for broadband lattice mixers as shown in Figure 6.17. The optimum termination at the i.f. port lies between 50Ω and 100Ω, while the r.f. source resistance is approximately 50Ω so that the minimum conversion loss than can be obtained in practice is of the order 5 dB. It is interesting to note that this value of minimum conversion loss is consistent with that claimed by the three manufacturers and summarised in Table 6.2.

Manufacturer	Minimum Conversion Loss
Hewlett-Packard	5.5 dB
Anzac	6.5 dB
Mini-Circuits	6.2 dB

Table 6.2

Broad-Band Mixer designed for 1.63GH$_z$
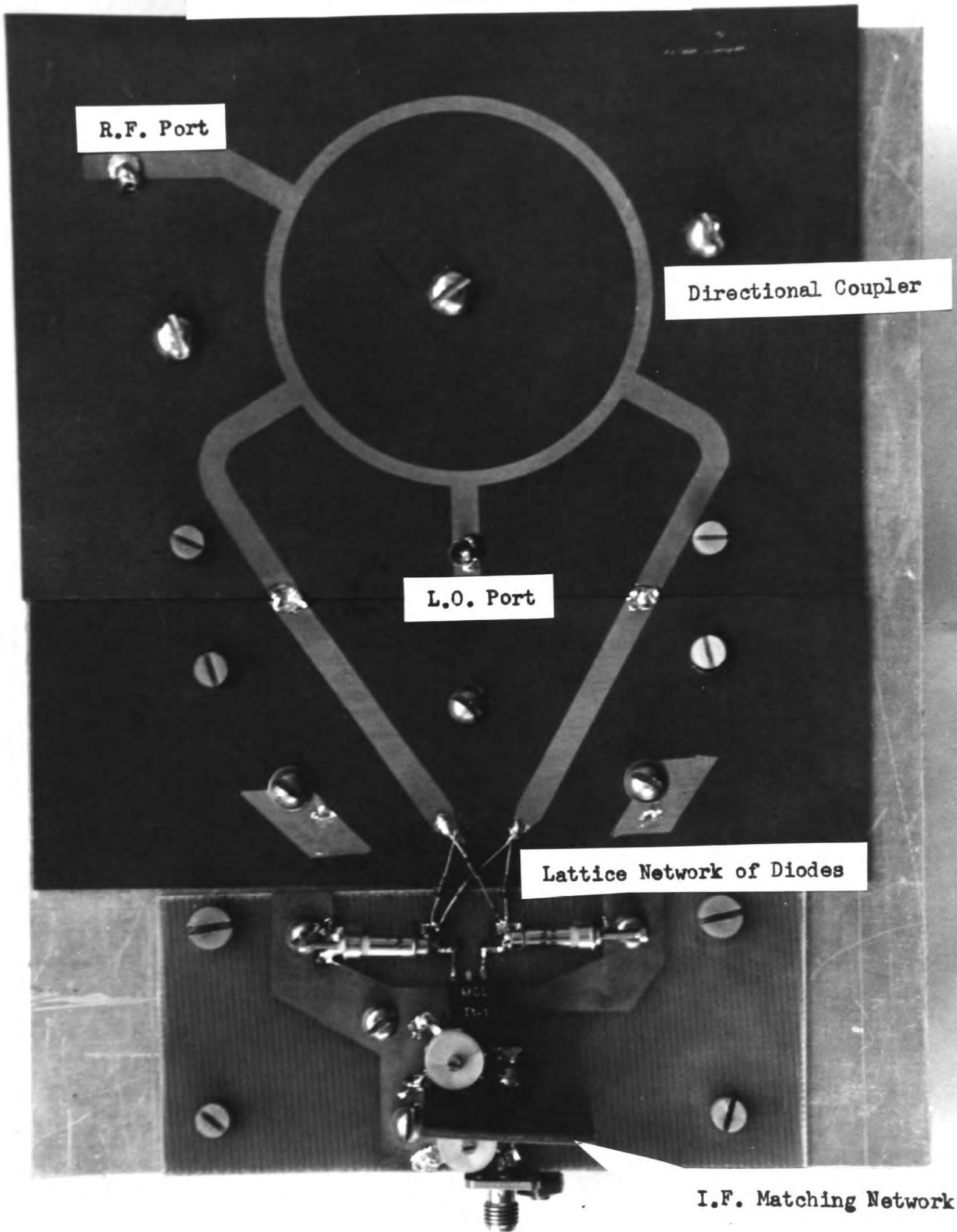
R.F. Port

Directional Coupler

L.O. Port

Lattice Network of Diodes

I.F. Matching Network

6.5 Conclusions

This chapter has discussed how in practice the diode parameters can be determined and, then in terms of those parameters, a relationship between the normalized current and the available local oscillator power was derived. This has been done in order that the mixers conversion loss measured in practice as a function of the available local oscillator power, can be compared with the predicted results. To verify the results a broadband lattice mixer was constructed and tested with different terminations at the i.f. port. It was found that there was a good agreement between the predicted and the results obtained in practice. The minimum conversion loss that can be obtained with realizable terminations at the r.f. and i.f. ports of the mixer is of the order of 5 dB and is consistent with the results claimed by different manufacturers.

6.6 References

1. Bethe, H.A., Theory of the Boundary Layer of Crystal Rectifiers, MIT Rad. Lab. Report, 43-12, 1942.

2. Rhoderick, E.H., Transport Processes in Schottky Diodes, Inst. of Physics Conference Series No. 22, Manchester, April 1974.

3. Kahng, D., Conduction Properties of the Av-n Type Si. Schottky Barrier, Solid State Electron, No. 6, 1963.

4. Katib, M.K., Evaluation of Harmonic Generating Properties of Schottky Barrier Diodes, Ph.D. Thesis, Durham University, 1976.

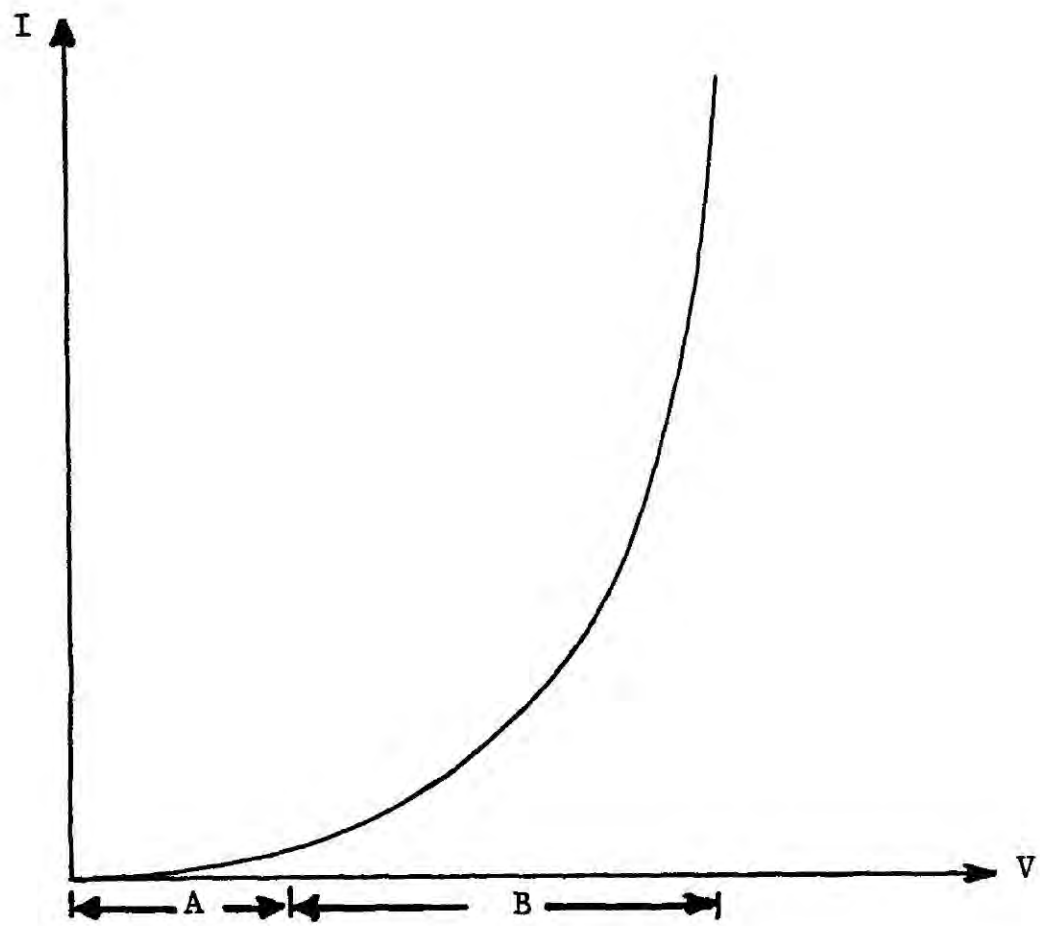5. Kulesza, B.L.J., General Theory of a Lattice Mixer, Proc. IEE 108, No. 7, 1971.

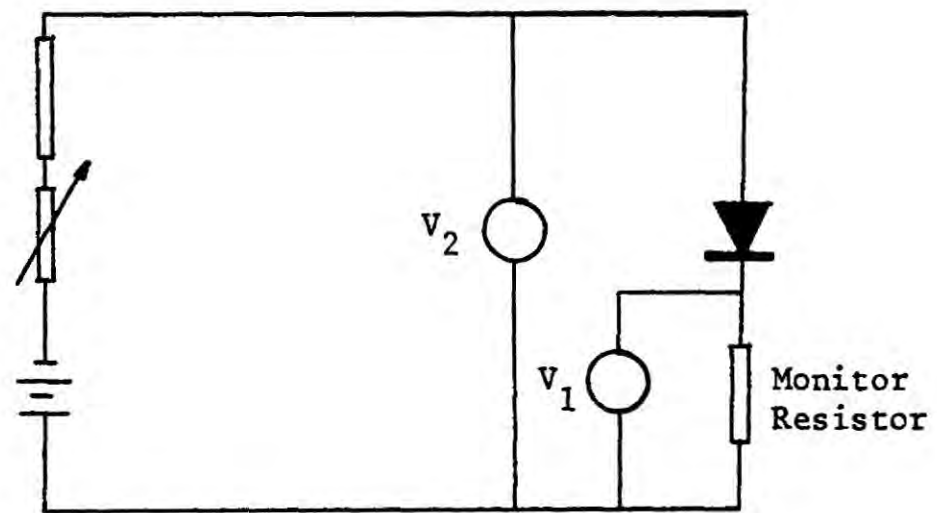Figure 6.1   Regions A and B of the Diode Static Characteristics

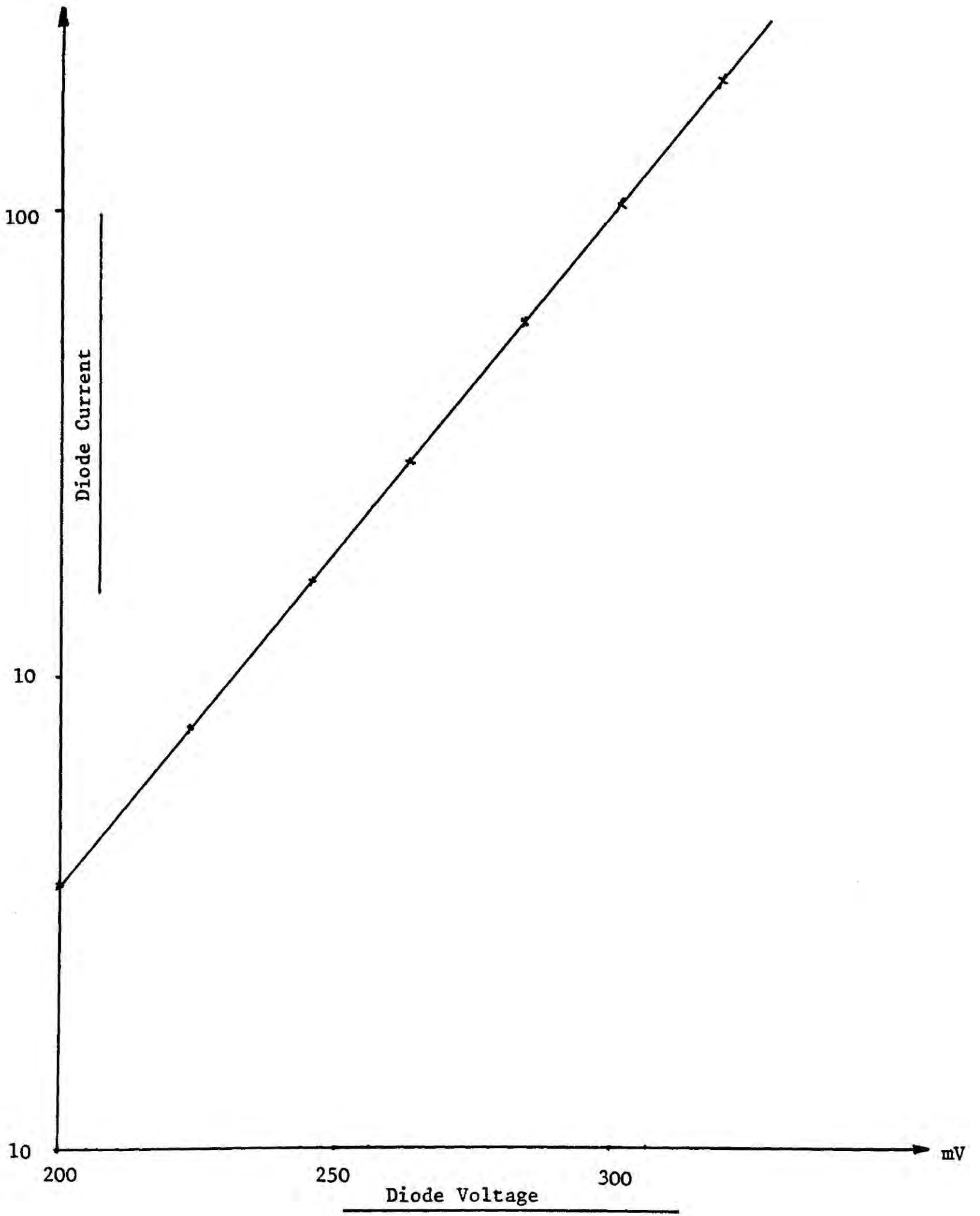Figure 6.2   Circuit Arrangement to Measure the Diode Parameters

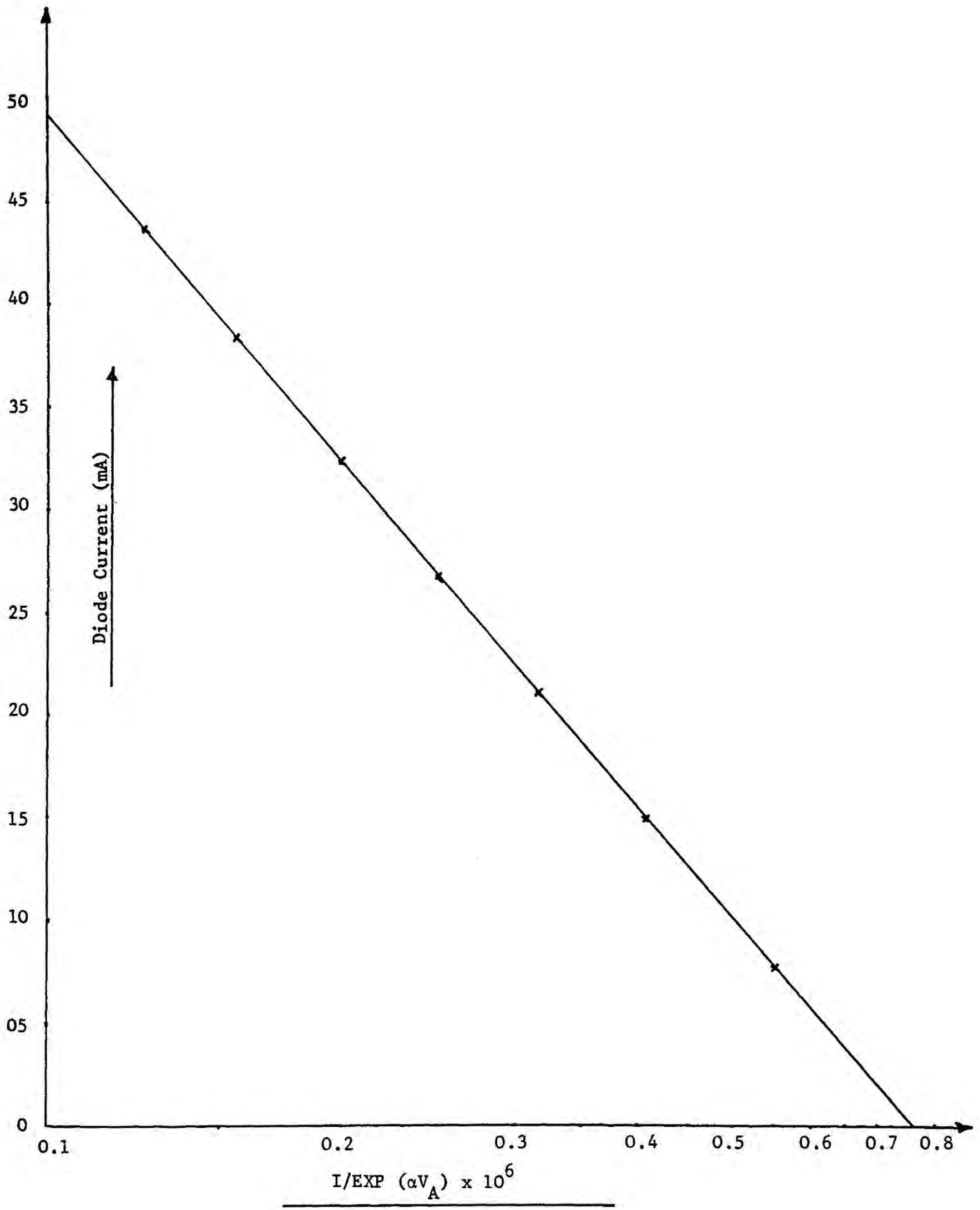Figure 6.3 Determination of the Diode Parameters α and I_s

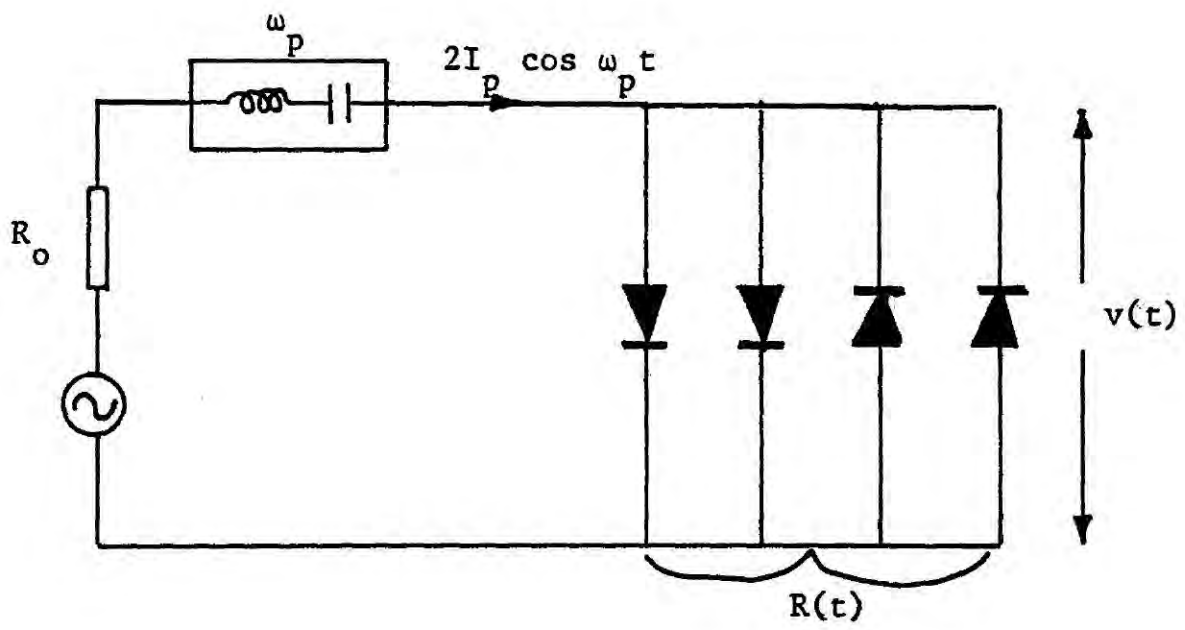Figure 6.4   Determination of the Diode Parameter r_s

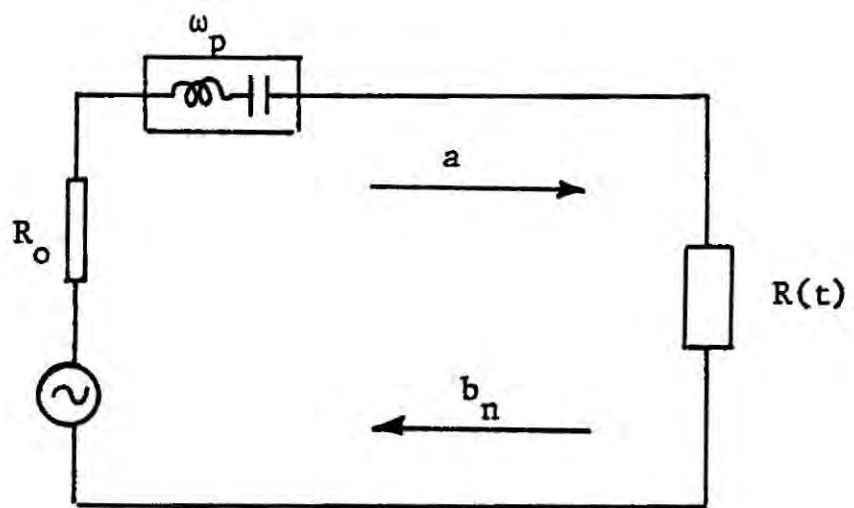Figure 6.5 Equivalent Diode Circuit as 'seen'
by the Local Oscillator

Figure 6.6 Time-Domain Equivalent Circuit of the Lattice
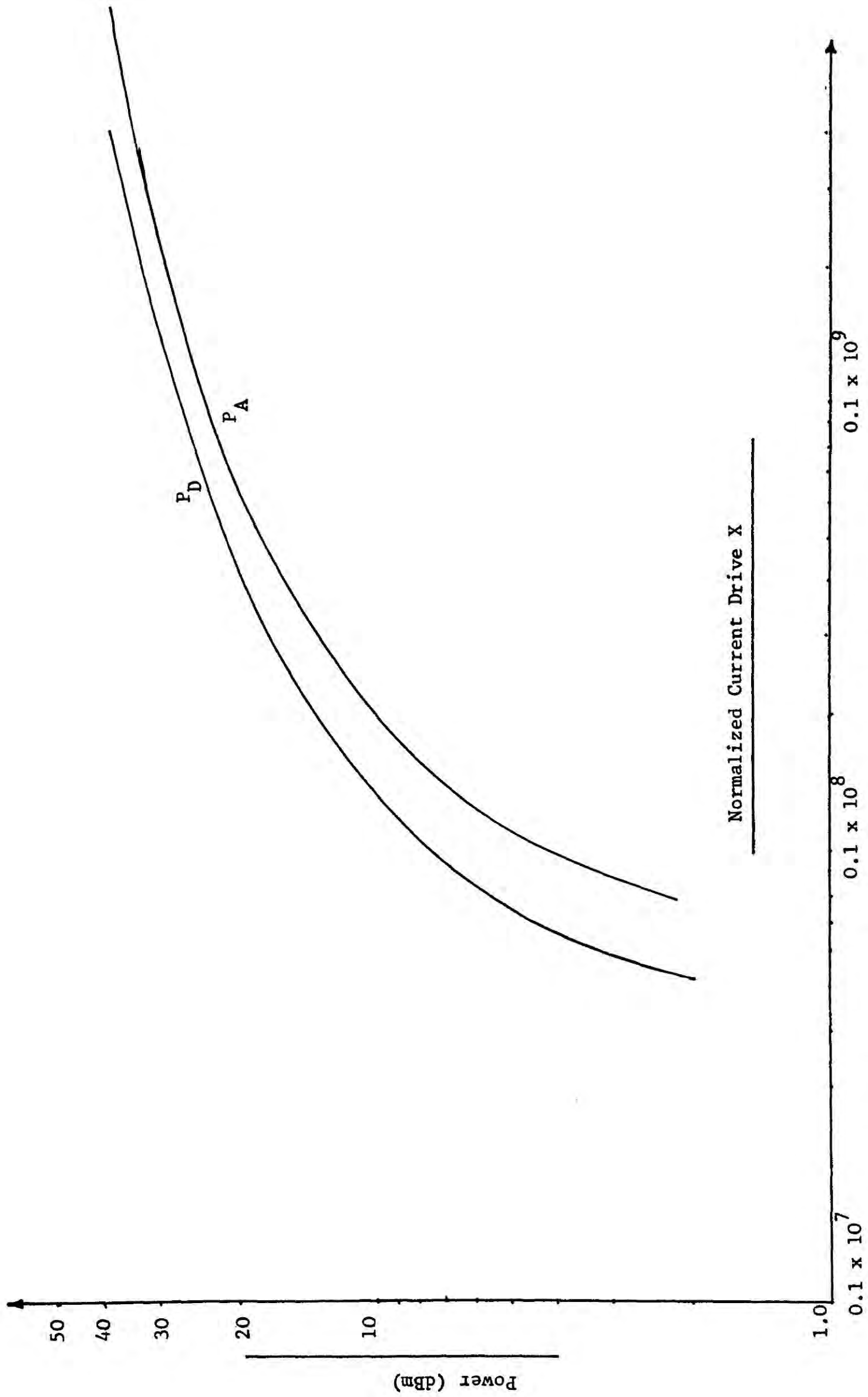Network of Diodes

Figure 6.7   Relationship Between P_A, P_D and the Normalised Current Drive X
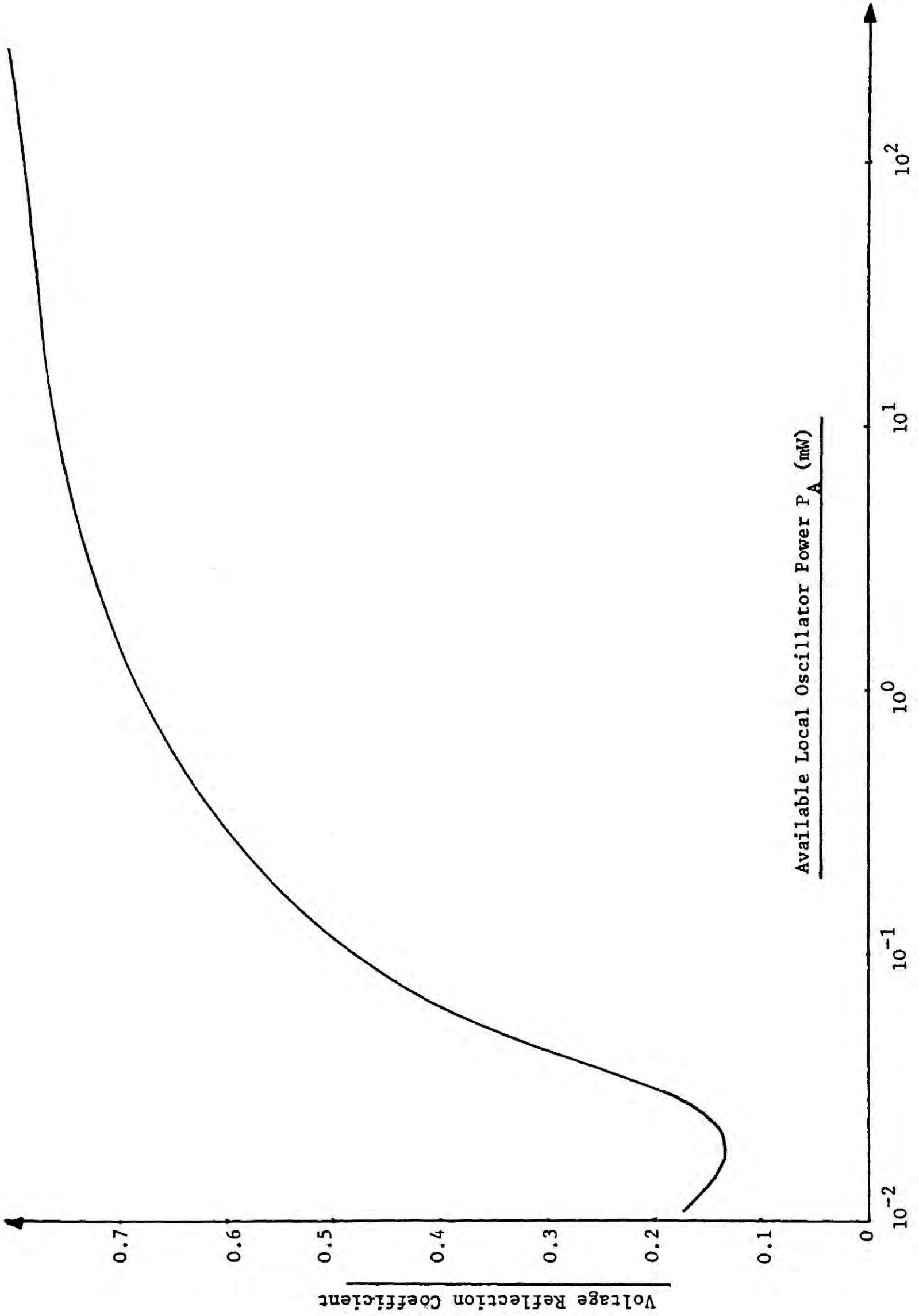
Figure 6.8 Relationship Between the Reflection Coefficient and Available Local Oscillator Power
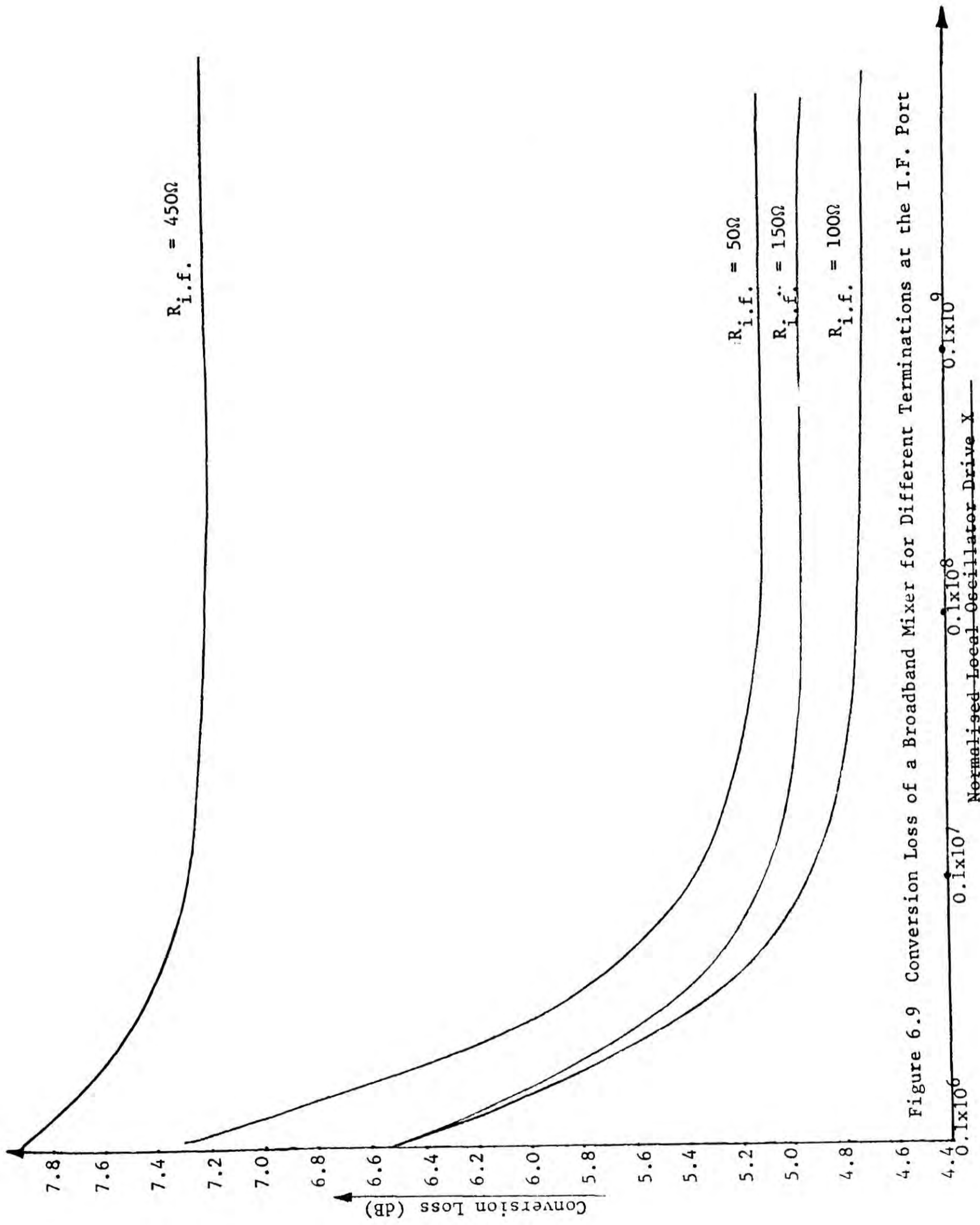
Figure 6.9   Conversion Loss of a Broadband Mixer for Different Terminations at the I.F. Port
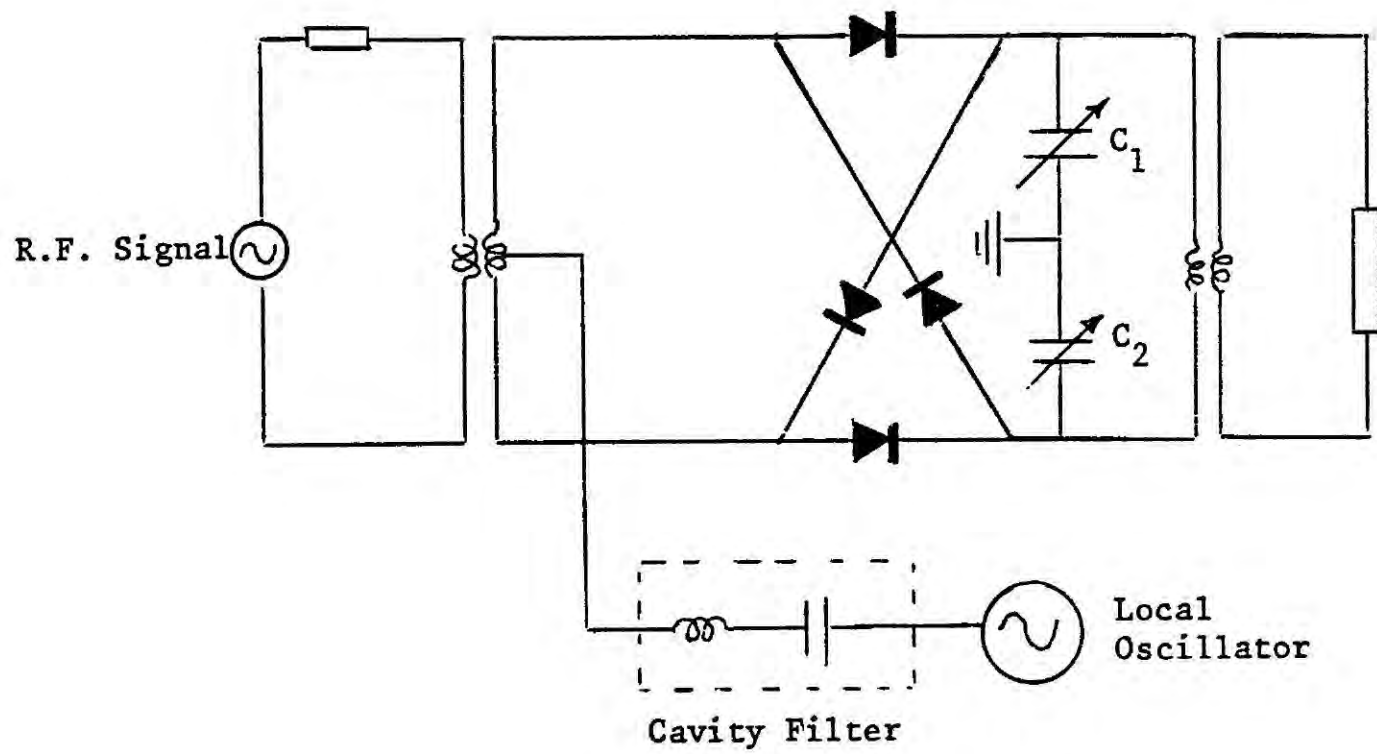
Figure 6.10 Low Frequency Model of a Broadband Mixer
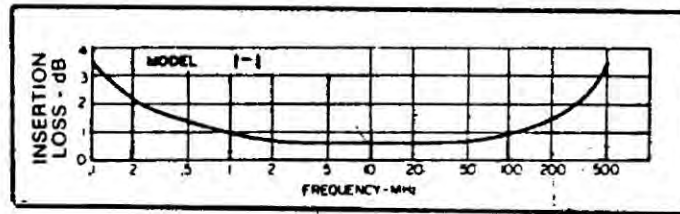
Impedance Ratio 50Ω: 50Ω
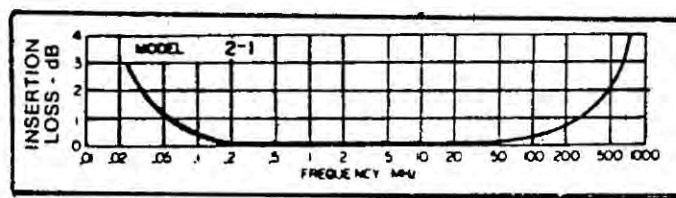
Impedance Ratio 50Ω: 100Ω
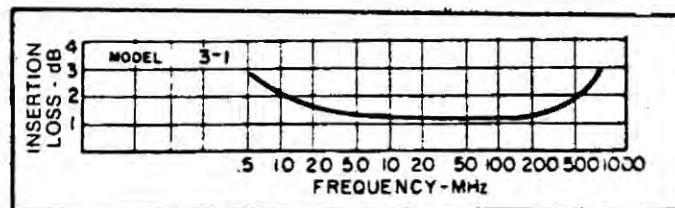
Impedance Ratio 50Ω: 150Ω
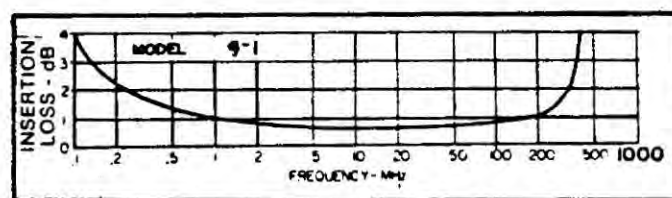
Impedance Ratio 50Ω: 450Ω

Figure 6.11   Manufacturer's Predicted Performance of the
IF Transformers
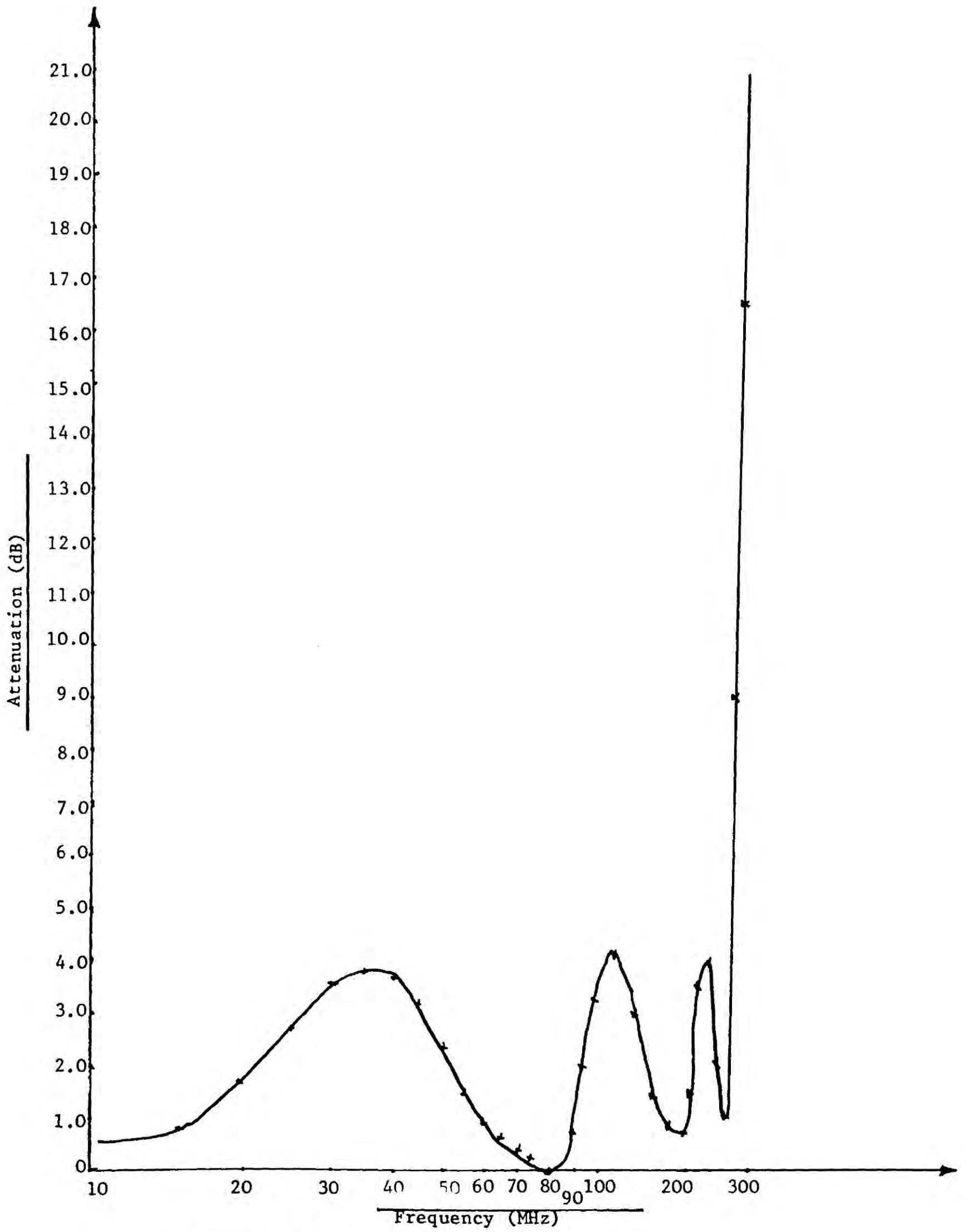
Figure 6.12   Frequency Response of the IF Filter
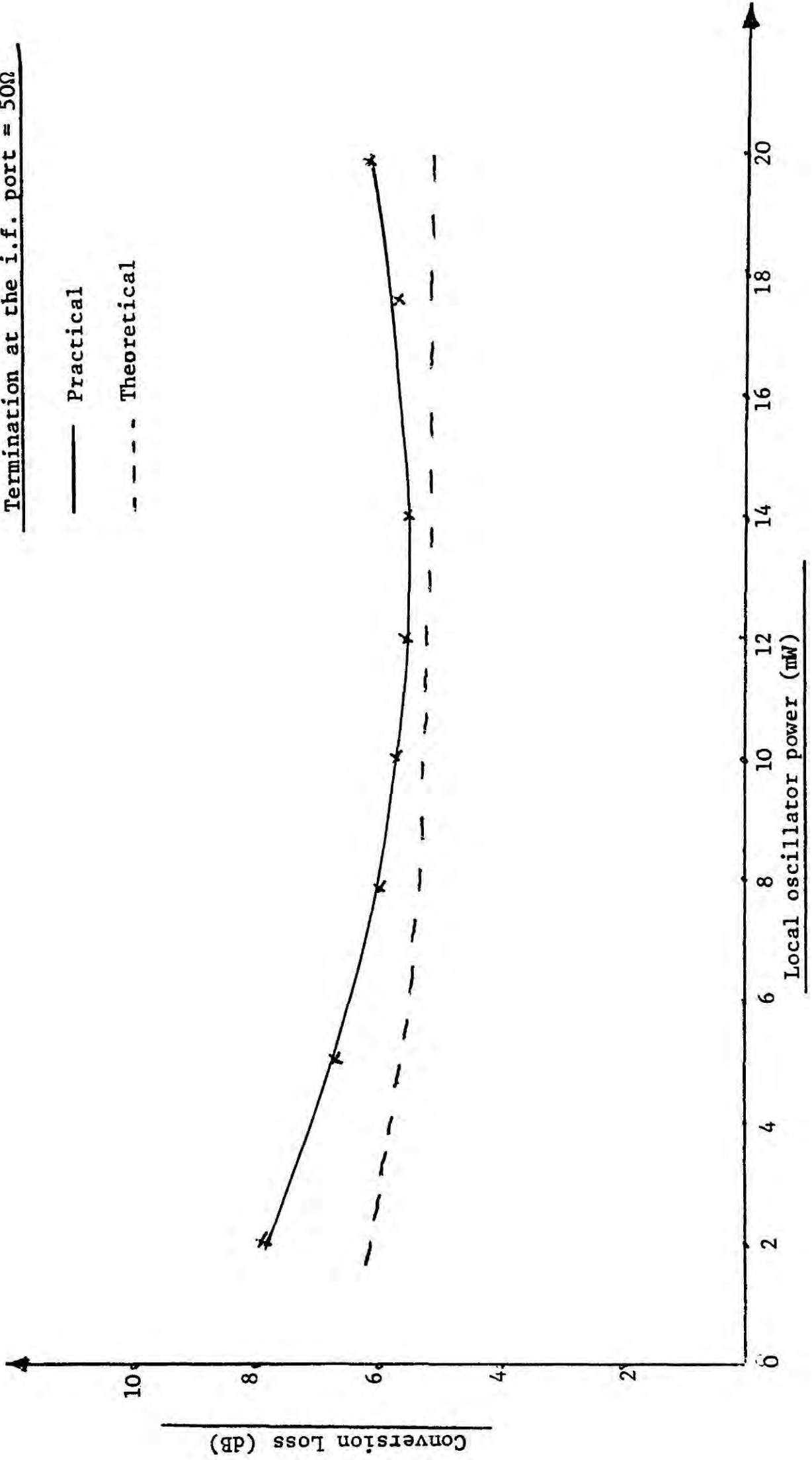
Figure 6.13 Practical and Predicted Performance of a Broadband Mixer
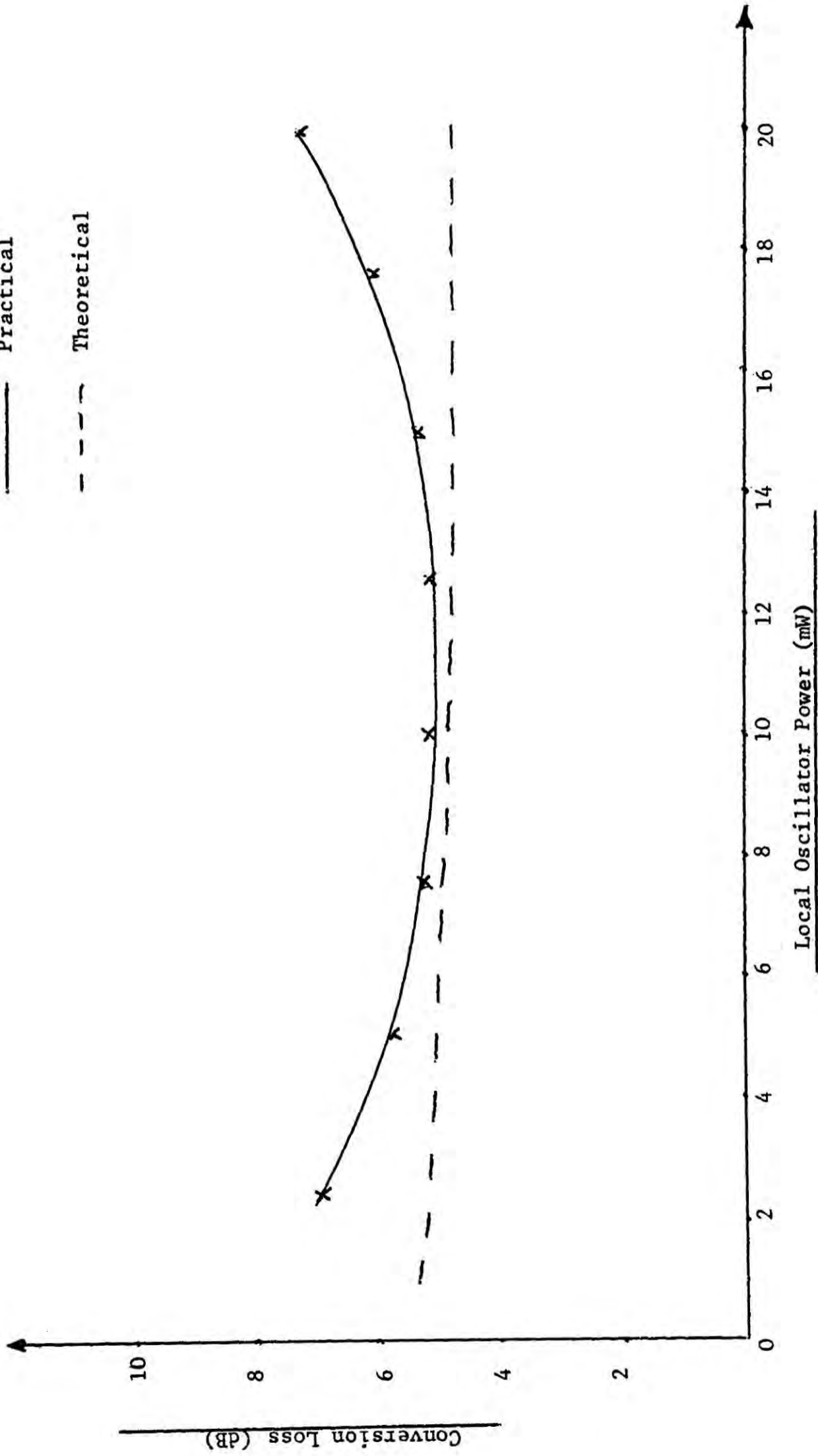
Figure 6.14 Practical and Predicted Performance of a Broadband Mixer
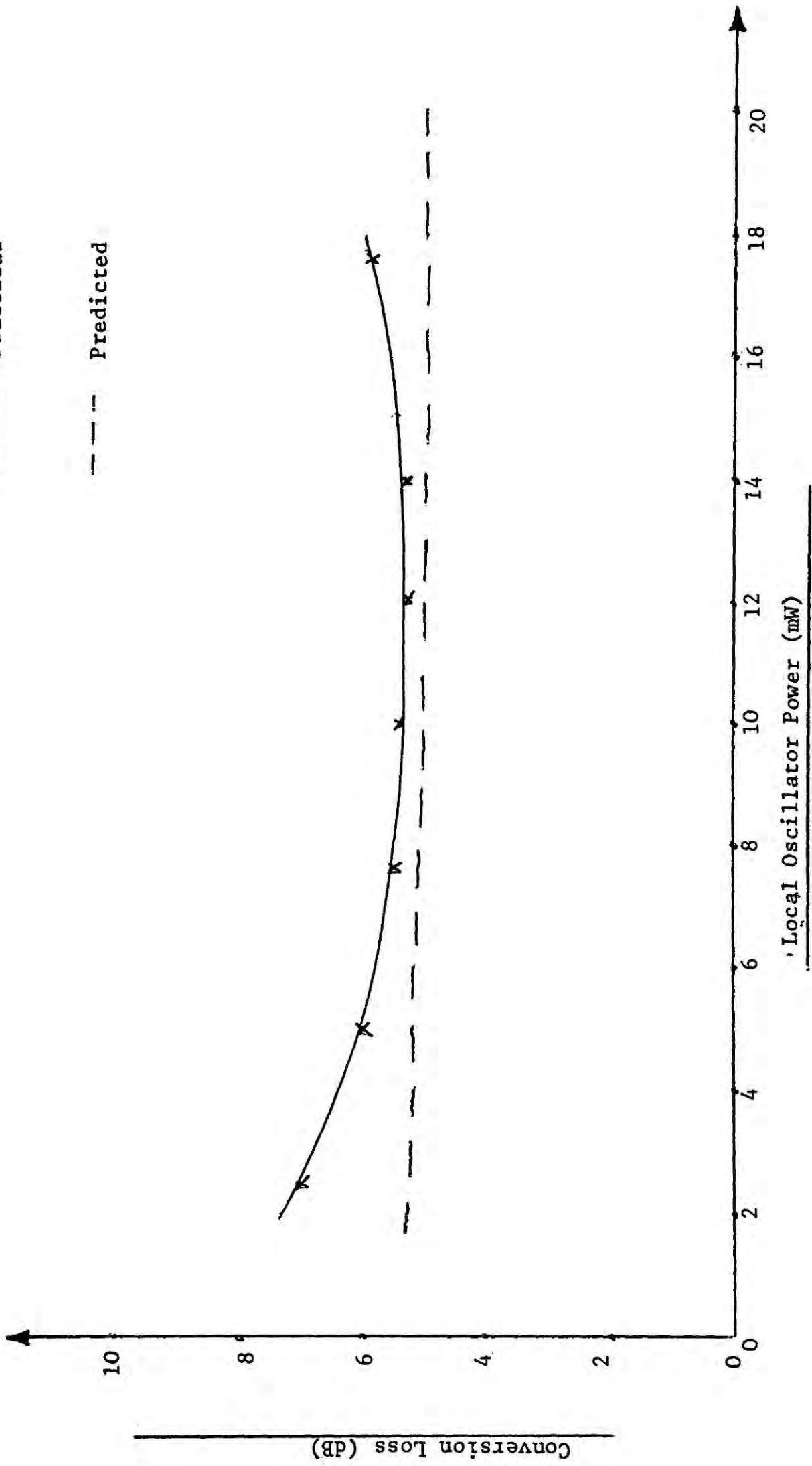
Figure 6.15 Practical and Predicted Performance of a Broadband Mixer
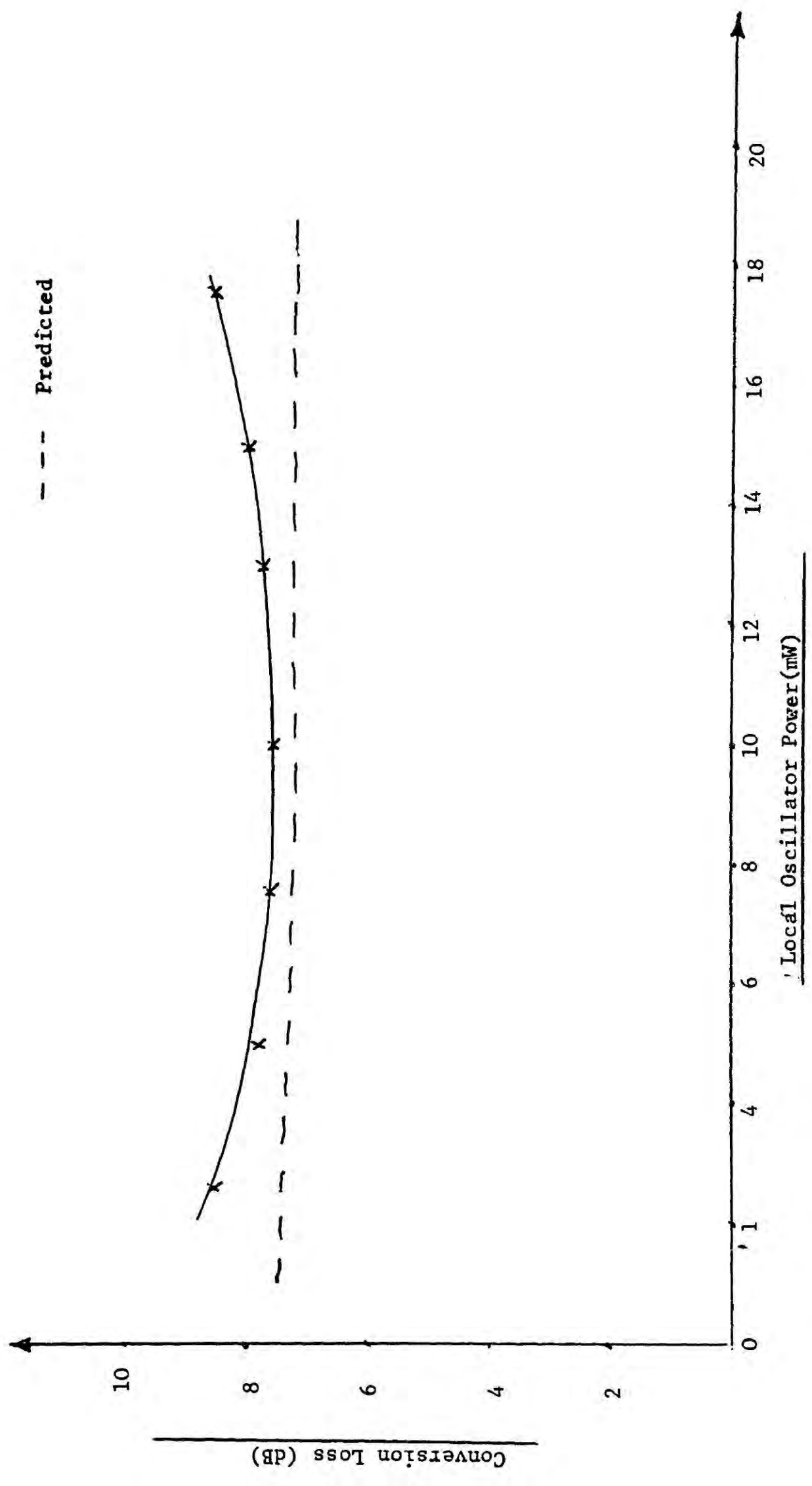
Figure 6.16 Practical and Predicted Performance of a Broadband Mixer

CONVERSION LOSS vs LO POWER

Conversion Loss, dB

4 at 1000 MHz

4 at 600 MHz

LO Power, dBm

Mini-Circuits

CONVERSION LOSS/LO POWER

CONVERSION LOSS (dB)

LO 1.060 GHz
RF 1.000 GHz @ -10 dBm

LO POWER (dBm)
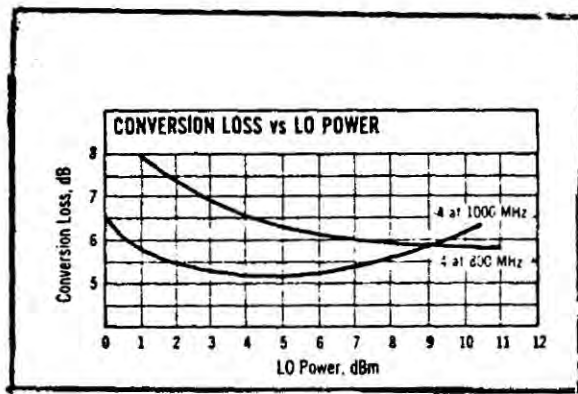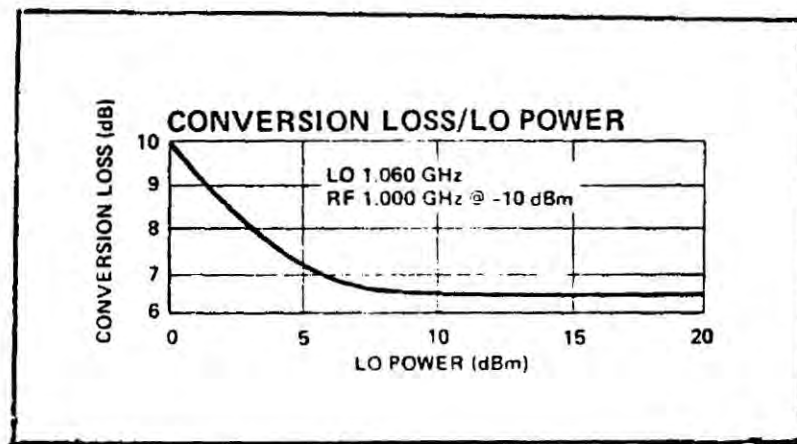
Anzac

Figure 6.17   Relationship Between Conversion Loss and Local

Oscillator for Broadband Mixers Produced   by

different Manufacturers

CHAPTER VII

Performance of Narrow-Band Lattice Mixers

7.1 Introduction

In the general analysis presented in Chapter III, it has been shown that using ideal diodes having zero forward resistance and infinite reverse resistance, it is theoretically possible to obtain zero conversion loss with narrow-band image open-circuit and image short-circuit mixers. It was further shown that, with practical diodes, it is still possible to obtain zero conversion loss in an image open-circuit mixer, provided it is matched at the r.f. and i.f. ports. The required terminations, however, are unrealistic and difficult to achieve in practice.

This chapter, therefore, initially examines the performance of narrow-band mixers when terminated by practically acceptable impedances. It is shown that out of all the mixers the image open-circuit mixer still offers the best possibility of obtaining lowest conversion loss. The design criteria and performance (in particular the losses) of the r.f. and i.f. circuits of the image open-circuit mixer are examined. Then, the performance of the practical image open-circuit mixer constructed using microstrip techniques is compared with that predicted by the theory.

7.2 Performance of Narrow-Band Mixers

7.2.1 Predicted Performance

It has been shown in section 3.3.3 that the required optimum techniques at the r.f. and i.f. ports to obtain minimum conversion loss (0 dB) for a lattice image open-circuit mixer are

$$R_{s_{opt}} \simeq \frac{2}{\pi} (r_s \, r_b)^{\frac{1}{2}}$$
<div align="right">3.40(a)</div>

$$G_{L_{opt}} \simeq \frac{2}{\pi} / (r_s \, r_b)^{\frac{1}{2}}$$
<div align="right">(3.40(b)</div>

If the diode's parameters given in Chapter VI are substituted into the above equations, then the required optimum terminations at the r.f. and i.f. ports are extremely large (approx 1 kΩ). Consequently, it is extremely difficult to realize these terminations in practice at high frequencies. For the lattice mixer with image short-circuit the corresponding optimum terminations at the r.f. and i.f. ports and the resulting conversion loss are a function of the local oscillator drive. However, these terminations are also large and hence difficult to realize.

To assess the performance of the two mixers it was decided to investigate the effect on the conversion loss when the i.f. port was terminated by the following impedances: 50Ω, 100Ω, 150Ω and 450Ω. These values were chosen as they can be obtained in practice using commercially available transformers (Mini-Circuits). Figures 7.1 to 7.8 show the computer-predicted results for the mixers over a wide range of local oscillator drive. The responses were computed for different terminations at the i.f. port and for two specific conditions at the r.f. port (corresponding to 50Ω and the required optimum impedance for a given i.f. termination).

In the case of the image open-circuit mixer, the conversion loss decreases as the L.O. drive and the impedance at the i.f. port increase. Further improvement of the conversion loss is obtained if for a given i.f. port termination, the r.f. port is matched. For the mixer with image short-circuit, the conversion loss increases with local oscillator drive and with increasing impedance at the i.f. port. The conversion loss of this mixer also improves, if, for a given termination at the i.f. port, the r.f. port is matched.

If practically realizable terminations are used at the r.f. and i.f. ports, the image open-circuit mixer still exhibits a lower conversion loss than the mixer with image short-circuit. It was therefore decided to investigate the performance of the former mixer in more detail.

7.2.2 R.F. Circuits of the Image Open-Circuit Mixer

Based on the design criteria discussed in Chapter V a microstrip circuit consisting of a rat-race directional coupler and two narrow-band bandstop filters were constructed on a low loss substrate (Duroid). The directional coupler was designed to operate at the frequency of 1.69 GHz and each bandstop filter was constructed to produce maximum attenuation at the image-frequency of 1.76 GHz. The resulting microstrip circuit is shown in Figure 7.9, where the filters were positioned so as the present an open-circuit at the diode terminals. The measured frequency response of the circuit is shown in Figure 7.10 where it can be seen that the isolation between ports 1 and 3 is in excess of 20 dB. The coupling between ports 3-4 and 1-4 match to within 0.3 dB at the signal frequency of 1.62 GHz. The overall fixed loss of the circuit is approx 0.7 dB and assuming that the fixed loss of directional coupler is 0.3 dB (as shown in Chapter VI), the filter by itself introduces a loss of only 0.4 dB. The tests were carried out with all ports of the circuit terminated in matching loads of 50Ω and the results obtained are in close agreement with those predicted by theory.

7.2.3 Performance of the Image Open-Circuit Mixer for Different Terminations at the I.F. Port

The i.f. circuit of the mixer was identical to the one described in paragraph 6.4.3 where four commercial transformers were used in turn to convert a 50Ω load to: 50Ω ; 100Ω ; 150Ω ; 450Ω as 'seen' by the mixer. The measured loss of the i.f. circuit of the mixer was about 1.2 dB at 70 MHz so that the total fixed loss in the mixer including that of the coupler and bandstop filters was about 1.9 dB. In the local oscillator circuit a co-axial cavity (tuned to 1.69 GHz) was included to ensure that the diodes are pumped by sinusoidal current drive. Figures 7.11

to 7.14 show the measured and predicted conversion losses as a function of the local oscillator drive for different terminations at the i.f. port, where the fixed loss in the mixer has been taken into account. Although good agreement is obtained between the predicted and measured results, there are still a number of problems associated with this mixer which are described below.

1. The conversion loss is high; it can be reduced if matching is introduced at the r.f. port.

2. With the lattice configuration of diodes connected to the microstrip circuit consisting of the coupler and filters, the termination 'seen' by the bandstop filters is no longer 50Ω and this mismatch will increase the conversion loss as indicated in Figures 7.11 to 7.14.

3. The i.f. termination 'seen' by the mixer depends on the transformer used. It is convenient to design the i.f. circuit so that matching is obtained at the i.f. port for any termination at the r.f. port.

The following paragraphs are therefore concerned with the possible solutions to the above problems in order to improve the performance of the image open-circuit mixer.

7.3 The I.F. Circuit of the Mixer

The intermediate frequency in a down converter is the lowest frequency involved and care must be taken in producing the output circuit. At this frequency the circuit is required to perform a number of functions in the part of the mixer where the signal level is lowest.

The i.f. output circuit of the mixer shown in Figure 7.15 consists of a wideband balanced-to-unbalanced transformer and a π section. The aim is to transform the required high i.f. output impedance of the mixer down to a standard 50Ω load. Such a matching network can be realized with lumped components and is conveniently designed by considering it as two inverted 'L' sections as shown in Figure 7.16. The common matching resistance R_m of the two sections is given by

$$R_m = R_s / (1 + Q_1^2) = R_L / (1 + Q_2^2) \qquad \qquad 7.1$$

where

$$Q_1 = X_{L1}/R_m \quad \text{and} \quad Q_2 = X_{L2}/R_m$$

Equation 7.1 shows that the node with the highest terminating resistance has the largest Q and hence dictates the bandwidth of the circuit. An interesting property of this π network is that the ratio of the terminating resistances is given by

$$\frac{R_L}{R_s} \simeq (\frac{C_1}{C_2})^2 \qquad \qquad 7.2$$

The above equation is independent of frequency so that C_1 and C_2 can be adjusted to obtain the desired impedance transformation. Although the components of the two 'L' sections are normally evaluated analytically, a greater insight into the properties of the π matching networks is obtained by using the Smith Chart. It is shown in Appendix VIII that the constant Q curves on the Smith Chart are defined by the following equation of a circle

$$U^2 + (V + \frac{1}{Q})^2 = 1 + \frac{1}{Q}^2 \qquad \qquad 7.3$$

where U and jV are the real and imaginary axes on the Smith Chart of the voltage reflection coefficient. Initially a π matching circuit was designed to transform 300Ω to 50Ω so that a Q of three at 70 MHz was obtained. The design procedure for the π network using the Smith Chart is given in Figure 7.17 and the values of the circuit components are shown in Figure 7.18(a). The required inductance of 0.26 μH was obtained using 9 turns of 18 gauge wire and following the design criteria derived in Appendix IX. The actual value of the inductance was checked using a Q meter (type IF 1245) and was found to be 0.27 μH. The final circuit

was constructed using two variable capacitors and the coil. The test

arrangement is shown in Figure 7.18(b): a 270Ω resistor (preferred value)

was placed in series with the signal generator to obtain matching. In

testing the circuit, the significant relationship is that of the available

power from the signal generator to the power measured at the output of

the circuit. The predicted loss from mismatch is 8.066 dB, but it was

found that the circuit introduced an extra loss of 2 dB. To reduce this

the π network was redesigned to have a Q of seven at 70 MHz, and an etched

spiral conductor was produced for the required inductance. The design of

the spiral inductance is described in Appendix IX and the values of the

components of the π network are shown in Figure 7.18(c). The inductance

was designed to be 148 nH and when checked a value of 150 nH was obtained.

Initially, this inductance was realized using a PCB and then using a low

loss (Duroid) substrate. As with stop-band filters, considerable

improvement was obtained with the low loss substrate indicating it is

important, when realizing r.f. networks employing electromagnetic coupling,

to utilize low loss substrates. The frequency response of the π section

is shown in Figure 7.19 indicating a minimum loss at 70 MHz of about 8 dB,

as an oscillator was used whose output impedance is 50Ω. The actual loss

of the π network only was accurately checked using a power meter and

disregarding the mismatch effect was found to be 0.2 dB. Figures 7.20(a)

and 7.20(b) show photographs of the complete i.f. section, consisting of

the broadband transformer and the π matching network. The frequency

response of the i.f. section is shown in Figure 7.21 where a minimum loss

of 1.5 dB is obtained at 70 MHz. This loss is made up of 0.2 dB produced

by the π network and 1.3 dB due to the broadband transformer.

7.4 The R.F. Circuit of the Mixer

Figures 7.1 to 7.4 show the computer predictions of the input impedance of the image open-circuit mixer as a function of the local oscillator drive for different terminations at the i.f. port. They indicate that in order to obtain minimum conversion loss (approx 2 dB) the required termination at the r.f. port should be approx 200Ω when the i.f. port is terminated in 450Ω. Consequently the condition for minimum conversion loss leads to the stopband filter being mismatched at its output port. Figure 7.22 shows the computer predicted frequency response of the filter over a wide range of terminations at its output port. The analysis indicates that although the attenuation in the stopband is not considerably affected, the main effect of the mismatch is to increase the attenuation (up to 1.4 dB) in the passband. This attenuation in the passband is not acceptable and therefore it is required to improve the match between the input impedance of the lattice network of diodes and the output port of the filters.

It was decided to achieve this by using two quarter-wave transformers with each transformer designed to operate at the radio frequency and to have a characteristic impedance of 100Ω. Figure 7.23 gives the computer predicted frequency response of the stopband filter and transformer over a wide range of terminations at the output port. As can be seen the attenuation in the stopband is still satisfactory but the attenuation in the passband is lowered (< 0.2 dB) over a wide range of terminations.

A microstrip circuit consisting of a rat-race coupler, bandstop filters and quarter-wave transformers was successfully realized on a Duroid substrate as shown in Figure 7.24. The measured frequency response of the circuit with each output port terminated in a 50Ω load is given in Figure 7.25 and agrees with that predicted by theory. Consequently, it was decided to use this form of r.f. circuit for the final version of an image open-circuit mixer.

7.5 Performance of the Image Open-Circuit Mixer

The previous paragraphs discussed the theoretical design criteria of
the r.f. and i.f. circuits used in an image open-circuit mixer, to obtain
minimum conversion loss. The block diagram of such a mixer in Figure 7.26
is followed by a photograph of the constructed circuit in Figure 7.27.
The r.f. section consisting of the rat-race coupler, bandstop filters and
quarter-wave transformers was fabricated on Duroid substrate. The bandstop
filters were designed to produce maximum attenuation at the image at
frequency of 1.76 GHz so that an open-circuit (theoretically) was obtained
at the diode terminals. The quarter wavelength transformers were designed
to produce a match at the output ports of the bandstop filters. The
measured insertion loss of the r.f. circuit at 1.62 GHz was 0.7 dB and
greater than 20 dB at the image-frequency.

The r.f. circuit consisted of a commercial (Mini-Circuit) 1:1 balanced-
to-unbalanced transformer and a π matching section. The latter was designed
on the lines of the discussion in section 7.3 and the measured insertion loss
of the complete i.f. circuit was 1.5 dB. The total loss of the embedding
networks of the mixer produced by the r.f. circuit (0.7 dB) and i.f. circuit
(1.5 dB) was about 2.2 dB.

The conversion loss of the mixer was measured by spectrum analyser as
discussed in section 6.4.3 with the r.f. signal level set to $- 10$ dB$_m$. The
measured conversion loss of the mixer taking into account the fixed losses
of the embedding networks is shown in Figure 7.28. The minimum conversion
loss obtained was 2.1 dB at a local oscillator drive of 15 dB$_m$ and compares
favourably with the predicted conversion loss of 1.6 dB indicated in
Figure 7.3. The extra loss of 0.5 dB is accounted for by the loss produced
by the diode stray inductance, imperfect image rejection and any mismatch
effects contributed by individual diodes and circuit.
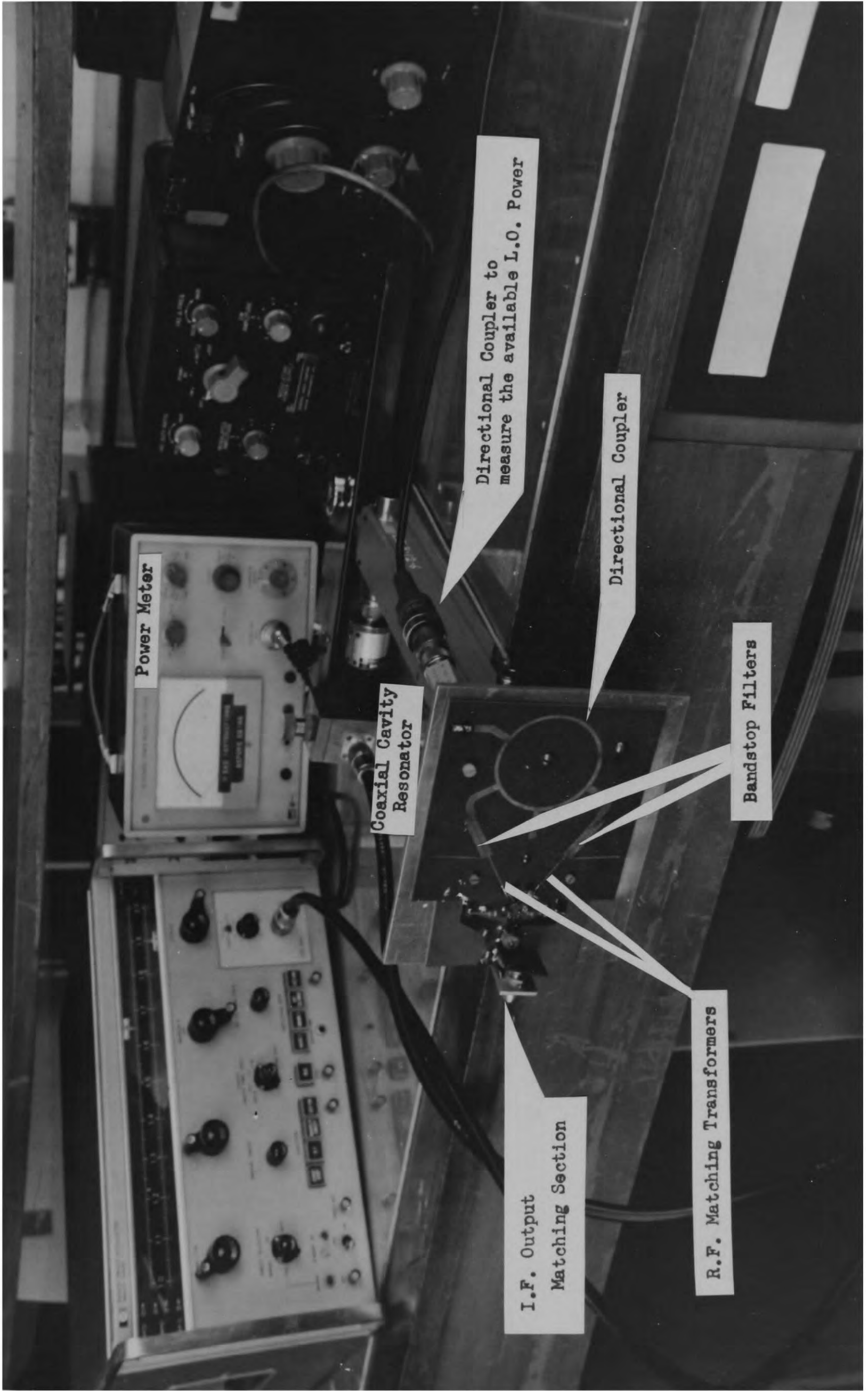
Power Meter

Directional Coupler to
measure the available L.O. Power

Directional Coupler

Coaxial Cavity
Resonator

Bandstop Filters

I.F. Output
Matching Section

R.F. Matching Transformers

Test Equipment and Mixer

7.6 Conclusions

In order to obtain a minimum conversion loss it is necessary to produce either an open or a short-circuit to the image-frequency component generated by the mixer circuit. It is shown that if practically realizable terminations are used at the r.f. and i.f. ports then the image open-circuit mixer offers the best possibility of obtaining the lowest conversion loss and consequently the properties of this mixer were investigated experimentally.

To obtain an image open-circuit mixer it is necessary to use an image-reject filter to ensure that a highly reactive termination is produced at the diode terminals. Such a filter was obtained with the design procedure discussed in Chapter V and the performance of the mixer was investigated for four different terminations at the i.f. port. The minimum conversion loss obtained for each i.f. termination is shown in the table below.

I.F. TERMINATION	MEASURED MINIMUM C.L. (dB)
50	7.1
100	5.9
150	5.1
450	5.9

As can be seen the conversion loss reaches a minimum value for an i.f. termination of 150Ω instead of the predicted i.f. termination of 450Ω. This is due to the attenuation introduced by mismatching the filter at its output port and the mixer at its r.f. port.

To overcome this problem and to reduce the conversion loss, the mixer was redesigned in order not only to produce a match at the r.f. and i.f. ports, but also to match the output port of the stopband filter. The matching at the i.f. port was obtained with the π network while at the r.f. port it was realized by using a quarter-wave transformer. The measured conversion loss of the final mixer was improved to 4.3 dB. Taking into account the losses of the imbedding networks of 2.2 dB the loss of 2.1 dB which is considered close enough to the predicted value of 1.6 dB.

The results obtained for the image open-circuit mixer indicate that the model of the diode and subsequent theoretical analysis adequately represent the practical conditions encountered.
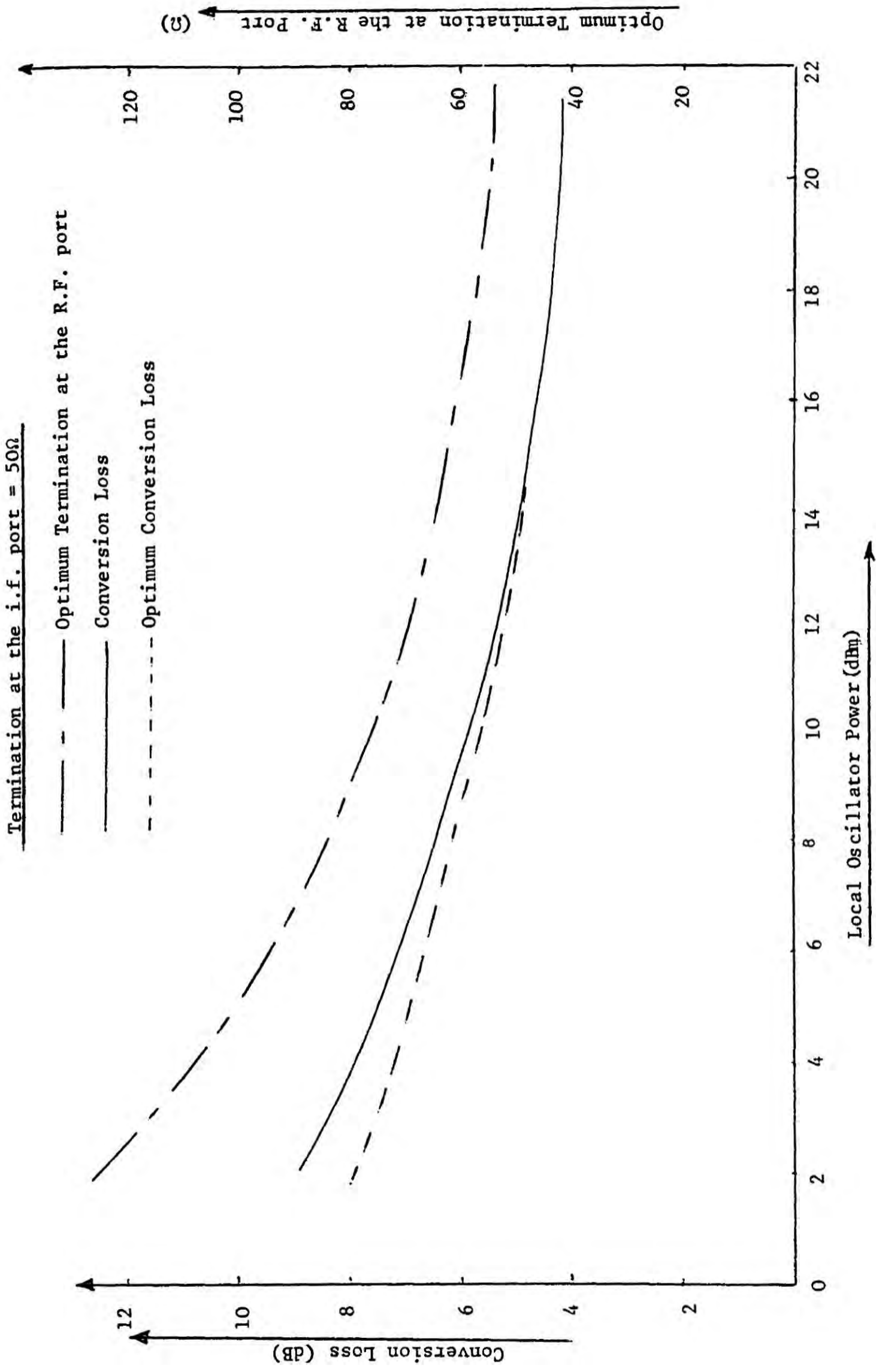
Figure 7.1 Predicted Performance of the Image Open-Circuit Mixer
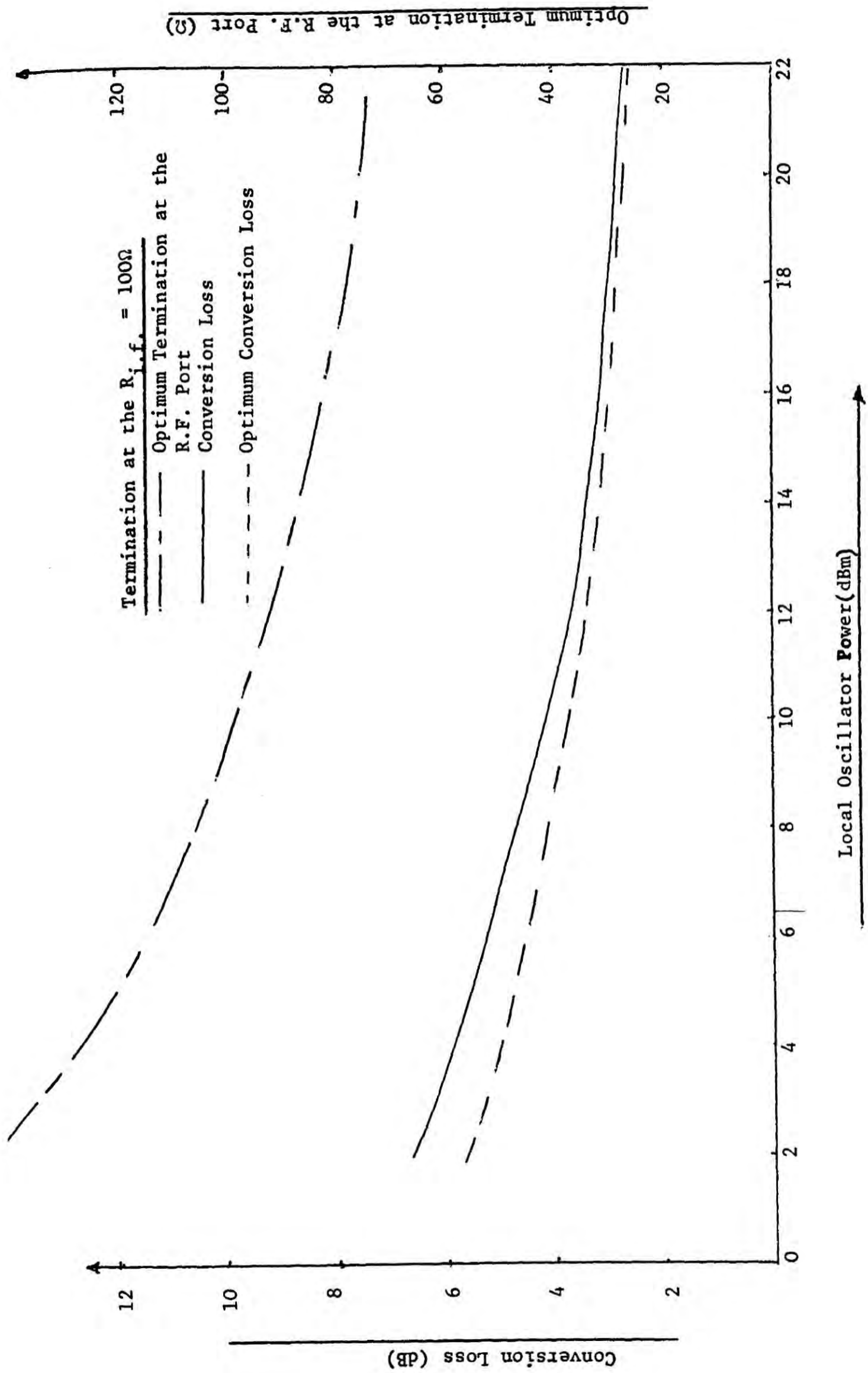
Figure 7.2 Predicted Performance of the Image Open-Circuit Mixer
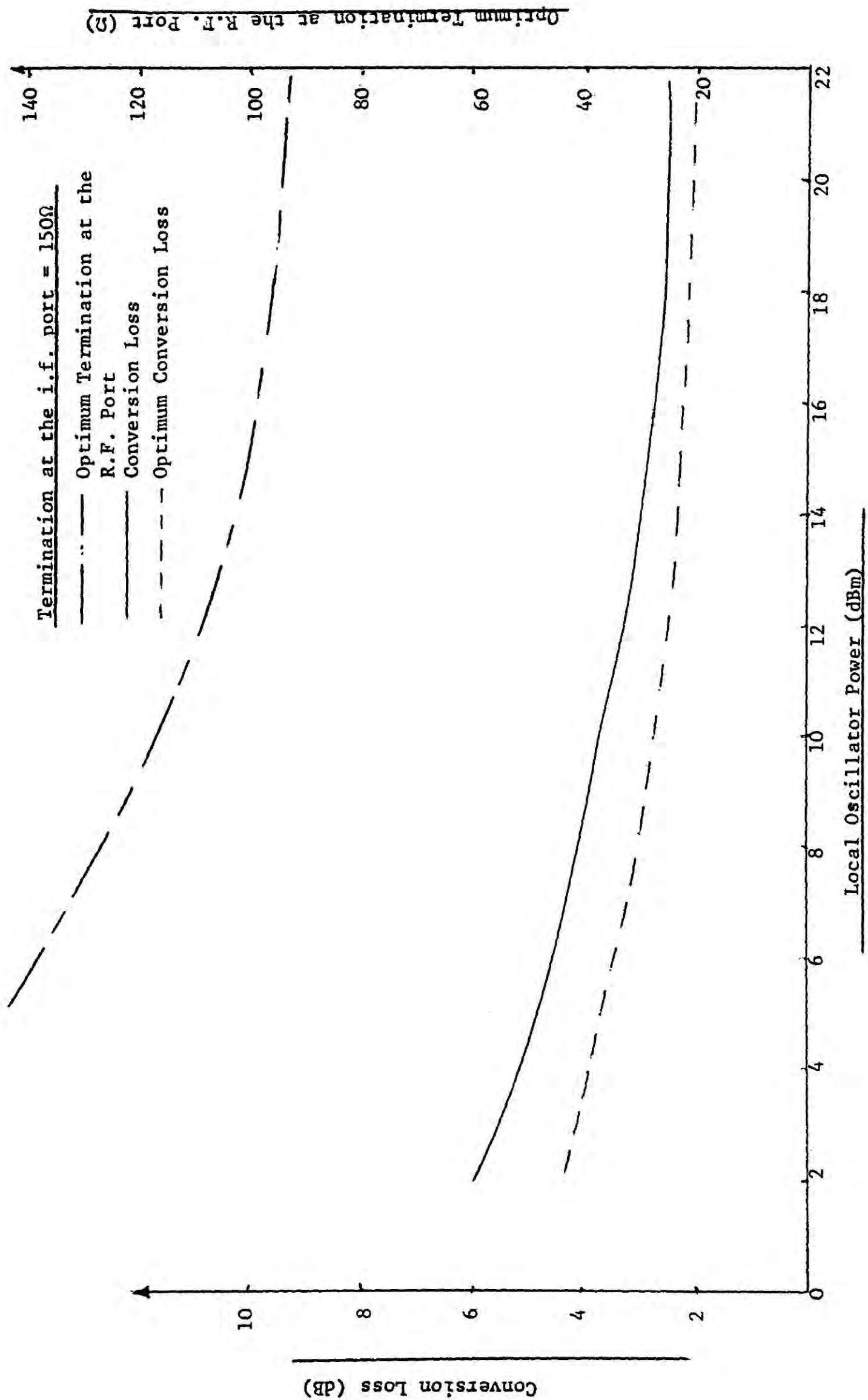
Figure 7.3 Predicted Performance of the Image Open-Circuit Mixer
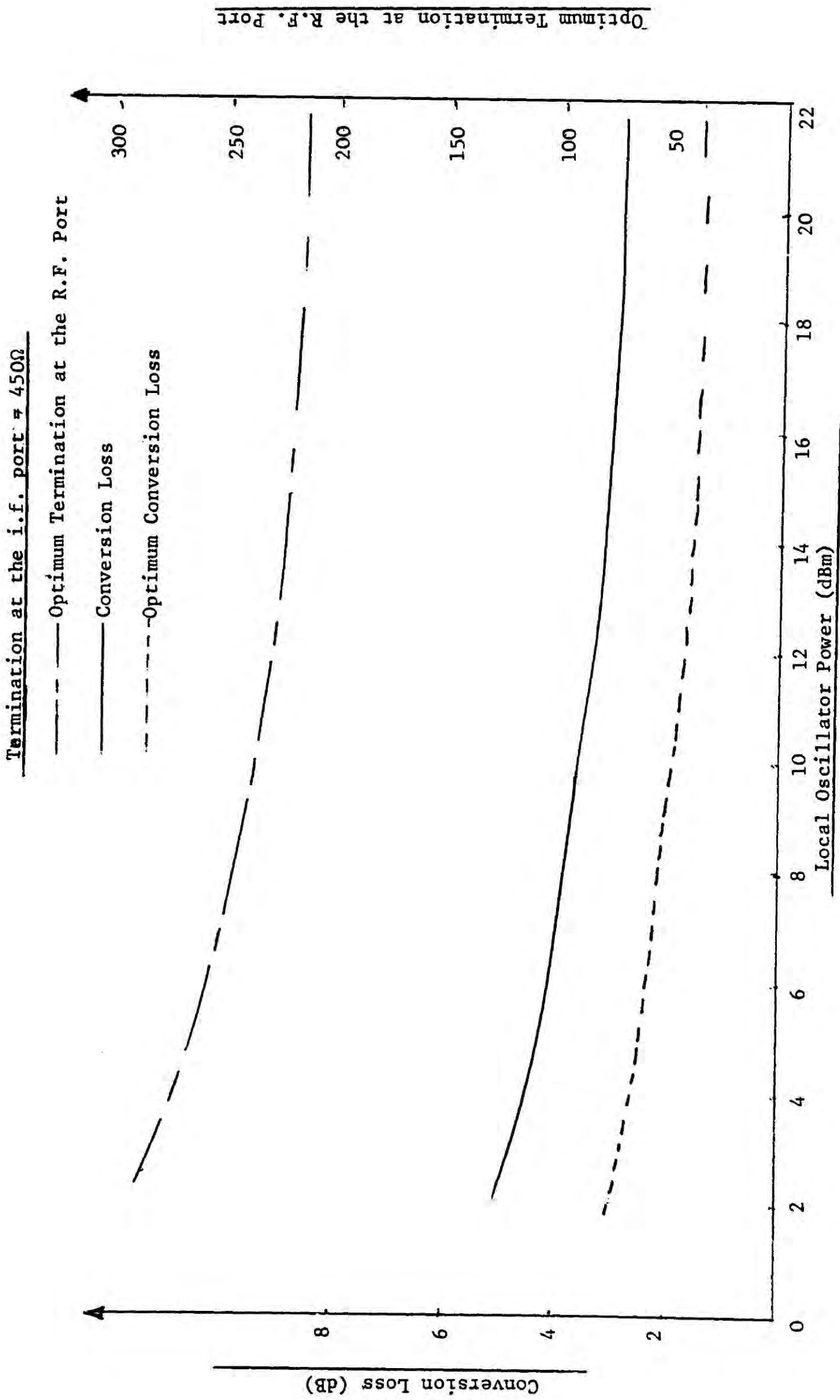
Figure 7.4 Predicted Performance of the Image Open-Circuit Mixer
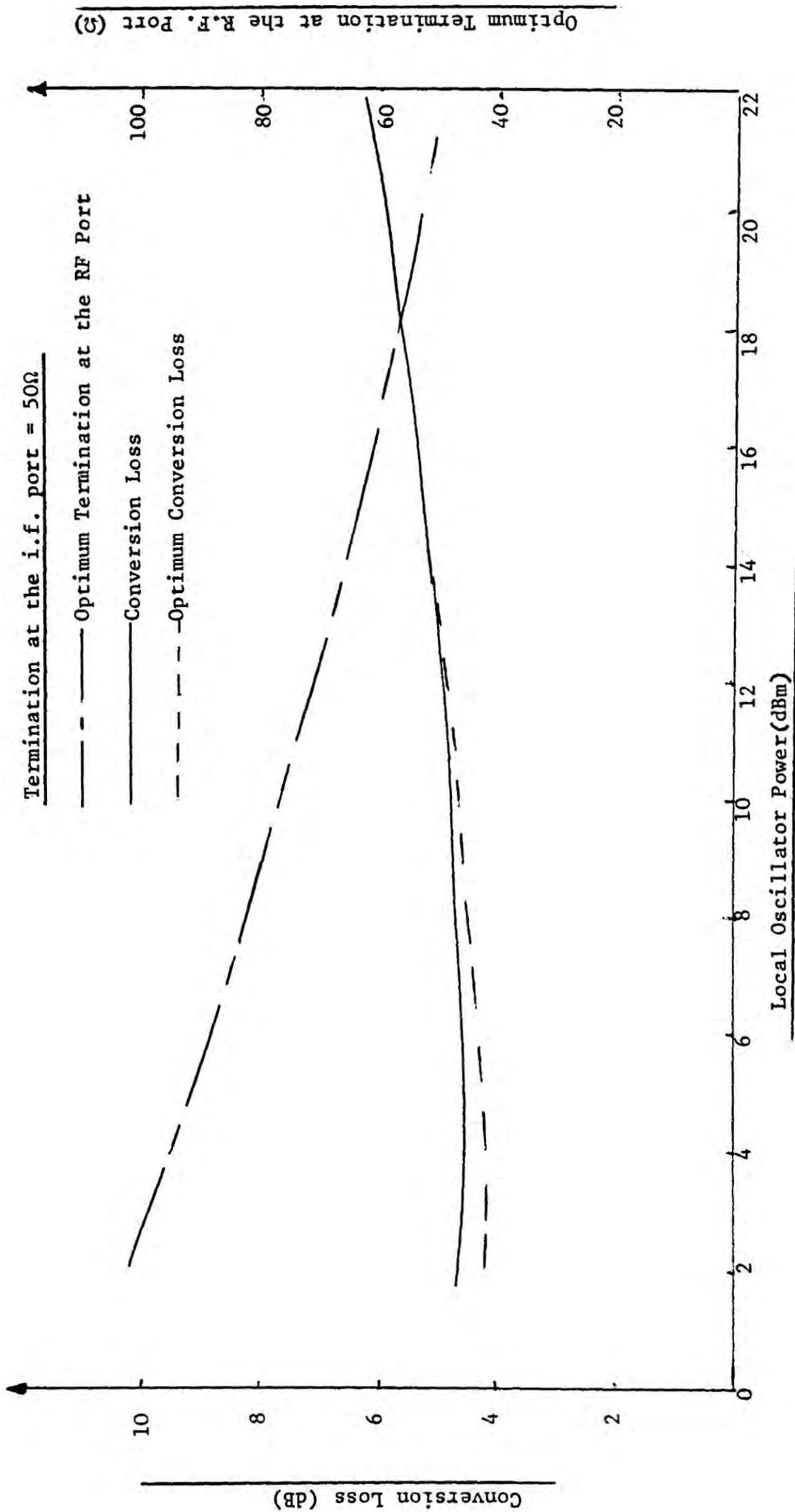
Figure 7.5 Predicted Performance of the Image Short-Circuit Mixer
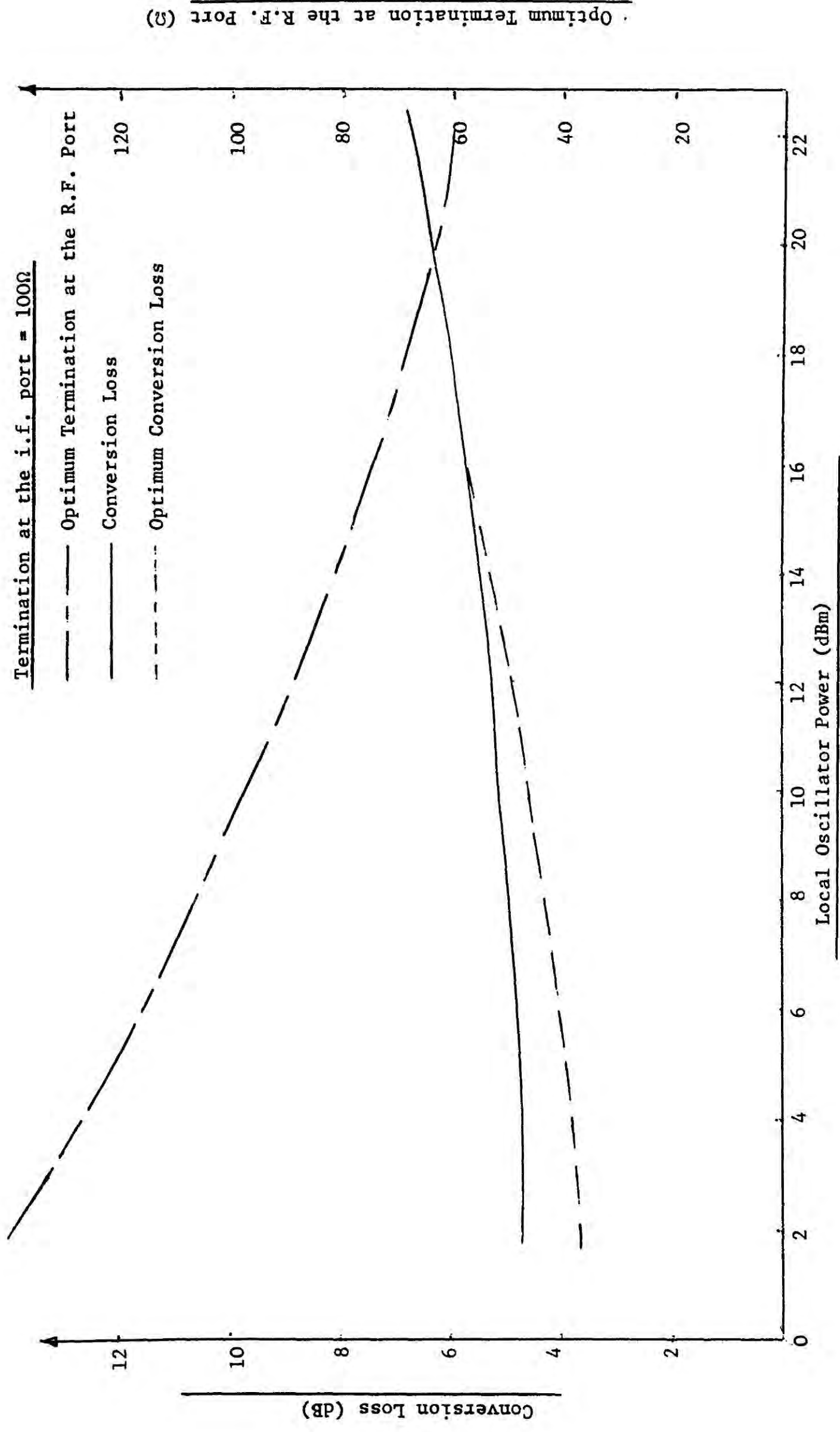
Figure 7.6 Predicted Performance of the Image Short-Circuit Mixer
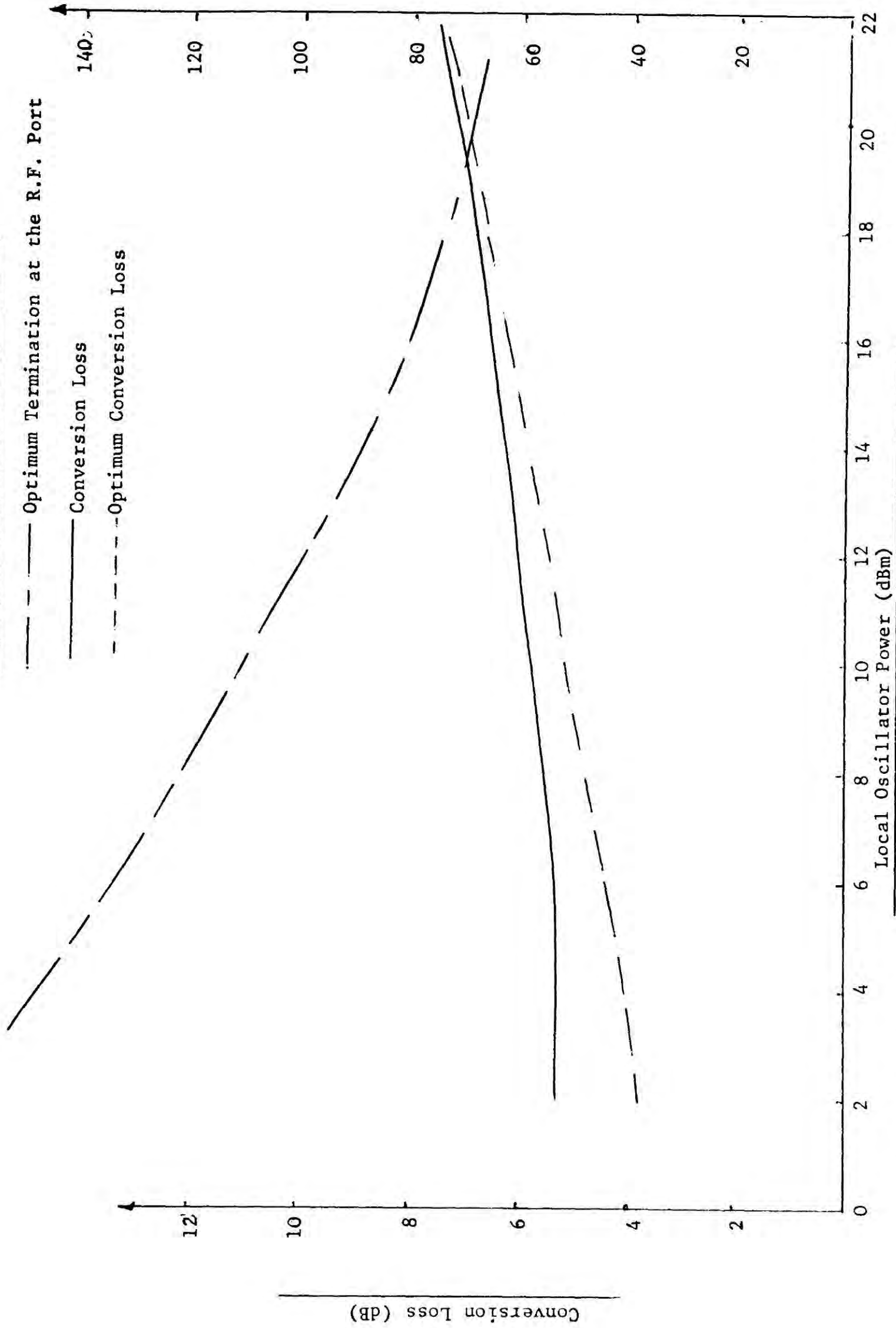
Figure 7.7 Predicted Performance of the Image Short-Circuit Mixer
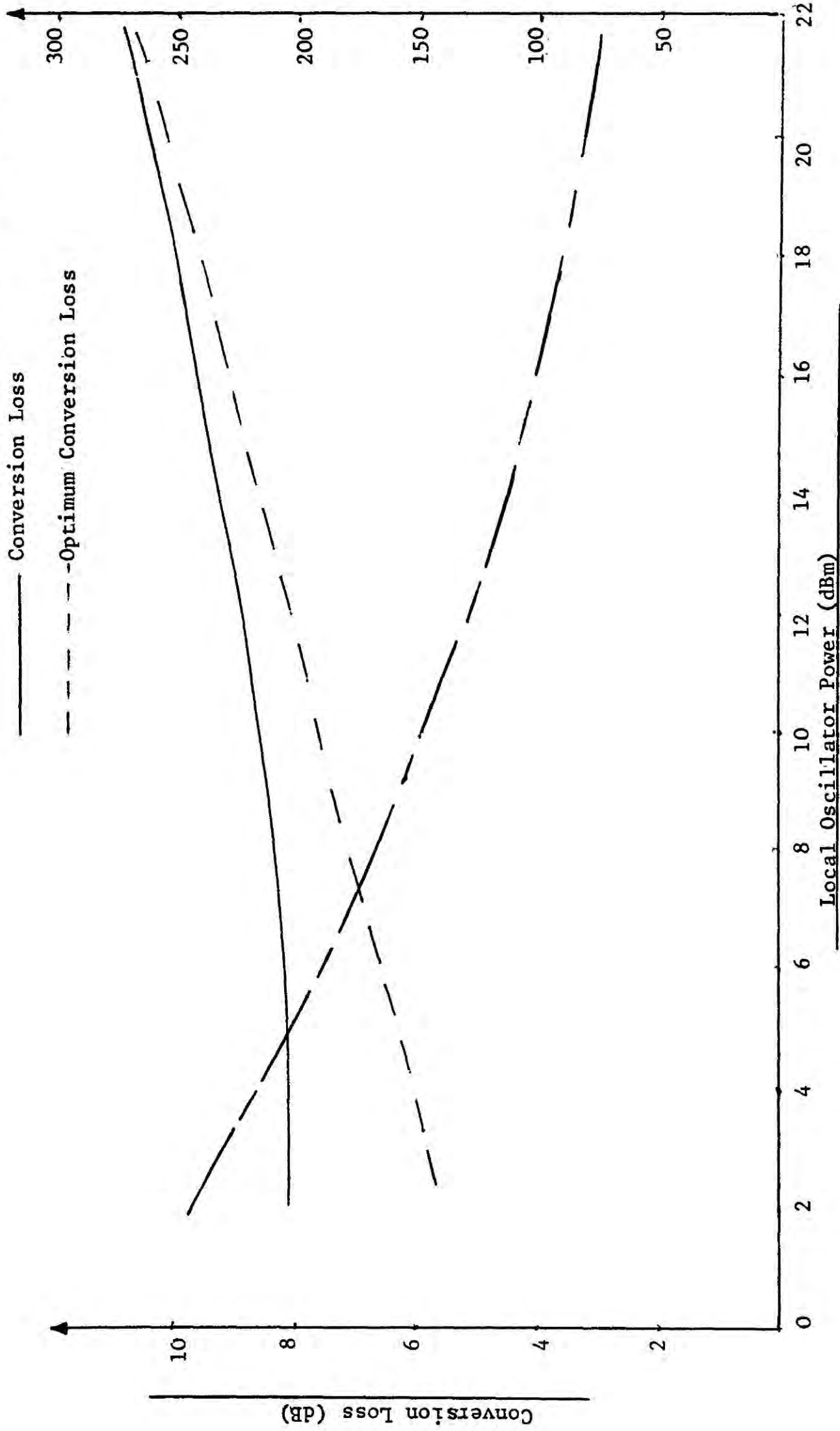
Figure 7.8 Predicted Performance of the Image Short-Circuit Mixer
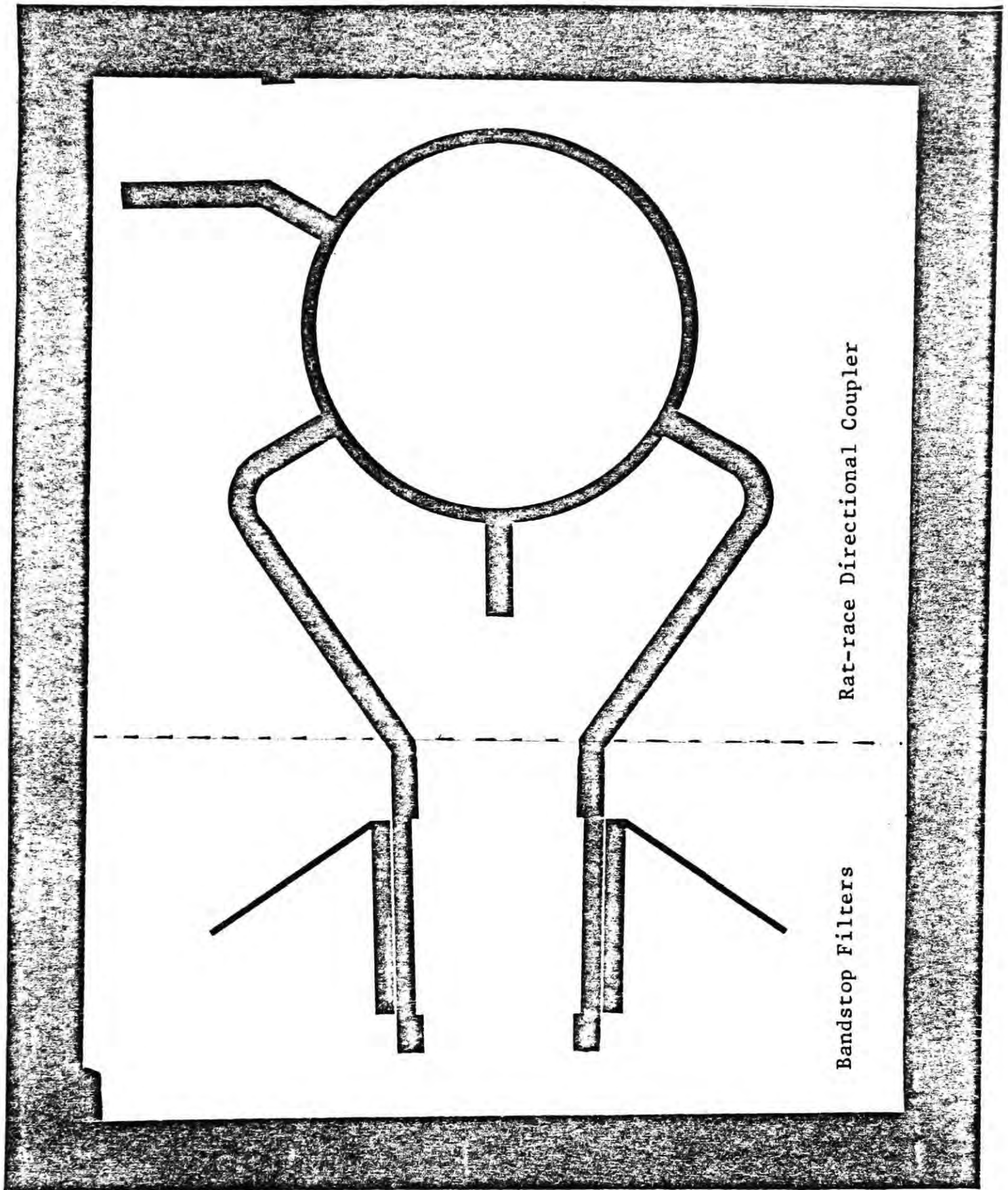
Figure 7.9 Rat-Race Directional Coupler and Bandstop Filters
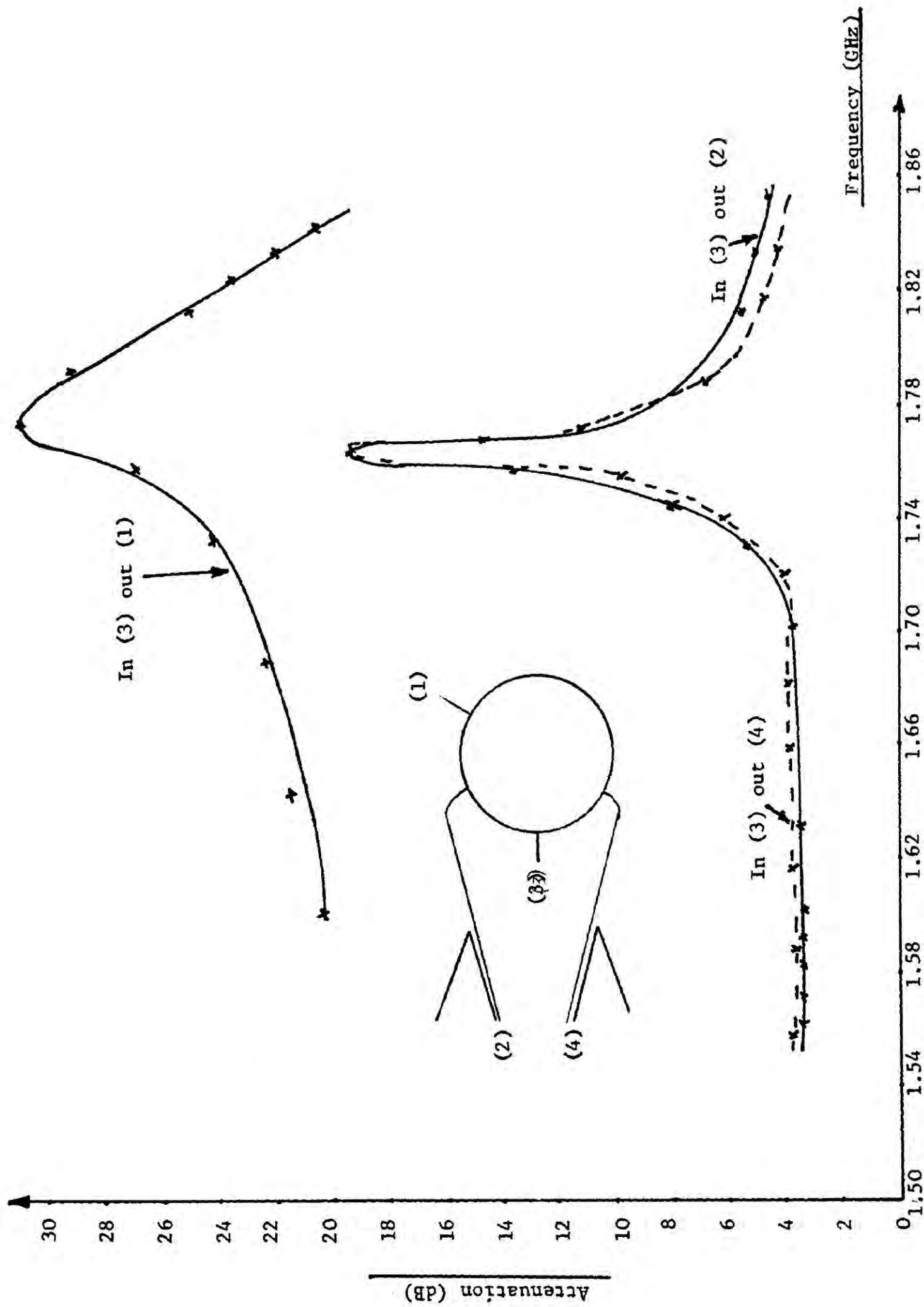
Figure 7.10 Measured Frequency Response of the Coupler and Bandstop Filters
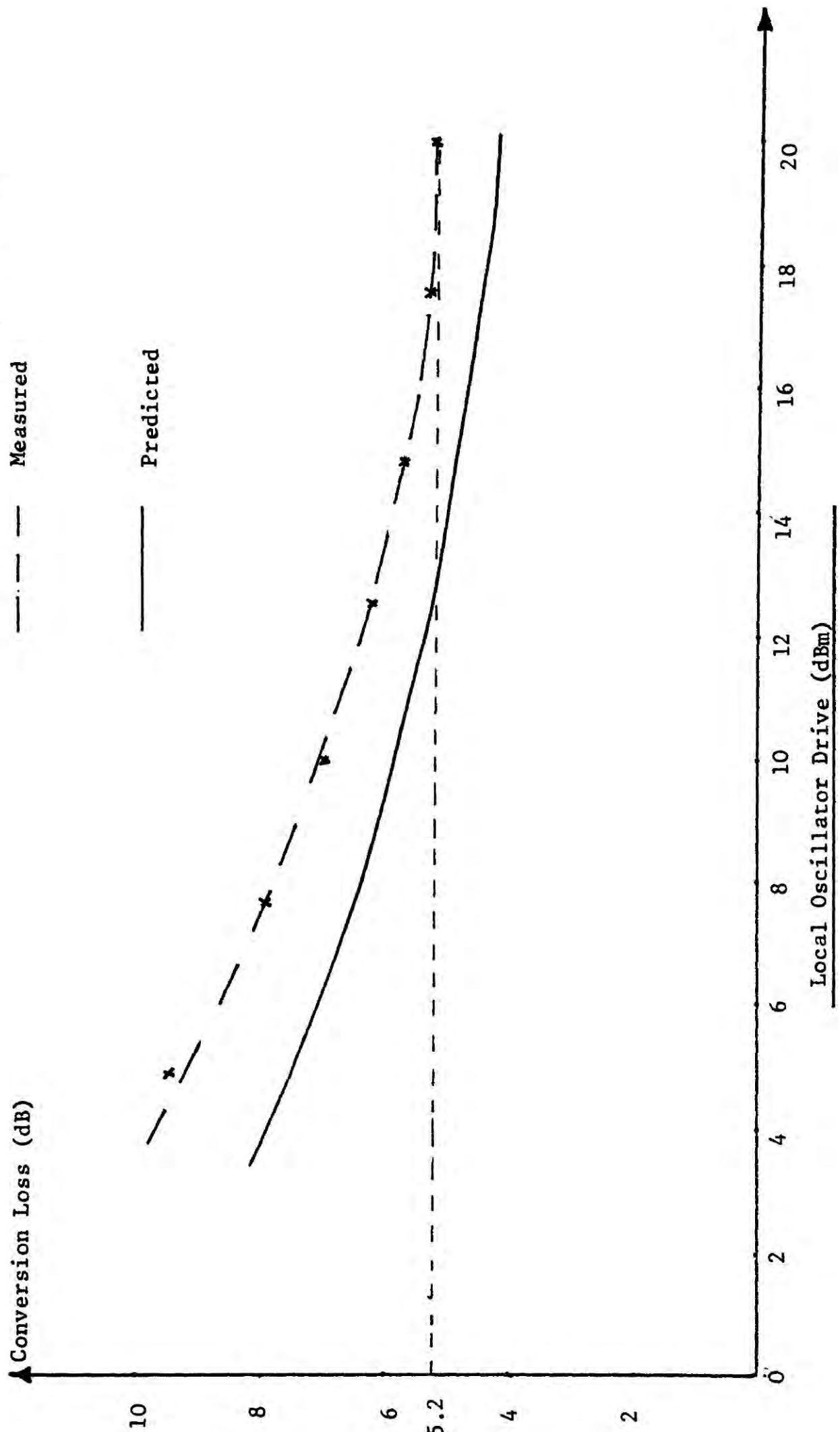
Figure 7.11 Measured and Predicted Performance of an Image Open-Circuit Mixer
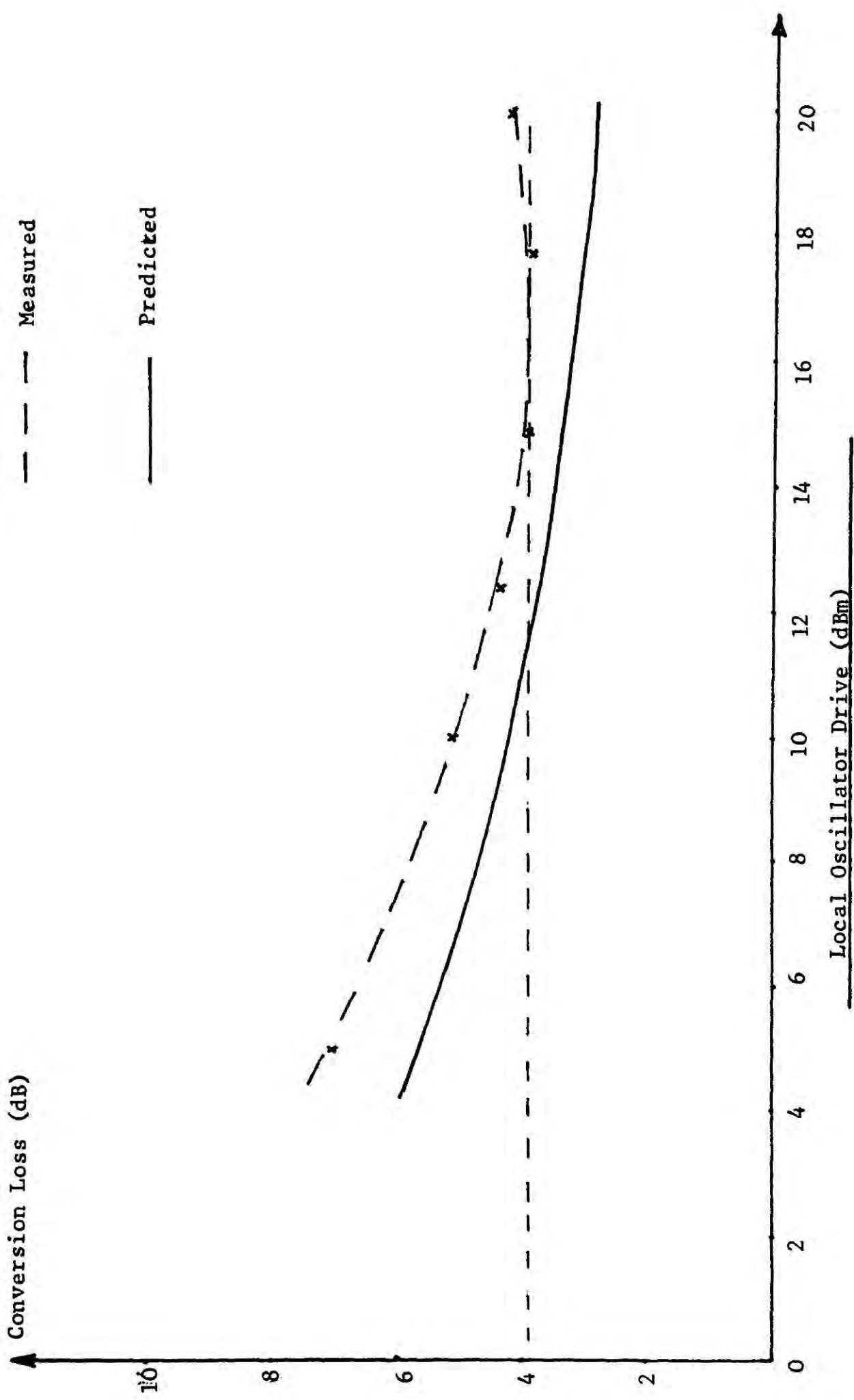
Figure 7.12 Measured and Predicted Performance of an Image Open-Circuit Mixer
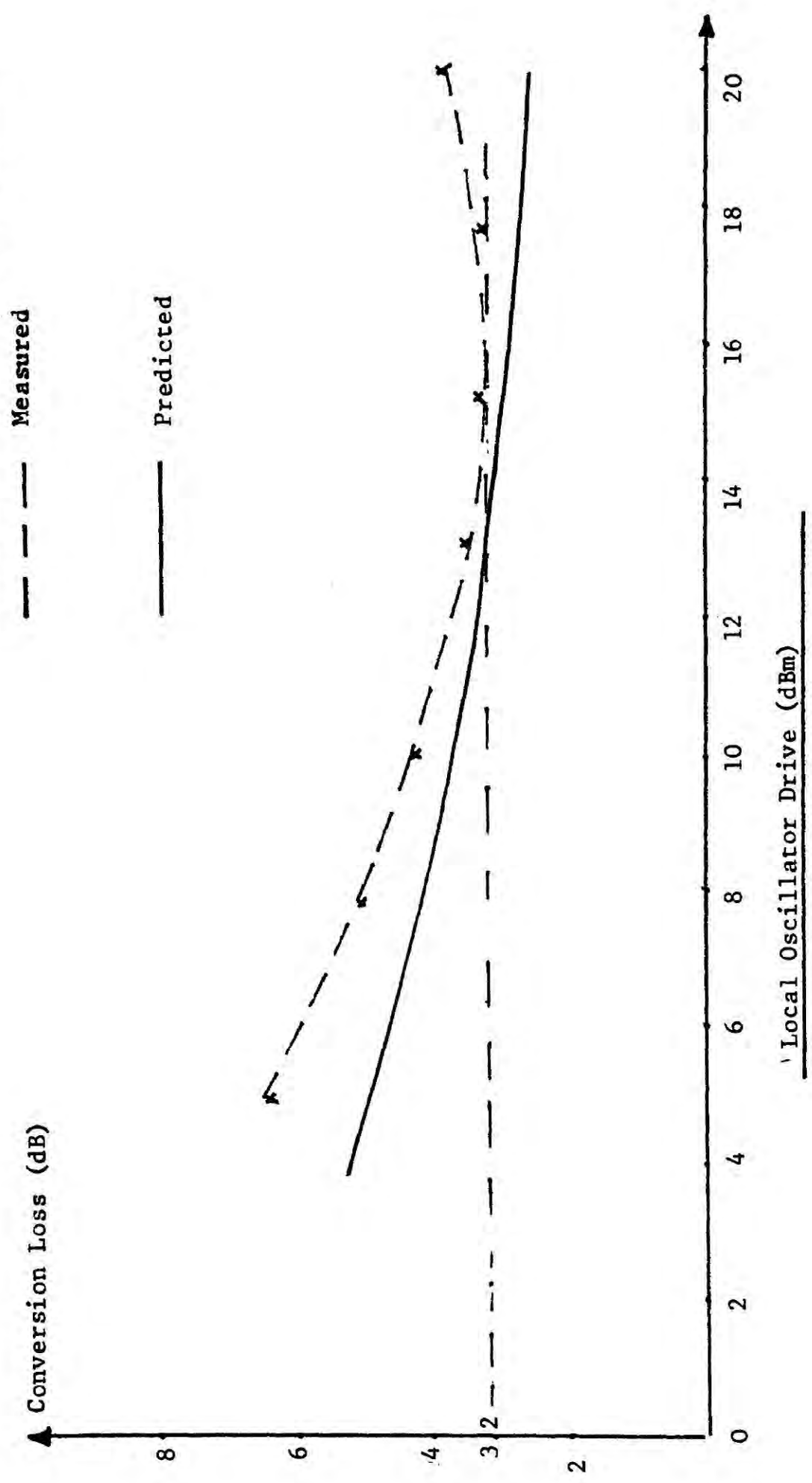
Figure 7.13   Measured and Predicted Performance of an Image Open-Circuit Mixer
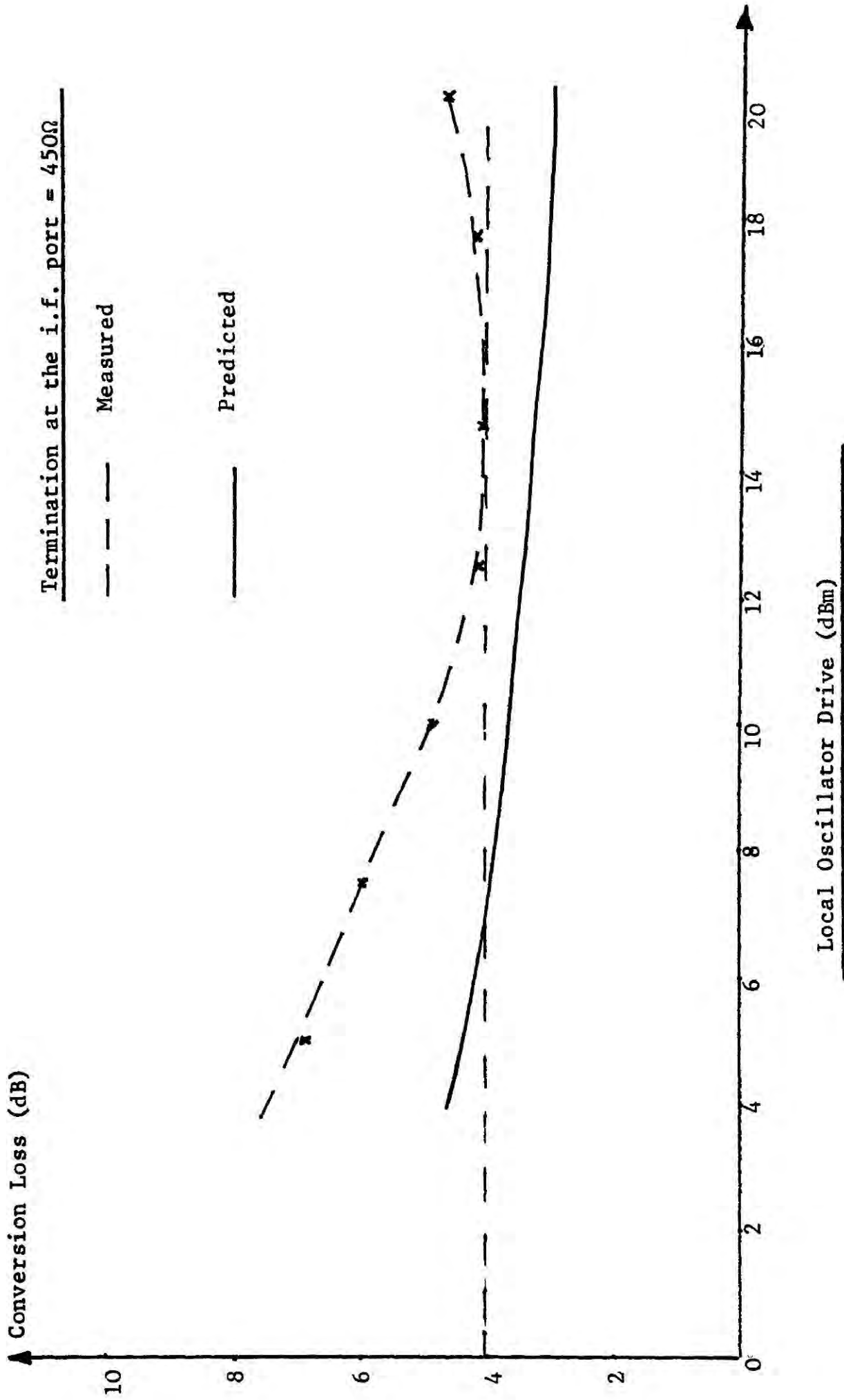
Figure 7.14 Measured and Predicted Performance of an Image Open-Circuit mixer
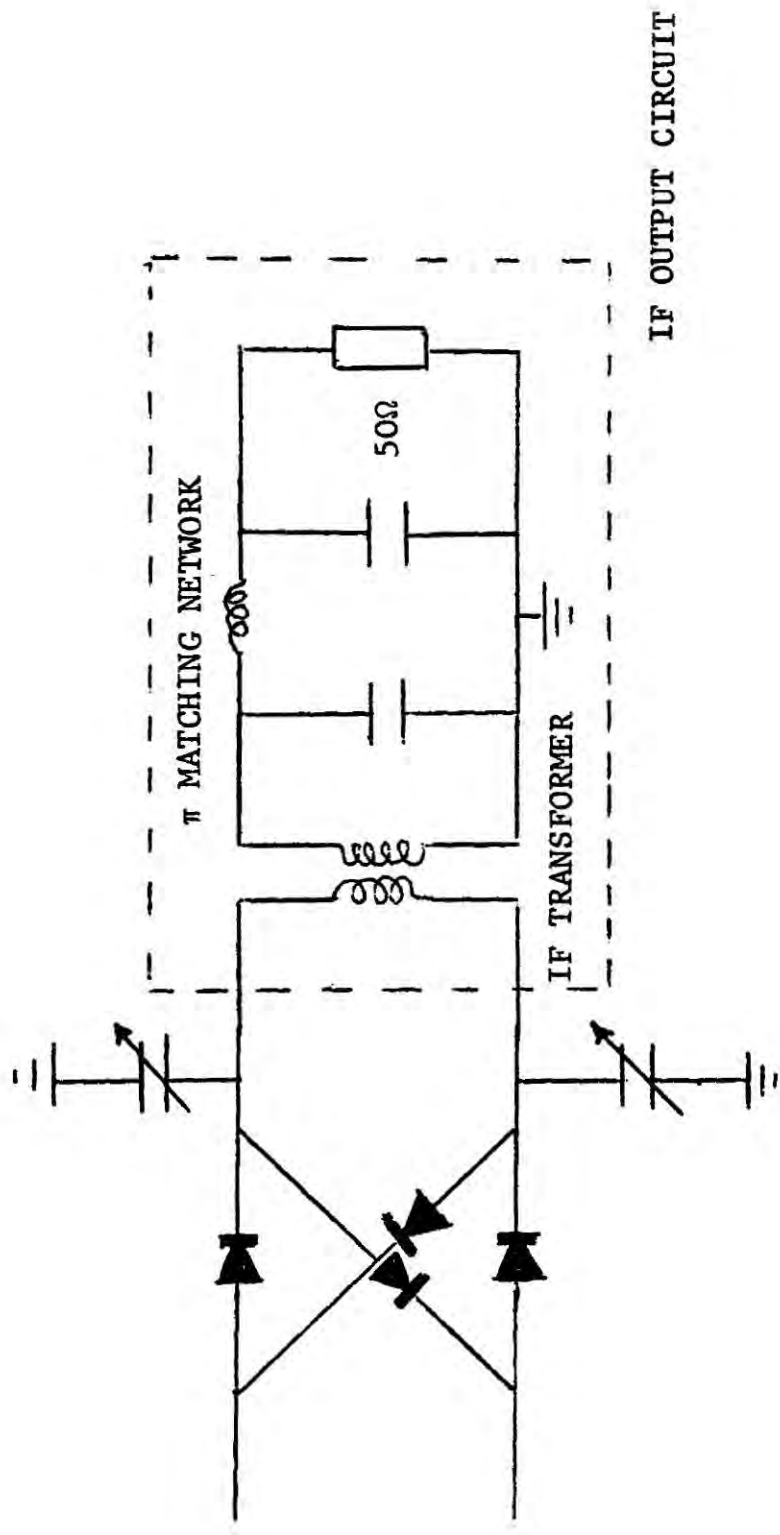
Figure 7.15 IF Output Circuit of the Mixer
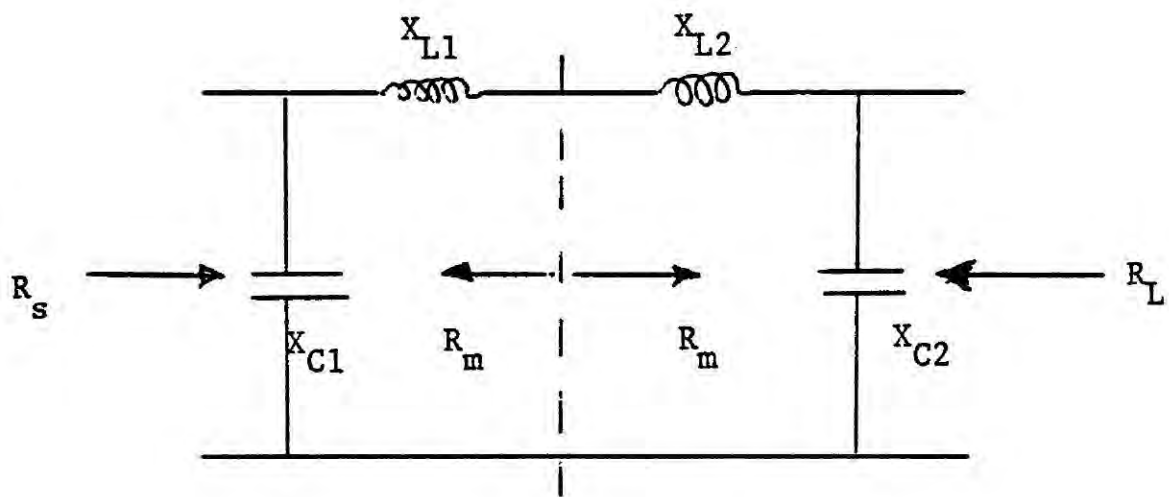
Figure 7.16 The π Matching Section
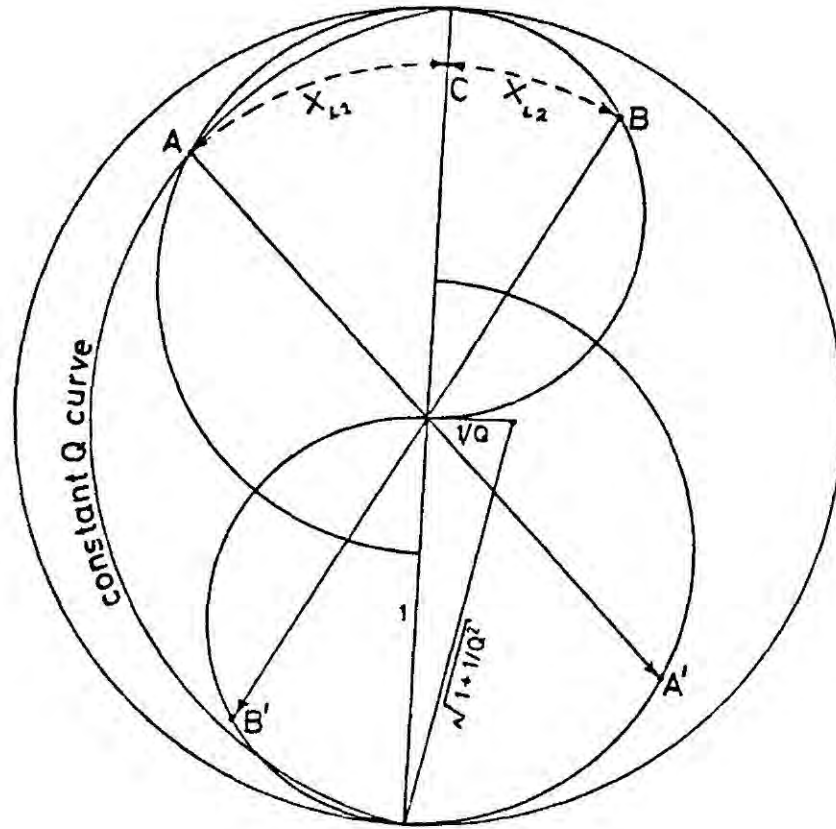
Figure 7.17 Design of the π Matching Network using the Smith Chart
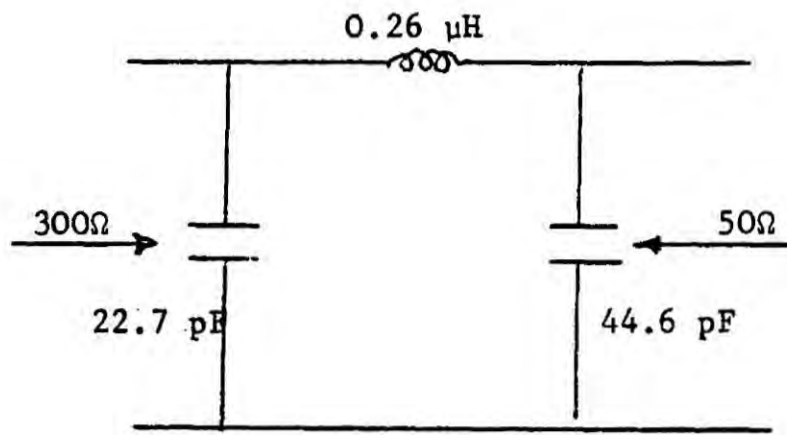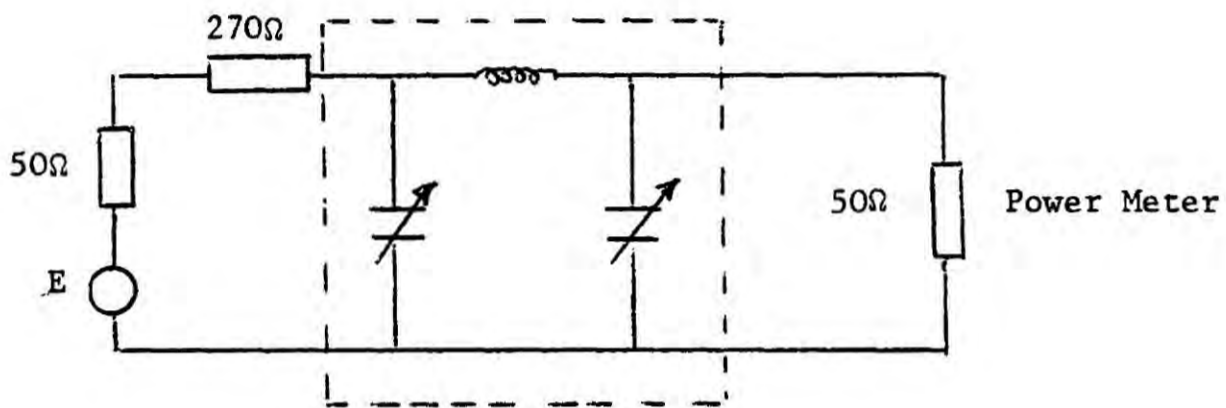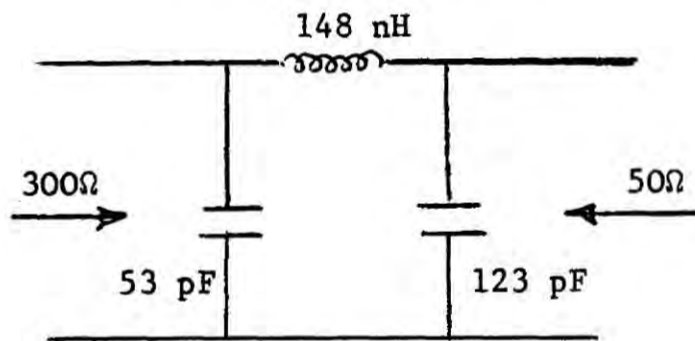
Figure 7.18 (a) π Matching Section with Q = 3

(b) Test Circuit

(c) π Matching Section with Q = 7
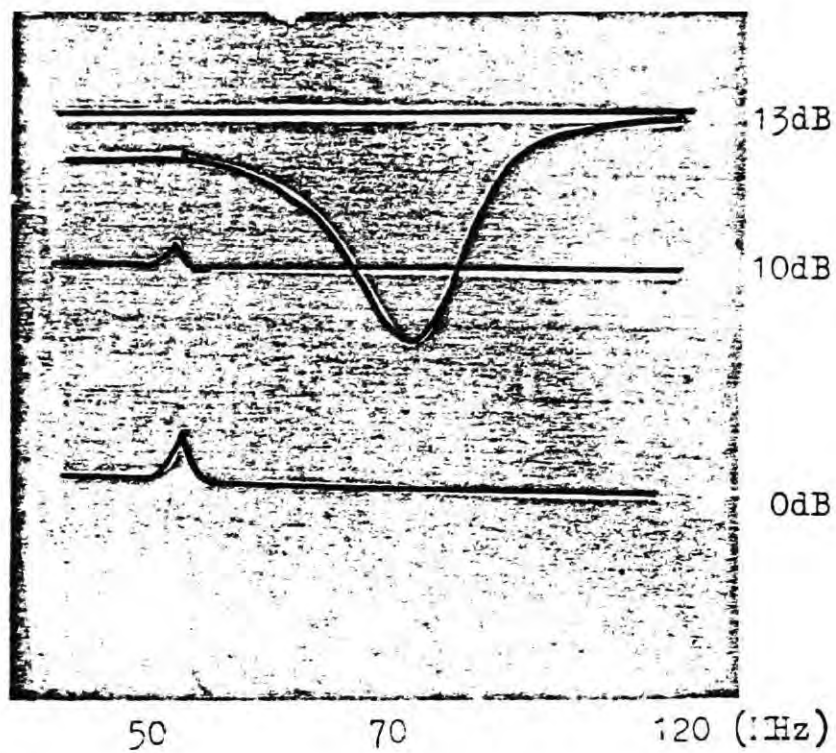
Figure 7.19 Frequency Response of the π Matching Section

Variable Capacitors

I.F. Transformer

MCL
TI-1

π Matching Network
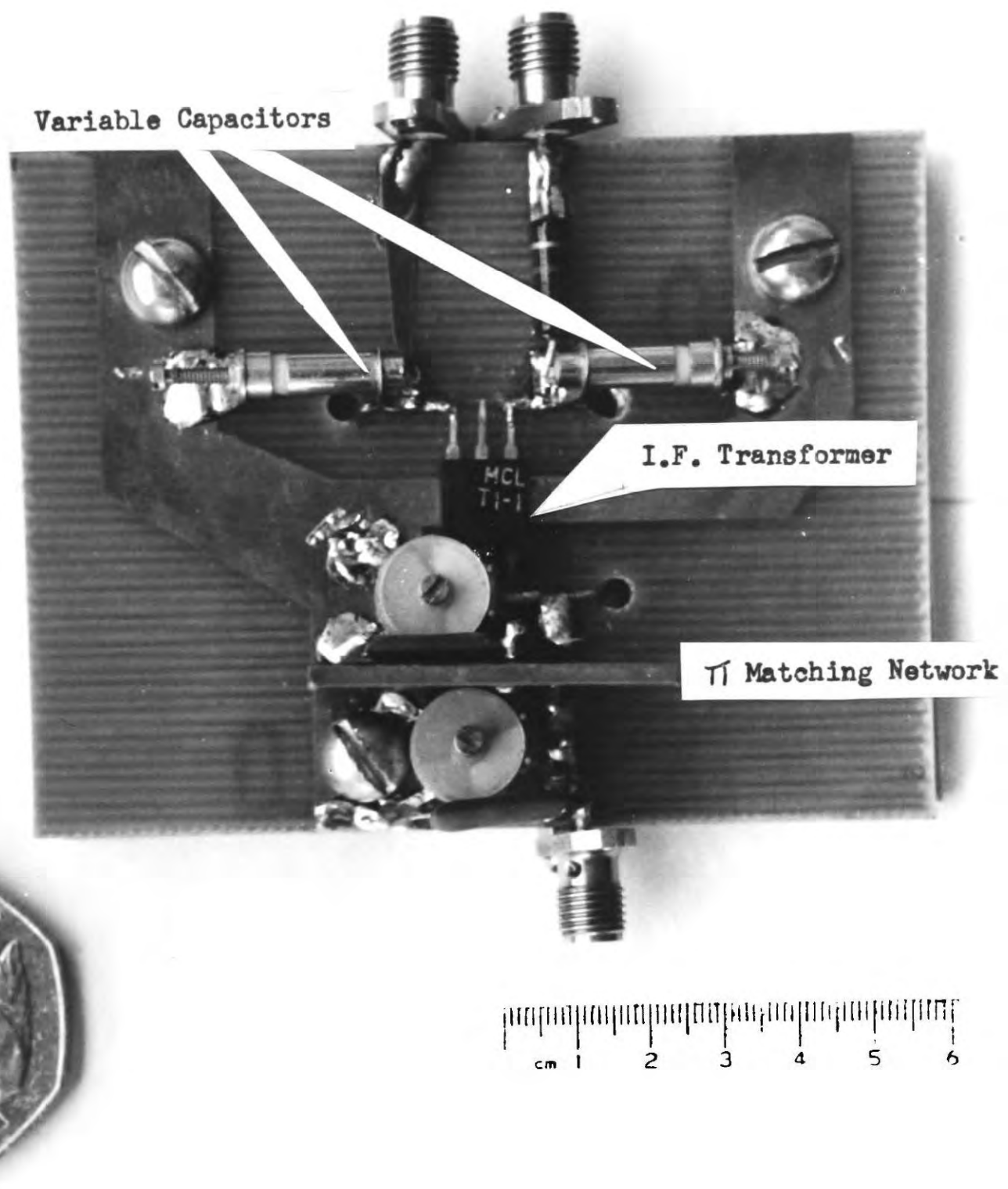
Figure 7.20(a) I.F. Output π Matching Section
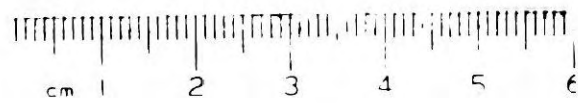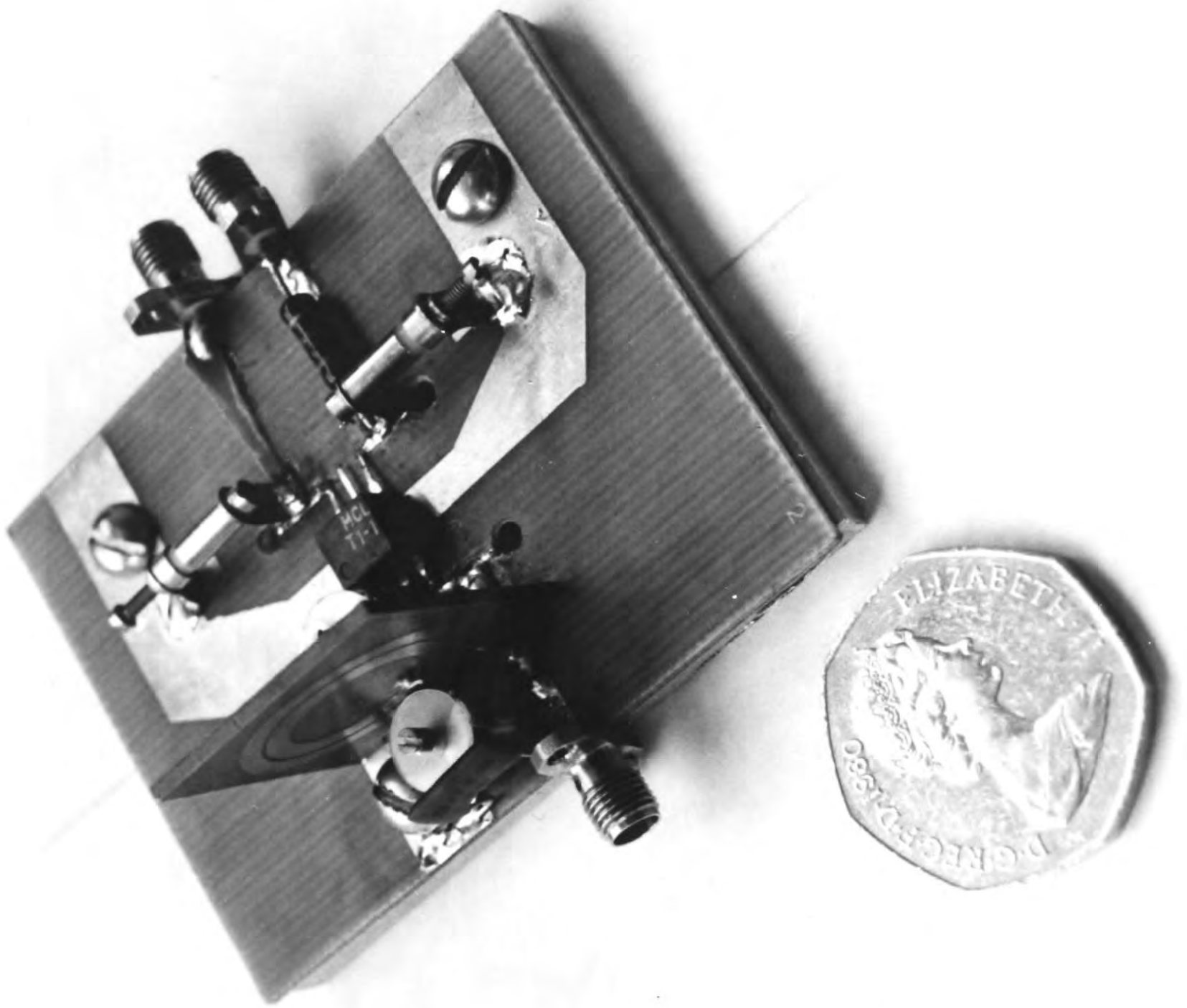
Figure 7.20(b) I.F. Output π Matching Section
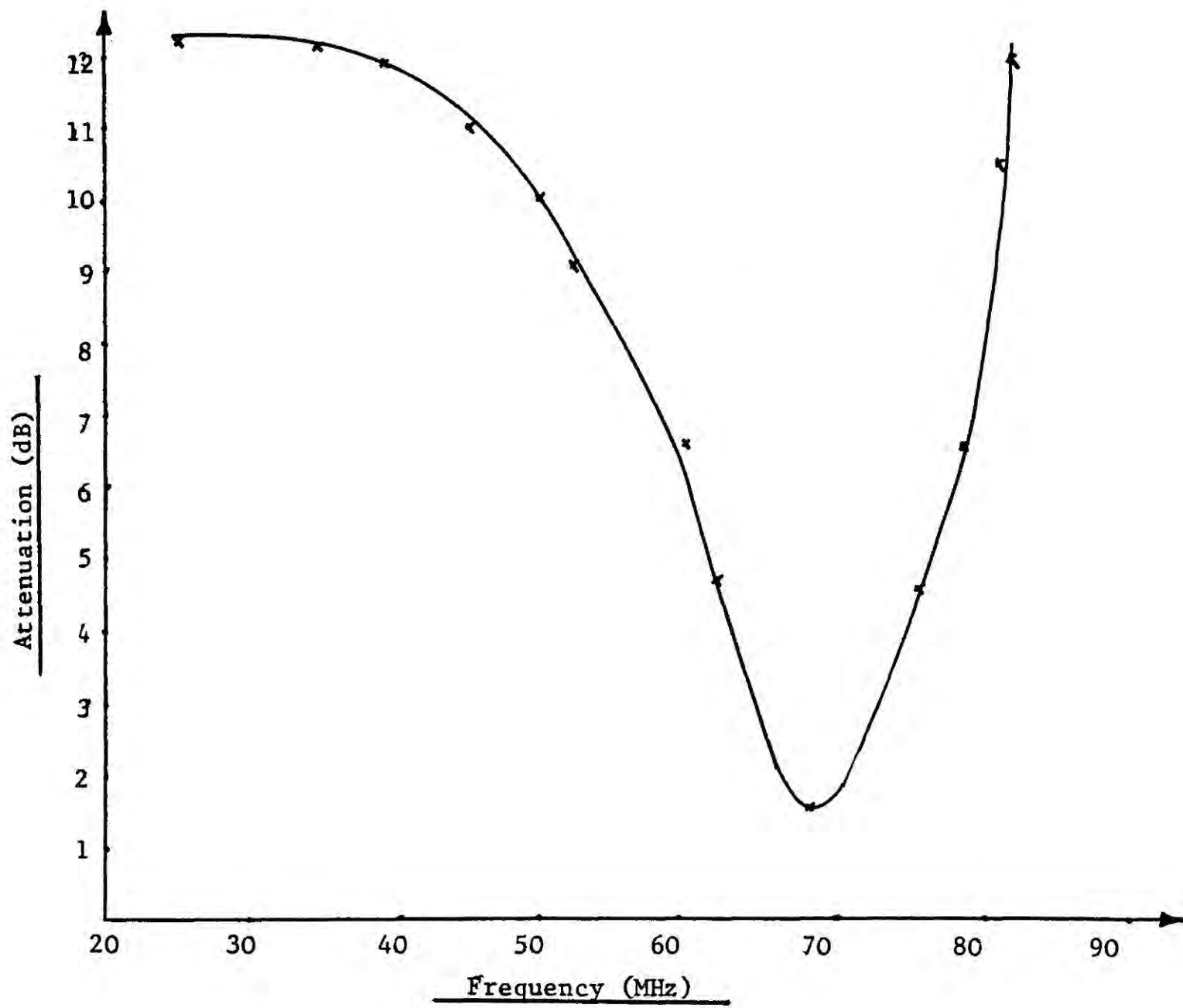
Figure 7.21 Measured Frequency Response of the IF Circuit
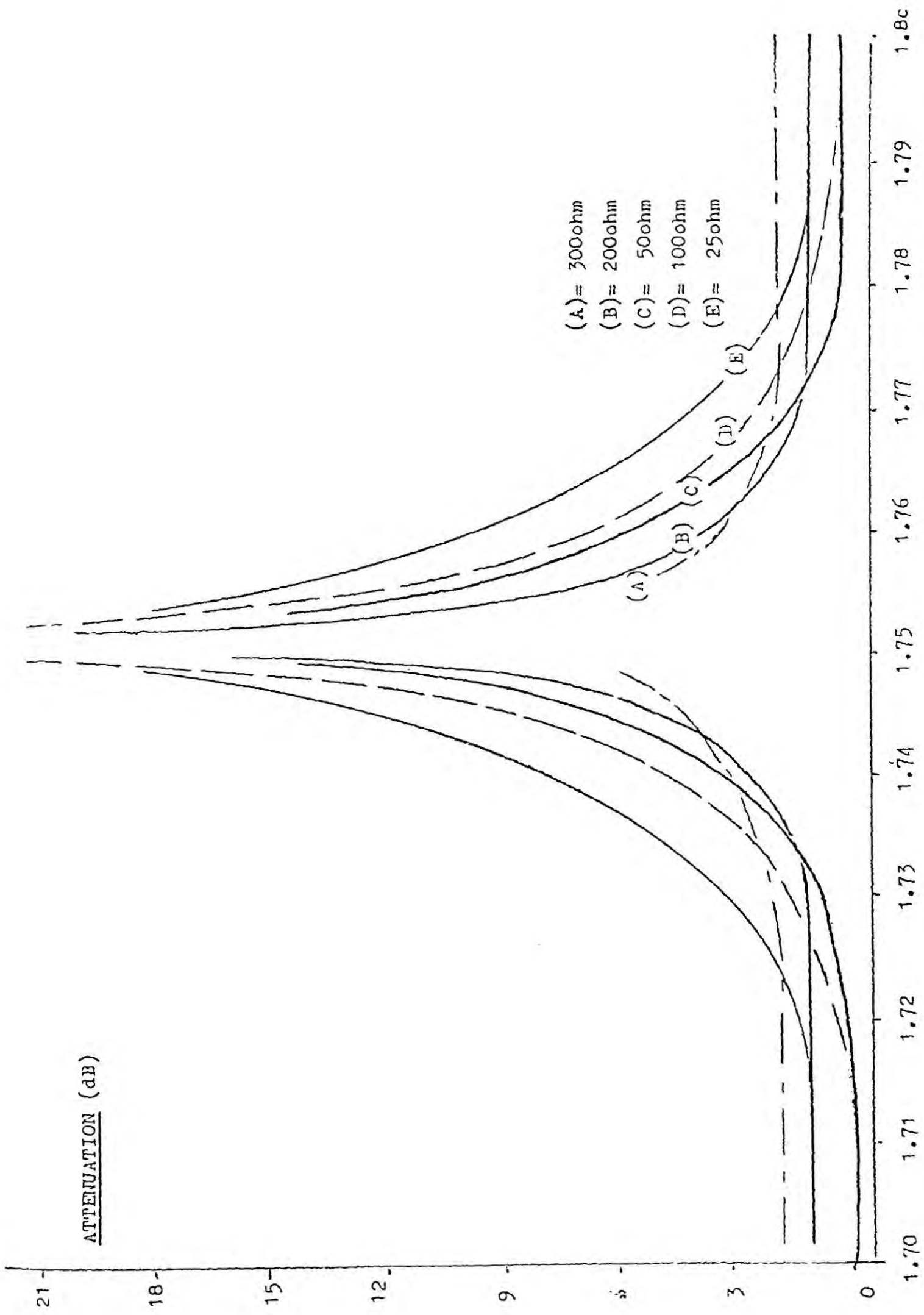
Figure 7.22 Effect of Mismatch on the Frequency Response of the Stopband Filter
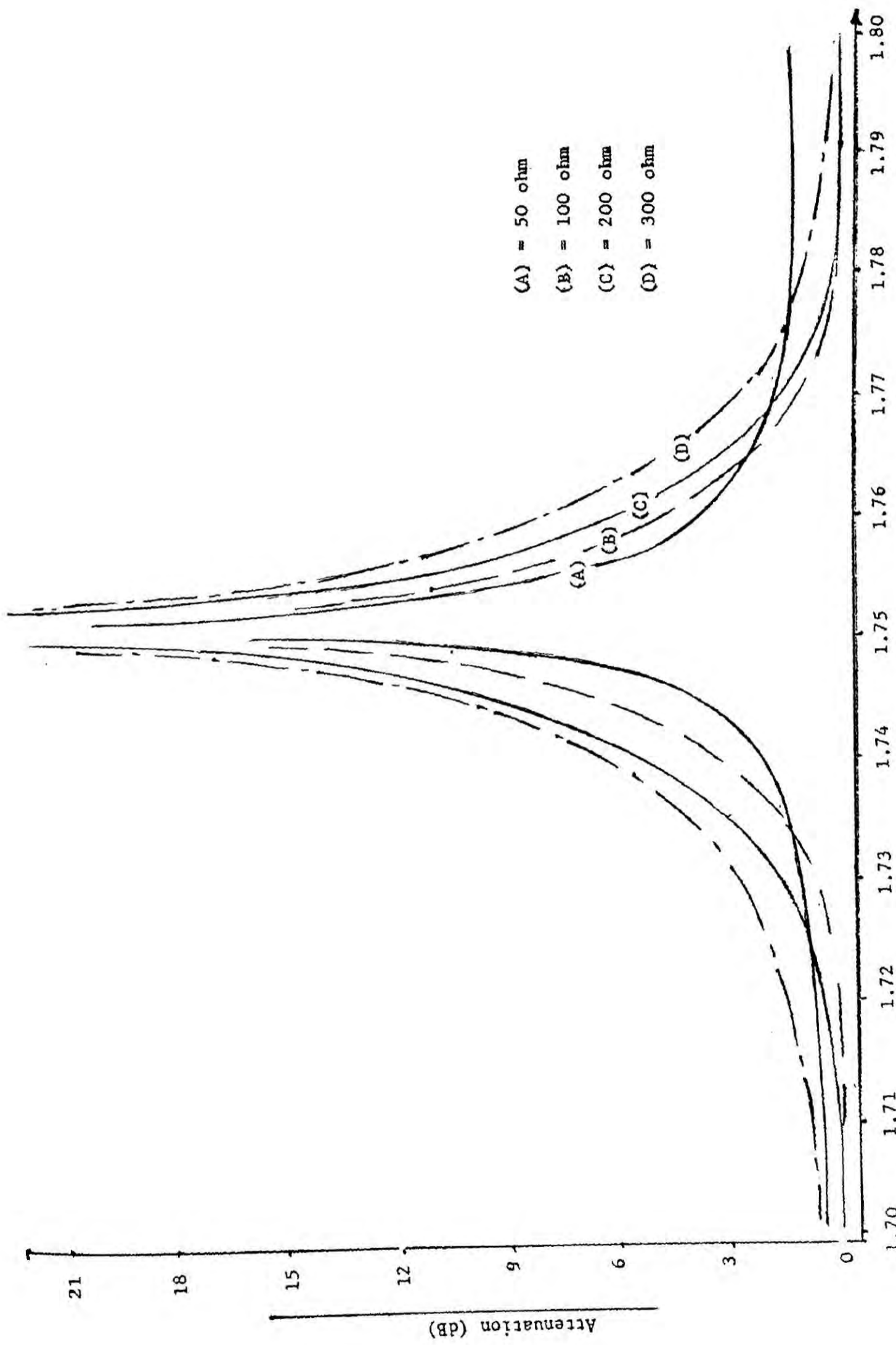
Figure 7.23 Computer Predicted Frequency Response of the Bandstop Filter and Transformer for Different Terminations at the Output Port.

(A) = 50 ohm
(B) = 100 ohm
(C) = 200 ohm
(D) = 300 ohm

Attenuation (dB)
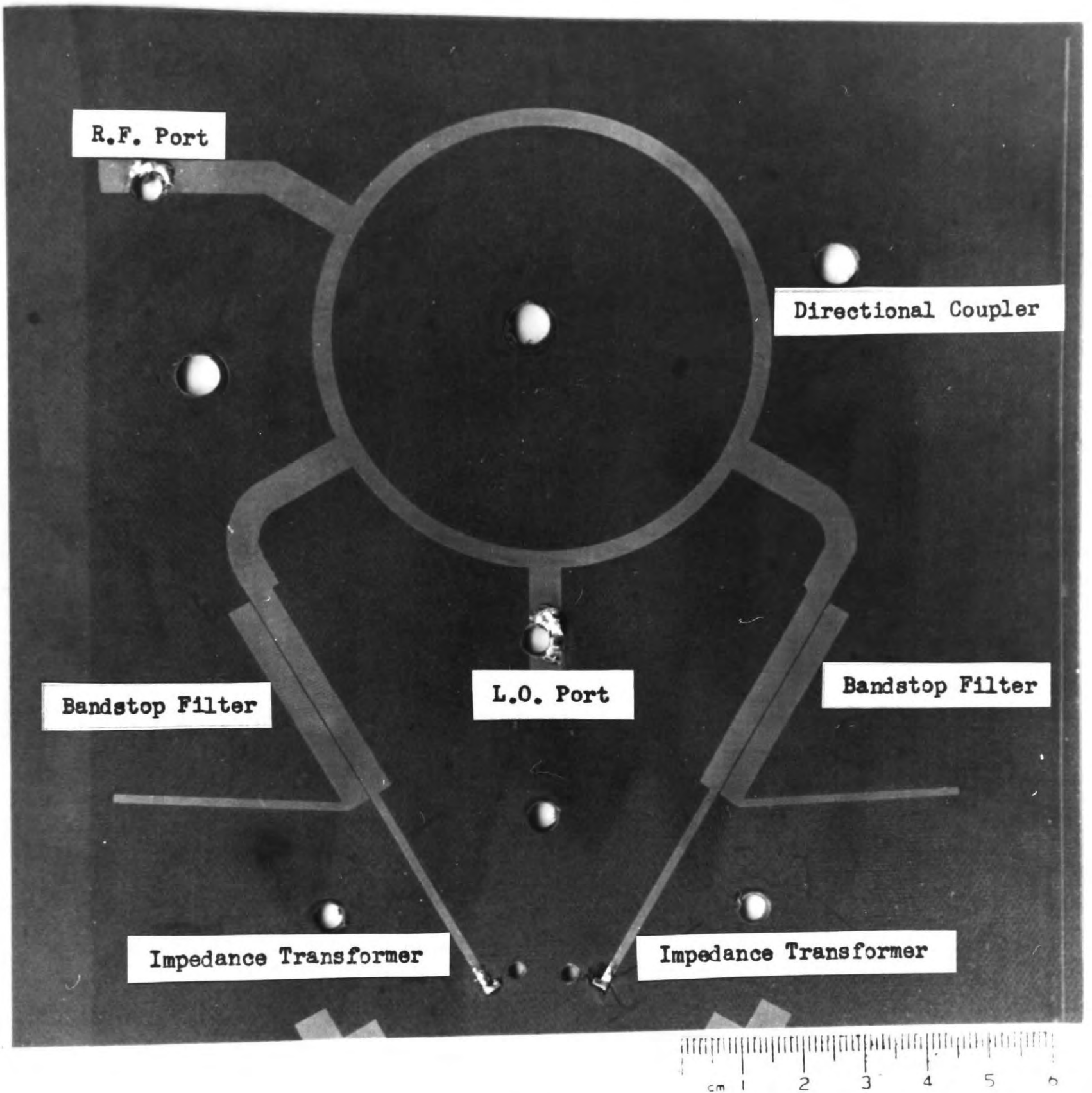
FREQUENCY (GHz)

Figure 7.24 Rat-Race Coupler, Filter and Impedance Transformer
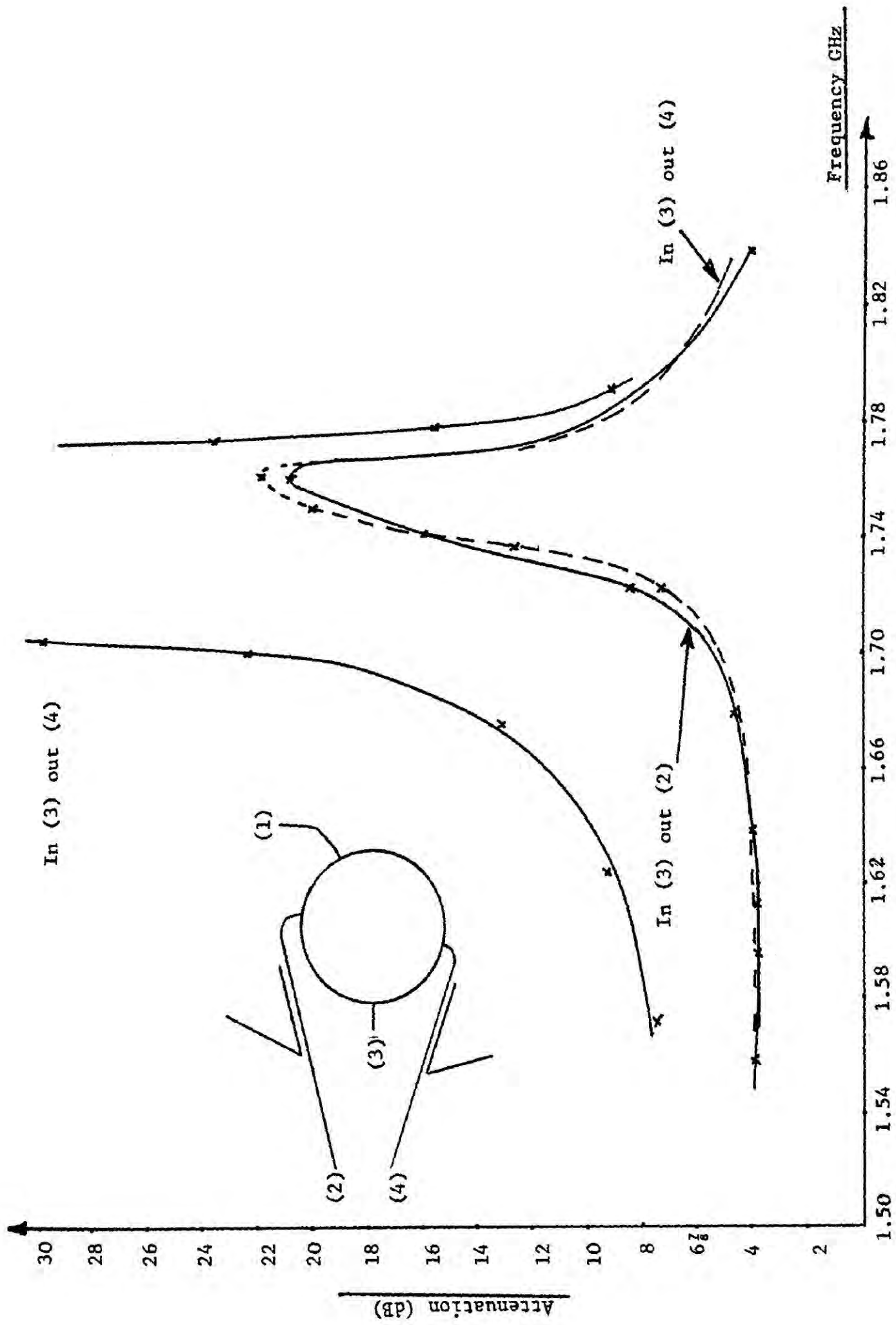
Figure 7.25 Measured Frequency Response of the Coupler, Bandstop Filters and Transformers
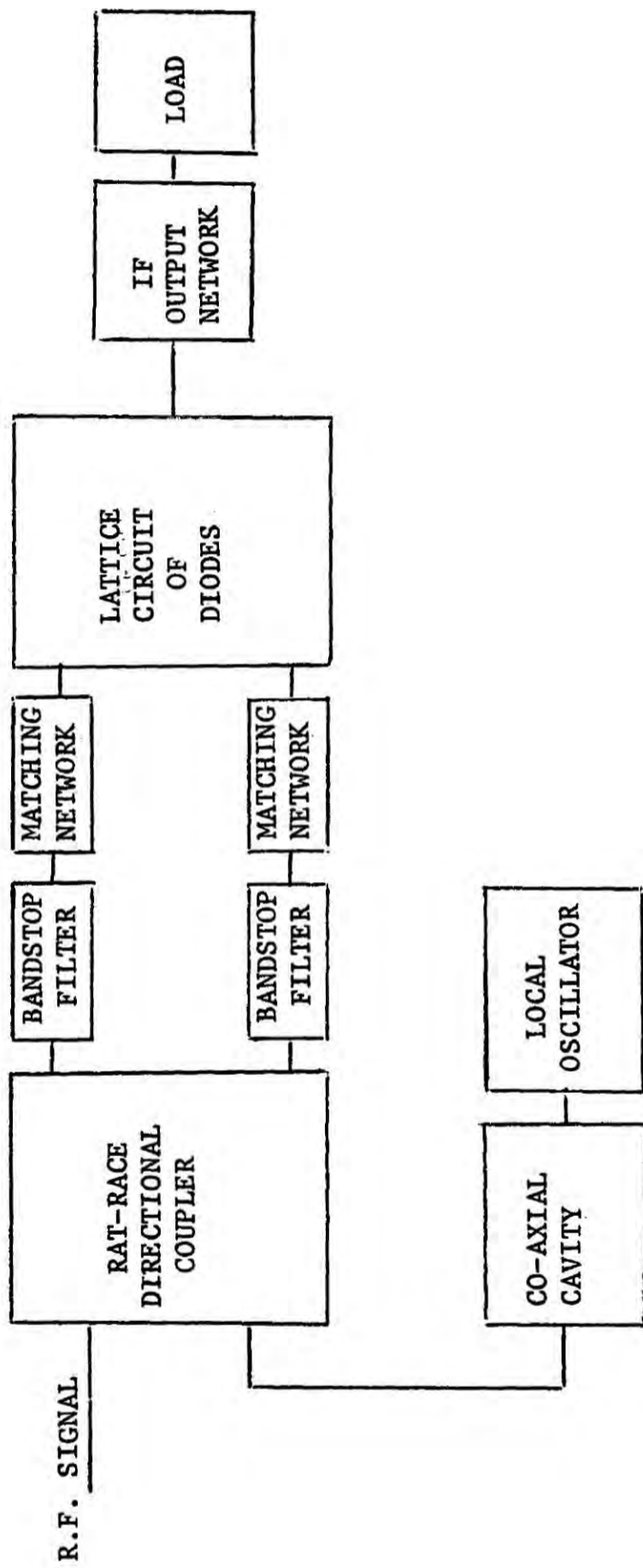
Figure 7.26 Block Diagram of the Image Open-Circuit Mixer
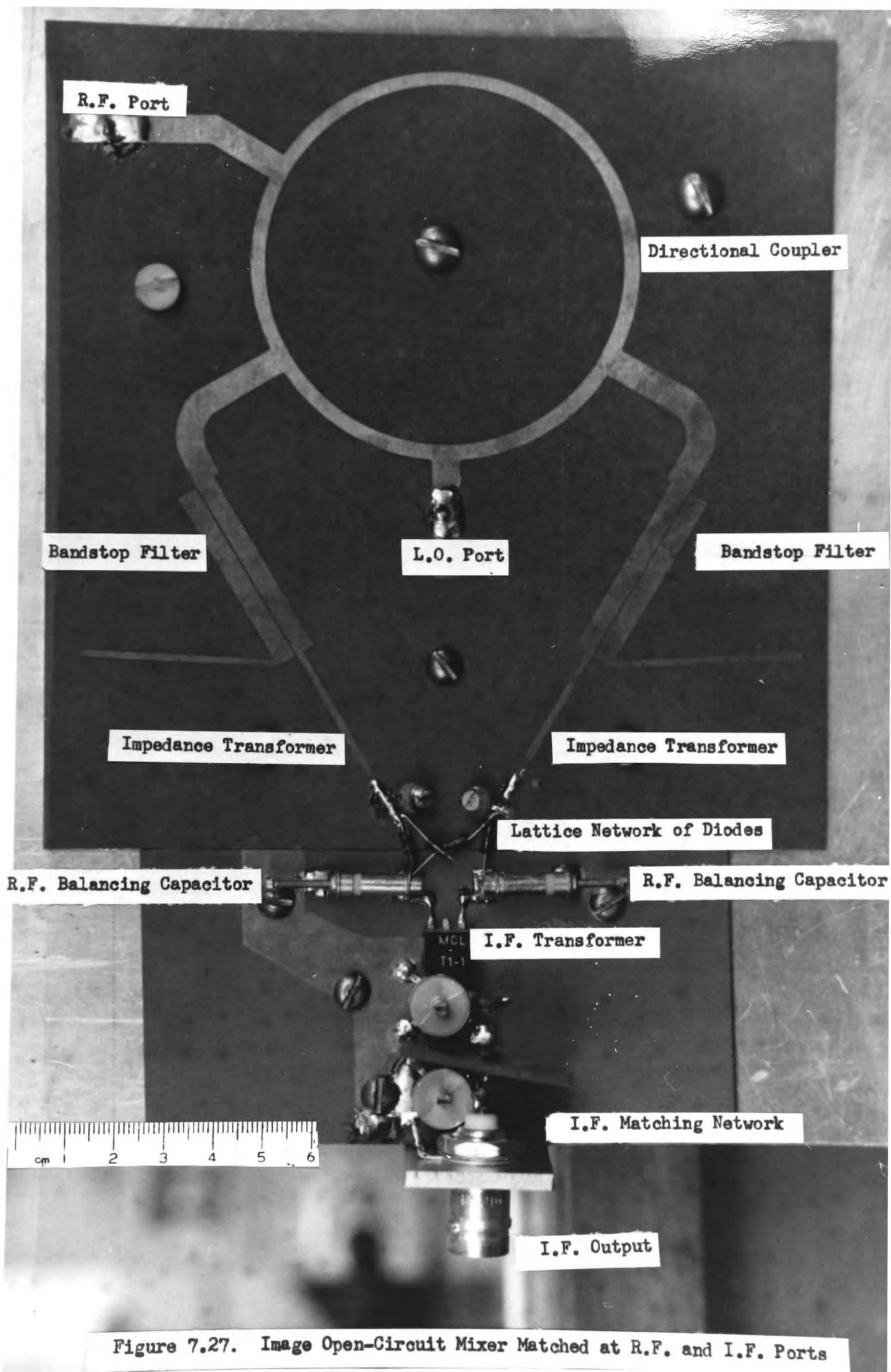
Figure 7.27.   Image Open-Circuit Mixer Matched at R.F. and I.F. Ports
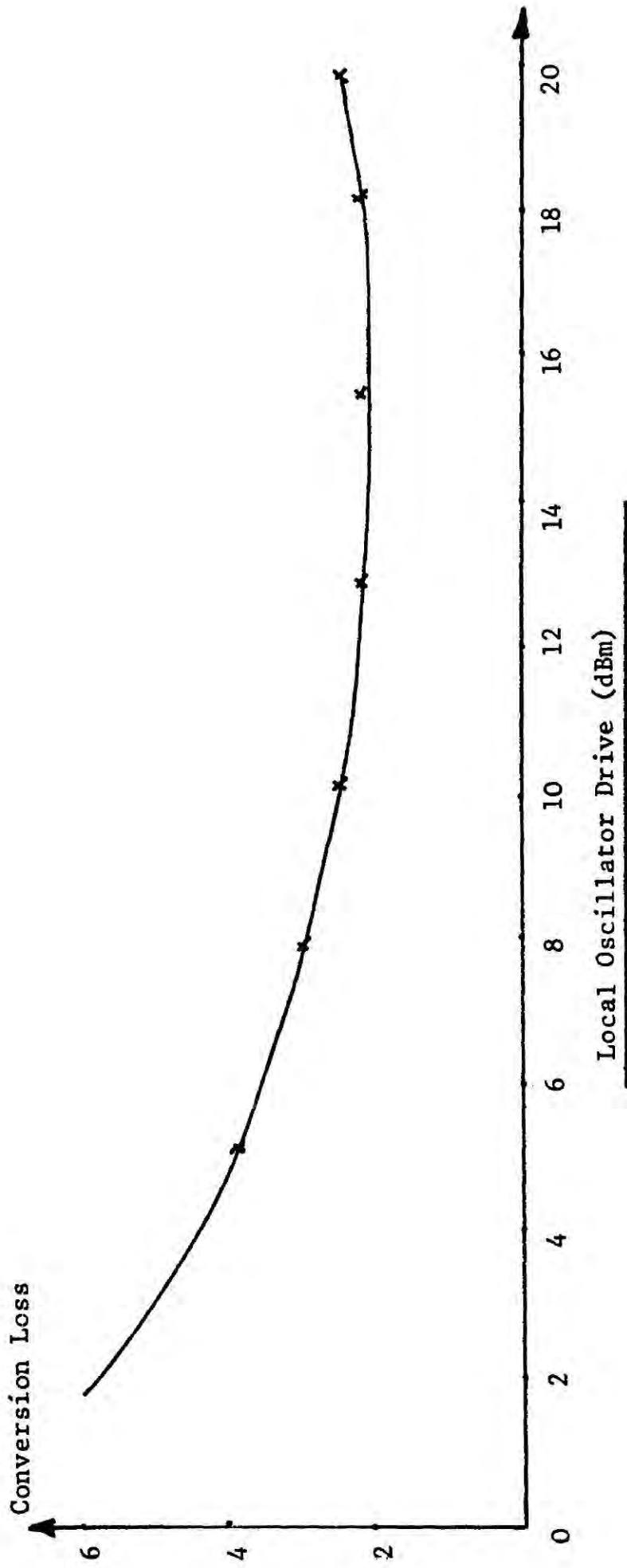
Figure 7.28 Measured C.L. of the Image Open-Circuit Mixed Matched at RF and IF Ports

CHAPTER VIII

Conclusions and Future Work

Single-balanced two-diode, and four-diode double-balanced, lattice mixers are usually preferred to single-diode mixers for high frequency applications as they generate a lower number of unwanted harmonic products and therefore reduce associated filtering problems. They also have the advantage of reducing the noise contribution from the local oscillator and eliminating the decoupling problems associated with the local oscillator circuit at the r.f. port of the mixer. A double balanced lattice mixer has a further advantage in that an inherent separation of odd and even harmonic products is obtained further reducing filter problems. Consequently the work presented here has been concerned with deriving the design criteria and properties of lattice mixers working at high frequencies where predictable losses are obtained.

The general analysis of mixers consists of two parts; one part is concerned with the behaviour of the diode when pumped by a large signal while the second part deals with the properties of the mixer in relation to the small signals. In Chapter I a review is carried out of the existing methods of large and small signal analysis. It is shown that the large signal analysis is concerned with the type of model which is to be used to represent the behaviour of the diode. The existing solutions that are readily available assume that the diode has either bi-linear or exponential characteristics and where the influence of diode parasitics is neglected. The effect of diode parasitics such as the series resistance and capacitance has, however, a considerable influence on the performance of mixers in practice and hence their presence cannot be neglected. The problem of obtaining analytical solutions to the large signal analysis where the effects of diode parasitics are included is formidable and this has lead to employing computer-aided analysis with various numerical by different workers. (Kerr, Cohn, Egami, Gwarek, Rustum and Howson).

When an r.f. signal is mixed with a local oscillator signal a whole
spectrum of harmonic modulation products is generated. Using pertubation
methods it is possible to analyse a non-linear circuit in terms of a number
of equations each corresponding to the harmonic modulation product present.
(Torrey and Whitmer). An alternative method to the classical frequency-
domain analysis of mixers is to adopt a time-domain approach to obtain the
scattering matrix of the complete mixer. This has been recently suggested
(Hines). Whichever method is employed it is generally recognised that to
improve the performance of the mixer it is essential that unwanted harmonic
modulation products generated by the diode are not allowed to dissipate
power externally or internally. The most important harmonic modulation
product is the image-frequency component, so named because of its relative
position to the r.f. signal in the frequency spectrum. As its magnitude
can be comparable to that of the signal and if its dissipation is not
reduced, high efficiency of conversion is not possible.

It is generally accepted that mixers are classified according to the
kind of termination that the image-frequency component 'sees' and normally
three types of mixers are considered: broadband; narrow-band image open-
circuit; narrow-band image short-circuit. In Chapter II a general analysis
is presented where the required terminations at the r.f. and i.f. ports
are determined in order to obtain minimum conversion loss for four types
of mixers; two narrow-band and two broadband. The inclusion of the fourth
type of mixer was felt to be necessary because it is generally not recognised
that a broadband mixer can be designed to either obtain minimum conversion
loss or to produce matching conditions at the r.f. and i.f. ports, a
condition appreciated by microwave engineers.

Frequency selective mixers can be used to realize Z, Y, G and H lattice mixers according to Saleh's classification and Chapter III is concerned with examining the properties of such mixers. The mixer analysis presented in Chapter III initially examined the properties of these mixers assuming that the diode has bi-linear characteristics. It is shown that there is a dual relationship between X and Y and G and H mixers, and that the conversion loss for G or H mixers is lower than the conversion loss for Z or Y mixers. Then for a sinusoidal current drive the performance of these mixers was examined assuming diodes have exponential characteristics and where the effect of the diode series resistance is included. It is shown that for this model of the diode, the duality property between the mixers no longer exists. It is therefore not possible to use the relationship $g(t) = r(t + \pi/\omega_p)$ for practical diodes, a relationship assumed by many researchers. That relationship is only valid if it is assumed that the diode obeys the bi-linear law or an exponential law where the effect of the diode series resistance is neglected. Finally in Chapter III the performance of the four types of lattice mixers, using the two models of the diode and for different image terminations, are compared. Such comparison and discussion of the performances has not been dealt with in any of the available literature. As a result of the work presented in Chapters II and III two papers have been published by the Institution of Electrical Engineers.

In large signal analysis it is very often assumed that the local oscillator waveform is sinusoidal at the diode junction so that the Fourier coefficients are only a function of the amplitude of the local oscillator drive. Chapter IV therefore initially examines the effect of diode capacitive parasitics on the waveshape of the current flowing in the diodes of a lattice mixer. It is shown that the effect of these parasitics is to produce a truncated half-wave rectified diode current. The parameters affecting the angle of truncation are analytically derived. The results found in this chapter are very important

as it has been suggested (neglecting the effect of diode capacitive parasitics), that the conversion loss and the noise figure of the mixer are considerably improved, for a lattice mixer pumped by an oscillator having a high output impedance (Howson, Stracca). A compromise must therefore be made in practice between the need to have a large output impedance to reduce the noise figure of the mixer, and the need to lower the output impedance of the local oscillator, so that the angle of truncation of the diode current can be minimized. Again as a result of the work done in Chapter IV two papers have been published by the Institution of Electrical Engineers.

Chapter V is concerned with the properties of microstrip planar transmission lines and their application in realizing filters and directional couplers. Coupled microstrip transmission lines form a basic building element in the realization of many microwave components but the information about their properties is usually presented in graphical forms and only for particular values of relative permittivities of the substrates. To overcome this problem an analytical solution has been suggested. Based on this solution bandpass and bandstop microstrip filters were realized and their properties examined. One interesting conclusion reached is that in realizing microwave components where electromagnetic coupling is employed, in order to obtain a good performance low loss substrate should be used.

Chapter VI is initially concerned with the evaluation of diode parameters of importance in the analysis of lattice mixers. Then using these diode parameters a theoretical relationship is derived between the normalized current drive and the available local oscillator power. This is done because it is not possible in practice to measure current directly but it is possible to measure power. Finally, Chapter VI examines the performance of a broadband mixer having different terminations at the i.f. port and the results obtained are compared with those theoretically predicted. It is found that good agreement is obtained between theory and practice.

In Chapter VII the performance of narrow-band mixers using realizable terminations is examined. It is concluded that the narrow-band image open-circuit mixer offers the best possibility of obtaining a low conversion loss figure. The realization and performance of this mixer are then considered for different terminations at the r.f. and i.f. ports. The design criteria and the performance obtained at the r.f. and i.f. stages are presented and finally the performance of the mixer obtained in practice is compared with that predicted by theory. Again a good agreement is obtained between the predicted performance and that actually obtained in practice.

The performance of this mixer can be improved if the losses caused by the r.f. and i.f. stages are reduced. Any further work on this mixer should therefore consider reducing the losses produced by the imbedding networks and in particular the loss produced by the i.f. transformer.

The optimum performance produced by the narrow-band image open-circuit has been obtained at a fixed frequency. It should be possible to realize image open-circuit mixers which are tunable over a limited range of frequencies by applying tunable bandstop filters (analysed in Chapter V).

The theory presented in this work has been concerned with examining the required terminations at the r.f., i.f. and image frequency in order to obtain minimum conversion loss. For the proposed model of the diode, an analytical solution should be possible to indicate the noise performance of the mixer.

It is suggested that this be done in terms of time-varying conductance and time-varying temperature as proposed by Dragone.

Appendix I

Derivation of the Coefficients for a Z Mixer

Substituting equations 3.4(a) and 3.4(b) into the general matrix equation 3.1 the following equations are obtained.

$$V_1 = \left(I_q \cos \omega_q t + I_I \cos (2\omega_p - \omega_q) t \right) \Sigma a_n \cos n\omega_p t$$
$$n \text{ even}$$

$$+ \left(I_{i.f.} \cos (\omega_p - \omega_q) t \right) \Sigma b_n \cos n\omega_p t$$
$$n \text{ odd}$$

A1.1

$$V_2 = \left(I_q \cos \omega_q t + I_I \cos (2\omega_p - \omega_q) t \right) \Sigma c_n \cos n\omega_p t$$
$$n \text{ odd}$$

$$+ \left(I_{i.f.} \cos (\omega_p - \omega_q) t \right) \Sigma d_n \cos n\omega_p t$$
$$n \text{ even}$$

A1.2

Extracting relations from the above equation at r.f., image and i.f. frequencies results in the matrix equation.

$$\begin{bmatrix} V_q \\ V_{i.f.} \\ V_I \end{bmatrix} = \begin{bmatrix} a_o & , & \frac{b_1}{2} & , & \frac{a_2}{2} \\ \frac{c_1}{2} & , & d_o & , & \frac{c_1}{2} \\ \frac{a_2}{2} & , & \frac{b_1}{2} & , & a_o \end{bmatrix} \begin{bmatrix} I_q \\ I_{i.f.} \\ I_I \end{bmatrix}$$

A1.3

Using equation 3.16 it can be shown that,

$$c_1 = b_1$$

The coefficients of equation A1.3 describing the Z mixer are derived as shown below

$$z_{11} = a_o = \frac{1}{2\pi} \int_{-\pi/2}^{3\pi/2} r_s + \frac{r_b \left(1 + X(t) \ s(t) \right)}{1 + 2X(t) \ s(t)} \ d(\omega_p t)$$

A1.4

The switching parameter s(t) is defined as,

$$s(t) = 1 \text{ for } {}^{-\pi}/2 \leqslant \omega_p t \leqslant {}^{\pi}/2 \qquad\qquad A1.5$$

$$s(t) = -1 \text{ for } {}^{\pi}/2 \leqslant \omega_p t \leqslant {}^{\pi}/2$$

The integral of equation 1.4 can be evaluated by sectioning it between the limits ${}^{-\pi}/2$ to ${}^{\pi}/2$ and ${}^{\pi}/2$ to ${}^{3\pi}/2$ i.e.

$$z_{11} = \frac{1}{2\pi} \int_{-\pi/2}^{\pi/2} (r_s + r_b \frac{1 + X \cos (\omega_p t)}{1 + 2X \cos \omega_p t}) d(\omega_p t) + \int_{\pi/2}^{3\pi/2} (r_s + r_b \frac{1 - X \cos(\omega_p t)}{1 - 2X \cos \omega_p t}) d(\omega_p t$$

$$= r_s + \frac{r_b}{2\pi} \left[\int_{-\pi/2}^{-\pi/2} (\frac{1}{2} + \frac{1}{2 (1 + 2X \cos (\omega_p t))}) \, d(\omega_p t) + \int_{\pi/2}^{3\pi/2} (\frac{1}{2} + \frac{1}{2 (1 - 2X \cos \omega_p t)}) \, d(\omega_p t) \right]$$

$$= \left(r_s + \frac{r_b}{2} \right) + \frac{r_b}{\pi} \left[\int_{-\pi/2}^{\pi/2} \frac{d(\omega_p t)}{1 + 2X \cos (\omega_p t)} \right] \qquad\qquad A1.6$$

The integral in equation A1.6 can now be evaluated using tables of integrals and reduces to the form shown below for $X \gg 1$.

$$z_{11} \approx \frac{r_b}{2} + \frac{r_b}{2\pi X} \log_e 4X \qquad\qquad A1.7$$

Similarly using equations 3.16 and A1.3 it can be shown that

$$z_{12} = \frac{b_1}{2} = \frac{r_b}{2\pi} \left[\int_{-\pi/2}^{3\pi/2} \frac{X \cos^2 (\omega_p t) \, d(\omega_p t)}{1 + 2X(t) \, s(t)} \right]$$

$$= \frac{r_b}{2\pi} \left[\int_{-\pi/2}^{\pi/2} \frac{X \cos^2 (\omega_p t) \, d(\omega_p t)}{1 + 2X \cos \omega_p t} + \int_{\pi/2}^{\pi/2} \frac{X \cos^2 (\omega_p t) \, d(\omega_p t)}{1 - 2X \cos \omega_p t} \right]$$

$$= \frac{r_b}{\pi} \left[\int_{-\pi/2}^{\pi/2} \frac{\left[X \cos^2 (\omega_p t) \right] d(\omega_p t)}{1 + 2X \cos (\omega_p t)} \right] \qquad A1.8$$

For $X \gg 1$ equation A1.8 can be evaluated to the form given below.

$$z_{12} = \frac{r_b}{\pi} X \left(\frac{1}{X} - \frac{\pi}{4X^2} + \frac{1}{4X^3} \log_e 4X \right)$$

$$\approx r_b/\pi \qquad A1.9$$

Using the same technique as above if can be shown that,

$$z_{13} = \frac{A_2}{2} = \frac{r_b}{2\pi} \left[\int_{-\pi/2}^{3\pi/2} \frac{\left[\left(1 + X(t) \ s(t) \right) \cos (2\omega_p t) \right] d(\omega_p t)}{1 + 2X(t) \ s(t)} \right] A1.10$$

Sectioning the above integral, equation A1.10 reduces to

$$z_{13} = \frac{r_b}{2\pi} \left[\int_{-\pi/2}^{\pi/2} \frac{\left[\cos (2\omega_p t) \right] d(\omega_p t)}{1 + 2X \cos (\omega_p t)} \right] \qquad A1.11$$

For $X \gg 1$ equation A1.11 can be evaluated and results in the following expression for z_{13}.

$$z_{13} = \frac{r_b}{2\pi} \left(\frac{1}{X} \log_e 4X + \frac{2}{X} - \frac{\pi}{2X^2} + \frac{1}{2X^3} \log_e 4X \right)$$

$$\approx \frac{r_b}{2\pi X} \left(2 + \log_e 4X \right) \qquad A1.12$$

Appendix II

Derivation of the Coefficients for a Y Mixer

Substituting equations 3.6(a) and 3.6(b) into the general matrix equation 3.1, the following equations can be obtained.

$$I_1 = \left(V_q \cos \omega_q t + V_I \cos (2\omega_p - \omega_q)t \right) \Sigma a_n \cos n\omega_p t$$
$$n \text{ even}$$

$$+ \left(V_{i.f.} \cos (\omega_p - \omega_q)t \right) \Sigma b_n \cos n\omega_p t \qquad \text{A2.1}$$
$$n \text{ odd}$$

$$I_2 = \left(V_q \cos \omega_q t + V_I \cos (2\omega_p - \omega_q)t \right) \Sigma c_n \cos n\omega_p t$$
$$n \text{ odd}$$

$$+ \left(V_{i.f.} \cos (\omega_p - \omega_q)t \right) \Sigma d_n \cos n\omega_p t \qquad \text{A2.2}$$
$$n \text{ even}$$

Extracting the relation from the above equations at r.f. image and i.f. frequencies and using equation 3.24, the coefficients of the matrix equation describing a Y mixer are derived below.

$$y_{11} = \frac{1}{2\pi} \int_{-\pi/2}^{\pi/2} \frac{\left(1 + X(t) \, s(t) \right) d(\omega_p t)}{r_b + 2r_s \, X(t) \, s(t)} \qquad \text{A2.3}$$

Splitting the above integral between the limits $^{-\pi}/2$ to $^{\pi}/2$ and $^{\pi}/2$ to $^{3\pi}/2$ the integral in equation A2.3 reduces to,

$$y_{11} = \frac{1}{\pi r_b} \int_{-\pi/2}^{\pi/2} \frac{\left(1 + X \cos \omega_p t \right) d(\omega_p t)}{1 + b \cos \omega_p t} \qquad \text{A2.4}$$

where the parameter b is given by,

$$b = 2r_s X/r_b \qquad \text{A2.5}$$

Depending on the local oscillator drive the parameter b can
have a value less, equal to, or greater than unity,

Similarly,

$$y_{12} = \frac{-1}{\pi r_b} \left[\int_{-\pi/2}^{3\pi/2} \frac{X\left[\cos^2(\omega_p t)\right] d(\omega_p t)}{1 + b \cos \omega_p t} \right] \qquad A2.6$$

and

$$y_{13} = \frac{1}{\pi r_b} \left[\int_{-\pi/2}^{3\pi/2} \frac{\left(\left[1 + X \cos \omega_p t\right] \cos 2\omega_p t\right) d(\omega_p t)}{1 + b \cos \omega_p t} \right] A2.7$$

Integrals given by equations A2.4, A2.6 and A2.7 can now be evaluated
over a complete range of local oscillator drive and are given by equations
3.26 to 3.30.

Appendix III

Derivation of the Coefficients for an H Mixer

For an H mixer the input current is restricted to frequencies given by equation 3.7(a) while the output voltage is restricted to frequency given by equation 3.7(b). Substituting equations 3.7(a) and 3.7(b) into the general matrix equation 3.1 the following equations are obtained.

$$
V_1 = \left(I_q \cos \omega_q t + I_I \cos (2\omega_p - \omega_q)t \right) \sum_{n \text{ even}} a_n \cos n\omega_p t
$$

$$
+ \left(V_{i.f.} \cos (\omega_p - \omega_q)t \right) \sum_{n \text{ odd}} b_n \cos n\omega_p t
$$

A3.1

$$
I_2 = \left(I_q \cos \omega_q t + I_I \cos (2\omega_p - \omega_q)t \right) \sum_{n \text{ odd}} c_n \cos n\omega_p t
$$

$$
+ \left(V_{i.f.} \cos (\omega_p - \omega_q)t \right) \sum d_n \cos n\omega_p t
$$

A3.2

Extracting relations from the above equations at r.f., image and i.f. frequencies and using equation 3.25 the coefficients describing the H mixer can be derived as shown below.

$$
h_{11} = 2r_s + \frac{r_b}{2\pi} \int_{-\pi/2}^{3\pi/2} \frac{d(\omega_p t)}{1 + X(t)\, s(t)}
$$

A3.3

$$
h_{12} = \frac{1}{2\pi} \int_{-\pi/2}^{3\pi/2} \frac{\left[\cos^2 (\omega_p t)\right] d(\omega_p t)}{1 + X(t)\, s(t)}
$$

A3.4

$$
h_{13} = \frac{r_b}{2\pi} \int_{-\pi/2}^{3\pi/2} \frac{\left[\cos (2\omega_p t)\right] d(\omega_p t)}{1 + X(t)\, s(t)}
$$

A3.5

$$h_{22} = \frac{1}{2r_b\pi} \int_{-\pi/2}^{\pi/2} \frac{\left(1 + 2\,X(t)\,s(t)\right)\,d(\omega_p t)}{1 + X(t)\,s(t)} \qquad \text{A3.6}$$

The integrals in the above equations can be evaluated by sectioning them between limits $^{-\pi}/2$ to $^{\pi}/2$ and $^{\pi}/2$ to $^{3\pi}/2$ i.e.,

$$h_{11} = 2r_s + \frac{r_b}{\pi} \int_{-\pi/2}^{\pi/2} \frac{d(\omega_p t)}{1 + X \cos \omega_p t} \qquad \text{A3.7}$$

$$h_{12} = \frac{1}{\pi} \int_{-\pi/2}^{\pi/2} \frac{\left[\cos^2 (\omega_p t)\right] d(\omega_p t)}{1 + X \cos \omega_p t} \qquad \text{A3.8}$$

$$h_{13} = \frac{r_b}{\pi} \int_{-\pi/2}^{\pi/2} \frac{\left[\cos (2\omega_p t)\right] d(\omega_p t)}{1 + X \cos \omega_p t} \qquad \text{A3.9}$$

$$h_{22} = \frac{1}{r_b\pi} \int_{-\pi/2}^{\pi/2} \frac{\left(1 + 2X \cos \omega_p t\right) d(\omega_p t)}{1 + X \cos \omega_p t} \qquad \text{A3.10}$$

Evaluating the above integrals results in the following expressions for the coefficients for the H mixer with $X \gg 1$.

$$h_{11} = 2(r_s + \frac{r_b}{X} \log_e 2X) \qquad \text{A3.11}$$

$$h_{12} = \frac{1}{\pi}\left(2 - \frac{\pi}{X} + \frac{2}{X^2} \log_e 2X\right)$$

$$\simeq {^2}/\pi \qquad \text{A3.12}$$

$$h_{13} = \frac{r_b}{\pi} \left(\frac{4}{X} - \frac{2\pi}{X^2} + \frac{4}{X^3} \log_e 2X - \frac{2}{X} \log_e 2X \right)$$

$$\simeq \frac{2r_b}{\pi X} \left(2 - \log_e 2X \right) \qquad\qquad\qquad A3.13$$

$$h_{22} = \frac{2}{r_b} \left(1 + \frac{2}{\pi X} \log_e 2X \right) \simeq \ ^2/r_b \qquad\qquad A3.14$$

Appendix IV

Derivation of the Coefficients for a G Mixer

Restricting the input voltage to frequencies given by equation 3.8(a) and the output current to the frequency given by equation 3.8(b) and using the general matrix equation 3.1, the following equations are obtained.

$$I_1 = \left(V_q \cos \omega_q t + V_I \cos (2\omega_p - \omega_q)t \right) \sum_{\substack{n \\ \text{n even}}} a_n \cos n\omega_p t$$

$$+ \left(I_{i.f.} \cos (\omega_p - \omega_q)t \right) \sum_{\substack{n \\ \text{n odd}}} b_n \cos n\omega_p t \qquad \text{A4.1}$$

$$V_2 = \left(V_q \cos \omega_q t + V_I \cos (2\omega_p - \omega_q)t \right) \sum_{\substack{n \\ \text{n odd}}} c_n \cos n\omega_p t$$

$$+ \left(I_{i.f.} \cos (\omega_p - \omega_q)t \right) \sum_{\substack{n \\ \text{n even}}} d_n \cos n\omega_p t \qquad \text{A4.2}$$

Extracting relations from the above equations at r.f., image and i.f. frequencies and using equation 3.53 the coefficients describing the G mixer can be derived as shown below.

$$g_{11} = \frac{1}{2\pi r_b} \int_{-\pi/2}^{3\pi/2} \left[2 - \frac{1}{1 + X(t) \, s(t)} \right] d(\omega_p t) \qquad \text{A4.3}$$

$$g_{22} = \frac{-1}{2\pi} \int_{-\pi/2}^{3\pi/2} \frac{\left[X(t) \cos \omega_p t \right]}{1 + X(t) \, s(t)} d(\omega_p t) \qquad \text{A4.4}$$

$$g_{13} = \frac{-1}{2\pi r_b} \int_{-\pi/2}^{3\pi/2} \frac{\left[\cos (2\omega_p t) \right] d(\omega_p t)}{1 + X(t) \, s(t)} \qquad \text{A4.5}$$

$$g_{22} = 2r_s + \frac{r_b}{2\pi} \int_{-\pi/2}^{3\pi/2} \frac{d(\omega_p t)}{1 + X(t) \ s(t)} \ d(\omega_p t) \qquad A4.6$$

The integrals in the above equations can be evaluated by sectioning them between limits $-\pi/2$ to $\pi/2$ and $\pi/2$ to $3\pi/2$ i.e.,

$$g_{11} = \frac{1}{\pi r_b} \int_{-\pi/2}^{\pi/2} \left(2 - \frac{1}{1 + X \cos \omega_p t} \right) d(\omega_p t) \qquad A4.7$$

$$g_{22} = \frac{-1}{\pi} \int_{-\pi/2}^{\pi/2} \left(\frac{X \cos \omega_p t}{1 + X \cos \omega_p t} \right) d(\omega_p t) \qquad A4.8$$

$$g_{13} = \frac{-1}{\pi r_b} \int_{-\pi/2}^{\pi/2} \left[\frac{\cos (2\omega_p t)}{1 + X(t) \ s(t)} \right] d(\omega_p t) \qquad A4.9$$

$$g_{22} = 2r_s + \frac{r_b}{\pi} \int_{-\pi/2}^{\pi/2} \frac{d(\omega_p t)}{1 + X(t) \ s(t)} \qquad A4.10$$

Evaluating the above integrals results in the following expressions for the coefficients of the G mixer if $X \gg 1$.

$$g_{11} = \frac{2}{r_b} \left(1 - \frac{1}{\pi X} \log_e 2X \right) \simeq 2/r_b \qquad A4.11$$

$$g_{12} = \frac{-X}{\pi} \left(\frac{2}{X} - \frac{\pi}{X^2} + \frac{2}{X^3} \log_e 2X \right) \qquad A4.12$$

$$\simeq -2/\pi$$

$$g_{13} = \frac{-1}{r_b \pi} \left(\frac{-2}{X} \log_e 2X + \frac{4}{X} - \frac{2\pi}{X^2} + \frac{4}{X^3} \log_e 2X \right) \simeq 0 \qquad A4.13$$

$$g_{22} = 2 \left(r_s + \frac{r_b}{\pi X} \log_e 2X \right) \qquad A4.14$$

APPENDIX $\overline{V}$

Derivation of the Angle of Truncation

The total current flowing through the diodes and the capacitor in Figure 4.3 at any instant of time is governed by the following differential equation.

$$C_e \frac{dv}{dt} + 2I_s (e^{\alpha v} - e^{-\alpha v}) = 2I_p \sin \omega_p t \qquad A5.1$$

where $\alpha = q/KT$ and I_s is the reverse saturating current of the diode. It is convenient to introduce the following normalized parameters,

$$\theta = \omega_p t \qquad A5.2(a)$$

$$K = I_s/I_p \qquad A5.2(b)$$

and a change in variable

$$y = Ke^{\alpha v} \qquad A5.2(c)$$

Equation A5.1 may now be expressed in the form,

$$\varepsilon \frac{dy}{d\theta} + y^2 - K^2 = y \sin \theta \qquad A5.3(a)$$

where

$$\varepsilon = \frac{\omega_p C_e}{2I_p \alpha} = \frac{\omega_p C_e r_b K}{2} \qquad A5.3(b)$$

$$= \frac{\omega_p C_e r_b}{4X} \qquad A5.3(c)$$

X has been defined as $I_p/2I_s$ and consequently $K = 1/2X$.

For typical Schottky-barrier diode parameters and current drive at microwave frequencies, ε and K^2 in equation A5.3(a) are both small. However $K^2 \ll \varepsilon$. To determine the general properties of equation A5.3(a) integral curves can be obtained over a range of y and θ by letting $dy/d\theta = 0$.

$$\therefore \ y = \frac{1}{2}\left(\sin \theta \pm (\sin^2 \theta + 4K^2)^{\frac{1}{2}}\right) \qquad \text{A5.4}$$

when $\qquad$ $K = 0$ $\qquad$ then $y = 0$ or $\sin \theta$

when $\qquad$ $\theta = 0$ $\qquad$ then $y = \pm K$

When $\sin \theta > 0$ and taking the negative sign then,

$$y \simeq - K^2$$

When $\sin \theta < 0$ and taking the positive sign then,

$$y \simeq K^2$$

When $\theta = \pi/2$ then $y \approx 1 + K^2$

The plots of the isocline curves of equation A5.3(a) are shown in Figure A5.1.

Outer Region Solution ($y \rightarrow y_o$ as $K^2 \rightarrow 0$)

In equation A5.3(a) both ε and K^2 are small but K^2 is much smaller than ε. An approximate solution of the equation may be obtained for a fixed value of ε and assuming that $K^2 \rightarrow 0$ hence $y \rightarrow y_o$. Equation A5.3(a) then becomes,

$$\varepsilon \frac{dy_o}{d\theta} = y_o \sin \theta - y_o^2 \qquad \text{A5.5}$$

Let $\qquad$ $y_o(\theta) = v(\theta) \ W(\theta)$ so that

$$\varepsilon(v^1 W + W^1 v) = vW \sin \theta - vW^2 \qquad \text{A5.6}$$

Let $\qquad$ $\varepsilon v^1 = v \sin \theta \qquad\qquad\qquad\qquad$ A5.7(a)

$\qquad\qquad$ $\varepsilon W^1 = -vW^2 \qquad\qquad\qquad\qquad$ A5.7(b)

Solving equation A5.7(a) $v = e^{-\frac{\cos \theta}{\varepsilon}}$
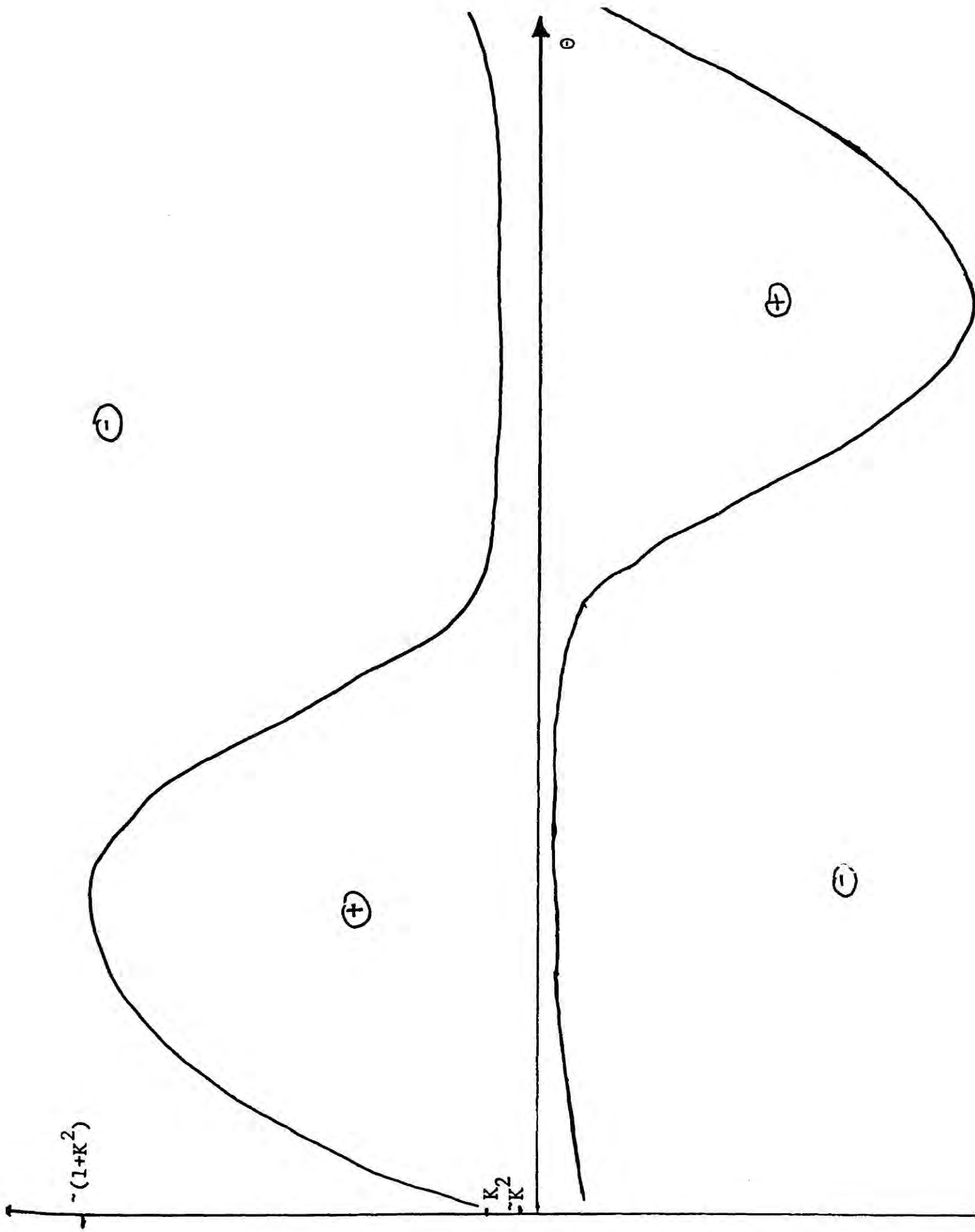
Figure A5.1 Isocline curves for the differential equation

and from equation A5.7(b) $\dfrac{\varepsilon}{W} = \displaystyle\int_0^\theta v(\theta)\ d\theta + A$

where A is a constant of integration.

Since $y_o(\theta) = vW$

$$y_o(\theta) = \frac{\varepsilon e^{-\dfrac{\cos\theta}{\varepsilon}}}{A + \displaystyle\int_0^\theta e^{\dfrac{\theta}{\varepsilon} - \dfrac{\cos\theta}{\varepsilon}}\ d\theta} \qquad\qquad A5.8$$

To determine the constant of integration A in the above equation let the initial value $y_o(0) = \hat{y}_o$, then from equation A5.8

$$\hat{y}_o = \frac{\varepsilon e^{-1/\varepsilon}}{A} \qquad\qquad A5.9$$

and equation A5.8 finally becomes,

$$y_o(\theta) = \frac{\hat{y}_o\ e^{\left(\dfrac{1 - \cos\theta}{\varepsilon}\right)}}{1 + \dfrac{\hat{y}_o}{\varepsilon}\ e^{+1/\varepsilon}\displaystyle\int_0^\theta e^{-\dfrac{\cos\theta}{\varepsilon}}\ d\theta} \qquad\qquad A5.10$$

Let

$$\hat{y}_o = e^{\dfrac{\cos\theta_c - 1}{\varepsilon}} \qquad\qquad A5.11$$

so that $\hat{y}_o$ is initially small having values in the range $(0 \leqslant \theta_c \leqslant \pi/2)$ of $(1 \geqslant y_o \geqslant e^{-1}/\varepsilon)$

Equation A5.10 becomes,

$$y_o = \frac{e^{\left(\dfrac{\cos\theta_c - \cos\theta}{\varepsilon}\right)}}{1 + \dfrac{1}{\varepsilon}\ e^{\dfrac{\cos\theta_c}{\varepsilon}}\displaystyle\int_0^\theta e^{-\dfrac{\cos\theta}{\varepsilon}}\ d\theta} \qquad\qquad A5.12$$

The solution of equation A5.12 for different ranges of θ and $\varepsilon \ll 1$ is given below.

(i) $y_o(0) = e^{\dfrac{Cos\ \theta_c - Cos\ \theta}{\epsilon}}$ in the range $0 \leqslant \theta_c \leqslant \pi/2$

(ii) y_o is exponentially small in the range $0 \leqslant \theta \leqslant \theta_c$ as the numerator of equation A5.12 is small.

(iii) Near $\theta = \theta_c$ let $\theta = \theta_c + \epsilon\tau$ so that equation A5.12 becomes,

$$y_o \simeq \frac{e^{\tau\ Sin\ \theta_c}}{1 + \dfrac{1}{\epsilon} e^{\dfrac{Cos\ \theta_c}{\epsilon}} \left(\displaystyle\int_0^{\theta_c} e^{-\dfrac{Cos\ \theta}{\epsilon}}\, d\theta + \int_{\theta_c}^{\theta_c + \epsilon\tau} e^{\dfrac{-Cos\ \theta}{\epsilon}}\, d\theta \right)} \qquad \text{A5.13}$$

Using Laplace's method for a supremum at $\theta = \theta_c$ it may be shown that the integral,

$$I(t,\epsilon) = \int_0^t e^{-\dfrac{1}{\epsilon} Cos\ t'}\, dt'$$

for $\epsilon \to 0^+$ is $\dfrac{\epsilon}{Sin\ t} e^{-\dfrac{cos\ t}{\epsilon}}$

Equation A5.13 therefore becomes,

$$y_o = \frac{e^{\tau\ Sin\ \theta_c}}{1 + \tau + \dfrac{1}{Sin\ \theta_c}}$$

Equation A5.14 indicates if $\tau < 0$ then y_o is exponentially small but if $\tau > 0$ then y_o is exponentially large provided $Sin\ \theta_c > 0$, i.e. there is a rapid rise in y_o as θ passes θ_c.

(iv) In the range $\theta_c < \theta < \pi$ since the numerator of equation A5.12 is exponentially large and,

$$\int_0^\theta e^{-\dfrac{Cos\ \theta}{\epsilon}}\, d\theta \simeq \frac{\epsilon}{Sin\ \theta} e^{-\dfrac{Cos\ \theta}{\epsilon}}$$

then,

$$y_o \approx \text{Sin } \theta \qquad\qquad A5.15$$

(v) In the range $\pi < \theta \leqslant 2\pi$

$$\int_0^\theta e^{-\frac{\text{Cos }\theta}{\varepsilon}}\, d\theta \approx 2\pi \, I_o\, (^1/\varepsilon)$$

$$\qquad\qquad A5.16$$

$$\approx \left(2\pi\varepsilon\right)^{\frac{1}{2}} e^{1/\varepsilon}$$

(using Lapace's method and noting there is a local maximum at $(\theta = \pi)$

Substituting equation A5.16 into equation A5.12,

$$y_o \approx \frac{e^{\frac{\text{Cos }\theta_c - \text{Cos }\theta}{\varepsilon}}}{\left(\frac{1}{\varepsilon}\, e^{\frac{\text{Cos }\theta_c}{\varepsilon}}\right)\left(2\pi\varepsilon\right)^{\frac{1}{2}} e^{1/\varepsilon}}$$

$$\approx \left(\frac{\varepsilon}{2\pi}\right)^{\frac{1}{2}} e^{-\frac{(1 + \text{Cos }\theta)}{\varepsilon}} \qquad\qquad A5.17(a)$$

where equation A5.17(a) is exponentially small.

Equation A5.17(a) may be evaluated at $\theta = \pi$ and $\theta = 2\pi$, i.e.

$$y_o\,(\pi) \approx \left(\frac{\varepsilon}{2\pi}\right)^{\frac{1}{2}} \qquad\qquad A5.18(a)$$

$$y_o\,(2\pi) \approx \left(\frac{\varepsilon}{2\pi}\right)^{\frac{1}{2}} e^{-2/\varepsilon} \qquad\qquad A5.18(b)$$

A graphical plot for $y_o(\theta)$ is shown in Figure A5.2. It is seen however, that $y_o(2\pi) \ll y_o(0)$ but in order to have a periodic solution of $y_o(\theta)$ these two quantities must be equal. The reason for the discrepency is that in the range $\pi < \theta < 2\pi$ the approximation of neglecting K^2 in equation A5.3(a) is no longer valid. For this range let,

$$y = K^2 Y \qquad\qquad A5.19(a)$$

so that equation A5.3(a) becomes,

$$\varepsilon \frac{dy}{d\theta} + K^2 Y^2 = 1 + Y \text{ Sin } \theta \qquad\qquad A5.19(b)$$

$y_0(\theta)$

1

$\frac{1}{\varepsilon}(\cos\theta - 1)$

$\sin\theta$

$\sqrt{\varepsilon/2\pi}$

$\sqrt{\varepsilon/2\pi}\, e^{-2/\varepsilon}$

$O(\varepsilon)$

θ_1

$\pi/2$

π

2π
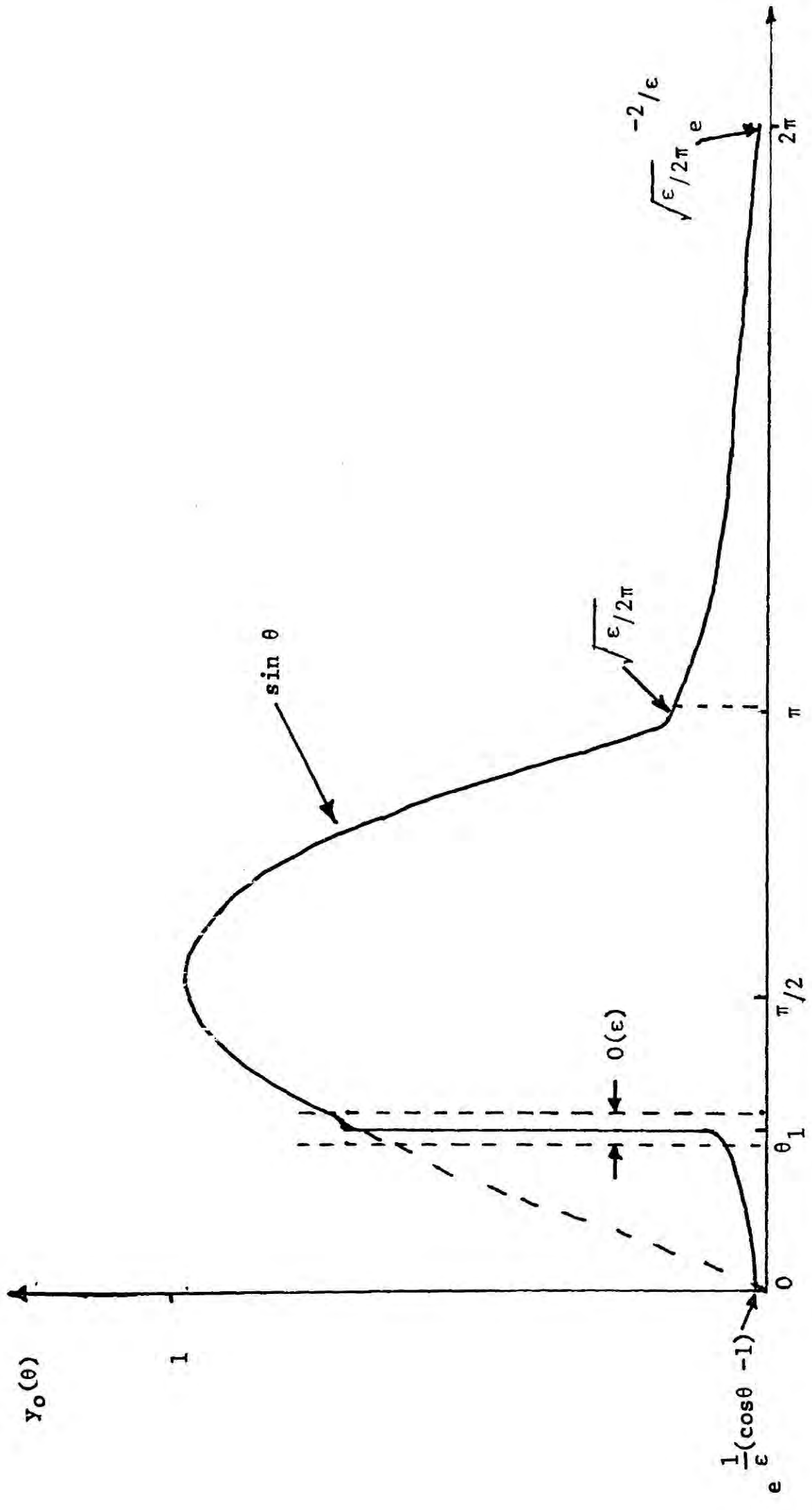
Figure A5.2 A graphical plot of $y_0(\theta)$

As $K^2 \to 0$ let $Y \to Y_o$ and to a first approximation equation A5.19(b) becomes,

$$\epsilon \frac{dY_o}{d\theta} = 1 - Y_o \sin \theta \qquad\qquad \text{A5.19(c)}$$

Expressing equation A5.19(c) in the form,

$$\frac{d}{d\theta} \left(e^{\frac{\cos \theta}{\epsilon}} \right) = \frac{1}{\epsilon} e^{\frac{\cos \theta}{\epsilon}}$$

$$\therefore Y_o = \frac{1}{\epsilon} e^{-\frac{\cos \theta}{\epsilon}} \int_{\theta_1}^{\theta} e^{\frac{\cos \theta}{\epsilon}} d\theta \qquad\qquad \text{A5.20}$$

The angle θ_1 in equation A5.20 plays a role of an arbitrary constant of integration and must satisfy two conditions;

(i)   must match with y_o

(ii)   give $K^2 Y_o (2\pi) \simeq y_o(o)$ so that a periodic solution is possible.

1.   Matching

$$\text{For } \epsilon \to 0 \quad Y_o = \frac{1}{\epsilon} e^{\frac{-\cos \theta}{\epsilon}} \frac{\epsilon e^{\frac{1}{\epsilon} \cos \theta_1}}{\sin \theta_1}$$

$$\text{A5.21}$$

$$Y_o \simeq e^{\frac{-\cos \theta + \cos \theta_1}{\epsilon}} \frac{}{\sin \theta_1}$$

In the range $\pi < \theta \leqslant 2\pi$ y_o must match $K^2 Y_o$. Using equations A5.21 and A5.17(a)

$$\frac{K^2 e^{\frac{\cos \theta}{\epsilon}}}{\sin \theta_1} = \left(\frac{\epsilon}{2\pi} \right)^{1/2} e^{-\frac{1}{\epsilon}} \qquad\qquad \text{A5.22}$$

2. Periodicity

To produce a periodic solution in y, $y_o(0) = K^2 Y_o(2\pi)$

i.e.

$$\frac{K^2}{\epsilon} e^{-\frac{1}{\epsilon}} \int_{\theta_1}^{2\pi} e^{\frac{\cos\theta}{\epsilon}} d\theta = e^{\frac{\cos\theta_c - 1}{\epsilon}} \qquad A5.23$$

as

$$\int_{\theta_c}^{2\pi} e^{\frac{\cos\theta}{\epsilon}} d\theta = \left(\frac{\pi\epsilon}{2}\right)^{\frac{1}{2}} e^{1/\epsilon}$$

$$K^2 \propto \left(\frac{2\epsilon}{\pi}\right)^{\frac{1}{2}} e^{\frac{\cos\theta_c - 1}{\epsilon}} \qquad A5.24$$

Using equations A5.24 and A5.22 leads to the following equation,

$$e^{\frac{\cos\theta_1 + \cos\theta_c}{\epsilon}} = \frac{1}{2} \sin\theta_1 \qquad A5.25$$

Equation A5.25 has roots near $\theta_1 = \pi$ and $\theta_1 = \pi - \theta_c$ where only the latter root leads to a realizable solution. (See equation 5.20 when $\theta_1 = \pi$)

Let $\qquad \theta_1 = \pi - \theta_c + \delta$

As $\delta \to 0$ equation A.23 reduces to,

$$\delta \approx \frac{-\epsilon \log_e \left(\frac{\sin\theta_c}{2}\right)}{\sin\theta_c} \qquad A5.26$$

In the range $0 < \theta < \pi$ and with $0 < \theta_c < \pi/2$ matching occurs for $\pi < \theta < \pi + \theta_c$.

The angle of truncation θ_c is governed by equation A5.24 which may be conveniently expressed in the form shown below.

$$\sin^2(\theta_c/2) = \frac{\epsilon}{2} \log_e\left(4X^2 \left(\frac{2\epsilon}{\pi}\right)^{\frac{1}{2}}\right) \qquad A5.27$$

APPENDIX $\overline{VI}$

Computer Programme for the Evaluation of the Odd
and Even-Mode Impedances

```
:========== EWATFIV ID=POLY
:==========
:========== $COMPILE POLY,TIME=2,PAGES=20

C       E.KORDLKIEWICZ
C        COUPLED MICROSTRIP LINES
        DIMENSION ZOO(20),ZOE(20),X(20),E1(20),E2(20)
        DIMENSION Z1(20),Z2(20)
        DIMENSION A(20)
        DO 2 J=1,20
        READ(5,1) A(J)
      1 FORMAT(E8.1)
      2 CONTINUE
        Z=10.0
        DO 30 K=1,20,1
        Y=0.1+(K-1)/10.0
        Y=ALOG10(Y)
        DO 10 J=1,20
        X(J)=A(J)
        E1(J)=5.5+(4.5)/(SQRT(1+10/(X(J))))
        E2(J)=1.675+(0.675)/(SQRT(1+10/(X(J))))
        Z1(J)=(60)*ALOG((8/X(J))+(X(J)/4))
        Z2(J)=(120*3.14)/(X(J)+2.42-0.44/X(J)+((1-1/X(J)**6))
        Z1(J)=Z1(J)/(SQRT(E2(J)))
        Z2(J)=Z2(J)/(SQRT(E2(J)))
        X(J)=ALOG10(X(J))
        ZOE(J)=(101.75-0.5766*Z+0.19595*Z**2)-(119.07-7.4693*Z+
       10.21756*Z**2)*(X(J))-(25.505-1.6742*Z+0.0493*Z**2)*(Y)+(18.011
       2-0.98016*Z+0.026015*Z**2)*(X(J)**2)
        ZOE(J)=ZOE(J)+(50.506-3.191*Z+0.093236*Z**2)*(Y)*(X(J))+(5.3831
       1-0.214*Z+0.00607*Z**2)*(Y**2)+(26.756-1.711*Z+0.046025*Z**2)*
       2(X(J)**3)-(10.512-0.55547*Z+0.014914*Z**2)*(Y)*(X(J)**2)
        ZOE(J)=ZOE(J)-(9.5443-0.46106*Z+0.01267*Z**2)*(Y**2)*(X(J))+
       1(22.467-1.5279*Z+0.037566*Z**2)*(Y**3)+(10.233-0.62118*Z+
       20.017796*Z**2)*(X(J)**4)
        ZOE(J)=ZOE(J)-(16.016-0.95732*Z+0.027278*Z**2)*(Y)*(X(J)**3)+
       1(15.094-0.95908*Z+0.028049*Z**2)*(Y**2)*(X(J)**2)-(15.76-
       20.93915*Z+0.026600*Z**2)*(Y**3)*(X(J))
        ZOE(J)=ZOE(J)+(9.2137-0.55252*Z+0.015099*Z**2)*(Y**4)
        ZOE(J)=ZOE(J)*(SQRT(E1(J)/(E2(J))))
        ZOO(J)=(75.656-4.6176*Z+0.14016*Z**2)-(77.979-4.7476*Z+0.13634*
       1Z**2)*(X(J))+(29.053-1.9514*Z+0.057938*Z**2)*(Y)+(10.502-
       20.65812*Z+0.019069*Z**2)*(X(J)**2)
        ZOO(J)=ZOO(J)-(49.071-3.075*Z+0.069438*Z**2)*(Y)*(X(J))-(12.4-
       10.656/6*Z+0.017558*Z**2)*(Y**2)-(2.1062-0.158*Z+0.0050311*Z**2)
       2*(X(J)**3)-(10.59-0.64*Z+0.0035*Z**2)*(Y)*(X(J)**2)
        ZOO(J)=ZOO(J)+(8.5285-0.41920*Z+0.010069*Z**2)*(X(J))*(Y**2)
       1-(22.236-1.3346*Z+0.038380*Z**2)*(Y**3)-(1.6076-0.11226*Z+
       20.0034528*Z**2)*(X(J)**4)
        ZOO(J)=ZOO(J)+(5.6445-0.50741*Z+0.014698*Z**2)*(Y)*(X(J)**3)-
       1(9.5457-0.61315*Z+0.01601*Z**2)*(X(J)**2)*(Y**2)+(11.5-0.65945
       2*Z+0.018530*Z**2)*(X(J))*(Y**3)
        ZOO(J)=ZOO(J)-(7.7155-0.47195*Z+0.015616*Z**2)*(Y**4)
        ZOO(J)=ZOO(J)*(SQRT(E1(J)/(E2(J))))
     10 CONTINUE
        WRITE(6,20)
     20 FORMAT(3X,'X(J)',12X,'ZOE(J)',12X,'ZOO(J)',12X,'E2(J)')
        WRITE(6,21)(X(J),ZOE(J),ZOO(J),E2(J),J=1,20)
     21 FORMAT(1X,E12.5,5X,E12.5,5X,E12.5,5X,E12.5)
        WRITE(6,22)
     22 FORMAT(3X,'X(J)',12X,'Z1(J)',12X,'Z2(J)')
        WRITE(6,23)(X(J),Z1(J),Z2(J),J=1,20)
     23 FORMAT(1X,E12.5,5X,E12.5,5X,E12.5)

     30 CONTINUE
        STOP
```

APPENDIX VII

Analysis of the Bandstop Filter

The ABCD parameters of a length of transmission line whose characteristic impedance is Z_0 are

$$\cos \theta \begin{bmatrix} 1 & , & Z_0 S \\ & & \\ S/Z_0 & , & 1 \end{bmatrix} \qquad \text{A7.1}$$

where $S = j \tan \theta$

and θ is the electrical length of the line.

The ABCD parameters of an open-circuit stub whose characteristic impedance is Z_1 are

$$\begin{bmatrix} 1 & , & 0 \\ & & \\ S/Z_1 & , & 1 \end{bmatrix} \qquad \text{A7.2}$$

Therefore using equations A7.1 and A7.2 the ABCD of the equivalent transmission line circuit of the bandstop filter shown in Figure 5.14(a) are

$$\cos \theta \begin{bmatrix} 1 + \dfrac{Z_0 S^2}{Z_1} & , & Z_0 S \\ & & \\ S\left(\dfrac{1}{Z_0} + \dfrac{1}{Z_1}\right) & , & 1 \end{bmatrix} \qquad \text{A7.3}$$

The microstrip bandstop filter using equation 5.18 is defined by

$$\begin{bmatrix} V_1 \\ \\ V_4 \end{bmatrix} = \begin{bmatrix} Z_{11} - \dfrac{Z_{13}^2 S}{Z_3 + S Z_{11}} & , & Z_{14} - \dfrac{Z_{13} Z_{12} S}{Z_3 + S Z_{11}} \\ & & \\ Z_{14} - \dfrac{Z_{13} Z_{12} S}{Z_3 + S Z_{11}} & , & Z_{11} - \dfrac{Z_{12}^2 S}{Z_3 + S Z_{11}} \end{bmatrix} \begin{bmatrix} I_1 \\ \\ I_4 \end{bmatrix} \qquad \text{A7.4}$$

where

$$Z_{11} = a/S$$

$$Z_{12} = b/S$$

A7.5

$$Z_{13} = b \ (1-S^2)^{\frac{1}{2}}/S$$

$$Z_{14} = a \ (1-S^2)^{\frac{1}{2}}/S$$

and

$$a = (Z_{OE} + Z_{OO})/2$$

A7.6

$$b = (Z_{OE} - Z_{OO})/2$$

Substituting the above equations into equation A7.4 results in

$$
\begin{bmatrix} V_1 \\ \\ V_4 \end{bmatrix} =
\begin{bmatrix}
\dfrac{a}{S} - \dfrac{b^2 \ (1-S^2)}{S(Z_3 + a)} & , & \dfrac{a \ (1-S^2)^{\frac{1}{2}}}{S} - \dfrac{b^2 \ (1-S^2)^{\frac{1}{2}}}{S \ (Z_3 + a)} \\ \\
\dfrac{a}{S} (1-S^2)^{\frac{1}{2}} - \dfrac{b^2 \ (1-S^2)^{\frac{1}{2}}}{S \ (Z_3 + a)} & , & \dfrac{a}{S} - \dfrac{b^2}{S \ (Z_3 + a)}
\end{bmatrix}
\begin{bmatrix} I_1 \\ \\ I_4 \end{bmatrix}
$$

A7.7

where Z_3 is the characteristic impedance of the open-circuit stub

Let

$$y = b^2/(Z_3 + a)$$

So that equation A7.7 becomes

$$
\begin{bmatrix} V_1 \\ \\ V_4 \end{bmatrix} =
\begin{bmatrix}
\dfrac{a - y \ (1-S^2)}{S} & , & \dfrac{(1-S^2)^{\frac{1}{2}} (a-y)}{S} \\ \\
\dfrac{(1-S^2)^{\frac{1}{2}} (a-y)}{S} & , & \dfrac{(a-y)}{S}
\end{bmatrix}
\begin{bmatrix} I_1 \\ \\ I_4 \end{bmatrix}
$$

A7.8

Finally to obtain the relationship between Z_{01} Z_1 and the odd and even-mode impedances and Z_3, it is necessary to establish the corresponding ABCD parameters of equation A7.9 by using the following

$$A = Z_{11}/Z_{12}, \quad B = \Delta Z/Z_{21}, \quad C = {}^1/Z_{21}, \quad D = Z_{22}/Z_{21}$$

The resulting ABCD parameters of equation A7.9 are

$$\begin{bmatrix} \dfrac{a-y\ (1-s^2)}{(1-s^2)^{\frac{1}{2}}(a-y)} & , & \dfrac{aS}{(1-s^2)^{\frac{1}{2}}} \\[4mm] \dfrac{S}{(a-y)(1-s^2)^{\frac{1}{2}}} & , & \dfrac{1}{(1-s^2)^{\frac{1}{2}}} \end{bmatrix} \qquad \text{A7.10}$$

Comparing the coefficients of the ABCD parameters of equations A7.10 and A7.3 results in

$$Z_0 = (Z_{OE} + Z_{OO})/2 \qquad \qquad \text{A7.11}$$

$$Z_1 = \frac{2\ (Z_{OO} + Z_{OE})\ \left(\dfrac{Z_3\ (Z_{OE} + Z_{OO})}{2} + Z_{OO}\ Z_{OE} \right)}{(Z_{OE} - Z_{OO})^2}$$

From equation A7.7 in order to make $Z_{12}{}' = 0$ then

$$a\ (Z_3 + a) - b^2 = 0 \qquad \qquad \text{A7.12}$$

Substituting equation A7.6 into equation A7.12 results in

$$\left(\frac{(Z_{OE} + Z_{OO})}{2} \right) X_c \tan\theta + 2Z_{OE}\ Z_{OO} = 0 \qquad \text{A7.13}$$

where $Z_3 = X_c \tan\theta$

APPENDIX VIII

Derivation of the Constant Q Equation

The relationship between normalized impedance $\bar{Z}$ and the voltage reflection coefficient ρ is

$$\rho = U + jV = \frac{\bar{Z} - 1}{\bar{Z} + 1} \qquad\qquad A1$$

Equation A1 can be expressed in the form

$$\bar{Z} = \bar{R} + j\bar{X} = \frac{(1 + U) + jV}{(1 - U) - jV} \qquad\qquad A2$$

Hence,

$$\bar{R} = \frac{1 - U^2 - V^2}{(1 - U)^2 + V^2} \qquad\qquad A3$$

and

$$\bar{X} = \frac{2V}{(1 - U)^2 + V^2} \qquad\qquad A4$$

The Q of a circuit is defined as $Q = \bar{X}/\bar{R}$ and hence from equation A3 and A4 it can be shown that

$$U^2 + (V + \frac{1}{Q})^2 = 1 + \frac{1}{Q^2} \qquad\qquad A5$$

which is an equation of a circle of radius $(1 + \frac{1}{Q^2})^{\frac{1}{2}}$ and whose centre is

$$U = 0 \text{ and } V = -\frac{1}{Q}$$

APPENDIX IX

Inductance Design

Single Layer Solenoid

The inductance L of a single layer solenoid is given by (STC "Ref Data for Radio Engineers" 4th Edition page 112).

$$L = n^2 \frac{r^2}{9r + 10l}$$

where

n = number of turns

r = radius of the solenoid (inches)

l = length of the solenoid (inches)

For an 18 guage enamelled wire of diameter 0.0422" the length of the solenoid is n x 0.0422. The radius of the former on which the coil is wound was 0.125"

The inductance is

$$L = \frac{n^2 \, 0.0156}{1.125 + 0.422n}$$

If L = 0.26 µH then

$$0.0156n^2 - 0.11n - 3 = 0$$

$$\therefore n = 8.9$$

$\therefore$ To obtain an inductance of 0.26 µH using 18 guage wire on a former of radius 0.125" requires 9 turns

Thick Film Spiral Inductance

The inductance L of a printed circuit circular spiral is given by (Lumped Elements in Microwave Circuits, IEEE Trans. MTT, Dec 1967, page 716).

$$L = \frac{a^2 n^2}{8a + 11c}$$

where

$$a = (r_o + r_i)/2$$

$$c = r_o - r_i$$

r_i is the inner radius of the spiral in mils

r_o is the outer radius of the spiral in mils

L is the inductance of the spiral in nanohenries

n is the number of turns

The basic design criteria for the realization of the etched circular inductor are:

1. It is important to provide as wide a conductor path as possible so that high value of Q is obtained.

2. The number of turns should be as small as possible.

3. The thickness of the conductor pattern is important as an increase in the print thickness increases Q of the coil.

To obtain 148 nH the following dimension of the circular spiral were used

r_o = 12 mm   a = 413

r_i = 9 mm   c = 118

n = 2
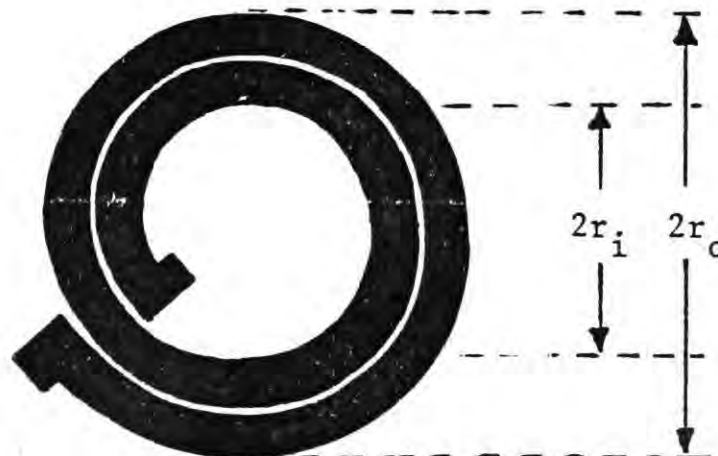
APPENDIX X

Publications

1. 'Large Signal Waveforms in Microwave Balanced Mixer with Capacitance' Proc. IEEE Vol. 125, No. 8, August 1978.

2. 'Effect of Source Resistance in Microwave Broadband Balanced Mixers' Microwaves, Optics and Acoustics, Vol. 2, No. 6, Nov. 1978.

3. 'Influence of Diode Capacitance on The Performance of Balanced Microwave Mixers' Electronic Letters, Vol. 17, No. 3, Feb. 1981.

4. 'Application of Resonant Circuit Theory to Matching Networks' Int. J. Elect. Eng. Ed., Vol. 18, Sept. 1981.

5. 'Fundamental Limitations in the Performance of Resistive Lattice H Mixer' IEE Proc., Vol. 129, Pt.H, No. 1, Feb. 1982.

LARGE SIGNAL WAVEFORMS IN A MICROWAVE BALANCED MIXER WITH CAPACITANCE

Indexing terms   Mixers (circuits), Solid-state microwave circuits

Abstract

The correspondence describes the effect of the diode capacitance on the current and voltage waveforms developed in a current-driven balanced mixer operating at microwave frequencies. It is shown that the current through the 'on' diode is a truncated halfwave sinewave, the angle of truncation being a function of the diode capacitance, drive level and the diode incremental resistance at the origin. The closed-form solution for the angle of truncation provides valuable insight into the deterioration in performance of balanced mixers at microwave frequencies owing to diode parasitic capacitance.

Introduction

A large variety of balanced mixers are available in integrated circuit form with operating frequency ranges of the order of 100 MHz. At microwave frequencies, however, the 2-diode balanced and the 4-diode double-balanced mixers are still inevitably used. These two mixer circuits have been comprehensively analysed in many publications assuming that the current through each diode is sinusoidal during conduction. At low frequencies this assumption is valid, but at microwave frequencies the diode parasitic capacitance considerably alters the large signal waveform, in that the current waveform through the 'on' diode is a truncated halfwave rectified sinewave, as shown in Fig. 1. This effect of the diode capacitance has not been observed and
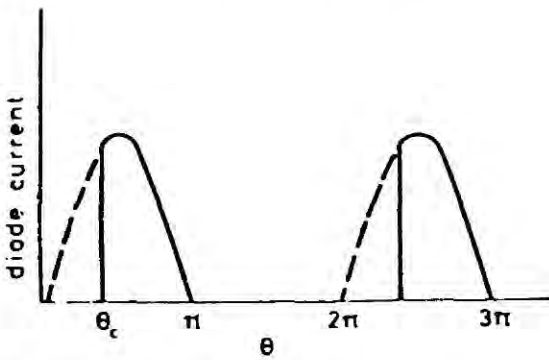
Fig. 1
Truncated half-wave rectified sinewave

analysed in any literature relating to mixer performance. Experimental results using a low-frequency model are found to be in good agreement with the theoretical predictions. A Fourier analysis on the diode current waveform shown in Fig. 1 and the resulting voltage waveform developed across each diode also shows good correlation with the practical results.
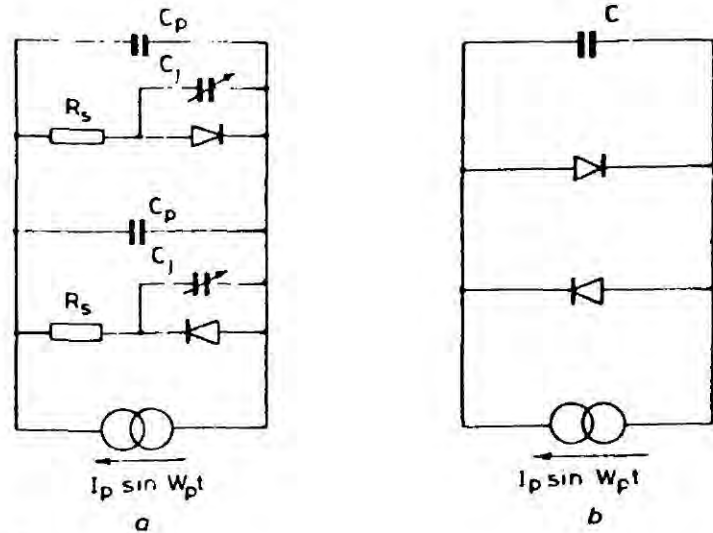
Fig. 2
Equivalent circuits of the mixer as seen by the local-oscillator current drive

Analysis

The circuit including the diode parasitics seen by the local-oscillator current drive for a balanced 2-diode mixer is shown in Fig. 2a. This circuit is also valid for a 4-diode double-balanced mixer if each diode shown in Fig. 2a represents the appropriate two diodes in parallel. Experimental investigations indicated that a 100% change in the value of the diode series resistance R_s did not significantly affect the current waveform and hence its effect has been neglected in the analysis. It has been shown[1,2] that the diode junction capacitance C_j can be approximated by a constant value given by

$$C_j \approx C(0) \approx |C_{j_{max}} - C_{j_{min}}|/2 \qquad (1)$$

where $C(0)$ is the value of C_j at zero voltage. The effective total capacitance across the diodes is therefore

$$C = 4C_p + 2C_j \qquad \text{(double-balanced mixer)}$$

or

$$C = 2C_p + C_j \quad \text{(balanced mixer)}, \tag{2}$$

where C_p is the diode package capacitance.

The equivalent circuit to be analysed therefore reduces to that shown in Fig. 2b and is governed by the following differential equation:

$$\frac{CdV}{dt} + nI_s \left[\exp(\alpha V) - \exp(-\alpha V)\right] = I_p \sin \omega_p t, \tag{3}$$

where $\alpha = q/KT$, I_s is the diode saturation current and $n = 2$ for a double-balanced mixer or $n = 1$ for a balanced mixer. It is convenient at this stage to introduce the following normalised parameters:

$$\theta = \omega_p t, \tag{4a}$$

$$K = nI_s/I_p, \tag{4b}$$

$$\epsilon = \omega_p C/\alpha I_p = \omega_p C r_b K/n \tag{4c}$$

where

$$r_b = \left.\frac{dV}{dI}\right|_{I=0} = \frac{1}{\alpha I_s}$$

Substituting the normalised parameters of eqn. 4 and a new variable defined by

$$y = K \exp(\alpha V) \tag{5}$$

eqn. 3 becomes

$$\epsilon \frac{dy}{d\theta} + y^2 - K^2 = y \sin \theta \tag{6}$$

The analytical solution to this nonlinear differential equation is difficult, but an approximate expression for the angle of truncation θ_c can be obtained by solving eqn. 6 in two regions:

$$K^2 \ll y^2$$

and

$$y^2 \ll K^2$$

and matching these two solutions to satisfy the condition of periodicity for y. The condition $K^2 \ll y^2$ corresponds to the part of the cycle when the diode is fully conducting and therefore the diode current is much greater than I_s. On the other hand, when the diode is
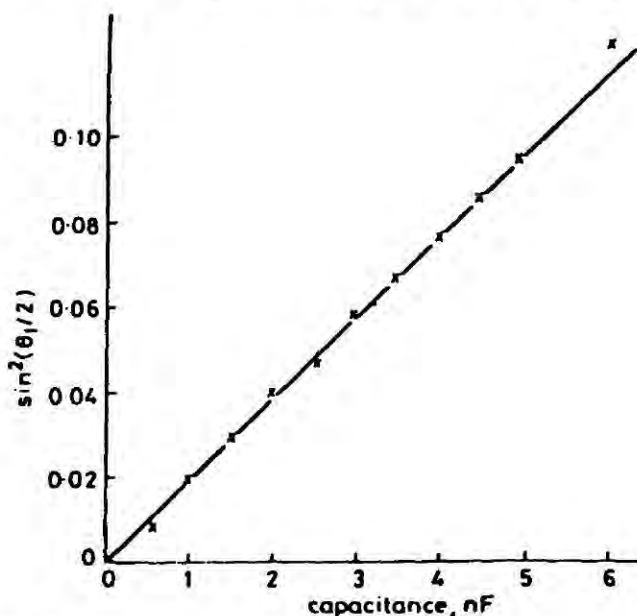

Fig. 3
Theoretical and measured values of delay angle against diode capacitance

X measured results
— theoretical results

in the reverse biased region the condition $y^2 \ll K^2$ is applicable. The angle of truncation θ_c is then given by

$$\sin^2(\theta_c/2) = \frac{\epsilon}{2} \log \{\exp[(2\epsilon/\pi)^{1/2}/K^2]\} \tag{7}$$

Eqn. 7 may be further simplified for a practical diode to

$$\sin^2(\theta_c/2) \simeq A\epsilon/2 \tag{8}$$

where A represents the logarithmic term in eqn. 7 and can be regarded as a constant since it varies slowly for large changes in ϵ.

Experimental results

A low-frequency equivalent circuit, shown in Fig. 2b, was constructed using Schottky barrier diodes. A test frequency of 50 kHz was chosen so that the inherent capacitive effect of the diodes was negligible. The high-frequency performance of the diodes was simulated by an external capacitor. The magnitude of this capacitor was determined by scaling a typical parasitic capacitive value in the ratio of working frequency (1 GHz) to the test frequency. Preliminary tests carried out on the diodes (type HP 2833) indicated that $I_s = 8 \times 10^{-7}$ A and $r_b = 3.4 \times 10^7 \Omega$. The current drive was adjusted so that the normalised current-drive factor K was 7×10^{-7}.

Fig. 3 shows a comparison of the theoretical values of θ_c with measured values for varying values of capacitance. The divergence between the theoretical and practical results for large values of capacitance may be explained by the fact that the assumption of a sharp turn on of the diode current is no longer valid in that region. The effect of the truncated angle θ_c on the frequency spectrum of the diode current and voltage was also found to be in close agreement with the measured results.

Conclusion

Saleh[3] has shown that the optimum performance of a balanced mixer in the absence of the diode parasitics is obtained when the time varying resistance $r(t)$ of the pumped diodes is a square wave. The diode capacitance in the case of practical microwave balanced mixer causes the current waveform to be truncated and hence the suggested optimum performance can never be practically obtained.

Acknowledgments

The authors wish to gratefully acknowledge the valuable assistance given by Prof. P.H. Roberts, Department of Mathematics, University of Newcastle upon Tyne.

1st March 1978

R. ARMSTRONG
E. KOROLKIEWICZ

Department of Electrical & Electronic Engineering
Newcastle upon Tyne Polytechnic
Ellison Building
Ellison Place
Newcastle upon Tyne NE7 8ST
England

B.L.J. KULESZA

Department of Physics & Electronics
University of Durham
South Road
Durham DH1 3LE
England

References

1 FEI, F.S., and MATTAUCH, R.J.: 'High frequency resistive mixer diode capacitance analysis', *Proc. IEEE*, 1976, 64, pp. 141–143
2 RAFUSE, R.P.: 'Low noise and dynamic range in symmetric mixer circuits'. Proceedings of the 1st Biennial Cornell conference, 1967, pp. 147–154
3 SALEH, A.A.M.: 'Theory of resistance mixers' (MIT Press, 1971), pp. 54–55

SPTC124E

Effect of source resistance in microwave broadband balanced mixers

E. Korolkiewicz and B.L.J. Kulesza

Abstract: A broadband mixer may be designed to obtain matched conditions at the r.f. port, or the r.f. port may be mismatched to produce a minimum conversion power loss. Using a practical diode law this paper compares the performance of a broadband balanced mixer designed by the above two methods and shows that, under certain conditions, the conversion loss can be made to be independent of the diode series resistance by mismatching the r.f. port.

1 Introduction

Mixers are classified according to the kind of termination that is 'seen' by the image frequency component. Three special cases called broadband, narrowband-image open circuit and narrowband-image short circuit mixers are usually considered. For narrowband (-image open circuit or -image short circuit) mixers the same results are obtained whether the source and load impedances are chosen to produce matched conditions at the r.f. and i.f. ports, a condition recognised in microwave circuits, or the expression for the conversion power loss is optimised and then the load and source impedances determined.[1-3] In the case of broadband mixers the two methods produce different results, although for single-diode series and shunt mixers the difference in the conversion power loss is small (less than 0·1 dB) over a wide range of bias conditions around the optimum.[4]

What is generally not recognised is that for broadband balanced mixers the two methods of design lead to a considerable difference in performance. This type of mixer is normally used in practice as it has the advantage over a single-diode mixer of producing a lower number of unwanted harmonic products and a lower noise contribution from the local oscillator. Balanced mixers are also increasingly applied as harmonically pumped downconvertors.[5,6] This paper analytically compares the performance of a balanced mixer designed to produce a minimum conversion loss with one designed to produce matched conditions at the input and output ports. A new approach is presented in that a practical diode law is assumed to include the effect of diode series resistance in the performance of the broadband balanced mixer.

2 Signal analysis of a broadband balanced mixer

A balanced H mixer (Reference 7), shown in Fig. 1a, may be treated as a passive linear network having three conceptual ports for signal, image and i.f. frequencies and may be described by the following matrix equation.

$$\begin{bmatrix} v_0 \\ i_{-1} \\ v_{-2} \end{bmatrix} = \begin{bmatrix} h_{11} & h_{12} & h_{13} \\ -h_{12} & h_{22} & -h_{12} \\ h_{13} & h_{12} & h_{11} \end{bmatrix} \begin{bmatrix} i_0 \\ v_{-1} \\ i_{-2} \end{bmatrix} \qquad (1)$$

In a broadband mixer the image and signal real R_s components 'see' the same termination (R_s) and, therefore, using the relationship

$$v_{-2} = -i_{-2}R_s$$

eqn. 1 may be expressed in the form

$$\begin{bmatrix} v_0 \\ i_{-1} \end{bmatrix} = \begin{bmatrix} H_{11} & H_{12} \\ -H_{12} & H_{22} \end{bmatrix} \begin{bmatrix} i_0 \\ v_{-1} \end{bmatrix} \qquad (2a)$$

where

$$H_{11} = h_{11}(1 - a^2/R) \qquad (2b)$$

$$H_{12} = h_{12}(1 - a/R) \qquad (2c)$$

$$H_{22} = h_{22}(1 + K_0/R) \qquad (2d)$$

$$K_0 = h_{12}^-/h_{11}h_{22} \qquad (2e)$$

$$a = h_{13}/h_{11} \qquad (2f)$$
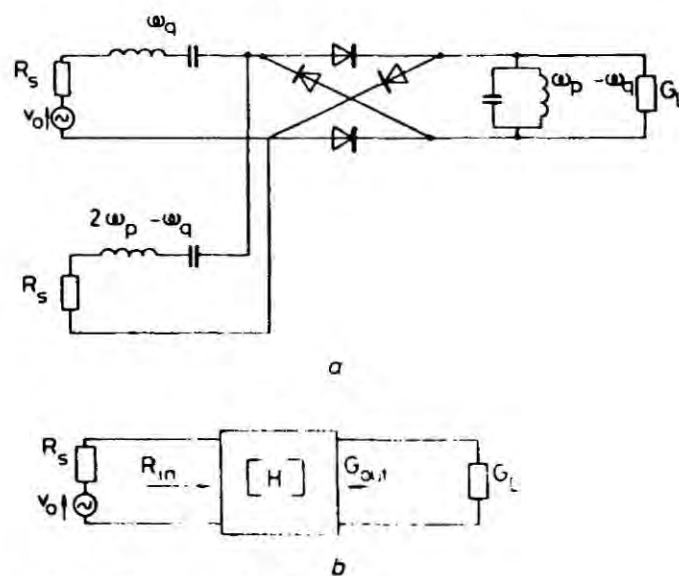
$$R = 1 + R_s/h_{11} \qquad (2g)$$

Fig. 1 Broadband balanced H mixer

The network described by eqn. 2a is shown in Fig. 1b. The conversion power loss (c.p.l.) is defined as

$$\text{c.p.l.} = 10 \log_{10}\left(\frac{\text{available input power}}{\text{output power}}\right) = 10 \log_{10}L. \qquad (3)$$

Using eqn. 2, L can be expressed in the form

$$L = \frac{\{(1 + y)(R + a) + 2K_0\}^2}{4K_0(R - 1)y} \tag{4a}$$

where

$$y = G_L/h_{22} \tag{4b}$$

The minimum conversion loss is obtained by setting the derivatives with respect to R and y to zero.

Setting $\partial L/\partial y = 0$ results in the expression for optimum y and G_L as follows:

$$y_{opt} = 1 + 2K_0/(R + a) \tag{5a}$$

and

$$G_{L_{opt}} = h_{22}\{1 + 2K_0/(R + a)\} \tag{5b}$$

Eqn. 5b corresponds to the condition of the i.f. port being matched, i.e. $G_{out} = G_{L_{opt}}$.

Substituting eqn. 5a into eqn. 4a for y_{opt} and setting $\partial L/\partial R = 0$ leads to the following equation in R:

$$R^2 - 2R - (1 + a)(2K_0 + a) = 0 \tag{6}$$

The optimum source resistance is obtained by using eqn. 2g and the positive root of eqn. 6 and is given by

$$R_{s_{opt}} = h_{11}(1 + a)\left\{1 + \frac{2K_0}{(1 + a)}\right\}^{1/2} \tag{7}$$

Finally, an expression for L_{opt} is obtained by substituting eqn. 7 into eqn. 4a,

$$L_{opt} = 2\left[\frac{1 + \{1 + 2K_0/(1 + a)\}^{1/2}}{-1 + \{1 + 2K_0/(1 + a)\}^{1/2}}\right] \tag{8}$$

This result is in agreement with Torrey and Whitmer[1] and gives a minimum conversion power loss of 3 dB when the parameter $2K_0/(1 + a)$ approaches infinity.

Eqn. 7 indicates, however, that, in the case of a mixer designed for optimum conversion loss, the signal port is not matched ($R_{s_{opt}} \neq R_{in}$). The source resistance R_{s_m} required to provide a matched condition at the input port ($R_{s_m} = R_{in}$) may be shown to be

$$R_{s_m} = h_{11}(1 - a^2/R)(1 + K_m)^{1/2} \tag{9a}$$

where

$$K_m = \left(\frac{K_0}{1 + K_0/R}\right)\left(\frac{1 - a/R}{1 + a/R}\right) \tag{9b}$$

Eqn. 9a may be shown, with the help of eqn. 2, to be a quartic equation in R of the form

$$R^4 + R^3(K_0 - 2) - 3K_0R + Ra\{2 + K_0(2 + a)\}$$
$$+ a^2\{K_0(1 - 2a) - a^2\} = 0 \tag{10}$$

An estimate of the largest real root (β) of eqn. 10 can be made using Tillots[8] criterion. The largest real root is limited by the following inequality:

$$\beta < 1 + \frac{|3K_0|}{K_0 - 2} \tag{11}$$

For most diodes the parameter K_0 (as discussed in Section 3) is much greater than 2 and, hence, the root $\beta < 4$. By approximation, therefore, eqn. 10 can be reduced to a cubic:

$$R^3 - 3R^2 + Ra(2 + a) + a^2(1 - 2a) = 0 \tag{12}$$

The roots of eqn. 12 are found using Cardan's formula,[8] where the largest root leading to a realisable source resistance is

$$R = 2\left(\frac{|(a + 3)(a - 1)|}{3}\right)^{1/2} \cos(\theta/3) + 1 \tag{12a}$$

where

$$\cos\theta = \frac{-27(1 + a^2)(a - 1)}{|(a + 3)(a - 1)|^{3/2}} \tag{12b}$$

The load conductance necessary to obtain a match at the output port is readily shown, using eqn. 2 to be

$$G_{L_m} = h_{22}(1 + K_0/R)(1 + K_m)^{1/2} \tag{13}$$

Finally, the corresponding expression for L, when both ports of the mixer are matched, is shown to be[1]

$$L_m = \frac{1 + (1 + K_m)^{1/2}}{-1 + (1 + K_m)^{1/2}} \tag{14}$$

By means of the relationships derived in this section, it is possible to compare the performance of a broadband mixer designed for minimum conversion loss with that of a similar mixer having matched conditions at input and output ports.
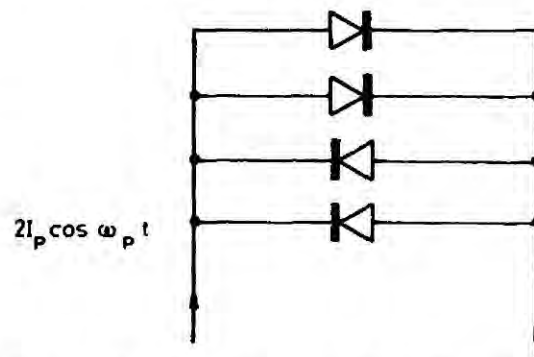
Fig. 2 *Diode circuit seen by the local oscillator drive*

3 Large-signal analysis of a broadband balanced mixer

The diode circuit seen by the local-oscillator current drive is shown in Fig. 2. The voltage developed across the diode's terminals may be expressed, using the diode practical v/i relationship, in the form

$$V = Ir_s + \frac{1}{\alpha}\log_e(1 + I/I_s) \tag{15}$$

where I is the current through each diode and α and I_s are the diode parameters. The time-varying diode incremental resistance is given, using eqn. 15 by

$$r(t) = \frac{1}{\alpha I_s}\left(\frac{1}{1 + I/I_s}\right) \tag{16}$$

The current through each diode may be conveniently written in the form

$$I = \tfrac{1}{2}I_p \cos\omega_p t\{1 + S(t)\} \tag{17}$$

where I_p is the peak amplitude of the local oscillator

current drive in each diode and $S(t)$ is a switching function defined as

$$S(t) = 1 \qquad -\pi/2 \leqslant \omega_p t \leqslant \pi/2$$
$$S(t) = -1 \qquad \pi/2 \leqslant \omega_p t \leqslant 3\pi/2 \qquad (18)$$

Substituting eqn. 17 into eqn. 16, the general expression for the time-varying incremental resistance becomes

$$r(t) = r_s + \frac{r_b}{1 + X(t) + X(t)S(t)} \qquad (19)$$

where $X(t) = X \cos \omega_p t$, $X = I_p/2I_s$ and r_b is the incremental diode resistance at the origin.

The balanced mixer shown in Fig. 1a may, taking into account the 180° phase difference of the local oscillator between two pairs of diodes, be described by the following relationship:

$$\begin{bmatrix} v_s \\ i_L \end{bmatrix} = \begin{bmatrix} 2r_s + \dfrac{r_b}{1 + X(t)S(t)} & \dfrac{X(t)}{1 + X(t)S(t)} \\ \dfrac{-X(t)}{1 + X(t)S(t)} & \dfrac{1}{r_b}\left[\dfrac{1 + X(t)S(t)}{1 + X(t)S(t)}\right] \end{bmatrix} \begin{bmatrix} i_s \\ v_L \end{bmatrix} \qquad (20)$$

provided $r_b \gg r_s$.

Frequency-selective circuits are normally used in a mixer and only the following signals are present:

$$i_s = i_0 \cos \omega_q t + i_{-2} \cos (2\omega_p - \omega_q)t \qquad (21a)$$

and

$$v_L = v_{-1} \cos (\omega_p - \omega_q)t \qquad (21b)$$

Substituting eqns. 21a and 21b into eqn. 20 and performing a frequency-balance operation results in the matrix equation (eqn. 1), where the Fourier coefficients are given by the following relationships:

$$h_{11} = 2r_s + \frac{r_b}{2\pi} \int_{-\pi.2}^{3\pi/2} \frac{d(\omega_p t)}{1 + X(t)S(t)} \qquad (22a)$$

$$h_{12} = \frac{1}{2\pi} \int_{-\pi/2}^{3\pi/2} \frac{\cos^2(\omega_p t)}{1 + X(t)S(t)} d(\omega_p t) \qquad (22b)$$

$$h_{13} = \frac{r_b}{2\pi} \int_{-\pi/2}^{3\pi/2} \frac{\cos(2\omega_p t)}{1 + X(t)S(t)} d(\omega_p t) \qquad (22c)$$

$$h_{22} = \frac{1}{2r_b\pi} \int_{-\pi/2}^{3\pi/2} \frac{1 + 2X(t)S(t)}{1 + X(t)S(t)} d(\omega_p t) \qquad (22d)$$

These integrals are evaluated[9] resulting in the following expressions for the h coefficients of eqn. 1:

$$h_{11} = 2\left(r_s + \frac{r_b}{\pi X} \log_e 2X\right) \qquad (23a)$$

$$h_{12} = 2/\pi \qquad (23b)$$

$$h_{13} = \frac{2r_b}{\pi X}(2 - \log_e 2X) \qquad (23c)$$

$$h_{22} = 2/r_b \qquad (23d)$$

4 Results

Practical microwave Schottky-barrier diode (HP 2833) parameters were measured and were found to be $r_b = 2.8 \times 10^7\ \Omega$ and $\alpha = 40\ V^{-1}$.

Common parameters influencing mixer performance are K_0 and a and are defined by eqns. 2e and 2f, respectively. The parameter K_0 may be expressed in terms of local oscillator drive X and diode parameters using eqn. 23, and is of the form

$$K_0 = \frac{r_b}{\pi^2}\left(r_s + \frac{r_b}{\pi X} \log_e 2X\right)^{-1} \qquad (24)$$
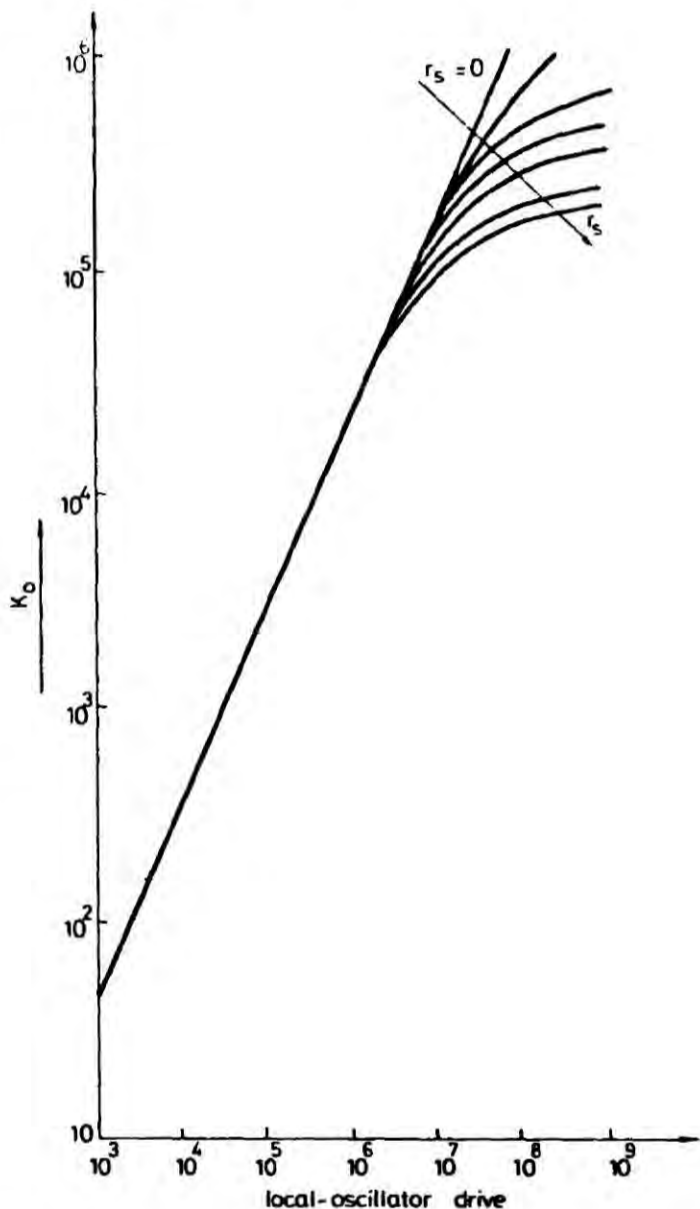
Fig. 3   *The parameter K_0 as a function of local-oscillator drive for diode series resistance 0–18 Ω*

Fig. 3 shows how the parameter K_0 behaves as a function of X. Examining eqn. 24 the parameter K_0 tends to a limiting value of $r_b/\pi^2 r_s$ at high local-oscillator drive.

The parameter a may also be expressed in terms of local-oscillator drive X and diode parameters, and using eqns. 2f and 23, is given by

$$a = \frac{r_b}{\pi X}\left[\frac{2 - \log_e 2X}{r_s + \frac{r_b}{\pi X} \log_e 2X}\right] \qquad (25a)$$

Fig. 4 shows the relationship between the parameter a and the local oscillator drive X. It is seen that a always lies be-

tween the limits 0 and −1. For finite diode series resistance r_s and high oscillator drive eqn. 25a tends to the following form.

$$a \simeq \frac{r_b}{r_s \pi X} [2 - \log_e 2X] \qquad (25b)$$

Figs. 5—7 show the effect of diode series resistance and local-oscillator drive on the conversion loss, source resistance and load conductance for both methods of design of broad-band balanced mixers.
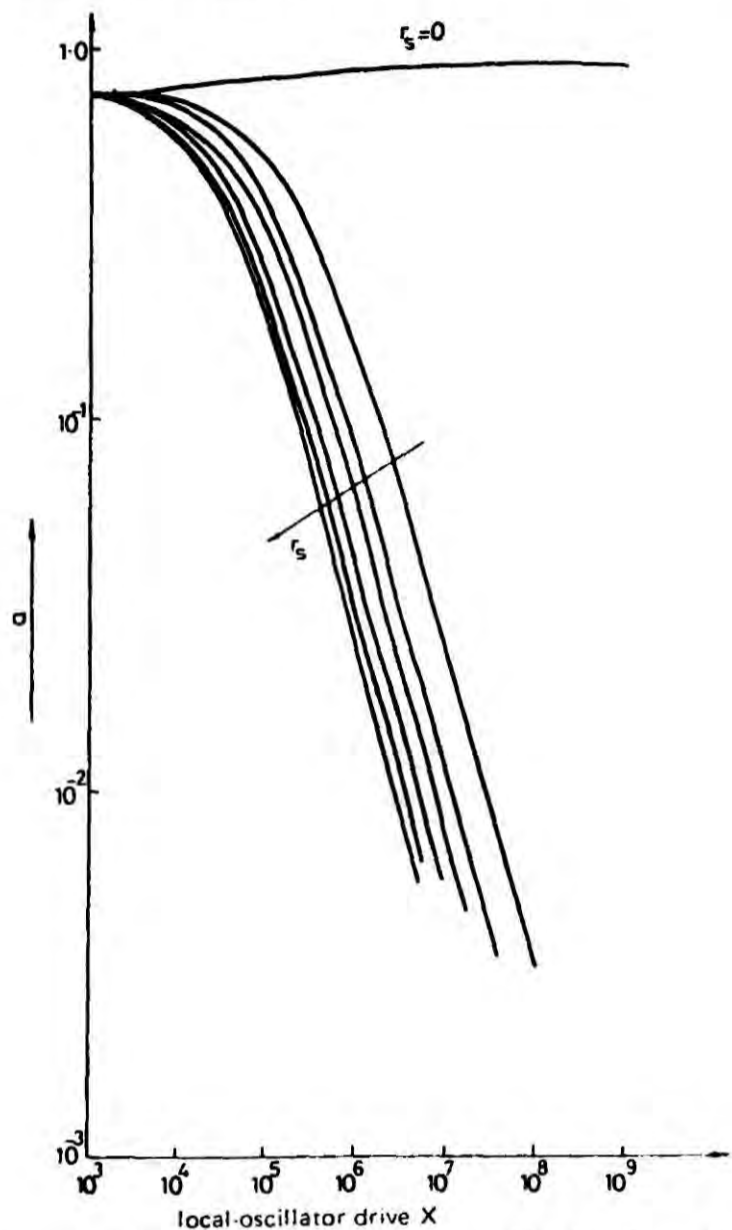
Fig. 4 *The parameter a as a function of local-oscillator drive for diode series resistance 0 - 18 Ω*
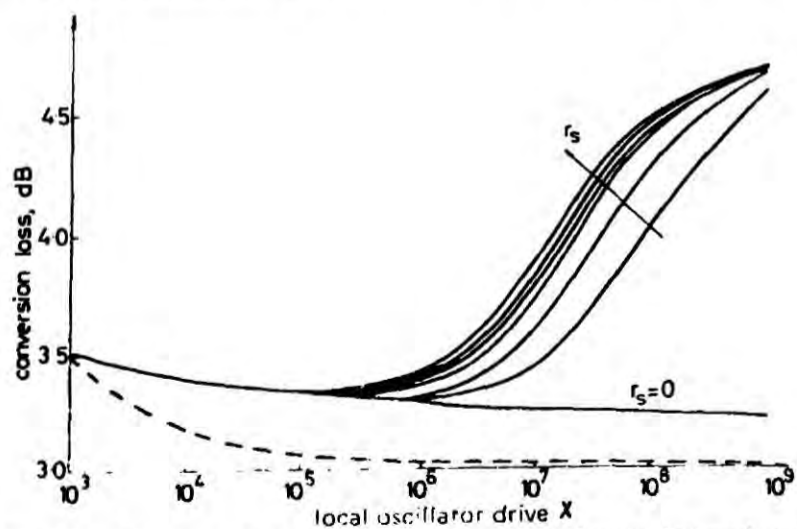
Fig. 5 *Computed conversion loss for an optimum designed and matched broadband balanced mixer for diode series resistance r_s 0 - 18 Ω*

optimum
matched

For a mixer designed to have a minimum conversion loss, the parameter $2K_0/(1 + a)$ tends, at high oscillator drive, towards a limiting value of $2r_b/\pi^2 r_s$ and, provided this limiting value is much greater than one, the conversion loss defined by eqn. 8 becomes independent of the diode series resistance (see Fig. 5). The conversion loss for a matched mixer is dependent on the diode-series resistance, and Fig. 5 shows that it passes a minimum value before reaching a limiting value at high oscillator drive. Examining eqn. 12 and Fig. 4 it is seen that, as the parameter a approaches zero, the root of eqn. 12 approaches three. Computer analysis indicates that this root remains approximately equal to three for a wide range of local-oscillator drive. Using this value for R in eqn. 9b, the local-oscillator drive X necessary to obtain minimum conversion loss may be shown to be governed by the following transcendental equation:

$$\frac{\pi X}{2} [\log_e 2X - 3] = \frac{r_b}{r_s} \qquad (26)$$
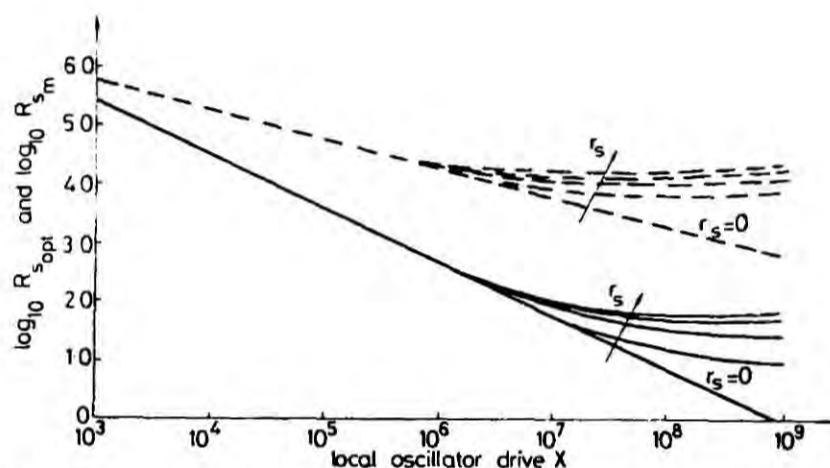
Fig. 6 *Computed source resistance for an optimum designed and matched broadband balanced mixer for diode series resistance r_s 0 - 18 Ω*

— — — optimum
—·—·— matched

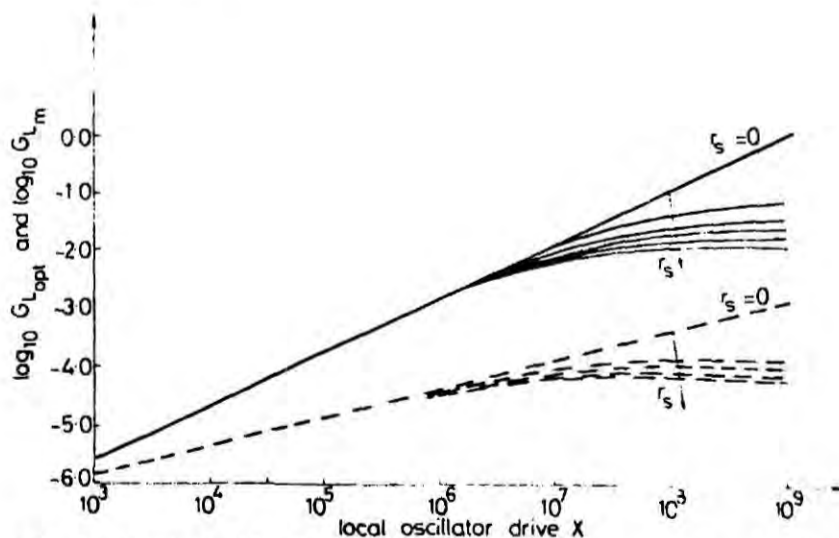**Fig. 7** *Computed load conductance for an optimum designed and matched broadband balanced mixer for diode series resistance 0 - 18 Ω*

— — — optimum
—·—·— matched

The limiting value of the conversion at high oscillator drive is, using eqn. 14, 4·7 dB.

Figs. 6 and 7 show the effect of diode series resistance and local-oscillator drive X on the source resistance and

load conductance for both methods of design of broadband mixers. In both cases the source resistance and load conductance tend to limiting values at high local-oscillator drive.

For a mixer designed for minimum conversion loss the limiting values of source resistance and load conductance are

$$R_{s_{opt}} \longrightarrow \frac{2}{\pi} [2 r_b r_s]^{1/2} \qquad (27a)$$

$$G_{L_{opt}} \longrightarrow \frac{2}{\pi} \left[\frac{2}{r_b r_s} \right]^{1/2} \qquad (27b)$$

For a broadband mixer designed to obtain a match at the input and output ports the limiting values are

$$R_{s_m} \longrightarrow 4 r_s \qquad (28a)$$

$$G_{L_m} \longrightarrow 4/(3\pi^2 r_s) \qquad (28b)$$

5 Conclusion

The performance of broadband balanced mixers is influenced by the choice of the source impedance at the r.f. port. An improvement in the conversion loss is obtained by mismatching the r.f. port and, as shown in Fig. 5, a theoretical limit of 3 dB can be approached for a large oscillator drive. The diode-series resistance does not significantly affect the conversion loss provided the diode incremental resistance at the origin (r_b) is large, a condition normally satisfied by Schottky-barrier diodes. The basic problem of achieving the theoretical limit of 3 dB at large local-oscillator drive is that large values of source impedance are required.

If the source is chosen to produce matched conditions at the r.f. port, the conversion loss is not only increased but is also influenced by the diode-series resistance (r_s) and the diode incremental resistance at the origin. The local-oscillator drive necessary to obtain a minimum conversion loss is governed by the transcendental equation (eqn. 26). Matching at the r.f. port has an advantage of requiring a lower source resistance as compared with a mixer designed to produce minimum conversion loss. It is interesting to note that the increase of the conversion loss at high local-oscillator drive for a matched mixer is not due to the diode series resistance, as has been assumed, but is actually due to the deviations of source resistance from its value to give minimum conversion loss.

6 References

1 TORREY, H.C., and WHITMER, C.A.: 'Crystal rectifiers' (MIT Press, 1948)
2 STRUM, P.D.: 'Some aspects of mixer crystal performance', *Proc. IRE*, 1953, 41, pp. 875–884
3 BURKLEY, C.J., and O'BRIEN, R.S.: 'Optimization of an 11 GHz mixer circuit using image recovery', *Int. J. Electron.*, 1975, 38, pp. 777–787
4 HOWSON, D.P.: 'Minimum conversion loss and input match conditions in the broad-band mixer', *Radio & Electron. Eng.*, 1972, 42, pp. 237–242
5 SCHNEIDER, M.V., and SNELL, W.W.: 'Harmonically pumped stripline down-converter', *IEEE Trans.*, 1975, MIT-23, pp. 271–275
6 BUCHS, J.D., and BEGEMANN, G.: 'Frequency conversion using harmonic mixers with resistive diodes', *IEE J. Microwaves, Opt. & Acoust.*, 1978, 2, pp. 71–76
7 SALEH, A.A.M.: 'Theory of resistive mixers' (MIT Press, 1971)
8 'Survey of applicable mathematics' (Iliffe, 1968)
9 BOIS, G.P.: 'Tables of indefinite integrals' (Dover, 1961)

Analysis of bulk waves in surface-acoustic wave devices

Ken'ichiro Yashiro and Naohisa Goto

Indexing term: *Wave propagation*

Abstract: A spurious response due to bulk waves has often been observed in surface-acoustic filters. This paper shows how bulk waves are radiated by the charge source on the surface of a semi-infinite piezoelectric solid. The expression for each component of bulk waves is evaluated asymptotically, in the form of the Fourier integral, by assuming that the observation point is located far from the source in comparison with a wavelength. In doing this, the method of steepest descents is used in order to integrate analytically. The numerical results are obtained for rotated Y-cut X-propagating LiNbO$_3$ and Y-Z LiNbO$_3$. These results are in good agreement with the experiment reported by Togami and Chiba.

1 Introduction

Surface-acoustic waves have been applied to commercial television i.f. filters.[1] In so doing there are some problems such as insertion losses, temperature properties and spurious response. A spurious response, which may be due to bulk waves, is one of the most important problems. There are two kinds of effects of bulk waves. One is due to bulk waves radiated along the surface by the transducer,[2] which

are detected directly by a receiving transducer. The other is caused by waves travelling down into the substrate, which can reach the receiving transducer only after reflection from the back surface. One may, therefore, use the radiation patterns to qualitatively predict the spurious frequency response from a knowledge of transducer positions and substrate thickness. In practice, reflections are often either reduced by using absorbers, or deflected away from the receiver by roughening or canting the back surface. However, bulk waves radiated into the substrate contribute to transducer impedance, thus affecting the electrical matching.

The problem of wave motion generated by a source at a surface of a semi-infinite solid has been studied by several

in las... ...by optical feedback. This effect
is sh... in Fig 2. The... ...on of the laser output with and
without ...ck shows th... ...duction in response speed as
well as ...ssed noise... ...d oscillations. At a feedback
level w...re the BER c...d no longer be reduced to 10^{-9}, the
excess noise power estimated at a received CW power of -37
dBm was at least twice as small as the receiver noise. The
oscillations are thought to be relatively unimportant because
they are out of band and appear to be small even at feedback
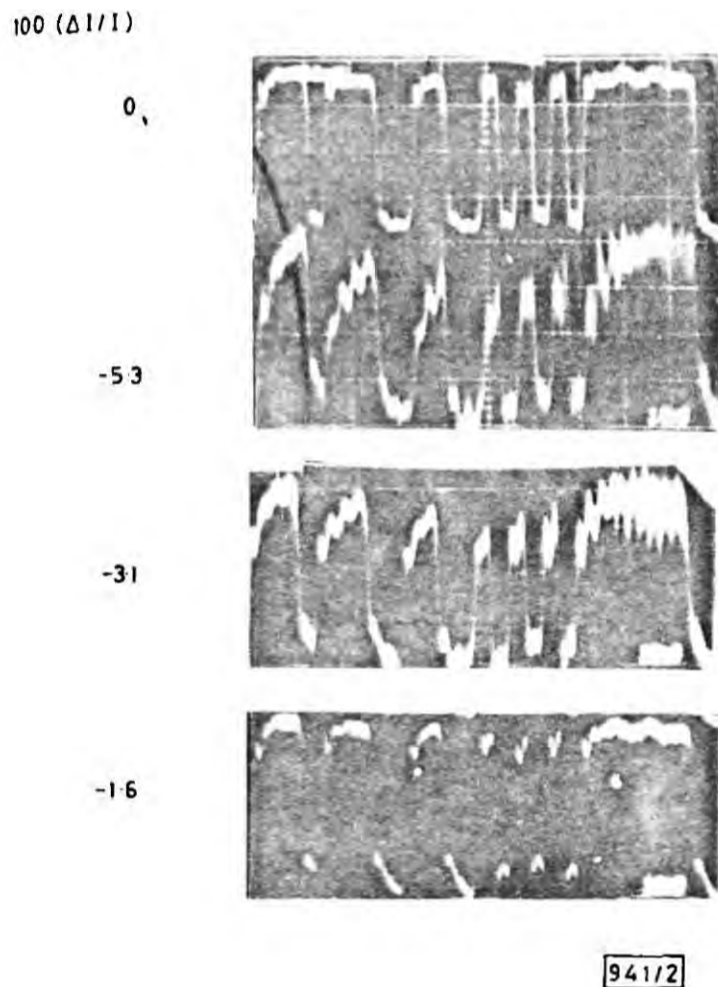levels where the penalty is already large.

100 (Δ1/1)

0,

-5·3

-3·1

-1·6

941/2

Fig. 2 *Pulse distortion caused by optical feedback*
As for Fig 1

The optical feedback produces a nonlinearity in the optical-
power current curve near the shifted threshold. When the DC
bias was varied (for fixed modulation voltage) so that the '0'
state passed through the nonlinearity, the BER passed through
a maximum. For a feedback level corresponding to a shift of
2%, the contribution to the penalty of this effect at its maxi-
mum, which coincided with $r = 0·1$, was estimated to be 0·5 dB
out of a total penalty of 2·2 dB.

Conclusion. Optical feedback produces several harmful effects
but the most important appear to be the generation of false '1'
states, reduction in the laser response speed and nonlinearity in
the light/current curve.

If the magnitude of the power penalty illustrated in Fig. 1 is
typical of BH lasers then it may be possible to avoid the use of
an isolator when the reflected power ratio can be kept low and
if there are no other substantial contributions to PN. For
example when $\eta^2 R = 0·01$ the penalty would be 0·7 dB
compared to the several dB insertion loss one might expect
from a production model isolator.

V. J. MAZURCZYK   *2nd January 1981*

Bell Laboratories
Holmdel, NJ 07733, USA

References

1 HIROTA, O., and SUEMATSU, Y.: 'Noise properties of injection lasers
   due to reflected waves', *IEEE J. Quantum Electron.,* 1979, **QE-15,**
   pp. 142 149
2 KOBAYASHI, K., *et al.:* '1·3 μm laser diode isolator module for a
   hybrid optical integrated circuit'. Topical Meeting on integrated
   and guided wave optics, 1981, Nevada, MD3

INFLUENCE OF DIODE CAPACITANCE ON PERFORMANCE OF BALANCED MICROWAVE MIXERS

Indexing terms: Microwave circuits, Mixers

The effect of the diode capacitance parasitics on the perfor-
mance of microwave double balanced lattice mixers, driven
by a local oscillator having a large internal resistance and a
current sinusoidal waveform, is examined. It is found that the
current present in the diodes is modified by the diode capaci-
tance and this in turn influences the performance of the
mixers. To reduce the effect of the diode capacitance on
the performance of the mixer it is necessary to reduce
the internal resistance of the local oscillator. There is there-
fore a compromise between the need of a low noise figure, and
hence a requirement of having a large internal resistance of
the local oscillator, and the undesired effect on the diode
current, and hence on the performance of the mixer.

Introduction: In the analysis of mixers the effect of the diode
parasitics on the waveform of the local oscillator has usually
been ignored. Rustom and Howson,[1] using a resistive diode
model, have confirmed the conclusion reached by Stracca[2] that
H and G mixers[3] driven by a local oscillator with a large
internal resistance and having a current waveform are the most
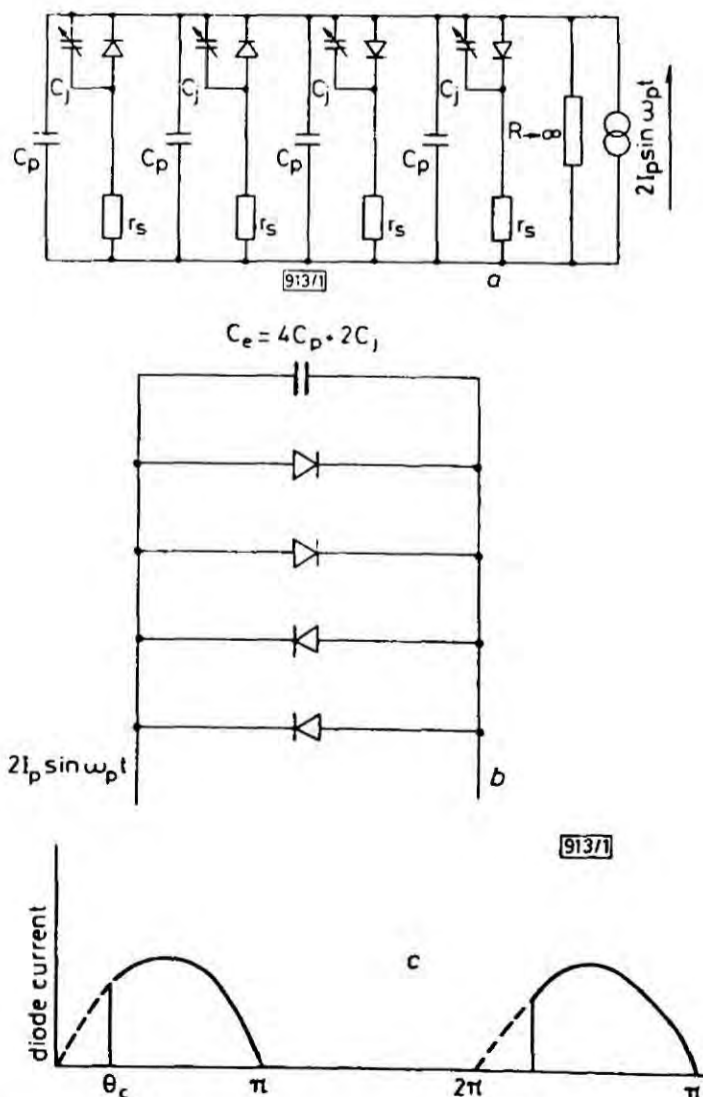promising mixer circuits for low system noise figure. This letter

$C_e = 4C_p + 2C_j$

$2I_p \sin \omega_p t$

b

θ_c π 2π π

c

93/7/1

Fig. 1

analytically examines the performance of lattice H mixers driven by a local oscillator having a current waveform and a large internal resistance when the effect of the diode capacitance parasitics is included.

Large signal analysis of a lattice mixer with capacitance: The effective circuit of a lattice configuration of the four diodes as 'seen' by the local oscillator is shown in Fig. 1a. Reducing the circuit to that shown in Fig. 1b. it can be shown that the current present in each diode to a first approximation is a truncated half-wave rectified sinewave shown in Fig. 1c, where the angle of truncation is given by[4]

$$\sin^2 \theta_{c\,2} = \frac{\varepsilon}{2} \log_e[4X^2(2\varepsilon/\pi)^{1\,2}]$$

where $\varepsilon = X_c r_b/4X$, X_c is the reactance of the capacitance C_e. r_b is the incremental diode resistance at the origin and X is the normalised current drive $(I_p/2I_s)$. The resultant current waveforms in the 'on' diode may be expressed in the form

$$i_1 = \tfrac{1}{2}[1 + S_1(t)]I_p \cos \omega_p t \qquad (2a)$$

and in the 'off' diode in the form

$$i_2 = \tfrac{1}{2}[1 + S_2(t)]I_p \cos \omega_p t \qquad (2b)$$

The two switching functions $S_1(t)$ and $S_2(t)$ are defined as

$$S_1(t) = \begin{cases} -1 \text{ for } -\pi/2 \le \omega_p t \le -\pi/2 + \theta_c \\ 1 \text{ for } -\pi/2 + \theta_c \le \omega_p t \le \pi/2 \\ -1 \text{ for } \pi/2 \le \omega_p t \le 3\pi/2 + \theta_c \end{cases} \qquad (3a)$$

$$S_2(t) = \begin{cases} 1 \text{ for } -\pi/2 \le \omega_p t \le \pi/2 + \theta_c \\ -1 \text{ for } \pi/2 + \theta_c \le \omega_p t \le 3\pi/2 \end{cases} \qquad (3b)$$

The time varying resistances of the 'on' and 'off' diodes, taking into account the 180° phase difference of the local oscillator current at the two pairs of the diodes are

$$r_+(t) = r_s + \frac{r_b}{1 + X(t) + X(t)S_1(t)} \qquad (4a)$$

$$r_-(t) = r_s + \frac{r_b}{1 - X(t) + X(t)S_2(t)} \qquad (4b)$$

where $X(t) = X \cos \omega_p t$.

Small signal analysis of a lattice H mixer: Using a bisection theorem, the equivalent circuit of a lattice mixer is found as shown in Fig. 2. In the case of an H mixer, the effective capacitance at the IF port can be incorporated in the parallel tuned circuit. The overall circuit matrix $[a]$ for the circuit in Fig. 2 is given by

$$[a] =$$
$$\begin{bmatrix} A + Cr_s & B + r_s[A + D + r_sC] \\ j(\omega/\omega_c)\dfrac{A}{r_s} + C[1 + j(\omega/\omega_c)] & j(\omega/\omega_c)\dfrac{B}{r_s} + D[1 + j(\omega/\omega_c)] \end{bmatrix} \qquad (5)$$

where $\omega_c = 1/C_e r_s$. Provided $(\omega/\omega_c) \ll 1$, eqn. 5 reduces to

$$[a] = \begin{vmatrix} A + Cr_s & r_s[A + D + r_sC] \\ C & D[1 + r_s] \end{vmatrix} \qquad (6)$$

and the effect of the diode capacitance C_e on the small signal analysis can be ignored. Thus a general matrix equation describing an H mixer is

$$\begin{vmatrix} V_1 \\ I_2 \end{vmatrix} = \begin{vmatrix} \Sigma a_n \cos n\omega_p t & \Sigma b_n \cos n\omega_p t \\ -\Sigma b_n \cos n\omega_p t & \Sigma c_n \cos n\omega_p t \end{vmatrix} \begin{vmatrix} I_1 \\ V_2 \end{vmatrix} \qquad (7)$$

By evaluating the Fourier coefficients of eqn. 7, it may be shown that the coefficients of the H matrix for a small but finite angle of truncation θ_c are given by

$$h_{11} \simeq 2r_s + \frac{r_b\theta_c}{\pi} \simeq \frac{r_b\theta_c}{\pi}; \quad h_{12} \simeq 2\pi$$

$$h_{13} \simeq \frac{-r_b}{2\pi} \sin 2\theta_c; \quad h_{22} \simeq 2/r_b \qquad (8)$$
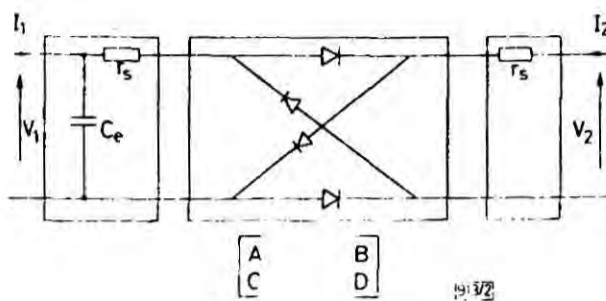
Fig. 2

Performance of lattice H mixers: Using the general expressions derived by Saleh[3] the performance of the lattice H mixers having different terminations at the image port can be readily determined. For a lattice H mixer with image open circuit the optimum terminations at the RF and IF ports and the resulting conversion loss are

$$R_{s_{opt}} \simeq \frac{r_b\theta_c}{\pi}[1 + (2/\pi\theta_c)]^{1/2}$$

$$G_{L_{opt}} \simeq \frac{2}{r_b}[1 + (2/\pi\theta_c)]^{1/2} \qquad (9)$$

$$L_{opt} \simeq \frac{1 + [1 + (2/\pi\theta_c)]^{1/2}}{-1 + [1 + (2/\pi\theta_c)]^{1/2}}$$

For a lattice H mixer with image short circuit the corresponding equations are

$$R_{s_{opt}} \simeq \frac{4r_b\theta_c^3}{3\pi}[1 + (3/\theta_c^2)]^{1/2}$$

$$G_{L_{opt}} \simeq \frac{2}{r_b}[1 + (3/\theta_c^2)]^{1/2} \qquad (10)$$

$$L_{opt} \simeq \frac{1 + [1 + (3/\theta_c^2)]^{1/2}}{-1 + [1 + (3/\theta_c^2)]^{1/2}}$$

Finally, for the broadband H mixer, the equations for optimum terminations and conversion loss are

$$R_{s_{opt}} \simeq \frac{2r_b\theta_c^3}{3}[1 + (6/\pi\theta_c^3)]^{1/2}$$

$$G_{L_{opt}} \simeq \frac{2}{r_b}[1 + (6/\pi\theta_c^3)]^{1/2} \qquad (11)$$

$$L_{opt} \simeq \frac{1 + [1 + (6/\pi\theta_c^3)]^{1/2}}{-1 + [1 + (6/\pi\theta_c^3)]^{1/2}}$$

Conclusion: The main effect of the diode effective capacitance is to considerably increase the conversion loss for low local oscillator drive and increase in magnitude the required terminations for the three types of lattice H mixers.

To minimise the effect of the diode capacitive parasitics on the performance of a lattice mixer, it is necessary to reduce the parameter ε. This can be done by lowering the frequency of the local oscillator and/or increase the local oscillator current drive X. There are, however, practical limitations to both these solutions. An alternative method is to allow the effective diode capacitance to discharge during the switching action of the four diodes by reducing the output resistance of the local oscillator. This effect was practically verified using an analogue model of a high frequency lattice mixer.

A compromise must be made in practice between the need to

have a large output impedance of the local oscillator to reduce the noise figure of the mixer, as suggested by Howson and Stracca, and the need to lower the output impedance of the local oscillator so that the angle of truncation of the diode current can be minimised.

E. KOROLKIEWICZ   22nd December 1980

School of Electronic Engineering
Faculty of Engineering
Newcastle upon Tyne Polytechnic, England

B. L. J. KULESZA

Department of Applied Physics and Electronics
University of Durham, Durham, England

References

1 RUSTOM, S., and HOWSON, D. P.: 'Mixer noise figure using an improved resistive model', Int. J. Electronics, 1976, 41
2 STRACCA, G. B.: 'Noise in frequency mixers using non-linear resistors', Alta Freq., 1971, 6
3 SALEH, A. A. M.: 'Theory of resistive mixers' (MIT Press, 1971)
4 ARMSTRONG, R., KOROLKIEWICZ, E., and KULESZA, B. L. J.: 'Large signal waveforms in microwave balanced mixers with capacitance', Proc. IEE, 1978, 125, (8), pp. 728–729

EXPERIMENTAL 30 GHz PRINTED ARRAY WITH LOW LOSS INSULAR GUIDE FEEDER

Indexing terms: Dielectric waveguides, Antenna arrays

Experimental results of a printed linear array using a low loss insular dielectric waveguide feed are presented. The array consists of etched dipoles excited by the magnetic field of the feed waveguide. Radiation patterns and plots of the field distributions in the feed waveguide are given, which are in good agreement with the simple theory used.

Introduction: The realisation of a compact antenna system is an important addition to dielectric waveguide integrated circuit technology. The design presented here exploits a low loss dielectric waveguide to feed an array of etched dipoles, forming a basically slow wave antenna: this should be contrasted with leaky wave designs[1] also exploiting periodically loaded dielectric waveguides. In the design presented in this letter, the dipole radiators are assumed not to perturb the slow wave in the guide. This design has potential in the realisation of low-cost moderately sized linear and planar arrays, since the low loss

Fig. 1 Linear array of dipole pairs fed by dielectric waveguide

nature of the dielectric waveguide feed offers considerable advantages over other low cost fabrication techniques such as microstrip, which are extremely lossy at millimetric frequencies.

Antenna configuration: This is shown in Figs. 1 and 2. An insular dielectric guide is covered with a further dielectric sheet, which supports an array of etched dipoles or patches.
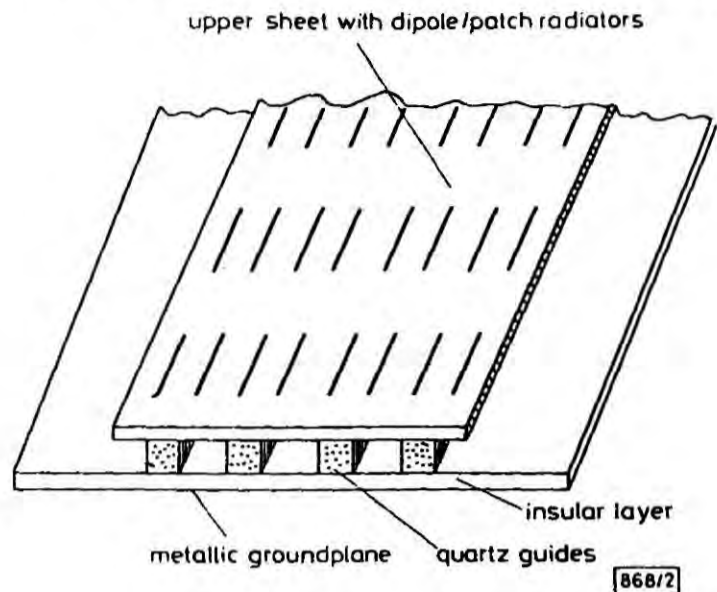

Fig. 2 Planar array configuration

Fig. 1 shows the radiators as pairs of dipoles. The H_x component of the approximately TM waveguide mode induces a current in each dipole, resulting in radiation. The radiation from all the dipoles sums to form the desired pattern in the far field. The design shown in Fig. 1 uses quartz ($\varepsilon_r = 3.8$) for the feed guide and RT Duroid ($\varepsilon_r = 2.2$) for the upper sheet supporting the dipole pattern. This forms a linear array: a planar array would consist of a number of parallel guides fed from an input dielectric or metallic waveguide (Fig. 2).

Theory: The design involves, first, the calculations of the waveguide dispersion and, second, the coupling from the waveguide mode to the dipoles. The former is done using a generalisation of the effective dielectric constant technique.[2] The presence of the lightly coupled dipoles is ignored. Fig. 3 shows the calculated dispersion curve; experimental values ob-
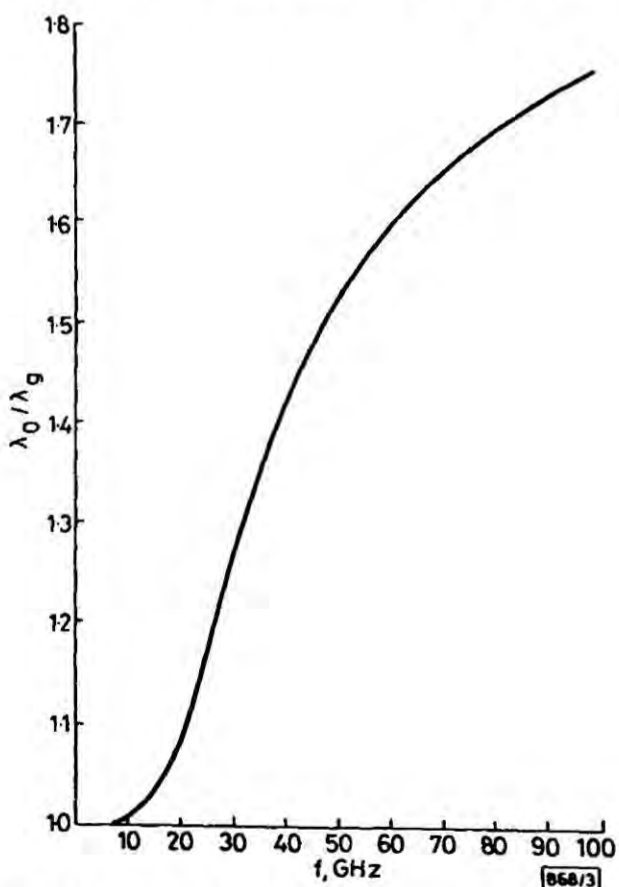

Fig. 3 Calculated dispersion for three-layer structure without dipoles
Line: 2 mm × 2 mm, $\varepsilon_r = 3.7$
Insular layer: 0.25 mm, $\varepsilon_r = 2.25$
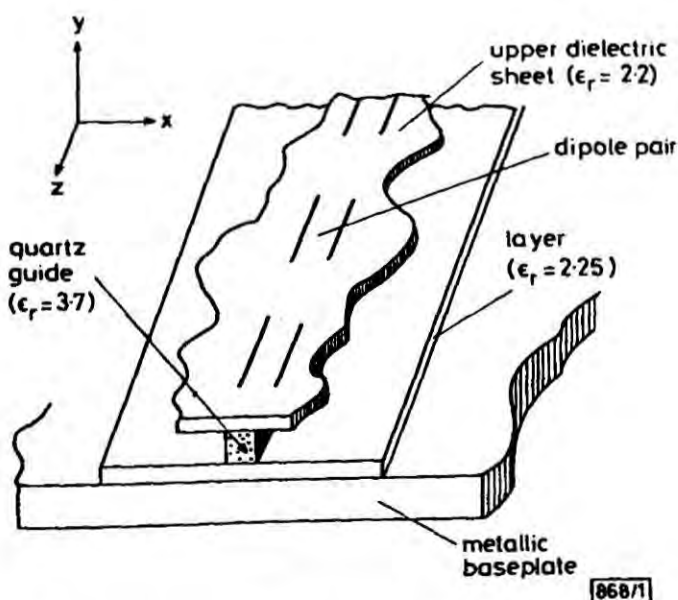Upper layer: 0.51 mm, $\varepsilon_r = 2.20$

APPLICATION OF RESONANT CIRCUIT THEORY TO MATCHING NETWORKS

R. ARMSTRONG and E. KOROLKIEWICZ

School of Electronic Engineering, Newcastle upon Tyne Polytechnic, England

1 INTRODUCTION

In high frequency communication systems, matching the source impedance to the load impedance is important, to prevent reflections and consequent distortion. Transmitters should transfer the maximum amount of power to the aerial, whilst in receiving systems low power levels also dictate maximum power transfer conditions. High frequency systems must accommodate modulated signals, and the bandwidth of a matching network must be adequate to allow the side bands to propagate. The basic building block of such matching networks is the parallel or series tuned circuit. This article shows how the theory of resonant circuits may be used to design apparently complex matching networks[1-3]. An example is given to illustrate the design process using both analytical and graphical methods. From an educational point of view the student sees the tuned circuit from a different aspect whilst the graphical method of solution is an excellent example on the use of a Smith Chart.

2 THE BASIC BUILDING BLOCK

Consider the problem of matching two resistors, R_s to R_m at a single frequency by means of the network shown in Fig. 1(a). As viewed from the terminals AB the matching network and the load appear as a parallel circuit as shown in Fig. 1(b). This network is equivalent to the three-element shunt network of figure 1(c).

The dynamic resistance is

$$R_D = (R_m^2 + X_{L1}^2)/R_m \tag{1}$$

and the equivalent parallel inductive reactance is

$$X_{LD} = (R_m^2 + X_{L1}^2)/X_{L1} \tag{2}$$

For matching at a single frequency it is required to choose values of X_{L1} and X_{C1} such that $R_D = R_S$ and from equation (1) it will be seen that X_{L1} must be given by,

$$X_{L1} = \sqrt{R_m(R_S - R_m)} \tag{3}$$

Equation (3) shows that R_S must be greater than R_m to make X_{L1} inductive. From Fig. 1(c) the magnitude of X_{C1} must equal the effective inductive re-
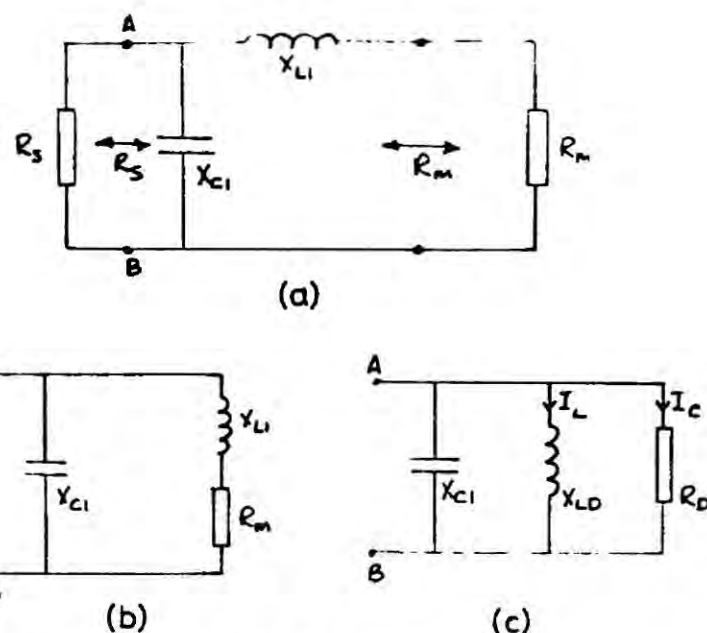
FIG. 1 LC matching section when $R_s > R_m$ and its equivalent parallel network.

actance at the working frequency and therefore,

$$X_{C1} = (R_m^2 + X_{L1}^2)/X_{L1} \tag{4}$$

The Q factor of the resonant circuit in Fig. 1(c) is defined as the ratio of the current I_L in the inductance to the current I_R in the resistance at resonance i.e.,

$$Q_1 = I_L/I_R = R_D/X_{LD} \tag{5}$$

Substituting equations (1) and (2) into equation (5), the Q factor of the resonant circuit in Fig. 1(c) is,

$$Q_1 = X_{L1}/R_m \tag{6a}$$

When R_s is connected across AB the loaded Q is given by,

$$Q_{1L} = Q_1/2 \tag{6b}$$

which determines the bandwidth of the network shown in Fig. 1(c).

If the terminating resistance values are specified, then the Q, and hence the bandwidth are automatically fixed. Alternatively, from equation (1) with $R_D = R_s$ it is easily shown that,

$$R_m = R_s/(1 + Q_1^2) \tag{7}$$

from which R_m may be determined if R_s and Q_1 are specified.

To match from a low resistance R_m to a high resistance R_L the matching network is reversed as shown in Fig. 2 and identical analysis yields,

$$X_{L2} = (R_m[R_L - R_m])^{\frac{1}{2}} \tag{8}$$
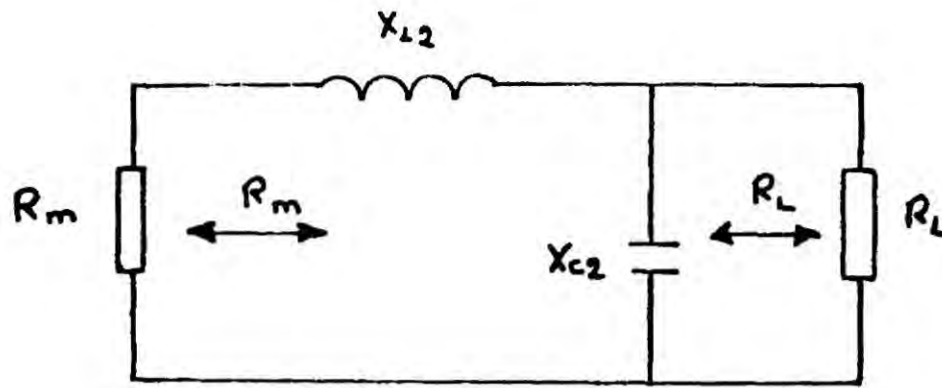
$$X_{C2} = (R_m^2 + X_{L2}^2)/X_{L2} \tag{9}$$

FIG. 2   LC matching section when $R_m < R_L$.

$$Q_2 = X_{L2}/R_m \tag{10}$$

$$R_m = R_L/(1 + Q_2^2) \tag{11}$$

In a majority of high frequency applications it is often necessary to match between a complex impedance and 50Ω. This can be done readily using the above theory. For example, if the source impedance is complex then the R_s of figure 1(a) is the effective parallel resistance of the source and the effective parallel susceptance is included as part of X_{C1}. Alternatively, in Fig. 2 the complex impedance may be regarded as a resistor R_m in series with a reactance which is included as part of X_{L1}. In both cases the above theory is sufficiently general to design the matching networks.

The range of complex impedances that can be matched to a 50Ω load by each of the two LC matching networks can be readily obtained[4] and are shown in Fig. 3.

3   π MATCHING NETWORKS

For the simple L-C networks analysed in section (2) the bandwidth is automatically fixed by the specified source and load resistances. If it is required to specify the bandwidth in addition, then the π network shown in Fig. 4(a) may be used. Such a network also has the advantage of being able to match any complex impedances. By splitting the π network into two simple LC sections as shown in Fig. 4(b) the value of R_m may be chosen to achieve the desired bandwidth. For matching, the required R_m is given by equations (7) and (11).

$$R_m = R_s/(1 + Q_1^2) = R_L/(1 + Q_2^2) \tag{12}$$

This equation shows that the node with the highest terminating resistance has the largest Q and hence dictates the bandwidth of the system.

It is shown in the appendix that constant Q curves on the Smith Chart are described by the following equation of a circle

$$U^2 + (V + 1/Q)^2 = 1 + 1/Q^2 \tag{13}$$

where U and jV are the real and imaginary axes on the Smith Chart of the
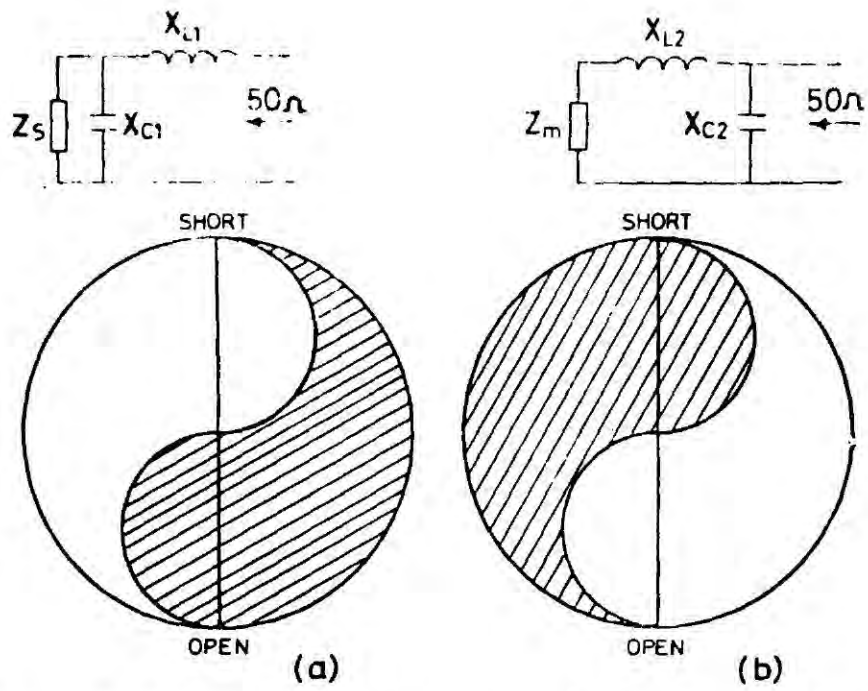
354

FIG. 3 (a) Shaded region shows range of complex impedance Z_s that can be matched to 50Ω using circuit shown in Fig. 1. (b) Shaded region shows range of complex impedance Z_m that can be matched to 50Ω using circuit shown in Fig. 2.
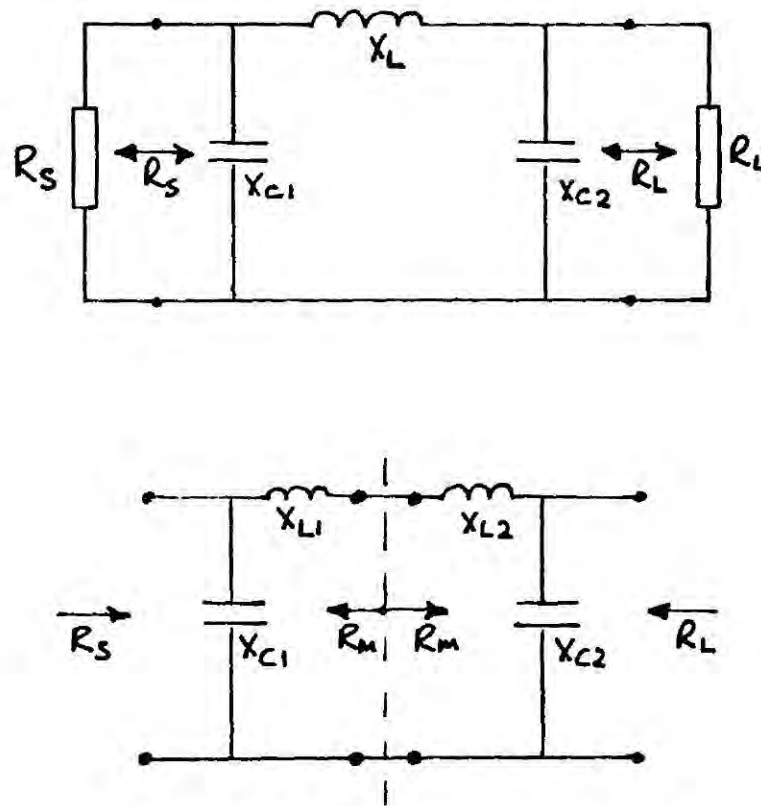

FIG 4 π matching section.

voltage reflection coefficient. It is possible therefore to use the Smith Chart to evaluate the elements of the π matching network as shown in the following example.

4 EXAMPLE

Suppose it is necessary to match an output admittance $(0.01 + j0.02)S$ of an amplifier to a 50Ω load and the required value of Q being 5 at the working frequency.

The output susceptance of the amplifier can be combined with the X_{C1} of the matching network to produce an equivalent reactance (X_{C1}) and therefore it is only necessary to match 100Ω to 50Ω. The Q is associated with the 100Ω node and the desired equations can be used to determine the required elements of the matching network as shown below.

$$R_m = R_s/(1 + Q_1^2) = 3.85\Omega$$

$$X_{L1} = \sqrt{R_m(R_s - R_m)} = 19.24\Omega$$

$$X_{C1} = \frac{R_m^2 + X_{L1}^2}{X_{L1}} = 20.0\Omega$$

$$X_{L2} = \sqrt{R_m(R_L - R_m)} = 13.32\Omega$$

$$X_{C2} = \frac{R_m^2 + X_{L2}^2}{X_{L2}} = 14.45\Omega$$

The required elements of the matching network are shown in Fig. 5.

The values of the elements of the series equivalent circuit of the parallel circuit consisting of a 100Ω resistance in parallel with X_{CT} is given by the intersection of the constant $Q (= 5)$ circle and constant conductance $(\bar{G} = 0.5)$ circle at point A. The required value of X_{C1} in parallel with the 100Ω resistance is found by moving diametrically opposite point A to point A', which gives the admittance values of the elements of the parallel network i.e. $\bar{G} = 0.5$ and $\bar{B}$ = 2.57, from which $\bar{X}_{C1} = 1/2.57 = 0.39$ and hence $X_{CT} = 19.5\Omega$.

The required normalized value of $\bar{X}_L$ is found by travelling from point A on the constant resistance circle (0.075) to the intersection of the constant con-
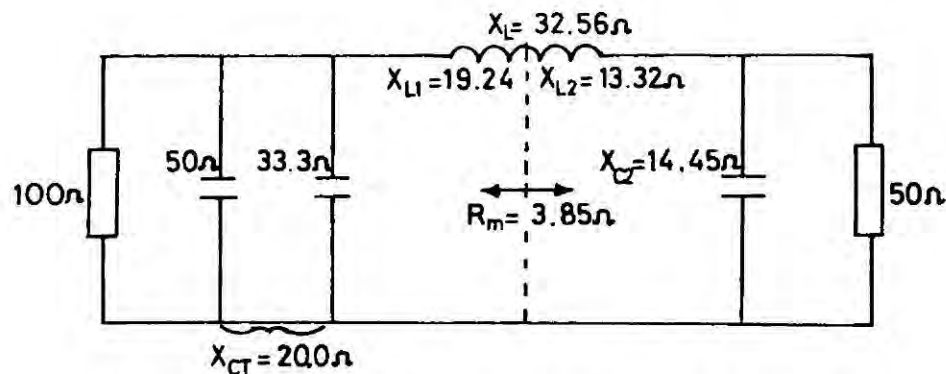

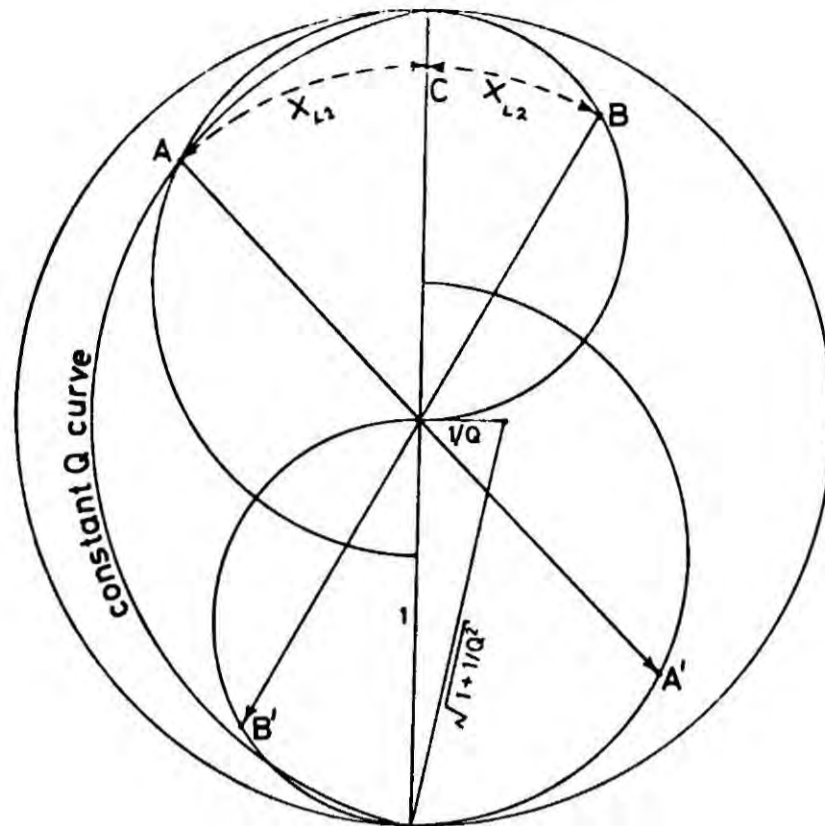FIG. 5 Required elements of the π matching section.

FIG. 6 Design of the π matching section using a Smith chart.
Point $A = 0.075 - j0.38$, point $A' = 0.5 + j2.55$,
point $B = 0.075 + j0.256$, point $B' = 1 - j3.7$ and point $C = 0.075 + j0$.

ductance ($\bar{G} = 1$) circle at point B. The normalized value of X_{C2} is obtained in a similar manner to that already described for X_{CT}, from a point diametrically opposite to B i.e. B.

Renormalizing the results determined from the Smith chart the values of the required elements of the π matching section are,

$R_m = 3.75\Omega$ (point C), $X_{CT} = 19.5\Omega$, $X_{L1} = 19.0\Omega$, $X_{L2} = 12.8\Omega$, $X_{C2} = 13.5\Omega$ As can be seen, the results obtained using the Smith chart are comparable with those given by the analytic method.

5 CONCLUSIONS

The aforegoing analysis has shown how parallel resonant circuits form the basis of π matching networks. The important point is to find the effective resistance R_m of the two back-to-back LC sections to give the desired bandwidth. If the source and load are complex the problem is reduced to matching resistive elements by combining the effective parallel susceptance with the capacitive shunt arms of the matching section. This concept may be used to explain how the first capacitive element of the matching network may be used as part of the tank circuit in an r.f. amplifier.

The same principles also apply to tee networks where the central element is

divided in such a manner as to produce the required bandwidth. In this case the effective resistance R_m will exceed both R_s and R_L and the design equations follow directly from the theory of series resonant circuits.

In an identical manner it is also possible to design matching networks with the inductance and capacitance interchanged on either one or both of the basic half sections. The choice of the form of the matching network may often depend on the nature of the source and load impedance. For example, if the output capacitance of an amplifier exceeds the value of X_1 in a π matching network then clearly the first shunt element of the network must be inductive.

It is considered that the results presented in this article give a valuable insight into the many apparently diverse matching networks used in practice. The graphical solution is another indication of the versatility of the Smith chart.

6 REFERENCES

[1]   Colussi, E. J., 'Internally matched R. F. power transistors', *Microwave Journal*, **21**, No. 4, pp. 81-84.

[2]   Przedpelski, A.B., 'Bandwidth of transmission line matching circuits'. *Microwave Journal*, **21**, No. 4, pp. 71-76.

[3]   Gelnovateh. V. G.. Burke, J. F.. 'Computer aided design of wide-band integrated microwave transistor amplifiers on high dielectric substrates' *IEEE Journal of Solid-State Circuits* (June, 1968).

[4]   Smith, P. H., *Electronic Applications of the Smith Chart*. McGraw-Hill, pp. 115-127 (1969).

APPENDIX

The relationship between normalized impedance $\bar{Z}$ and the voltage reflection coefficient p is given by,

$$p = U + jV = \frac{\bar{z} - 1}{\bar{z} + 1} \tag{A1}$$

Equation (A1) can also be expressed in the form shown below,

$$\bar{z} = \bar{r} + j\bar{x} = \frac{(1 + U) + jV}{(1 - U) - jV} \tag{A2}$$

Hence,

$$\bar{r} = \frac{1 - U^2 - V^2}{(1 - U)^2 + V^2} \tag{A3}$$

and,

$$\bar{x} = \frac{2V}{(1 - U)^2 + V^2} \tag{A4}$$

The Q of a circuit is defined as,

$$Q = \bar{x}/\bar{r}$$

and hence from equations (A3) and (A4) it can be shown that,

$$U'^2 + \left(1 + \frac{1}{Q}\right)^2 = 1 + \frac{1}{Q^2} \tag{A5}$$

which is an equation of a circle of radius $\left[1 + \frac{1}{Q^2}\right]^{\frac{1}{2}}$ and centre $U' = 0$ and $V = -1\,Q$.

In a similar manner it may be shown that when dealing with admittance equation (A5) is modified to,

$$U^2 + \left(V - \frac{1}{Q}\right)^2 = 1 + \frac{1}{Q^2} \tag{A6}$$

which is a circle centred on,

$$U = 0 \text{ and } V = +\frac{1}{Q}$$

ABSTRACTS-ENGLISH, FRENCH, GERMAN, SPANISH

Application of resonant circuit theory to matching networks
A wide variety of matching networks are used in high frequency communication systems and this paper shows how such networks can be conveniently designed using the theory of resonant circuits. A graphical method is also included which provides a valuable insight into the properties of the Smith Chart.

Application de la théorie des circuits résonnants aux réseaux adaptateurs
Une grande variété de réseaux adaptateurs est utilisée dans les systèmes de communication à haute fréquence. Cet article montre comment de tels réseaux peuvent être calculés de façon commode par la théorie des circuits résonnants. Une méthode graphique utilisée donne en outre un précieux aperçu des propriétés de l'abaque de Smith.

Anwendung der Resonanzkreistheorie auf Anpassungsnetzwerke
Eine grosse Vielfalt von Anpassungsnetzwerken wird in Hochfrequenz-Fernmeldesystemen verwendet; diese Arbeit zeigt, wie derartige Netzwerke bequem bei Benutzung der Theorie von Resonanzkreisen entworfen werden können. Ferner wird eine graphische Methode angegeben, die einen wertvollen Einblick in die Eigenschaften des Smithschen Leitungsdiagramms gibt.

Aplicación de la teoria de circuitos resonantes para redes de acoplamiento
Una amplia variedad de redes de acoplamiento se utilizan en los sistemas de comunicación de alta frecuencia. En este articulo se muestra cómo tales redes pueden calcularse apropiadamente utilizando la teoria de circuitos resonantes. Se incluye un método gráfico que proporciona una valiosa profundización en las propiedades de la carta de Smith.

Fundamental limitations in performance of a resistive lattice *H* mixer

B.L.J. Kulesza, Dip.E.E., Ph.D., C.Eng., M.I.E.E., and E. Korolkiewicz, M.Sc.

Abstract: The main objective of the paper is to present in one place all the performance curves for the various modes of operation of the resistive lattice *H* mixer. Four distinct cases are considered; two narrowband mixers with open- and short-circuit terminations at the image frequency, and two broadband circuits with matched and mismatched conditions at the RF port. The design formulas are tabulated, and the expected minimum conversion power loss, as well as the optimum terminations required over a wide range of operational levels, are plotted for each type of mixer.

1 Introduction

Single-balanced two-diode and double-balanced four-diode lattice mixers are usually preferred to single-diode circuits for high-frequency applications, as they generate less unwanted harmonic products, and therefore reduce associated filtering problems. They also have the advantage of reducing the noise contribution from the local oscillator and eliminating the decoupling problems associated with the local oscillator circuit at the RF port of the mixer. A double-balanced lattice mixer has a further advantage, in that inherent separation of odd and even harmonic products is obtained, which further reduces filtering problems [1]. The disadvantage of a more complicated diode circuitry for multidiode mixers, especially at microwave frequencies, has largely been overcome by modern MIC technology [2–4]. In fact, a *K*-band double-balanced lattice mixer has recently been constructed using a combination of microstrip lines, slotlines and coupled slotlines, thereby eliminating the crossing problem of transmission lines [5].

When an RF signal is mixed with a local oscillator a whole spectrum of harmonic modulation products are generated. Using perturbation methods, it is possible to analyse a nonlinear circuit in terms of a number of equations, each corresponding to the harmonic modulation product present [6–9]. An alternative method to the classical frequency-domain analysis of mixers has recently been suggested [10–12], using a time-domain approach to obtain the scattering matrix of the complete mixer. Whichever method is used, the total power available in the harmonic modulation products can never be greater than that generated by the RF source [13]. Consequently, the local oscillator power necessary to drive the non-linear elements is not available as the output power at any of the harmonic modulation product frequencies generated. To improve the performance of a mixer, it is essential to ensure that unwanted harmonic modulation products generated within the nonlinear elements are not allowed to dissipate power externally or internally. The most important parasitic is the image frequency component, so named because of its relative position to the signal in the frequency spectrum. As its magnitude can be comparable to that of the signal, and unless its dissipation is reduced, high efficiencies of conversion are not possible.

It is generally accepted that mixers are classified according to the kind of termination the image frequency component 'sees'. For resistive mixers there are three special cases, called the 'broadband' the 'narrowband open-circuit' and 'narrowband short-circuit' mixers. In the broadband circuit the resistive components of the terminations at the input are identical at signal and image frequencies. In the narrowband cases the termination at the image frequency is either infinite or zero, i.e. open circuit or short circuit.

Stracca [14] has considered the performance of balanced mixers when the local oscillator is coupled to the diode through a series resonator. The resonator presents a high impedance to the local oscillator harmonics, and so the mixer is pumped by a sinusoidal current. He showed that an improvement in the conversion loss can be obtained if a mixer is pumped by a sinusoidal current waveform rather than a sinusoidal voltage one. Rustom and Howson [15] have also investigated the mixer noise figure of *Z, Y, G* and *H* mixers, according to the Saleh classification [9], using an improved resistive diode model.

A computer-based analysis confirmed the conclusion reached by Stracca, that *H* and *G* mixers having a local oscillator current drive are the most promising mixer circuits if it is desired to obtain a low system noise figure.

A variety of diode models are generally used in the analysis of mixers, ranging from that of an ideal diode (having zero forward resistance and infinite reverse resistance), a bilinear diode (with finite forward and reverse resistance), and an ideal exponential diode where the effect of the diode series resistance is neglected. It can be shown that the diode series resistance has a profound effect on the harmonic generator properties of a diode. By restricting the local oscillator to a sinusoidal current drive, this paper examines the performance of resistive lattice *H* mixers, where the effect of the diode series resistance has been included, analytically (as compared with the usual computer-aided analysis using various numerical techniques). In the general analysis of mixers, three distinct cases are normally considered: two narrowband (image open- and short-circuit) mixers, and a broadband mixer designed to obtain minimum conversion loss. In this paper, a fourth case is included where a broadband mixer is analysed with matched conditions at the RF and IF ports.

2 Analysis

A basic circuit of a lattice *H* mixer, according to the Saleh classification [9], is shown in Fig. 1a. Assuming inherent separation of the odd and even harmonic modulation products [1], such a mixer may be described by the following general

matrix equation:

$$
\begin{bmatrix} v_1 \\ I_2 \end{bmatrix} \approx \begin{bmatrix} \sum_{n\ even} a_n \cos n\omega_p t & \sum_{n\ odd} b_n \cos n\omega_p t \\ \sum_{n\ odd} c_n \cos n\omega_p t & \sum_{n\ even} d_n \cos n\omega_p t \end{bmatrix} \begin{bmatrix} I_1 \\ V_2 \end{bmatrix}
$$

(1)

To evaluate the coefficients of the above equation, consider the circuit as 'seen' by the local oscillator, shown in Fig. 1b. Let the mixer be pumped by a sinusoidal current

$$ i = 2I_p \cos \omega_p t \tag{2} $$

The current i_D flowing through each diode of the mixer is given by

$$ i_D = \tfrac{1}{2}\{1 + s(t)\} \cos \omega_p t \tag{3a} $$

where $s(t)$ is the switching function, defined as

$$ s(t) = \frac{4}{\pi}(\cos \omega_p t - \tfrac{1}{3} \cos 3\omega_p t + \ldots) \tag{3b} $$

The voltage v developed across the terminals of a diode, using the practical diode law, can be expressed in the form

$$ v = i_D r_s + \frac{1}{\alpha}\{\ln(1 + i_D/I_s)\} \tag{4a} $$

where r_s is the diode series resistance, and α and I_s are the diode parameters. The time varying resistance of the pumped diode, using the above equations, is given by

$$ r(t) = \frac{dv}{di_D} = r_s + \frac{r_b}{1 + X(t) + X(t)s(t)} \tag{4b} $$

where

$$ r_b = \frac{dv}{di_D}\bigg|_{i_D=0} $$

$$ X(t) = X \cos \omega_p t $$

and

$$ X = I_p/2I_s $$

Substituting eqn. 4b into eqn. 1, and taking into account the 180° phase difference of the local oscillator between the two
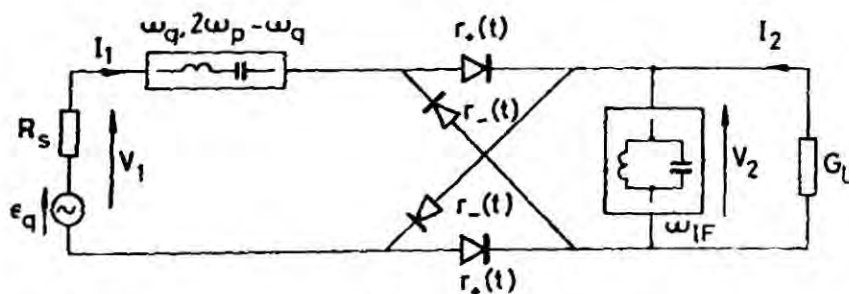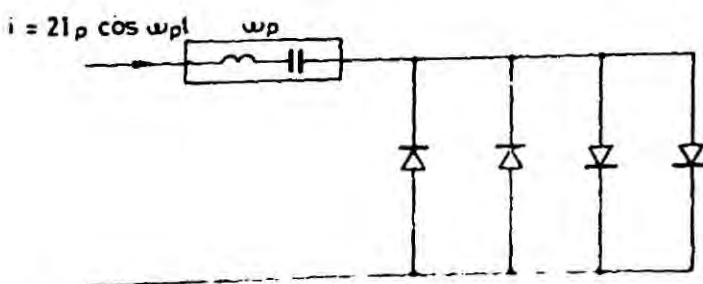

Fig. 1A *Four-diode lattice H mixer*

Fig. 1B *Equivalent local oscillator circuit*

pairs of diodes, the following equation can be obtained, provided $r_b \gg r_s$

$$
\begin{bmatrix} V_1 \\ I_2 \end{bmatrix} = \begin{bmatrix} 2r_s + \dfrac{r_b}{1+X(t)s(t)} & \dfrac{X(t)}{1+X(t)s(t)} \\[2mm] \dfrac{-X(t)}{1+X(t)s(t)} & \dfrac{1}{r_b}\dfrac{1+2X(t)s(t)}{1+X(t)s(t)} \end{bmatrix} \begin{bmatrix} I_1 \\ V_2 \end{bmatrix}
$$

(5)

For the H mixer, filters placed at the RF and IF ports restrict the input current I_1 to RF and image frequencies, and the output voltage V_2 to intermediate frequency only, i.e.

$$ I_1 = I_q \cos \omega_q t + I_{-2} \cos(2\omega_p - \omega_q)t \tag{6a} $$

and

$$ V_2 = V_{-1} \cos(\omega_p - \omega_q)t \tag{6b} $$

Substituting eqns. 6a and b into eqn. 5, and performing a frequency balance operation at ω_q, $2\omega_p - \omega_q$ and $\omega_p - \omega_q$, the following three-port matrix is obtained:

$$
\begin{bmatrix} V_q \\ I_{-1} \\ V_{-2} \end{bmatrix} \begin{bmatrix} h_{11} & h_{12} & h_{13} \\ -h_{12} & h_{22} & -h_{12} \\ h_{13} & h_{12} & h_{11} \end{bmatrix} \begin{bmatrix} I_q \\ V_{-1} \\ I_{-2} \end{bmatrix}
$$

(7)

The elements of the above three-port matrix are the Fourier coefficients of the time-varying parameters in eqn. 5 and can be shown to be [16]

$$ h_{11} \simeq 2\left(r_s + \frac{r_b}{\pi X}\ln 2X\right) $$

$$ h_{12} \simeq 2/\pi $$

$$ h_{13} \simeq \frac{2r_b}{\pi X}(2 - \ln 2X) $$

$$ h_{22} \simeq 2/r_b \tag{8} $$

If the image termination is defined as R_{-2}, then

$$ V_{-2} = -I_{-2}R_{-2} \tag{9} $$

Substituting eqn. 9 into eqn. 7, the following two-port matrix equation describing the mixer is obtained:

$$
\begin{bmatrix} V_q \\ I_{-1} \end{bmatrix} = \begin{bmatrix} H_{11} & H_{12} \\ -H_{12} & H_{22} \end{bmatrix} \begin{bmatrix} I_q \\ V_{-1} \end{bmatrix}
$$

(10)

where

$$ H_{11} = h_{11}\{1 - a^2/(1+R)\} $$

$$ H_{12} = h_{12}\{1 - a/(1+R)\} $$

$$ H_{22} = h_{22}\{1 + K_0/(1+R)\} \tag{11} $$

and

$$ a = h_{13}/h_{11} $$

$$ K_0 = h_{12}^2/h_{11}h_{22} $$

$$ R = R_{-2}/h_{11} $$

3 Performance parameters of lattice H resistive mixers

The conversion power loss (cpl) of a mixer is defined as

$$ cpl = 10 \log_{10} \frac{\text{available RF power}}{\text{output IF power}} \tag{12} $$

$$ = 10 \log_{10} L $$

For the H mixer, using eqn. 10, it can be shown that

$$L = \frac{\{(R_s + H_{11})(G_L + H_{22}) + H_{12}^2\}^2}{4H_{12}^2 R_s G_L} \quad (13)$$

where R_s is the source resistance at the RF port and G_L is the load conductance at the IF port.

One method of determining the necessary terminations at the RF and IF ports to obtain minimum conversion loss is to set the derivatives of eqn. 10 with respect to R_s and G_L to zero. This results in the following general equations:

$$R_{s_{opt}} = H_{11}(1 + K)^{1/2}$$

$$G_{L_{opt}} = H_{22}(1 + K)^{1/2} \quad (14)$$

$$L_{min} = \frac{1 + (1 + K)^{1/2}}{-1 + (1 + K)^{1/2}}$$

where

$$K = H_{12}^2/H_{11}H_{22}$$

It can also be shown that, provided the H coefficients are independent of R_s and G_L, then the above equations also correspond to the condition that the mixer is simultaneously matched at the RF and IF ports, i.e.

$$R_{s_{opt}} = R_{IN} \quad \text{and} \quad G_{L_{opt}} = G_{OUT}$$

where R_{IN} is the input resistance and G_{OUT} is the output conductance of the two port network defined by eqn. 10.

Examining eqn. 11, it can be seen that the H coefficients are independent of R_s and G_L only for $R_{-2} = \infty$ or $R_{-2} = 0$. Substituting eqn. 11, for the two conditions, into eqn. 14, general performance parameters for the two narrowband mixers can be obtained, and these are given in Table 1.

For a broadband mixer, however, $R_{-2} = R_s$, and hence the H coefficients are a function of the source resistance. Setting the derivatives of eqn. 13 with respect to R_L and G_L to zero, and using eqn. 11, it can be shown that, to obtain minimum conversion loss, the necessary terminations at the RF and IF ports are

$$R_{s_{opt}} = h_{11}(1 + a)(1 + K_B)^{1/2} \quad (15)$$

$$G_{L_{opt}} = h_{22}(1 + K_B)$$

where

$$K_B = 2K_0/(1 + a)$$

The resulting expression for the conversion loss is then

$$L_{min} = \frac{2\{1 + (1 + K_B)^{1/2}\}}{-1 + (1 + K_B)^{1/2}} \quad (16)$$

Considering eqns. 15, it can be shown that, when the broadband mixer is designed to obtain minimum conversion loss, the mixer is matched at the IF port but mismatched at the RF port. This conclusion is in agreement with Kelly [10], who analysed a general mixer using a time-domain approach, assuming that the diodes are perfect, i.e. having zero forward resistance and an infinite reverse resistance. The requirement of mismatching the RF port in the case of a broadband mixer is therefore valid whether the mixer is regarded as lossless or not. This condition results from the fact that the coefficients of the two-port network are functions of the source resistance. If the diodes in the lattice mixer are assumed to be approaching ideal, the parameter K_B becomes much greater than one, so that $L_{min} = 2$ and CPL = 3 dB, as predicted by Kelly using time-domain analysis and Torrey and Whitmer [8] using frequency-domain analysis.

An alternative method of designing a broadband mixer is to obtain matched conditions at the RF and IF ports. Using eqns. 11 and 14, it can be shown that the RF port is matched if the source resistance is

$$R_{IN} = R_s = h_{11}\{1 - a^2/(1 + R)\}\{1 + K_m\}^{1/2} \quad (17)$$

where

$$K_m = \left\{\frac{K_0}{1 + K_0/(1 + R)}\right\}\left\{\frac{[1 - a/(1 + R)]^2}{1 - a^2/(1 + R)}\right\}$$

Table 1

Mixer Parameter	Narrowband image open-circuit ($R_{-2} = \infty$)	Narrowband image short-circuit ($R_{-2} = 0$)	Broadband mixer mismatched at the RF port ($R_{-2} = R_s$)	Broadband mixer matched at the RF port ($R_{-2} = R_s$)
Minimum conversion loss	$\dfrac{1 + (1 + K_0)^{1/2}}{-1 + (1 + K_0)^{1/2}}$	$\dfrac{1 + (1 + K_s)^{1/2}}{-1 + (1 + K_s)^{1/2}}$	$\dfrac{2\{1 + (1 + K_B)\}^2}{-1 + (1 + K_B)}$	$\dfrac{1 + (1 - K_m)^{1/2}}{-1 + (1 + K_m)^{1/2}}$
Optimum source resistance	$h_{11}(1 + K_0)^{1/2}$	$h_{11}(1 - a^2)(1 + K_s)^{1/2}$	$h_{11}(1 + a)(1 + K_B)^{1/2}$	$h_{11}\left(1 - \dfrac{a^2}{1 + R}\right)(1 + K_m)^{1/2}$
Optimum load conductance	$h_{22}(1 + K_0)^{1/2}$	$h_{22}(1 + K_0)(1 + K_s)^{1/2}$	$h_{22}(1 + K_B)^{1/2}$	$h_{22}(1 + K_0)(1 + K_m)^{1/2}$
K_0	$h_{12}^2/h_{11}h_{22}$			
K_s		$\left(\dfrac{K_0}{1 + K_0}\right)\left(\dfrac{1 - a}{1 + a}\right)$		
K_B			$2K_0/(1 + a)$	
K_m				$\left\{\dfrac{K_0}{1 + K_0/(1 + R)}\right\}\left\{\dfrac{[1 - a/(1 + R)]^2}{1 - a^2/(1 + R)}\right\}$

$a = h_{13}/h_{11}$

$$R = 2\left\{\frac{(a + 3)(a - 1)}{3}\right\}^{1/2}\cos(\theta/3) \quad \text{and} \quad \cos\theta = \frac{\sqrt{27}(1 + a^2)(a - 1)}{[(a + 3)(a - 1)]^{3/2}}$$

and results in the following quartic expression in R:

$$(1 + R)^4 + (K_0 - 2)(1 + R)^3 - 3K_0(R + 1) + a(1 + R) \times$$
$$\{2a + K_0(e + a)\} + a^2\{K_0(1 - 2a) - a^2\} = 0 \quad (18)$$

For practical diodes the parameter $K_0 \gg 1$, so that the value of R is given by [17]

$$R = 2\left\{\frac{(a + 3)(a - 1)}{3}\right\}^{1/2} \cos(\theta/3) \quad (19)$$

where

$$\cos\theta = \frac{\sqrt{27}(1 - a^2)(a - 1)}{\{(a + 3)(a - 1)\}^{3/2}}$$

The particular performance parameters for the narrowband and broadband H mixers are summarised in Table 1, and are in agreement with the general forms derived in other papers [8, 9, 17]. Hines [11] initially cast doubts on the validity of the frequency-domain analysis of mixers, attributing errors to inadmissible matrix truncation. However, in his recent paper [12] he showed that the time-domain and frequency-domain approaches produce similar results provided the same conditions prevail. He further showed that it is possible to obtain low losses in two-frequency single-diode mixers, in which all other responses are reactively suppressed. To obtain this condition, the impedance presented to the local oscillator must be much greater or much smaller than that of the two signals (RF and IF). For a lattice mixer this is obtained inherently as, at any in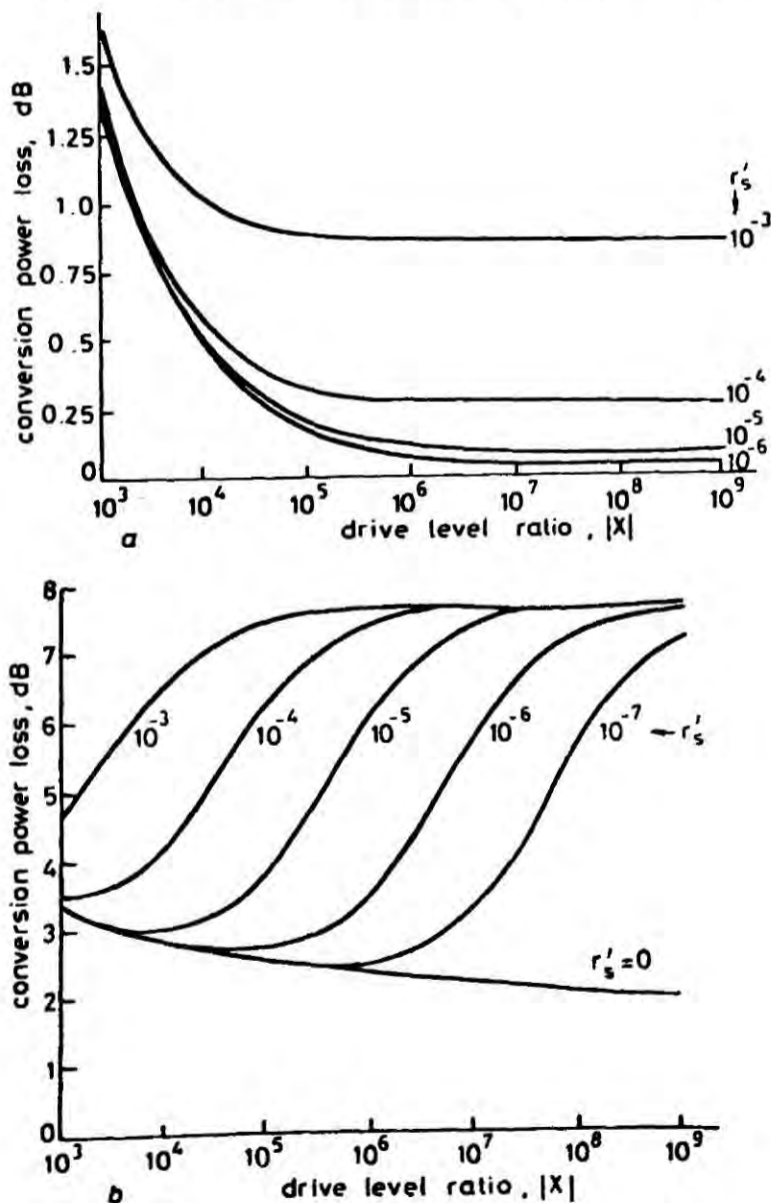stant of time, two diodes in parallel are always lower than that to the two signals. Consequently, as discussed in Section 4, it is possible to obtain low conversion loss in the case of the narrowband image-open-circuit lattice mixer.

4 Narrowband mixers

Complete rejection of the image frequency current at the RF port of the mixer, using conventional filter techniques, can never be obtained in practice. However, this type of mixer still offers the best possibility of a very efficient convertor. Even at low signal-to-image current ratios, conversion losses below 3 dB are theoretically attainable. The performance of the open-circuit mixer can be obtained by letting the image resistance R_{-2} tend to infinity in the general expressions for the H parameters of eqn. 11. The resultant expressions, describing the performance of the open-circuit mixer, are shown in Table 1. For practical mixers, because $h_{11}h_{22} \ll h_{12}^2, K_0 \gg 1$, and further simplifications are possible, which eventually leads, at high drive levels, to

$$R_{s_{opt}} \to \frac{2}{\pi}\sqrt{r_b r_s} \qquad R_{L_{opt}} \to \frac{\pi}{2}\sqrt{r_b r_s}$$

and

$$L_{min} \to \frac{1 + \pi\sqrt{r_s'}}{1 - \pi\sqrt{r_s'}} \quad \text{where} \quad r_s' = r_s/r_b \quad (20)$$

For a narrowband image short-circuit ($R_{-2} = 0$), although there is no dissipation at the image frequency externally (zero voltage), greater losses are incurred within the lattice of the mixer for nonideal diodes, i.e. $r_s' \neq 0$. Using the general equations given in Table 1, it can be shown that the limiting values of the terminations at the RF and IF ports, and
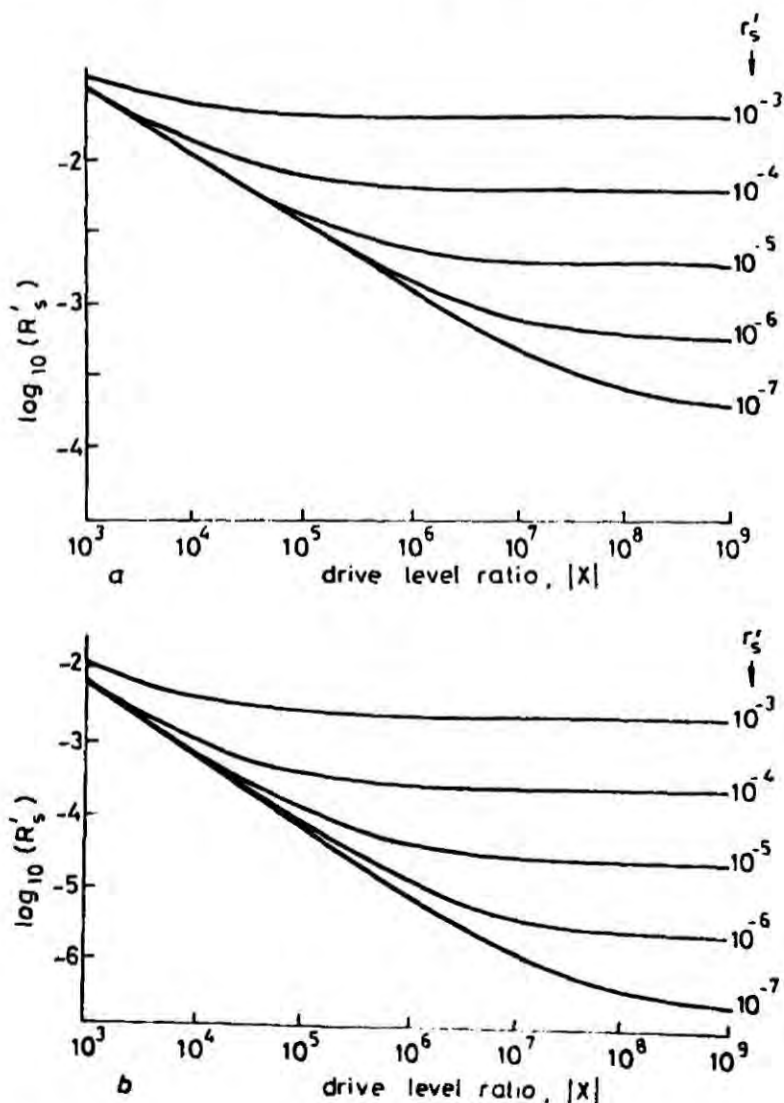

Fig. 2 *Minimum conversion power for narrowband mixers*

a Narrowband open-circuit mixer
b Narrowband short-circuit mixer

Fig. 3 *Optimum normalised source resistance for narrowband mixers*

a Narrowband open-circuit mixer
b Narrowband short-circuit mixer

resulting conversion loss at large drive, are

$$R_{s_{opt}} \rightarrow 2\sqrt{2}r_s \qquad R_{L_{opt}} \rightarrow \pi^2 r_s/2\sqrt{2}$$

$$L_{min} \rightarrow 5.8 \,(7.6\,dB) \tag{21}$$

The performances of the narrowband mixers are shown in Figs. 2–4, with normalised loss resistance of the diodes r_s', as the running parameter, and the optimum terminations normalised with respect to r_b ($R_s' = R_s/r_b$ and $R_L' = R_L/r_b$) where very low losses are predicted for the image open-circuit, as can be seen from Fig. 2a. The plot shows clearly that below a certain value of r_s' (e.g. 10^{-5}) the reduction in the conversion loss is negligible and may not justify the additional search and expense for lower loss diodes. In the case of image short-circuit there is a minimum of conversion loss, which occurs at certain drive levels, owing to the internal optimisation process.
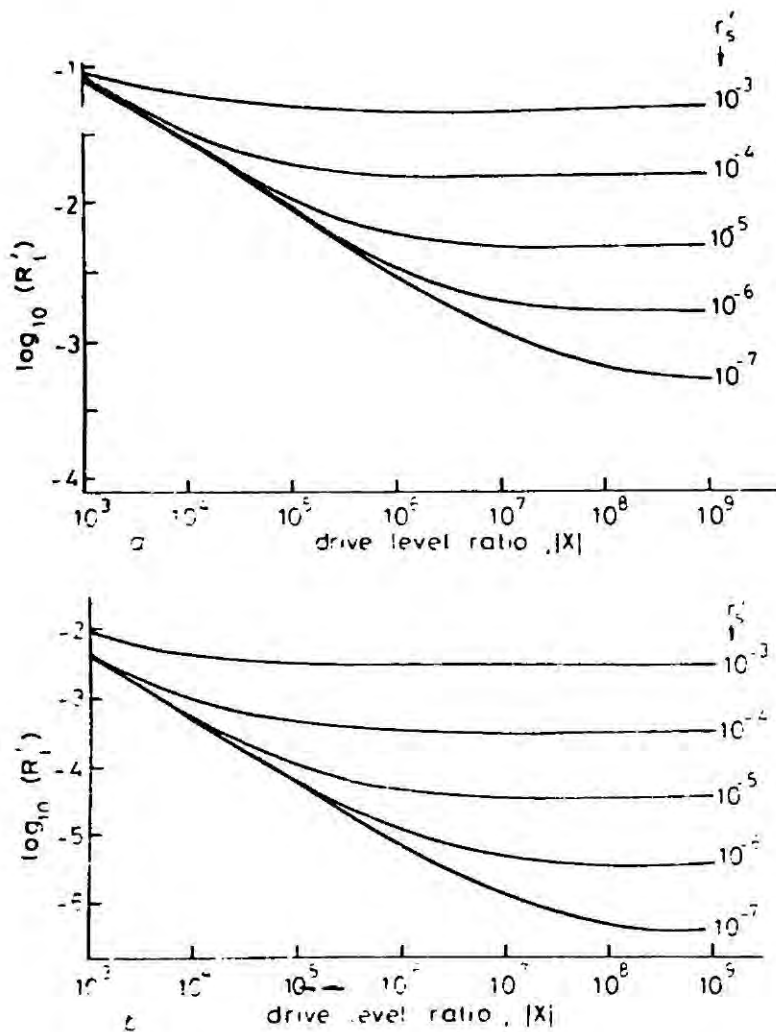
Fig. 4 Optimum normalised load resistance for narrowband mixers

a Narrowband open-circuit mixer
b Narrowband short-circuit mixer

The following transcendental equation defines the necessary drive to obtain minimum conversion loss

$$\ln(2X) - 3 = \frac{2}{\pi X}\left(\frac{r_b}{r_s}\right) \tag{22}$$

The conversion loss for this type of mixer, in general, is greater than for the one with image open-circuit.

5 Broadband mixers

It is normally difficult to approximate the ideal open or short-circuit conditions for the image frequency components in practical mixers. The problem becomes even more acute when the RF signal lies in the microwave frequency range (e.g. 10 GHz), and low values of IF are employed (e.g. 70, 45 or 30 MHz). Very often, therefore, because of relatively wide

bandwidths of practical filters, the impedance presented to the image frequency components may be very close to or equal in value to the terminating impedance at the RF signal frequency. The mixers which satisfy this latter equal impedance are known as broadband or double-sideband mixers.

One method of design of a broadband mixer is to produce a mismatch at the RF port in order to obtain minimum conversion loss. Using the general relationship shown in Table 1, the limiting values of terminations and the resulting conversion loss for large local oscillator drive are shown below:

$$R_{s_{opt}} \rightarrow \frac{2}{\pi}\sqrt{2r_b r_s} \qquad R_L \rightarrow \frac{\pi}{2}\sqrt{\frac{r_b r_s}{2}}$$

$$L_{min} \rightarrow 2\frac{1 + \pi\sqrt{r_s'}}{1 - \pi\sqrt{r_s'}} \rightarrow 2\,(3\,dB)$$

The alternative approach in the design of a broadband mixer is to obtain matching conditions at the RF and IF ports. Equating the signal and image terminating impedances, i.e. $R_s = R_{-2}$, results in a reduced cubic equation (eqn. 17) from which the value of the optimum source resistance at the RF port is finally determined.

For this mixer there is also a minimum of conversion loss, which occurs at certain drive levels and is defined by the transcendental eqn. 22. For large local oscillator drive the optimum terminations at the RF and IF ports and the resulting conversion losses are

$$R_{s_{opt}} \rightarrow 4r_s \qquad R_{L_m} \rightarrow 3\pi^2 r_s/4$$

$$L_{min} \rightarrow 4.7\,dB$$

The effect of the diode series resistance and the local oscillator drive on the normalised RF and IF resistance, and the con-
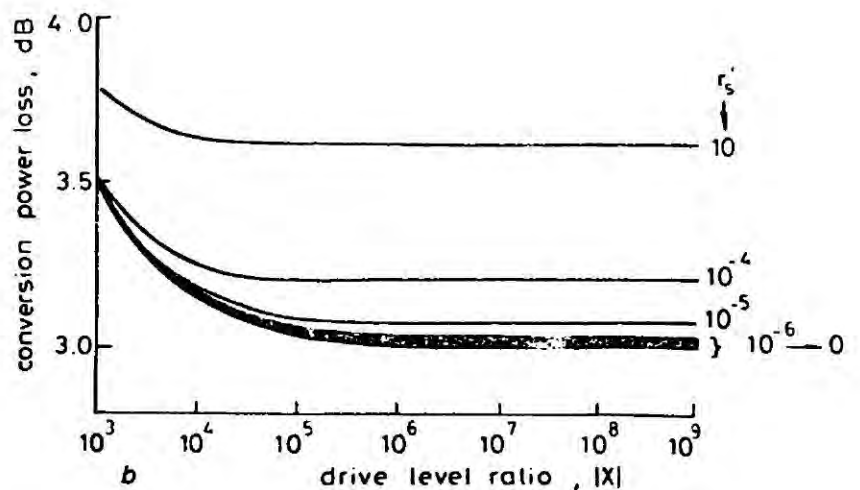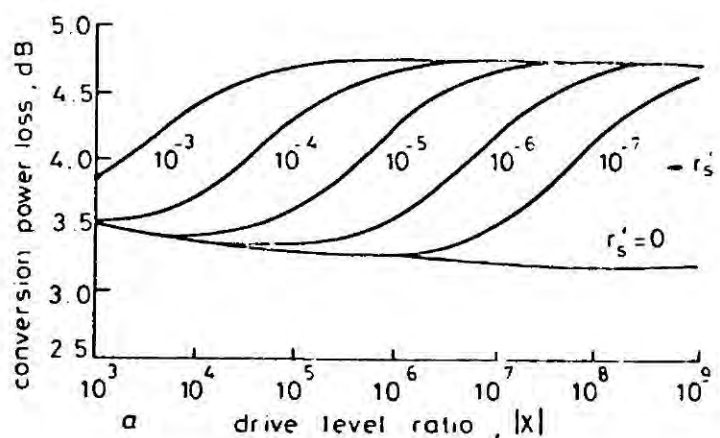
Fig. 5 Minimum conversion loss for matched and mismatched broadband mixers

a Broadband mixer (matched case)
b Broadband mixer (mismatched case)

version loss for the matched and mismatched broadband mixers, is shown in Figs. 5–7.

6 Conclusions

The performances of the practical lattice H mixers considered in this paper will depend to a large extent on the quality of
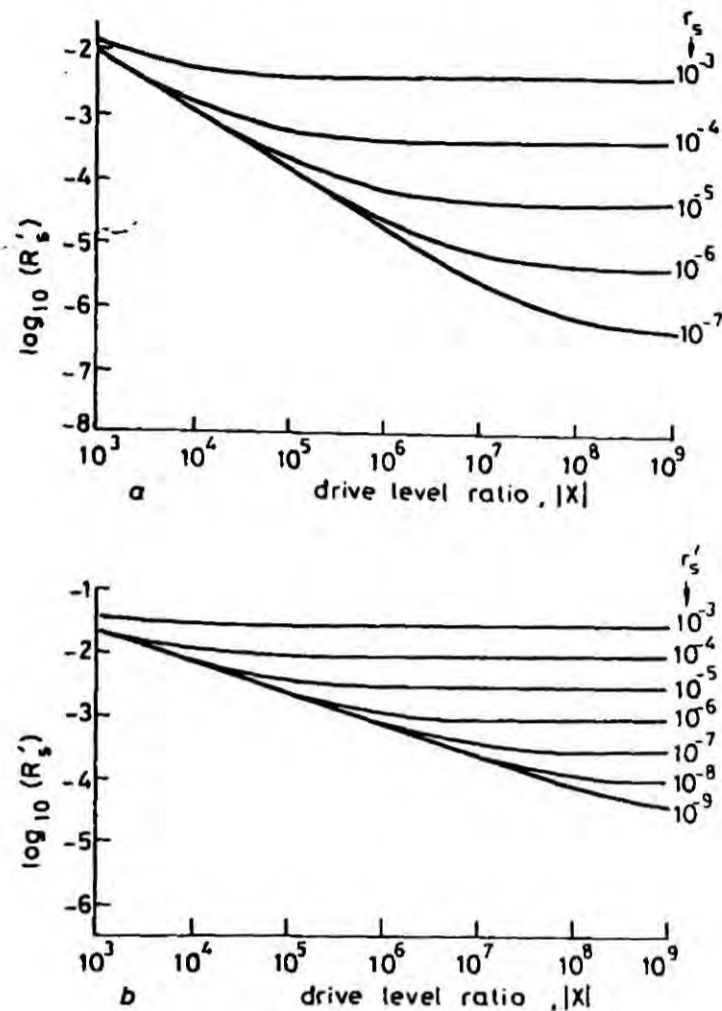

Fig. 6 *Optimum normalised source resistance for matched and mismatched broadband mixers*

a Broadband mixer (matched case)
b Broadband mixer (mismatched case)

the imbedding networks employed. In every case, an assumption was made that the frequency-selective terminations were ideal and nondissipative outside the required frequencies. To simplify the analysis further, the effect of the diode and circuit parasitics was assumed to be negligible at the frequencies of interest. It is apparent, therefore, that only with such constraints would these special cases have predicted input and output impedances which are purely resistive and a minimum conversion power loss when the mixer works between optimum terminations.

The narrowband image open-circuit mixer theoretically offers the lowest conversion loss at practical local oscillator drive levels, i.e. for X between 10^4 and 10^6. It can also be shown that, even at the image current rejection ratio of 4:1 with conjugate optimum terminations, loss below 2 dB is still possible. A useful practical feature of this type of mixer is that the ratios of the optimum input and output impedances remain reasonably constant for any drive level. As the drive is increased, however, the absolute values of the required terminations become lower.

The predicted performance of a narrowband short-circuit mixer does not compare favourably with the performance in the open-circuit case. Apart from the higher conversion power losses at similar operational levels, the required optimum terminations are much lower. This latter fact could create

matching difficulties if used with existing practical systems. Although this type of mixer is less likely to be considered, in practice, it is an interesting case as it displays an optimisation process that takes place within the lattice network of diodes.

Broadband mixers may find wider applications in communicating systems, especially where large bandwidths are of importance. The performance will depend on the choice of terminating resistance at the RF port. When matching conditions at the RF and IF ports are maintained, the conversion
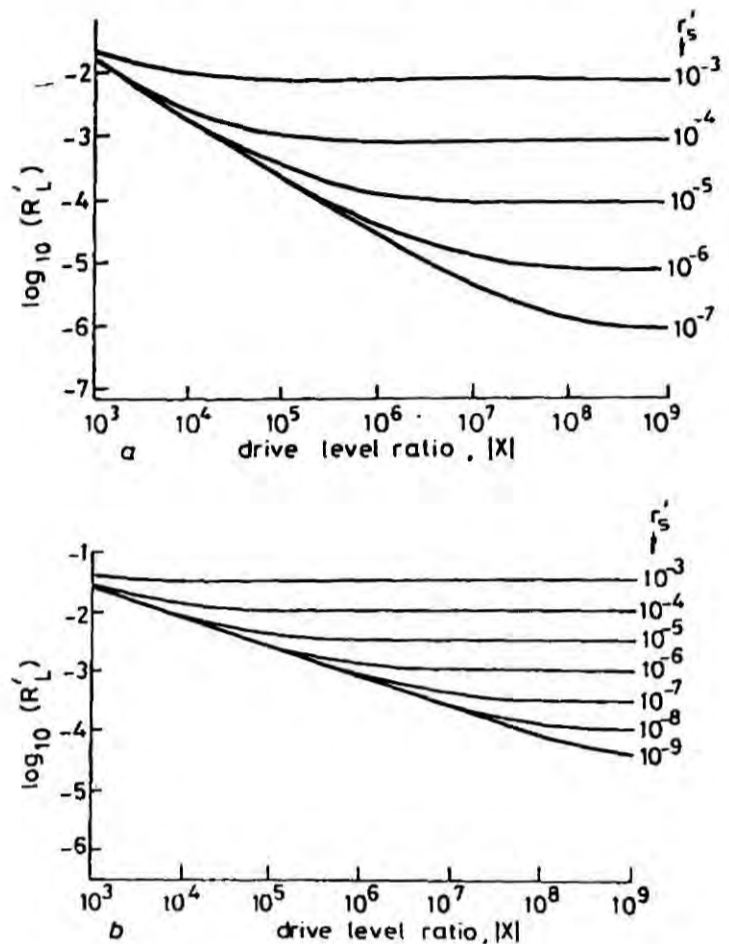

Fig. 7 *Optimum normalised load resistance for matched and mismatched broadband mixers*

a Broadband mixer (matched case)
b Broadband mixer (mismatched case)

power loss plot also shows the presence, although somewhat reduced, of the optimisation effect previously encountered in the narrowband short-circuit case. An improvement in the conversion loss is obtained if the mixer is mismatched at the RF port, and, as can be seen, the optimisation effect disappears; whether a troublesome mismatch at the signal is worthwhile in order to gain a lower loss will depend on the merit of individual applications and the frequency of operation. In both cases, with lossless diodes at infinite drive, the conversion loss reaches a theoretical limit of 3 dB. If the diode is considered as having exponential characteristics and zero series resistance, then the results obtained for the mixers designed for minimum conversion loss agree with those obtained by Saleh.

7 References

1 TUCKER, D.G.: 'Elimination of even-order modulation rectifier modulators', *J. Br. IRE*, 1961, 21, pp 161 167.
2 JOHNSON, K.M.: 'X-band integrated circuit mixer with reactively terminated image', *IEEE Trans.*, 1968, MTT-16, pp. 388–397
3 ARAKI, T., and HIRAYAMA, M.: 'A 20 GHz integrated balanced mixer', *ibid.*, 1971, MTT-19, pp. 638–643
4 SCHNEIDER, M.V., and SNELL, W.W.: 'Harmonically pumped stripline down-converter', *ibid.*, 1975, MTT-23, pp. 271–275
5 OGAWA, H., AIKAWA, M., and MORITA, K.: 'K-band integrated double-balanced mixer', *ibid.*, 1980, MTT-28, pp 180 185

6 PETERSON, L.C., and LLEWELLYN, L.B.: 'The performance and measurement of mixers in terms of linear-network theory', *Proc. IRE*, 1945, 33, pp. 458-476

7 DUINKER, J.: 'General properties of frequency converting networks', Philips Research Report 13, 1958, pp. 37-38, 101-148

8 TORREY, C.T., and WHITMER, C.A.: 'Crystal rectifiers', MIT Radiation Laboratory Series (McGraw-Hill, New York, 1948)

9 SALEH, A.A.M.: 'Theory of resistive mixers' (MIT Press, 1971)

10 KELLY, A.J.: 'Fundamental limits on conversion loss of double sideband resistive mixers', *IEEE Trans.*, 1977, MTT-25, pp. 867-869

11 HINES, M.: 'Failure of the classical circuit model in the analysis of low-loss band-limited mixers', IEE MTT-S Conference Proceedings, International Microwave Symposium Digest, Ottawa, Canada, 1978, pp. 402-404

12 HINES, M.: 'Inherent signal losses in resistive-diode mixers', *IEEE Trans.*, 1981, MTT-29, pp. 281-292

13 PAGE, C.H.: 'Frequency conversion with positive non-linear resistors', *J. Natl. Bur. Stand.*, 1956, 56, pp. 179-182

14 STRACCA, G.B., ASPESI, I., and D'ARCANGELO, T.: 'Low-noise microwave down-converter with optimum matching at idle frequencies', *IEEE Trans.*, 1973, MTT-21, pp. 544-547

15 RUSTOM, S., and HOWSON, D.P.: 'Mixer noise figure using an improved resistive model', *Int. J. Electron.*, 1976, 41, pp. 159-167

16 KULESZA, B.L.J.: 'General theory of a lattice mixer', *Proc. IEE*, 1971, 118, (7), pp. 864-870

17 KOROLKIEWICZ, E., and KULESZA, B.L.J.: 'Effect of source resistance in microwave broad-band balanced mixers', *IEE J. Microwaves, Opt. & Acoust.*, 1978, 2, (6), pp. 183-187